

**A Morphological Assessment of the Health Status of a Cadaver Population at
the Faculty of Health Sciences, Stellenbosch University, with Special
Reference to Tuberculosis (TB) Lesion Distribution**

By

Elsje-Márie Geldenhuys

Dissertation presented for the degree of Doctor of Philosophy in Medical Sciences
(Morphological Sciences) in the Faculty of Medicine and Health Sciences, Stellenbosch
University



Supervisor: Prof. Sanet Kotzé
Co-Supervisor: Dr. Lené Burger

December 2014

DECLARATION

By submitting this dissertation electronically, I declare that the entirety of the work contained herein is my own, original work, that I am the sole author thereof (save to the extent explicitly otherwise stated), that reproduction and publication thereof by Stellenbosch University will not infringe any third party rights and that I have not previously in its entirety or in part submitted it for obtaining any qualification.

Signature.....

Date: 30 July 2014

ABSTRACT

Tuberculosis (TB) is a chronic pulmonary infection characterized by granulomatous inflammation, caseating necrosis and a propensity to develop fibrosis and cavitations. Pulmonary TB (PTB) lesions may develop in a variety of ways and can be grouped into primary, secondary, progressive primary and miliary TB based on their pathogenesis and morphological appearance. The Western Cape Province, South Africa, has a high TB burden with increasing TB notification rates. At Stellenbosch University (SU), approximately 90% of cadavers used for medical dissections come from impoverished communities where TB is a major health problem in terms of morbidity.

The aim of the present study was to assess the health status of a cadaver population (n=127) at the Faculty of Medicine and Health Sciences (FMHS), SU, with special reference to TB lesion distribution and prevalence.

For this study, full-body digital X-rays of 127 cadavers (87 males; 40 females; average age, 47.1 years) were obtained with the Lodox[®] Statscan[®] Imaging System after embalming and prior to dissection. A complete pathology report of six organ systems including the skeletal system was used in combination with histological examination, molecular analysis and radiological findings to investigate the prevalence and association between TB and systemic pathology. Samples for histological purposes were removed from organs with pathology lesions. For molecular studies, five different nucleic acid extraction methods were used to extract DNA from the formalin-fixed paraffin-embedded cadaver samples. Pulmonary samples were subjected to a line probe assay (LPA) and polymerase chain reactions (PCR) to determine mycobacterial genotypic distribution.

Two independent radiologists examined the chest X-rays and their findings were compared with the pulmonary findings.

PTB was a common finding in the cadaver population (76.4%) with males more commonly affected. A female predilection was observed for extrapulmonary TB. Statistically, TB was associated with pulmonary pathology, including pneumonia and bronchiectasis. Systemic pathology commonly encountered in the present study included neoplasms, coronary artery disease, colonic diverticula, hepatic triaditis, cirrhosis, glomerulosclerosis, pyelonephritis and a variety of healed maxillofacial and appendicular skeletal fractures. Extracted nucleic acid concentrations, as determined with the NanoDrop[®] spectrophotometer, ranged between 10ng/μl and 1000ng/μl. The standard salting-out method was found to be the most cost-effective and therefore the preferred method for nucleic acid extraction. The HAIN[®] MTBDR^{plus}[®] kit was effective in determining the presence of mycobacterial species belonging to the *Mycobacterium tuberculosis* complex (MTBC). The sensitivity to first-line drugs could not be determined as a result of DNA degradation. Spoligotyping was unsuccessful, as incomplete and unidentifiable hybridization of the 43 spacers occurred. The RD105 and MUB02/RD105 PCR results were non-reproducible and non-specific. Pulmonary cavitation and pleural thickening were the only findings that were positively correlated with the radiological findings ($p < 0.05$).

To our knowledge, this is the first study to extensively investigate TB and systemic pathology including histopathology, molecular techniques and postmortem radiology in cadavers from low socio-economic backgrounds from a high TB burden area. This study therefore provides a more complete and thorough understanding of the prevalence, distribution and morphology of TB lesions as well as the association between TB and systemic pathology.

ABSTRAK

Tuberkulose (TB) is a kroniese, pulmonêre infeksie gekenmerk deur granulomateuse ontsteking, verkasende nekrose en 'n neiging om fibrose en kavitasies te ontwikkel. Pulmonêre TB (PTB) letsels kan op verskeie wyses ontwikkel en kan, gebaseer op patogenese en morfologiese voorkoms, geklassifiseer word as primêre, sekondêre, progressiewe primêre of miliêre TB. Die Wes-Kaap provinsie, Suid-Afrika, het 'n hoë TB las met toenemende TB aanmeldingskoerse. Ongeveer 90% van die kadawers wat by die Universiteit Stellenbosch (US) gebruik word vir mediese disseksies kom van verarmde gemeenskappe waar TB 'n groot gesondheidsprobleem is in terme van die siektesyfer.

Die doel van hierdie studie was om die gesondheidstoestand te bepaal van 'n kadawerpopulasie (n=127) by die Fakulteit Geneeskunde en Gesondheidswetenskappe (FGG), US, met spesifieke verwysing na die verspreiding en voorkoms van TB letsels.

Digitale X-strale van die hele liggaam van 127 kadawers (87 manlik; 40 vroulik; gemiddelde ouderdom, 47.1 jaar) na balseming en voor disseksie is met behulp van die Lodox[®] Statscan[®] Imaging System bekom. 'n Volledige patologie-verslag van ses orgaanstelsels, die skeletstelsel ingesluit, is in kombinasie met histologiese ondersoeke, molekulêre ontleding en radiologiese bevindinge gebruik om die voorkoms van en assosiasie tussen TB en sistemiese patologie te ondersoek. Monsters vir histologiese studie is van organe met patologiese letsels geneem. Vir molekulêre studies is vyf verskillende nukleïensuur ekstraksie-metodes gebruik om DNS uit die formalien-gefikseerde paraffien-ingebed kadawermonsters te ekstraheer. Pulmonêre monsters is onderwerp aan 'n lyn-onderzoek-toets ("line probe assay") en polimerase-kettingreaksies (PKR)

om mikobakteriële genotipiese verspreiding te bepaal. Twee onafhanklike radioloë het die bors X-strale ondersoek en hulle bevindinge is vergelyk met die pulmonêre bevindinge.

PTB is 'n algemene bevinding in die kadawerpopulasie (76.4%) met mans wat meer dikwels geaffekteer is. 'n Vroulike voorkeur vir ekstrapulmonêre TB is waargeneem. TB is statisties geassosieër met pulmonêre patologie, longontsteking en brongiëktase. Sistemiese patologie wat algemeen gevind is in die huidige studie sluit in neoplasmas, koronêre hartsiekte, kolon divertikula, lewer triaditis, sirrose, glomerulosklerose, piëlo нефритis en 'n verskeidenheid geneesde maksillofasiale en appendikulêre skeletale frakture. Geëkstraheerde nukleïensuur-konsentrasies, soos bepaal met die NanoDrop[®] spektrofotometer, het gewissel tussen 10ng/μl en 1000ng/μl. Daar is gevind dat die standaard uitsoutings-metode die mees koste-effektief en dus die voorkeur-metode nukleïensuur ekstraksie-metode was. Die HAIN[®] MTBDR^{plus}[®] toets was effektief om die aanwesigheid van mikobakteriële spesies wat aan die *Mycobacterium tuberculosis* kompleks behoort, te bepaal. Sensitiwiteit vir eerste-linie middels kon nie bepaal word nie as gevolg van DNS degradasie. Spoligotipering was onsuksesvol omdat onvoltooide en onidentifiseerbare hibridisasie van die 43 merkers plaasgevind het. Die RD105 en MUB02/RD105 PCR resultate was nie-herhaalbaar en nie-spesifiek. Pulmonêre kavitasie en pleurale verdikking was die enigste bevindinge wat positief gekorreleer is met die radiologiese bevindinge ($p < 0.05$).

Na ons wete is hierdie studie die eerste een wat TB en sistemiese patologie ekstensief ondersoek en gebruik maak van histopatologie, molekulêre tegnieke en nadoodse radiologie in kadawers van lae sosio-ekonomiese agtergronde vanaf 'n area met 'n hoë TB las. Hierdie studie verskaf dus 'n meer volledige en deeglike begrip van die voorkoms, verspreiding en morfologie van TB letsels sowel as die assosiasie tussen TB en sistemiese patologie.

This thesis is dedicated to those, who even in death, teach us.

“hic locus est ubi mors gaudet succurrere vitae”

This is the place where death delights to help the living

ACKNOWLEDGEMENTS

My most humble and sincere thanks to:

First and foremost, my supervisors and mentors: Prof. Sanet Kotzé and Dr. Lené Burger, for their dedication, guidance, support and endless patience over the past four years. The Division of Anatomy and Histology, SU; in particular Prof. Ben Page, Prof. Paul van Helden, Mandi Alblas, Linda Greyling (“Mrs. G”), Madeleine Hanekom, Bertha Bastiaanse, Paul Pretorius, Marie de Beer, Basil Veenendaal, Warren Uithaler, Shumaya Uithaler, Jonathan Goliath, Logan Williams, Anthony Marthie, Lionel du Toit, Sara Seronne, Suhail Varachia, Danette van der Walt and Hannes du Toit (research assistants). The MBChB second and third years and cadavers of 2011 to 2013. The staff at the Western Cape Forensic Pathology Service medico-legal mortuary (Tygerberg Hospital), in particular Ms. Prudence Flaendorp, Mr. Stef Steiner, Lodox Systems and Mr. André du Toit, Forensic Pathology Histology Laboratory. The Histology lab, Prof. Tommie Victor’s lab and Prof. Rob Warren’s lab, FISAN Building, in particular, Reggie Williams, Elsa Garbett, Annemie Jordaan, Melanie Grobbelaar, Margaretha de Vos and Lizma Streicher. Profs Martin Kidd (biostatistician), Jan Lotz, Richard Pitcher and Dr. Michelle da Silva (Department Radiodiagnosis) as well as Dr. Johan Dempers (forensic pathologist) and Dr. Noor Mohamed (anatomical pathologist). Most of all, my mom and dad, Mandie and Stephan and brother, Christoff, for their constant support, encouragement, patience and love. Without you, this work would’ve been impossible to complete. My trusted friends, Julia Boonzaier, Elzet Kirsten, Leanie Kleynhans, Lizaan Ehlers, Lani Thiart, William Haylett, Francois Swanepoel, Carol Todd, Nabeela Kajee, Wilmaré van Wyk, Carika Hanekom and the Theunissen sisters (Christine, Anina and Tricia). And finally, my Heavenly Father for allowing me to see how He has “knitted the human body together in a mother’s womb” (Psalm 139), for His constant grace and for guiding me every single day of my life.

“I can do all this through Him who gives me strength.” ~ Philippians 4:13

RESEARCH OUTPUTS:

PUBLICATIONS AND PRESENTATIONS BASED ON THIS WORK

International Conferences:

1. **Kotzé SH, Geldenhuis E, Vorster W, Hoogland PVJM.** 2012. A morphological study of the vertebral venous plexus (VVP) and its connections in the macaque monkey, *Macacamulatta*. [Poster presentation at the Anatomical Society of Southern Africa (ASSA), Windhoek, Namibia – April 2012]
2. **Geldenhuis E, Burger EH, Kotzé SH.** 2012. The morphology of multiple Kaposi's sarcoma lesions in a cadaver: a case report. *International Journal of Experimental and Clinical Anatomy*, Volume6/2012 (S76) [Oral presentation at the Anatomical Society of Southern Africa (ASSA), Windhoek, Namibia – April 2012]. *Speaker was second runner up in the category "First time presenter"*.
3. **Geldenhuis E, Burger EH, Kotzé SH.** 2012. The morphology of multiple Kaposi's sarcoma lesions in a cadaver: a case report. *International Journal of Experimental and Clinical Anatomy*, Volume6/2012 (S76) [Poster presentation at the International Symposium for Clinical and Applied Anatomy (ISCAA), Ankara, Turkey – June 2012]
4. **Geldenhuis E, Burger EH, Jordaan AM, Van Helden PD, Kotzé SH.** 2013. The prevalence of emphysema in association with pulmonary tuberculosis in a cadaver population: a morphological study. [Poster presentation at the International Symposium for Clinical and Applied Anatomy (ISCAA), Graz, Austria – May 2013]
5. **Geldenhuis E, Burger EH, Greyling LM, Kotzé SH.** 2013. Mean cardiac valve circumference in a cadaver population at the Faculty of Medicine and Health Sciences,

Stellenbosch University. [Poster presentation at the International Symposium for Clinical and Applied Anatomy (ISCAA), Graz, Austria – May 2013]

National Conferences

1. **Geldenuys E, Burger EH, Jordaan AM, Van Helden PD, Kotzé SH.** 2013. The prevalence of emphysema in association with pulmonary tuberculosis in a cadaver population: a morphological study. [Oral presentation at the Anatomical Society of Southern Africa (ASSA), Durban, South Africa – April 2013]. *Speaker was second runner up in the category “Best presenter under the age of 35”*
2. **Geldenuys E, Burger EH, Greyling LM, Kotzé SH.** 2013. Mean cardiac valve circumference in a cadaver population at the Faculty of Medicine and Health Sciences, Stellenbosch University. [Poster presentation at the Anatomical Society of Southern Africa (ASSA), Durban, South Africa – April 2013]
3. **Geldenuys E, Burger EH, Jordaan AM, Streicher EM, Hanekom M, Warren RM, Victor TC, Van Helden PD, Kotzé SH.** 2014. An evaluation of five different mycobacterial DNA extraction methods from formalin-fixed paraffin-embedded (FFPE) pulmonary tissue removed from previously embalmed cadavers. [Poster presentation at the Anatomical Society of Southern Africa (ASSA), Stellenbosch, South Africa – April 2014]. *Speaker was first runner up in the category “Best Poster”*
4. **Geldenuys E, Burger EH, Jordaan AM, Streicher EM, Hanekom M, Warren RM, Victor TC, Van Helden PD, Kotzé SH.** 2014. Genotypic analysis of mycobacterial DNA from formalin-fixed paraffin-embedded (FFPE) pulmonary tissues from previously embalmed cadavers. [Poster presentation at the Anatomical Society of Southern Africa (ASSA), Stellenbosch, South Africa – April 2014]

5. **Da Silva MB, Geldenuys E, Burger EH, Lotz JW, Pitcher RD, Kotzé SH.** 2014. Standardizing the criteria for the examination of chest X-rays in embalmed cadavers. [Poster presentation at the Anatomical Society of Southern Africa (ASSA), Stellenbosch, South Africa – April 2014]

Annual Academic Year Day at the Faculty of Medicine and Health Sciences, Stellenbosch University:

1. **Kotzé SH, Geldenuys E, Vorster W, Hoogland PVJM.** 2012. A morphological study of the vertebral venous plexus (VVP) and its connections in the macaque monkey, *Macacamulatta*. [Poster presentation at Tygerberg Campus – August 2011]
2. **Geldenuys E, Burger EH, Kotzé SH.** 2012. The morphology of multiple Kaposi's sarcoma lesions in a cadaver: a case report. [Oral presentation at Tygerberg Campus – August 2012]
3. **Geldenuys E, Burger EH, Jordaan AM, Van Helden PD, Kotzé SH.** 2013. The prevalence of emphysema in association with pulmonary tuberculosis in a cadaver population: a morphological study. [Poster presentation at Tygerberg Campus – August 2013]
4. **Geldenuys E, Burger EH, Greyling LM, Kotzé SH.** 2013. Mean cardiac valve circumference in a cadaver population at the Faculty of Medicine and Health Sciences, Stellenbosch University. [Poster presentation at Tygerberg Campus – August 2013]
5. **Da Silva MB, Geldenuys E, Burger EH, Kotzé SH, Lotz JW, Pitcher RD.** 2013. A study correlating the chest radiographic features with the pulmonary dissection findings in embalmed cadavers. [Oral presentation at Tygerberg Campus – August 2013]

WORKSHOPS AND COURSES COMPLETED:

1. Successfully completed and passed the module *Anatomical Pathology for Non-Pathology Disciplines* (10391 871) which was orchestrated by the Division Anatomical Pathology, Department Pathology, Faculty of Medicine and Health Sciences, Stellenbosch University.
2. Attended the Bone Pathology Symposium from the 12 to 15 May 2014, which was hosted by the Department of Anatomy, School of Medicine, Faculty of Health Sciences, University of Pretoria, South Africa.

TABLE OF CONTENTS

Declaration.	i
Abstract.	ii
Abstrak.	iv
Acknowledgements.	viii
Research Outputs.	ix
List of Figures.	xxiii
List of Tables.	xxix
Abbreviations.	xxxiii
CHAPTER 1: Introduction.	1
1.1 General introduction.	2
1.1.1 The Study Location: Cape Town, Western Cape, South Africa.	3
1.2 Hypotheses, Aims and Objectives of the Study.	5
1.2.1 Morphologic Assessment: Hypotheses.	5
1.2.2 Morphologic Assessment: Aims.	6
1.2.3 Morphologic Assessment: Objectives.	6
1.2.4 Molecular Analysis: Hypotheses.	7
1.2.5 Molecular Analysis: Aims.	7
1.2.6 Molecular Analysis: Objectives.	8
1.2.7 Radiology Analysis: Hypothesis.	8
1.2.8 Radiology Analysis: Aim.	9
1.2.9 Radiology Analysis: Objective.	9
CHAPTER 2: Literature review.	10
2.1 History of Tuberculosis.	11
2.2 Tuberculosis in South Africa.	11
2.3 High-Risk Groups and Predisposing Conditions.	12
2.4 Etiology.	13
2.4.1 <i>Mycobacterium tuberculosis</i>	13
2.5 Pathogenesis and Pathology of Tuberculosis.	14
2.6 Spectrum of Tuberculosis.	14
2.6.1 Primary Tuberculosis.	14
2.6.2 Progressive Primary TB.	16
2.6.3 Secondary Tuberculosis (Post-Primary Tuberculosis).	16
2.6.4 Miliary Tuberculosis.	17
2.7 Morphology and Histopathology of Pulmonary Tuberculosis.	17
2.8 Complications of Tuberculosis.	18
2.9 Extrapulmonary Manifestations of Tuberculosis in Adults.	20
2.9.1 Tuberculous Lymphadenitis.	21
2.9.2 Tuberculosis of the Central Nervous System in Adults.	21

2.9.3 Tuberculous Pericarditis and Myocarditis in Adults.	22
2.9.4 Gastrointestinal Tract Tuberculosis in Adults.	24
2.9.4.1 Tuberculosis of the Oral Cavity.	25
2.9.4.2 Esophageal Tuberculosis.	25
2.9.4.3 Gastroduodenal Tuberculosis.	25
2.9.4.4 Ileocaecal Tuberculosis.	26
2.9.4.5 Colonic Tuberculosis.	27
2.9.4.6 Rectal and Anal Tuberculosis.	28
2.9.4.7 Hepatobiliary and Pancreatic Tuberculosis.	28
2.9.5 Tuberculosis of the Genitourinary System in Adults.	29
2.9.5.1 Renal Tuberculosis.	29
2.9.5.2 Male Genital Tuberculosis.	30
2.9.5.3 Female Genital Tuberculosis.	31
2.9.6 Tuberculosis of the Skeletal System in Adults.	31
2.9.6.1 Spinal Tuberculosis.	32
2.9.6.2 Peripheral Osteoarticular Tuberculosis.	32
2.10 Tuberculosis in Children.	33
2.11 Literature Survey of the Genotypic Characteristics of <i>M. tuberculosis</i>	34
2.11.1 The <i>M. tuberculosis</i> Beijing Genotype.	36
2.11.2 Mixed Infections.	38
2.11.3 Multidrug-Resistant Tuberculosis (MDR-TB).	38
2.11.4 Extensively Drug-Resistant Tuberculosis (XDR-TB).	39
2.12 Imaging of Tuberculosis in Adults: A Literature Survey.	40
2.12.1 Conventional Radiography (X-Ray).	40
2.12.2 Ultrasonography.	41
2.12.3 Computed Tomography (CT) and Magnetic Resonance Imaging (MRI).	41
2.12.4 Conventional Radiographical Imaging Findings: Primary TB.	41
2.12.5 Computed Tomography (CT) Imaging Findings: Primary TB.	43
2.12.6 Conventional Radiographical Imaging Findings: Progressive Primary TB.	43
2.12.7 Conventional Radiographical Imaging Findings: Secondary TB.	44
2.12.8 Computed Tomography (CT) Imaging Findings: Secondary TB.	45
2.12.9 Conventional Radiographical Imaging Findings: MDR-TB versus XDR-TB.	45
2.12.10 Lodox [®] Statscan [®] (Digital Imaging System).	48
CHAPTER 3: Materials and Methods.	51
3.1 Study Subjects.	52
3.2 Ethical Considerations.	56
3.3 Embalming by Intra-Arterial Injection into the Carotid Artery.	56
3.4 Lodox [®] Statscan [®]	57
3.5 Radiologists' Examination.	57
3.5.1 Evaluating the Cadaver Chest X-Ray.	59

3.6 Intra-arterial Injection of Latex into the Carotid Artery.	60
3.7 Anatomy Dissections by Medical Students.	60
3.8 Instruments and Equipment.	61
3.9 Cadaveric Dissections and Internal Examination.	61
3.9.1 Lungs.	62
3.9.2 Neck and Anterior Mediastinal Organs.	64
3.9.3 Heart and Pericardial Sac.	64
3.9.4 Hepatobiliary System.	64
3.9.5 Spleen.	65
3.9.6 Stomach and Small Intestine.	65
3.9.7 Pancreas.	66
3.9.8 Cecum, Appendix and Large Intestine.	66
3.9.9 Kidneys.	67
3.9.10 Lower Genitourinary Tract (Male).	67
3.9.11 Lower Genitourinary Tract (Female).	68
3.9.12 Male and Female External Genitalia.	68
3.9.13 Brain Removal and Examination.	68
3.9.14 Skeletal Evaluation.	69
3.10 Determination of Body Mass Index (BMI) of the Cadavers.	69
3.11 Pathologists' Examination.	70
3.12 Histology Procedures.	71
3.12.1 Histology Stains.	73
3.12.1.1 Hematoxylin and Eosin (H&E) Stain.	73
3.12.1.2 Ziehl-Neelsen (ZN) Stain.	73
3.12.1.3 Perls' Prussian Blue Stain.	74
3.12.1.4 Martius Scarlet Blue (MSB) Stain.	74
3.12.1.5 McManus's PAS Method for Glycogen and Fungal Cell Walls.	75
3.12.1.6 Verhoeff's Method for Elastic Methods.	76
3.12.2 Histology Controls.	76
3.13 Molecular Analysis.	78
3.13.1 Pulmonary Tissue Samples.	78
3.13.2 Wax Removal and Heating Procedures.	78
3.13.3 Nucleic Acid Extraction.	79
3.13.3.1 NucliSens [®] miniMag [®] Kit.	79
3.13.3.2 QIAamp [®] DNA Mini kit for Formalin-Fixed Paraffin-Embedded (FFPE) Tissue.	80
3.13.3.3 "Salting-out" Procedure (according to Miller <i>et al.</i> , 1988).	80
3.13.3.4 Genotype DNA Isolation (HAIN [®]) Kit.	81
3.13.3.5 Phenol/Chloroform Method.	81
3.13.4 Quantitation of Extracted DNA.	82

3.13.5 <i>Taq</i> Polymerase Enzymes.	82
3.13.6 Molecular Applications.	83
3.13.6.1 Spoligotyping.	83
3.13.6.2 HAIN [®] MTBDRplus [®] DNA Kit (version 2.0).	84
3.13.6.3 IS6110 PCR Protocol.	85
3.13.6.4 RD105 PCR Protocol.	86
3.13.6.5 Mtub02/RD105 PCR Protocol (according to Tsolaki <i>et al.</i> , 2005).	86
3.13.7 Agarose Gel Electrophoresis (AGE).	86
CHAPTER 4: Results.	88
4.1 Pulmonary System.	89
4.1.1 Tuberculosis.	89
4.1.1.1 Prevalence of Tuberculosis in the Study Subjects.	89
4.1.1.2 Pulmonary Tuberculosis Lesions.	89
4.1.1.3 Distribution of Pulmonary TB Lesions.	94
4.1.1.4 Distribution of Pulmonary TB Bronchopneumonia.	95
4.1.1.5 Histopathology of Pulmonary TB.	98
4.1.2 Pneumonias.	105
4.1.2.1 Tuberculous Bronchopneumonia.	105
4.1.2.2 Bronchopneumonia.	105
4.1.2.2.1 Distribution of Bronchopneumonia in the Cadavers.	106
4.1.2.3 Lobar Pneumonia.	108
4.1.2.4 Community-Acquired Atypical Pneumonia.	109
4.1.2.5 Lymphocytic Interstitial Pneumonitis (LIP).	110
4.1.2.6 Aspiration Pneumonia.	111
4.1.3 Chronic Obstructive Pulmonary Disease (COPD).	111
4.1.3.1 Emphysema.	111
4.1.3.1.1 Distribution of Emphysema in the Cadavers.	112
4.1.3.2 Chronic Bronchitis.	113
4.1.3.3 Bronchiectasis.	115
4.1.4 Acute Lung Injury.	115
4.1.4.1 Microbial Causes of Acute Lung Injury.	117
4.1.4.1.1 Viral Infections: <i>Cytomegalovirus</i>	117
4.1.4.1.2 Fungal Infections: <i>Pneumocystis jiroveci</i> (formerly <i>P. carinii</i>).	118
4.1.5 Pulmonary Neoplasms.	120
4.1.6 Pneumoconiosis.	123
4.1.7 Hemosiderosis.	125
4.1.8 Diseases of the Pulmonary Vascular Circulation.	126
4.1.8.1 Pulmonary Hypertension (PH).	126
4.1.8.2 Bone Marrow Embolism.	127
4.1.9 Pulmonary Edema.	128

4.2 Cardiovascular System.	130
4.2.1 Cardiac Tuberculosis.	130
4.2.2 Cardiomegaly.	130
4.2.3 Congenital Heart Disease.	131
4.2.4 Valvular Heart Disease.	131
4.2.4.1 Aortic Valvular Stenosis.	131
4.2.4.2 Mitral Valvular Stenosis.	132
4.2.4.3 Mitral Valve Replacement.	133
4.2.4.4 Pulmonary Stenosis.	133
4.2.4.5 Tricuspid Disease.	134
4.2.5 Ischemic Heart Disease (IHD).	134
4.2.5.1 Atheromatous Disease of the Coronary Arteries.	134
4.2.5.2 Healed Fibrotic Lesions.	136
4.2.6 Myocarditis.	137
4.2.7 Lipochrome (Lipofuscin) Deposition.	138
4.2.8 Hypertrophic Obstructive Cardiomyopathy (HOCM).	139
4.2.9 Vascular Pathology.	140
4.2.9.1 Arterial Atherosclerosis.	140
4.2.9.2 Arterial Aneurysms.	141
4.2.9.3 Venous Aneurysms.	143
4.2.9.4 Hemangiomas.	144
4.2.9.5 Kaposi's Sarcoma.	145
4.3 Gastrointestinal System.	147
4.3.1 Diseases of the Stomach.	147
4.3.1.1 Gastric Tuberculosis.	147
4.3.1.2 Gastric Ulcers.	147
4.3.1.3 Gastritis.	148
4.3.2 Diseases of the Intestines.	149
4.3.2.1 Intestinal Tuberculosis.	149
4.3.2.2 Benign Neoplastic Polyps of Intestinal Mucosa.	150
4.3.2.3 Intestinal Ulcers.	151
4.3.2.4 Intestinal Neoplasms.	152
4.3.2.4.1 Gastrointestinal Stromal Tumor (GIST).	152
4.3.2.5 Diverticular Disease.	153
4.3.2.6 Volvulus and Strangulation.	154
4.3.2.7 Parasitic Infestation.	155
4.3.2.7.1 <i>Ascaris lumbricoides</i>	155
4.3.3 Diseases of the Pancreas.	156
4.3.3.1 Pancreatic Tuberculosis.	156
4.3.3.2 Acute Pancreatitis.	157

4.3.3.3 Chronic Pancreatitis.	158
4.4 Hepatobiliary System.	159
4.4.1 Hepatic Tuberculosis.	159
4.4.2 Acute Triaditis.	161
4.4.3 Alcoholic Hepatitis.	161
4.4.4 Chronic Hepatitis.	162
4.4.5 Liver Cirrhosis.	163
4.4.6 Hepatic Steatosis.	165
4.4.7 Hepatic Neoplasms.	166
4.4.7.1 Hepatocellular Carcinoma.	167
4.4.7.2 Metastatic Carcinoma.	168
4.4.8 Tuberculosis of the Gallbladder.	169
4.4.9 Cholelithiasis.	170
4.4.10 Benign Gallbladder Neoplasms.	171
4.4.11 Chronic Cholecystitis.	173
4.5 Renal System.	174
4.5.1 Renal Tuberculosis.	174
4.5.2 Glomerulosclerosis.	175
4.5.3 Acute Pyelonephritis.	176
4.5.4 Chronic Pyelonephritis.	177
4.5.5 Cystic Renal Disease.	179
4.5.6 Hypertensive Nephrosclerosis.	181
4.5.7 Healed Fibrotic Scars.	182
4.5.8 Renal Neoplasms.	183
4.6 Male Genital System.	186
4.6.1 Diseases of the Prostate.	186
4.6.1.1 Benign Prostatic Hyperplasia.	186
4.6.1.2 Prostatic Adenocarcinoma.	187
4.6.1.3 Corpora Amylacea.	188
4.6.1.4 Prostatitis.	189
4.6.2 Diseases of the Testis.	190
4.6.2.1 Testicular Tuberculosis.	190
4.6.2.2 Hydrocele.	191
4.6.2.3 Varicocele.	191
4.7 Female Genital System.	192
4.7.1 Uterine Fibroid Leiomyomas.	192
4.7.2 Cervical Intraepithelial Neoplasia (CIN).	193
4.8 Lymphoreticular System.	194
4.8.1 Lymph Node Involvement.	194
4.8.1.1 Tuberculous Lymphadenitis.	194

4.8.1.2 Lymphomatous Malignancy.	196
4.8.2 Spleen.	196
4.8.2.1 Splenic Tuberculosis.	196
4.9 Brain.	198
4.9.1 Tuberculosis of the Brain.	198
4.9.2 Hydrocephalus.	199
4.9.3 Cerebrovascular Disease.	199
4.9.3.1 Cerebral Infarction.	199
4.9.4 Bacterial Infections.	200
4.9.4.1 Bacterial Meningitis.	200
4.10 Breast.	201
4.10.1 Fibrocystic Change.	201
4.10.2 Fibroadenoma.	202
4.11 Skeletal System.	203
4.11.1 Study Subjects.	203
4.11.2 Skull.	203
4.11.2.1 Maxillofacial Fractures.	203
4.11.2.2 Maxillary and Mandibular Apical Periodontal Cysts.	205
4.11.2.3 Mandibular Trauma.	206
4.11.2.4 Mandibular Implants.	207
4.11.3 Spine.	209
4.11.3.1 Vertebral Tuberculosis.	209
4.11.3.2 Surgical Fusion.	210
4.11.3.3 Diffuse Idiopathic Skeletal Hyperostosis (DISH).	210
4.11.3.4 Spina Bifida (Rachischisis).	212
4.11.3.5 Vertebral Osteophytes.	213
4.11.3.6 Spondylolysis.	215
4.11.3.7 Sacral Trauma.	216
4.11.3.8 Transitional Vertebrae at the Lumbosacral Level.	217
4.11.4 Thorax.	218
4.11.4.1 Rib Lesions.	218
4.11.4.1.1 Prevalence and Distribution of Rib Lesions.	220
4.11.4.1.2 Morphology of the Rib Lesions.	222
4.11.4.2 Rib Trauma.	224
4.11.4.3 Sternum.	226
4.11.4.3.1 Pectus Carinatum (Pigeon Breast).	226
4.11.4.4 Clavicle.	227
4.11.4.4.1 Clavicular Trauma.	227
4.11.5 Upper Limb.	228
4.11.5.1 Healed Trauma of the Upper Limb.	228

4.11.5.2 Scapula.	230
4.11.5.2.1 Scapular Trauma.	230
4.11.5.2.2 Dislocation in the Shoulder Joint.	231
4.11.5.2.3 Degenerative Joint Disease of the Upper Limb.	232
4.11.6 Lower Limb.	233
4.11.6.1 Healed Trauma of the Lower Limb.	233
4.11.6.2 Patellar Fractures.	235
4.11.6.3 Degenerative Joint Disease of the Hip Joint.	235
4.11.6.4 Bilateral Total Hip Arthroplasty (THA).	236
4.11.6.5 Pelvic Trauma.	237
4.11.6.6 Sacroiliac Joint (SIJ) Fusion.	238
4.11.6.7 Degenerative Joint Disease of the Knee Joint.	239
4.11.7 Infectious Diseases.	240
4.11.7.1 Osteomyelitis.	240
4.11.8 Circulatory Disorders.	241
4.11.8.1 Hypertrophic (Pulmonary) Osteoarthropathy (HPOA).	241
4.11.9 Hematological Disorders.	243
4.11.9.1 Cribra Orbitalia (CO).	243
4.11.10 Miscellaneous Bone Conditions.	244
4.11.10.1 Paget's Disease of the Bone (Osteitis Deformans).	244
4.11.10.2 Internal Frontal Hyperostosis (IFH).	245
4.11.12 Distribution of Skeletal Pathology in the Cadaver Cohort.	247
4.12 Statistical Analysis.	248
4.12.1 Risk Factors for Tuberculosis.	248
4.12.1.1 Sex.	248
4.12.1.1.1 Association between Sex Disparity and Pulmonary TB.	248
4.12.1.1.2 Association between Sex Disparity and Extrapulmonary TB.	248
4.12.1.2 Body Mass Index.	249
4.12.2 Pulmonary TB versus Pulmonary Disease.	250
4.12.2.1 Association between Pulmonary TB and Bronchopneumonia.	250
4.12.2.2 Association between Pulmonary TB and Bronchiectasis.	251
4.12.2.3 Association between Pulmonary TB and Pleural Thickening.	252
4.12.2.4 Association between Pulmonary TB and Emphysema.	253
4.12.3 Statistically Independent Pulmonary Findings in the Cadaver Cohort.	254
4.12.4 Correspondence Analysis.	255
4.12.5 Association between Pulmonary TB and Rib Lesions.	256
4.12.6 Correspondence Analysis.	258
4.12.6.1 Association between the Prevalence of Pulmonary and Extrapulmonary TB, Sex and Risk Factors.	258
4.13 Molecular Analysis.	259

4.13.1	Quantitation of Nucleic Acids.	259
4.13.2	Molecular Techniques to Demonstrate <i>M. tuberculosis</i>	260
4.13.2.1	HAIN [®] MTBDRplus [®] DNA kit (ver. 2.0).	260
4.13.2.2	IS6110 PCR.	262
4.13.3	Molecular Techniques for Typing of <i>M. tuberculosis</i>	263
4.13.3.1	Spoligotyping.	263
4.13.3.2	RD105 and Mtub02/RD105 PCR.	264
4.13.4	Overall Combination of Macroscopic and Molecular Results.	265
4.14	Radiological Analysis: Chest X-Ray Evaluation.	267
4.14.1	Pulmonary Analysis.	267
4.14.1.1	Pulmonary Cavitation.	267
4.14.1.2	Emphysematous Appearance.	268
4.14.1.3	Consolidation.	268
4.14.1.4	Pneumothorax.	269
4.14.2	Statistical Findings.	270
4.14.2.1	Radiology versus Pathology: Segments 1-6.	270
4.14.2.2	Radiology versus Pathology: Segment 1.	272
4.14.2.3	Radiology versus Pathology: Segment 2.	273
4.14.2.4	Radiology versus Pathology: Segment 3.	274
4.14.2.5	Radiology versus Pathology: Segment 4.	275
4.14.2.6	Radiology versus Pathology: Segment 5.	276
4.14.2.7	Radiology versus Pathology: Segment 6.	277
4.14.3	Evaluation: Cardiovascular Findings.	278
4.14.3.1	Cardiomegaly.	278
4.14.3.2	Hyperattenuation of Aortas.	279
CHAPTER 5: Discussion and Conclusion.		281
5.1	Main Findings: Morphological Analysis.	282
5.1.1	Pulmonary Tuberculosis.	282
5.1.2	Systemic (Extrapulmonary) Tuberculosis.	283
5.1.3	Risk Factors for Tuberculosis.	294
5.1.4	Systemic Pathology.	298
5.1.4.1	Pulmonary System.	298
5.1.4.2	Cardiovascular System.	305
5.1.4.3	Gastrointestinal Tract System.	312
5.1.4.4	Hepatobiliary System.	319
5.1.4.5	Renal System.	323
5.1.4.6	Genital System.	326
5.1.4.7	Lymphoreticular System.	329
5.1.4.8	Brain.	330
5.1.4.9	Breast.	333

5.1.4.10 Skeletal System.	333
5.1.5 Statistically Significant Trends Observed in the Present Study.	349
5.2 Main Findings: Molecular Analysis.	357
5.3 Main Findings: Radiological Analysis.	364
5.4 Postmortem Changes Mimicking Disease.	365
5.5 Impact of the Study.	369
5.6 Limitations of the Study.	372
5.7 Future Research.	374
5.8 Conclusion.	376
REFERENCE LIST.	381
ADDENDA.	442
Addendum A: Standard formula for embalming at the Division Anatomy and Histology, SU..	443
Addendum B: Weights of the lungs and hearts of the cadaver cohort (n=127).	444
Addendum C: Cardiac valve measurements in the 2012 cadaver cohort (n=43).	446
Addendum D: Cardiac valve measurements in the 2013 cadaver cohort (n=44).	447
Addendum E: Body weights and estimated body mass index (BMI) of the cadavers (n=127). .	448
Addendum F: Protocol for the standard Hematoxylin and Eosin technique for paraffin sections.	449
Addendum G: Protocol for the Ziehl-Neelsen technique for acid-fast bacteria.	450
Addendum H: Protocol for the Perls' Prussian blue reaction for ferric iron.	451
Addendum I: Protocol for the Martius Scarlet Blue (MSB) stain for fibrin.	452
Addendum J: Protocol for the Periodic Acid-Schiff (PAS) technique.	454
Addendum K: Protocol for the Verhoeff's method for elastic fibers.	455
Addendum L: A summary of the distribution of systemic TB lesions in the cadaver cohort (n=127).	456

LIST OF FIGURES

Figure 1.1. Nine provinces of South Africa.	3
Figure 2.1. An example of a granuloma and a Langhans multinucleated giant cell.	18
Figure 2.2. Examples of lymphadenopathy and Ranke Complex.	46
Figure 2.3. Primary Tuberculosis.	46
Figure 2.4. Secondary Tuberculosis.	47
Figure 2.5. Miliary Tuberculosis.	47
Figure 2.6. Lodox [®] Statscan [®]	48
Figure 3.1. Lung segments of the cadaver cohort (n = 40).	58
Figure 3.2. Example of a cadaver chest X-ray (K05/11), posterior-anterior (PA) view.	59
Figure 3.3. Instruments used during the dissections.	61
Figure 3.4. Photographs of the pulmonary system of cadaver K36/10.	62
Figure 3.5. Photographs indicating the dissection process to investigate the pulmonary parenchyma.	63
Figure 3.6. Photograph indicating the dissection process to investigate the hepatic parenchyma.	65
Figure 3.7. Photograph indicating the dissection process to investigate the splenic and pancreatic parenchyma.	66
Figure 3.8. Photograph indicating the dissection process to investigate the renal parenchyma.	67
Figure 3.9. Histology laboratory.	71
Figure 3.10. Sample sectioning.	72
Figure 3.11. Summary of the experimental design of the study.	77
Figure 3.12. Samples for molecular analyses.	78
Figure 4.1. Overall distribution of pulmonary TB lesions in the cadaver cohort.	94
Figure 4.2. Overall distribution of TB bronchopneumonia in the cadaver cohort.	95
Figure 4.3. Macroscopic appearance of superior lobe cavities in the pulmonary system.	96
Figure 4.4. Macroscopic appearance of granulomatous inflammation in the pulmonary system.	97
Figure 4.5. Macroscopic appearance of caseous necrosis.	98
Figure 4.6. Macroscopic appearance of tuberculous bronchopneumonia.	98
Figure 4.7. Microscopic appearance of TB granulomas in the pulmonary tissue.	103
Figure 4.8. Microscopic appearance the Langhans cells in the TB lesions.	104
Figure 4.9. Ziehl-Neelsen stains.	105
Figure 4.10. Overall distribution of bronchopneumonia in the cadaver cohort.	107
Figure 4.11. Macroscopic appearance of bronchopneumonia.	107
Figure 4.12. Microscopic appearance of bronchopneumonia.	108
Figure 4.13. Microscopic appearance of interstitial pneumonia.	109

Figure 4.14. Microscopic appearance of lymphocytic interstitial pneumonitis (LIP).	110
Figure 4.15. Overall distribution of emphysema in the cadaver cohort.	112
Figure 4.16. Macroscopic appearance of emphysema in the cadavers.	113
Figure 4.17. Microscopic appearance of emphysema in the cadavers.	113
Figure 4.18. Microscopic appearance of chronic bronchitis.	114
Figure 4.19. Macroscopic appearance of bronchiectasis.	115
Figure 4.20. Fibrin deposition in acute lung injury.	117
Figure 4.21. Microscopic appearance of cytomegalovirus infection.	118
Figure 4.22. Microscopic appearance of <i>Pneumocystis jiroveci</i> infection.	119
Figure 4.23. Radiologic appearance of pulmonary tumors.	121
Figure 4.24. Macroscopic appearance of sarcomatoid and squamous cell carcinoma.	122
Figure 4.25. Microscopic appearance of pulmonary neoplasms.	122
Figure 4.26. Macroscopic appearance of anthracosis.	124
Figure 4.27. Microscopic appearance of anthracotic pigmentation within pulmonary tissue. ...	125
Figure 4.28. Microscopic difference between carbon-laden macrophages and siderophages. ...	126
Figure 4.29. Microscopic appearance pulmonary hypertension in cadaver K10/10.	127
Figure 4.30. Microscopic appearance of a bone marrow embolism of cadaver K30/10.	128
Figure 4.31. Pulmonary edema.	129
Figure 4.32. Cardiomegaly.	130
Figure 4.33. Atrial septal defect.	131
Figure 4.34. Mitral valve replacement.	133
Figure 4.35. Coronary artery atherosclerosis.	135
Figure 4.36. Microscopic appearance of coronary artery atherosclerosis.	136
Figure 4.37. Microscopic appearance of fibrotic lesions in the cardiac wall.	137
Figure 4.38. Microscopic appearance of myocarditis.	138
Figure 4.39. Microscopic appearance of lipofuscin.	138
Figure 4.40. Microscopic appearance of hypertrophic obstructive cardiomyopathy (HOCM)..	140
Figure 4.41. Aortic atherosclerosis superior to the aortic valve.	141
Figure 4.42. Aortic cholesterol slits.	141
Figure 4.43. Fusiform abdominal aneurysm.	142
Figure 4.44. Arterial dissection.	143
Figure 4.45. Popliteal venous aneurysms.	144
Figure 4.46. Benign hemangioma in the liver.	145
Figure 4.47. Morphology of Kaposi's Sarcoma lesions in an embalmed cadaver.	146
Figure 4.48. The morphology of gastric ulcers.	148
Figure 4.49. Microscopic appearance of chronic gastritis.	149
Figure 4.50. Microscopic appearance of intestinal TB.	150
Figure 4.51. Benign neoplastic polyps in the cadaver cohort.	151
Figure 4.52. The microscopic appearance of intestinal ulcers.	152
Figure 4.53. Gastrointestinal stromal tumor.	153

Figure 4.54. Distribution of colonic diverticula in the cadaver cohort.	153
Figure 4.55. Microscopic appearance of diverticula.	154
Figure 4.56. Intestinal volvulus.	155
Figure 4.57. <i>Ascaris lumbricoides</i>	156
Figure 4.58. Microscopic appearance of pancreatic tuberculosis.	157
Figure 4.59. Acute pancreatitis.	158
Figure 4.60. Chronic pancreatitis.	159
Figure 4.61. Hepatic tuberculosis.	160
Figure 4.62. Microscopic appearance of acute triaditis.	161
Figure 4.63. Microscopic appearance of alcoholic hepatitis.	162
Figure 4.64. Microscopic appearance of chronic hepatitis.	163
Figure 4.65. Morphology of liver cirrhosis.	165
Figure 4.66. Microscopic appearance of hepatic steatosis.	166
Figure 4.67. Morphology of hepatocellular carcinoma.	168
Figure 4.68. Hepatic metastases.	169
Figure 4.69. Tuberculosis of the gallbladder.	170
Figure 4.70. Cholelithiasis.	171
Figure 4.71. Adenomyoma of the gallbladder.	172
Figure 4.72. Adenoma of the gallbladder.	172
Figure 4.73. Microscopic appearance of chronic cholecystitis.	173
Figure 4.74. Microscopic appearance of renal tuberculosis.	175
Figure 4.75. Microscopic appearance of sclerosis of glomeruli.	176
Figure 4.76. Microscopic appearance of acute pyelonephritis.	177
Figure 4.77. Microscopic appearance of chronic pyelonephritis.	179
Figure 4.78. Macroscopic appearance of simple renal cysts.	180
Figure 4.79. Microscopic appearance of simple renal cysts.	181
Figure 4.80. Microscopy of nephrosclerosis.	182
Figure 4.81. Healed fibrotic renal infarction.	183
Figure 4.82. Macroscopic appearance of renal tumors in our cadaver cohort.	184
Figure 4.83. Microscopic appearance of renal tumors in our cadaver cohort.	185
Figure 4.84. Immunohistochemistry of the renal tumor in cadaver K106/12.	185
Figure 4.85. PAS stain of the tumor in cadaver K106/12.	186
Figure 4.86. Benign prostatic hyperplasia (BPH).	187
Figure 4.87. Prostatic adenocarcinoma.	188
Figure 4.88. Corpora amylacea.	189
Figure 4.89. Microscopy of chronic prostatitis.	190
Figure 4.90. Testicular TB.	190
Figure 4.91. Hydrocele.	191
Figure 4.92. Microscopic appearance of varicocele.	192
Figure 4.93. Uterine leiomyoma.	193

Figure 4.94. Microscopic appearance of cervical intraepithelial neoplasia (CIN).	194
Figure 4.95. Morphologic appearance of tuberculous lymphadenitis.	195
Figure 4.96. Microscopic appearance of lymphomatous malignancy.	196
Figure 4.97. Splenic TB.	198
Figure 4.98. Cerebral infarction.	200
Figure 4.99. Purulent leptomeningitis.	201
Figure 4.100. Fibrocystic change of the female breast.	202
Figure 4.101. Fibroadenoma of the female breast.	202
Figure 4.102. Healed maxillofacial trauma.	205
Figure 4.103. Maxillary apical periodontal cysts.	206
Figure 4.104. Healed mandibular fractures.	207
Figure 4.105. Fixed mandibular prosthesis.	208
Figure 4.106. Vertebral tuberculosis (Pott's disease).	209
Figure 4.107. Anterior cervical fixation.	210
Figure 4.108. Diffuse idiopathic skeletal hyperostosis (DISH).	211
Figure 4.109. Spinal fusion as a result of DISH in cadaver K62/11.	212
Figure 4.110. Spina bifida.	213
Figure 4.111. Osteophytic changes.	215
Figure 4.112. Spondylolysis.	216
Figure 4.113. Fracture of the sacrum.	216
Figure 4.114. Sacralisation and lumbarisation.	218
Figure 4.115. Parietal pleural attachment.	220
Figure 4.116. Position of periostotic lesions on each individual rib.	221
Figure 4.117. The position and number of periostotic lesions on each individual rib.	221
Figure 4.118. The number of rib lesions affecting the right and left side, unilaterally, as well as the number of bilateral involvement.	222
Figure 4.119. Subperiosteal rib lesions.	223
Figure 4.120. Proliferative rib lesions.	223
Figure 4.121. Proliferative rib lesions.	223
Figure 4.122. Plaque-like rib lesion.	223
Figure 4.123. Healed rib trauma.	226
Figure 4.124. Pectus carinatum.	227
Figure 4.125. Clavicular trauma.	227
Figure 4.126. Healed upper limb fractures.	229
Figure 4.127. Upper limb fractures and repair.	229
Figure 4.128. Healed scapular fractures.	230
Figure 4.129. Permanent shoulder dislocation.	231
Figure 4.130. Osteoarthritis in the upper limb.	233
Figure 4.131. Tibial and fibular repair.	234
Figure 4.132. Patellar fractures.	235

Figure 4.133. Bilateral total hip arthroplasty (K106/09).	236
Figure 4.134. Pelvic trauma.	237
Figure 4.135. Fusion of sacrum to os coxae.	238
Figure 4.136. Osteoarthritis in the knee joint.	239
Figure 4.137. Osteomyelitis.	240
Figure 4.138. Hypertrophic pulmonary osteoarthropathy (HPOA) in cadaver K83/09.	242
Figure 4.139. Hypertrophic (pulmonary) osteoarthropathy (HPOA).	243
Figure 4.140. Cribriform orbitalia in the cadaver cohort.	244
Figure 4.141. Paget's Disease (Osteitis deformans).	245
Figure 4.142. Internal frontal hyperostosis.	246
Figure 4.143. Summary of skeletal pathology.	247
Figure 4.144. Association between sex and prevalence of extrapulmonary TB.	249
Figure 4.145. Association between body mass index (BMI) and prevalence of pulmonary TB.	250
Figure 4.146. Association between pulmonary TB and bronchopneumonia.	251
Figure 4.147. Association between pulmonary TB and bronchiectasis.	252
Figure 4.148. Association between pulmonary TB and pleural thickening.	253
Figure 4.149. Association between pulmonary TB and emphysema.	254
Figure 4.150. A graphical representation of the association between pulmonary TB and pulmonary findings.	255
Figure 4.151. Association between pulmonary TB and rib lesions.	257
Figure 4.152. A graphical representation of the association between pulmonary TB and rib lesions.	257
Figure 4.153. A graphical representation of the association between pulmonary TB, extrapulmonary TB, sex and general risk factors for TB.	259
Figure 4.154. HAIN [®] MTBDRplus [®] DNA kit results.	261
Figure 4.155. HAIN [®] MTBDRplus [®] DNA kit results.	261
Figure 4.156. IS6110 PCR gel electrophoresis.	263
Figure 4.157. Spoligotyping patterns of some of the isolates analysed in the present study. ...	264
Figure 4.158. Cross-tabulation to determine the statistical significance between the molecular and pathology results.	266
Figure 4.159. Pulmonary cavitation on the chest X-ray of the first cadaver cohort (n=40). ...	267
Figure 4.160. Emphysema on the chest X-ray of the first cadaver cohort (n=40).	268
Figure 4.161. Consolidation on the chest X-ray of the first cadaver cohort (n=40).	269
Figure 4.162. Pneumothorax on the chest X-ray of the first cadaver cohort (n=40).	269
Figure 4.163. Association between radiology and pathology: pulmonary cavitation.	270
Figure 4.164. Association between radiology and pathology: pleural thickening.	271
Figure 4.165. Association between radiology and pathology: pulmonary cavitation.	272
Figure 4.166. Association between radiology and pathology: pleural thickening.	273
Figure 4.167. Association between radiology and pathology: pulmonary cavitation.	274

Figure 4.168. Association between radiology and pathology: pulmonary cavitation.	276
Figure 4.169. Association between radiology and pathology: pulmonary cavitation.	277
Figure 4.170. Association between radiology and pathology: pleural thickening.	278
Figure 4.171. Cardiac features on the cadaver CXR.	279
Figure 4.172. Hyperattenuation of the aortas on the CXR.	280

LIST OF TABLES

Table 3.1. Demographic information of the 2011 cadaver cohort.	53
Table 3.2. Demographic information of the 2012 cadaver cohort.	54
Table 3.3. Demographic information of the 2013 cadaver cohort.	55
Table 3.4. Modules covered in the anatomy curricula at the Division Anatomy and Histology.	60
Table 3.5. The intercept and slope values for race and gender.	70
Table 3.6. Total number of tissue samples stained with the standard H&E.	72
Table 3.7. Histology stains used in the present study.	73
Table 3.8. Controls used in the present study.	76
Table 4.1. The prevalence of tuberculosis in the cadaver cohort (n=127).	89
Table 4.2. Macroscopical appearance of tuberculosis in the cadaver cohort (n=127).	90
Table 4.3. Microscopy and Ziehl-Neelsen (ZN) results in the cadaver cohort (n=127).	99
Table 4.4. The prevalence of bronchopneumonia in the cadaver cohort (n=127).	106
Table 4.5. Interstitial pneumonia in the cadaver cohort (n=127).	109
Table 4.6. Lymphocytic interstitial pneumonitis in the cadaver cohort (n=127).	110
Table 4.7. Aspiration pneumonia in the cadaver cohort (n=127).	111
Table 4.8. The prevalence of emphysema in the cadaver cohort (n=127).	112
Table 4.9. Chronic bronchitis in the cadaver cohort (n=127).	114
Table 4.10. Acute lung injury in the cadaver cohort (n=127).	116
Table 4.11. Cytomegalovirus infection in the cadaver cohort (n=127).	118
Table 4.12. <i>Pneumocystis jiroveci</i> infection in the cadaver cohort (n=127).	119
Table 4.13. Types of pulmonary tumors in the cadaver cohort (n=127).	121
Table 4.14. Pulmonary hypertension (PH) in the cadaver cohort (n=127).	127
Table 4.15. Cardiomegaly in the cadaver cohort (n=127).	130
Table 4.16. Aortic stenosis in the cadaver cohort (n=127).	132
Table 4.17. Mitral stenosis in the cadaver cohort (n=127).	132
Table 4.18. Pulmonary stenosis in the cadaver cohort (n=127).	134
Table 4.19. Percentage occlusion in the coronary arteries of the cadavers (n=127).	135
Table 4.20. Fibrotic lesions in the cardiac wall in the cadaver cohort (n=127).	136
Table 4.21. Myocarditis in the cadaver cohort (n=127).	137
Table 4.22. Hypertrophic obstructive cardiomyopathy in the cadaver cohort (n=127).	139
Table 4.23. Measurement of the cardiac chamber walls of the cadavers with HOCM.	139
Table 4.24. Arterial atherosclerosis in the cadaver cohort (n=127).	140
Table 4.25. Arterial aneurysms in the cadaver cohort (n=127).	142
Table 4.26. Arterial dissection in the cadaver cohort (n=127).	142
Table 4.27. Venous aneurysm in the cadaver cohort (n=127).	143
Table 4.28. Hemangioma in the cadaver cohort (n=127).	144

Table 4.29. Organs affected by Kaposi's sarcoma (KS) lesions in cadaver K02/10.	145
Table 4.30. Gastric ulcers in the cadaver cohort (n=127).	147
Table 4.31. Gastritis in the cadaver cohort (n=127).	148
Table 4.32. Tuberculous involvement of the intestines in the cadaver cohort (n=127).	149
Table 4.33. Intestinal polyps and their anatomical locations in the cadaver cohort (n=127).	150
Table 4.34. Intestinal ulcers and their anatomical locations in the cadaver cohort (n=127).	152
Table 4.35. Gastrointestinal stromal tumor (GIST) in the cadaver cohort (n=127).	152
Table 4.36. Colonic diverticula in the cadaver cohort (n=127).	154
Table 4.37. Intestinal volvulus in the cadaver cohort (n=127).	154
Table 4.38. <i>Ascaris lumbricoides</i> infestation of the intestines in the cadaver cohort (n=127). .	155
Table 4.39. Pancreatic tuberculosis in the cadaver cohort (n=127).	157
Table 4.40. Acute pancreatitis in the cadaver cohort (n=127).	157
Table 4.41. Chronic pancreatitis in the cadaver cohort (n=127).	158
Table 4.42. Tuberculosis involvement of the liver in the cadaver cohort (n=127).	160
Table 4.43. Acute triaditis in the cadaver cohort (n=127).	161
Table 4.44. Alcoholic hepatitis in the cadaver cohort (n=127).	162
Table 4.45. Chronic hepatitis in the cadaver cohort (n=127).	163
Table 4.46. Cirrhosis in the cadaver population (n=127).	164
Table 4.47. Hepatic steatosis in the cadaver cohort (n=127).	165
Table 4.48. Hepatic neoplasms in the cadaver cohort (n=127).	167
Table 4.49. Cholelithiasis in the cadaver cohort (n=127).	171
Table 4.50. Benign neoplasms of the gallbladder in the cadaver cohort (n=127).	172
Table 4.51. Cholecystitis in the cadaver cohort (n=127).	173
Table 4.52. Renal tuberculosis in the cadaver cohort (n=127).	174
Table 4.53. Sclerosis of glomeruli in the cadaver cohort (n=127).	175
Table 4.54. Acute pyelonephritis in the cadaver cohort (n=127).	177
Table 4.55. Chronic pyelonephritis in the cadaver cohort (n=127).	178
Table 4.56. Simple renal cysts in the cadaver cohort (n=127).	180
Table 4.57. Hypertensive nephrosclerosis in the cadaver cohort (n=127).	182
Table 4.58. Healed fibrotic renal scars in the cadaver cohort (n=127).	183
Table 4.59. Renal tumors in the cadaver cohort (n=127).	184
Table 4.60. Benign prostatic hyperplasia in the cadaver cohort (n=56).	187
Table 4.61. Prostatic adenocarcinoma in the cadaver cohort (n=56).	188
Table 4.62. Corpora amylacea in the cadaver cohort (n=56).	188
Table 4.63. Prostatitis in the cadaver cohort (n=56).	189
Table 4.64. Testicular TB in the cadaver cohort (n=56).	190
Table 4.65. Hydrocele in the cadaver cohort (n=56).	191
Table 4.66. Varicocele in the cadaver cohort (n=56).	191
Table 4.67. Uterine leiomyomas in the cadaver cohort (n=40).	192
Table 4.68. Cervical intraepithelial neoplasia in the cadaver cohort (n=40).	193

Table 4.69. Tuberculous lymphadenitis in the cadaver cohort (n=127).	195
Table 4.70. Lymphomatous Malignancy.	196
Table 4.71. Tuberculosis involvement of the spleen in the cadaver cohort (n=127).	197
Table 4.72. Hydrocephalus in the cadaver population (n=80).	199
Table 4.73. Cerebral infarctions in the cadaver cohort (n=80).	199
Table 4.74. Bacterial meningitis in the cadaver cohort (n=80).	201
Table 4.75. Fibrocystic change in the female cadaver cohort (n=40).	201
Table 4.76. Fibroadenoma in the female cadaver cohort (n=40).	202
Table 4.77. Maxillofacial trauma in the cadaver cohort (n=124).	204
Table 4.78. Maxillary and mandibular apical periodontal cysts in the cadaver cohort (n=124)...	206
Table 4.79. Mandibular trauma in the cadaver cohort (n=124).	207
Table 4.80. Mandibular implants in the cadaver cohort (n=124).	208
Table 4.81. DISH in the cadaver cohort (n=124).	211
Table 4.82. Spina bifida in the cadaver cohort (n=124).	213
Table 4.83. Vertebral osteophytosis in the cadaver cohort (n=124).	213
Table 4.84. Spondylolysis in the cadaver cohort (n=124).	215
Table 4.85. Lumbarisation and sacralisation in the cadaver cohort (n=124).	217
Table 4.86. Rib lesions in the cadaver cohort (n=124).	218
Table 4.87. Rib trauma in the cadaver cohort (n=124).	224
Table 4.88. Pectus carinatum in the cadaver cohort (n=124).	226
Table 4.89. Clavicular trauma in the cadaver cohort (n=124).	227
Table 4.90. Upper limb fractures in the cadaver cohort (n=124).	228
Table 4.91. Scapular fractures in the cadaver cohort (n=124).	230
Table 4.92. Degeneration of the upper limb in the cadaver cohort (n=124).	232
Table 4.93. Lower limb fractures in the cadaver cohort (n=124).	233
Table 4.94. Patellar fractures in the cadaver cohort (n=124).	235
Table 4.95. Pelvic osteoarthritis in the cadaver cohort (n=124).	236
Table 4.96. Pelvic trauma in the cadaver cohort (n=124).	237
Table 4.97. Sacral fusion to os coxae in the cadaver cohort (n=124).	238
Table 4.98. Degeneration of the knee joint in the cadaver cohort (n=124).	239
Table 4.99. Osteomyelitis of the skeleton in the cadaver cohort (n=124).	240
Table 4.100. Hypertrophic (pulmonary) osteoarthropathy in the cadaver cohort (n=124).	241
Table 4.101. Cribra orbitalia (CO) in the cadaver cohort (n=124).	243
Table 4.102. Internal frontal hyperostosis (IFH) in the cadaver cohort (n=124).	246
Table 4.103. Pulmonary findings that were statistically independent from pulmonary TB.	254
Table 4.104. A summary of the extraction methods used in this study.	260
Table 4.105. Observed frequencies in all of the segments in the first cadaver cohort (n=40)...	271
Table 4.106. Observed frequencies in the first segment in the first cadaver cohort (n=40).	273
Table 4.107. Observed frequencies in the second segment in the first cadaver cohort (n=40)...	274

Table 4.108. Observed frequencies in the third segment in the first cadaver cohort (n=40). ... 275
Table 4.109. Observed frequencies in the fourth segment in the first cadaver cohort (n=40). ..275
Table 4.110. Observed frequencies in the fifth segment in the first cadaver cohort (n=40).276
Table 4.111. Observed frequencies in the sixth segment in the first cadaver cohort (n=40). ... 277

ABBREVIATIONS

%	percentage
®	registered sign
°C	degrees celsius
µl	microliter
µm	micrometer
A	adenine
AAA	abdominal aortic aneurysm
AC	aortic calcification
ACA	adenocarcinoma
aDNA	ancient DNA
AFB	acid-fast bacilli
AGE	agarose gel electrophoresis
AIDS	acquired immunodeficiency syndrome
AIP	acute interstitial pneumonia
AIS	adenocarcinoma <i>in situ</i>
ALD	alcoholic liver disease
ALI	acute lung injury
ANOVA	analysis of variance
AM-A	amplification mix A
AM-B	amplification mix B
AP	acute pancreatitis
APC	antigen presenting cell
ARDS	adult respiratory distress syndrome
ASD	atrial septal defect
AS	ankylosing spondylitis
BA	blunt assault
BAC	bronchioloalveolar carcinoma
BAF	bronchial anthracofibrosis
BCG	<i>Mycobacterium bovis</i> bacilli Calmette-Guérin
BE	bronchiectasis
BFT	blunt force trauma
BM	bacterial meningitis
BMI	body mass index
BNF	buffered neutral formalin
bp	base pairs
BPH	benign prostatic hyperplasia
C	cytosine

CA	carcinoma
CAD	coronary artery disease
CAP	community-acquired pneumonia
CD31	cluster of differentiation 31
CD34	cluster of differentiation 34
CF	cystic fibrosis
CHD	coronary heart disease
CHF	congestive heart failure
CK7	cytokeratin 7
CK20	cytokeratin 20
CLB	cell lysis buffer
CMV	cytomegalovirus
CNS	central nervous system
CO	cribra orbitalia
COD	cause of death
CON	conjugate buffer
COPD	chronic obstructive pulmonary disease
CP	chronic pancreatitis
CRF	chronic renal failure
CSF	cerebrospinal fluid
CSSR	Centre for Social Science Research
CT	computed tomography
CVD	cardiovascular disease
CVS	cardiovascular system
CWP	coal worker's pneumoconiosis
CXR	chest X-ray
DAD	diffuse alveolar damage
DCM	dilated cardiomyopathy
DISH	diffuse idiopathic skeletal hyperostosis
DJD	degenerative joint disease
DNA	deoxyribonucleic acid
DOTS	directly observed therapy, short-course
DPX	di-n-butylphthalate (in xylene)
DR	direct repeat
DTH	delayed-type hypersensitivity
DVR	direct variable repeat
DVT	deep venous thrombosis
ECL	enhanced chemiluminescence
ECM	extracellular matrix
EBV	Epstein-Barr virus

EDTA	ethylene-diamine-tetra-acetic acid
EPTB	extrapulmonary tuberculosis
ESRD	end-stage renal disease
FA	fibroadenoma
FES	fat embolism syndrome
FFPE	formalin-fixed paraffin-embedded
FMHS	Faculty of Medicine and Health Sciences
G	guanine
g	gram
GERD	gastro-esophageal reflux disease
GIST	gastrointestinal stromal tumor
GIT	gastrointestinal tract
GN	glomerulonephritis
GT	gallbladder tuberculosis
H	isoniazid
HAART	highly active antiretroviral therapy
HCC	hepatocellular carcinoma
HCM	hypertrophic cardiomyopathy
HCV	hepatitis C virus
HHV-8	human herpesvirus 8
<i>H. pylori</i>	<i>Helicobacter pylori</i>
HIV	human immunodeficiency virus
HOCM	hypertrophic obstructive cardiomyopathy
HPOA	hypertrophic (pulmonary) osteoarthropathy
HPV	human papillomavirus
hr	hour
HREC	Health Research Ethics Committee
HYB	hybridization buffer
H&E	hematoxylin and eosin
IBD	inflammatory bowel disease
IFI	invasive fungal infection
IHD	ischemic heart disease
IL-1	interleukin-1
IL-3	interleukin-3
IL-4	interleukin-4
IL-6	interleukin-6
INH	isoniazid
IPF	idiopathic pulmonary fibrosis
IPH	intraparenchymal hemorrhage
ISH	<i>in situ</i> hybridization

KS	Kaposi's sarcoma
KSHV	Kaposi's sarcoma herpesvirus
L	liter
LAD	left anterior descending
LCA	left coronary artery
LCC	low-copy clade
LCX	left circumflex coronary artery
LGV	lymphogranuloma venereum
LH	liver hemangioma
LIP	lymphocytic interstitial pneumonitis
LPA	line probe assay
LS	Lodox [®] Statscan [®]
LSP	large sequence polymorphism
LSTV	lumbosacral transitional vertebrae
LTBI	latent tuberculosis infection
LUTS	lower urinary tract symptoms
MAC	<i>Mycobacterium avium</i> complex
MAI	<i>Mycobacterium avium-intracellulare</i>
<i>M. bovis</i>	<i>Mycobacterium bovis</i>
MDR-TB	multidrug-resistant tuberculosis
MI	myocardial infarction
MIRU-VNTR	mycobacterial interspersed repetitive-unit-variable number tandem repeat
mL	milliliter
MRC	Medical Research Council
MRI	magnetic resonance imaging
MSB	martius scarlet blue
Mtb.	<i>Mycobacterium tuberculosis</i>
MUT	mutant
MVA	motor vehicle accident
MTBC	<i>Mycobacterium tuberculosis</i> complex
NAFLD	non-alcoholic fatty liver disease
ng	nanogram
NHL	non-Hodgkin's lymphoma
NLB	nuclei lysis buffer
NSAIDs	non-steroidal anti-inflammatory drugs
nsSNP	non-synonymous single nucleotide polymorphism
NTM	non-tuberculous mycobacteria
OA	osteoarthritis
PA	posterior-anterior

PAS-D	periodic acid-schiff with diastase
PCP	pneumocystis pneumonia
PCR	polymerase chain reaction
PFO	patent foramen ovale
PH	pulmonary hypertension
PMCT	postmortem computed tomography
PT	pancreatic tuberculosis
PTB	pulmonary tuberculosis
PTH	parathyroid hormone
PVA	popliteal venous aneurysm
RBC	red blood cell
RCA	right coronary artery
RD	regions of difference
RFLP	restriction fragment length polymorphism
RIF	rifampicin
RIN	rinse buffer
RMP	rifampicin
RNA	ribonucleic acid
RT-PCR	real-time polymerase chain reaction
RVD	rheumatic valvular disease
SAH	subarachnoid hemorrhage
SAS	subarachnoid space
SBO	spina bifida occulta
SCC	squamous cell carcinoma
SCLC	small-cell lung carcinoma
SDS	sodium dodecyl sulphate
SES	socio-economic status
SIJ	sacroiliac joint
SNP	single nucleotide polymorphism
SSA	sessile serrated adenoma
SSPE	saline-sodium phosphate-EDTA
STR	stringent buffer
SU	Stellenbosch University
SUB	substrate buffer
T	thymine
TB	tuberculosis
TBE	tris-borate EDTA
TBM	tuberculous meningitis
TEG	tri-ethylene glycol
THA	total hip arthroplasty

TIN	tubulo-interstitial nephritis
TNF	tumor necrosis factor
TSH	total skeletal height
UIP	usual interstitial pneumonia
UTI	urinary tract infection
UV	ultraviolet
VNTR	variable nucleotide tandem repeats
VSD	ventricular septal defect
WHO	World Health Organization
WT	wild type
XDR-TB	extensively drug-resistant tuberculosis
ZN	ziehl-neelsen stain

Introduction

“If we knew what it was we were doing, it would not be called research, would it?”

Albert Einstein

1.1 General Introduction

Since the time of Hippocrates (460-370 BC), tuberculosis (TB) has been one of the most common chronic granulomatous pulmonary diseases known to man. More than 2000 years later, in the 1980's, a profound increase in the global prevalence of TB brought about a renewed interest in TB-related research. Today, TB remains a major cause of morbidity and mortality worldwide. Currently, 182 countries are implementing the directly observed therapy, short-course (DOTS) strategy which is the worldwide recommended approach for TB control. There is a current global decline in TB prevalence and mortality, but the rapid spread of HIV and its co-infection with TB in South Asian and sub-Saharan African countries, threaten to exacerbate TB incidence rates. South Africa currently is the country with the highest number of people infected with HIV and acquired immune-deficiency syndrome (AIDS), worldwide (Karim *et al.*, 2009). Despite consisting of approximately 0.7% of the entire world's population, South Africa had an overall HIV burden of about 17.0% at the end of 2007 (Karim *et al.*, 2009). This high HIV burden in part has resulted in South Africa being one of the countries with the worst TB epidemics in the world. Tuberculosis rates in South Africa are over two times more than observed in other third world countries and up to 60 times higher than observed in first world countries, such as the United States (US) and Europe (Fourie, 2011). Tuberculosis drug resistance has recently emerged as a very serious health problem in South Africa. The combination of increasing TB prevalence, HIV/TB coinfection rates, drug-resistance and mortality constitutes a major problem that has led to an increasing demand for rapid and effective diagnosis for TB with an appropriate therapeutic approach.

1.1.1 The Study Location: Cape Town, Western Cape, South Africa

South Africa, the southernmost country on the African continent, has a total surface area of approximately 1.2 million km² with a population of more than 52 million. This middle-income country with a heterogeneous population consisting of black, white and mixed ancestry (Sitas et al., 2004), is divided into nine provinces (Figure 1.1). The life expectancy is on average between 49 and 53 years, which is mostly due to the effects of HIV and AIDS (Den Boom, 2007).

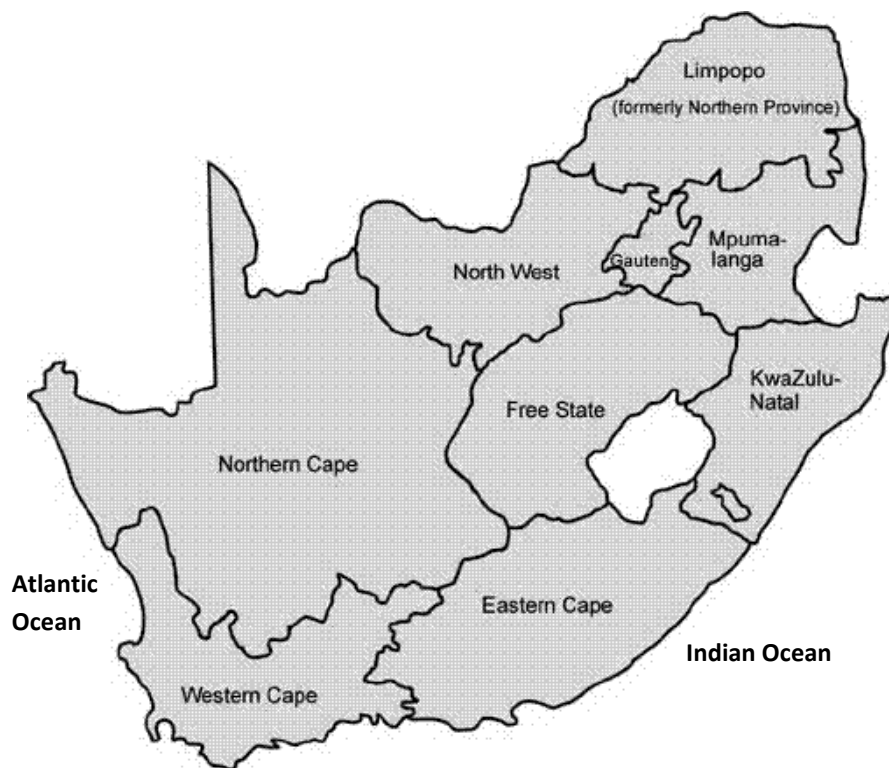


Figure 1.1. Nine provinces of South Africa. The Western Cape is the southwestern province in South Africa (South African Provincial Map, S.a.).

The Western Cape Province houses approximately 5.8 million people, which constitutes roughly 11.2% of the total South African population. The Western Cape, currently has the third highest TB incidence rate in South Africa with approximately 909 new cases per 100 000 (Western Cape Government Health, 2013). Despite having the third highest incidence in South Africa, TB

remains a major problem in the Western Cape. The present study was performed at the Faculty of Medicine and Health Sciences (FMHS), Stellenbosch University (SU), located in the northern suburbs in Cape Town, the second most populous city in South Africa.

In recent years at the FMHS, SU, an increase in pathology lesions (especially in the pulmonary system, presumed to be as a result of TB) as well as a decrease in the average age over the last 10 years was observed in the cadavers used for dissection by medical students. These cadavers therefore make an ideal study cohort as current literature lacks information regarding TB lesion distribution relating to mycobacterial species and the morphology of the lesions as well as information of TB lesions in association with other systemic diseases. In addition, little is available in the literature on extraction of nucleic acids, both human and mycobacterial DNA, from previously embalmed cadavers. Therefore, by incorporating pathology, molecular biology and radiology into a study on cadavers used in anatomy dissections, a void can be filled in the literature.

In this study, the health status of a cadaver population (n=127) originating primarily from the Western Cape, was evaluated. Approximately 90% of the cadavers are unclaimed bodies from low socio-economic backgrounds. The remaining 10% of cadavers is donations for medical dissection and research purposes. Special reference was given to tuberculosis (TB) lesion distribution and morphology in the cadaver population. In addition, a complete pathology report of systemic pathology including extrapulmonary TB lesions in the organ systems was studied. With the use of histological procedures, including six different histochemical stains, certain cells or conditions were selectively stained and illustrated. In addition, the Ziehl-Neelsen (ZN) stain

was employed to demonstrate acid-fast bacilli (AFB) and subsequently *Mycobacterium tuberculosis*, the organism responsible for causing TB, in lung sections with pulmonary TB (PTB). Sections from systemic organs with signs of extrapulmonary TB (EPTB) were furthermore stained with the ZN stain.

To our knowledge, little exists in the literature regarding exact TB lesion distribution relating to the different mycobacterial strains present in the Western Cape, South Africa. The presence of species belonging to the *Mycobacterium tuberculosis* complex (MTBC) was demonstrated using a variety of molecular techniques. Different polymerase chain reactions (PCR's), including the IS6110, RD105, Mtub02/RD105 PCRs were employed to differentiate the mycobacterial species.

1.2 Hypotheses, Aims and Objectives of the Study

1.2.1 Morphologic Assessment: Hypotheses

As the cadaver cohort in this division of Anatomy and Histology is mostly unclaimed cadavers from the Western Cape Province, South Africa, we hypothesize that the majority of the cadavers are expected to be infected with pulmonary TB (PTB). In addition to PTB, extrapulmonary TB (EPTB) involvement is expected to be observed frequently, as the immune systems of the majority of the cadavers are likely to be compromised due to several factors, including, chronic infections, alcohol, smoking and HIV/AIDS (Yach, 1988).

Concerning systemic pathology, Labuschagne and Mathey (2000) profiled the cadaver population from 1956-1999 at the same Division. It was found that apart from PTB in some cadavers, cardiovascular disease, including coronary artery disease (CAD), pneumonia, chronic

obstructive pulmonary disorder (COPD) and neoplasms were the most common causes of death (COD) in their cadaver population. Neoplasms were the most common COD in their cadaver population. Now, more than 15 years after this study by Labuschagne and Mathey (2000), we hypothesize that a radical different scenario regarding the COD in our cadaver population will be observed. Pulmonary TB and consequently other pulmonary disorders such as pneumonia and COPD will be more commonly observed than neoplasms.

1.2.2 Morphologic Assessment: Aims

The aims of the study are:

1. To investigate, illustrate and describe the morphology of pathology lesions in the cadaver population (Morphology includes both macroscopy and microscopy).
2. To describe the morphology and distribution of TB lesions in both the pulmonary and extrapulmonary systems.
3. To statistically evaluate the association between TB and risk factors in our cadaver population, including age, ethnicity and body mass index (BMI).
4. To statistically determine significant trends between TB and other systemic diseases.

1.2.3 Morphologic Assessment: Objectives

In order to achieve the aims, the following objectives were set:

1. To use embalmed cadavers (n=127) dissected by medical students as part of their anatomy teaching.

2. To do concurrent and subsequent detailed dissections and investigations of soft organ systems as well as the skeletal system (to be confirmed by Dr. E.H. Burger, a forensic pathologist).
3. Detailed gross photographs (*Sony Cybershot*) and microphotographs (*Zeiss Axioskop* light microscope and *Zeiss Axioscam*) of pathology lesions will be taken.
4. Standard histological procedures will be performed, including hematoxylin and eosin (H&E) stains, as well as six different special stains. The histopathologic findings will be confirmed by a forensic pathologist (Dr. E.H. Burger).
5. Statistical tests to determine significant trends include contingency tables (cross-tabulations), correspondence analyses and McNemar's test.

1.2.4 Molecular Analysis: Hypotheses

The focus of several nucleic acid extraction studies has been on the extraction of nucleic acids from formalin-fixed paraffin-embedded (FFPE) biopsied material. This was previously done with success and illustrated the use of archival samples for molecular research. We therefore hypothesize that extraction of mycobacterial nucleic acids from previously embalmed cadavers will be possible. In addition to the nucleic acid extraction, we hypothesize that the mycobacterial species will be identified and differentiated with several molecular applications.

1.2.5 Molecular Analysis: Aims

The aim of this study is:

1. To determine and describe the TB lesion distribution associated with specific *Mycobacterium tuberculosis* strains as determined by mycobacterial genetic testing. The

data obtained from these tests may contribute in helping to identify a specific pattern in the distribution of the TB cases and the appearance of the TB lesions.

1.2.6 Molecular Analysis: Objectives

The objectives of this study are:

1. Five different extraction methods will be applied to not only evaluate the efficiency of the methods, and to extract and detect mycobacterial nucleic acids. The methods are a) NucliSens[®] miniMag[®] kit (bioMérieux, France); b) QIAamp[®] DNA extraction kit for formalin-fixed paraffin-embedded (FFPE) tissue (Qiagen, Germany), c) “salting out”, d) Genotype DNA isolation (HAIN[®]) method and e) phenol/chloroform method.
2. The molecular applications which will be used to identify mycobacterial species, include spoligotyping, HAIN[®] MTBDRplus[®] DNA kit (ver. 2.0), IS6110, RD105 and MTUB02/RD105 polymerase chain reactions (PCRs).

1.2.7 Radiology Analysis: Hypothesis

The chest X-ray (CXR) is the gold standard in detecting pulmonary pathology in living patients. The Lodox[®] Statscan[®] Imaging System has been applied in trauma centers and forensic mortuaries worldwide. We hypothesize that the Lodox[®] full-body digital X-rays can be applied to diagnose pulmonary pathology in the embalmed cadavers.

1.2.8 Radiology Analysis: Aim

The aim of this study is to:

1. To determine the diagnostic effectiveness of full-body digital X-rays (Lodox[®] Statscan[®] images) of formalin-embalmed cadavers by retrospectively comparing chest X-rays to pathology observed during dissection.

1.2.9 Radiology Analysis: Objective

The objective of this study is:

1. The diagnostic effectiveness of full-body digital X-rays (Lodox[®] Statscan[®] images) of formalin-embalmed cadavers will be evaluated by statistical analyses such as descriptive and cross-tabulation statistics.

Literature Review

“From my numerous observations, I conclude that these tubercle bacilli occur in all tuberculous disorders and that they are distinguishable from all other microorganisms”

Robert Koch, 1882

2.1 History of Tuberculosis

Hippocrates (460-370 BC) suggested that pulmonary tuberculosis (or “phthisis”) was the “greatest and most terrible disease” ever. Historically and archeologically, it is evident that tuberculosis (TB) was prevalent in early Hindu, Greek and Roman societies. This disease, also referred to as the “white plague” in a book written by Gandy (2003), was regarded as the main cause of death in Europe and Northern Africa in the early nineteenth century. Over the following years, scientists performed various experiments in an attempt to understand the etiopathogenesis of TB. Some researchers proposed that TB was inherited from parents, while others suggested that it was due to unhygienic living conditions, but it was only in 1882, when Robert Koch, a Prussian bacteriologist, discovered that the single organism, *Mycobacterium tuberculosis*, was responsible for TB (Gandy, 2003).

In the previous century, first world countries experienced an overall decline in the incidence of TB, however the less developed countries have not been so fortunate and an increase in incidence of TB was evident in the densely inhabited regions of third world countries.

2.2 Tuberculosis in South Africa

Tuberculosis is a major health problem in South Africa, with disease rates more than twice observed in other third world countries and up to 60 times higher than those observed in first world countries, such as the US and Europe (Fourie, 2011). The high incidence has been ascribed to poor nutrition, historical or political background and neglect, as well as inefficient management and poor health systems (Yach, 1988; Fourie, 2011). According to the World Health Organization (WHO), South Africa was regarded as one of the five countries in 2009 with

the highest TB incidence rates in the world (World Health Organization, 2010) In terms of HIV incidence rates, South Africa was regarded as one of the African countries with the lowest HIV rates, but this scenario changed in the last 8 years with incidence and reporting rates increasing exponentially. TB/HIV co-infection in South African provinces such as KwaZulu-Natal, Mpumalanga, Gauteng and the Western Cape is a rising problem. If it is not controlled and managed properly, it will change the epidemiological profile of TB in South Africa significantly. The Western Cape was until recently regarded as the epicenter of TB in South Africa with one of the highest rates in the world (Fourie, 2011). According to Statistics South Africa, TB was the single disease that caused the most deaths in South Africa in 2010 (Statistics South Africa, 2013).

2.3 High-Risk Groups and Predisposing Conditions

The preponderance of people affected by TB is found predominantly in third world or developing countries. Infants, the elderly, immigrants from developing countries and individuals from low socio-economic backgrounds are regarded as high-risk groups for the development of TB (Churg *et al.*, 2005). Predisposing conditions include human immunodeficiency virus (HIV) infection, poor nutrition, overcrowded housing, alcoholism and poor health systems (Yach, 1988, Churg *et al.*, 2005). In acquired immune deficiency syndrome (AIDS)-stricken areas, TB incidence is approximately 50 to 100 times more than in Northern American and European developed countries (Daniel, 2009).

2.4 Etiology

Mycobacterium is a genus of gram-positive bacteria with acid-fast properties. Acid-fastness refers to the aptitude of the bacteria to retain specific stains even when it is strongly decolourised with alcohol or an acid (Youmans, 1979). Mycobacteria can be divided into two groups based on pathogenicity namely, *Mycobacterium tuberculosis* complex (MTBC) and non-tuberculous mycobacteria (NTM). *Mycobacterium tuberculosis* complex is a closely related group of organisms and comprises *M. tuberculosis*, *M. bovis*, *M. africanum*, and *M. microti*, which are responsible for causing diseases in man and animal. The NTMs are ubiquitous environmental organisms which are not transmittable from person to person but can cause several opportunistic diseases in immune-compromised patients (Frothingham *et al.*, 1998; Leslie *et al.*, 2005).

2.4.1 *Mycobacterium tuberculosis*

Mycobacterium tuberculosis is a highly successful pathogen and is regarded as the most virulent, obligate pathogen of the mycobacterial species, responsible for pulmonary and extra-pulmonary TB (Ilyas *et al.*, 2002; Churg *et al.*, 2005; Leslie *et al.*, 2005). *M. tuberculosis* has the ability to persist in a dormant state for extended periods of time within the host, regardless of the specialized host immune cells to keep bacterial infections at bay. *M. tuberculosis* is an aerobic organism, meaning that it thrives at high levels of oxygen, making the respiratory system the ideal site for an infection (Leslie *et al.*, 2005). It is a slightly coiled, rod-shaped bacterium (bacillus) approximately 4-5 μm in length and is almost always found in the lining of cavities and granulomas in the affected tissue (Leslie *et al.*, 2005).

2.5 Pathogenesis and Pathology of Tuberculosis

Tuberculosis in general presents in the respiratory system and may lead to extensive destruction of pulmonary parenchyma and consequently pulmonary dysfunction (Bezuidenhout and Schneider, 2009). To understand the pathogenesis of *M. tuberculosis*, it is necessary to investigate the behavior of the infectious pathogen. Species belonging to the MTBC are transmitted between individuals by means of aerosolized droplets, which are generated by coughing of an infected individual. The inhaled bacteria move through the respiratory tract until they reach the distal air spaces of the lung. If alveolar macrophages succeed in the task of destroying the invading bacteria, the infection will be prevented and the individual will not develop TB. On the other hand, if macrophages fail to destroy the bacteria, they will multiply inside the alveolar macrophages and ultimately overcome and destroy these defensive cells (Glickman and Jacobs, 2001; Gandy, 2003).

2.6 Spectrum of Tuberculosis

2.6.1 Primary Tuberculosis

Primary TB is the form of disease which develops in previously unexposed hosts, with or without a compromised immune system (Youmans, 1979; Leslie *et al.*, 2005; Kumar *et al.*, 2007). Primary TB originates as a result of bacterial replication at the site of pulmonary entry, where bacteria may enter the hilar lymph nodes and ultimately disseminate to the rest of the body (Glickman and Jacobs, 2001). The description of the early stages of primary TB is based exclusively on animal models, as it has seldom been observed in humans (Bezuidenhout and Schneider, 2009).

Primary pulmonary tuberculosis (PTB) develops when the airborne bacteria is inhaled, phagocytosed and then stimulates an innate immunity (Bezuidenhout and Schneider, 2009). The competent human immune response against *M. tuberculosis* is extremely effective, but the pathogen is almost never eliminated and may enter a stage of dormancy (Glickman and Jacobs, 2001). The phagocytosed bacteria are transported to the hilar lymph nodes where they are presented to immune cells and ultimately elicit an immune reaction (Bezuidenhout and Schneider, 2009).

The best aerated areas of the lung include the superior lobes (antero-lateral segments), the lingula and right middle lobe. *M. tuberculosis* is an aerobic organism, making these areas the ideal site for initial infection (Kumar *et al.*, 2007). As a consequence, the characteristic granulomatous pattern generally develops near the periphery of the lung, adjacent to the pleura. It will present as a grayish-white consolidated lesion, measuring approximately 1 to 1.5cm in diameter and is more commonly referred to as the Ghon focus (Kumar *et al.*, 2007; Bezuidenhout and Schneider, 2009). The combination of the parenchymal and lymph node involvement is collectively known as the Ghon complex. In individuals with competent immune systems lympho-hematogenous spread can be contained and the Ghon complex will undergo fibrosis. In some cases, a calcium salt may be deposited in the focus (Bezuidenhout and Schneider, 2009). Radiologically, this area can be recognized as a calcified lesion and may be referred to as the Ranke complex (Leslie *et al.*, 2005; Kumar *et al.*, 2007).

The main implications of primary TB are that it elicits a hypersensitivity reaction and thereby increases resistance to the pathogen. Viable bacilli may be found in the foci of inactive TB scars

and may be the precursor for reactivation, or may develop uninterrupted into progressive primary tuberculosis (Kumar *et al.*, 2007). The latter is a specific type of primary TB and can be found in individuals with a suppressed or compromised immune system as a result of AIDS or with nonspecific host defense impairments. These individuals are prone to develop progressive primary TB as they have an inability to induce a hypersensitivity reaction resulting in non-caseating granulomas (Kumar *et al.*, 2007). Active disease will develop directly after the primary infection and often leads to dissemination of TB. The granulomatous inflammation and resulting necrosis will cause erosion of the infected necrotic fragments into blood vessels (resulting in miliary TB) or bronchi (resulting in a TB bronchopneumonia) (Bezuidenhout and Schneider, 2009).

2.6.2 Progressive Primary TB

Progressive primary TB develops within one year in about 5% of infected individuals with compromised immune systems (American Thoracic Society, 1990; Leung, 1999; Jeong and Lee, 2008). Although this form of TB often results in TB dissemination (Bezuidenhout and Schneider, 2009); it typically leads to focal disease progression and cavity formation (Leung, 1999). The morphology of progressive primary TB is therefore similar to post-primary TB (Leung, 1999).

2.6.3 Secondary Tuberculosis (Post-Primary Tuberculosis)

Secondary tuberculosis also referred to as post-primary or reactivation tuberculosis occurs in hosts with prior exposure to *M. tuberculosis*. This can either be due to reinfection, or they may experience reactivation of the dormant Ghon-complex due to a compromised immune system (Glickman and Jacobs, 2001; Leslie *et al.*, 2005; Kumar *et al.*, 2007; Bezuidenhout and

Schneider, 2009). This is the most common form of TB in adults with previous exposure to *M. tuberculosis* (Churg *et al.*, 2005). Secondary TB generally affects the apices of the superior lobes as *M. tuberculosis* is a strict aerobe and these lobes are well aerated as previously described (Bezuidenhout and Schneider, 2009). Extensive caseating necrosis, cavity formation with accompanying fibrosis and parenchymal destruction are synonymous with secondary TB (Bezuidenhout and Schneider, 2009). The bacilli may disseminate via the bloodstream, lymphatics and airways to other main organ systems (Churg *et al.*, 2005).

2.6.4 Miliary Tuberculosis

Miliary tuberculosis develops when bacteria drain via the lymphatic capillaries into the lymphatic ducts. In turn these empty into the right side of the heart and ultimately the pulmonary circulation. Small foci of consolidation measuring approximately 2 mm in diameter are found dispersed through the lung parenchyma and may expand and merge into larger regions of consolidation (Kumar *et al.*, 2007). This pattern of pulmonary TB is typically seen in individuals with compromised immune systems (Hoffmann and Churchyard, 2009).

2.7 Morphology and Histopathology of Pulmonary Tuberculosis

In a typical secondary tuberculosis infection, the lungs are affected bilaterally with the tendency of one side being more affected than the other. Large cavities, often containing caseous remnants, are more generally observed in the superior lobes, while the superior regions of the inferior lobes usually contain smaller cavities (Bezuidenhout and Schneider, 2009). The cavity walls have a distinct fibrotic appearance. Histological examination of the wall demonstrates the

presence of caseous material immediately adjacent to the lining of the wall with consolidating granulomatous inflammation and fibrosis (Bezuidenhout and Schneider, 2009) (Figure 2.1).

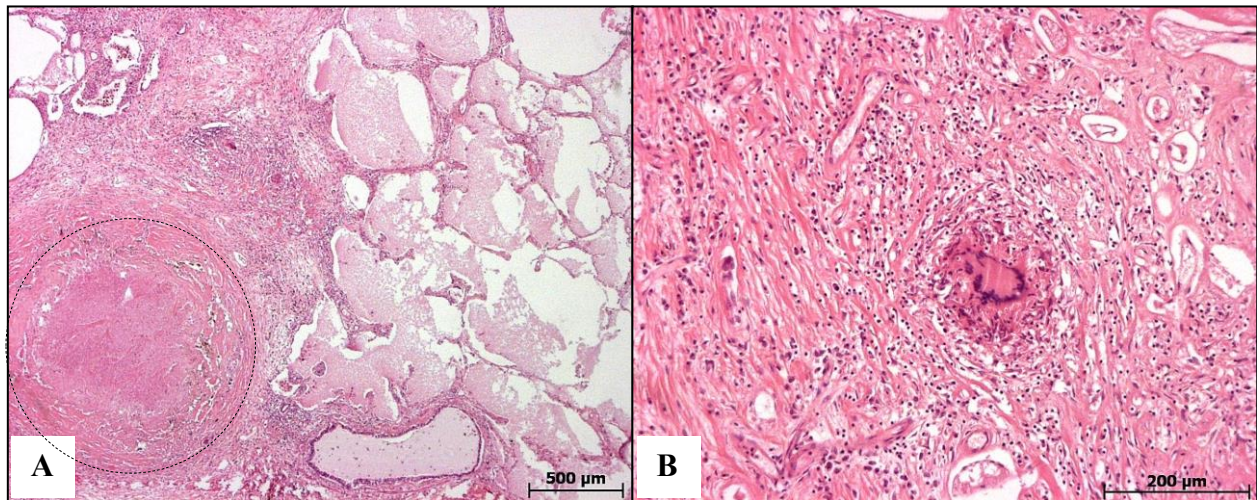


Figure 2.1. An example of a granuloma and a Langhans multinucleated giant cell. A) Tuberculous granuloma with central caseation. The periphery of the granuloma contains epithelioid cells, lymphocytes and variable amounts of Langhans multinucleated giant cells, (K89/09) H&E, (25x); B) The development and manifestation of Langhans giant cells indicate the presence of indigestible bacteria, in this case *M. tuberculosis*, (K89/09) H&E, (100x) (Ioachim, 1983; Leslie and Wick, 2005).

2.8 Complications of Tuberculosis

The following conditions are examples of complications that may arise due to pulmonary TB.

- Extensive damage and loss of lung parenchyma with a subsequent decrease in lung capacity, is usually associated with a typical pulmonary secondary TB infection (Bezuidenhout and Schneider, 2009).
- Emphysema is an obstructive pulmonary disease associated with the abnormal irreversible enlargement of the respiratory bronchioles. It may be categorized into four different types based on the anatomical position within the lobule (a cluster of three to five acini). One type of emphysema called irregular emphysema, may occur in the setting of inflammatory processes and is almost always associated with lung scars. Tuberculosis,

as a chronic inflammatory process, is ideal for the development of emphysematous lesions adjacent to fibrotic changes (Leslie *et al.*, 2005; Kumar *et al.*, 2007).

- Bronchiectasis is the abnormal loss of lung parenchyma due to an increase in the size of the bronchi and bronchioles. The loss of lung parenchyma may be due to destruction of muscular and elastic supporting tissue. During severe respiratory infections, aspiration of mucus into small peripheral bronchi may occur. This may lead to lung collapse as the bronchial lumen is obstructed. Expansion of the bronchi may occur as result of collapsed alveoli and increased pressures in the lung due to obstruction. It may also occur due to contraction of myofibroblasts at some point in organization of the affected area during the wound healing process (Kumar *et al.*, 2007).
- Pleural effusion is a characteristic complication of pulmonary TB and generally occurs unilaterally. The effusion develops when the Ghon focus erodes into the adjacent pleural cavity with accompanying discharge of bacilli and tuberculo-protein. A hypersensitivity reaction to the tuberculo-protein will be the outcome (Gie *et al.*, 2009). This may lead to lung collapse, or atelectasis (Stead *et al.*, 1955).
- Tuberculous empyema is defined as the buildup of fluid, usually of high protein levels in the pleural space (Churg *et al.*, 2005). Empyema can involve the entire pleural space or it may be localized (Crofton *et al.*, 1975).
- Fibrothorax, a relatively common cause of empyema, is used to describe prominent collagenous deposits which bind the parietal and visceral pleurae and thereby immobilize a portion of the lung or in more severe cases, the entire lung.
- Large caseous cavities may develop as a result of secondary TB. These may rupture leading to a spontaneous pneumothorax (Bezuidenhout and Schneider, 2009).

- A common complication of TB occurs when a pulmonary cavity erodes into a neighboring pulmonary artery and causes severe hemorrhage and consequently hemoptysis (Bezuidenhout and Schneider, 2009).
- Tuberculous pneumonia occurs in the setting of an uncontrolled, underlying pulmonary tuberculous infection. It develops when the infection disseminates through the lung parenchyma as a typical bronchopneumonia. Tuberculous pneumonia differs from primary TB lesions in that tissue necrosis with accompanying calcification are absent until the very late stages (Leong *et al.*, 2011).
- Chylothorax can be defined as a milky pleural effusion with a high lipid content and is relatively rare. It is generally associated with any surgery or trauma to the thoracic duct, however spontaneous chylothorax has been implicated as a complication in pulmonary tuberculosis (Churg *et al.*, 2005).
- The thick, fibrous lining of the large cavities caused by TB may undergo squamous or columnar metaplasia which predisposes the cyst to the development of a squamous cell carcinoma. In rare cases the cavities may contain keratin and may mimic an epidermoid cyst (Bezuidenhout and Schneider, 2009).

2.9 Extrapulmonary Manifestations of Tuberculosis in Adults

The prevalence of extrapulmonary tuberculous lesions in individuals with AIDS is much higher than in individuals without the syndrome (Rieder *et al.*, 1990). It is thought that approximately 50% of individuals with concurrent AIDS and TB infections have extrapulmonary lesions (Golden and Vikram, 2005).

2.9.1 Tuberculous Lymphadenitis

Tuberculous involvement of the cervical, axillary, inguinal and mesenteric lymph nodes is regarded as the most common manifestation of extrapulmonary tuberculosis (Dandapat *et al.*, 1990). Asymmetrical adenomegaly with an increase in the size of the nodes, compressible or fluctuant lymph nodes with focal inflammation and hilar and mediastinal lymphadenopathy are clinical presentations which may be indicative of tuberculous involvement. *Mycobacterium tuberculosis* is the main causative agent responsible for mycobacterial lymphadenitis in adults (Reuter and Wood, 2009).

Tuberculous lymphadenitis of the peripheral cervical lymph nodes typically presents as a palpable mass situated along the superior border of the sternocleidomastoid muscle, however more than one region containing lymph nodes may be affected (Geldmacher *et al.*, 2002). During the onset of tuberculous lymphadenitis the lymph nodes feel firm and well circumscribed, however, with time, they may form a fluctuant abscess which may involve the adjacent structures, such as overlying skin. In the chronic setting, fibrosis may occur as a sign of healing. Acute lymphadenitis resembling a pyogenic infection is typically observed in HIV-positive individuals. As mentioned earlier, mediastinal lymphadenopathy is typical of primary TB. On computed tomography (CT) scans, tuberculous mediastinal lymph nodes appear as enlarged, heterogeneous soft tissue abnormalities with peripheral enhancement (Pastores *et al.*, 1993).

2.9.2 Tuberculosis of the Central Nervous System in Adults

Approximately 1% of active TB cases involve the central nervous system (CNS). Tuberculosis of the CNS may affect the brain as well as the spinal cord and may be either localized, forming

characteristic tuberculomas, or it may be diffuse, such as tuberculous meningitis (TBM) (Thwaites, 2009). Tuberculous meningitis is the most common form of tuberculosis involving the central nervous system (Bernaerts *et al.*, 2003). The pathogen is transported via the bloodstream to the CNS where it enters through the blood vessels of the choroid plexus. Initially, small granulomas, also known as Rich's foci, develop in the subependymal or subpial region of the CNS (Thwaites, 2009). A granulomatous meningeal inflammation will develop when the Rich focus ruptures into the subarachnoid space. An exudate containing a variety of inflammatory cells will develop at the base of the brain. This will lead to the formation of basal adhesions which may result in hydrocephalus as they cause obstruction of the subarachnoid cisterns (Thwaites, 2009).

2.9.3 Tuberculous Pericarditis and Myocarditis in Adults

Approximately 1-8% of active TB cases involve the pericardium (Lorell, 1997). Pericardial tuberculosis is a serious manifestation of extrapulmonary tuberculosis and is linked to a high morbidity due to the resultant complications (Mayosi, 2009). Tuberculous pericarditis is, according to Mayosi *et al.* (2005), typically prominent in countries with a high TB prevalence, especially in African countries. In a study conducted in 2005, in the Western Cape region of, South Africa, 69.5% of all TB patients were affected by tuberculous pericarditis (Reuter *et al.*, 2005). In epidemiological studies done in Cameroon, Nigeria and South Africa an increase in the incidence of tuberculous pericarditis had been observed in association with an increase in the HIV incidence (Mayosi, 2009).

Dissemination of *M. tuberculosis* bacilli to the pericardium occurs either via retrograde lymphatic flow from peritracheal, peribronchial and mediastinal lymph nodes or via the bloodstream from a primary tuberculous infection (Mayosi *et al.*, 2005). Tuberculous pericarditis elicits four distinct pathological stages:

1. Mycobacteria induce granuloma formation with accompanying macrophages and T-cells. Furthermore, polymorphonuclear leukocytosis occurs with an associated fibrinous exudate.
2. A serosanguineous effusion containing lymphocytes, monocytes and foam cells develop (foam cells are cells loaded with lipids which are derived from macrophages); caseating granulomas develop when the effusion is absorbed.
3. Fibrosis occurs as a result of thickening of fibrin.
4. Fibrosis of the parietal and visceral pericardium causes constriction of the cardiac chambers and may inhibit diastolic filling. The fibrosis is often accompanied by calcification (Mayosi, 2009).

Chest radiographs reveal cardiomegaly as a result of the pleural effusion and in some cases calcification of the pericardium is visible (Mayosi, 2009; Reuter *et al.*, 2009).

Three manifestations of tuberculous myocarditis exist, namely; 1) granuloma formation with caseation, 2) miliary type and 3) a diffuse infiltrative type (López Gude *et al.*, 2006; Mayosi, 2009). The latter pattern manifests more commonly in individuals with HIV coinfection (Mayosi, 2009).

Myocardial tuberculosis is very uncommon occurring in less than 0.3% of active TB cases, especially since the development of effective treatment against TB (Bali *et al.*, 1990; López Gude *et al.*, 2006). Isolated tuberculous myocarditis on the other hand, is extremely uncommon and is associated with a high mortality (Mayosi, 2009). Several complications may develop including arrhythmias, congestive heart failure and sudden death (Bali *et al.*, 1990).

2.9.4 Gastrointestinal Tract Tuberculosis in Adults

According to Paustian (1964), tuberculosis of the gastrointestinal tract (GIT) is the sixth most common manifestation of extrapulmonary tuberculosis. Approximately 10-12% of active TB cases is extrapulmonary TB, and between 11-16% of these is observed in the abdomen (Aston, 1997; Wang *et al.*, 1998; Singhal *et al.*, 2005). It is regarded as a disease affecting young adults. The typical age of patients with active gastrointestinal TB is between 21 and 40 years and it affects males and females equally (Sharma and Ahuja, 2009). Mycobacteria may infect any part of the GIT from mouth to anus, the pancreatobiliary system and the peritoneum (Sharma and Bhatia, 2004; Sharma and Ahuja, 2009). Gastrointestinal TB can have a diverse appearance commonly imitating diseases such as cancerous malignancies (Sharma and Bhatia, 2004).

It is believed that *Mycobacterium tuberculosis* bacilli disseminate to the gastrointestinal tract by means of four pathways:

1. Reinfection of disseminated bacilli from a primary lesion
2. Sputum with active bacilli may be ingested.
3. Contiguous infected organs may cause seeding of bacilli.
4. Lymphohematogenous dissemination (Sharma and Ahuja, 2009).

Intestinal, peritoneal and lymph nodal tuberculosis involvement are described (Sharma and Ahuja, 2009). Intestinal TB may be found in approximately 50-78% of active abdominal TB cases and peritoneal TB is found in approximately 43% of the cases (Geake *et al.*, 1981; Khan *et al.*, 2006). Gastrointestinal tuberculosis may manifest as either tuberculous ulcers, hypertrophic nodules or a combination of both (Hoon *et al.*, 1950; Hawley *et al.*, 1968). According to Sharma and Ahuja (2009), tuberculous ulcers in the GIT are associated with emaciated individuals, whereas hypertrophic nodules are commonly observed in well-nourished individuals.

2.9.4.1 Tuberculosis of the Oral Cavity

Oral tuberculosis is not common, however, due to increased HIV coinfections, TB may manifest in the mouth. Tuberculous lesions of the lip are uncommon, nonetheless TB of the tongue, gingivae or palate are more commonly observed (Ilyas *et al.*, 2002).

2.9.4.2 Esophageal Tuberculosis

Esophageal tuberculosis is a very uncommon condition and may account for approximately 0.2% of all TB cases. Esophageal TB may be either primary or secondary. It develops primarily due to extension of the disease from neighboring lymph nodes and typically mimics esophageal carcinoma (Sharma and Bhatia, 2004; Sharma and Ahuja, 2009).

2.9.4.3 Gastroduodenal Tuberculosis

Tuberculosis of the stomach makes up approximately 1% of all the cases of abdominal tuberculosis (Sharma and Bhatia, 2004). Sullivan and coworkers (1940) stated that a deficiency in gastric acidity secretions is observed in patients with pulmonary TB. The authors suspected

that the decrease in gastric acid secretion would be a suitable medium for *M. tuberculosis* growth; however, this is not the case. According to Sullivan *et al.* (1940), the stomach seems to have some form of a natural immunity, making it difficult for the bacilli to thrive under these conditions. Stomach TB may manifest as either miliary or ulcerative tuberculosis. Miliary TB presents as single caseating tubercles in the submucosa or the serosa, whereas ulcerative TB is characterized by several irregularly-shaped ulcers which hardly ever infiltrate the muscular layer. The latter form may cause scarring due to fibrosis with accompanying shrinkage of the stomach. Gastric TB may mimic syphilis or gastric carcinoma (Sullivan *et al.*, 1940; Sharma and Bhatia, 2004).

Duodenal tuberculosis, like stomach tuberculosis, is very uncommon and is found in approximately 1% of cases of abdominal TB. In a study done in India, obstruction of the duodenum was observed which was typically due to inflamed lymph nodes, rather than duodenal TB lesions (Gupta *et al.*, 1988). Barium studies demonstrated evidence of segmental narrowing and CT scans showed thickening of the wall as well as lymphadenopathy (Sharma and Bhatia, 2004).

2.9.4.4 Ileocaecal Tuberculosis

The ileocaecal area is the most common site for gastrointestinal TB primarily due to the ample lymphoid tissue in this particular region (Hawley *et al.*, 1968; Sharma and Ahuja, 2009). Ileocaecal involvement was observed in 86% of the patients with abdominal TB in Hong Kong, while in the United Kingdom, only 40% of the abdominal TB cases showed ileocaecal involvement (Singhal *et al.*, 2005; Leung *et al.*, 2006). Bhansali (1977) studied abdominal

tuberculosis in 196 patients in India, in which 102 patients had ileum involvement, while only 100 patients had caecal involvement. Ileocaecal tuberculosis is typically associated with lymphadenitis and may manifest either in the mesenteric or in the para-aortic or iliac group of lymph nodes. Adhesions, hyperplastic tuberculous nodules or strictures of the small intestine may lead to bowel obstruction (Sharma and Ahuja, 2009).

2.9.4.5 Colonic Tuberculosis

Colonic tuberculosis usually refers to isolated TB of the sigmoid, ascending or transverse colon, without involvement of the ileocaecal region. Approximately 9.2% of patients with abdominal TB have isolated colonic involvement (Sharma and Ahuja, 2009). Since intestinal TB may mimic serious illnesses, such as carcinomas or chronic ulcerative colitis, it is of great importance that clinicians include tuberculous involvement in the differential diagnosis (Sato *et al.*, 2004). In a colonoscopy study done by Sato and colleagues (2004) over a period of 14 years, treating a total of 18,499 patients, 11 patients had colonic TB. Ten of the 11 patients showed none of the typical symptoms associated with colonic TB. In these cases, colonoscopy played a vital role in the diagnosis of the TB lesions.

Of the 11 patients, four cases (36%) had type 1 (multiple nodular lesions with circumferential ulcers) in the right hemi-colon. Type 1 is the characteristic manifestation of colonic TB. Type 2 colonic TB was observed in four (36%) cases and includes circumferentially arranged ulcers without any nodular lesion involvement; while type 3 usually occurs in the sigmoid colon and results in a number of erosions in this area. Type 3 was seen in only one case (9%). Type 4 on the other hand, involves the distal part of the ileum and includes solitary erosion in these areas

and was observed in two cases (18%) (Sato *et al.*, 2004). Studies have shown that the incidence rate of colonic TB has increased in the past two decades (Chatzicostas *et al.*, 2002). Even though this is a very rare condition, it is treatable and can be cured. With the aid of a colonoscopy, diagnosis of these infections can be made more rapidly (Sato *et al.*, 2004).

2.9.4.6 Rectal and Anal Tuberculosis

The earliest research on hypertrophic tuberculosis of the GIT started in 1891, when Hartman and Pilliet demonstrated thickening of the submucosa as well as an edematous mucosa in the rectal regions (Hawley *et al.*, 1968). The manifestation of rectal tuberculosis is somewhat different from the more proximal manifestation of the disease in that it tends to cause submucosal thickening (Sharma and Ahuja, 2009). Rectal TB is relatively uncommon, but it may arise in the absence of pulmonary and abdominal TB (Hawley *et al.*, 1968; Sharma and Bhatia, 2004).

Anal tuberculosis occurs more frequently and develops when *M. tuberculosis* bacilli disseminate via lymphatics or the bloodstream or it may be secondary to a primary lesion elsewhere. The clinical presentation of ano-perianal tuberculosis includes: pilonidal abscess formation, ulceration with accompanying inguinal lymphadenopathy and anal strictures (Gupta, 2005). Anal TB may typically mimic conditions such as Crohn's disease, syphilis, sarcoidosis and lymphogranuloma venereum (LGV) (Sharma and Ahuja, 2009).

2.9.4.7 Hepatobiliary and Pancreatic Tuberculosis

Hepatic tuberculosis may manifest as a miliary, nodular or an abscess-like TB (Chien *et al.*, 1995). Tuberculosis of the gallbladder may present as an acute cholecystitis as a result of a

bacterial infection or obstructive jaundice due to contiguous, enlarged pericholedochal lymph nodes (Saluja *et al.*, 2007). Several clinical presentations of pancreatic tuberculosis exist, such as acute pancreatitis due to a sudden, intense inflammation of the pancreas, portal vein thrombosis as well as obstructive jaundice (Foo *et al.*, 2007).

2.9.5 Tuberculosis of the Genitourinary System in Adults

Genitourinary tuberculosis is a relatively common manifestation of extrapulmonary TB. The renal and urinary tracts of immune compromised individuals, such HIV-positive as well as AIDS patients, are more likely to be infected by the bacilli (Shafer *et al.*, 1991). The worldwide prevalence of genitourinary tract TB is difficult to determine as several cases go unreported, especially in developing countries (Eastwood and Corbishley, 2009).

2.9.5.1 Renal Tuberculosis in Adults

The kidney is usually the initial site for infection due to the hematogenous dissemination of *M. tuberculosis* bacilli from a primary site of infection (Eastwood and Corbishley, 2009). Tuberculous involvement of the kidneys may be either unilateral or bilateral. The morphology of renal tuberculosis depends on the host's immune system along with the virulence of the *M. tuberculosis* strain. The characteristic granulomatous inflammatory pattern with or without caseation is typically observed in renal TB and will develop in the glomeruli situated in the cortex, due to increased blood flow and oxygen pressures. The granulomas with the accompanying bacilli often become enlarged and rupture into the Loops of Henle via the adjacent proximal tubules. The subsequent inflammation may lead to extensive tissue necrosis. Disseminated renal TB typically presents primarily in the cortex as small whitish-yellow

nodules, which is characteristic of miliary TB. A more diffuse type of the miliary pattern is generally seen in individuals with compromised immune systems. Secondary tuberculous lesions may develop in the ureters and bladder due to dissemination from the primary focus. Scarring is typically seen in both ureteric and bladder involvement, which may result in obstruction or segmental dilatation (Eastwood and Corbishley, 2009).

2.9.5.2 Male Genital Tuberculosis

The most common sites in the male genital system infected by tuberculosis are the prostate gland and the epididymis. The testicles are not commonly affected (Gorse *et al.*, 1985; Çek, 2009). Three main pathways through which the bacilli enter the male genital system include hematogenous dissemination, extension by contiguous infection from adjacent granulomas and direct descending infection from primary renal tuberculosis. Epididymal TB is primarily a venereal disease typically affecting men aged 35 and older, while prostatic TB generally affects men under the age of 50 years. Other sites which are less likely to develop TB include the vas deferens, scrotal skin, seminal vesicles, urethra and penis (Çek, 2009).

The morphological appearance of tuberculous prostatitis includes multiple granulomas with caseating centers in the posterior and lateral regions of the prostate. Unilateral and less frequently, bilateral involvement has been reported (Muttarak *et al.*, 2001; Çek, 2009). Langhans multinucleated giant cells are usually observed in conjunction with caseating granulomas, while abscesses develop as a result of a suppurative (purulent) inflammation (Çek, 2009).

2.9.5.3 Female Genital Tuberculosis

The fallopian tubes are regarded as the primary site for female genital TB development, while the endometrium and the ovaries are less frequently infected (Botha and Van Der Merwe, 2009). Cervical, vaginal and vulval TB is relatively uncommon (Saracoglu *et al.*, 1992). In a study done over a period of 31 years by Nogales-Ortiz and colleagues (1979), bilateral fallopian tube involvement was observed in all the patients with genital TB. Granuloma formation is observed in endometrial TB, while vaginal and vulvar TB manifests as ulcers with the appearance of a chancre (a painless, red papule which may erode to form an ulcer with a raised border). Cervical TB presents with ulcers and caseating granulomas and may mimic the appearance of a cervical carcinoma (Botha and Van Der Merwe, 2009).

2.9.6 Tuberculosis of the Skeletal System in Adults

Skeletal tuberculosis in the form of bone and joint TB manifests in approximately 35% of individuals with extrapulmonary TB (Golden and Vikram, 2005). Almost 50% of individuals with skeletal TB do not necessarily have a concomitant pulmonary infection and may go unnoticed, as it is difficult to ascertain diagnosis in active cases (Davidson *et al.*, 1970). Skeletal TB most commonly includes spinal TB, followed by tuberculous arthritis in joints and tuberculous osteomyelitis (Davidson *et al.*, 1970; Golden and Vikram, 2005). The pathogenesis of skeletal TB appears to be similar to what is observed in other extrapulmonary manifestations of TB. The bacilli either reach the bone via hematogenous dissemination or an area with tuberculous involvement may infect adjacent skeletal structures due to lymphatic drainage or direct erosion into the bone. The joint spaces are infected either due to direct hematogenous dissemination or erosion of epiphyseal bone into the joint space (Davidson *et al.*, 1970).

The typical skeletal tuberculous lesion is generally a mixture of arthritis and osteomyelitis. The synovium of the joint space typically develops an inflammatory reaction which may lead to the formation of granulation tissue. Fibrin deposits, also called “rice bodies”, start to develop once the effusion is well developed. The granulation tissue may start to erode and destroy adjacent cartilage and ultimately erode cancellous bone. Demineralization and caseating necrosis will be the end result (Davidson *et al.*, 1970).

2.9.6.1 Spinal Tuberculosis

Approximately 50% of patients with skeletal TB have spinal involvement (Souhami and Moxham, 1990). Tuberculous involvement of the spine, also known as Pott’s disease, generally manifests inferiorly in the thoracic and superiorly in the lumbar spine (Golden and Vikram, 2005). The infection usually develops anterior and inferior of the vertebral body with accompanying bone collapse and destruction of the intervertebral discs and nearby vertebrae, resulting in kyphosis. In some instances, paraspinal and psoas abscesses may develop adjacent to the site of the infection (Golden and Vikram, 2005).

2.9.6.2 Peripheral Osteoarticular Tuberculosis

Tuberculous arthritis is defined as a gradually progressive monoarticular disease in the main weight-bearing joints, like knee and hip joints. Approximately 50% of patients with tuberculous arthritis have shown evidence of prior pulmonary TB on chest radiographs (Reuter *et al.*, 2009). *Mycobacterium tuberculosis* is the typical organism responsible for tuberculous arthritis; however, other members of the MTBC, such as *M. bovis* and atypical non-tuberculous bacteria (e.g. *M. kansasii* and *M. trivale*) have been implicated (Souhami and Moxham, 1990). X-ray

imaging findings of tuberculous arthritis include soft tissue swelling with accompanying juxta-articular osteopenia, subchondral erosions and joint destruction (Watts and Lifeso, 1996). Tuberculous osteomyelitis, on the other hand, manifests with a typical cold abscess and associated swelling. The lesions may present as either single or multiple and may involve bones such as the skull, ribs, pelvis and long bones (Reuter *et al.*, 2009).

2.10 Tuberculosis in Children

Childhood tuberculosis is a major health problem especially in developing countries and particularly in communities with a high incidence of TB (Graham *et al.*, 2009). It is regarded as an important cause of chronic morbidity and mortality in children worldwide (Van Rie *et al.*, 1999; Hesselning *et al.*, 2002). The most common manifestation of childhood TB is pulmonary TB; however, 20 to 25% of all childhood TB is extrapulmonary TB (Graham *et al.*, 2009). Tuberculous lymphadenitis, vertebral TB, abdominal TB and tuberculous meningitis are the most common forms of childhood extrapulmonary TB (Marais *et al.*, 2006).

In the past, much attention has been given to the diagnosis, management, treatment and control of adult tuberculosis as it is regarded as the most infectious. Children rarely develop sputum smear-positive disease due to the paucibacillary nature of childhood TB and consequently hardly ever contribute to transmission. As a result, research on childhood TB, has been neglected in the past (Marais *et al.*, 2009). The socio-economic status and age of a child is often of crucial importance in diagnosing TB. There are four challenges to consider when diagnosing TB in children under the age of five: a) childhood TB presents with non-specific symptoms; b) children are prone to other infectious diseases, and may also suffer from HIV; c) children from low socio-

economic backgrounds tend to be malnourished and d) childhood TB are usually paucibacillary (Graham *et al.*, 2009). In addition, pulmonary TB in children is difficult to diagnose due to non-specific radiological findings on chest X-rays (Andronikou and Wieselthaler, 2009).

Primary pulmonary TB in children manifests as mediastinal and hilar adenopathy. Miliary nodules and pleural disease are often observed. Children often present with morphological changes similar to those observed in adult secondary TB, while progressive primary disease is more common in infants (Andronikou and Wieselthaler, 2009). According to ElTayeb *et al.* (2008), children are more susceptible to the development of extrapulmonary TB and may present with severe forms of miliary disease and tuberculous meningitis.

2.11 Literature Survey of the Genotypic Characteristics of *M. tuberculosis*

Mycobacterium tuberculosis belongs to a group of related species known as the *Mycobacterium tuberculosis* complex (MTBC) which is responsible for disease in humans and animals. The members include *M. tuberculosis*, *M. bovis*, *M. africanum*, *M. caprae*, *M. canetti*, *M. pinnipedii* and *M. microti* (Frothingham *et al.*, 1998). These genetic monomorphic bacterial pathogens, display extremely low DNA sequence diversity, with more than 99.9% of the DNA being shared between the members (Comas *et al.*, 2009). Despite this fact, their genomes have unique genotypic and phenotypic characteristics, making differentiation and classification possible between the members (Sreevatsan *et al.*, 1997; Frothingham *et al.*, 1998).

In 1998, sequencing of the complete genome of the *M. tuberculosis* H37Rv strain was completed. The analysis demonstrated a total of 4,000 coding genes constituting approximately

4,411,529 base pairs (bp) with a G-C content of about 65.6%. This genome is regarded as the second largest bacterial genome after *Escherichia coli* (Cole *et al.*, 1998).

Advances in molecular epidemiology were established in 1992, when DNA repetitive elements (such as polymorphic GC repetitive sequences) were used as genetic markers to differentiate between pathogenic TB isolates (Cole *et al.*, 1998). It was only then that genotyping with the IS6110 insertion element by means of the restriction fragment length polymorphism (RFLP) method was used for strain differentiation (Van Embden *et al.*, 1993; Behr *et al.*, 1997). Although it is currently the most commonly used method for strain differentiation, RFLP is time-consuming and up to 40 days of bacterial culturing is necessary to obtain sufficient amounts of mycobacterial DNA (Gori *et al.*, 2005).

The IS6110 insertion sequences consists of 1,355 bp and is dispersed throughout the genome of *M. tuberculosis* in highly variable copy numbers reaching up to 25 copies. The genomic DNA is digested into smaller fragments with the enzyme *PvuII* and the fragments are subsequently separated according to size by means of agarose gel electrophoresis. The fragments are allowed to hybridize with the probe for IS6110 and chemoluminescent exposure reveals the fragments with the IS6110 sequence. Each *M. tuberculosis* strain has a unique IS6110 banding pattern or RFLP (Behr *et al.*, 1997). According to Van Rie *et al.* (1999), IS6110 RFLP may help to understand the mechanism behind endogenous and exogenous TB reinfection in persistent cases.

A polymerase chain reaction (PCR)-based genotypic technique, the spoligotyping method, was developed (Kamerbeek *et al.*, 1997; Supply *et al.*, 2000). It was designed as a fast, cost effective

and accurate technique used to identify and characterize the composition of the direct repeat (DR) region. The *M. tuberculosis* complex genome consists of DR regions each containing a 36 base pair (bp) DR locus and unique non-repetitive spacer sequences varying from 35 to 41 bps. The non-repetitive spacer sequences are termed direct variable repeats (DVR) (Van Embden *et al.*, 2000). Homologous recombination between the direct repeats in the genome results in variability in the DR locus. Amplification and hybridization of genomic DVRs to a probe containing 43 different DVR sequences are used to determine the presence or absence of specific *M. tuberculosis* strains.

The fourth international spoligotyping database (SpolDB4) is used to investigate pathogenic transmission and evolutionary changes between the members of MTBC (Brudey *et al.*, 2006). This database consists of 39,295 isolated strains from patients in 141 countries worldwide. They are differentiated into 62 evolutionary lineages based on their unique spoligotyping pattern, using computer software. The Beijing evolutionary lineage is present in the majority of countries worldwide indicating their unique ability for worldwide dissemination (Brudey *et al.*, 2006). Some lineages of *M. tuberculosis* are limited to defined geographical locations, usually the country of origin (Brudey *et al.*, 2006).

2.11.1 The *M. tuberculosis* Beijing Genotype

The *M. tuberculosis* Beijing strain was first isolated and described in the People's Republic of China and Mongolia in the mid-nineties and is regarded as one of the most successful family strains in the current TB epidemic (Van Soolingen *et al.*, 1995; Parwati *et al.*, 2010). This

genotype has been shown to be frequently associated with drug-resistant TB, especially multidrug-resistant (MDR) TB (Parwati *et al.*, 2010).

In South Africa, a spoligotyping study revealed the absence of Beijing strains in samples obtained from 1930 to 1965, while there was an increase in strain occurrence in the samples from 1965 to 1995 and the strain was increasingly common in samples from 1996 to 2005. The percentage of the Beijing strain responsible for TB in children increased from 13% in 2000 to 33% in 2003. The Beijing strain genotype is consequently one of the most predominant strains in South Africa, especially in the Western Cape (Parwati *et al.*, 2010). It is currently believed that the success of the Beijing genotype can be attributed to its ability to evade the protective effect of the *Mycobacterium bovis* bacilli Calmette-Guérin (BCG) vaccine (Van Soolingen *et al.*, 1995). The Beijing genotype lack spacers 1 to 34 in their DR locus and have highly analogous RFLP patterns. The Beijing genotype has a very conserved spoligotyping pattern and according to a study done in 2004, will hybridize to no less than three of the spacers 35-43 in the DR locus, while spacers 1-34 will remain unhybridized (Kremer *et al.*, 2004).

In addition to spoligotyping and the IS6110 insertion sequence RFLP, several additional molecular techniques have been developed to differentiate and predict *M. tuberculosis* Beijing strains. The RD105 genomic deletion is a large sequence polymorphism (LSP) consisting of 3,467 bp and is used as a marker for the Beijing strain family (Tsolaki *et al.*, 2005; Flores *et al.*, 2007). The Mtub02 locus on the other hand, is a mycobacterial interspersed repetitive-unit (MIRU) that consists of 9 bp repeated sequence situated 25 bp before the RD105 deletion (Luo *et al.*, 2011). By applying a PCR assay using the RD105 deletion or the Mtub02 MIRU locus in the

genome of *M. tuberculosis*, identification of the different strains may be accomplished (Tsolaki *et al.*, 2005).

2.11.2 Mixed Infections

Several mycobacterial strains may be concurrently present in an individual during active disease. This may occur either as a result of multiple infections, or an infection in conjunction with reactivation. In the case of a mixed infection, one strain will dominate the bacterial population (McEvoy, *et al.*, 2009). In a study done by Warren *et al.* (2004) in an area with a high incidence of TB in Cape Town, Western Cape, South Africa, it was found that 19% of individuals were infected simultaneously with both Beijing and non-Beijing strains, while 57% of individuals with a Beijing strain were furthermore infected with a non-Beijing strain. This study was performed using the IS6110 insertion element located within the Rv2820 gene. They have concluded that mixed infections may also play a significant role in the development of drug resistance.

2.11.3 Multidrug-Resistant Tuberculosis (MDR-TB)

Multidrug-resistant tuberculosis is defined as disease that is resistant to at least isoniazid (INH) and rifampicin (RMP) (Andrews *et al.*, 2007). Strains of *M. tuberculosis* that are classified as MDR-TB threaten the effective control and prevention of TB. Resistance to anti-TB drugs is mainly attributed to mutations in the drug-target genes (Rattan *et al.*, 1998). Multidrug-resistance incidence rates are difficult to determine, nonetheless mathematical modelling (multiple logistic regression) studies in 2004 have indicated that the global burden of MDR-TB was approximately 430,000 cases (Zignol *et al.*, 2006).

Multidrug-resistance and HIV coinfection could lead to a significant increase in the burden of MDR-TB (Wells *et al.*, 2007). Between 1965 and 1995, a decrease in the prevalence of both primary and acquired drug-resistant TB was observed. This was mainly ascribed to 25 annual surveys on drug-resistance that were conducted by the *Tuberculosis Research Institute of the Medical Research Council of South Africa* (MRC). These surveys were suspended in 1995 due to budgetary restrictions, however, a significant increase in the prevalence of MDR-TB was observed in the second half of the 90's (Andrews *et al.*, 2007). High rates of MDR-TB within a country point to major problems with the present tuberculosis program (Drobniewski and Khanna, 2009).

2.11.4 Extensively Drug-Resistant Tuberculosis (XDR-TB)

Extensively drug-resistant tuberculosis is defined as MDR-TB with an additional resistance to a fluoroquinolone as well as at least one second-line anti-tuberculous drug, such as kanamycin, amikacin or capreomycin (Moll *et al.*, 2009; World Health Organisation Report, 2010). According to Moll and colleagues (2009), the appearance of XDR-TB strains is mainly an artificial occurrence and is a sign of failing TB programs. The mortality rate of patients diagnosed with XDR-TB is extremely high (98%) (Andrews *et al.*, 2007). Increased nosocomial outbreaks of MDR-TB and XDR-TB in populations infected with HIV and AIDS, may be observed if not managed effectively. Precautions must therefore be taken to prevent outbreaks in hospitals (Andrews *et al.*, 2007).

2.12 Imaging of Tuberculosis in Adults: A Literature Survey

The diagnosis and subsequent assessment of TB infections in patients by means of imaging have been in use since the development of radiography at the end of the nineteenth century (Daley and Gotway, 2009). Screening of chest radiographs of individuals suspected of TB infection has played a central role in the identification, diagnosis and treatment of tuberculosis. Lately, newly designed modalities, such as magnetic resonance imaging (MRI) and CT have been used for screening of TB.

Several factors influence the radiographical presentation of TB. These include a) prior exposure to mycobacteria, in particular *M. tuberculosis*; b) age at the onset of infection and c) host immunity (Leung, 1999). Imaging manifestations of primary, progressive primary and secondary TB have been described in the literature and several distinct patterns can be distinguished based on the pathological, clinical and radiological presentations (Daley and Gotway, 2009).

2.12.1 Conventional Radiography (X-Ray)

Screening of the thorax in the HIV-uninfected is the most common method used for diagnosing TB. In HIV-infected individuals, especially children, AIDS-defining respiratory illnesses may simulate the presence of TB and therefore make it less helpful for diagnosis. Osteoarticular TB, in particular spinal TB lesions, can be diagnosed when bone radiographs are screened for TB. The radiographic appearance of TB on abdominal radiographs is highly non-specific and may indicate bowel obstruction, intussusception, ascites development and calcified granulomas (Sharma and Bhatia, 2004).

2.12.2 Ultrasonography

Thoracic ultrasound is currently being used to determine the presence of pleural and pericardial effusions and for characterization thereof. Thickening of the pericardium as well as the pleura may be highly indicative of TB; however other diagnostic procedures must be implemented to confirm the findings (Kiehn *et al.*, 1993). Abdominal ultrasounds are used mainly for diagnosing the presence of enlarged lymph nodes (either in the calcified or the caseating form), ascites as a complication of hepatobiliary TB, fibrotic thickening of the ileocecal region as well as granulomas in the liver and/or spleen (Saczek *et al.*, 2001; Sharma and Batia, 2004). An ultrasound of the neck region is often used to identify enlarged cervical lymph nodes; however, this is not a reliable procedure to distinguish between lymphadenopathy due to TB or due to malignancies (Morgan *et al.*, 1983).

2.12.3 Computed Tomography (CT) and Magnetic Resonance Imaging (MRI)

Computed tomography is valuable for the investigation of intrathoracic and abdominal TB, while MRI can be used as a tool in determining the diagnosis and prognosis of tuberculous meningitis and vertebral TB (Schaaf and Reuter, 2009).

2.12.4 Conventional Radiographical Imaging Findings: Primary TB

As described earlier, primary tuberculosis develops directly after the first exposure to *M. tuberculosis*, where the initial granulomatous formation (also termed Ghon-focus) will develop near the periphery of the lung, usually subpleural (Daley and Gotway, 2009). The granuloma in a host with an uncompromised immune system will undergo fibrosis as a result of healing and may in some cases calcify. The Ghon-complex (or in some instances also termed

Ranke complex, when observed on an X-ray) develops in cases where the parenchyma is infected in conjunction with the neighboring lymph nodes. Enlarged intrathoracic lymph nodes, termed lymphadenopathy, are the most common clinical and radiological manifestation of primary TB which is generally seen in the right paratracheal and hilar regions (Figure 2.2). Ipsilateral to the enlarged lymph nodes, ill-defined parenchymal opacities are sometimes observed and may be focal or affect the entire lobe. In some cases the opacification may extend to the pleural region and may include air bronchograms (McAdams *et al.*, 1995). Areas of opacification resembling that of bronchopneumonia may also be seen (Figure 2.3) (Leung, 1999).

Miliary tuberculosis results from lymphohematogenous dissemination to areas of the lung and other organs. In 1986, Woodring and coworkers observed miliary dissemination in 2-6% of the patients (n=90) with primary TB and it was more commonly encountered in the patients with compromised immune systems. Initially, chest X-rays of patients with miliary TB appear normal, however, as the disease progresses, small, well-circumscribed nodules can be seen throughout the lung in a diffuse pattern (Figure 2.4) (Woodring *et al.*, 1986). The miliary nodules typically do not calcify and lymphadenopathy may be observed in these cases (McAdams *et al.*, 1995).

Pleural effusion, as a manifestation of primary TB, is typically observed on X-rays ipsilaterally to the region where the Ghon-focus is located and is generally unilateral, however cases with bilateral effusion have been reported (Leung, 1999; Woodring *et al.*, 1986). With effective treatment; pleural effusion may resolve, although pleural thickening and calcification may also develop (McAdams *et al.*, 1995).

2.12.5 Computed Tomography (CT) Imaging Findings: Primary TB

High-resolution computed tomography (HRCT) is ideal for detecting small lesions characteristic of miliary TB. They can be visualized as diffuse, small, well circumscribed nodules measuring up to 3mm in diameter. The nodules may be visualized in areas adjacent to the visceral pleura (Daley and Gotway, 2009). Enlarged TB lymph nodes have a characteristic low-attenuation with a marginal rim enhancement in the general CT setting. It is important to note, however, that lymphadenopathy with central low-attenuation in the clinical setting may also be indicative of other conditions such as metastatic carcinomas, lymphomas and Crohn's disease in the intestines (Leung, 1999; Daley and Gotway, 2009).

Pleural effusions are commonly associated with primary TB, and even though effective treatment may lead to complete resolution of the effusion, pleural thickening and calcification may occur. If the pleural thickening on the CT scan is 2cm or more in diameter, it may indicate the presence of a pleural exudate (McAdams *et al.*, 1995; Daley and Gotway, 2009).

2.12.6 Conventional Radiographical Imaging Findings: Progressive Primary TB

Primary TB may progress directly to secondary TB in some individuals with compromised immune systems. This may occur at the Ghon-focus and at the site of hematogenous dissemination (Daley and Gotway, 2009). Consolidation and cavity formation are synonymous with progressive primary TB and may manifest at the Ghon-focus or in the apices of both superior lobes. Opacification and typical miliary TB lesions may be observed (McAdams *et al.*, 1995; Daley and Gotway, 2009).

2.12.7 Conventional Radiographical Imaging Findings: Secondary TB

As described earlier, secondary tuberculosis is defined as the reactivation of a latent *M. tuberculosis* infection. During the course of the secondary TB infection, severe tissue destruction as a result of caseating necrosis occurs, producing the characteristic cavities (Daley and Gotway, 2009).

In the apices and posterior regions of the superior lobes, as well as the superior regions of the inferior lobes, ill-defined areas of consolidation are observed (Figure 2.5). Due to severe tissue destruction, cavity formation is inevitable. Multiple cavities are often seen in areas of consolidation and may range from millimeters to centimeters (Woodring *et al.*, 1986; McAdams *et al.*, 1995). The thickness of the cavity walls indicates the stage of development of the cavity. Initially, the cavities have irregular, thick walls, but following healing, the walls may become thinned and may resemble that of emphysematous bullae (Woodring *et al.*, 1986).

Cavity formation is the trademark of postprimary TB and is indicative of communication between infected parenchymal lesions and tracheobronchial structures (Figure 2.5). The caseous material from the cavities may be expelled to other regions of the lung via smaller airways, suggesting an endobronchial spread. Evidence of this type of infection can be seen on a chest radiograph as small, ill-defined lesions. They are often referred to as “acinar” or “acino-nodose” lesions (McAdams *et al.*, 1995).

The pleura are rarely affected in postprimary TB and if a pleural effusion occurs, it is generally small and is often found in conjunction with ipsilateral parenchymal abnormalities (McAdams *et*

al., 1995; Leung, 1999). In the event of a large convex-shaped effusion, a tuberculous empyema should be considered, however this complication is rarely seen in secondary TB (Woodring *et al.*, 1986). Another unusual presentation of secondary TB is lymphadenopathy. According to Woodring *et al.* (1986), lymphadenopathy was seen in less than 5% of individuals with secondary TB. Miliary TB may be observed (Daley and Gotway, 2009).

2.12.8 Computed Tomography (CT) Imaging Findings: Secondary TB

On high-resolution computed tomography, secondary TB presents as ill-defined nodules with branching patterns, resembling that of a tree budding in spring. The branching is indicative of impaction of smaller airways with pus and caseating necrosis. Cavities of variable sizes are often seen in conjunction with consolidation (Daley and Gotway, 2009). Smaller cavities are more easily identified when CT and HRCT scans are used in comparison with conventional chest X-rays. Computed tomography is regarded as highly sensitive for the visualization of typical findings associated with tuberculous involvement of airways, such as volume loss, overinflation, mucoid impaction and post-obstructive consolidatory pneumonia (Lee *et al.*, 1995; Daley and Gotway, 2009).

2.12.9 Conventional Radiographical Imaging Findings: MDR-TB versus XDR-TB

It has been proposed by Kim *et al.* (2004) that extensive cavity formation is usually associated with MDR-TB, however, no apparent differences can be seen between chest radiographs of patients infected with drug-susceptible or multidrug-resistant *M. tuberculosis* (Daley and Gotway, 2009).

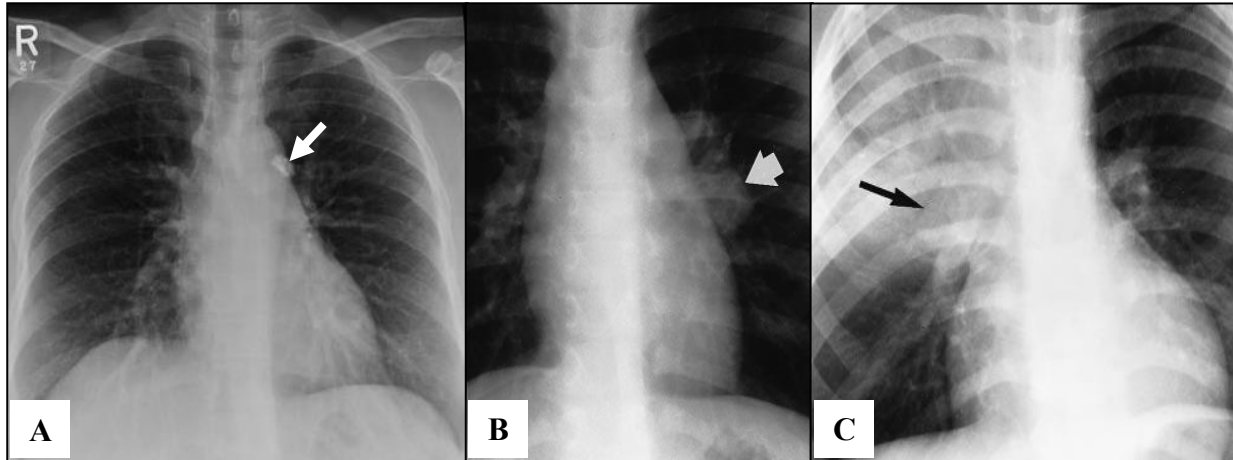


Figure 2.2. Examples of lymphadenopathy and Ranke Complex. A) Chest radiograph shows a Ranke complex (arrow) situated in the left hemithorax adjacent to the left primary bronchus (Radiopaedia.org, <http://radiopaedia.org/images/831487>); B) Left hilar lymphadenopathy (arrow) in a 4-year old patient (Leung, 1999); C) Right hilar lymphadenopathy (arrow) in conjunction with a typical bronchopneumonic pattern in a 4 year-old patient (Leung, 1999).

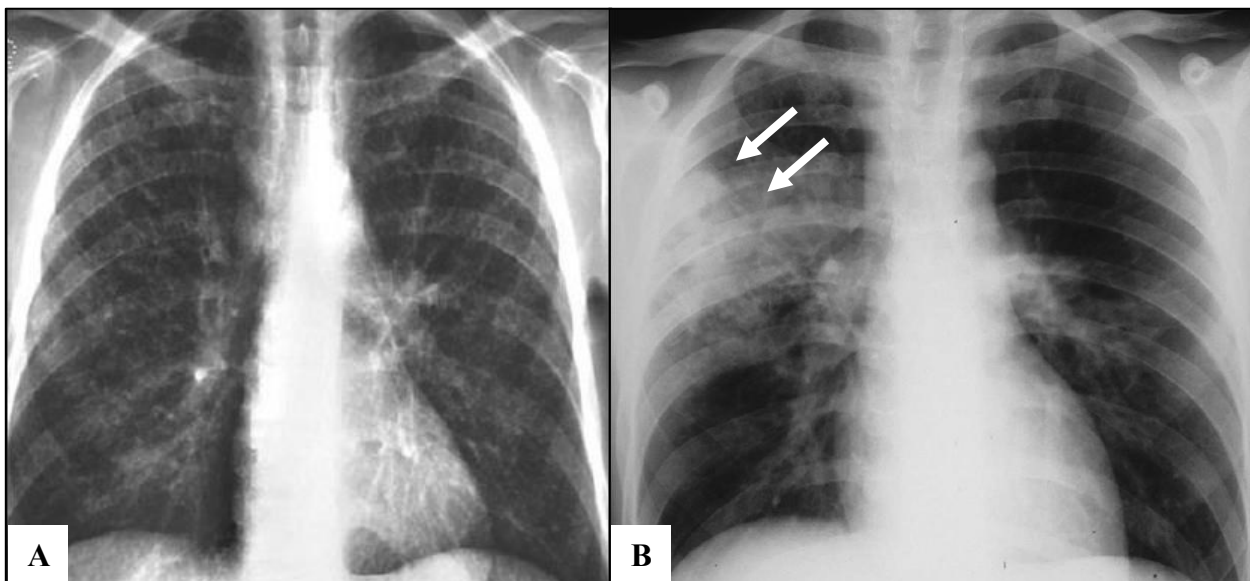


Figure 2.3. Primary Tuberculosis. A) Chest X-ray shows small nodules throughout the lung parenchyma of a HIV positive patient; B) Right superior lobe consolidation (arrows) with accompanying adenopathy can be seen (Annals of Thoracic Medicine, <http://www.thoracicmedicine.org/>).

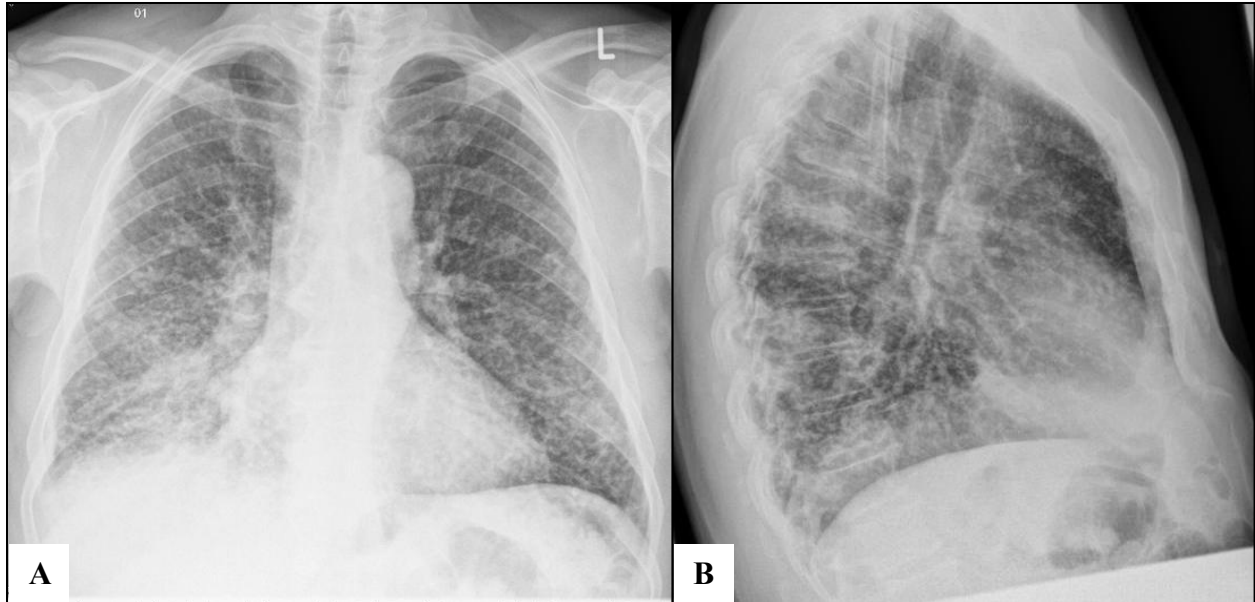


Figure 2.4. Miliary Tuberculosis. A) Chest radiograph shows several nodules scattered throughout the lung (Radiopaedia.org, <http://radiopaedia.org/cases/miliary-tuberculosis-2>), (B) A lateral view of the same patient (Radiopaedia.org, <http://radiopaedia.org/cases/miliary-tuberculosis-2>).

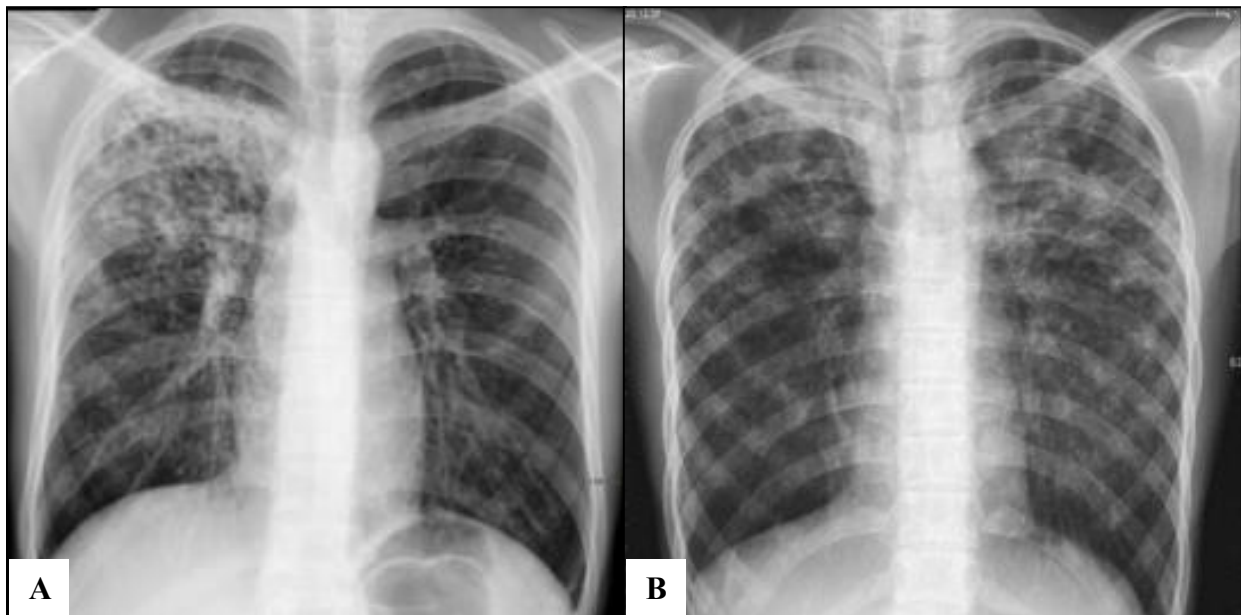


Figure 2.5. Secondary Tuberculosis. A) Chest X-ray shows a patchy and ill-defined area of consolidation with several cavities in the right superior lobe of a 16-year-old male, (B) Ill-defined patches of consolidation can be observed in both superior lobes of a 14-year-old girl (Ho *et al.*, 2011).

2.12.10 Lodox® Statscan® (Digital Imaging System)

Lodox® Statscan® (LS) is a fast and cost-effective digital imaging system that can produce a clear diagnostic full-body digital image in 13 seconds (Lodox.com, 2012). It was initially developed in South Africa for non-medical purposes but is currently used in trauma centers and mortuaries across the world (Chen *et al.*, 2010). The LS system emits up to 10 times less harmful quantities of radiation from an X-ray tube which is attached to the one side of a C-arm, while the X-ray detector is positioned on the opposite side (Figure 2.6). An anterior-posterior full-body digital image is taken while the C-arm moves along the length of the table and a lateral full-body image can be produced when the C-arm is rotated 90° axially around the patient (Evangelopoulos *et al.*, 2010; Lodox.com, 2012).

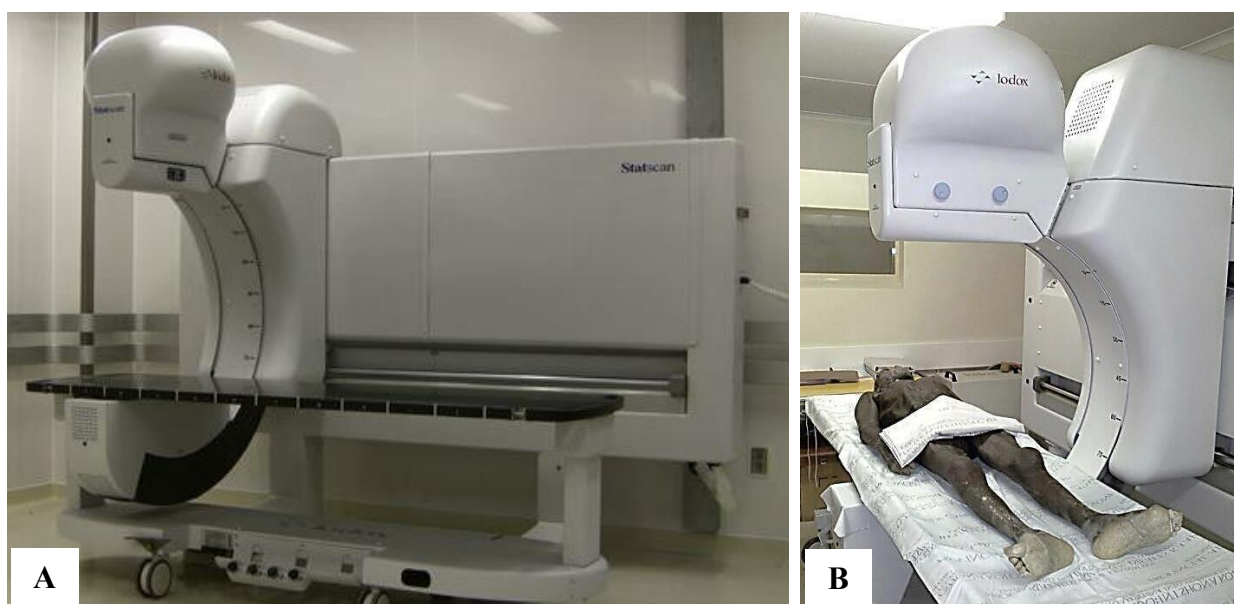


Figure 2.6. Lodox® Statscan®. A) The Lodox® Statscan® Imaging System produces full-body digital images of high quality by moving the C-arm along the length of the table (www.health 24.com); B) a cadaver used for the present study is being scanned.

The efficacy of the LS digital imaging system has been described in the literature. The detection of bone fractures, peripheral vascular injuries distal to the site of injury and foreign bodies such as bullet fragments have been reported (Mulligan *et al.*, 2006; Ball *et al.*, 2007). Evangelopoulos

and coworkers (2010) evaluated the efficacy of LS and indicated 54% sensitivity and 99% specificity for pleural abnormalities, while 45% sensitivity and 100% specificity were observed for lung parenchymal abnormalities. They concluded their study by indicating that the LS not only provides high-speed full-body digital images and low dose of radiation but also produces high quality images in a single scan.

The use of conventional radiography during anatomical dissections for education purposes has been known for several decades (Miles, 2005; Kotzé *et al.*, 2012). However, little information exists in the literature regarding the incorporation of cadaveric radiographs during dissections (Kotzé *et al.*, 2012). Dissection of cadavers for anatomical education have several advantages and it is believed that with the advantages of radiology, a combination of both anatomy and radiology may offer a more effective way to observe and study gross anatomy and pathology (Gunderman and Wilson, 2005). Stitching of conventional X-rays to produce a full-body X-ray was a time-consuming practice and was therefore seldom performed. With the development of the Lodox[®] Statscan[®] digital imaging system, full-body digital X-rays were easy to obtain (Lodox.com, 2012). In a novel study done by Kotzé and colleagues (2012) the efficacy of integrating full-body digital X-rays of each cadaver in the dissection program at Stellenbosch University, South Africa were examined. The integrated systems-based program is being used at Stellenbosch University where systemic anatomy and pathology modules are taught within weeks of each other. The researchers have concluded that students were able to effectively identify and observe the internal structures of the cadaver, including giving them a three dimensional perspective of the cadaver during dissections. In addition, students were given the opportunity to identify and observe gross pathology, for example skeletal and major soft-tissue

abnormalities in cadavers and on X-rays (Kotzé *et al.*, 2012). To our knowledge, this study is the first of its kind in which full body scans of cadavers were incorporated into an educational dissection program. The Lodox[®] Statscan[®] digital imaging system is therefore not only invaluable as a diagnostic tool in trauma centers and mortuaries worldwide, but can also play an important role in medical education.

Materials and Methods

“For the things we have to learn before we can do them, we learn by doing them.”
Aristotle, Nicomachean Ethics

3.1. Study Subjects

To assess the health status of the cadaver cohort for medical dissection at Stellenbosch University, three cohorts of embalmed cadavers were dissected and examined over a three year period. The first cohort of cadavers (n=40) was dissected during 2011, the second (n=43) in 2012, and the third (n=44) during 2013. The demographic information available on these cadavers is summarized in tables 3.1, 3.2 and 3.3.

The male to female ratio in the 2011, 2012 and 2013 cadaver cohorts were 4.4:1, 1.4:1 and 2.5:1, respectively. The ages ranged from 28 years to 82 years (average age: 45.0 years) in the 2011 cohort, 29 to 83 (average age: 49.7 years) in the 2012 cohort and 22 to 73 (average age: 52.4 years) in the 2013 cohort. For the total cadaver population over three years, the male-to-female ratio was 2.2:1 and average age was 49.2 years. Approximately 90% of the dissected cadavers are unclaimed bodies from low socio-economic backgrounds, primarily from the Western Cape and surrounding areas. The medical histories of the cadavers were not available to the researchers.

Table 3.1. Demographic information of the 2011 cadaver cohort

<i>Ref. Number</i>	<i>Sex</i>	<i>Age</i>	<i>Ethnicity</i>	<i>Ref. Number</i>	<i>Sex</i>	<i>Age</i>	<i>Ethnicity</i>
K01-10	Male	53	Mixed Race	K81-09	Male	44	*
K02-10	Male	31	Mixed Race	K82-09	Male	47	Mixed Race
K03-10	Male	34	Mixed Race	K83-09	Male	60	Mixed Race
K04-10	Female	39	Mixed Race	K87-09	Male	*	*
K05-10	Male	30	Black	K89-09	Male	41	Mixed Race
K06-10	Female	53	Black	K95-09	Male	*	Black
K10-10	Male	36	Black	K96-09	Male	*	Mixed Race
K12-10	Male	37	Black	K99-09	Female	70	White
K13-10	Male	47	Black	K100-09	Male	45	Mixed Race
K16-10	Female	45	Mixed Race	K101-09	Male	48	Mixed Race
K18-10	Female	32	Mixed Race	K102-09	Female	28	Mixed Race
K19-10	Female	63	Mixed Race	K104-09	Male	*	Mixed Race
K30-10	Male	*	White	K106-09	Male	*	Mixed Race
K36-10	Male	82	Mixed Race	K108-09	Male	42	Black
K38-10	Male	39	Black	K110-09	Female	49	Black
K40-10	Male	47	Mixed Race	K112-09	Male	58	Mixed Race
K42-10	Male	*	Mixed Race	K113-09	Male	40	Mixed Race
K45-10	Male	43	Mixed Race	K115-09	Male	32	Mixed Race
K47-10	Male	43	Mixed Race	K118-09	Male	*	Mixed Race
K80-09	Male	31	Black	K119-09	Female	50	Black

[* no information available]

Table 3.2. Demographic information of the 2012 cadaver cohort

<i>Ref. Number</i>	<i>Sex</i>	<i>Age</i>	<i>Ethnicity</i>	<i>Ref. Number</i>	<i>Sex</i>	<i>Age</i>	<i>Ethnicity</i>
K05-11	Female	41	Mixed Race	K65-11	Female	52	Mixed Race
K06-11	Male	37	Mixed Race	K69-11	Female	63	White
K10-11	Female	45	Mixed Race	K70-11	Female	*	Mixed Race
K13-11	Female	47	Black	K72-11	Male	*	Black
K15-11	Male	33	Black	K74-11	Male	70	White
K18-11	Female	76	*	K75-11	Male	36	Black
K31-11	Male	53	Black	K76-11	Female	*	Black
K38-11	Male	68	Black	K80-11	Male	38	Black
K40-11	Female	*	Mixed Race	K82-11	Female	39	Black
K41-11	Female	29	*	K101-11	Male	50	Mixed Race
K42-11	Male	*	Mixed Race	K116-11	Female	*	Mixed Race
K43-11	Female	32	Mixed Race	K120-11	Female	53	Mixed Race
K44-11	Male	48	White	K121-11	Male	50	Mixed Race
K46-11	Male	30	*	K124-11	Female	*	Black
K47-11	Male	64	*	K125-11	Male	39	Mixed Race
K52-11	Male	48	Mixed Race	K126-11	Male	45	Mixed Race
K53-11	Male	*	Mixed Race	K129-11	Male	65	Mixed Race
K55-11	Male	43	Black	K130-11	Female	81	White
K59-11	Male	34	*	K138-11	Male	57	Mixed Race
K62-11	Male	83	White	K140-11	Female	42	Mixed Race
K63-11	Male	*	Black	K148-11	Male	49	Mixed Race
K64-11	Female	48	*				

[* no information available]

Table 3.3. Demographic information of the 2013 cadaver cohort

<i>Ref. Number</i>	<i>Sex</i>	<i>Age</i>	<i>Ethnicity</i>	<i>Ref. Number</i>	<i>Sex</i>	<i>Age</i>	<i>Ethnicity</i>
K25-12	Male	39	Black	K74-12	Female	52	Mixed Race
K26-12	Male	*	Mixed Race	K75-12	Male	52	Mixed Race
K27-12	Male	66	Mixed Race	K76-12	Male	*	Mixed Race
K28-12	Female	62	Black	K77-12	Female	32	Mixed Race
K31-12	Male	45	White	K78-12	Male	61	Mixed Race
K42-12	Female	*	Black	K79-12	Female	49	Mixed Race
K43-12	Male	*	Mixed Race	K81-12	Male	49	Mixed Race
K46-12	Male	46	Mixed Race	K82-12	Male	63	Mixed Race
K49-12	Male	*	Black	K83-12	Male	59	Mixed Race
K50-12	Female	*	Mixed Race	K86-12	Female	24	Mixed Race
K51-12	Male	56	Mixed Race	K87-12	Male	24	Mixed Race
K52-12	Male	57	Mixed Race	K93-12	Male	72	Mixed Race
K57-12	Male	51	Mixed Race	K94-12	Male	60	Mixed Race
K58-12	Male	70	Mixed Race	K97-12	Male	*	Black
K59-12	Female	*	Black	K98-12	Male	42	Black
K60-12	Female	22	Mixed Race	K99-12	Male	47	Mixed Race
K61-12	Male	52	Mixed Race	K100-12	Female	46	Mixed Race
K62-12	Female	73	Mixed Race	K101-12	Male	58	Mixed Race
K64-12	Male	50	Mixed Race	K104-12	Female	61	Mixed Race
K66-12	Female	55	Mixed Race	K106-12	Male	44	Mixed Race
K69-12	Male	*	Black	K107-12	Female	62	White
K70-12	Male	60	Black	K119-11	Male	*	Mixed Race
K73-12	Male	72	Mixed Race	K124-12	Male	55	White

[* no information available]

	Cadaver was removed for forensic investigation due to suspicious cause of death discovered during dissection process
--	--

	Claimed by the family
--	-----------------------

3.2 Ethical Considerations

In South Africa, sections 61 to 64 of the National Health Act, No 61 of 2003, allows for the use of cadavers, both unclaimed and donated, for medical training and research purposes (National Health Act, 2003). At the Faculty of Medicine and Health Sciences, Stellenbosch University, South Africa, approximately 40 cadavers are used annually for anatomy dissections by the second and third year medical students as part of their anatomy training. Procurement of cadavers for the Division of Anatomy and Histology is done according to the departmental protocol which has been approved by the Inspector of Anatomy for the Western Cape.

The present study (N10/10/333) was approved by the Health Research Ethics Committee (HREC) of Stellenbosch University which conforms to the principles defined in the 1964 Declaration of Helsinki.

3.3 Embalming by Intra-Arterial Injection into the Carotid Artery

A standardized method for embalming cadavers is used at the Division of Anatomy and Histology, Stellenbosch University (*Addendum A*). Each cadaver for the present study was embalmed by making a superficial incision in the carotid triangle of the neck, starting from approximately 1cm superior from the border of the clavicle. The fascia between the sternal and clavicular heads of the sternocleidomastoid muscle as well as underlying muscles was reflected to expose the carotid sheath. The carotid artery, a component of the carotid sheath, lies more posterior and medial to the jugular vein. Care was taken in selecting the common carotid artery without damaging surrounding anatomical structures. With the use of an aneurysm hook, the carotid artery was selected and raised to the surface by placing the aneurysm hook in a resting position with both ends on the skin surface. This was followed by

an incision made across the width of the artery. A cannula connected to a tap connected to the container with embalmed fluid was carefully placed in the artery to prevent air bubble formation. The embalming fluid was then introduced via the cannula while maintaining the correct pressures. The embalmed cadavers were kept for at least three months at temperatures ranging from 18° to 20°C prior to dissection.

3.4 Lodox® Statscan®

Full-body digital X-rays were obtained using the Lodox® Statscan® digital imaging system which is located at the Western Cape Forensic Pathology Service medico-legal mortuary near the Tygerberg Hospital, Cape Town. The imaging software used is DVS®, version 2.8 and allows for the development and observation of DICOM® format images. Additional software, lucid™, was used to adjust for soft tissue and bone by enhancing image processing (Lodox Systems, 2012). The software, ImageJ® 1.46r, was used to access and observe the acquired DICOM® images. The scans were evaluated for macroscopic pathology both prior to dissections (prospectively) and during and after dissections (retrospectively). Correlations were made between the observations made on the X-rays and macroscopic pathology observed during dissections. The candidate correlated the observed pathology with a registrar from the Division of Radiodiagnosis, Dr. Michelle da Silva, under the guidance of Prof. RD Pitcher and Prof. J Lotz from that division.

3.5 Radiologists' Examination

The chest X-ray findings were reviewed by two independent radiologists without prior knowledge of the morphological pathology observed during the dissections. Each pair of cadaveric lungs was divided into six segments (designated segment 1 to 6) (Figure 3.1). Criteria were developed to compare the dissection findings with the radiological features. The

criteria included opacification, nodularity, collapse, bronchiectasis, cavities and pleural thickening. Statistical tests used to compare the findings included description statistics, cross-tabulation statistics and correspondence analyses.

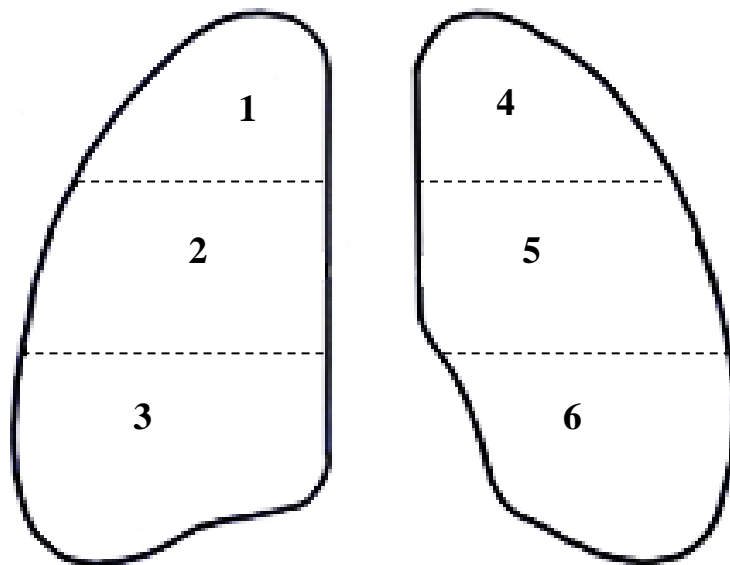


Figure 3.1. Lung segments of the cadaver cohort (n = 40). The right and left lungs were divided into six segments to compare the radiology and pathology.

3.5.1 Evaluating the Cadaver Chest X-Ray

The chest X-rays of the first cadaver cohort was evaluated using the following standard criteria (Figure 3.2):

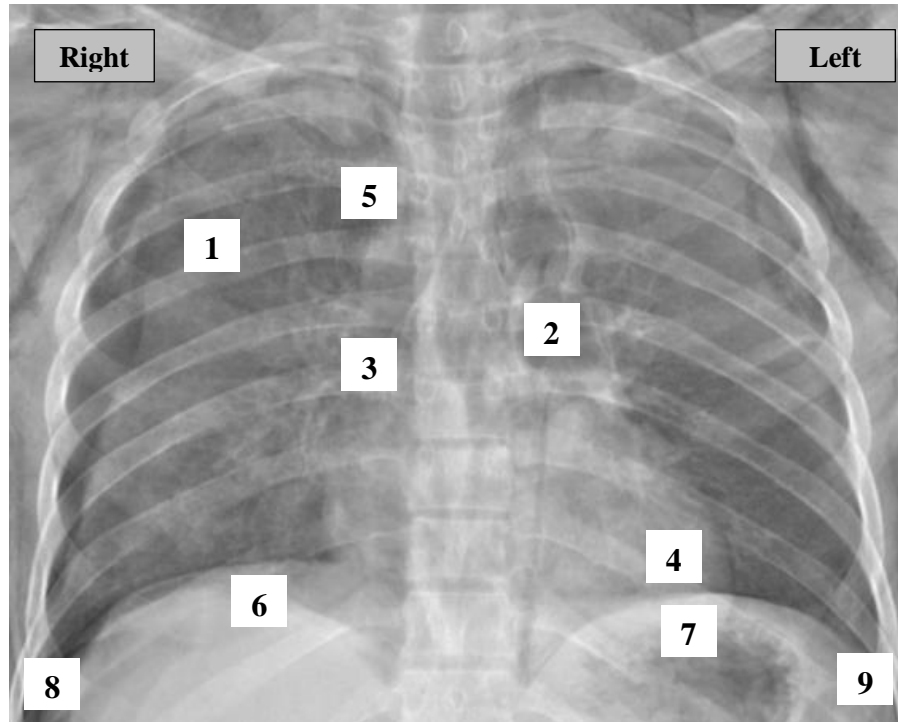


Figure 3.2. Example of a cadaver chest X-ray (K05/11), posterior-anterior (PA) view.

- A: The lung fields (1) were examined for equal transradiancy. Ideally, a displaced oblique fissure indicated atelectasis.
- B: The hilar area was inspected. Anatomically, the left hilum (2) is located more superior than the right hilum (3) and should be concave in shape.
- C: The heart (4) was inspected for normal shape and size (for this study, cardiomegaly was diagnosed when the maximum cardiac diameter was more than 50.0% of the transthoracic diameter).
- D: The right side of the trachea (5) was inspected for signs of peritracheal lymphadenopathy.
- E: The domes of the diaphragm were evaluated. The right part of the diaphragm (6) should be more superior compared to the left part of the diaphragm (7).
- F: The costophrenic angles (8 and 9) were evaluated, however in the majority of the cadavers the angles were difficult to identify.

3.6 Intra-Arterial Injection of Latex into the Carotid Artery

The cadavers of the 2011 and 2012 cohorts were each injected with red-colored liquid latex approximately four to six weeks after embalming and prior to the acquisition of the digital X-rays. This was done for improved demonstration of arteries during dissection. For practical purposes, this procedure was not repeated in the 2013 cohort.

3.7 Anatomy Dissections by Medical Students

The MBChB II and III students dissected different organ systems of the same cadaver cohort during the course of one year. These dissections formed part of their anatomy practical sessions during their pre-clinical training. The program is indicated in Table 3.4.

Table 3.4. Modules covered in the anatomy curricula at the Division Anatomy and Histology

<i>Group</i>	<i>Month</i>	<i>Module</i>
MBChB II	January	Respiratory system
	February	Cardiovascular system
	May	Gastrointestinal tract system
	Mid-July	Urogenital system
MBChB III	January	Brain
	June	Musculoskeletal system

In order to make the investigation more thorough, evaluation of the brain, prostate gland, cervix and oral cavity of each cadaver was included in the two years that followed.

3.8 Instruments and Equipment

The following instruments were used to dissect and examine the internal organs of the cadavers (Figure 3.3).

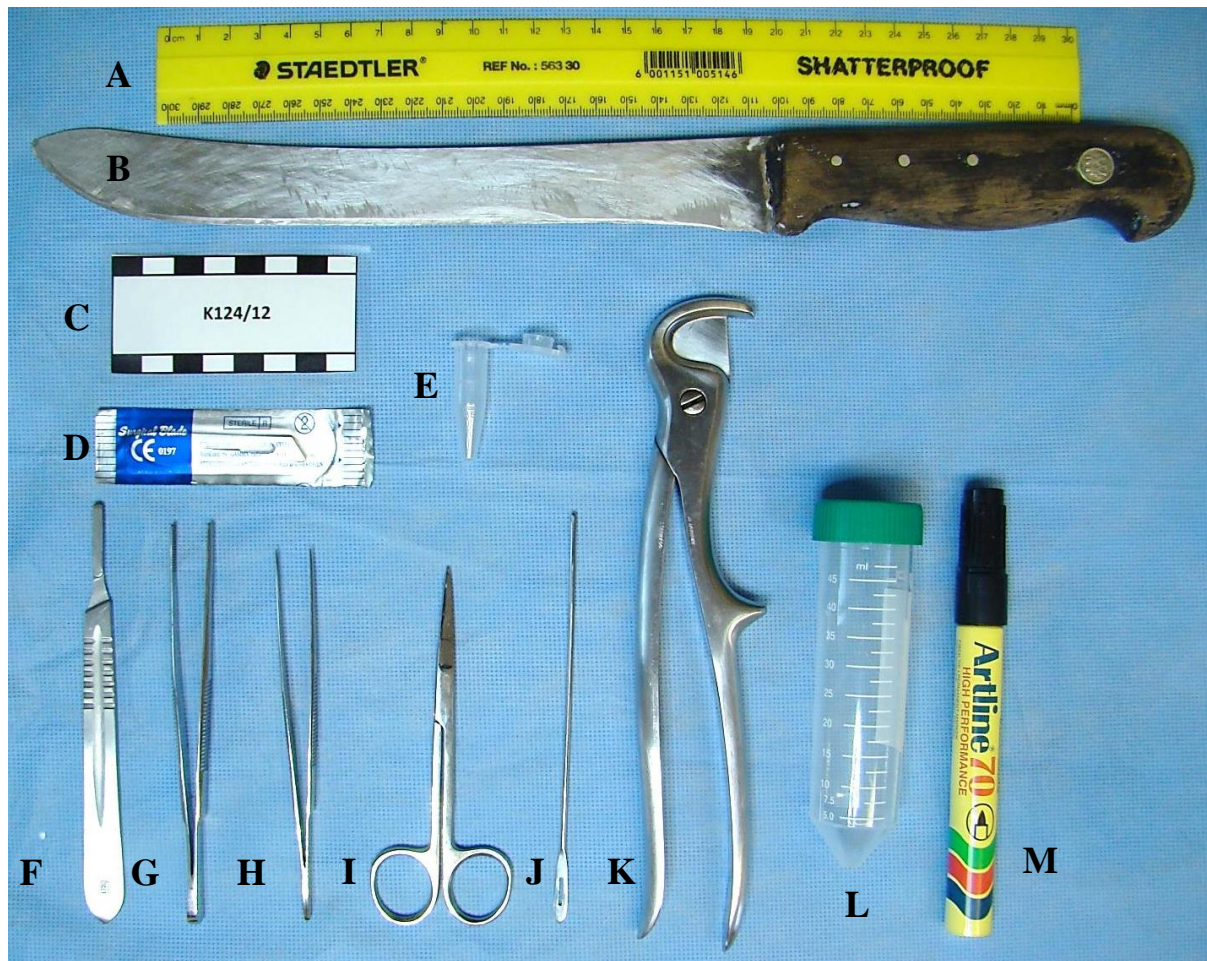


Figure 3.3. Instruments used during the dissections. A) 30-cm ruler; B) organ knife, 240mm/9.5 inches; C) cadaver reference number; D) nr. 22 disposable blade; E) Eppendorf® microtube, 1.5ml; F) scalpel knife holder; G) forceps, serrated tips, 125mm/4.9 inches; H) forceps, serrated tips, 115mm/4.5 inches; I) scissors, Mayo abdominal, straight 110mm/4.3 inches; J) probe, 1mm; K) rib shears; L) specimen container, 50ml; M) permanent marker.

3.9 Cadaveric Dissections and Internal Examination

Cadavers were dissected according to the departmental protocol as described in Grant's Dissector, fifteenth edition (Tank, 2013). At the beginning of each year, the Ph.D. candidate was introduced to the class and medical students were alerted to the fact that their dissections

would be used for further studies. They were asked to carefully dissect the structures in order to maintain the normal structural architecture and decrease any artifactual changes.

3.9.1 Lungs

During the medical dissections, the anterior thoracic wall was dissected and reflected to expose the thoracic organs. The lungs were photographed *in situ* (Figure 3.4) and carefully removed and weighed using a standard weighing scale (*Addendum B*). Subsequently the pleural surfaces were inspected for pathology lesions and the pulmonary parenchyma was palpated for nodular lesions.

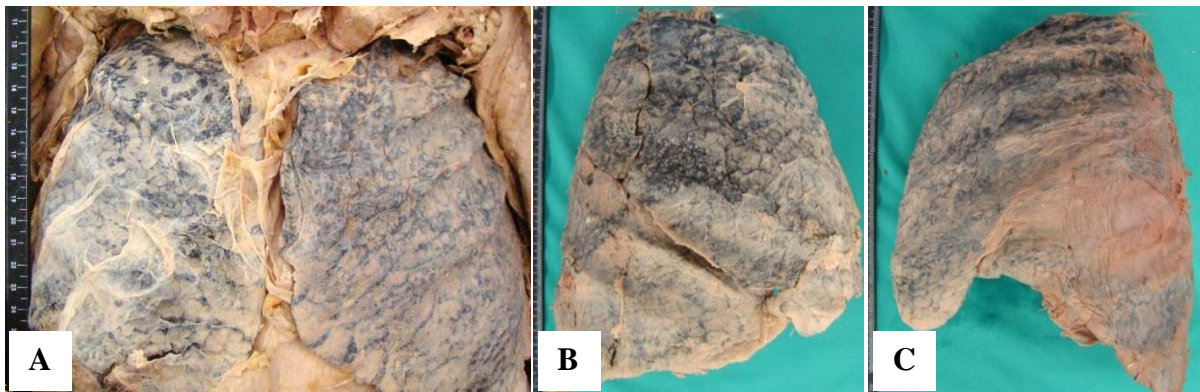


Figure 3.4. Photographs of the pulmonary system of cadaver K36/10. A) Photograph presenting the *in situ* appearance of the lungs after the anterior thoracic wall has been removed during dissections; B) *ex vivo* photograph of the right lung after organ removal and C) *ex vivo* photograph showing the left lung.

The lungs were then placed on a cutting board and 1- to 2-cm sections were made along the short axis with a clean postmortem knife (Figure 3.5). The parenchymal features were subsequently exposed and the researcher inspected the lung parenchyma to identify any abnormalities, such as areas of consolidation and scarring. Care was taken to prevent cross-contamination by replacing the scalpel blades and cleaning the instruments with 70% alcohol.

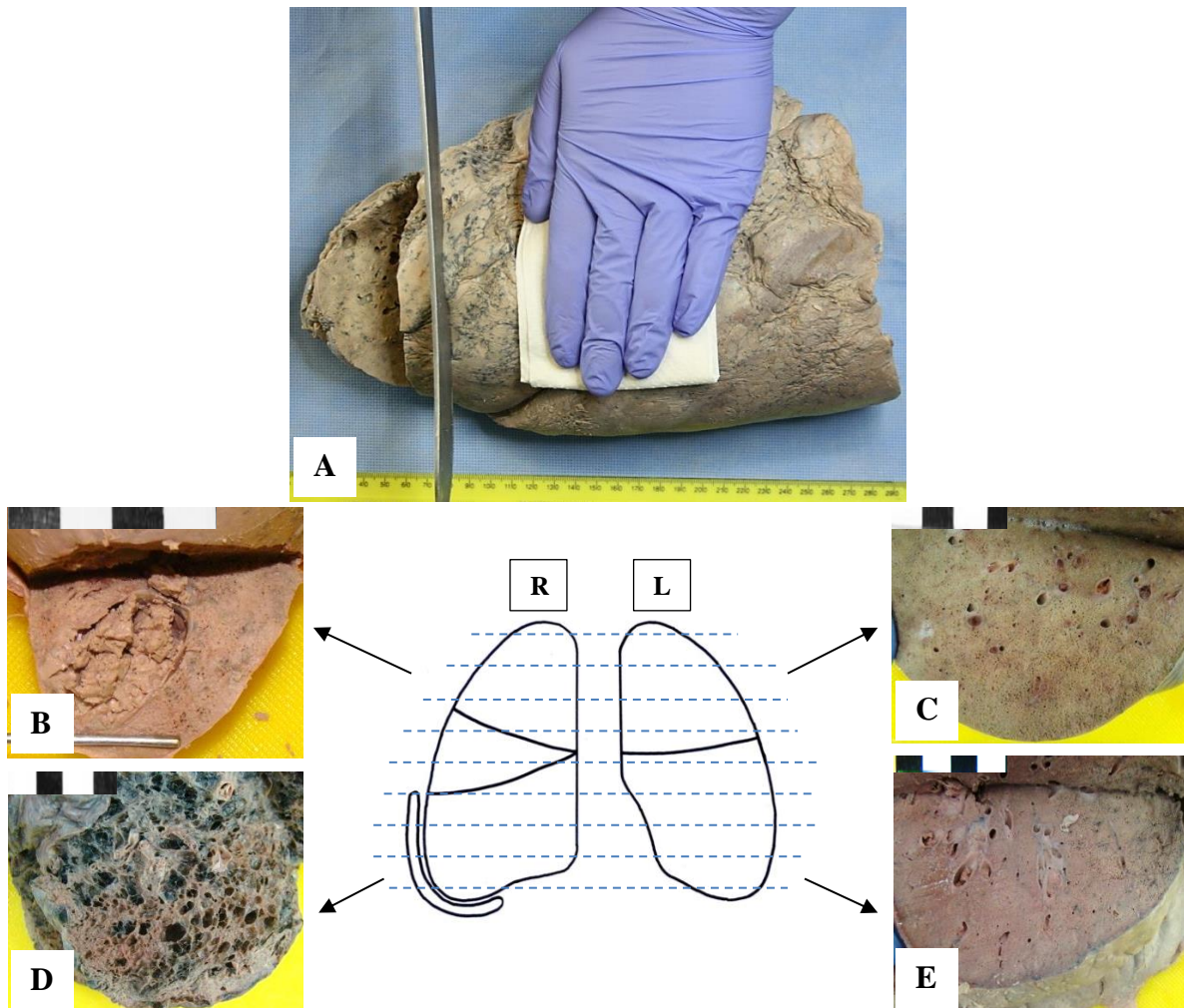


Figure 3.5. Photographs indicating the dissection process to investigate the pulmonary parenchyma. A) Transverse (horizontal) sections were made of each lung. B) The superior region of the right lung of cadaver K25/12; C) the superior lobe of K75/12, showing the parenchyma. Each section was evaluated for visible pathology; D) the inferior region of the right lung of cadaver K46/12 showing emphysematous changes and E) the inferior lobe of the left lung of cadaver K97/12. [The dashed lines indicate the sections that were made to observe the parenchyma]

Samples were removed from areas which showed macroscopical pathology or abnormalities. For the pulmonary system, a total of five samples (one for each lobe of the lungs) were removed with a clean scalpel blade from the affected organs to avoid crushing or tearing of the tissue. These samples were used for histology. The tissue was placed in correctly labeled specimen bottles containing adequate volumes of 10% neutral buffered formalin (pH 7.5). The formalin was prepared according to standard histological procedures.

3.9.2 Neck and Anterior Mediastinal Organs

The anterior mediastinum was inspected and any abnormal lymph nodes were removed for histological examination. The tongue, larynx, trachea and esophagus were subsequently removed and opened lengthwise along the posterior aspects. The mucosal surfaces were inspected for any abnormalities and removed for histology when pathology was suspected.

3.9.3 Heart and Pericardial Sac.

The heart was removed from the cadaver according to the dissection protocol after which the remnants of the pericardium and excess fat was removed to expose the extramural coronary arteries. These arteries were examined by making cross-sections at 3- to 5-mm intervals to determine atherosclerotic plaques within the lumen. The heart was then placed on a cutting board and cut into 2- to 3-cm slices along the short axis (horizontal plane) starting at the apex of the heart to just inferior to the atrioventricular valvular margin. The myocardium was carefully inspected for fibrosis or colour changes which may indicate the presence of a myocardial infarction. The atrial chambers were opened to investigate the fossa ovale and the atria. Measurements of the circumferences of each of the semilunar and atrioventricular valves were taken and recorded on a data sheet (*Addendum C and D*). The width of the left ventricle, right ventricle and septum was also measured. The ascending aorta, its arch with accompanying branches, and the descending aorta was opened along its length *in situ* with a scalpel to determine the presence of atherosclerotic plaques and aneurysms.

3.9.4 Hepatobiliary System.

In situ photographs were taken of the abdominal organs once the skin and the underlying abdominal wall muscles were dissected and reflected. The organs were then removed and each of the organs was photographed and inspected individually. The liver was weighed and

cut with a clean post mortem knife into sections of approximately 2- to 3-cm wide along the short axis (parasagittal sections) (Figure 3.6). The parenchyma was inspected and photographed. A sample was taken from each liver for histology. The gallbladder was opened, the contents removed and examined for calculi. The common bile duct was inspected by extending the incision through the duct.



Figure 3.6. Photograph indicating the dissection process to investigate the hepatic parenchyma. The liver was weighed and cut with a clean post mortem knife into sections of approximately 2- to 3-cm each along the short axis (parasagittal sections).

3.9.5 Spleen

The spleen was removed by severing the attachment at the hilum prior to being inspected. The capsule was inspected after the spleen was weighed and photographed. Multiple transverse cuts of approximately 1- to 2-cm wide were made along the short axis of the spleen to inspect the parenchymal appearance (Figure 3.7, A). A sample was taken of the spleen to inspect the microscopic appearance of the parenchymal features.

3.9.6 Stomach and Small Intestine

The distal part of the esophagus was separated from the cardia of the stomach prior to opening the stomach along the greater curvature, antero-laterally. The incision was extended

through the pylorus and continued through the duodenum, jejunum and ileum, along the entire length of the intestine on the antimesenteric borders in order to expose and inspect the intestinal mucosa. Any abnormalities were noted, photographed and samples for histology were taken from the corresponding lesions.

3.9.7 Pancreas

The pancreas was identified within the C-shaped bend of the duodenum at the level of L1 to L3 in each cadaver. The pancreatic parenchyma was inspected by making transverse (parasagittal) sections along the short axis (Figure 3.7, B). A sample for histology was taken to observe the microscopical features.

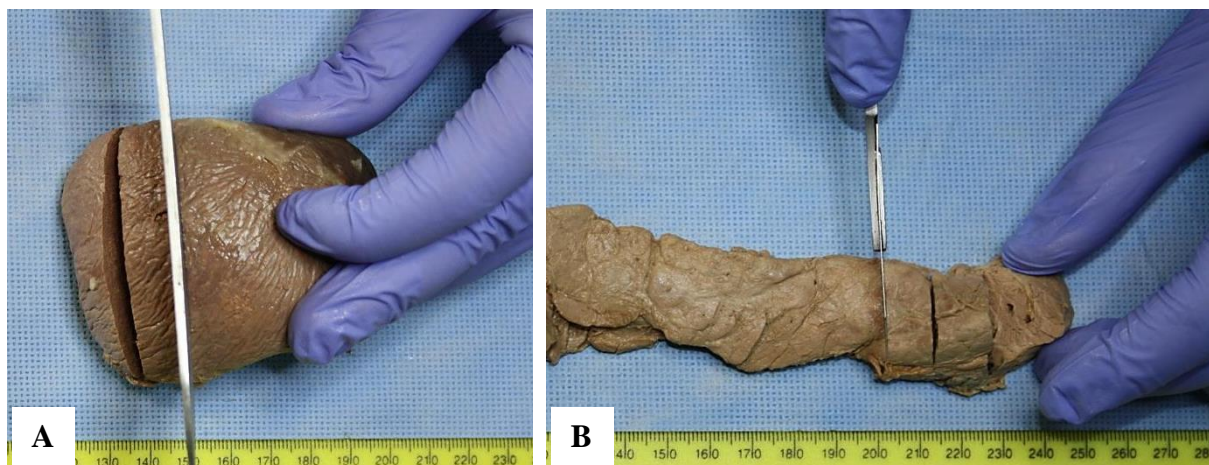


Figure 3.7. Photograph indicating the dissection process to investigate the splenic and pancreatic parenchyma. A) After the capsular surface of the spleen was inspected, multiple sections measuring approximately 1- to 2-cm in width were made along the short axis; B) transverse (parasagittal) sections were made with a scalpel blade along the short axis.

3.9.8 Cecum, Appendix and Large Intestine

After the appendix was inspected, an incision was made in the cecum and extended along the antimesenteric borders to the distal part of the sigmoid colon, proximal to the rectum. The mucosal surfaces were washed to remove fecal material to inspect for abnormalities. Samples were taken for histology if any abnormalities were noted.

3.9.9 Kidneys

The kidneys were removed by separating the renal capsule from the perinephric fat and severing the blood vessels and ureters near the renal hilum. The kidneys were weighed and the capsules were removed. The kidneys were cut longitudinally along its lateral border to inspect the internal parenchyma (Figure 3.8). The cortex, medullary pyramids, pelvis as well as the major and minor calices were inspected for abnormalities. Photographs and samples for histology were taken of each of the kidneys. In addition, the cortical surfaces were inspected for any irregularities, scarring or cystic features.



Figure 3.8. Photograph indicating the dissection process to investigate the renal parenchyma. The kidney was sliced through their coronal (longitudinal) axis starting at the lateral aspect to inspect the internal parenchyma.

3.9.10 Lower Genitourinary Tract (Male)

The prostate together with the bladder was removed from the cadaver by separating bladder from the pubic symphysis on the anterior aspect. The prostate was examined and the size was measured in three dimensions, prior to being cut to inspect the parenchyma. Samples were removed for histology when benign prostatic hyperplasia (BPH) or any other abnormalities were suspected. The bladder was opened on the antero-lateral aspect to inspect the inner mucosa. Both testes were removed from the scrotum and cut in the sagittal plane to inspect parenchymal features.

3.9.11 Lower Genitourinary Tract (Female)

The bladder was separated from the uterus and opened lengthwise on the superior aspect to inspect the mucosa. The cervix and uterus were removed and inspected for any abnormalities, such as venereal warts (*condylomata acuminata*) or erosions. Samples were taken when pathological lesions were observed on macroscopic inspection. The uterus was opened in the sagittal plane to inspect the thickness of the endometrium. The fallopian tubes and ovaries were also examined for macroscopical pathology.

3.9.12 Male and Female External Genitalia

Male external genitalia were inspected by making a midline incision on the dorsum and an additional coronal incision through the body of the penis to inspect the interior penile features. The female external genitalia were visually examined for pathology such as *condylomata acuminata*.

3.9.13 Brain Removal and Examination

The head of the cadaver was placed on a wooden block. Two incisions were made on the scalp perpendicular to each other. The scalp was incised down to the bone prior to peeling the skin and subcutaneous tissue back. An oscillating saw (HEBU®) was used to cut and remove the calvarium. Care was taken to prevent dural or brain penetration. The brain and cerebellum was removed and examined externally for any abnormalities, prior to sectioning. The base of the brain was examined for possible tuberculous meningitis (TBM) lesions. The brain was placed on a flat surface and a sagittal section was made to separate the two hemispheres for inspection of the medial surface of each of the hemispheres. Starting at the frontal lobe, serial coronal sections measuring 2- to 3-cm were made to inspect the brain parenchyma. Abnormalities were noted and samples were taken for histology.

3.9.14 Skeletal Evaluation

The soft tissue was removed from each cadaver by means of dissection by trained technical staff at the Division of Anatomy and Histology. The skeletal remains were placed in a container with water and sodium bicarbonate for a minimum of three days at constant temperatures of approximately 80°C. This was done to remove soft tissues that was unable to be removed during dissection. Defatting of the bones was achieved using tri-ethylene glycol (TEG). The skeletal remains were subsequently evaluated for congenital abnormalities, variations and pathology. The skeletal findings were recorded on a customized data sheet and detailed photographs were taken of the abnormalities.

3.10 Determination of Body Mass Index (BMI) of the Cadavers

The body mass index (BMI) of each cadaver was measured. The cadavers were weighed with a *Pa 6110 B2007 Indicator* scale prior to embalming (*Addendum E*). As we did not have the heights of the cadavers, the physiological length of each cadaver's left femur was measured using a calibrated osteometric board. The value obtained (in centimeters) were used to estimate the total skeletal height (TSH) of the cadaver. The following equation was used:

$$\text{TSH} = (\text{length of left femur (cm)} \times \text{intercept}) + \text{slope} = \text{length (cm)}$$

The intercept and slope values were used based on the sex and race of the cadavers (Table 3.5). Limited research has been done on stature estimation in the mixed race population. It was decided for the purpose of this study to use intercept and slope values by Lundy and Feldsman (1987) to estimate TSH in the mixed population group. This notion was confirmed by Prof. Maryna Steyn, a forensic anthropologist at Pretoria University (Personal interview, June 2, 2014).

Table 3.5. The intercept and slope values for race and sex

Population Group and Sex	Intercept Value	Slope Value	Reference
Males			
Black	45.72	2.40	Lundy and Feldesman, 1987
Mixed Race	45.72	2.40	Lundy and Feldesman, 1987
White	51.17	2.30	Dayal, 2003
Females			
Black	27.42	2.77	Lundy and Feldesman, 1987
Mixed Race	27.42	2.77	Lundy and Feldesman, 1987
White	34.69	2.64	Dayal, 2003

The BMI was subsequently determined using the following equation:

$$\text{BMI} = (\text{weight})/(\text{height})^2$$

Where weight is measured in kilograms (kg) and height in meters (m).

3.11 Pathologists' Examination

After the parenchymal findings of each of the organ system were evaluated a differential diagnosis was made of each cadaver by the researcher. Dr. E.H. Burger, a forensic pathologist, was consulted to correlate the researcher's diagnoses. In 2011 and 2012, Dr. Burger assisted the candidate with evaluating and describing the morphological appearances of the pathology observed in the cadavers. The morphological appearance of systemic pathology and in particular TB lesions as well as its distribution was thoroughly described in the pathology report. In 2013, the researcher registered for the module "*Anatomical Pathology for Non-Pathology Disciplines (10391 871)*". The module was successfully completed and gave the researcher the opportunity to become more self-reliant with diagnosing pathology in the anatomical setting.

3.12 Histology Procedures

In all organs where histology samples were harvested, the following procedure was used to process the samples;

Thin sections (5mm in width) were taken using a sharp trimming blade. Every specimen was handled on a clean surface to avoid cross-contamination between sections. The section was placed in a correctly labeled cassette with appropriate perforations. Processing was performed by the *Shandion Elliot Duplex* processor overnight for 17 hours (Figure 3.9). Following processing, the specimens were orientated in an appropriate mold and were filled with liquid paraffin wax by the *Leica EG 1160* embedder (Figure 3.9). After the blocks containing the tissue samples were trimmed to expose the tissue, sections ranging from 4 to 7 μ m were cut with a *Leica TM2125RT* microtome (Figure 3.10). The sections were placed in a water bath with added STA-ON[®] tissue section adhesive (Merck, Germany) to prevent section lifting. The temperature was maintained at approximately 42°C. One section (5 μ m) was cut from each block. The sections were incubated for approximately 1 hour at 60°C prior to staining with the *Leica Autostainer XL* (Figure 3.9).



Figure 3.9. Histology laboratory. 1) *Shandion Elliot Duplex* processor; 2) *Leica EG 1160* embedder; 3) *Leica Autostainer XL*

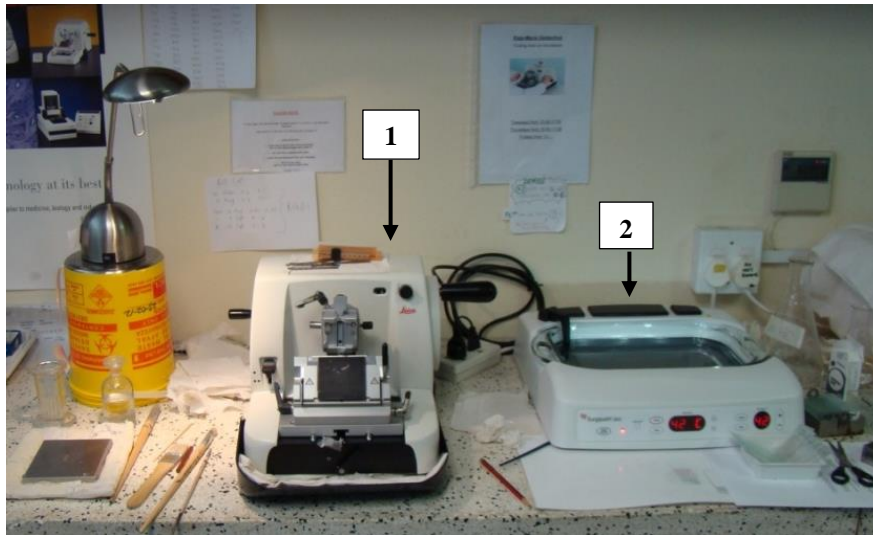


Figure 3.10. Sample sectioning. 1) *Leica TM2125RT* microtome ; 2) water bath

Staining was done with the *Leica Autostainer XL* using Mayer's hematoxylin (Merck, Germany) and eosin yellowish (Merck, Germany) for the hematoxylin and eosin (H&E) stain (Figure 3.9) (*Addendum F*). Specific special stains were performed whenever a pathological lesion or abnormality was evident during histological evaluation. These included the Ziehl-Neelsen (ZN), Martius Scarlet Blue (MSB), Perls' Prussian, McManus periodic acid Schiff (PAS) and Verhoeff's (EVG) stains. The stain was selected based on the histopathological needs to identify and diagnose a condition. The coverslips were applied using DPX (Merck, Germany), a high quality mounting medium. An *Axioskop Zeiss* light microscope system, with a *Zeiss Axiocam* camera attached, was used to view the slides.

The total number of tissue sections removed is summarized in Table 3.6.

Table 3.6. Total number of tissue samples stained with the standard H&E

<i>Total number of cassettes per year</i>	<i>Respiratory System</i>	<i>Central Nervous System</i>	<i>Cardiovascular system</i>	<i>Gastrointestinal Tract System</i>	<i>Urogenital Tract System</i>
<i>2011</i>	200	*	20	34	35
<i>2012</i>	215	39	106	194	139
<i>2013</i>	225	20	132	182	138
<i>TOTAL</i>	640	59	258	410	312

* Not part of the pilot study

3.12.1 Histology Stains

The following histology stains were used in the present study (Table 3.7).

Table 3.7. Histology stains used in the present study

<i>Histology Stain</i>	<i>Tissue Type</i>
Hematoxylin and Eosin	All tissue types
Ziehl-Neelsen	Pulmonary tissue (n=127 cadavers) and extrapulmonary tissue with macroscopical signs of TB
Perls' Prussian Blue	Pulmonary tissue
Martius Scarlet Blue	Pulmonary/extrapulmonary tissues suspected of containing fibrin (as a result of acute inflammation)
McManus' PAS Method	Pulmonary tissue with microscopical signs of fungal infections
Verhoeff's Method	Blood vessels walls

3.12.1.1 Hematoxylin and Eosin (H&E) Stain

Hematoxylin and Eosin (H&E) stain is the most widely used stain to demonstrate histological features of tissue as well as cellular cytoplasmic characteristics. The alum hematoxylin component, or Mayer's hematoxylin (Merck, Germany), stains nuclei purple-blue, while the eosin (Merck, Germany) counterpart stains cellular cytoplasm and connective tissue an orange pink color (Bancroft and Gamble, 2011). This stain was therefore selected to show the general histological tissue structure. The protocol for the H&E stain can be found in *Addendum F*.

3.12.1.2 Ziehl-Neelsen (ZN) Stain

Mycobacteria have a surrounding lipid capsule and are therefore difficult to demonstrate with the standard Gram stain. The surrounding capsule must therefore be penetrated by a stain that is resistant to removal by acid or alcohol. The Ziehl-Neelsen stain is ideal for demonstrating acid-fast bacteria (AFB). The staining method makes use of two reagents; carbol-fuchsin (Merck, Germany) and acidified methylene blue (Merck, Germany). Carbol-fuchsin, a red dye, is forced into the AFB lipid capsule using heat. In addition, surrounding structures are also stained red. The carbol-fuchsin is removed from surrounding structures with the use of

an acid, while the lipid layer of the AFB resists the effects of the acid. The bacteria are therefore stained red, while the background is stained with a counterstain, namely acidified methylene blue (Bancroft and Gamble, 2011). This stain was selected for this study to demonstrate the presence of acid-fast bacteria (such as mycobacteria) in granulomatous lesions. The protocol for the ZN stain is described in *Addendum G*.

3.12.1.3 Perls' Prussian Blue Stain

The Perls' Prussian blue method makes use of an acidic ferro-cyanide solution to expose ferric iron in the form of ferric hydroxide, $\text{Fe}(\text{OH})_3$. Ferric ferro-cyanide, an insoluble blue compound, is produced when diluted potassium ferro-cyanide reacts with the exposed ferric iron (Bancroft and Gamble, 2011). Pulmonary samples were stained in order to determine for the presence of iron-containing macrophages (so-called "heart failure cells") in the sections. This stain can be used to distinguish between iron-positive macrophages and carbon-positive macrophages (Bancroft and Gamble, 2011). The latter is formed as a result of anthracosis, a smoking-related manifestation, where carbon particles are phagocytosed by alveolar macrophages. The protocol is described in *Addendum H*.

3.12.1.4 Martius Scarlet Blue (MSB) Stain

The Martius Scarlet blue method makes use of a small-molecule yellow dye (Martius yellow) in conjunction with phosphotungstic acid dissolved in 96% alcohol. The phosphotungstic acid is used to prevent staining of muscle cells, collagen and other connective tissues, while newly developed fibrin is stained yellow. Subsequent treatment with a red medium-molecule (brilliant crystal scarlet) stains mature fibrin and muscle cells red, while a blue large-

molecule dye (methyl blue) is used to demonstrate old fibrin as well as collagen fibers (Bancroft and Gamble, 2011).

When acute inflammation develops on a serosal surface, a fibrinous inflammatory response may occur with a resultant increased vascular permeability and increased flow of large molecules (such as fibrinogen) across the endothelial barrier. This results in an exudate with high plasma protein content. In some instances the exudate may be cleared by means of fibrinolysis and macrophages. If the resolution phase fails, the fibrinogen (from the plasma) is converted to fibrin (Burkitt *et al.*, 1996). The fibrin will ultimately be replaced by fibroblasts with accompanying angiogenesis which may lead to scar formation with important clinical consequences (Kumar, 2013). The MSB stain is therefore specifically designed to stain for fibrin in inflamed tissue and in ante-mortem thrombi. This stain was chosen for the present study to illustrate fibrin in tissues which showed signs of inflammation. The protocol for the MSB stain can be found in *Addendum I*.

3.12.1.5 McManus's PAS Method for Glycogen and Fungal Cell Walls

Fungal growth may either be present in the primitive asexual form (spherical spores) or in the vegetative form (cylindrical hyphae). These morphological features make it possible to distinguish between the different types of fungi (Bancroft and Gamble, 2011). Fungi are relatively large eukaryotic organisms with cell walls consisting of polysaccharides. These polysaccharides can be oxidized to dialdehydes, which are demonstrated by Schiff's reagent (Bancroft and Gamble, 2011). This periodic acid-Schiff (PAS) method is usually used to demonstrate glycogen and mucus in sections. It can therefore be used to demonstrate opportunistic fungal growth in pulmonary tissue sections or it may be a diagnostic indicator

for serous and mucinous carcinomas (Aalto, 1986, Bancroft and Gamble, 2011). The protocol describing the McManus's PAS technique used in the present study is found in *Addendum J*.

3.12.1.6 Verhoeff's Method for Elastic Fibers

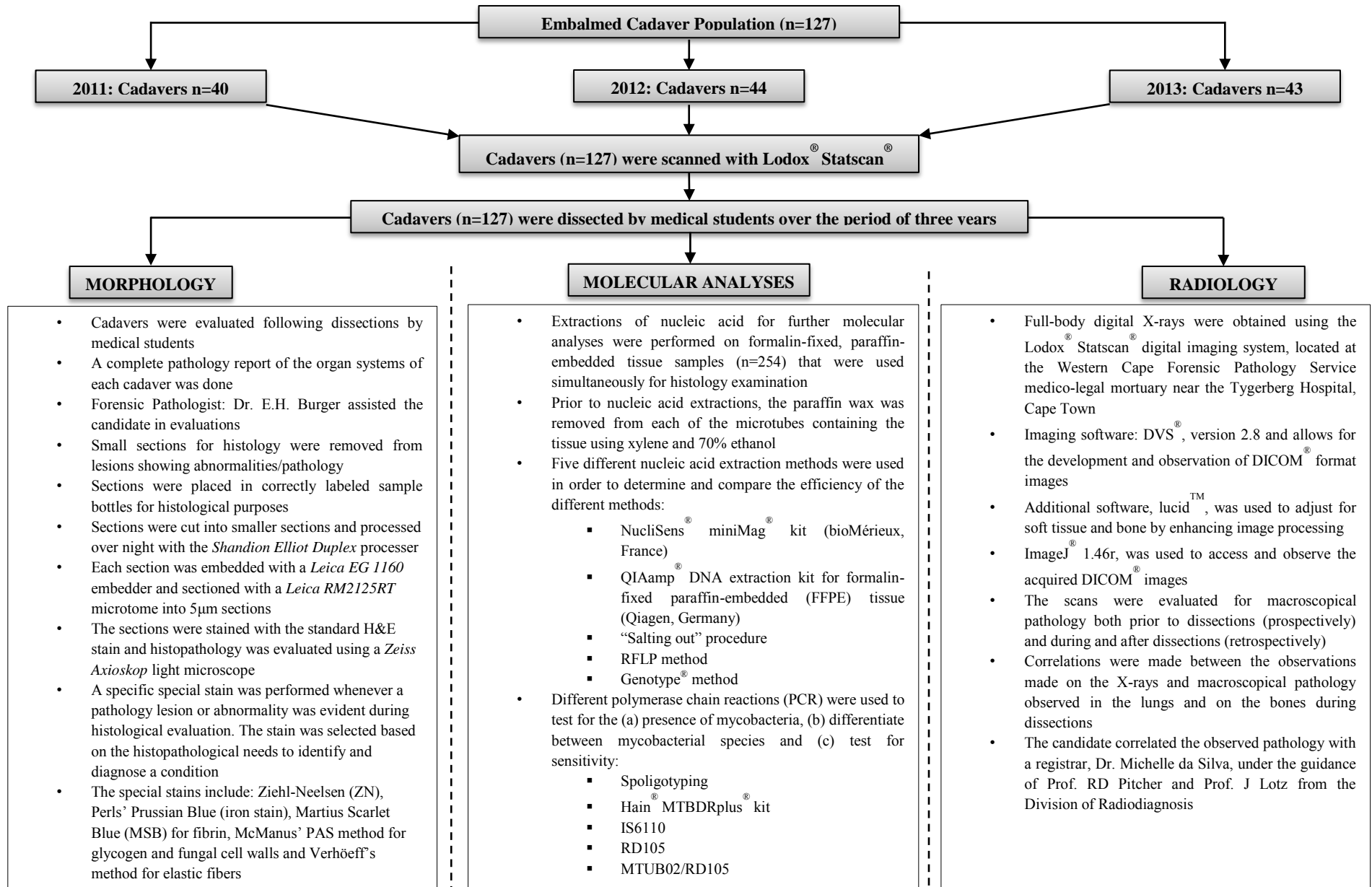
The Verhoeff's method is used to demonstrate elastic fibers in the tunica media of arterial walls. Tissue sections of arterial walls showing significant thickening or hardening (arteriosclerosis) as well as abnormal dilations of the arteries (aneurysms) were stained with the Verhoeff's method (Burkitt *et al.*, 1996). Abnormalities in the general architecture of the elastic fibers may indicate an underlying pathological process. This stain may therefore indicate abnormalities in the blood vessel walls of the cadavers. The Verhoeff's method can be found in *Addendum K*.

3.12.2 Histology Controls

The following histology controls were used in the present study (Table 3.8).

Table 3.8. Controls used in the present study

<i>Histology Stain</i>	<i>Control – Tissue Type</i>
Hematoxylin and Eosin	No control necessary
Ziehl-Neelsen	Positive control – Pulmonary tissue from Forensic Pathology Service histopathology laboratory, Clinical Building, SU
Perls' Prussian Blue	Positive control – Splenic tissue from histology laboratory, FISAN Building, SU
Martius Scarlet Blue	Positive control – tissue with signs of acute inflammation (fibrin)
McManus' PAS Method	Positive control – liver tissue
Verhoeff's Method	Quality control - artery



A summary of the experimental design of the present study can be found on page 77 (Figure 3.11).

3.13 Molecular Analysis

3.13.1 Pulmonary Tissue Samples

Extractions of nucleic acid for molecular analyses were performed on the formalin-fixed, paraffin-embedded tissue samples which were used for histology examination. Each paraffin block containing pulmonary tissue was cut with a sterile microtome blade at 5 μ m. Two serial sections were cut from each lobe of the right lung and were collected in a 1.5ml microtube. The same procedure was repeated for the left lung; however three sections were cut from each lobe to ensure an equivalent amount of sections in each microtube (Figure 3.12). Pulmonary sections from all three cadaver cohorts (2011-2013) were used while the total number of samples used for molecular analysis was 254 samples.

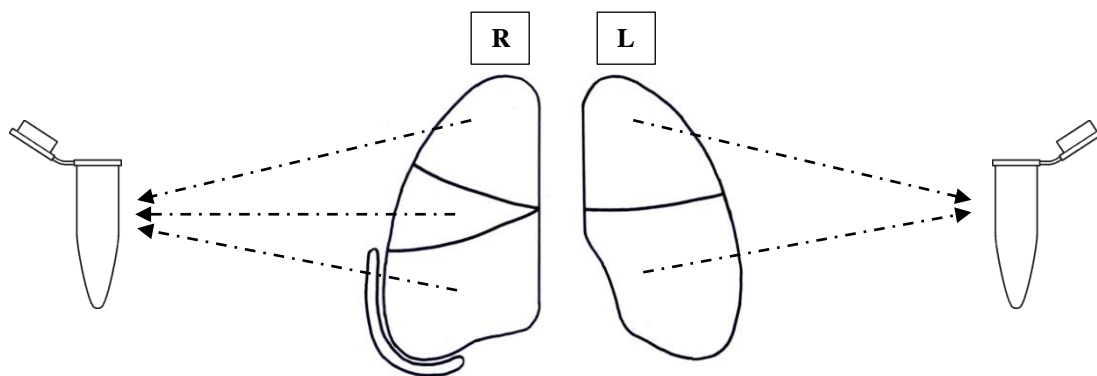


Figure 3.12. Samples for molecular analyses. Formalin-fixed, paraffin-embedded tissue samples were sectioned at 5 μ m and collected in a microtube. Two microtubes containing equal sections from the left and right lung per cadaver were obtained.

3.13.2 Wax Removal and Heating Procedures

After the sections were collected in the microtubes, 1000 μ l xylene (Merck, Germany) was added to each microtube and heated for 5 minutes at 40 $^{\circ}$ C, shaking at 1400 rpm, to dissolve the majority of the wax. This step was repeated twice. The tubes were centrifuged at 13,000

rpm for 1 minute and the supernatant was carefully removed. Once the wax was entirely removed, 1ml 100% ethanol was added to each tube followed by centrifugation at 13,000 rpm for 1 minute and decanted. This step was repeated for a second time with 70% ethanol. The tubes were placed on a heating block until the ethanol had completely evaporated.

3.13.3 Nucleic Acid Extraction

Five different nucleic acid extraction methods were used in order to determine and compare the efficiency of the different methods, namely: (i) NucliSens[®] miniMag[®] kit (bioMérieux, France); (ii) QIAamp[®] DNA extraction kit for formalin-fixed paraffin-embedded (FFPE) tissue (Qiagen, Germany), (iii) “salting out”, (iv) Genotype DNA isolation (HAIN[®]) method and (v) phenol/chloroform method.

3.13.3.1 NucliSens[®] miniMag[®] Kit

The NucliSens[®] miniMag[®] kit (bioMérieux, France) is based on the use of magnetic silica particles and handles up to 12 samples in parallel in a semi-automated setting. Prior to being extracted with the NucliSens[®] kit, the samples were digested overnight with 500µl proteinase K. The samples were lysed with 500µl of the lysis buffer containing guanidine thiocyanate. The nucleic acids were allowed to bind to a mixture of 50µl magnetic silica particles and the mixture was incubated at room temperature for 10 minutes. These particles were washed with a variety of wash buffers as instructed by the manufacturer (bioMérieux, France). The NucliSens[®] miniMAG[®] platform was used to wash the silica particles. The samples were placed in a thermomixer (Eppendorf, Germany) for 5 minutes at 60°C after 50µl of elution buffer was added. A magnetic rack was used to separate the silica particles from the extracted nucleic acid and the latter was transferred to clean 1.5ml microtubes.

3.13.3.2 QIAamp[®] DNA Mini kit for formalin-fixed paraffin-embedded (FFPE) tissue

The QIAamp[®] DNA Mini kit (Qiagen, Germany) was used according to the manufacturer's instructions. The dewaxed tissue samples were suspended in 180µl ATL buffer and 20µl proteinase K after which they were incubated overnight at 56°C to allow for sufficient digestion. After digestion, 200µl AL buffer was added to each sample and vortexed. Following the vortex step, 200µl of 96% ethanol was added for nucleic acid precipitation. The lysate was transferred to a 2ml QIAamp[®] MinElute[®] and centrifuged at 8000rpm for 1 minute. The lysate was washed with different wash buffers according to instructions by the manufacturer (Qiagen, Germany). The lysate was transferred to clean 1.5ml microtubes in which the nucleic acid was eluted with 60µl of ATE buffer.

3.13.3.3 “Salting-out” Procedure (according to Miller *et al.*, 1988)

The third technique used for nucleic acid extraction from the tissue samples was the “salting out” procedure. The tissue samples in the microtubes were crushed with a mortar and pestle after liquid nitrogen (-196°C) was added to each of the samples. Care was taken to prevent cross-contamination. After the samples were thoroughly crushed in the mortar, 1500µl of cell lysis buffer (CLB) was added and collected in a clean microtube (2.0ml). The tubes were subsequently centrifuged at 3000 rpm for 15 minutes at 4°C where after the supernatant was decanted. The resulting pellet was resuspended in 534µl nuclei lysis buffer (NLB), 60µl sodium dodecyl sulphate (SDS) and 20µl proteinase K. The tubes were incubated overnight at 37°C. When no visible particulate matter was present in the microtubes after digestion, 200µl saturated sodium chloride (NaCl >6M) was added. The tubes were mixed thoroughly by hand using gentle wrist action. Subsequently the tubes were centrifuged at 11,000 rpm for 20 minutes at 4°C. The resulting supernatant was collected in clean microtubes (1.5ml) and

1200µl absolute ethanol was added. The DNA was washed with 500µl 70% ethanol which was subsequently discarded to let the DNA pellet dry out.

3.13.3.4 Genotype DNA Isolation (HAIN®) Kit

Tissue samples were added into correctly labeled microtubes (1.5ml). Briefly, 100µl Lysis Buffer M along with 10µl proteinase K was added. The mixtures were vortexed for a minimum of 10 seconds. The samples were incubated in a thermomixer at 800rpm for 30 minutes at 56°C. The samples were subsequently centrifuged for 2 minutes at maximum speed. The supernatant was then transferred to new microtubes (1.5ml) before 100µl Binding Buffer B6 was added. The lysate was transferred onto a membrane consisting of a spin filter and RTA Receiver Tube. The tubes were centrifuged for 1 minute at 13,000rpm. After the tubes were centrifuged, a total of 300µl Wash Buffer I was added on the membrane and centrifuged for 30 seconds at 13,000rpm. The Receiver Tubes with the filtrates of each of the samples were discarded. A new 2.0 ml RTA Receiver Tube was used and 750µl Wash Buffer II was added. The tubes were subsequently centrifuged for 30 seconds at 13,000rpm after which the filtrates were discarded. The Spin Filter was centrifuged for 2 minutes at 13,000rpm to eliminate ethanol. The Spin Filters were transferred to a labeled 1.5 ml Receiver Tube prior to adding 200µl pre-warmed Elution Buffer onto the membrane of the filter. The samples were incubated at room temperature for 1 minute. DNA elution was achieved by centrifuging for 1 minute at 6000rpm.

3.13.3.5 Phenol/Chloroform Method

The tissue samples were crushed with a mortar and pestle after liquid nitrogen (-196°C) were added to the samples. Caution was taken to prevent cross-contamination. Briefly, 600µl extraction buffer and 50µl lysozyme were added to each of the samples after which they were

incubated form 37°C for 2 hours. A total of 65µl 10x proteinase K and 30µl proteinase K (10mg/µl) were added and incubated overnight at 45°C. A volume of 1ml phenol/chloroform/isoamyl alcohol (25:24:1) was added, inverted and centrifuged for 10 minutes at 10,000 rpm. The top phase was collected and transferred to a microtube containing chloroform/isoamyl alcohol (24:1). The tubes were again centrifuged at 10,000 rpm for 10 minutes. The pH was maintained at 5.2. The top phase was collected and transferred to a microtube containing 1/10 volumes of 3M sodium acetate. The DNA was precipitated using 2/3 volumes of chilled isopropanol. The samples were kept overnight at -70°C. The samples were centrifuged for 10 minutes at 13,000 rpm after which they were washed with 70% chilled ethanol. The resultant pellets were dried and 40µl of H₂O was added prior to incubating at 65°C for 2 hours to dissolve the DNA.

3.13.4 Quantitation of extracted DNA

The purity of the extracted nucleic acids was determined using the:

- a) 260nm/280nm ratio which is indicative of organic matter residues and
- b) 260nm/230nm ratio which indicates residues of organic solvents (Wahlberg *et al.*, 2012).

A spectrophotometer (ND-1000 Spectrophotometer, NanoDrop®) was used to determine the amount of nucleic acids at 260nm.

3.13.5 *Taq* Polymerase Enzymes

Different *Taq* polymerase enzymes were used and tested for their efficiency during the PCR applications. The different *Taq* polymerase enzymes were FastStartTaq (Roche, Switzerland), Hotstartaq (Qiagen, Germany), and TaKaRa *Ex Taq* (TaKaRa, Japan). The Faststart *Taq*

enzyme was shown to be more specific and effective and was used in all of the PCR applications.

3.13.6 Molecular Applications

3.13.6.1 Spoligotyping

Mycobacterial isolates were prepared using the standard international PCR protocol with primers DRa and DRb. Care was taken to prevent cross-contamination. Negative controls were included to ascertain potential amplicon contamination. Positive controls such as H37Rv and Bacille Calmette Guerin (BCG) DNA were included to determine the reproducibility of the spoligotyping.

The DR region was amplified using two primers, DRa and DRb. Each primer consisted of 18 base pairs with the following sequences, DRa: 5'-GGT TTT GGG TCT GAC GAC-3' and DRb: 5'-CCG AGA GGG GAC GGA AAC-3'. The 5'-end of the DRa primer was biotinylated. The PCR conditions were 1 minute at 94°C, followed by 30 cycles of 30 seconds at 94°C, 1 minute at 55°C and 30 seconds at 72°C, after which the samples were exposed to 72°C for 10 minutes.

Briefly, 160µl PCR products were loaded onto a specifically designed membrane and hybridized for 60 minutes at 60°C followed by two post-hybridization washes for 5 minutes each at 60°C. Subsequently, a streptavidin-peroxidase step was done for 60 minutes at 42°C followed by a membrane wash with 250ml 2xSSPE-0.5% SDS for 10 minute twice at 42°C. A final rinse for 5 minutes with 250ml of 2xSSPE at room temperature was done. A chemiluminescent ECL detection liquid (GE Healthcare, United Kingdom) was added prior to exposure to X-ray film. A hyperprocessor (GE Healthcare, United Kingdom) was used to

develop the exposed film. The worldwide database was used to determine the geographical distribution of the isolates.

3.13.6.2 HAIN[®] MTBDRplus[®] DNA Kit (version 2.0)

The HAIN[®] MTBDRplus[®] DNA kit was used to determine mycobacterial resistance to rifampicin and/or isoniazid in the cadaver samples. All 254 samples were subjected to the MTBDRplus[®] assay. The MTBDRplus[®] strip contains 22 probes. This includes 5 hybridization and amplification probes which serve as controls for the test and 17 probes for resistance hybridization. Eight *rpoB* wild-type probes (WT1 to WT8) are included to test for Rifampicin (RIF) resistance. Four more probes MUT1, MUT2A, MUT2B and MUT3 target specific mutations in the *rpoB* gene. To determine Isoniazid (INH) resistance, one wild type probe of the *katG* gene and two probes for specific mutations in this gene, MUT T1 and MUT T2, were used. The promoter region of the *inhA* gene is included in the strip and contains two wild-type probes (WT1 and WT2) and four mutation probes (MUT1, MUT2, MUT3A and MUT3B).

For PCR amplification, two mixtures were supplied by the manufacturer. Briefly, 35µl AM-A mixture, a primer-nucleotide mixture, 10µl of AM-B mixture containing 2.5mM MgCl₂ and 1.25 U hot start Taq polymerase (Qiagen, Germany) and 5µl extracted chromosomal DNA were added to a microtube to make a final volume of 50µl. The PCR conditions were 15 minutes at 95°C, followed by 10 cycles of 30 seconds at 95°C, 2 minutes at 58°C and 30 seconds at 72°C, after which the samples were exposed to 72°C for 10 minutes.

Hybridization was done using a tray containing 12 wells in parallel in the Twincubator (Hain Lifesciences, Germany). The hybridization (HYB) and stringent (STR) buffers were

preheated to 45°C. Briefly, 20µl DEN-blue, a denaturing buffer, was added to 20µl of the amplified samples and was incubated at room temperature for 5 minutes. Afterwards, 1ml of the preheated HYB buffer was added to each of the wells. Correctly labeled DNA test strips were added to the mixtures in the wells and were incubated for 30 minutes at 45°C. Following incubation, the mixtures were completely aspirated and 1ml STR buffer was added to each of the wells. The strips were incubated at 45°C for 15 minutes. Following incubation and aspiration, 1ml of a rinsing (RIN) buffer was added to each strip and incubated at room temperature. Following the rinsing step, 1ml diluted conjugate (CON) buffer (1:12) was added and incubated for 30 minutes. The strips were subsequently rinsed twice with RIN buffer after which 1ml diluted substrate (SUB) buffer (1:12) was added. The strips were incubated at room temperature for approximately 5 minutes or until the banding pattern was clearly observable. The reaction was subsequently stopped by adding distilled water to the strips. An MTBDRplus 2.0 evaluation sheet (Hain Lifesciences, Germany) was used for interpreting the DNA strips.

3.13.6.3 IS6110 PCR Protocol

The IS6110 region is a 1,361 base pair repetitive insertion sequence. The present PCR method amplifies a target sequence consisting of 123 base pairs within IS6110. The sequences of the primers were: Tr-F1: 5'-ACA TCC TAC ACA CGC TC tcg ccc gtc tac ttg gtg-3' and Tr-R1: 5'-CAA GCA GAA GAC GGC ATA CG cac tta cgc acc gtc tcc-3'. The target size is 46 base pairs, while the final product size is 83 base pairs. The PCR conditions were 15 minutes at 95°C, followed by 30 cycles of 1 minute at 94°C, 1 minute at 62°C and 1 minute at 72°C, after which the samples were exposed to 72°C for 10 minutes. The amplicons (amplified products) were visualized using an ethidium-bromide-stained agarose gel.

3.13.6.4 RD105 PCR Protocol

The RD105 region is regarded as one of the four common large sequence polymorphisms (LSP) observed in Beijing genotypes (Tsolaki *et al.*, 2005). This region consists of 3467 base pairs and can be used to distinguish Beijing and non-Beijing genotypes. The primer sequences for the Beijing genotype were: B-F1: 5'-ACA TCC TAC ACA CAC GCT C-3' and B-R2: 5'-CAA GCA GAA GAC GGC ATA CG-3'. The sequences for non-Beijing genotypes are NB-F2: 5'-ACA TCC TAC ACA CAC GCT C-3' and NB-R2: 5'-CAA GCA GAA GAC GGC ATA CG-3'. The PCR conditions were 15 minutes at 95°C, followed by 40 cycles of 30 seconds at 94°C, 30 seconds at 68°C and 45 seconds at 72°C, after which the samples were exposed to 72°C for 10 minutes. Following the 10 minutes, the samples were kept at 4°C while the agarose gel was prepared for loading.

3.13.6.5 Mtub02/RD105 PCR Protocol (According to Tsolaki *et al.*, 2005)

Mycobacterial isolates can be separated into Beijing- and non-Beijing genotypes by combining two different PCRs with primers flanking either the deletion Mtub02Beij or the deletion Mtub02. The sequences of the primers were: Mtub02F: 5'-CGT GCA CAG TTG GGT GTT TA-3' and Mtub02R: 5'-TTC GTT CAG GAA CTC CAA GG-3'. The PCR conditions were 4 minutes at 95°C, followed by 35 cycles of 30 seconds at 94°C, 30 seconds at 60°C and 45 seconds at 72°C, after which the samples were exposed to 72°C for 10 minutes. Following the 10 minutes, the samples were kept at 4°C while the agarose gel was prepared for loading.

3.13.7 Agarose Gel Electrophoresis (AGE)

The PCR products were visualized with the use of an ethidium-bromide stained agarose gel. The 1% agarose gel was prepared by mixing 100g of agarose powder (Merck, Germany) into

100ml prepared 1xTBE solution. The solution was heated until it reached boiling point prior to adding 4 μ l ethidium bromide (Sigma-Aldrich, USA). The solution was poured into a casting tray and combs were placed in the correct positions. The solution was allowed to cool resulting in a malleable gelatin-like block which was placed in an electrophoresis chamber. Briefly, 2 μ l loading dye was mixed with each of the samples prior to loading. A total of 13 μ l samples were loaded into each well of the agarose gel submerged in 1xTBE buffer. Following the loading of samples, an electric current measuring 100mV was applied to the gel. This resulted in the separation of the DNA based on their band size. The agarose gel was viewed and photographed with the *UV Transilluminator 2000 Bio-Rad* and *Kodak[®] Digital Science[®] (ver. 3.0.2.)* software, respectively.

Results

“You cannot separate passion from pathology any more than you can separate a person's spirit from his body.”

Richard Selzer, Letters to a Young Doctor

For the purpose of this study, when a group of photos illustrate a particular systemic pathology, the sequence of the photos will start with the least severe to the most severe pathology observed.

4.1 Pulmonary System

4.1.1 Tuberculosis

4.1.1.1 Prevalence of Tuberculosis in the Study Subjects

The prevalence of pulmonary tuberculosis (TB) was determined in 127 cadavers at the Division of Anatomy and Histology, Department Biomedical Sciences, Stellenbosch University during 2011-2013. The overall prevalence of pulmonary TB in the cadaver cohort was 97/127 (76.4%) (Table 4.1) as determined using gross anatomy dissections, histological examination and molecular biology (*Addendum L*). The average age of the affected cadavers was 47.1 years and the male to female ratio was 1.1:1.

Table 4.1. The prevalence of tuberculosis in the cadaver cohort (n=127)

<i>Sex</i>	<i>Total</i>	<i>Pulmonary Tuberculosis</i>	<i>Prevalence (%)</i>
Female	40	29	72.5
Male	87	68	79.3
TOTAL	127	97	76.4

4.1.1.2 Pulmonary Tuberculosis Lesions

The TB lesions were most commonly observed bilaterally in the apical and/or sub-apical regions (Figures 4.1, 4.3); however the anterior segments of the superior lobes, lingula and middle lobes and sometimes the basal segments of the inferior lobes were also affected. Unilateral TB involvement was seen in 12/73 (16.4%) cadavers.

Typical pulmonary tuberculous lesions observed in the cadavers included:

- Bilateral apical or sub-apical cavities with or without caseous necrosis
- Extensive fibrosis in the cavity wall and adjacent to the cavities

- White-yellowish confluent areas of granulomatous inflammation
- Hilar lymph node involvement
- Tuberculous bronchopneumonia

Depending on the resistance of the host, the cavities sometimes extended into the superior region of the inferior lobe. In more severe cases, extensive destruction of the lung tissue was observed (Figure 4.3). Extensively thickened pleurae and hilar lymphadenopathy were common findings. Tuberculous bronchopneumonia, as a result of caseous debris inhalation into the bronchi, was seen as small, confluent, whitish nodules which resulted in a consolidated appearance (Figure 4.6). A summary of the tuberculous lesions in the pulmonary system of the cadaver population can be seen in Tables 4.2 and 4.3.

Table 4.2. Macroscopical appearance of tuberculosis in the cadaver cohort (n=127)

<i>Cadaver Ref. Nr.</i>	<i>Macroscopic Pulmonary Tuberculosis (PTB) Findings</i>	
	<i>Right Lung</i>	<i>Left Lung</i>
K81/09	Fibrosis with consolidation in superior lobe	Fibrosis with consolidation in superior lobe
K82/09	Tuberculous nodules (calcified) in superior lobe	Tuberculous nodules (calcified) in superior and inferior lobes
K83/09	Whitish nodules and fibrosis in superior lobe	Whitish nodules and fibrosis in superior lobe (Fig. 4.4, C)
K87/09	Tuberculous nodules in both lobes (Fig. 4.4, A)	Tuberculous nodules in both lobes
K89/09	Cavities with caseation in superior lobe	Small, white tuberculous nodules in superior lobe (Fig. 4.4, D)
K95/09	Fibrosis with consolidation in both lobes	Fibrosis with consolidation in superior lobe
K96/09	Large, fibrous cavity with caseation in superior lobe, apical cavities with caseation	TB bronchopneumonia in both lobes with cavitation in the apex
K100/09	Necrotizing cavity in apex	Necrotizing cavities in both lobes with severe disruption of lung tissue (Fig. 4.3, B)
K101/09	Necrotizing cavities with fibrosis in superior lobe	Hemorrhagic TB nodule with blood aspiration in the left inferior lobe
K102/09	Large apical cavities (Fig. 4.3 D)	Large cavity with very little lung tissue in superior lobe; smaller cavities in posterior aspects of inferior lobe
K104/09	Small cavities adjacent to fibrous scars in superior lobe	Large necrotizing cavity in superior lobe
K106/09	Tuberculous necrosis in apex	Tuberculous necrosis in apex
K110/09	Tuberculous granulomas in apical region, necrosis	Necrotizing TB cavities in both lobes with fibrous cavities in the anterior aspects of inferior lobe
K112/09	*	Necrotizing TB cavities with pleural adhesions in inferior part of superior lobe
K113/09	TB bronchopneumonia in apex	TB bronchopneumonia in inferior lobe and posterior inferior aspect of superior lobe
K115/09	Small cavitation in superior lobe	Small cavitation in superior lobe

<i>Cadaver Ref. Nr.</i>	<i>Macroscopical Pulmonary Tuberculosis (PTB) Findings</i>	
	<i>Right Lung</i>	<i>Left Lung</i>
K01/10	Cavities in superior lobe; consolidation in the antero-medial aspect of the inferior lobe	The left lung was massively destructed with a thickened pleura (Fig. 4.3, A)
K02/10	Large cavity in the apex	*
K03/10	Consolidated appearance in apex; two smaller cavities in inferior lobe	Superior lobe showed a very large necrotizing cavity; consolidated appearance in inferior lobe
K04/10	*	One large cavity with caseation in apex with an extensively thickened pleura
K06/10	Large cavity surrounded by emphysematous lung in superior lobe	Superior lobe contains a consolidated area consistent with TB bronchopneumonia
K10/10	Entire lung appears consolidated – TB bronchopneumonia	Entire lung appears consolidated – TB bronchopneumonia; extensive cavitation with caseation in superior lobe
K12/10	Large cavity with extensive necrosis in superior lobe; inferior lobe appears consolidated – TB bronchopneumonia	Cavities were present in apex; in the central area of the inferior lobe, consolidation consistent with TB bronchopneumonia is present
K13/10	Consolidated appearance (TB bronchopneumonia) in superior lobe	Consolidated appearance (TB bronchopneumonia) in superior lobe
K16/10	Superior lobe had a consolidated appearance (TB bronchopneumonia), apical cavities with caseation	Superior lobe had a consolidated appearance (TB bronchopneumonia)
K18/10	Superior lobe had a large central cavity with caseation	Entire superior lobe and superior part of inferior lobe was destroyed by tuberculous cavitation; inferior lobe had a consolidated appearance
K19/10	Fibrosis with consolidation in both lobes	Fibrosis with consolidation in superior lobe
K30/10	Nodular appearance in inferior lobe (Fig. 4.4, B)	Small calcified nodules in superior lobe
K38/10	Fibrosis with consolidation in superior lobe	Fibrosis with consolidation in superior lobe
K40/10	Necrotizing cavities in both lobes with consolidation – TB bronchopneumonia	Small lesion present on periphery of superior lobe – Ghon focus
K42/10	Large, central necrotizing cavity in superior lobe and superior part of inferior lobe; consolidation – TB bronchopneumonia	*
K45/10	Large, fibrous cavity present in superior lobe; superior aspect of inferior lobe contains necrotizing cavities (Fig. 4.3, C)	Large cavity with prominent pleural adhesions in apex; necrotizing TB nodules in superior and inferior lobes
K05/11	Consolidated appearance in both lobes	Antimortem pneumonectomy
K13/11	Cavitation in apical region with caseating necrosis, consolidated appearance in postero-lateral region of inferior lobe	Small cavities in superior lobe with caseating necrosis, consolidation in antero-medial part of superior lobe, small cavity in the inferior region of inferior lobe
K15/11	Fibrosis with consolidation in both lobes	Fibrosis with consolidation in both lobes
K31/11	Extensive cavitation in superior lobe with caseation	Small cavity in apical region
K41/11	Small, tuberculous nodules in apical region, cavitation with caseation in superior lobe, atelectasis	*
K46/11	Cavitation with tuberculous nodules and caseating necrosis in superior lobe	Extensive cavitation with caseating necrosis affecting entire lung. Large exudate present
K47/11	Fibrotic lesions in superior lobe, with a consolidated appearance in inferior lobe – TB bronchopneumonia	Cavities in apical region, with fibrosis in both lobes
K52/11	Cavity with caseating necrosis in apical region and fibrosis, cavitation in inferior lobe	Cavities of varying sizes in both lobes, caseation was seen, nodular appearance
K53/11	Fibrotic lesions in superior lobe, with a consolidated appearance in inferior lobe – TB bronchopneumonia	Fibrosis with consolidation in both lobes

<i>Cadaver Ref. Nr.</i>	<i>Macroscopical Pulmonary Tuberculosis (PTB) Findings</i>	
	<i>Right Lung</i>	<i>Left Lung</i>
K55/11	Fibrosis with consolidation in both lobes - TB bronchopneumonia	Fibrotic lesions in superior lobe, with a consolidated appearance in inferior lobe
K59/11	Several cavities throughout the entire lung, caseating necrosis was observed	Consolidation in superior lobe with small cavities
K62/11	Extensive tuberculous nodules in superior lobe	Tuberculous nodules in both lobes with caseating necrosis
K64/11	Tuberculous nodules in apical region, caseating necrosis	Consolidated appearance with focal caseation in superior lobe and diffuse caseating in inferior lobe
K65/11	Fibrosis with consolidation in both lobes	Superior lobe had a consolidated appearance (TB bronchopneumonia)
K69/11	Fibrosis with consolidation in both lobes	Fibrosis with consolidation in both lobes
K70/11	Extensive cavitation in superior lobe	Extensive cavitation in superior lobe with caseating necrosis
K75/11	Cavities in inferior part of superior lobe and superior part of inferior lobe	Small cavity in apical region, area of consolidation in superior lobe
K80/11	*	Tuberculous granuloma in postero-lateral region of inferior part of inferior lobe
K82/11	Tuberculous nodules in apical region	Tuberculous nodules in both lobes
K101/11	Cavities of various sizes in superior lobe associated with consolidation – TB bronchopneumonia	Cavitation in superior lobe
K116/11	Extensive cavitation with caseating necrosis in entire lung, consolidation in superior lobe	Cavitation in superior lobe and inferior lobe
K119/11	Granulomas distributed through entire lung	Granulomas distributed through entire lung
K120/11	Fibrosis with consolidation in both lobes	Fibrotic lesions in superior lobe, with a consolidated appearance in inferior lobe – TB bronchopneumonia
K121/11	Extensive cavitation in apex and inferior lobe, caseating necrosis is seen with tuberculous nodules throughout lung	Caseating necrosis in apical region, extensive cavitation, nodular appearance (tuberculous nodules)
K124/11	*	Consolidated appearance in apex – TB bronchopneumonia, similar appearance in superior part of inferior lobe
K125/11	*	Cavitation with caseation in superior lobe
K126/11	Two tuberculous nodules with caseating necrosis in superior lobe	Cavitation with caseation in apical region; extensive cavitation in inferior lobe, nodular appearance
K129/11	*	Consolidated appearance in the inferior lobe
K138/11	Extensive cavitation in apical region, smaller cavities in rest of superior lobe	Extensive cavitation in superior lobe as well as superior aspect of inferior lobe
K140/11	Cavities in apical region and inferior lobe (surrounded by a consolidated appearance)	Cavities in apical region, consolidation in inferior lobe
K148/11	Cavitation and caseation with accompanying fibrosis in superior lobe, smaller nodules in inferior lobe	Tuberculous nodules in inferior lobe
K25/12	Extensive cavitation in entire superior lobe	Two cavities in apex; four small nodules in superior aspect of inferior lobe
K26/12	Nodules in superior lobe with consolidation	Antero-medial aspect of superior lobe and lingual
K27/12	Six cavities with caseating necrosis in apex; seven small nodules on inferior antero-lateral aspect	Five cavities in superior part of superior lobe; two cavities in superior part of inferior lobe (caseating necrosis)
K28/12	Fibrosis with consolidation in both lobes	Fibrotic lesions in superior lobe, with a consolidated appearance in inferior lobe – TB bronchopneumonia
K42/12	Consolidated appearance extending through lung – TB bronchopneumonia	Consolidated appearance extending through lung – TB bronchopneumonia

<i>Cadaver Ref. Nr.</i>	<i>Macroscopical Pulmonary Tuberculosis (PTB) Findings</i>	
	<i>Right Lung</i>	<i>Left Lung</i>
K43/12	Extensive cavitation in superior lobe with caseating necrosis and consolidation; inferior lobe appears consolidated (Fig. 4.6, B)	Extensive cavitation in apex with consolidation and calcification; four cavities with caseation in inferior lobe (Fig. 4.6, A)
K46/12	Consolidated appearance extending through lung – TB bronchopneumonia	Fibrosis with consolidation in both lobes
K49/12	Small cavity in apex with extensive fibrosis	Small cavity in superior part of inferior lobe
K50/12	Small cavities with extensive fibrosis in apex	Small cavity in apex
K51/12	Caseating necrosis in apex; five smaller cavities in base of lung	Large cavity in apex on antero-medial aspect
K52/12	Four cavities in superior lobe; five smaller cavities with surrounding consolidation in base of lung	*
K57/12	Fibrosis with consolidation in both lobes	Fibrosis with consolidation in both lobes
K60/12	Two cavities with caseating necrosis and surrounding consolidation in superior part	One large cavity with caseation on antero-medial aspect; small nodules on peripheral part of superior part of inferior lobe
K61/12	Three cavities (without caseation) and fibrosis in superior lobe	*
K64/12	One small cavity with caseation in apex; small cavity with caseation on postero-lateral aspect of inferior lobe	One large cavity with caseation, has a hemorrhagic appearance
K66/12	Two cavities with caseation in superior lobe; caseating cavity in superior aspect of inferior lobe – consolidation is prominent (TB bronchopneumonia)	Three cavities with caseation in superior lobe with caseation; one cavity with caseation in superior part of inferior lobe – consolidation is prominent (TB bronchopneumonia)
K69/12	Four cavities with caseation in superior lobe	Consolidation in superior part of inferior lobe
K73/12	Five cavities surrounded by extensive emphysema; small area of consolidation in superior part of inferior lobe	Nine cavities (three cavities with caseation) in superior lobe; large cavity with caseation on postero-lateral aspect
K74/12	Superior lobe has a miliary appearance with one large necrotic cavity	Three cavities with caseation and surrounding consolidation in superior lobe
K75/12	Consolidation in lower 2/3 rd of superior lobe	Consolidation in superior part of inferior lobe
K76/12	Fibrotic lesions in superior lobe, with a consolidated appearance in inferior lobe – TB bronchopneumonia	Fibrotic lesions in superior lobe, with a consolidated appearance in inferior lobe – TB bronchopneumonia
K77/12	Consolidation in the lower 2/3 rd of superior lobe with five cavities with caseation (Fig. 4.5)	Entire superior lobe is necrotic
K78/12	Consolidated appearance extending through lung – TB bronchopneumonia	Consolidated appearance extending through lung – TB bronchopneumonia
K81/12	One large cavity in superior lobe with surrounding consolidation	One large cavity with necrosis in superior lobe with surrounding consolidation; two smaller cavities in superior part of inferior lobe with a large surrounding area of consolidation
K82/12	Fibrotic lesions in superior lobe, with a consolidated appearance in inferior lobe – TB bronchopneumonia	Fibrosis with consolidation in both lobes
K87/12	Consolidated appearance extending through lung – TB bronchopneumonia	Fibrosis with consolidation in superior lobe
K97/12	Fibrosis with consolidation in both lobes	*
K98/12	Consolidated appearance extending through lung – TB bronchopneumonia	Consolidated appearance extending through lung – TB bronchopneumonia
K99/12	Small granulomas in inferior part of superior lobe	Small granulomas in superior lobe
K100/12	Fibrosis with consolidation in both lobes	Fibrosis with consolidation in both lobes
K101/12	Several cavities with caseation in superior lobe; several necrotic cavities in inferior lobe	*
K106/12	Nodular appearance through entire lung; area of calcification in base of lung	Nodular appearance through entire lung

<i>Cadaver Ref. Nr.</i>	<i>Macroscopical Pulmonary Tuberculosis (PTB) Findings</i>	
	<i>Right Lung</i>	<i>Left Lung</i>
K107/12	Fibrosis with consolidation in both lobes	Fibrotic lesions in superior lobe, with a consolidated appearance in inferior lobe – TB bronchopneumonia
K124/12	Consolidated appearance extending through lung – TB bronchopneumonia	Consolidated appearance extending through lung – TB bronchopneumonia

* Typical granulomatous pattern suggestive of TB was absent

4.1.1.3 Distribution of Pulmonary TB Lesions

For the purpose of this study, the right middle lobe was included in the right superior lobe. The distribution of the tuberculous inflammation was noted in the different lobes of the pulmonary system. The right superior lobe was involved in 60/127 (47.2%) of the cases, while the left superior lobe was involved in 58/127 (45.7%) (Figure 4.1, D). The right and left inferior lobes were involved in 28/127 (22.0%) and 36/127 (28.3%), respectively (Figure 4.1, D).

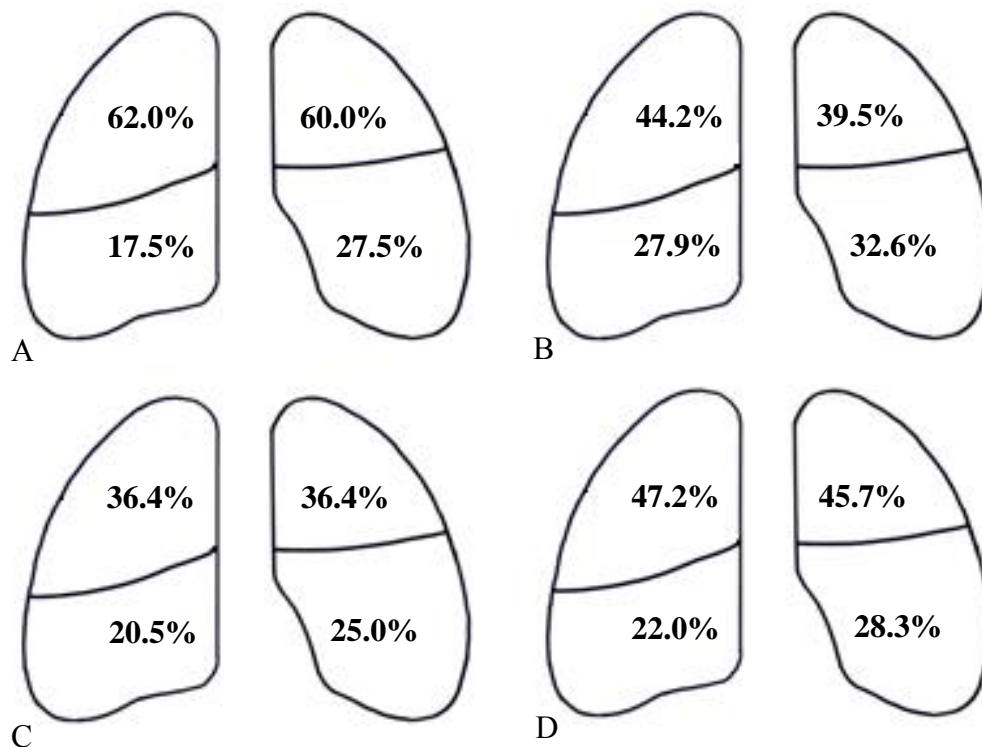


Figure 4.1. Overall distribution of pulmonary TB lesions in the cadaver cohort. A) 2011 cohort; B) 2012 cohort; C) 2013 cohort and D) total distribution over the three years. For the purpose of the schematic diagram, the right middle lobe was included in the right superior lobe.

4.1.1.4 Distribution of Pulmonary TB Bronchopneumonia

For the purpose of this study, the right middle lobe was included in the right superior lobe. Tuberculous bronchopneumonia was observed in the right superior and left superior lobes of 29/127 (22.8%) cadavers and 15/127 (11.8%) cadavers, respectively (Figure 4.2, D). The right and left inferior lobes were involved in 12/127 (9.4%) cadavers and 12/127 (9.4%) cadavers, respectively (Figure 4.2, D).



Figure 4.2. Overall distribution of TB bronchopneumonia in the cadaver cohort. A) 2011 cohort; B) 2012 cohort; C) 2013 cohort and D) total distribution over the three years. For the purpose of the schematic diagram, the right middle lobe was included in the right superior lobe.

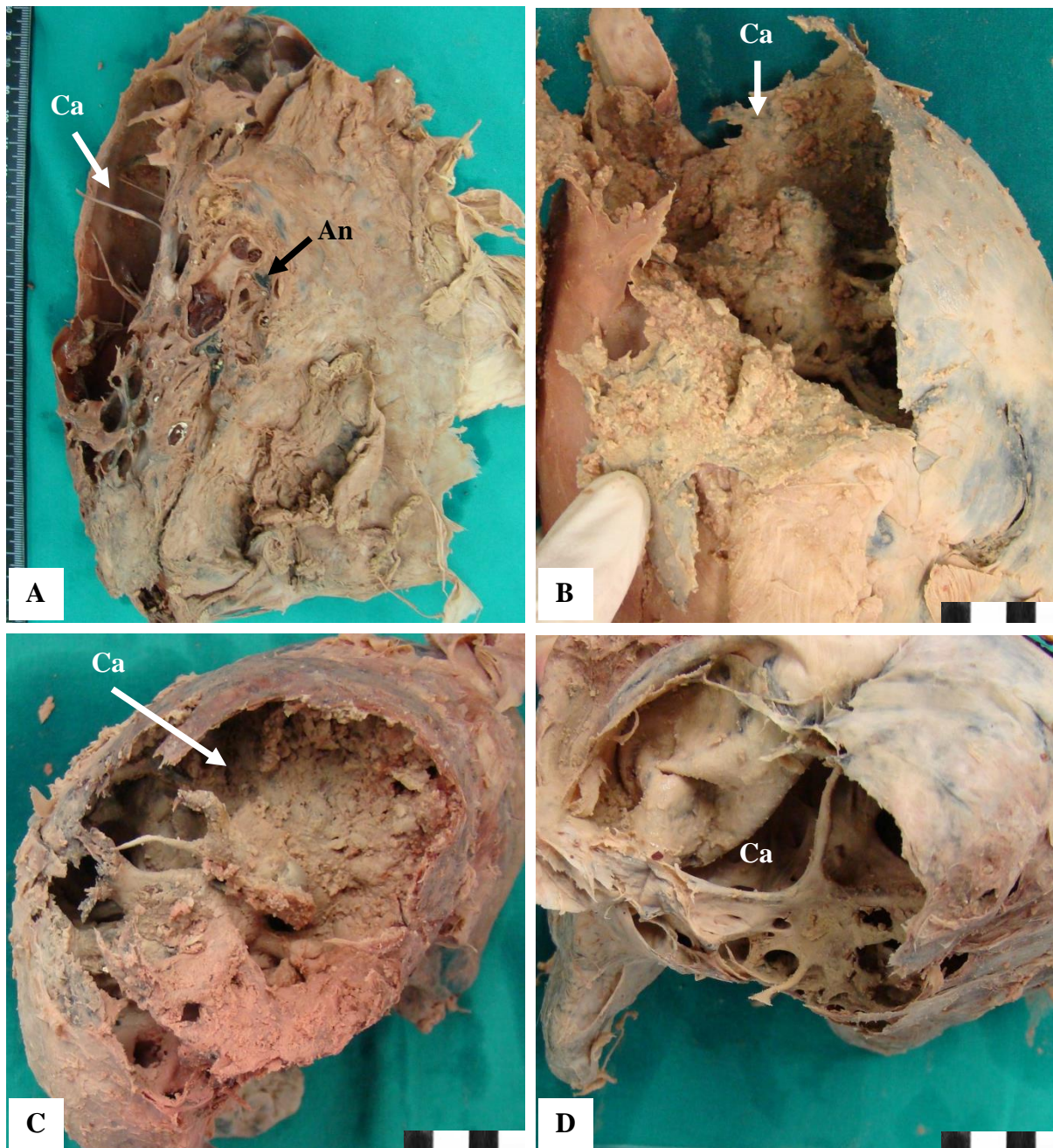


Figure 4.3. Macroscopical appearance of superior lobe cavities in the pulmonary system. A) extensive cavitation in the superior lobe of the left lung of cadaver K01/10, postero-medial view; B) cavitation in the superior lobe of the left lung of cadaver K100/09, antero-lateral view; C) cavitation in the superior lobe of the right lung of cadaver K45/10, superior view; D) cavitation of the superior lobe of the right lung of cadaver K102/09, superior view; anthracotic lymph node (An), cavity (Ca).

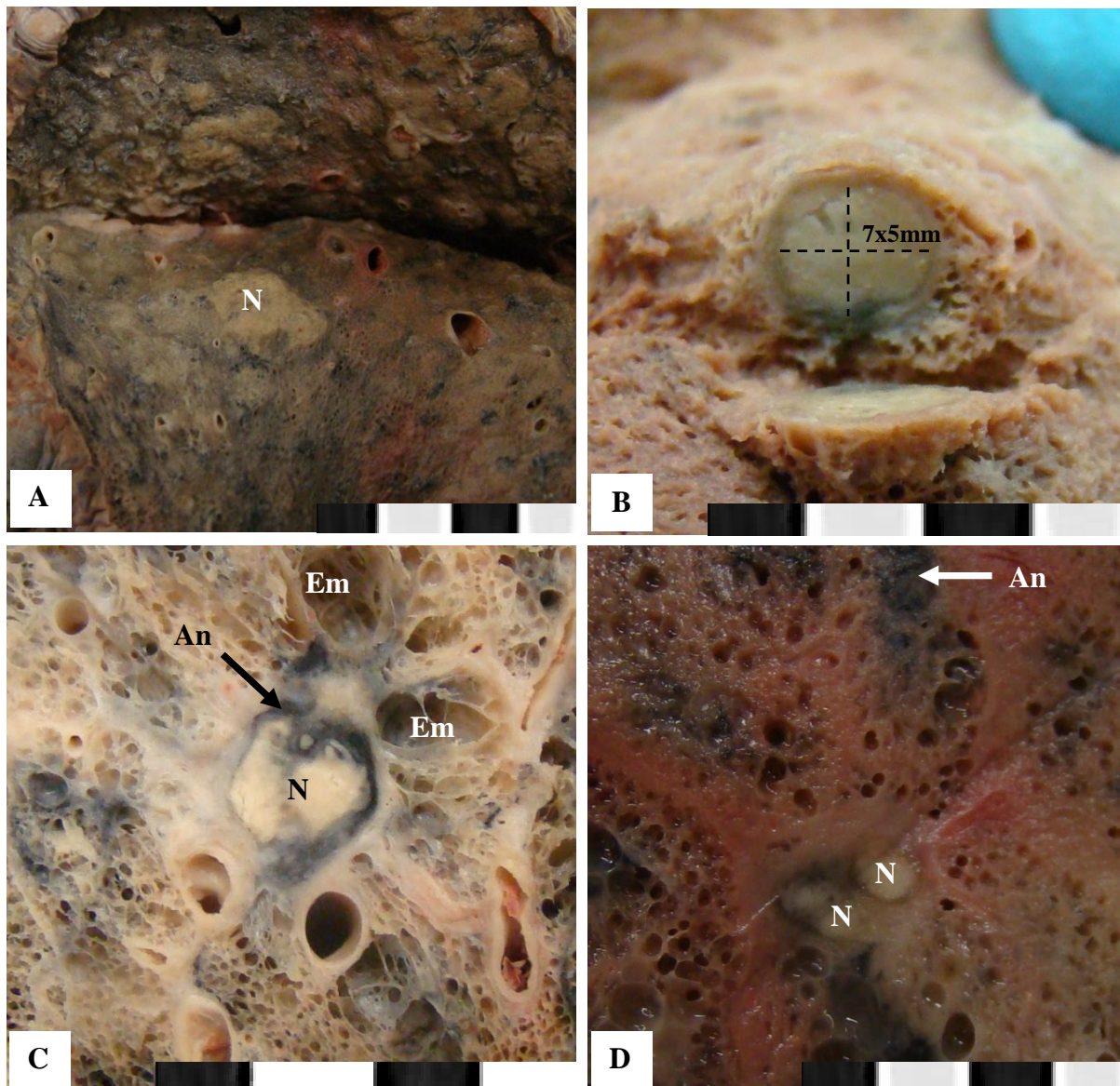


Figure 4.4. Macroscopic appearance of granulomatous inflammation in the pulmonary system. A) confluent necrotizing granulomatous inflammation in the right superior lobe of cadaver K87/09; B) nodule measuring 7x8mm in the superior left lobe of cadaver K30/10; C) small TB nodule in the apical region of the left lobe of cadaver K83/09; D) small tuberculous nodules measuring approximately 7x5mm in the left lung of cadaver K89/09; anthracosis (An), emphysema (Em), nodule (N).



Figure 4.5. Macroscopic appearance of caseous necrosis. Extensive caseating necrosis in a cavity in the right superior lobe of cadaver K77/12; cavity (Ca).

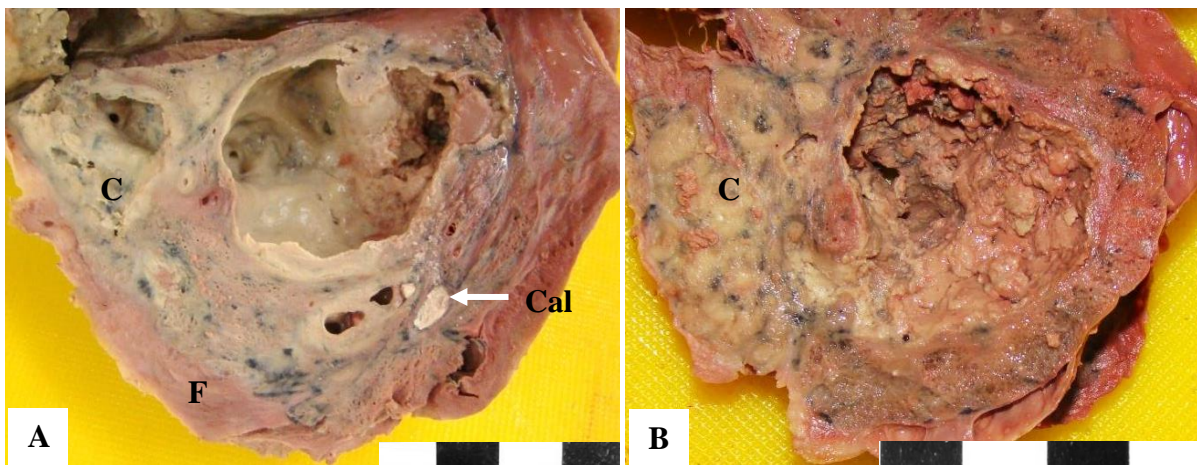


Figure 4.6. Macroscopic appearance of tuberculous bronchopneumonia. A) yellow-whitish consolidation with adjacent cavities in the left apex of cadaver K43/12; B) tuberculous consolidation surrounding a cavity in the apex of the right lung of cadaver K43/12; calcification (Cal), consolidation (C), fibrosis (F).

4.1.1.5 Histopathology of Pulmonary TB

The typical histological appearance of a granulomatous lesion seen in all cadavers was a characteristic central area of caseation (necrosis) surrounded by a rim of palisaded activated “epithelioid” macrophages, scattered lymphocytes with plasma cells and collagen fibrils (Figure 4.7). Large cells with multiple peripheral nuclei arranged in a horseshoe pattern (Langhans’ giant cells) were observed on the H&E sections. Both the Langhans’ cell and epithelioid cells were derived from macrophages. A variable degree of fibrosis was observed

in the areas adjacent to the granulomas (Figure 4.7). The caseated areas healed completely by calcification in 2/127 (1.6%) cadavers. The microscopic picture of the tuberculous cavities had the same wall structure in all the cadavers depending on the host's immune response. Polymorphonuclear leukocytes were often seen in the lining of the cavity. Usually a nonspecific pneumonia with blood vessel involvement accompanied the tuberculous granuloma.

A wide spectrum of tuberculous lesions was seen in the cadaver population, ranging from “hard” paucibacillary granulomas with non-caseating centers to necrotic multibacillary granulomas with few epithelioid macrophages at the edges of the granuloma.

Acid-fast bacilli were most easily found in the walls of the cavities or in the central necrotic debris (Figure 4.9). The ZN stain demonstrated acid-fast bacilli in 34/97 (35.1%) of the cadavers (Table 4.3).

Table 4.3. Microscopy and Ziehl-Neelsen (ZN) results in the cadaver cohort (n=127)

<i>Cadaver Ref. Nr.</i>	<i>Microscopical Pulmonary Tuberculosis (PTB) Findings in the Cadaver Cohort (n=127)</i>		<i>ZN Results</i>
	<i>Right Lung</i>	<i>Left Lung</i>	
K81/09	Chronic (and acute) inflammatory cells, predominantly lymphocytes, fibrosis in parenchyma	Chronic (and acute) inflammatory cells, predominantly lymphocytes, fibrosis in parenchyma	-
K82/09	Fibrotic (inactive) granuloma, prominent fibrosis in parenchyma	*	-
K83/09	Granuloma, chronic inflammatory cells, necrosis, multinucleated giant cells, fibrotic (inactive) granuloma (Fig. 4.8, A)	*	-
K87/09	Fibrotic (inactive) granuloma, prominent fibrosis in parenchyma	Granulomas, necrosis, chronic inflammatory cells, fibrosis	+
K89/09	Granuloma, necrotic, multinucleated giant cells (Fig. 4.7, C; Fig. 4.8, B)	Granulomas of variable sizes, some necrotic, some fibrotic (inactive), multinucleated giant cells (Fig. 4.7, A)	-
K95/09	Consolidation with mixture of chronic and acute inflammatory cells – TB bronchopneumonia	Consolidation with mixture of chronic and acute inflammatory cells – TB bronchopneumonia	-
K96/09	Fibrosis, granulomas, chronic inflammatory infiltrate (Figure 4.9)	Thickened pleura, granulomas, necrosis, chronic inflammatory infiltrate	+
K100/09	Necrotic granulomas, chronic inflammatory infiltrate	Cavity, fibrosis, thickened pleura, multinucleated giant cells, granulomas	+

<i>Cadaver Ref. Nr.</i>	<i>Microscopical Pulmonary Tuberculosis (PTB) Findings in the Cadaver Cohort (n=127)</i>		<i>ZN Results</i>
	<i>Right Lung</i>	<i>Left Lung</i>	
K101/09	Massive, necrotic granulomas, fibrosis, thickened pleura, lymphocytes	Thickened pleura, necrosis, granulomas, hemorrhage in cavity	+
K102/09	Acute and chronic inflammatory cells, cavities, fibrosis – TB bronchopneumonia	Focal areas of chronic inflammatory cells, granulomas, fibrosis, necrosis	-
K104/09	Extensive fibrosis, several granulomas, chronic inflammatory cells, necrosis	Granulomas in parenchyma and pleura, cavities, fibrosis, necrosis, lymphocytes	+
K106/09	Extensive fibrosis, granulomas, chronic inflammatory cells	Extensive fibrosis, granulomas, chronic inflammatory cells	-
K110/09	Granulomas of variable sizes, necrosis, fibrosis	Several granulomas, necrosis, large cavities	+
K112/09	*	Large granulomas, fibrosis, chronic inflammatory cells, necrosis	+
K113/09	Large granuloma, thickened pleura, fibrosis, necrosis, chronic inflammatory cells	*	+
K115/09	Granulomas of variable sizes, necrosis, fibrosis, lymphocytes (Fig. 4.8, D)	*	+
K01/10	Several cavities, granulomas, thickened pleura	Epithelioid macrophages, extensive fibrosis, multinucleated giant cells	-
K02/10	Thickened pleura, few granulomas scattered in parenchyma, fibrosis	Thickened pleura, few granulomas scattered in parenchyma, fibrosis	-
K03/10	Granulomas, epithelioid macrophages, necrosis, chronic inflammatory cells	Chronic (and acute) inflammatory cells, necrosis, fibrosis	-
K04/10	*	Chronic inflammatory cells, fibrosis, granulomas, thickened pleura	-
K06/10	Granulomas, fibrosis, chronic inflammatory cells	Several granulomas, necrosis, chronic inflammatory infiltrate	+
K10/10	Granulomas with fibrosis, large cavity, lymphocytes (Fig. 4.8, E)	Large, granulomatous lesion, chronic inflammatory cells	+
K12/10	Granulomas, thickened pleura, fibrosis	Chronic (and acute) inflammatory cells, necrosis, fibrosis	-
K13/10	Chronic inflammatory cells (lymphocytes) present, granulomas	*	-
K16/10	Necrosis, fibrosis, chronic inflammatory cells	Granulomatous inflammation with chronic inflammatory cells, fibrosis	+
K18/10	Granulomas, necrosis, fibrosis, chronic inflammatory cellular infiltrate	Fibrotic (inactive) granuloma, prominent fibrosis in parenchyma	+
K19/10	Chronic (and acute) inflammatory cells, necrosis, fibrosis – TB Bronchopneumonia	*	-
K30/10	Multinucleated giant cells, granuloma, fibrosis	Ill-circumscribed granulomas, fibrosis, chronic inflammatory cells	+
K38/10	*	Granulomas, fibrosis, chronic inflammation	+
K40/10	Lymphocytes, granulomas, necrosis, multinucleated giant cells, fibrosis	Lymphocytes, granulomas, necrosis, multinucleated giant cells, fibrosis	+
K42/10	Granulomas, necrosis, fibrosis, multinucleated giant cells, thickened pleura	Fibrotic (inactive) granuloma, prominent fibrosis in parenchyma	+
K45/10	Granuloma, necrosis, epithelioid macrophages, fibrosis, lymphocytes	Several granulomas, chronic inflammation, fibrosis, necrosis	+
K05/11	Granulomas, chronic inflammatory cells	*	-
K13/11	Necrosis, granulomas, fibrosis, lymphocytic infiltrate	*	-
K15/11	Chronic inflammatory infiltrate, fibrosis, cavities, LIP	Chronic inflammatory infiltrate, fibrosis, cavities, LIP	-
K31/11	Cavities, fibrosis, lymphocytes	Granulomas, chronic inflammatory cells	-
K41/11	Several granulomas, fibrosis, necrosis, chronic inflammatory infiltrate (Fig. 4.7, D; Fig. 4.8, F)	*	-

<i>Cadaver Ref. Nr.</i>	<i>Microscopical Pulmonary Tuberculosis (PTB) Findings in the Cadaver Cohort (n=127)</i>		<i>ZN Results</i>
	<i>Right Lung</i>	<i>Left Lung</i>	
K46/11	Several granulomas with caseating necrosis and chronic inflammatory cells, fibrosis	Necrosis, granulomas, lymphocytes, fibrosis	+
K47/11	Granuloma with caseating necrosis, fibrosis, lymphocytes (Fig. 4.7, B)	Granuloma, extensive fibrosis, lymphocytes	-
K52/11	Necrosis, granulomas, multinucleated giant cells, fibrosis, chronic inflammatory cells	Necrosis, granulomas, fibrosis, multinucleated giant cells, chronic inflammatory cells	+
K53/11	Several granulomas with caseating necrosis and chronic inflammatory cells, fibrosis	Necrosis, granulomas, fibrosis, lymphocytic infiltrate	-
K55/11	Necrosis, granulomas, fibrosis, lymphocytic infiltrate	Necrosis, granulomas, fibrosis, lymphocytic infiltrate	+
K59/11	Fibrosis, chronic inflammatory cells, granulomas, necrosis	*	-
K62/11	Necrosis, granulomas, fibrosis, lymphocytic infiltrate	Necrosis, granulomas, fibrosis, lymphocytic infiltrate	+
K64/11	Necrotic granuloma, multinucleated cells, fibrosis, lymphocytes (Fig. 4.8, C)	Granuloma, necrosis, fibrosis, lymphocytes	-
K65/11	Granulomas, fibrosis, lymphocytes, thickened pleura	*	-
K69/11	Cavities, mixture of chronic and acute inflammatory cells, predominantly lymphocytes – TB bronchopneumonia	*	-
K70/11	Fibrotic (inactive) granuloma, prominent fibrosis in parenchyma	*	-
K75/11	Granulomas, multinucleated giant cells, fibrosis, chronic inflammatory cells	*	-
K80/11	Fibrotic (inactive) granuloma, prominent fibrosis in parenchyma	Fibrotic (inactive) granuloma, prominent fibrosis in parenchyma	-
K82/11	Granulomas, fibrosis, necrosis, scattering of chronic inflammatory cells	Necrosis, granulomas, lymphocytes, fibrosis	-
K101/11	Extensive fibrosis, lymphocytes, cavities	Fibrosis, foci of chronic inflammatory cells, particularly lymphocytes	-
K116/11	Granulomas, multinucleated giant cells, necrosis, fibrosis, bronchiectasis, chronic inflammatory cells	Fibrosis, necrotic granulomas, bronchiectasis, chronic inflammatory cells	-
K119/11	Necrosis, granulomas, multinucleated giant cells, fibrosis, lymphocytes	Multinucleated giant cells, granulomas, necrosis, fibrosis, lymphocytes	-
K120/11	Fibrotic (inactive) granuloma, prominent fibrosis in parenchyma	Fibrotic (inactive) granuloma, prominent fibrosis in parenchyma	-
K121/11	Fibrosis, pleural thickening, necrosis, granulomas, chronic inflammatory cells	Granuloma, necrosis, fibrosis, chronic inflammatory cells	+
K124/11	Granuloma, lymphocytes, fibrosis, calcifications	Large granulomas, lymphocytes, fibrosis, calcifications	-
K125/11	Cavities, fibrosis, lymphocytes	Cavities, fibrosis, lymphocytes	-
K126/11	Lymphocytes, ill-circumscribed granulomas, fibrosis	*	+
K129/11	*	Several granulomas, fibrosis, multinucleated giant cells, chronic inflammatory cells	-
K138/11	Several granulomas, thickened pleura, fibrosis, chronic inflammatory cells	Granulomas, extensive fibrosis, no necrosis	+
K140/11	Granulomas, fibrosis, necrosis, scattering of chronic inflammatory cells	Granulomas, fibrosis, necrosis, chronic inflammatory cells	+
K148/11	Necrosis, granulomas, lymphocytes, fibrosis	Necrosis, granulomas, lymphocytes, fibrosis	-
K25/12	Fibrosis, lymphocytes, thickened pleura, bronchiectasis, granulomas	Fibrosis, lymphocytes, thickened pleura, bronchiectasis, granulomas	-

<i>Cadaver Ref. Nr.</i>	<i>Microscopical Pulmonary Tuberculosis (PTB) Findings in the Cadaver Cohort (n=127)</i>	<i>ZN Results</i>	
	<i>Right Lung</i>	<i>Left Lung</i>	
K26/12	Necrosis, chronic inflammatory cells, granulomas, multinucleated giant cells, bronchiectasis	Necrosis, granulomas, chronic inflammatory infiltrate	-
K27/12	Fibrotic granulomas, no caseation, multinucleated giant cells, cavity, bronchiectasis	Fibrotic granulomas, necrosis, bronchiectasis, fibrosis, mixture of acute and chronic inflammatory cells	-
K28/12	Fibrosis, lymphocytes, thickened pleura, bronchiectasis – TB bronchopneumonia	Fibrosis, lymphocytes, thickened pleura, bronchiectasis – TB bronchopneumonia	-
K42/12	Necrosis, granulomas, foci of TB bronchopneumonia, chronic inflammatory infiltrate	Granulomas, TB bronchopneumonia	-
K43/12	Large, necrotic granuloma, several smaller granulomas, multinucleated giant cells, necrosis and fibrosis	Caseating necrosis, several granulomas, multinucleated giant cells, fibrosis	-
K46/12	Fibrosis, chronic inflammatory cells, bronchiectasis – TB bronchopneumonia	Fibrosis, chronic inflammatory cells, bronchiectasis – TB bronchopneumonia	-
K49/12	Fibrosis, chronic inflammatory cells – TB bronchopneumonia	Fibrosis, chronic inflammatory cells, bronchiectasis – TB bronchopneumonia	-
K50/12	*	Chronic inflammatory cells, extensive fibrosis, thickened pleura	+
K51/12	Inactive, fibrotic granuloma, chronic inflammatory cells, bronchiectasis, fibrosis	Bronchiectasis, fibrosis, cavity	+
K52/12	Necrosis, fibrosis, chronic inflammatory cells, particularly lymphocytes	Necrosis, fibrosis, chronic inflammatory cells, particularly lymphocytes	-
K57/12	Bronchiectasis, thickened pleura, cavities, fibrosis	Bronchiectasis, thickened pleura, cavities, fibrosis	-
K60/12	Necrosis, several granulomas, fibrosis, chronic inflammatory cells	Granulomas, necrosis, fibrosis, chronic inflammatory cells	-
K61/12	Granulomas, fibrosis, necrosis, multinucleated giant cells,	Extensive fibrosis	-
K64/12	Mixture of chronic and acute inflammatory cells, fibrosis – TB bronchopneumonia	*	-
K66/12	Granulomas, fibrosis, chronic inflammatory cells, necrosis	Granulomas, necrosis, cavity, fibrosis, lymphocytes	+
K69/12	Granulomas, fibrosis, necrosis,	Granulomas, fibrosis, necrosis,	-
K73/12	Chronic inflammation, cavity, necrosis, fibrosis, multinucleated giant cells	Chronic inflammation, cavity, necrosis, fibrosis, multinucleated giant cells	+
K74/12	Several granulomas, necrosis, fibrosis, lymphocytes	Several granulomas, necrosis fibrosis, lymphocytes	+
K75/12	Chronic inflammation, necrosis, fibrosis	Granulomas, necrosis, fibrosis, chronic inflammatory cells	-
K76/12	Fibrosis, cavity, little functional parenchyma, foci of lymphocytes	Fibrosis, little functional parenchyma, foci of lymphocytes	+
K77/12	Necrosis, fibrosis, chronic inflammatory cells, particularly lymphocytes	Fibrosis, foci of chronic inflammatory infiltrate, cavities	+
K78/12	Fibrosis, foci of chronic inflammatory infiltrate, cavities	Granulomas, necrosis, fibrosis, chronic inflammatory cells	-
K81/12	Granulomas, necrosis, fibrosis, chronic inflammatory cells	*	+
K82/12	Necrosis, fibrosis, chronic inflammatory cells, particularly lymphocytes	Fibrosis, foci of chronic inflammatory infiltrate, cavities	-
K87/12	Fibrosis, foci of chronic inflammatory infiltrate, cavities	Fibrosis, foci of chronic inflammatory infiltrate, cavities	-
K97/12	Fibrosis, foci of chronic (and acute) inflammatory infiltrates – TB bronchopneumonia	Fibrosis, foci of lymphocytic inflammatory infiltrates – TB bronchopneumonia	-
K98/12	Fibrosis, foci of chronic inflammatory infiltrate, particularly lymphocytes	Fibrosis, foci of chronic inflammatory infiltrate, particularly lymphocytes	-

<i>Cadaver Ref. Nr.</i>	<i>Microscopical Pulmonary Tuberculosis (PTB) Findings in the Cadaver Cohort (n=127)</i>	<i>ZN Results</i>	
	<i>Right Lung</i>	<i>Left Lung</i>	
K99/12	Granulomas, fibrosis, lymphocytes	Granulomas, multinucleated giant cells, fibrosis, necrosis, lymphocytes	-
K100/12	Fibrosis, foci of chronic inflammatory infiltrate, particularly lymphocytes	Fibrosis, foci of chronic inflammatory infiltrate, particularly lymphocytes	-
K101/12	Granulomas, fibrosis, lymphocytes, necrosis, cavities,	*	-
K106/12	Fibrosis, foci of chronic inflammatory infiltrate, particularly lymphocytes	Fibrosis, lymphocytes, granulomas, necrosis	-
K107/12	Fibrosis, foci of chronic (and acute) inflammatory infiltrates – TB bronchopneumonia	Fibrosis, foci of chronic (and acute) inflammatory infiltrates – TB bronchopneumonia	-
K124/12	Fibrosis, lymphocytes, granulomas, necrosis	Fibrosis, lymphocytes, granulomas, necrosis	-

* Typical granulomatous pattern suggestive of TB was absent

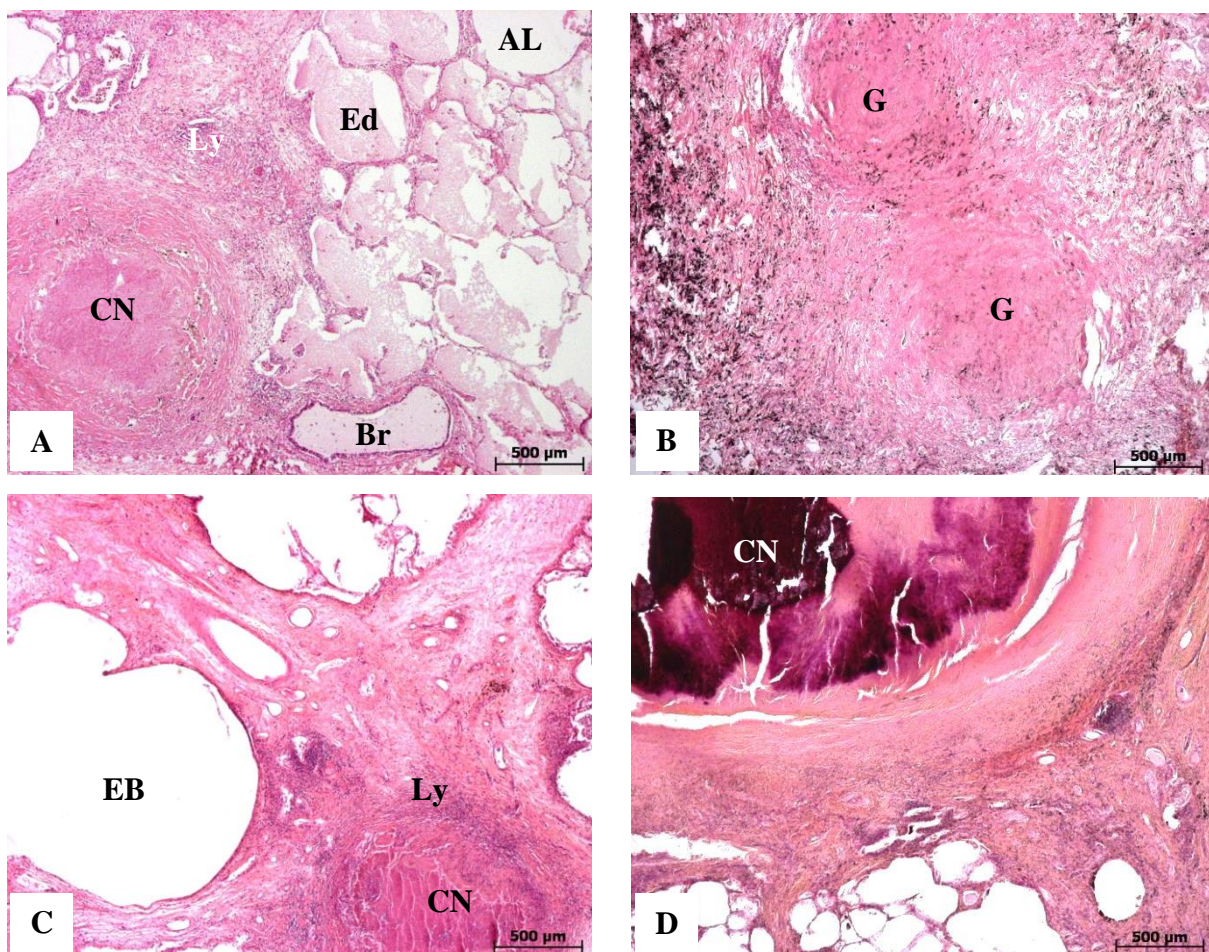


Figure 4.7. Microscopic appearance of TB granulomas in the pulmonary tissue. A) caseating granuloma in the left superior lobe of cadaver K89/09, H&E (25x); B) tuberculous granulomas with surrounding anthracosis in the right superior lobe of cadaver K47/11, H&E (25x); C) caseating granuloma in right superior lobe of cadaver K89/09, H&E (25x); D) caseating granuloma in the right superior lobe of cadaver K41/11, H&E (25x); alveoli (AL), bronchiole (Br); caseous necrosis (CN), edematous remnants in the alveoli (Ed), emphysematous bullae (EB); granuloma (G), lymphocytes (Ly).

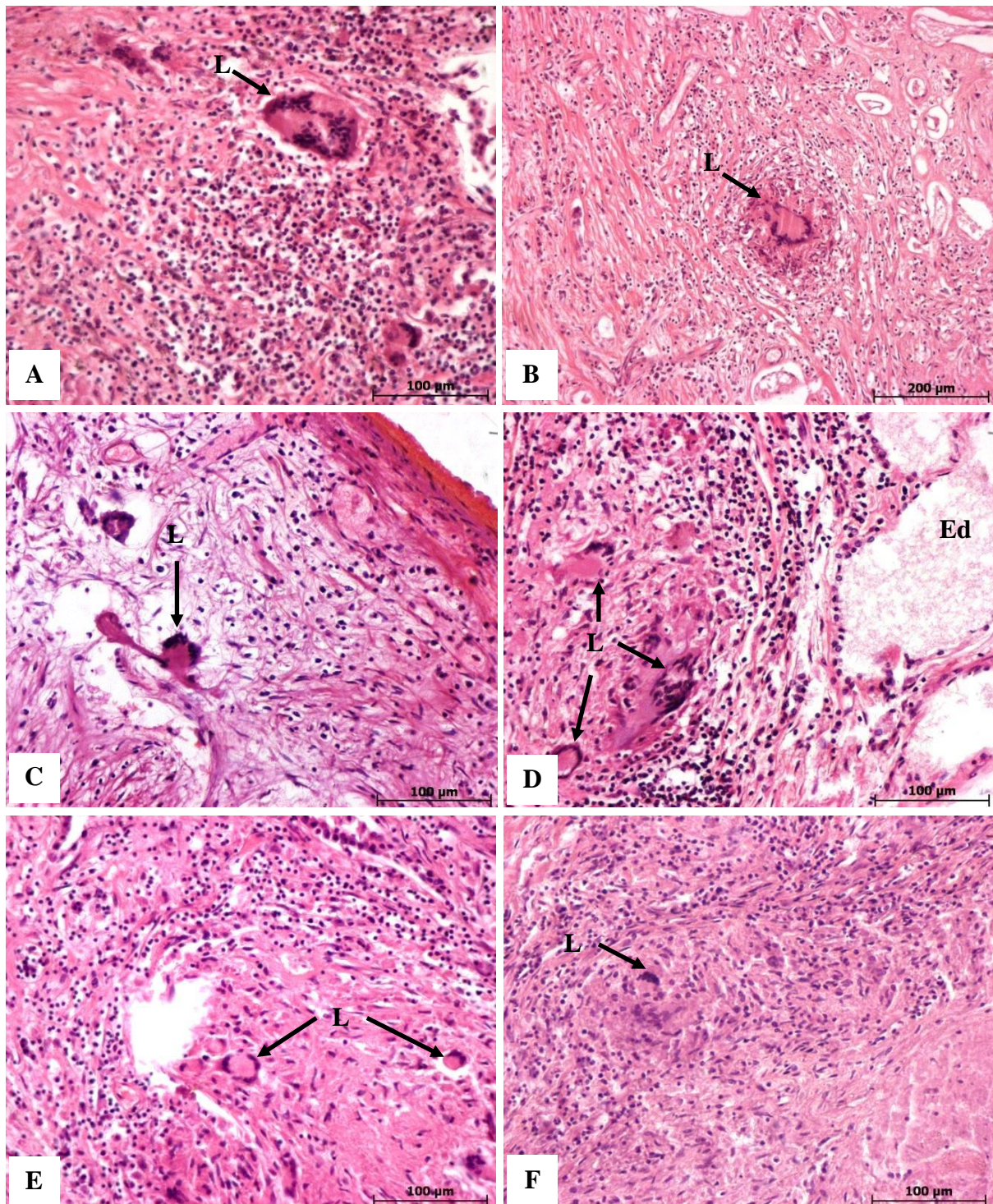


Figure 4.8. Microscopic appearance the Langhans cells in the TB lesions. A) right superior lobe of cadaver K83/09, H&E (200x); B) right superior lobe of cadaver K89/09, H&E (100x); C) right superior lobe of cadaver K64/11, H&E (200x); D) right superior lobe of cadaver K115/09, H&E (200x); E) right superior lobe of cadaver K10/10, H&E (200x); F) right superior lobe of cadaver K41/11; alveoli (AL); edematous remnants in the alveoli (Ed), Langhans giant cell (L).

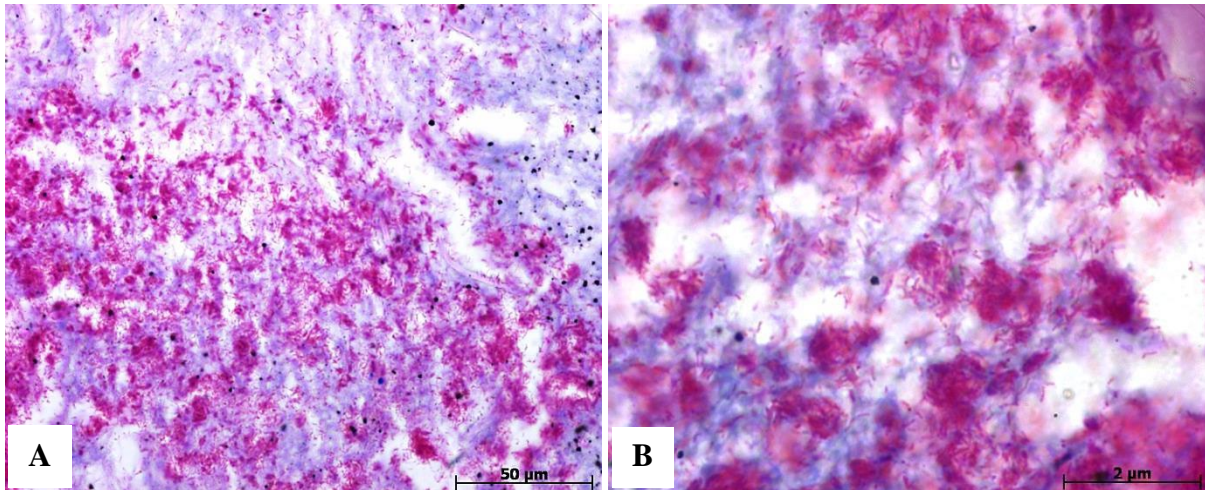


Figure 4.9. Ziehl-Neelsen stains. A) Right inferior lobe of cadaver K96/09, Ziehl-Neelsen (400x); B) right inferior lobe of cadaver K96/09, Ziehl-Neelsen (1000x).

4.1.2 Pneumonias

Six types of pneumonias were noted in this study of which bronchopneumonia was the most frequently observed.

4.1.2.1 Tuberculous Bronchopneumonia

Tuberculous bronchopneumonia was seen in 27/97 (27.8%) cadavers. Macroscopically, the lung was consolidated with cavities present. Microscopically, large numbers of the mycobacterial bacilli were discharged into the bronchus. The lung appeared consolidated due to the presence of an inflammatory exudate within the alveoli. In addition, the alveoli were filled with abundant eosinophilic exudate which consisted of macrophages. Should this necrotic tissue be coughed up, cavities would form.

4.1.2.2 Bronchopneumonia

Microbial infection of the pulmonary parenchyma adjacent to infected bronchioles formed a patchy pattern of purulent pneumonic consolidation. This consolidation, termed bronchopneumonia, was observed in 62/127 (48.8%) cadavers (Table 4.4). Numerous localized foci of acute inflammation consisting mainly of polymorphonuclear leukocytes and

a smaller number of red blood cells (RBC's) were observed adjacent the infected bronchioles (Figure 4.12). The alveolar capillaries were dilated and congested. In some instances, the neighboring alveoli became confluent and occasionally the process was so extensive that an entire lobe was consolidated. The bronchioles were often acutely inflamed and in some cases were filled with pus. Edematous changes together with polymorphonuclear leukocytes were seen in some alveoli, while others were filled with a dense fibrinous exudate (Figure 4.12). In 11/127(8.7%) cadavers, the alveoli were collapsed as a result of “absorption atelectasis”, a process where absorption of air distal to the filled alveoli occurred. Other alveoli were distended due to compensation. This disease was usually observed in the inferior lobes and in most cases occurred bilaterally, however the entire lung was involved in some of the cadavers.

4.1.2.2.1 Distribution of Bronchopneumonia in the Cadavers

For the purpose of this study, the right middle lobe was included in the right superior lobe. The right superior lobe was involved in 38/127 (30.0%) cadavers, while the left superior lobe was involved in 26/127 (20.5%) (Figure 4.10, D). The right and left inferior lobes were involved in 32/127 (25.2%) cadavers and 53/127 (41.7%) cadavers, respectively (Figure 4.10, D).

Table 4.4. The prevalence of bronchopneumonia in the cadaver cohort (n=127)

<i>Sex</i>	<i>Total</i>	<i>Bronchopneumonia</i>	<i>Prevalence (%)</i>
Female	40	19	47.5
Male	87	43	49.4
TOTAL	127	62	48.8

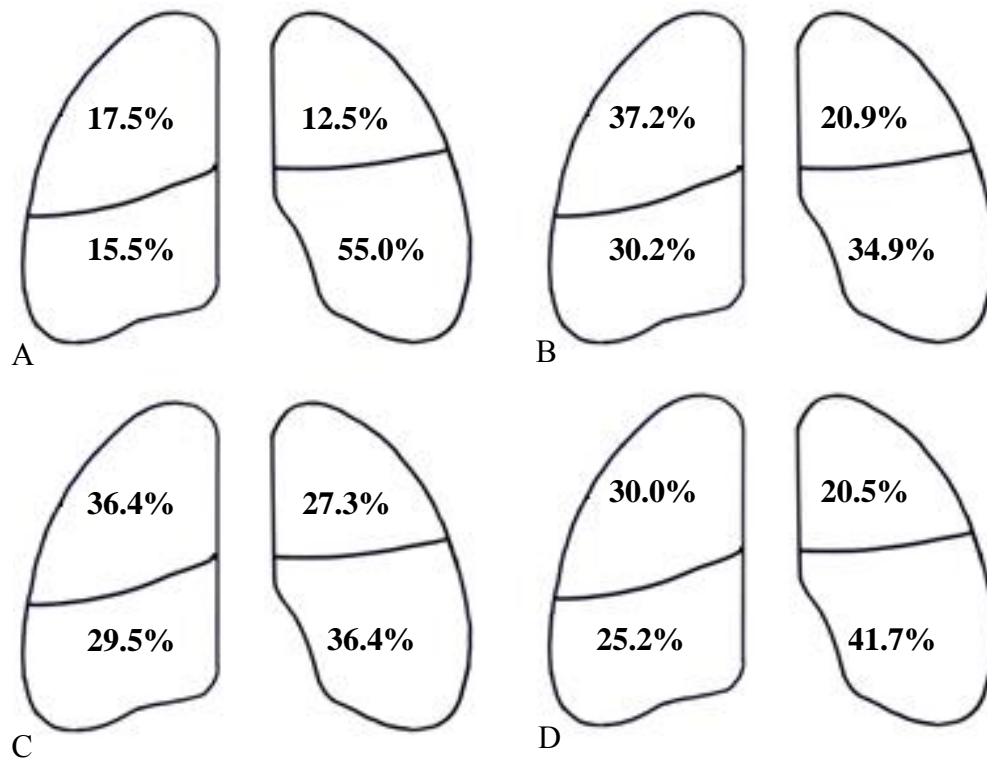


Figure 4.10. Overall distribution of bronchopneumonia in the cadaver cohort. A) 2011 cohort; B) 2012 cohort; C) 2013 cohort and D) total distribution over the three years. For the purpose of the schematic diagram, the right middle lobe was included in the right superior lobe.

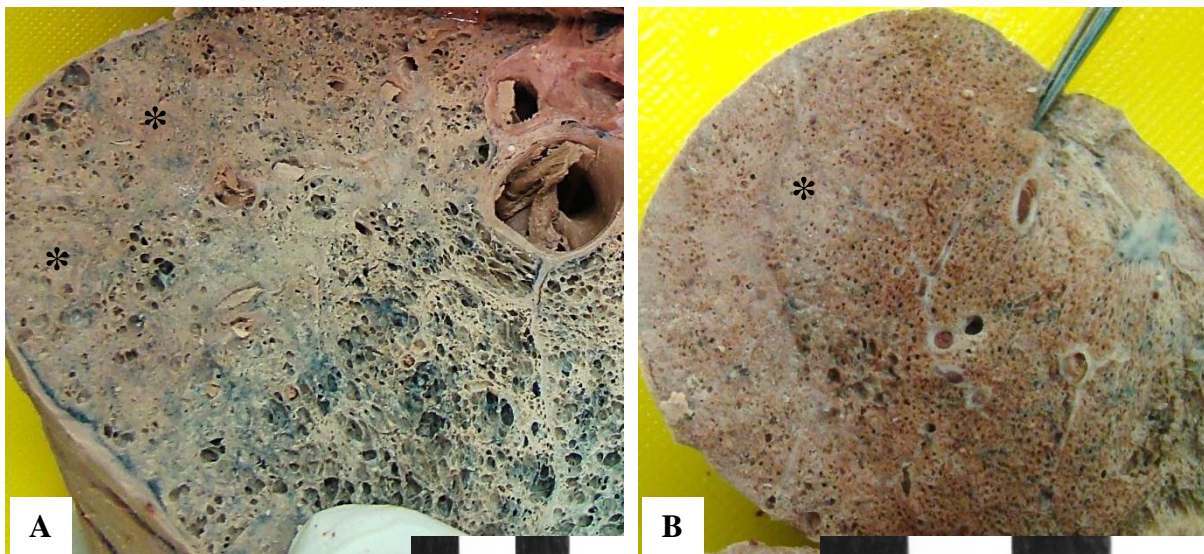


Figure 4.11. Macroscopic appearance of bronchopneumonia. A) Consolidation in the right superior lobe of cadaver K38/11, superior view; apex of the left superior lobe of cadaver K63/11 showing consolidation, superior view; area of consolidation (asterisks) B) Consolidation in the right superior lobe of cadaver K63/11, superior view; area of consolidation (asterisk)

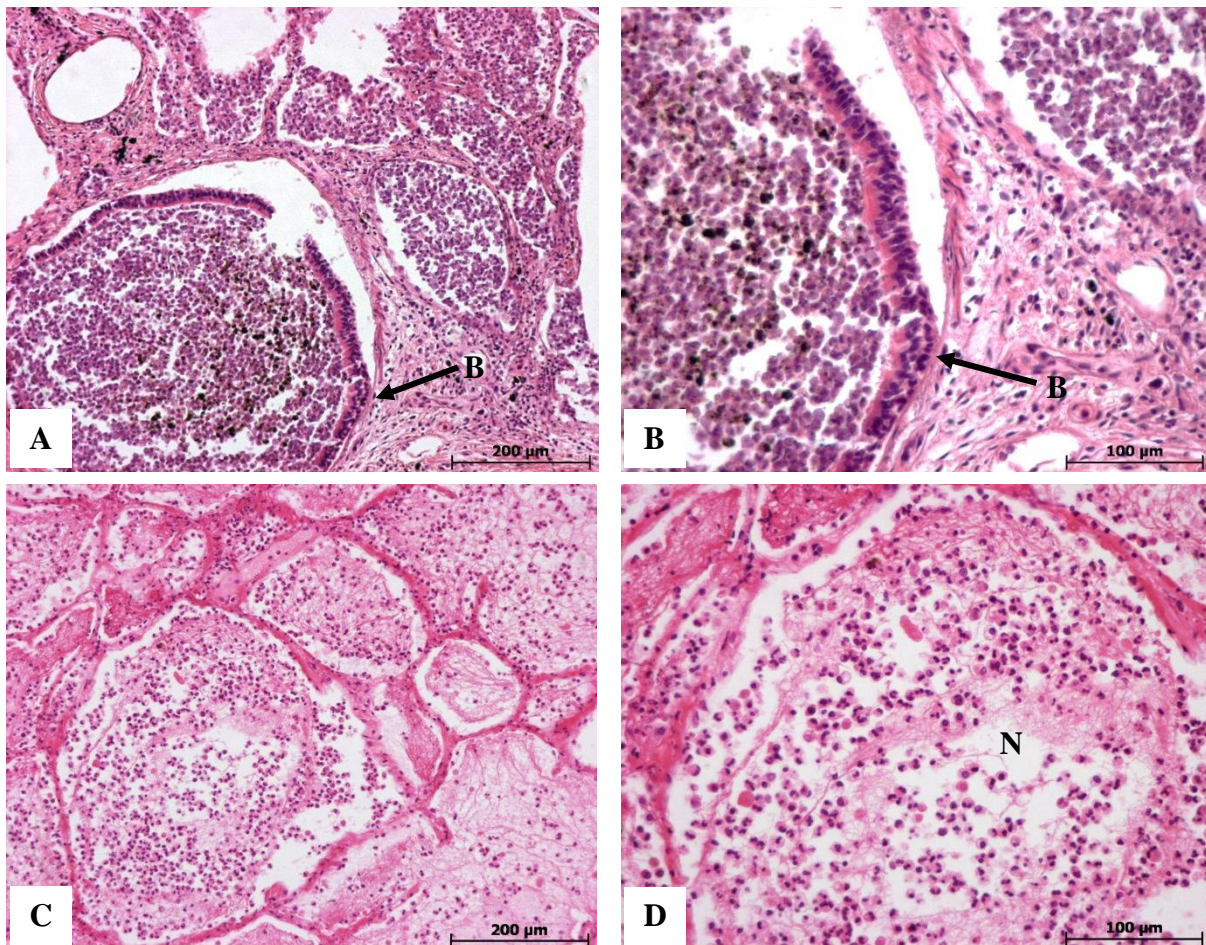


Figure 4.12. Microscopic appearance of bronchopneumonia. A) Inflammatory infiltrate in the alveoli adjacent to the bronchiole in the right superior lobe of cadaver K38/10, H&E (100x); B) right superior lobe of cadaver K38/10, H&E (200x); C) neutrophilic infiltrate in the alveoli of the right superior lobe of cadaver K19/10, H&E (100x); D) right superior lobe of cadaver K19/10, H&E (200x); bronchiole (B), neutrophilic infiltrate (N).

4.1.2.3 Lobar Pneumonia

Acute inflammatory involvement of an entire lobe of a lung, termed lobar pneumonia, was observed in 1/127 (0.8%) cadaver. As with bronchopneumonia, the route of infection with lobar pneumonia was via the bronchi and bronchioles. Within the lung, the infection was more acute and the inflammatory exudate disseminated more directly through the lung tissue to the pleural surface. This cadaver, K118/09, presented with a darker, brownish-red consolidated and wet left inferior lobe. Histologically, the alveoli were packed with an acute inflammatory infiltrate consisting of neutrophils, RBCs, degenerated macrophages and fibrin.

As with bronchopneumonia, the alveolar capillaries were dilated and congested. This stage of pneumonia is known as red hepatization.

4.1.2.4 Community-Acquired Atypical Pneumonia

Primary community-acquired atypical pneumonia was observed in 2/127 (1.6%) cadavers (Table 4.5). Both cadavers affected were males with unavailable age. Macroscopically, the affected region in the lobes was consolidated. Both cases presented with unilateral involvement. Microscopically, patchy inflammatory changes consisting of lymphocytes and plasma cells were largely confined to the alveolar septa which were widened and edematous (Figure 4.13). The alveolar spaces were spared and free of an inflammatory exudate. No acute lung injury with resulting hyaline membrane formation was noted in the cases. This case was indicative of a mild atypical pneumonia.

Table 4.5. Interstitial pneumonia in the cadaver cohort (n=127)

<i>Cadaver Ref. Nr.</i>	<i>Sex</i>	<i>Macroscopical Findings</i>	<i>Microscopical Findings</i>	<i>Absolute Weight (g)</i>	<i>Adapted Weight (g)</i>
K53/11	Male	Consolidated right superior lobe with fibrosis	Mononuclear infiltrate (i.e. lymphocytes) in the interstitium of right superior lobe	870.0	870.0
K49/12	Male	Consolidated right superior lobe with fibrosis	Chronic inflammatory infiltrate in interstitium of right superior lobe	620.0	620.0

* Mean percent change with formalin fixation = + 0.0% (according to Finkbeiner *et al.*, 2004)

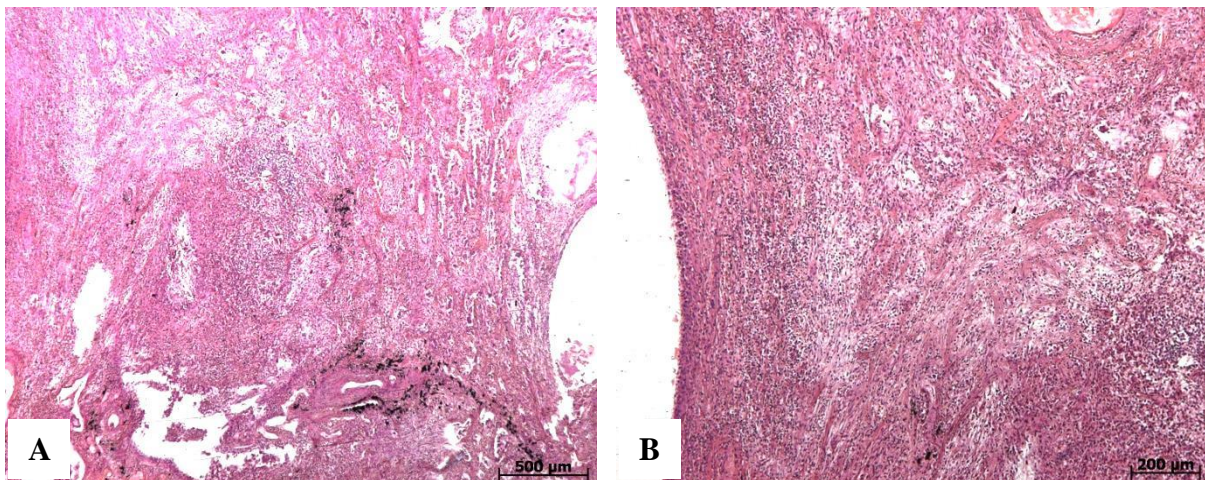


Figure 4.13. Microscopic appearance of interstitial pneumonia. A) Right superior lobe of cadaver K53/11, H&E (25x); B) right superior lobe of cadaver K53/11, H&E (50x).

4.1.2.5 Lymphocytic Interstitial Pneumonitis (LIP)

Lymphocytic interstitial pneumonitis (LIP) was observed in the right superior lobe of 2/127 (1.6%) cadavers (Table 4.6). The male to female ratio was 1:2.3 and the average of the affected cadavers was 48.0 years. The cadaver (K05/11) underwent a pneumonectomy of the left lung prior to death. Histologically, the diagnosis of LIP was made based on the presence of a dense and diffuse alveolar septal lymphocytic infiltrate (Figure 4.14). Plasma cells and histiocytes were also noted amongst the lymphocytes. The right inferior lobe presented with a typical bronchopneumonia with accumulated polymorphonuclear cells within the alveoli. Similar findings were observed in cadaver K124/12.

Table 4.6. Lymphocytic interstitial pneumonitis in the cadaver cohort (n=127)

<i>Cadaver Ref. Nr.</i>	<i>Sex</i>	<i>Age</i>	<i>Anatomical Involvement and Macroscopical Findings</i>	<i>Microscopical Findings</i>	<i>Absolute Weight (g)</i>	<i>Adapted Weight (g)*</i>
K05/11	Female	41	Consolidation in right lung	Lymphocytic infiltrate in alveolar septa, no cellular infiltrate in alveoli	950.0	950.0
K124/12	Male	55	Consolidation in right lung	Lymphocytic infiltrate in interstitium, alveoli are spared	870.0	870.0

* Mean percent change with formalin fixation = + 0.0% (according to Finkbeiner *et al.*, 2004)

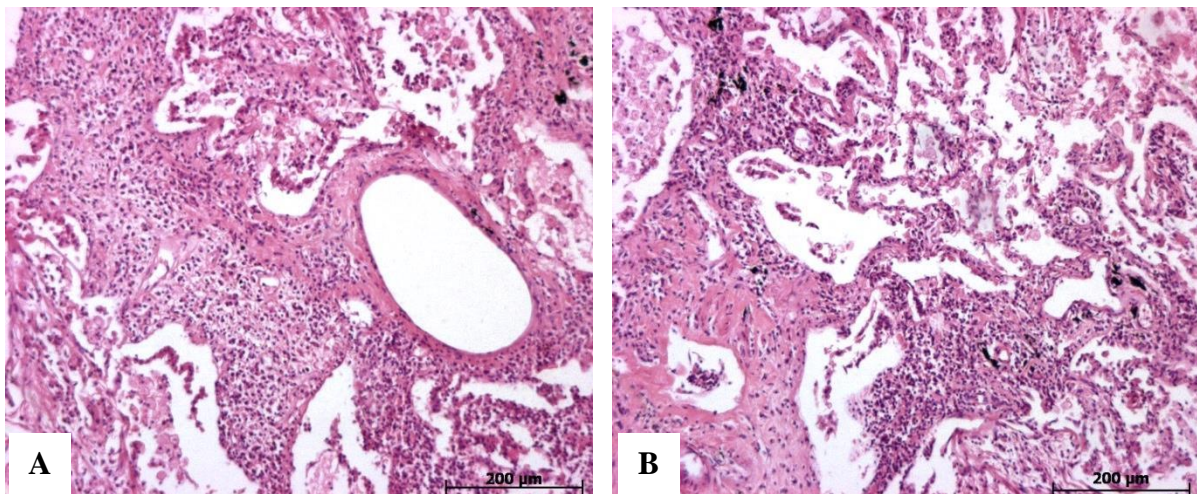


Figure 4.14. Microscopic appearance of lymphocytic interstitial pneumonitis (LIP). A) right superior lobe of cadaver K05/11, H&E (100x); B) right superior lobe of cadaver K05/11, H&E (100x)

4.1.2.6 Aspiration Pneumonia

Aspiration pneumonia was observed in 3/127 (2.4%) cadavers (Table 4.7). All the cadavers affected were males and an average of 40.5 years was observed. Histologically, foci of acute inflammatory cells, including polymorphonuclear cells, were seen adjacent to the foreign material. Cadaver K30/10 presented with a typical foreign body granuloma and accompanying multinucleated giant cells.

Table 4.7. Aspiration pneumonia in the cadaver cohort (n=127)

<i>Cadaver Ref. Nr.</i>	<i>Sex</i>	<i>Age*</i>	<i>Pulmonary Involvement</i>	<i>Microscopical Findings</i>	<i>Foreign Object Present</i>
K82/09	Male	47	Left inferior lobe	Acute inflammatory cells	Stomach contents
K30/10	Male	*	Right superior lobe	Multinucleated giant cells, granulomas	Possible hair/fiber
K59/11	Male	34	Left inferior lobe	Polymorphonuclear cells	Stomach contents

* Age is unavailable

4.1.3 Chronic Obstructive Pulmonary Disease (COPD)

Chronic obstructive pulmonary disease (COPD) is a collective term describing emphysema, chronic bronchitis, bronchiectasis and asthma. The former three diseases, emphysema, chronic bronchitis and bronchiectasis have all been noted in the cadaver cohort.

4.1.3.1 Emphysema

Large, pale voluminous lungs (some cases obscuring the heart *in situ*) were observed in 54/127 (42.5%) cadavers (Table 4.8). Prominent air spaces due to the destruction of the alveolar walls were seen during gross dissections (Figure 4.16). Emphysematous changes were most prominent in the superior lobes and especially in the lingula. Subpleural bullae which are associated with emphysema were often observed. None of these bullae were ruptured and no resulting pneumothorax was associated with a rupture bullous.

4.1.3.1.1 Distribution of Emphysema in the Cadavers

For the purpose of this study, the right middle lobe was included in the right superior lobe. The right superior and left superior lobes were involved in 60/127 (47.2%) and 55/127 (43.3%) cadavers, respectively (Figure 4.15, D). The right and left inferior lobes were involved in 32/127 (25.2%) and 42/127 (33.1%) cadavers, respectively (Figure 4.15, D).

Table 4.8. The prevalence of emphysema in the cadaver cohort (n=127)

<i>Sex</i>	<i>Total</i>	<i>Emphysema</i>	<i>Prevalence (%)</i>
Female	40	12	30.0
Male	87	42	48.3
TOTAL	127	54	42.5

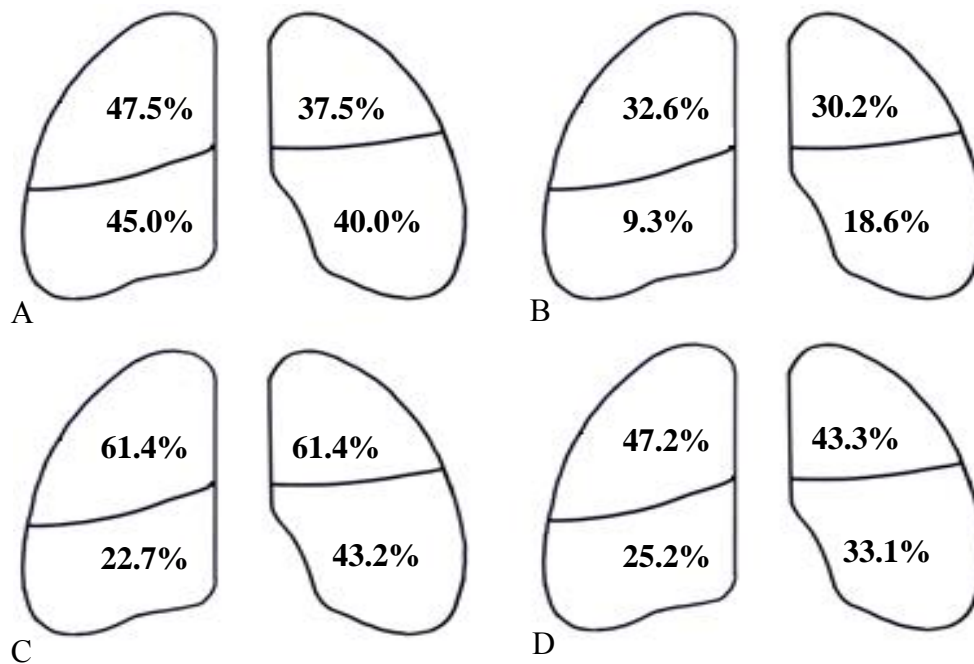


Figure 4.15. Overall distribution of emphysema in the cadaver cohort. A) 2011 cohort; B) 2012 cohort; C) 2013 cohort and D) total distribution over the three years. For the purpose of the schematic diagram, the right middle lobe was included in the right superior lobe.

Histologically, a marked increase in the alveolar volume was noted (Figure 4.17). The alveolar walls were thinner than the normal alveoli. In the advanced states of this disease, the alveoli may become confluent, giving rise to the large and prominent airspaces (Figure 4.17). In some cases the alveoli were collapsed as a result of loss of elastic support within the

alveolar wall. In addition, a decrease in the amount of alveolar capillaries was noted. Emphysema was often associated with chronic infection, such as bronchitis or TB.

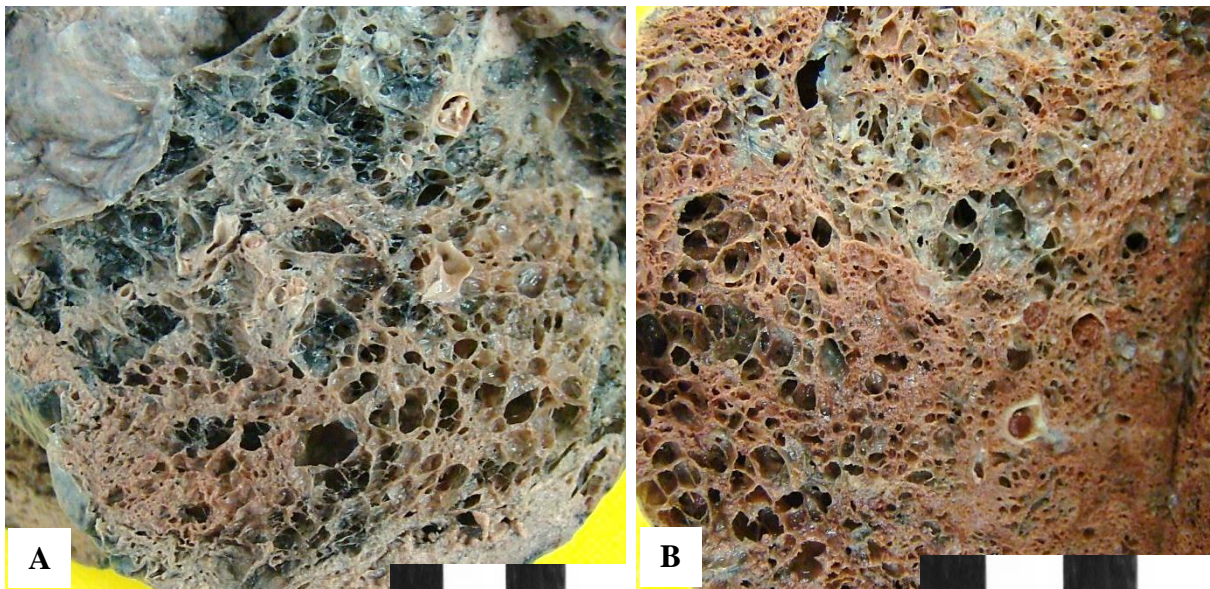


Figure 4.16. Macroscopic appearance of emphysema in the cadavers. A) Extensively enlarged alveoli in the right inferior lobe of cadaver K46/12, superior view; B) large, confluent alveoli in the right superior lobe of cadaver K99/12, superior view.

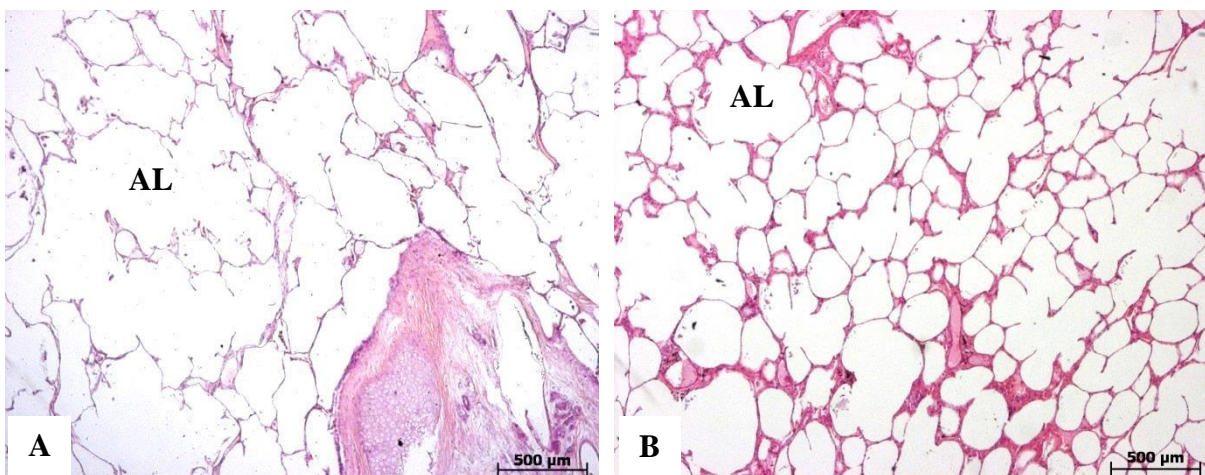


Figure 4.17. Microscopic appearance of emphysema in the cadavers. A) an increased volume of the alveolar spaces with thin alveolar walls in the right superior lobe of cadaver K69/11, H&E (25x); large and prominent air spaces in the right inferior lobe of cadaver K80/09, H&E (25); alveoli (AL).

4.1.3.2 Chronic Bronchitis

Chronic bronchitis, defined clinically as a persistent and productive cough for at least 3 months in 2 consecutive years (Kumar *et al.*, 2013), was observed in 9/127 (7.1%) cadavers (Table 4.9). The male to female ratio was 1.6:1 and the average age of the affected cadavers

was 49.0 years. Diagnosis was made based on histological appearance where an increasing thickness of the bronchial wall was observed. A prominently thickened basal membrane was noted with a marked infiltration of the submucosa by acute or chronic inflammatory cells (Figure 4.18). Prominent hypertrophy of the mucosal smooth muscle cells were seen and in some cases copious amounts of mucous was observed due to hyperplastic mucous glands.

Table 4.9. Chronic bronchitis in the cadaver cohort (n=127)

<i>Cadaver Ref. Nr.</i>	<i>Sex</i>	<i>Age*</i>	<i>Pulmonary Involvement</i>	<i>Microscopical Findings</i>
K89/09	Male	41	Left inferior lobe	Thickening of bronchial basement membrane, mucous
K30/10	Male	*	Left inferior lobe	Thickening of bronchial basement membrane, mucous
K05/11	Female	41	Right inferior lobe	Thickening of bronchial basement membrane, mucous
K44/11	Male	48	Left superior lobe	Thickening of bronchial basement membrane, mucous
K53/11	Male	*	Left inferior lobe	Mucosal smooth muscle hypertrophy, thickening of bronchial basement membrane
K120/11	Female	53	Right superior lobe; left inferior lobe	Thickening of bronchial basement membrane
K25/12	Male	39	Left inferior lobe	Thickening of bronchial basement membrane, mucosal smooth muscle hypertrophy
K76/12	Male	*	Right inferior lobe	Thickening of bronchial basement membrane, mucosal smooth muscle hypertrophy
K93/12	Male	72	Right inferior lobe; Left superior and inferior lobes	Thickening of bronchial basement membrane

* Age is unavailable

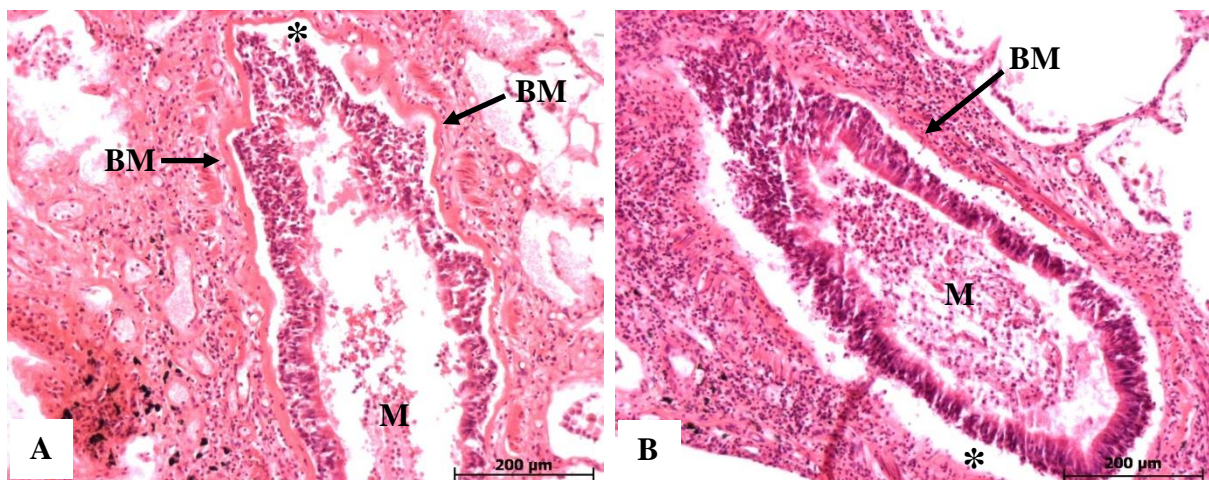


Figure 4.18. Microscopic appearance of chronic bronchitis. A) Thickened basement membrane of the bronchiole in the right superior lobe of cadaver K89/09, H&E (100x); B) thickened bronchiolar basement membrane and mucus within bronchiole in the right superior lobe of cadaver K89/09, H&E (100x); basal membrane (BM), mucus in the bronchioles (M), artifactual tearing (asterisks).

4.1.3.3 Bronchiectasis

Bronchiectasis, defined as an abnormal and permanent dilatation of the bronchi was observed in 43/127 (33.9%) cadavers. Bilateral involvement was seen in 35/43 (81.4%). The bronchi were dilated (up to three times their normal diameter) and could be followed beyond a point 1cm from the pleural surfaces (Figure 4.19). The bronchial walls were thickened and fibrotic. Associated fibrosis of the adjacent pulmonary parenchyma may occur. Tuberculous bronchiectasis was observed most frequently in the apices of both lungs. Histologically, a mixture of acute and chronic inflammatory cells within the bronchi and bronchial walls were noted. In addition, loss of the supporting elastic tissue was noted. In the more chronic cases, fibrosis was observed within the bronchiolar walls.

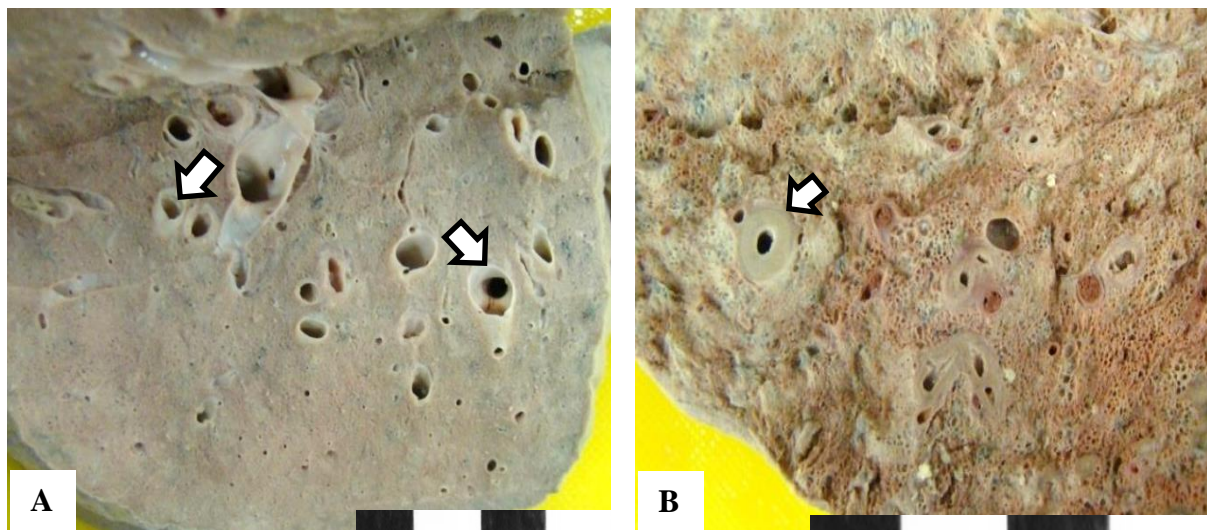


Figure 4.19. Macroscopic appearance of bronchiectasis. A) Large, prominent and abnormal bronchi in the inferior lobe of the left lung of cadaver K60/12, superior view; B) prominent and abnormal bronchi inferior lobe of the right lung of cadaver K43/12, superior view; dilated bronchi (blocked arrows).

4.1.4 Acute Lung Injury

Diffuse alveolar damage (DAD), the morphological prototype of acute lung injury, was observed in 25/127 (19.7%) cadavers (Table 4.10). The male to female ratio was 1:1 and the average age of the affected cadavers was 47.2 years. Cell injury to the endothelium and alveolar epithelium was accompanied by fluid exudation. Fibrin deposition and hyaline

membranes was commonly observed lining the alveolar walls (Figure 4.20). Consequently, the resultant fibroblastic proliferation is complemented by pneumocyte type II hyperplasia which was observed in the pulmonary sections (Figure 4.20). Some interstitial mononuclear inflammatory infiltrates were seen in the arteries surrounding the damaged tissue.

Table 4.10. Acute lung injury in the cadaver cohort (n=127)

<i>Cadaver Ref. Nr.</i>	<i>Sex</i>	<i>Age*</i>	<i>Pulmonary Involvement</i>	<i>Microscopic Findings</i>	<i>Phase of ALI</i>
K82/09	Male	47	Left superior lobe	Foamy exudate in alveoli, fibrin deposition in alveolar walls	Phase I
K95/09	Male	*	Right superior lobe	Fibrinous deposition in alveolar walls, hyaline membranes	Phase I
K96/09	Male	*	Left inferior lobe	Fibrinous deposition in alveolar walls, alveolar exudate	Phase II
K100/09	Male	45	Left lung	Focal fibrinous deposition, hyaline membranes	Phase III
K112/09	Male	58	Right inferior lobe	Hyaline membranes in alveolar walls	Phase I - II
K02/10	Male	31	Entire right lung	Fibrinous deposition, alveolar exudate	Phase I
K03/10	Male	34	Right superior lobe	Focal areas of alveolar exudates, fibrin deposition	Phase I
K12/10	Male	37	Right superior lobe	Alveolar exudates with hyaline membranes lining alveoli	Phase II
K13/10	Male	47	Right superior lobe	Fibrinous exudate in alveoli, hyaline membranes	Phase III
K40/10	Male	47	Right inferior lobe	Alveolar exudate, hyaline membrane	Phase I
K05/11	Female	41	Right inferior lobe	Alveolar exudate with hyaline membranes	Phase I
K10/11	Female	45	Right superior lobe	Fibrinous exudate lining alveolar walls	Phase I
K47/11	Male	64	Right and left inferior lobes	Fibrinous exudate lining the alveolar walls	Phase I
K64/11	Female	48	Both lungs	Fibrinous exudate in alveoli, hyaline membranes	Phase II
K65/11	Female	52	Right superior lobe; Left inferior lobe	Fibrinous deposition lining alveolar walls	Phase II
K72/11	Male	*	Both lungs	Fibrinous deposition in alveoli, hyaline membranes	Phase III
K121/11	Male	50	Both lungs	Fibrinous deposition in alveoli, hyaline membranes	Phase II
K124/11	Female	*	Right lung	Fibrinous exudate lining alveolar walls	Phase II
K26/12	Male	*	Right lung	Fibrinous deposition lining alveolar walls	Phase I
K43/12	Male	*	Right middle and inferior lobes; left inferior lobe	Thickened septa with alveolar exudate	Phase III
K66/12	Female	55	Left inferior lobe	Fibrinous deposition in the lining of the alveoli	Phase I
K69/12	Male	*	Right lung	Fibrinous exudate in alveoli, lining alveolar walls	Phase II

<i>Cadaver Ref. Nr.</i>	<i>Sex</i>	<i>Age*</i>	<i>Pulmonary Involvement</i>	<i>Microscopic Findings</i>	<i>Phase of ALI</i>
K73/12	Male	72	Right inferior lobe	Acute inflammation, fibrin lining the alveolar walls	Phase I
K74/12	Female	52	Right lung	Fibrinous exudate in alveoli, lining alveolar walls	Phase I
K86/12	Female	24	Right superior lobe; left superior lobe	Fibrinous deposition in alveolar walls, alveolar exudate	Phase II

* Age is unavailable

Phase I – mild; Phase II – moderate; Phase III – severe

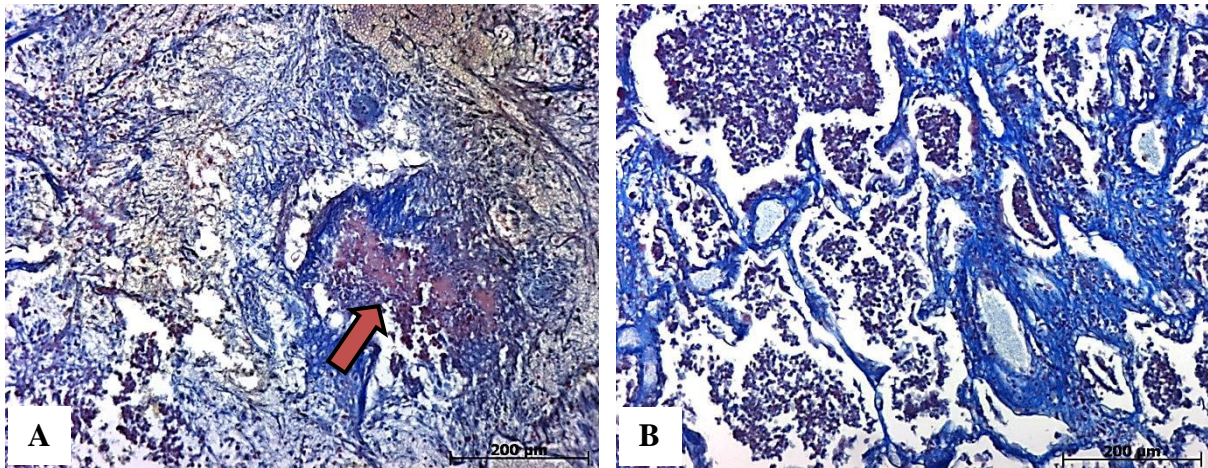


Figure 4.20. Fibrin deposition in acute lung injury. A) Red (arrow) and blue fibrin deposition with yellow erythrocytes in the superior left lobe of cadaver K75/12; Martius Scarlet Blue (MSB) stain (100x); B) blue fibrin deposition in the alveolar walls in the superior left lobe of cadaver K75/12; MSB stain (100x).

4.1.4.1 Microbial Causes of Acute Lung Injury

4.1.4.1.1 Viral Infections: *Cytomegalovirus*

Cytomegalovirus (CMV) infection in the pulmonary system was observed in 2/127 (1.6%) cadavers (Table 4.11). Both cadavers infected with CMV were females. This type of infection is a common cause of symptomatic pneumonia in immune-compromised individuals, such as those infected with HIV. The histopathologic findings include little to no inflammation and DAD (Figure 4.21). Large cytomegalic cells with large, round “owl eye” intranuclear inclusions and cellular gigantism, the latter being the hallmark of CMV infection were seen in the cadavers (Figure 4.21). In 1/2 (50.0%), miliary small nodules with or without central caseation were observed. Interstitial and alveolar edema, alveolar fibrin and cellular debris and in some cases type II pneumocyte hyperplasia were observed.

Table 4.11. Cytomegalovirus infection in the cadaver cohort (n=127)

<i>Cadaver Ref. Nr.</i>	<i>Sex</i>	<i>Age*</i>	<i>Pulmonary Involvement</i>	<i>Microscopic Findings</i>
K124/11	Female	*	Entire right lung	Thick exudate in alveoli, areas of calcification, large oval cells with an “owl eye” appearance within the parenchyma, fibrin deposition in alveolar walls
K74/12	Female	52	Both lungs	Thick exudate in alveoli, septic granulomas, large oval cells with inclusion bodies, fibrinous deposition in alveolar walls

* Age is unavailable

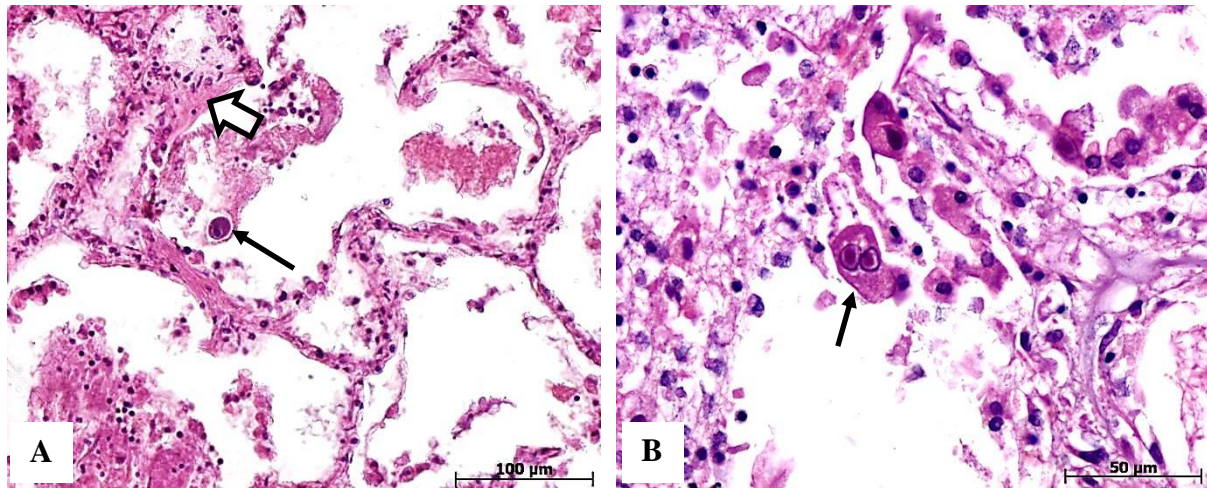


Figure 4.21. Microscopic appearance of cytomegalovirus infection. A) A cell with the characteristic “owl-eye” appearance in the right inferior lobe of cadaver K124/11, H&E (200x); B) right superior lobe of cadaver K74/12 showing cells infected with CMV (arrow), H&E (400x); cytomegalovirus (small arrows), hyaline membrane (blocked arrow).

4.1.4.1.2 Fungal Infections: *Pneumocystis jiroveci* (formerly *P. carinii*)

Pneumocystis jiroveci was the most commonly observed opportunistic fungal infection in the cadaver cohort and was seen in 5/127 (3.9%) cadavers. The male to female ratio was 1.8:1 and the average age of the infected cadavers was 34.0 years. Frothy or foamy eosinophilic intra-alveolar exudates with organisms were seen in the alveoli of the infected cadavers. The alveolar septa were thickened and a mononuclear infiltrate was minimal if not absent. This histological picture is synonymous with profound immunodeficiency. A silver stain was performed on one tissue section and revealed round cystic structures reaching up to 10μm in diameter.

Table 4.12. *Pneumocystis jiroveci* infection in the cadaver cohort (n=127)

<i>Cadaver Ref. Nr.</i>	<i>Sex</i>	<i>Age*</i>	<i>Pulmonary Involvement</i>	<i>Microscopic Findings</i>	<i>PAS Findings</i>
K82/09	Male	47	Left superior lobe	Foamy exudate in alveoli, fibrin deposition in alveolar walls	Round, cystic structures in pulmonary parenchyma
K96/09	Male	*	Left inferior lobe	Fibrinous deposition in alveolar walls, alveolar exudate	Round, cystic structures within alveoli
K02/10	Male	31	Entire right lung	Fibrinous deposition, alveolar exudate	Small, round, cystic structures within alveoli
K43/12	Male	*	Right middle and inferior lobes; left inferior lobe	Thickened septa with alveolar exudate (Fig. 4.22, A and B)	Small, cystic structures within alveoli (Fig. 4.22, C and D)
K86/12	Female	24	Right superior lobe; left superior lobe	Fibrinous deposition in alveolar walls, alveolar exudate	Round, cystic structures within alveoli

* Age is unavailable

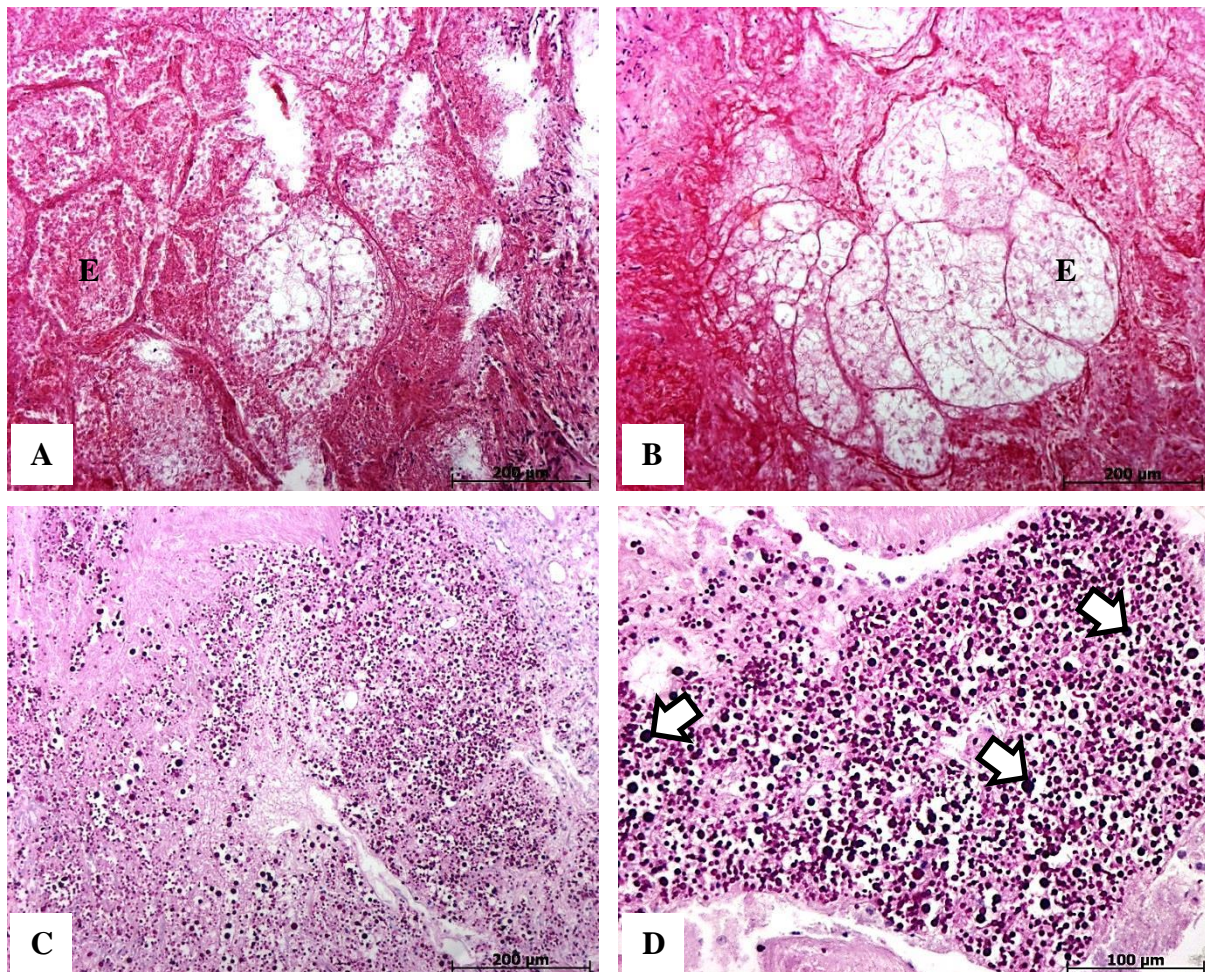


Figure 4.22. Microscopic appearance of *Pneumocystis jiroveci* infection. A) Inferior part of the superior lobe of cadaver K43/12, H&E (100x); B) right inferior lobe of cadaver K43/12, H&E (100x); alveolar exudates (E); C) small, cystic spaces within the right superior lobe of cadaver K43/12, PAS stain (100x); D) a higher magnification of C illustrating the darker stained, cystic spaces (blocked arrows), PAS stain (200x).

4.1.5 Pulmonary Neoplasms

Pulmonary neoplasms were observed in 7/127 (5.5%) cadavers (Table 4.13). The male to female ratio was 2.8:1 and the average age of the affected cadavers was 52.1 years. Adenocarcinoma *in situ* (AIS) (previously termed bronchioloalveolar carcinoma (BAC)) was observed in 1/7 (14.3%) cadaver. In this cadaver (K01/10), cuboidal cells (representing pneumocyte type II cells) and columnar cells (representing bronchial cells) grew along the alveolar walls of (Figure 4.25, A). No evidence of stromal, vasculature or pleural invasion was observed. Pulmonary adenocarcinoma (ACA) was observed in 3/7 (42.9%) cadavers. The ACA's of the cadavers were not associated with the bronchial tree and manifested as peripheral nodules of more than 3 cm in diameter. They were invasive, underwent necrosis and fibrosis and did not show cavitation. Glandular differentiation was observed (Figure 4.25, B). Metastasis to the both kidneys was observed in cadaver K106/12. A primary sarcomatoid carcinoma was observed in 1/7 (14.3%) cadaver. This invasive carcinoma was a located centrally. Histologically, sarcoma or sarcoma-like elements were observed. Squamous cell carcinoma (SCC) was observed in 1/127 (0.8%) cadaver. This cadaver (K94/12) presented with bilateral masses without atelectasis (lung collapse) (Figure 4.24, B). The mass was visible of the CXR (Figure 4.23, A) Necrosis with cavitation was noted. Keratinization, a common feature of SCC, was observed within the lung. Histologically, keratin pearls were observed in the lung sections. A poly-differentiated tumor was observed in 1/127 (0.8%) cadaver. This cadaver (K125/11) presented with a massive mediastinal tumour measuring 120x110mm in maximum dimensions. The mass had a firm and granular texture, was adherent to the superior vena cava (SVC) and infiltrated the neighboring pulmonary parenchyma. This mass was visible on the CXR (Figure 4.23, B). Histologically, ill-defined anaplastic cells were observed with fibrous bands separating the malignant cells (Figure 4.25, C, D). Necrosis was a common feature.

Table 4.13. Types of pulmonary tumors in the cadaver cohort (n=127)

<i>Cadaver Ref. Nr.</i>	<i>Sex</i>	<i>Age</i>	<i>Anatomical Region</i>	<i>Macroscopical Findings</i>	<i>Microscopical Findings</i>	<i>Type of Tumor</i>
K83/09	Male	60	Right inferior lobe	Scarring in inferior part of right inferior lobe (incidental finding)	Atypical, pleomorphic, malignant, growing along the alveolar walls (infiltrating)	ACA
K01/10	Male	53	Right inferior lobe	Fibrosis (scarring), large alveolar spaces, consolidation	Pleomorphic, ill-defined, lining alveolar spaces; non-mucinous (Fig. 4.25, A)	ACA <i>in situ</i> (Previously BAC)
K06/10	Female	53	Right superior lobe	Well-circumscribed nodules, fibrosis, necrosis	Mitotic figures, pleomorphic, infiltrating, malignant (Fig. 4.25, B)	ACA
K125/11	Male	39	Right superior lobe	Massive mediastinal tumor (120x110mm), texture is firm and gritty, adherent to superior vena cava (SVC)	Low-grade and ill-defined, dysplastic, anaplastic, fibrous bands amongst malignant cells, necrosis, calcification (Fig. 4.25, C and D)	Poly-differentiated tumor
K51/12	Male	56	Right lung	Fibrosis, infiltration into surrounding parenchyma, necrosis (Fig. 4.24, A)	Malignant, low-grade and ill-defined, sarcoma or sarcoma-like elements	Sarcoma-toid
K94/12	Male	60	Both lungs	Fibrous thickening, necrosis in parenchyma, nodules, extensive fibrosis (Fig. 4.24, B)	Well-defined border, necrosis, keratinization ("keratin pearls"), squamous cells, infiltrating	Squamous cell CA
K106/12	Male	44	Both lungs	Nodular appearance	Dysplastic, low-grade, ill-defined	ACA

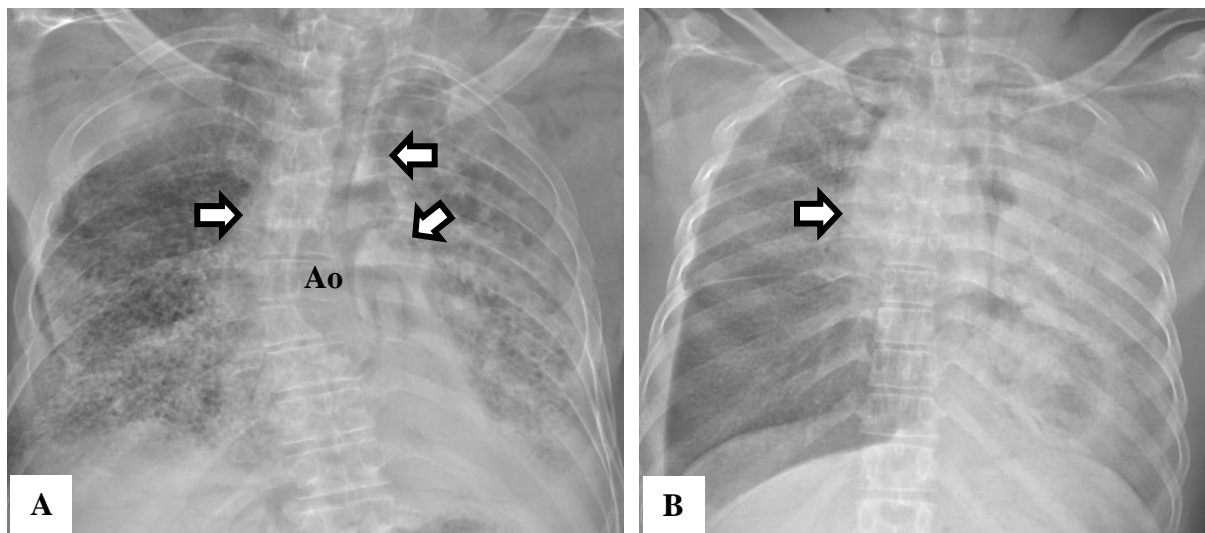


Figure 4.23. Radiologic appearance of pulmonary tumors. A) A large mass (blocked arrows) in the hilar areas of both lungs, posterior to the heart (cadaver K94/12); B) large mediastinal tumor in the middle of the chest X-ray (blocked arrow), obscuring the heart of cadaver K125/11; ascending aorta (Ao).

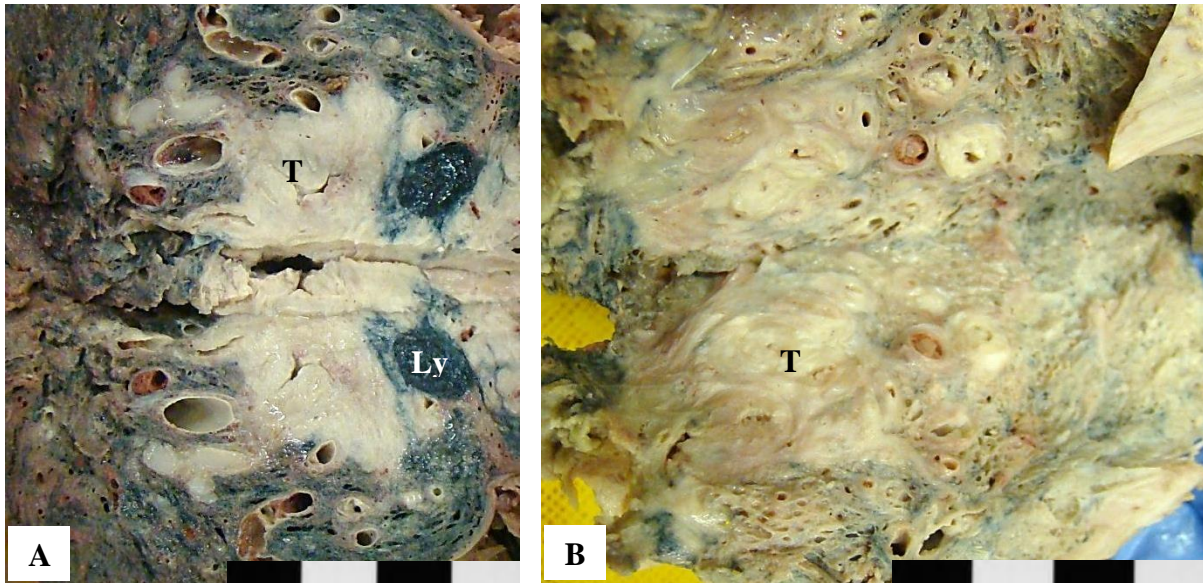


Figure 4.24. Macroscopic appearance of sarcomatoid and squamous cell carcinoma. A) Infiltrating mass (T) with accompanying lymphadenopathy (Ly) in the right inferior lobe of cadaver K51/12, superior and inferior view; B) large mass (T) with a thick, fibrotic appearance in the hilum of the left lung of cadaver K94/12, superior and inferior view.

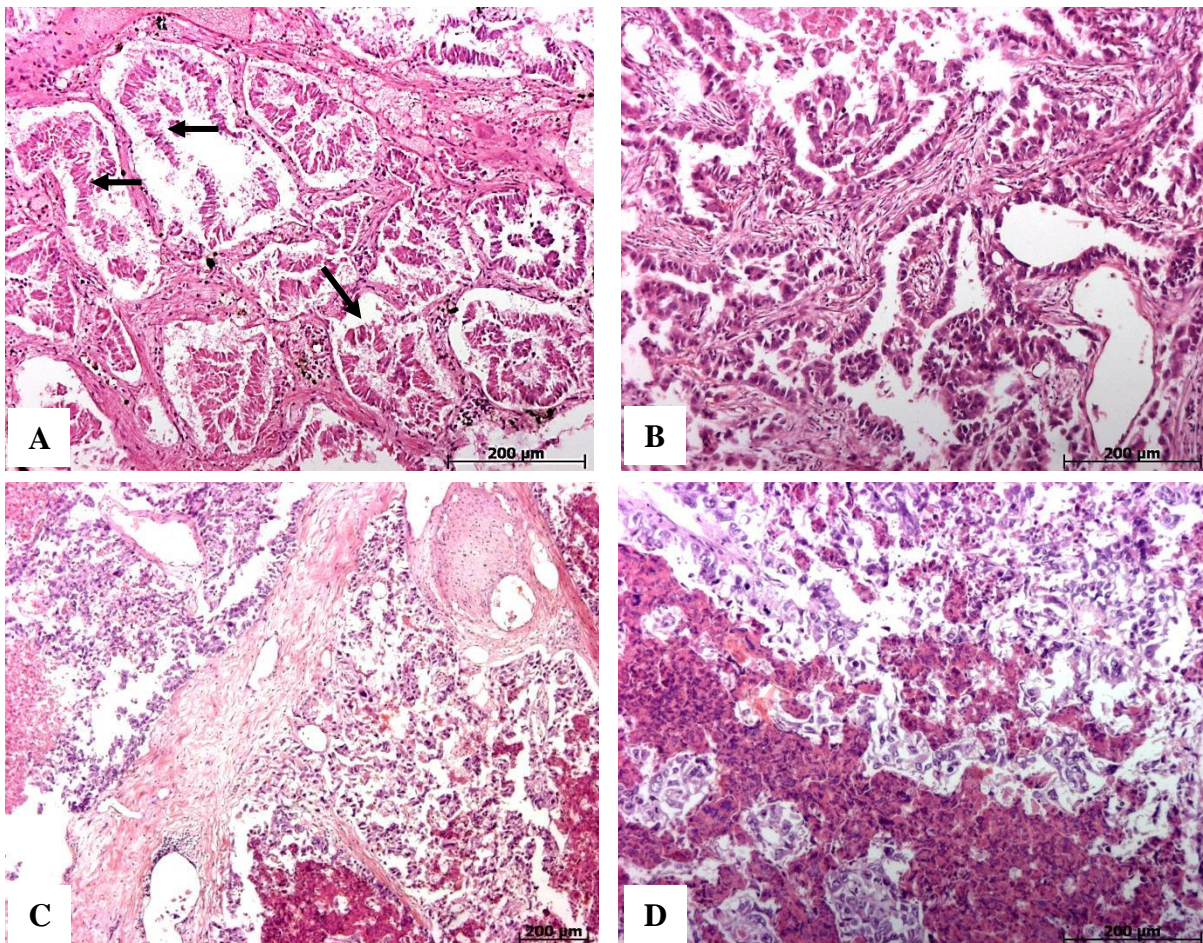


Figure 4.25. Microscopic appearance of pulmonary neoplasms. A) Adenocarcinoma *in situ* (AIS) (arrows) in the right inferior lobe of cadaver K01/10, H&E (100x); B) invasive adenocarcinoma (ACA) in the alveoli of cadaver K06/10, H&E (100x); C) poly-differentiated carcinoma in cadaver K125/11, H&E (25x); D) magnification of the poly-differentiated carcinoma in K125/11, H&E (100x).

4.1.6 Pneumoconiosis

Coal-worker's pneumoconiosis (CWP) was observed in 91 (71.7%) of the cadavers. This disease is also known as "black lung disease" due to the darker discoloration of the pulmonary parenchyma as a result of inhalation of carbon particles. Black pigmentation (anthracosis) of the lungs was seen in the cadavers, ranging from foci of accentuated pigmentation to increased pigmentation throughout the entire lung. In some cases, anthracosis was a common incidental finding. The pigmentation was present on the pleura, parenchyma or both and was most extensive in the superior zones of the lung (Figure 4.26). The lungs with CWP often presented with palpable nodules. Histologically, the spectrum of CWP ranged from minimal pigmentation within the interstitium to larger, coal dust macules (Figure 4.27). These macules consisted of focal interstitial pigment deposition close to the respiratory bronchioles. Focal emphysematous lesions were found neighboring these macules. In some instances, carbon pigment-laden alveolar macrophages were found within the airspaces, while deposition of pigment was seen along the route of lymphatic drainage. Hilar lymph nodes were frequently affected as a result of the accumulation of pigment-laden macrophages within the nodes.



Figure 4.26. Macroscopic appearance of anthracosis. A) Black pigmentation of the left lung of cadaver K42/10, antero-lateral view; B) extensively anthracotic pigmentation in the right lung of cadaver K18/10, antero-lateral view; C) postero-medial view of the right lung of K89/09; D) postero-medial view of the right lung of cadaver K82/09; Bronchus (Br), lymph node, inferior pulmonary vein (IV), lymph node (L), pulmonary artery (PA), superior pulmonary vein (S).

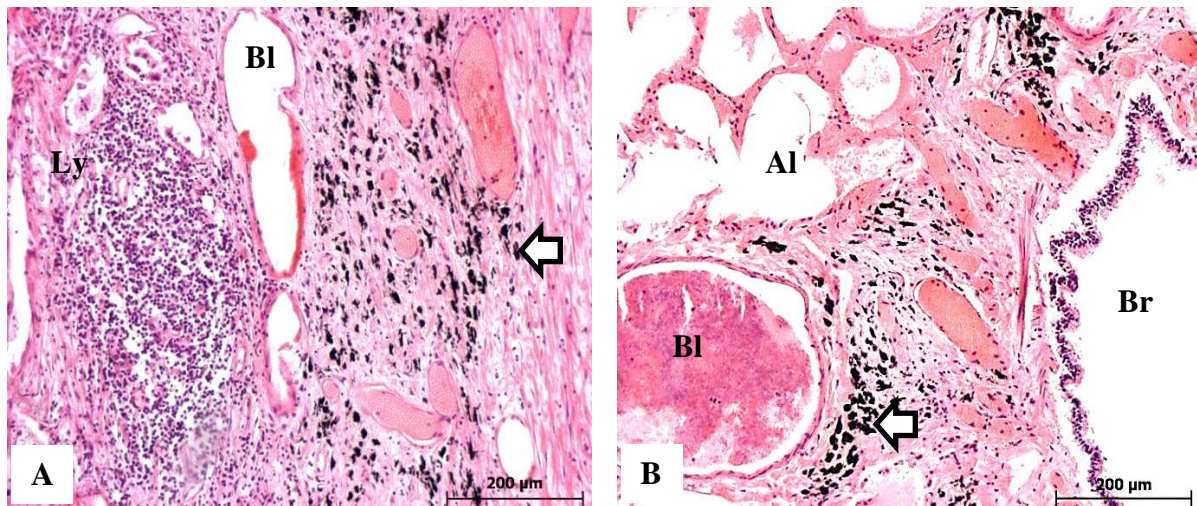


Figure 4.27. Microscopic appearance of anthracotic pigmentation within pulmonary tissue. A) Right superior lobe of cadaver K12/10, H&E (100x); B) left superior lobe of cadaver K47/10, H&E (200x); alveoli (Al); anthracosis (blocked arrows); blood vessel (Bl); bronchiole (Br); lymphocytes (Ly).

4.1.7 Hemosiderosis

Endogenous iron pigment accumulation was observed in 7/127 (5.5%) cadavers. This was seen in cases with pulmonary hemorrhage, either as a localized or diffuse disease. The alveolar macrophages contained phagocytosed hemosiderin (a product of hemoglobin breakdown from red blood cells). These macrophages (also referred to as siderophages) were distinguished from carbon pigment-laden macrophages based on their microscopical appearance (Figure 4.28). In contrast with carbon pigment-laden macrophages, siderophages have a granular, refractive appearance within which the hemosiderin accumulated into larger and smaller granular particles. The Perls Prussian blue stain was used to differentiate between hemosiderin and carbon pigmented macrophages (Figure 4.28, D).

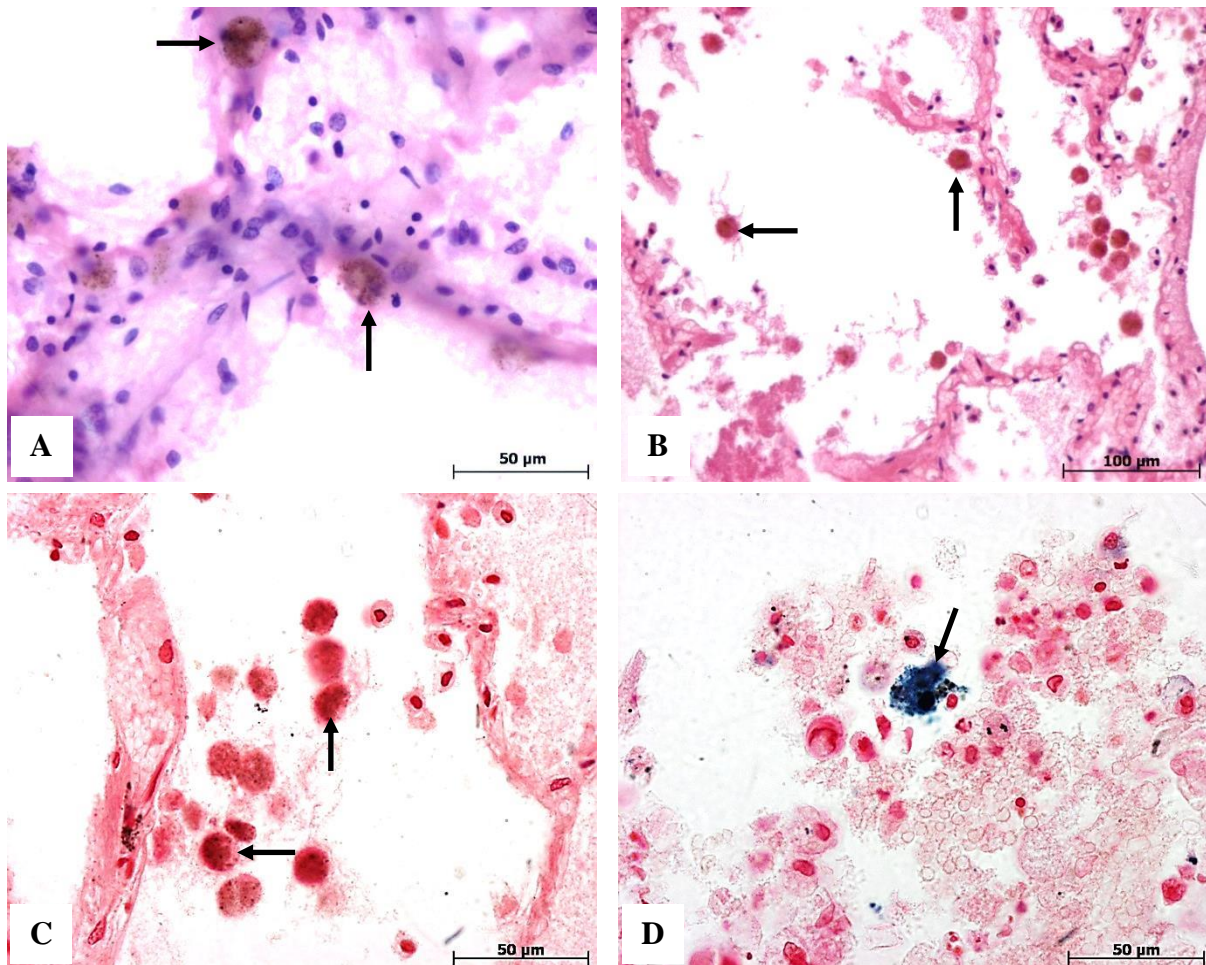


Figure 4.28. Microscopic difference between carbon-laden macrophages and siderophages. A) carbon-laden macrophages (arrows) in the alveolar septa in cadaver K03/10, H&E (400x); B) siderophages (arrows) in the alveolar spaces of cadaver K13/10, H&E (200x); C) Perls' Prussian blue stain with absent iron (K03/10), PPB (400x); D) Perls' Prussian blue with the presence of iron (K06/10), PPB (400x).

4.1.8 Diseases of the Pulmonary Vascular Circulation

4.1.8.1 Pulmonary Hypertension (PH)

Pulmonary hypertension (PH) was observed in 3/127 (2.4%) cadavers (Table 4.14). The male to female ratio was 1.4:1 and the average age of the affected cadavers was 47.7 years. Muscular hypertrophy of the pulmonary arteries were seen in the right superior lobe in 3/4 (75.0%) of the cadavers, while the right inferior lobe was affected in 1/4 (25.0%) cadaver. Histologically, prominent thickening of the arterial tunica media was observed with obvious narrowing of the lumen (Figure 4.29).

Table 4.14. Pulmonary hypertension (PH) in the cadaver cohort (n=127)

<i>Cadaver Ref. Nr.</i>	<i>Sex</i>	<i>Age*</i>	<i>Pulmonary Involvement</i>	<i>Microscopic Findings</i>
K83/09	Male	60	Right superior lobe	Muscular hypertrophy (tunica media)
K10/10	Male	36	Right superior lobe	Muscular hypertrophy of pulmonary arteries
K40/11	Female	*	Right inferior lobe	Muscular hypertrophy (tunica media)
K99/12	Male	47	Right superior lobe	Atherosclerosis of pulmonary artery

* Age is unavailable

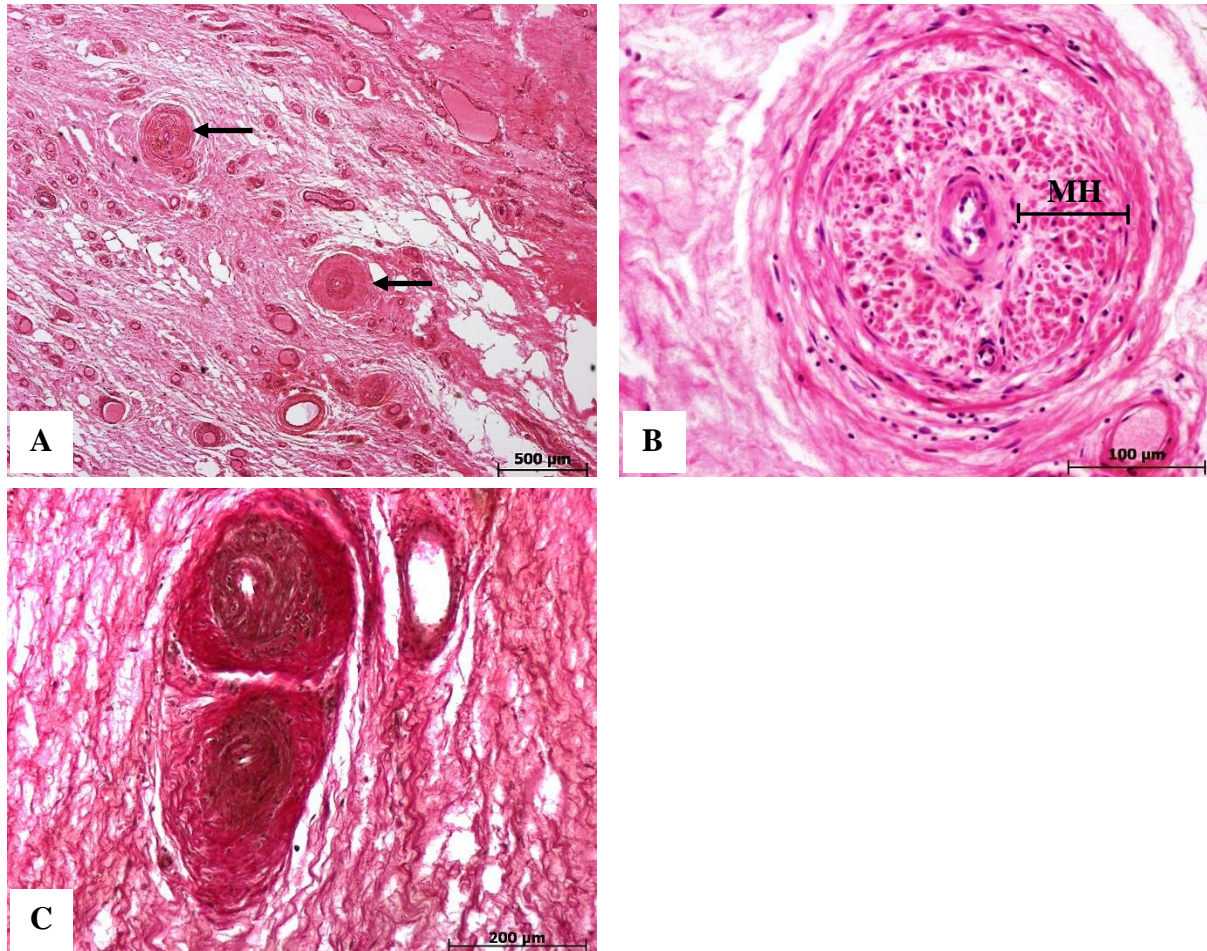


Figure 4.29. Microscopic appearance pulmonary hypertension in cadaver K10/10. A) several pulmonary arteries with muscular hypertrophy in the right superior lobe, H&E (25x); B) muscular hypertrophy (MH) of the tunica media of a pulmonary artery in the right superior lobe, H&E (200x); C) extensive thickening of the pulmonary arterial walls in the right superior lobe, Verhoeff's stain (100x).

4.1.8.2 Bone Marrow Embolism

Pulmonary embolism was observed in 1/127 (0.8%) cadaver. Cadaver K30/10 presented with several bone marrow emboli in the right inferior lobe. Macroscopically (and visible on the Lodox[®] scan), this cadaver appeared to have fractured the right 6th rib prior to his death. The bone marrow consisting of fat elements and hematopoietic tissue dislodged from the fractured

rib entered the arterial circulation which terminated in the pulmonary circulation of the right lung. Histologically, the fat and hematopoietic tissue was observed in the pulmonary arterial system (Figure 4.30). This was an incidental finding during routine histopathological evaluation.

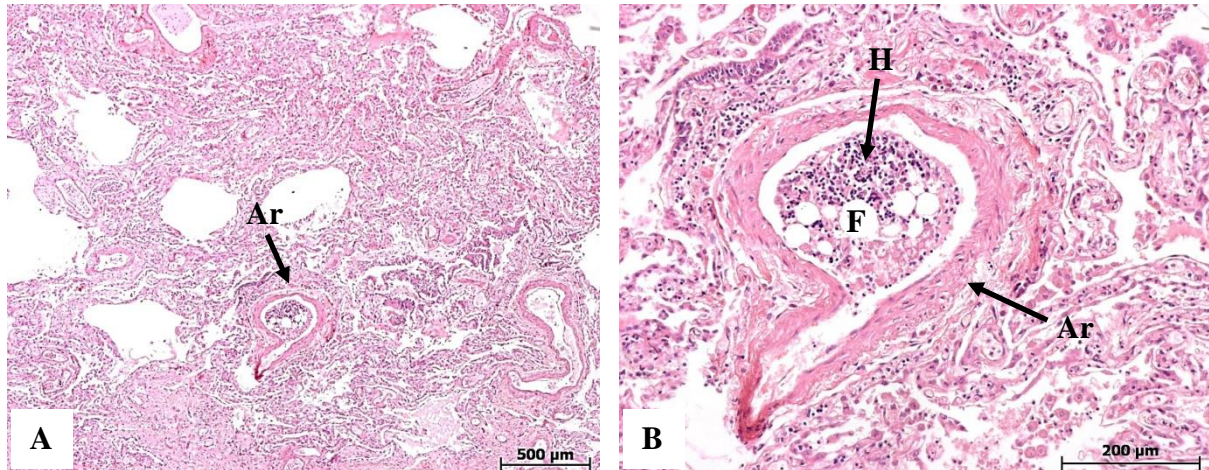


Figure 4.30 Microscopic appearance of a bone marrow embolism of cadaver K30/10. A) a low magnification of a pulmonary artery with bone marrow in the right superior lobe, H&E (25x); B) a higher magnification showing the fat elements and hematopoietic tissue in the pulmonary artery in the right superior lobe, H&E (100x); Artery (Ar), fat elements (F), hematopoietic tissue (H).

4.1.9 Pulmonary Edema

Pulmonary edema was observed microscopically in 95/127 (74.8%) cadavers. The alveoli were filled with a smooth to grainy pink homogenous material (Figure 4.31). In 7/95 (7.4%) cadavers, congested capillaries and erythrocytes within the alveoli were observed. The presence of hemosiderin in the alveoli of these 7 cadavers was illustrated with the Perls Prussian blue stain (Figure 4.28, D) and was indicative of an underlying disease, including left-sided heart failure.

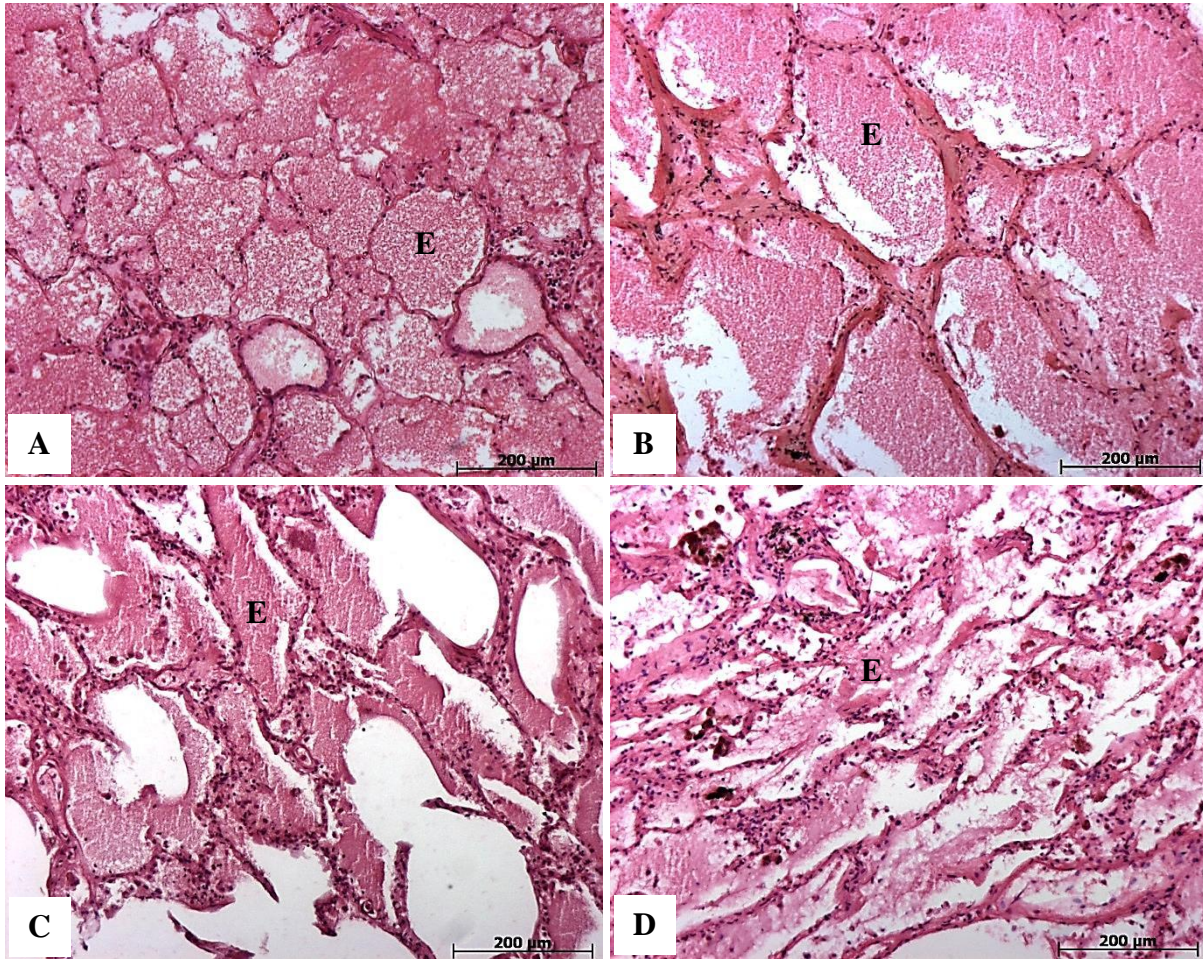


Figure 4.31. Microscopic appearance of pulmonary edema. A) Pulmonary edema within the alveolar spaces of the right inferior lobe of cadaver K04/10, H&E (100x); B) edematous changes within the alveoli of the left inferior lobe of cadaver K42/10, H&E (100x); pulmonary edema in the left superior lobe of cadaver K12/10, H&E (100x); pink, homogenous edematous material in the alveoli of the right superior lobe of cadaver K13/10, H&E (100x); edema (E).

4.2 Cardiovascular System

4.2.1 Cardiac Tuberculosis

No TB lesions were observed in the pericardium, myocardium and the epicardium of the hearts of any of the 127 cadavers.

4.2.2 Cardiomegaly

Extensive cardiomegaly, or extensive enlargement of the heart, was observed in 2/127 (1.6%) of the cadavers (Table 4.15). The male to female ratio was 1:2.3. The CXR of the cadavers with cardiomegaly showed the edge of the left side of the heart appearing far into the left hemithorax (Figure 4.32, A). Cadavers with an adapted heart weight of more than 500g were diagnosed as cardiomegaly.

Table 4.15. Cardiomegaly in the cadaver cohort (n=127)

<i>Cadaver Ref. Nr.</i>	<i>Sex</i>	<i>Underlying Cause</i>	<i>Absolute Weight (g)</i>	<i>Adapted Weight (g)*</i>
K95/09	Male	Stenotic aortic valve	570.0	603.1
K99/12	Female	Hypertrophic heart (Fig. 4.32)	600.0	634.8

* Mean percent change with formalin fixation = + 5.8% (according to Finkbeiner et al., 2004)

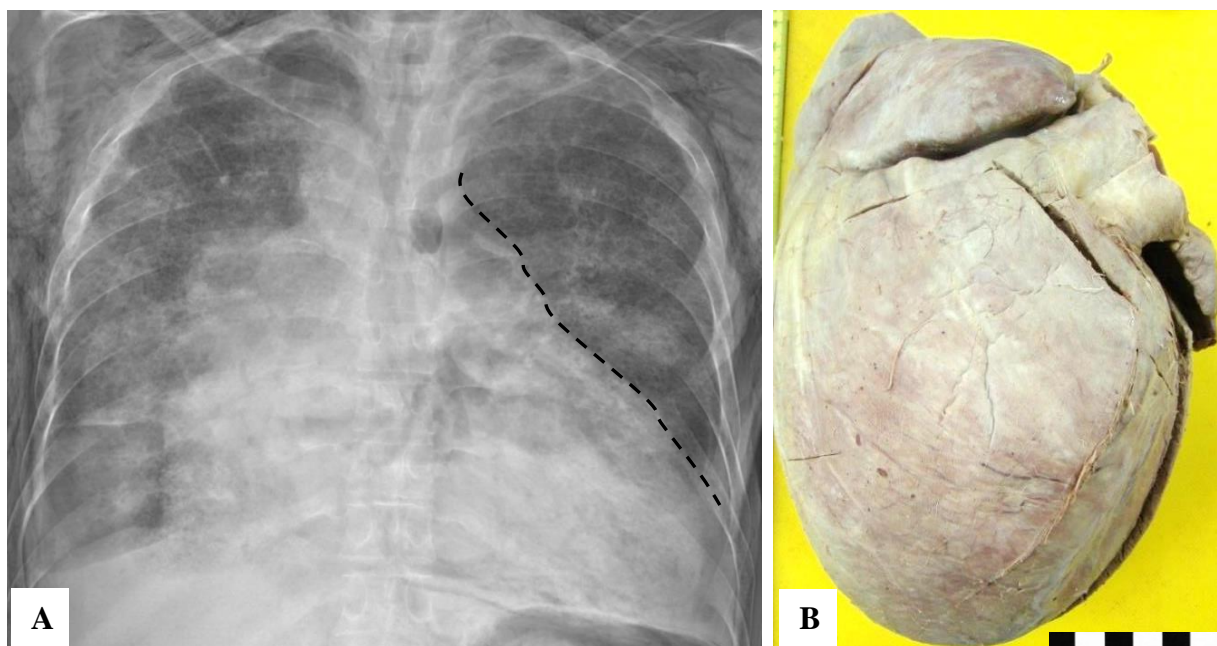


Figure 4.32. Cardiomegaly. A) The chest X-ray (CXR) of cadaver K99/12 is showing the enlarged heart (dashed line); B) the heart measuring 565.2g was removed during gross dissection.

4.2.3 Congenital Heart Disease

One cadaver (1/127; 0.8%) presented with a large atrial septal defect (ASD) measuring 20mm x 30mm (Figure 4.33). The right atrium was dilated possibly as a result of compensation (Figure 4.33, A). The septal defect appeared to be congenital in origin.

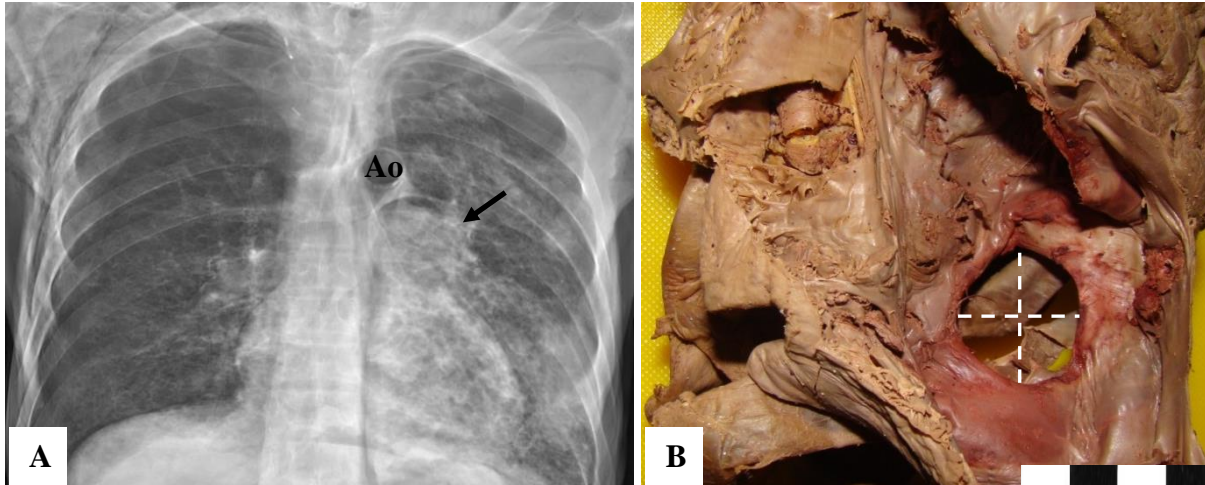


Figure 4.33. Atrial septal defect. A) The heart of cadaver K118/09 is within normal limits on the chest X-ray (CXR), while the right atrium appeared relatively dilated (arrow); B) atrial septal defect (ASD) in the atrial wall of cadaver K118/09 indicated with dotted lines; aortic arch (Ao).

4.2.4 Valvular Heart Disease

The measurements of the cardiac valves of the cadavers can be found in *Addenda C* and *D*. Valvular disease was observed in 34/127 (26.8%) cadavers. The atrioventricular valves were affected in 24/34 (70.6%) cadavers (mitral (100.0%); tricuspid, 0.0%) and the semilunar valves were affected in 22/34 (64.7%) cadavers (aortic (54.5%), pulmonary (45.5%)).

4.2.4.1 Aortic Valvular Stenosis

Aortic valvular stenosis was observed in 12/127 (9.4%) cadavers (Table 4.16). Of the 12 cadavers, atherosclerotic degeneration and calcification of the aortic valve was observed in 3/12 (25.0%) cadavers.

Table 4.16. Aortic stenosis in the cadaver cohort (n=127)

<i>Cadaver Ref. Nr.</i>	<i>Sex</i>	<i>Age†</i>	<i>Measurement (cm)</i>	<i>Absolute Weight (g)</i>	<i>Adapted Weight (g)*</i>	<i>Data from Sunderman et al., 1949 and Kitzman et al., 1988 (mcm)**</i>
K43/11	Female	32	5.0	170.0	179.9	67.0 (60.0-71.0)
K69/11	Female	63	6.0	140.0	148.1	76.0 (73.0-79.0)
K120/11	Female	53	5.5	140.0	148.1	67.0 (60.0-71.0)
K52/12	Male	57	5.4	220.0	232.8	67.0 (60.0-71.0)
K58/12	Male	70	7.0	400.0	423.2	83.0 (81.0-85.0)
K62/12	Female	73	6.5	280.0	296.2	76.0 (73.0-79.0)
K73/12	Male	72	6.8	190.0	201.0	83.0 (81.0-85.0)
K74/12	Female	52	4.6	140.0	148.1	67.0 (60.0-71.0)
K77/12	Female	32	5.5	150.0	158.7	67.0 (60.0-71.0)
K78/12	Male	61	6.0	270.0	285.7	83.0 (81.0-85.0)
K83/12	Male	59	5.8	340.0	359.7	67.0 (60.0-71.0)
K94/12	Male	60	5.7	300.0	317.4	83.0 (81.0-85.0)

* Mean percent change with formalin fixation = + 5.8% (according to Finkbeiner *et al.*, 2004);

** Valvular circumferences comparison (according to Sunderman *et al.*, 1949 and Kitzman *et al.*, 1988);

† Cadavers with unknown age were excluded

4.2.4.2 Mitral Valvular Stenosis

The mitral valvular circumferential measurements in the present study were compared with autopsy specimen measurements done by Sunderman *et al.* (1949) and Kitzman *et al.* (1988).

According to the measurements, mitral stenosis was observed in 24127 (18.9%) cadavers (Table 4.17). One cadaver (0.8%) presented with signs of rheumatic mitral valvulitis. On gross inspection, diffuse fibrous thickening of the mitral leaflets was observed.

Table 4.17. Mitral stenosis in the cadaver cohort (n=127)

<i>Cadaver Ref. Nr.</i>	<i>Sex</i>	<i>Age†</i>	<i>Measurement (cm)</i>	<i>Absolute Weight (g)</i>	<i>Adapted Weight (g)*</i>	<i>Data from Sunderman et al., 1949 and Kitzman et al., 1988 (cm)**</i>
K05/10	Male	30	6.5	220.0	232.8	96.0 (94.0-99.0)
K06/11	Male	37	8.4	150.0	158.7	96.0 (94.0-99.0)
K13/11	Female	47	7.5	130.0	137.5	86.0 (82.0-91.0)
K41/11	Female	29	6.9	220.0	232.8	86.0 (82.0-91.0)
K44/11	Male	48	8.6	280.0	296.2	96.0 (94.0-99.0)
K52/11	Male	48	8.4	250.0	264.5	96.0 (94.0-99.0)
K55/11	Male	43	8.5	230.0	243.3	96.0 (94.0-99.0)
K62/11	Male	83	6.8	190.0	201.0	95.0 (92.0-98.0)
K69/11	Female	63	7.2	140.0	148.1	86.0 (82.0-90.0)
K101/11	Male	50	8.0	220.0	232.8	96.0 (94.0-99.0)
K120/11	Female	53	7.7	140.0	148.1	86.0 (82.0-91.0)
K121/11	Male	50	8.4	220.0	232.8	96.0 (94.0-99.0)
K25/12	Male	39	8.1	210.0	222.2	96.0 (94.0-99.0)
K31/12	Male	45	8.6	210.0	222.2	96.0 (94.0-99.0)
K57/12	Male	51	8.6	230.0	243.3	96.0 (94.0-99.0)
K61/12	Male	52	8.8	250.0	264.5	96.0 (94.0-99.0)
K73/12	Male	72	8.5	190.0	201.0	95.0 (92.0-98.0)

<i>Cadaver Ref. Nr.</i>	<i>Sex</i>	<i>Age</i> †	<i>Measurement (cm)</i>	<i>Absolute Weight (g)</i>	<i>Adapted Weight (g)*</i>	<i>Data from Sunderman et al., 1949 and Kitzman et al., 1988 (mm)**</i>
K74/12	Female	52	7.4	140.0	148.1	86.0 (82.0-91.0)
K75/12	Male	52	8.1	290.0	306.8	96.0 (94.0-99.0)
K93/12	Male	72	7.4	390.0	412.6	95.0 (92.0-98.0)
K94/12	Male	60	8.3	300.0	317.4	95.0 (92.0-98.0)
K99/12	Male	47	8.3	600.0	634.8	96.0 (94.0-99.0)
K101/12	Male	58	7.9	160.0	169.3	96.0 (94.0-99.0)
K104/12	Female	61	7.7	270.0	285.7	86.0 (82.0-90.0)

* Mean percent change with formalin fixation = + 5.8% (according to Finkbeiner *et al.*, 2004);

** Valvular circumferences comparison (according to Sunderman *et al.*, 1949 and Kitzman *et al.*, 1988);

† Cadavers with unknown age were excluded

4.2.4.3 Mitral Valve Replacement

A mechanical mitral valvular replacement was observed in 1/127 (0.8%) cadaver. A double tilting disc valve (*St. Jude Valve*) had been implanted in the mitral valve (Figure 4.34). A fibrotic growth was seen on the lateral disc of the mechanical valve, resulting in an incompetent mitral valve.

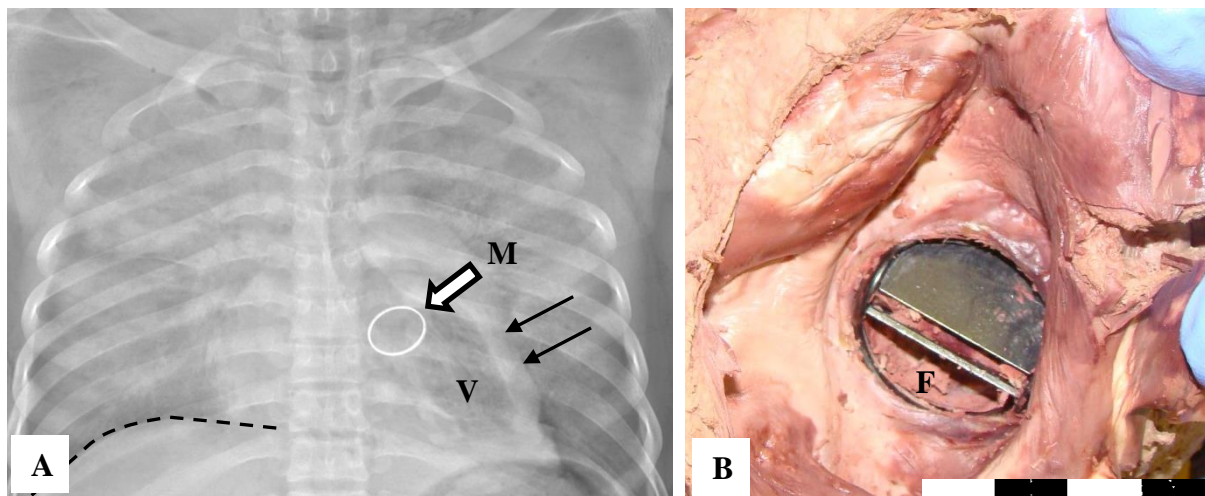


Figure 4.34. Mitral valve replacement. A) chest X-ray of cadaver K87/12; B) mechanical mitral valve replacement; fibrotic tissue (F), left ventricle (V); left ventricle wall (arrows), dome of diaphragm (dashed line).

4.2.4.4 Pulmonary Stenosis

The pulmonary valve circumferential measurements from our cadaver cohort were compared with autopsy specimen measurements performed by Sunderman *et al.* (1949) and Kitzman *et al.* (1988). According to our findings, pulmonary stenosis was observed in 10/127 (7.9%) cadavers (Table 4.18). The pulmonary stenosis was valvular in origin and no ventricular

septal defect was observed in the cadavers with pulmonary stenosis. No subvalvular and supra-avalvular stenosis were observed.

Table 4.18. Pulmonary stenosis in the cadaver cohort (n=127)

<i>Cadaver Ref. Nr.</i>	<i>Sex</i>	<i>Age†</i>	<i>Measurement (cm)</i>	<i>Absolute Weight (g)</i>	<i>Adapted Weight (g)*</i>	<i>Data from Sunderman et al., 1949 and Kitzman et al., 1988 (mm)**</i>
K18/11	Female	76	6.0	225.0	238.1	71.0 (68.0-74.0)
K69/11	Female	63	5.6	140.0	148.1	71.0 (68.0-74.0)
K74/11	Male	70	6.3	170.0	179.9	73.0 (72.0-75.0)
K130/11	Female	81	6.0	150.0	158.7	71.0 (68.0-74.0)
K60/12	Female	22	5.6	110.0	116.4	62.0 (57.0-67.0)
K62/12	Female	73	6.2	280.0	296.2	71.0 (68.0-74.0)
K74/12	Female	52	5.3	140.0	148.1	62.0 (57.0-67.0)
K78/12	Male	61	6.7	270.0	285.7	73.0 (72.0-75.0)
K83/12	Male	59	5.6	340.0	359.7	62.0 (57.0-67.0)
K94/12	Male	60	5.2	300.0	317.4	73.0 (72.0-75.0)

* Mean percent change with formalin fixation = + 5.8% (according to Finkbeiner *et al.*, 2004);

** Valvular circumferences comparison (according to Sunderman *et al.*, 1949 and Kitzman *et al.*, 1988);

† Cadavers with unknown age were excluded

4.2.4.5 Tricuspid Disease

No tricuspid valvular disease was observed in any cadavers in the present study.

4.2.5 Ischemic Heart Disease (IHD)

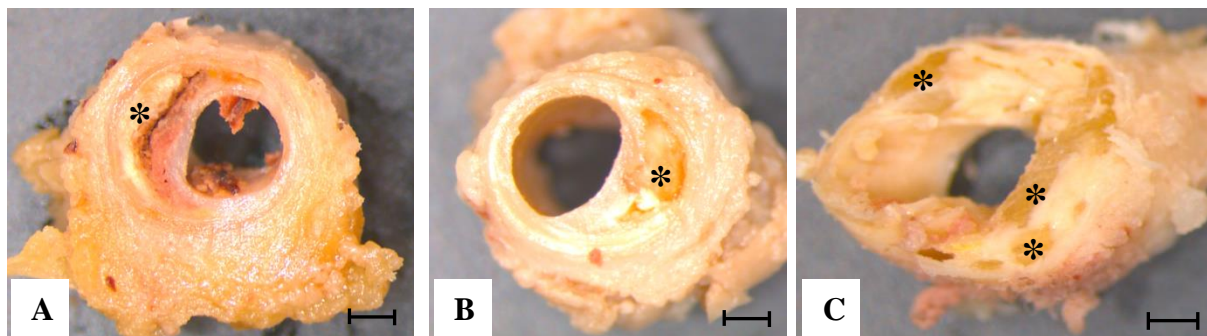
4.2.5.1 Atheromatous Disease of the Coronary Arteries

Atheromatous disease of the coronary arteries were observed in 42/127 (33.1%) cadavers (Table 4.19). The male to female ratio was 1.3:1. The average age was 54.4 years. Atheromatous plaques of varying sizes were observed within the coronary arteries (Figure 4.34). Histological examination revealed that the lumen of the epicardial coronary arteries were narrowed due to the accumulation of lipids, macrophages and smooth muscle cells (Figure 4.35). Critical stenosis ($\geq 70\%$ reduction in arterial lumen) was observed in 11/42 (26.2%) cadavers with coronary atherosclerosis. In 2/42 (4.8%) cadavers, complete obstruction of one coronary artery was observed. No macroscopically obvious atheromatous plaque rupture was observed in any of the cadavers.

Table 4.19. Percentage occlusion in the coronary arteries of the cadavers (n=127)

Cadaver Ref. Nr.	Sex	Age*	Percentage Occlusion in the Epicardial Coronary Arteries			
			LAD (%)	LCx (%)	LCA (%)	RCA (%)
K81/09	Male	44	50	40	*	40
K83/09	Male	60	60	*	50	40
K96/09	Male	*	50	*	*	30
K100/09	Male	45	*	*	*	20
K101/09	Male	48	20	*	*	*
K102/09	Female	28	30	*	*	*
K104/09	Male	*	60	50	*	30
K106/09	Male	*	75	70	*	70
K112/09	Male	58	*	*	*	60
K118/09	Male	*	20	60	*	40
K119/09	Female	50	60	40	*	50
K06/10	Female	53	95	*	*	60
K13/10	Male	47	30	*	*	*
K16/10	Female	45	70	*	*	*
K19/10	Female	63	20	*	*	50
K30/10	Male	*	60	30	*	60
K36/10	Male	82	30	60	*	30
K40/10	Male	47	75	40	*	60
K31/11	Male	53	60	70	*	75
K40/11	Female	*	60	50	*	90
K44/11	Male	48	75	*	*	*
K53/11	Male	*	*	*	*	50
K74/11	Male	70	30	70	*	*
K120/11	Female	53	40	40	*	40
K126/11	Male	45	*	40	*	*
K129/11	Male	65	50	*	*	30
K138/11	Male	57	*	*	*	50
K140/11	Female	42	50	*	*	50
K26/12	Male	*	*	*	70	70
K50/12	Female	*	20	*	*	*
K51/12	Male	56	*	*	*	30
K62/12	Female	73	*	60	*	100
K64/12	Male	50	*	50	*	40
K75/12	Male	52	90	100	*	*
K76/12	Male	*	20	*	*	*
K81/12	Male	49	50	*	*	*
K82/12	Male	63	40	95	*	30
K83/12	Male	59	*	*	*	20
K93/12	Male	72	50	*	*	40
K100/12	Female	46	10	10	*	20
K107/12	Female	62	40	30	*	60
K124/12	Male	55	30	*	*	*

* Patent coronary artery

**Figure 4.35. Coronary artery atherosclerosis.** A) Left anterior descending of cadaver K83/09; B) right coronary artery of cadaver K104/09; C) right coronary artery of cadaver K30/10; calcification (*); bar = 2mm.

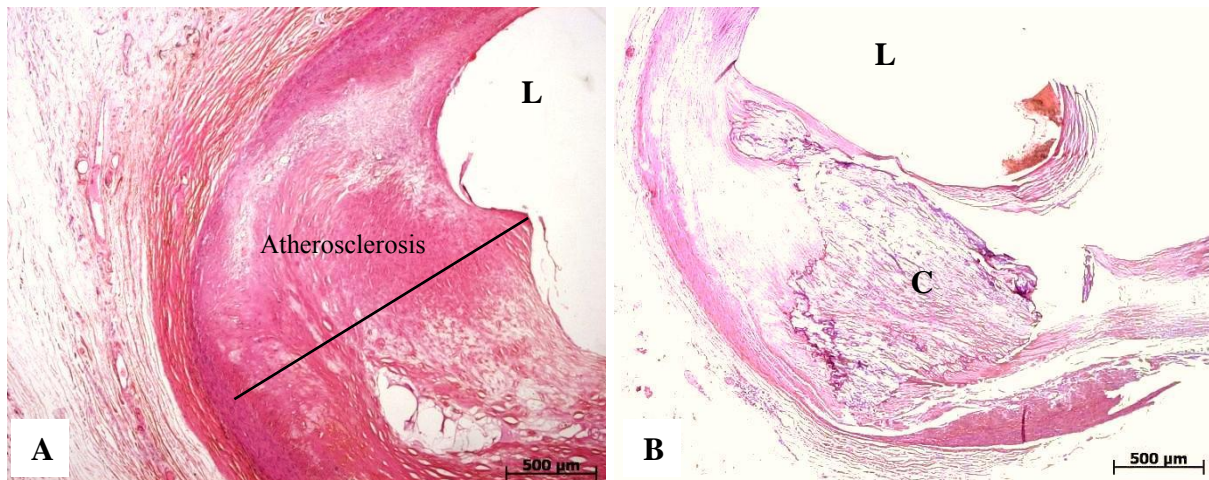


Figure 4.36. Microscopic appearance of coronary artery atherosclerosis. A) Left anterior descending (LAD) coronary artery of cadaver K40/10 showing a prominent thickening of the arterial wall; B) left circumflex (LCx) coronary artery of cadaver K36/10 with calcification; calcification (C), lumen (L).

4.2.5.2 Healed Fibrotic Lesions

Healed fibrotic lesions were observed in 5/127 (3.9%) cadavers (Table 4.20). The male to female ratio was 1.5:1 and the average age of the affected cadavers was 52.8 years. All of these lesions of the myocardium appeared as old, fibrotic infarcts. Macroscopically, fibrotic lesions were seen in myocardium as yellowish-white lesions in the myocardium. Histologically, necrotic muscle fibers with accompanying fibrosis stained light pink with the H&E stain (Figure 4.36).

Table 4.20. Fibrotic lesions in the cardiac wall in the cadaver cohort (n=127)

<i>Cadaver Ref. Nr.</i>	<i>Sex</i>	<i>Age</i>	<i>Macroscopic Appearance</i>	<i>Microscopic Findings</i>	<i>Absolute Weight (g)</i>	<i>Adapted Weight (g)*</i>
K06/10	Female	53	Fibrous lesion in antero-lateral wall of left ventricle	Prominent fibrosis between myocytes (Fig. 4.36)	205.0	216.9
K13/11	Female	47	Thickened/fibrotic left ventricle	Vacuolization, loss of nuclei, fibrosis	130.0	137.5
K44/11	Male	48	Thickened/fibrotic right ventricular wall	Shrunken, irregular myocytes, loss of nuclei, vacuolization	280.0	296.2
K47/11	Male	64	Fibrosis in anterior left ventricle	Fibrosis, irregular myocytes, vacuolization	390.0	412.6
K75/12	Male	52	Extensively thickened anterior left ventricle	Irregular myocytes, loss of nuclei, fibrosis	290.0	306.8

* Mean percent change with formalin fixation = + 5.8% (according to Finkbeiner et al., 2004);

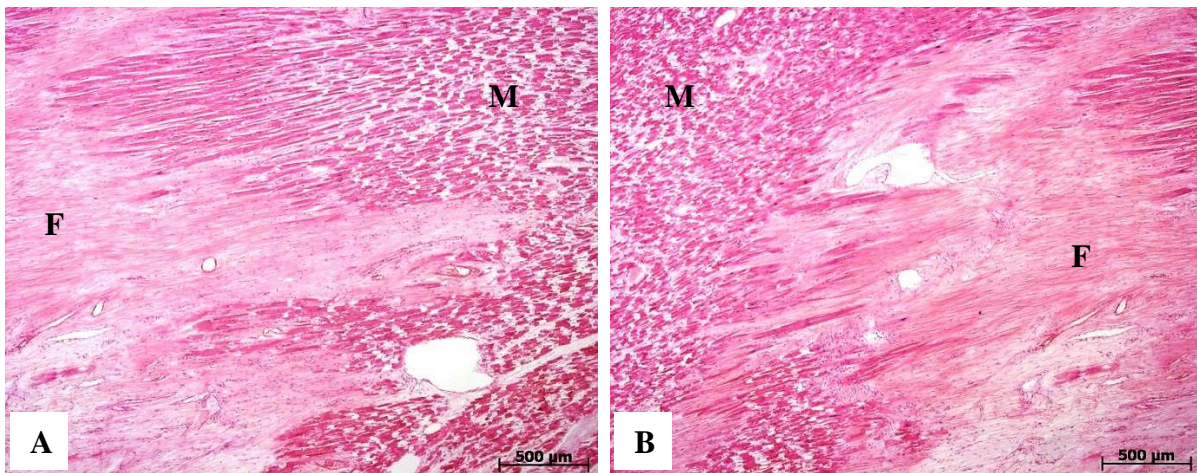


Figure 4.37. Microscopic appearance of fibrotic lesions in the cardiac wall. A) Fibrotic infarction in the left ventricular wall of cadaver K06/10, H&E (25x); B) fibrotic infarction in the left ventricular wall of cadaver K06/10, H&E (25x); fibrosis (F), myocardium (M).

4.2.6 Myocarditis

Myocarditis was observed in 4/127 (3.1%) cadavers (Table 4.21). The male to female ratio was 1.4:1 and the average age of the affected cadavers was 47.0 years. Macroscopically, the affected ventricles were thickened but the final diagnosis was made on microscopic level. Histologically, the myocardium was injured due to the inflammation with a fibrinous exudate on the surface. An inflammatory infiltrate consisting of a mixture of polymorphonuclear neutrophils and lymphocytes was seen amongst the myocytes (Figure 4.37). One cadaver (K124/11) presented with a fibrinopurulent exudate on the surface of the heart. The inflammatory process extended into the myocardial wall (Figure 4.37, B).

Table 4.21. Myocarditis in the cadaver cohort (n=127)

<i>Cadaver Ref. Nr.</i>	<i>Sex</i>	<i>Age*</i>	<i>Macroscopic Appearance</i>	<i>Microscopic Findings</i>	<i>Absolute Weight (g)</i>	<i>Adapted Weight (g)**</i>
K47/10	Male	43	Thickened left ventricular wall	Two small foci of chronic inflammatory infiltrate	205.0	216.9
K44/11	Male	48	Thickened right ventricular wall	Fibro-purulent exudate on surface extending into myocardium, myocyte injury	280.0	296.2
K121/11	Male	50	Thickened left ventricular wall (Fig. 4.37, A)	Foci of myocyte injury, inflammatory infiltrate	220.0	232.8
K124/11	Female	*	Thickened right ventricular wall (Fig. 4.37, B)	Mixed inflammatory infiltrate, fibrinous exudate	160.0	169.3

* Age is unavailable

** Mean percent change with formalin fixation = + 5.8% (according to Finkbeiner et al., 2004)

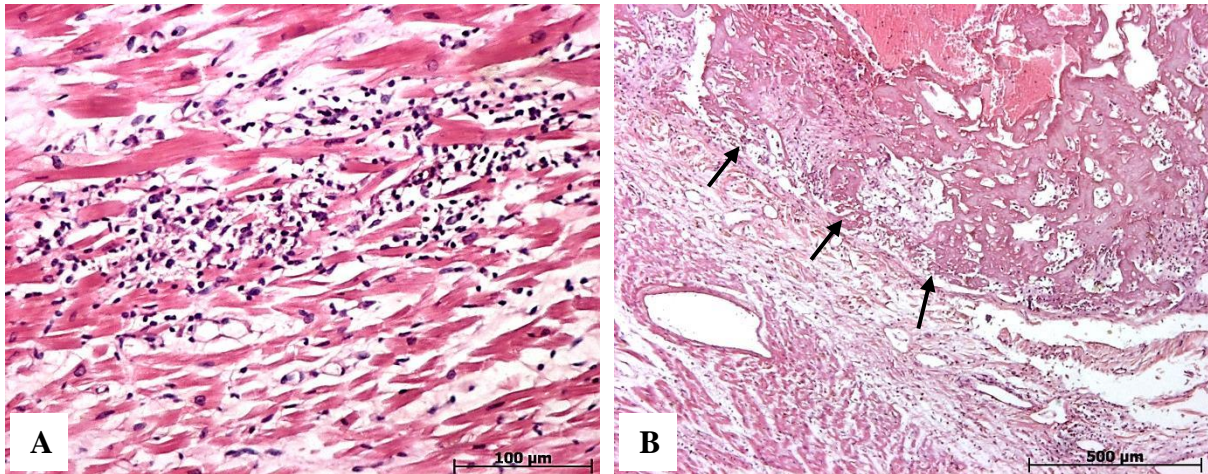


Figure 4.38. Microscopic appearance of myocarditis. A) Chronic inflammatory infiltrate within the left ventricular wall of cadaver K121/11, H&E (200x); B) right ventricle of cadaver K124/11 presented with a fibrinopurulent exudate on the surface of the heart, H&E (50x).

4.2.7 Lipochrome (Lipofuscin) Deposition

The “wear-and-tear” pigment known as lipochrome or lipofuscin was seen histologically in 13/127 (10.2%) cadavers. The male to female ratio was 1 and the average age of the cadavers with lipofuscin deposition within their hearts was 51.1 years. The intracytoplasmic yellow-brown pigment was found mainly in a perinuclear location within the myocardial fibers (Figure 4.39).

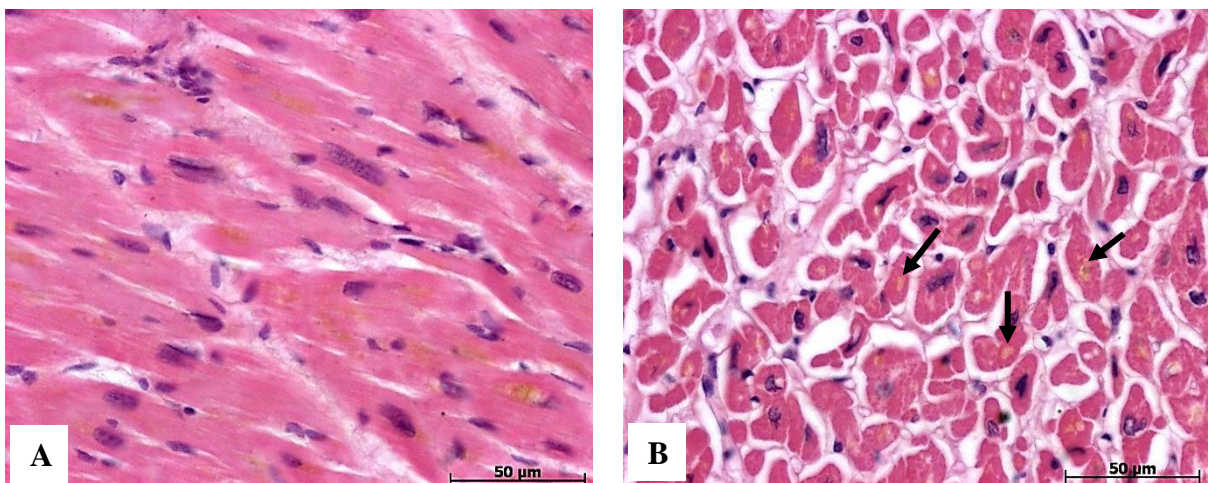


Figure 4.39. Microscopic appearance of lipofuscin. A) Slightly granular yellow-brown pigmentation within the myocardial fibers of the left ventricle of cadaver K76/11, H&E (400x), longitudinal section; B) the yellow-brown pigmentation is visible in a perinuclear location in the left ventricle of cadaver K76/11 (black arrows), H&E (400x) cross-section.

4.2.8 Hypertrophic Obstructive Cardiomyopathy (HOCM)

Hypertrophic obstructive cardiomyopathy (HOCM) was observed in 3/127 (2.4%) cadavers (Table 4.22). The male to female ratio was 1.1:1 and the average age of the affected cadaver was 35.5 years. Myocardial hypertrophy without ventricular dilatation, resulting in smaller than normal ventricular cavities was observed. The septum of the heart was disproportionately thickened. Histologically, myocyte hypertrophy and excessive myocyte branching was seen with box-like nuclei (Figure 4.40). Fibrosis and edema were commonly seen in the HOCM cases.

Table 4.22. Hypertrophic obstructive cardiomyopathy in the cadaver cohort (n=127)

<i>Cadaver Ref. Nr.</i>	<i>Sex</i>	<i>Age*</i>	<i>Macroscopic Appearance</i>	<i>Microscopic Findings</i>	<i>Absolute Weight (g)</i>	<i>Adapted Weight (g)**</i>
K95/09	Male	*	Large heart, thickened ventricular wall and septum	Box-shaped nuclei, fibrosis, myocyte hypertrophy	570.0	603.1
K05/10	Male	30	Left ventricular wall and septum thickened	Edema, fibrosis, box-shaped nuclei, hypertrophy	220.0	232.8
K05/11	Female	41	Left atrium was small, small left ventricular lumen	Branching in cardiac muscle (myocyte disarray)	170.0	179.9

* Age is unavailable

** Mean percent change with formalin fixation = + 5.8% (according to Finkbeiner et al., 2004);

Table 4.23. Measurement of the cardiac chamber walls of the cadavers with HOCM

<i>Cadaver Ref. Nr.</i>	<i>Sex</i>	<i>Age*</i>	<i>Left Ventricle (mm)**</i>	<i>Septum (mm)**</i>	<i>Right Ventricle (mm)**</i>	<i>Data from Sunderman et al. 1988 (mm)***</i>
K95/09	Male	*	17	14	5	LV = 12.0; S = 13.0; RV = 4.0
K05/10	Male	30	18	20	3	LV = 12.0; S = 13.0; RV = 4.0
K05/11	Female	41	14	13	5	LV = 12.0; S = 13.0; RV = 4.0

* Age is unavailable

** Wall thickness measured in the area with the largest width

*** Wall thickness comparison based on age and sex (according to Sunderman *et al.*, 1988); left ventricle (LV), septum (S), right ventricle (RV)

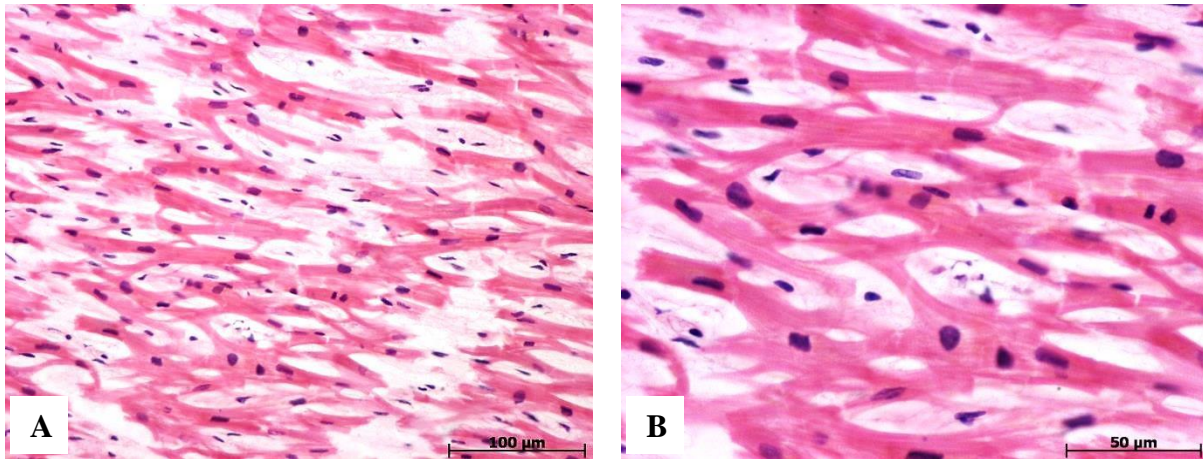


Figure 4.40. Microscopic appearance of hypertrophic obstructive cardiomyopathy (HOCM). A) Myocyte branching in the septum of cadaver K05/10, H&E (200x); B) prominent myocyte branching in the septum of cadaver K05/10, H&E (400x).

4.2.9 Vascular Pathology

4.2.9.1 Arterial Atherosclerosis

Atherosclerotic plaques in the ascending aorta (Figure 4.40) were observed in 28/127 (22.0%) cadavers, 18/127 (14.2%) in the aortic arch and 18/127 (14.2%) in the descending aorta (Table 4.24). Abdominal aortic atherosclerosis was observed in 29 (22.8%) cadavers. In the abdominal region, the plaques were more noticeable inferior to the origins of the large arterial branches supplying the GIT and kidneys. The atherosclerotic plaques were also prominent in the area where the aorta bifurcates into the common iliac arteries. The right and left common iliac arteries were affected by atherosclerosis in 9/127 (7.1%) cadavers, respectively. Histologically, cholesterol slits (Figure 4.41, A) were observed as well as calcification (Figure 4.41, B) within the atheromatous plaques.

Table 4.24. Arterial atherosclerosis in the cadaver cohort (n=127)

<i>Cohort</i>	<i>Ascending Aorta</i>	<i>Aortic Arch</i>	<i>Descending Thoracic Aorta</i>	<i>Abdominal Aorta</i>	<i>R Common Iliac</i>	<i>L Common Iliac</i>
2011	8/40 (20.0%)	4/40 (10.0%)	5/40 (12.5%)	9/40 (22.5%)	6/40 (15.0%)	7/40 (17.5%)
2012	7/43 (16.3%)	7/43 (16.3%)	8/43 (18.6%)	10/43 (23.3%)	1/43 (2.3%)	0%
2013	13/44 (29.5%)	7/44 (15.9%)	5/44 (11.4%)	10/44 (22.7%)	2/44 (4.5%)	2/44 (4.5%)
TOTAL	28/127 (22.0%)	18/127 (14.2%)	18/127 (14.2%)	29/127 (22.8%)	9/127 (7.1%)	9/127 (7.1%)

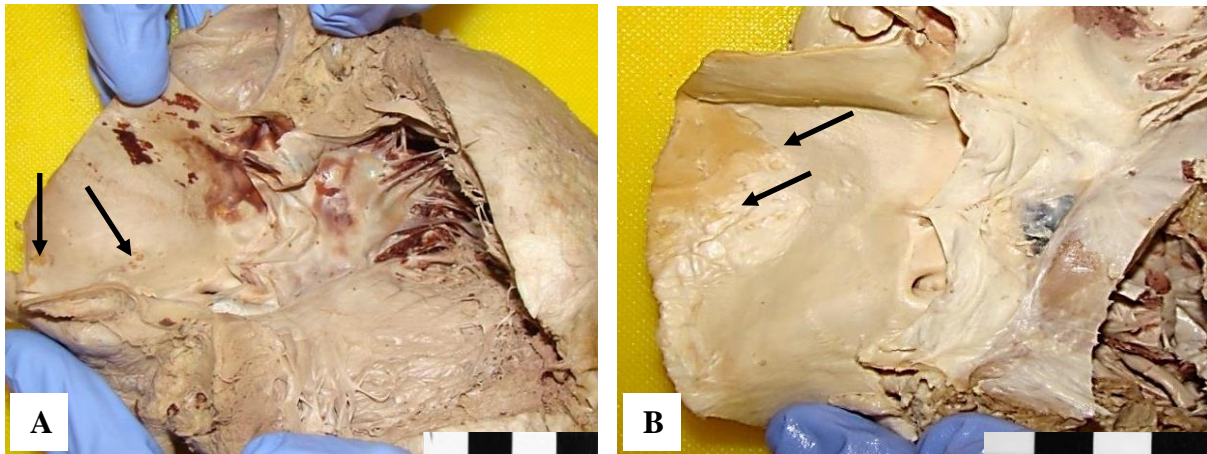


Figure 4.41. Aortic atherosclerosis superior to the aortic valve. A) Small atherosclerotic plaques superior to the aortic valvular cusps (K50/12); B) atherosclerosis superior to the aortic valvular cusps (K58/12).

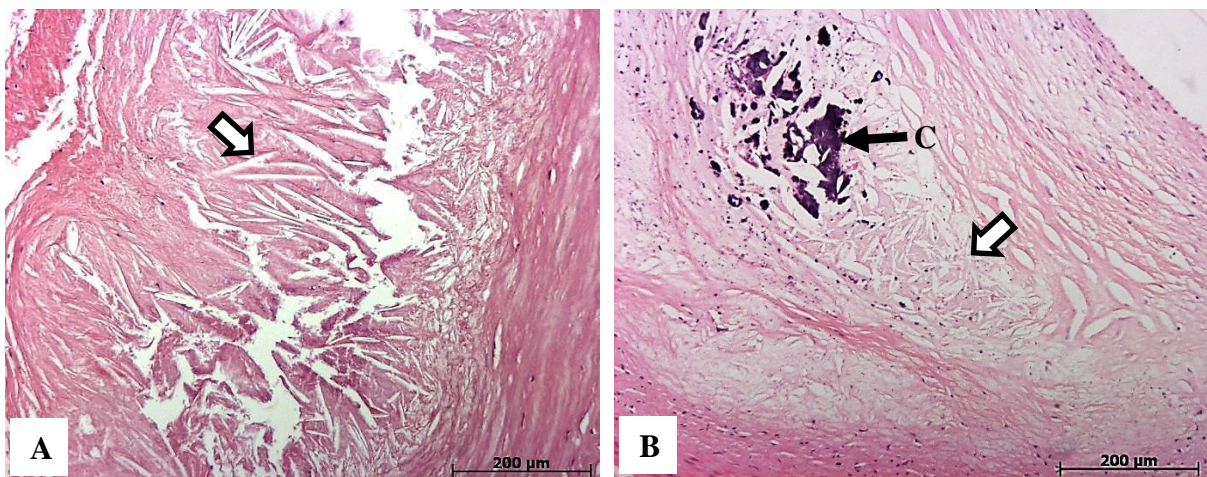


Figure 4.42. Aortic cholesterol slits. A) Cholesterol slits (blocked arrow) in the aortic atheroma of cadaver K101/09, H&E (100x); B) cholesterol slits (blocked arrow) in the tunica media of the left anterior descending (LAD) with concomitant calcification (C) of cadaver K119/09, H&E (100x).

4.2.9.2 Arterial Aneurysms

The types of arterial aneurysms observed in the cadavers included fusiform aneurysms and arterial dissections. The abdominal aorta between the renal and iliac arteries was affected in 9/127 (7.1%) cadavers (Table 4.25). The right common iliac artery was affected in 8/127 (6.3%) cadavers, while 10/127 (7.9%) cadavers had aneurysms in their left common iliac arteries (Table 4.25). Atherosclerotic plaques were commonly found in conjunction with aneurysms. The aneurysms were of the fusiform type (Figure 4.43). Abdominal aortic

aneurysm repair was noted in 1/127 (0.8%) of the cadavers (K78/12). The repair was done by inserting a Dacron[®] graft into the abdominal aorta. The suture lines were all intact.

Table 4.25. Arterial aneurysms in the cadaver cohort (n=127)

<i>Cohort</i>	<i>Ascending Aorta</i>	<i>Aortic Arch</i>	<i>Descending Thoracic Aorta</i>	<i>Abdominal Aorta</i>	<i>Right Common Iliac</i>	<i>Left Common Iliac</i>
2011	0%	0%	0%	5/40 (12.5%)	4/40 (10.0%)	6/40 (15.0%)
2012	0%	0%	0%	3/43 (7.0%)	3/43 (7.0%)	2/43 (4.7%)
2013	0%	0%	0%	1/44 (2.3%)	1/44 (2.3%)	1/44 (2.3%)
TOTAL	0%	0%	0%	9/127 (7.1%)	8/127 (6.3%)	10/127 (7.9%)



Figure 4.43. Fusiform abdominal aneurysm. This cadaver (K106/09) presented with a fusiform abdominal aneurysm in the area superior to the aortic bifurcation (blocked arrow) and a fusiform aneurysm in the right iliac artery (dashed line).

A dissecting aneurysm was seen in 1/127 (0.8%) of the cadavers (Table 4.26). Cadaver K113/09 presented with a blood-filled channel in the external iliac arterial wall (Figure 4.44).

Table 4.26. Arterial dissection in the cadaver cohort (n=127)

<i>Cadaver Ref. Nr.</i>	<i>Sex</i>	<i>Age</i>	<i>Anatomical Region</i>	<i>Macroscopical Appearance</i>
K113/09	Male	40	Right inguinal fossa	Right external iliac artery

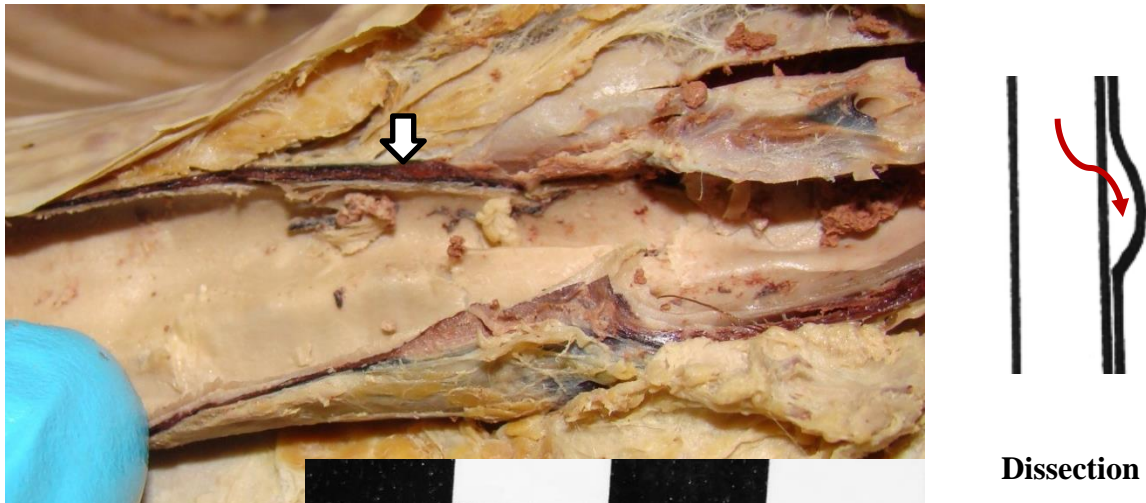


Figure 4.44. Arterial dissection. This cadaver (K113/09) presented with a “dissecting aneurysm” in the right external iliac artery located in the right inguinal fossa.

4.2.9.3 Venous Aneurysms

Large, bilateral popliteal venous aneurysms were observed in cadaver K82/09 (Table 4.27). These aneurysms were of the saccular-type (Figure 4.45). The largest of the venous aneurysms were noted on the right and measured approximately 25x15mm in maximum dimensions. Smaller saccular aneurysms were noted in the right gastrocnemius muscle. A slightly smaller saccular venous aneurysm was noted in the left popliteal vein. No other aneurysms were noted in the venous drainage of the left limb.

Table 4.27. Venous aneurysm in the cadaver cohort (n=127)

<i>Cadaver Ref. Nr.</i>	<i>Sex</i>	<i>Age</i>	<i>Anatomical Region</i>	<i>Macroscopical Appearance</i>
K82/09	Male	47	Popliteal fossa	Bilateral saccular aneurysms in popliteal veins

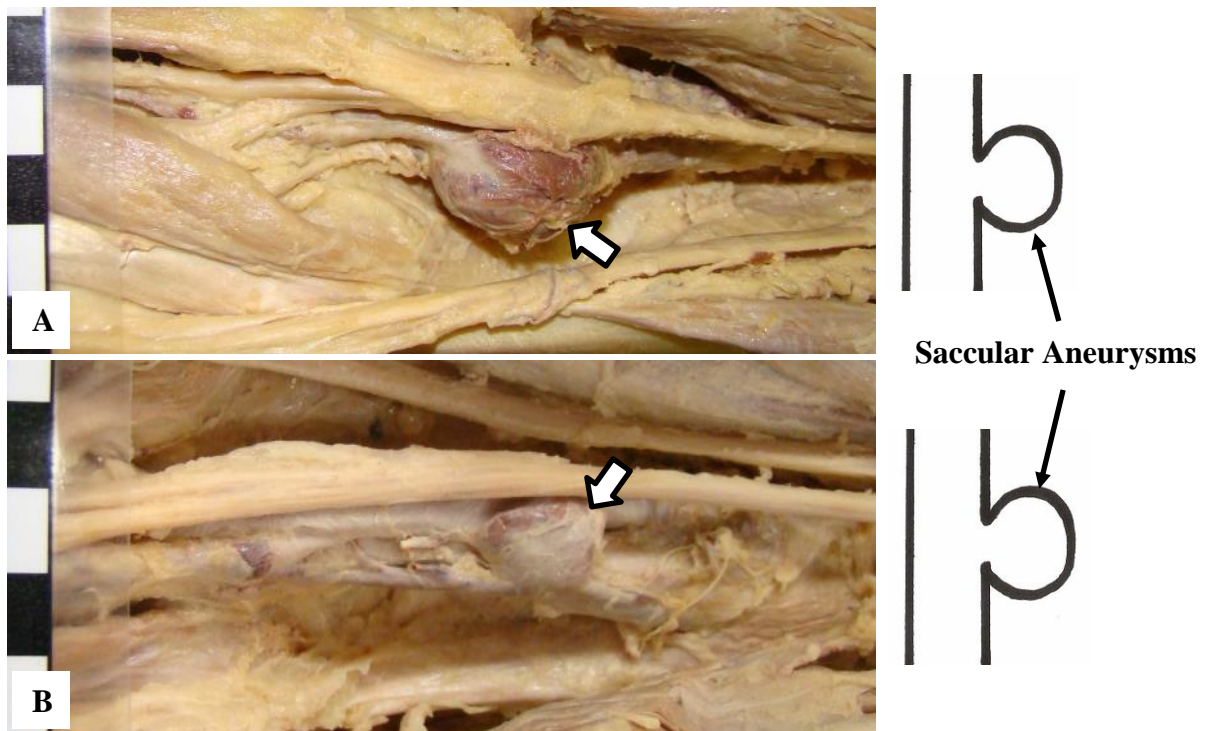


Figure 4.45. Popliteal venous aneurysms. Bilateral popliteal venous aneurysms (K82/09). A) right popliteal venous aneurysm (blocked arrow), posterior view; B) left popliteal venous aneurysm (blocked arrow), posterior view.

4.2.9.4 Hemangiomas

Hemangiomas, a hamartomatous malformation, are not a true tumor and were found in 1/127 (0.8%) cadaver (Table 4.28). The hepatic hemangioma was an incidental finding during gross anatomy dissection. The hemangioma was a well-circumscribed, solitary lesion and appeared dark and reddish-brown compared to the adjacent normal hepatic parenchyma (Figure 4.46, A). No sign of central caseation was seen. Histologically, the hepatic hemangioma consisted of a mass of vascular channels, some of which contained blood (Figure 4.46, B). The channels were supported by fibrous septa. The vascular channels were capacious (*cavernous hemangioma*) which consisted of loose strands of endothelium-lined connective tissue.

Table 4.28. Hemangioma in the cadaver cohort (n=127)

<i>Cadaver Ref. Nr.</i>	<i>Sex</i>	<i>Age</i>	<i>Anatomical Region</i>	<i>Macroscopical Appearance</i>
K38/10	Male	39	Liver	30x15mm in maximum dimensions enlarged blood-filled spaces

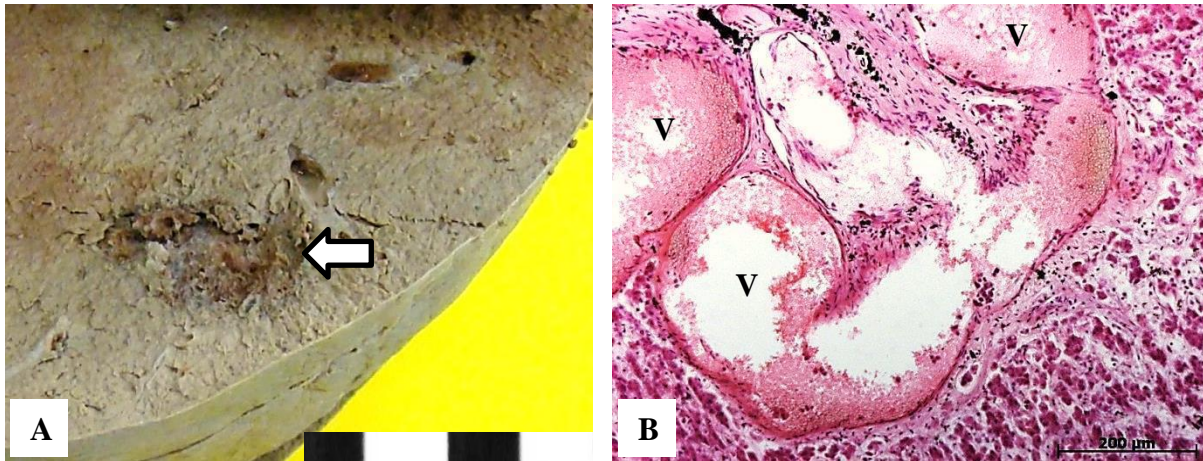


Figure 4.46. Benign hemangioma in the liver. A) Benign hepatic hemangioma in the liver of cadaver K38/10 (blocked arrow); B) prominent blood vessels (V) within the hepatic parenchyma.

4.2.9.5 Kaposi Sarcoma

Kaposi's sarcoma (KS) presented in 1/127 (0.8%) cadaver (Table 4.29). Cadaver K02/10 presented with multiple Kaposi's sarcoma lesions in multiple organs. The lesions manifested in different patterns, ranging from a reddish-brown discoloration (Figure 4.47, A) to black nodules (Figure 4.47, B). The organs that were affected are listed in Table 4.29.

Table 4.29. Organs affected by Kaposi's sarcoma (KS) lesions in cadaver K02/10.

<i>Site of Involvement</i>	<i>Macroscopical Appearance</i>	<i>Histological Appearance</i>
Hard palate (adjacent to the left secondary maxillary molar)	Reddish-brown lesion	Spindle-shaped cells immediately adjacent to vascular spaces of differing sizes (Fig. 4.47, C). Cleft-like spaces containing extravasated erythrocytes (Fig. 4.47, D) (a typical findings of KS). Mild chronic inflammation and hyaline bodies were present (Fig. 4.47, D). In some sections, fibrotic bands reaching into the unaffected tissue were prominent.
Skin on the upper and lower extremities	Small, round, well circumscribed greyish-white lesions	
Superior lobe of the right lung	Nodular on palpation and red-coloured patches	
Pulmonary hilar lymph nodes	Darker discoloration	
Epicardium	Thickened epicardium (up to 13mm in width)	
Left lobe of the liver	Hemorrhagic appearance (resembles hemangioma) (Fig. 4.47, A)	
Greater curvature of the stomach	Dark discoloration (Fig. 4.47, B)	
Spleen	Dark discoloration	
Tail of the pancreas	Dark discoloration	
Proximal jejunum	Black punctate lesions	
Superficial inguinal lymph nodes	Darker discoloration	
Left adrenal gland	Dark discoloration	
Medial aspect of the vastus medialis muscle	Hemorrhagic appearance	
Neurovascular bundle	Hemorrhagic appearance	

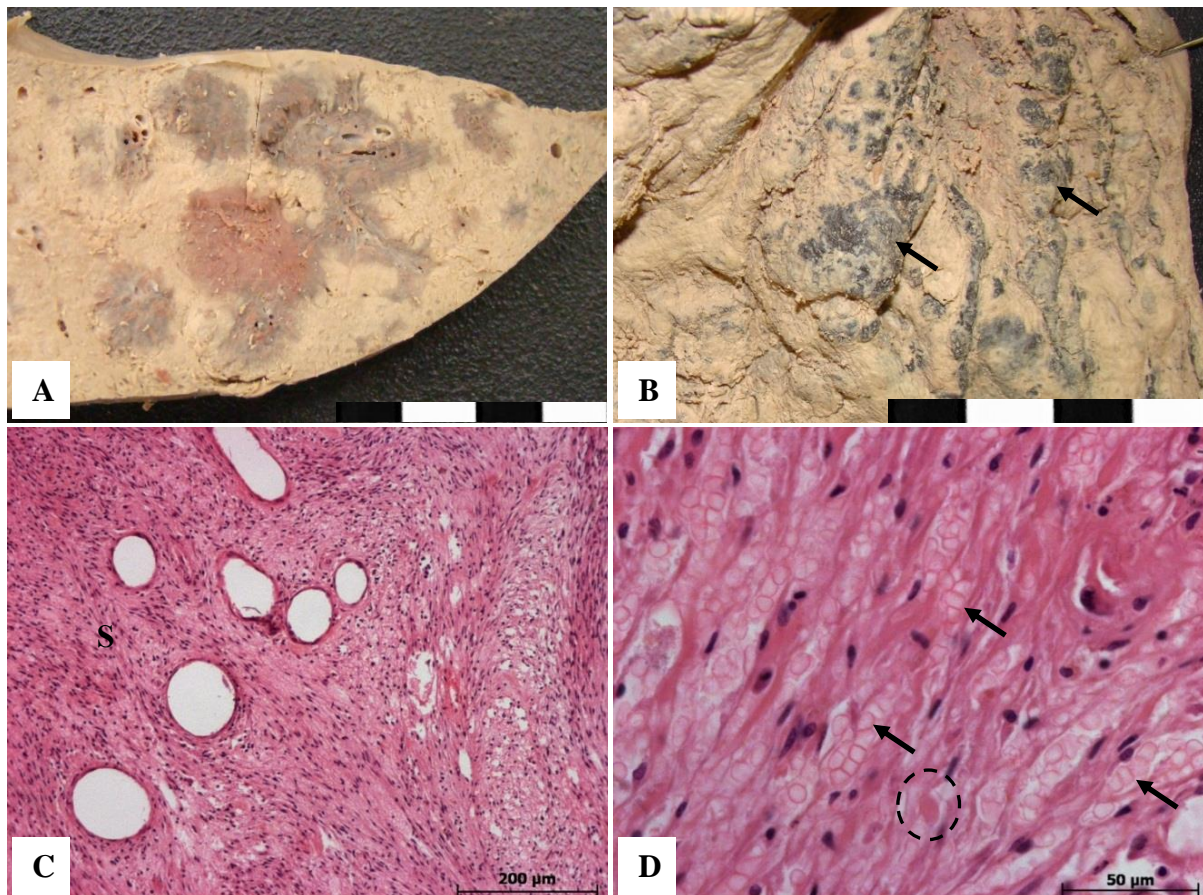


Figure 4.47. Morphology of Kaposi's Sarcoma lesions in an embalmed cadaver. A) Abnormal vascular changes in the left lobe of the liver manifesting as hemorrhagic lesions; B) black lesions (arrows) in the greater curvature of the stomach, C) antero-superior epicardium of the right and left ventricle revealing spindle-shaped cells, H&E (25x); D) hard palate, H&E (400x). A hyaline globule (circle) and extravasated red blood cells (arrows) are typical of KS lesions; spindle-shaped cells (S).

4.3 Gastrointestinal System

4.3.1 Diseases of the Stomach

4.3.1.1 Gastric Tuberculosis

No tuberculous involvement of the stomach of the 127 cadavers was noted.

4.3.1.2 Gastric Ulcers

Gastric ulcers were observed in 5/127 (3.9%) cadavers (Table 4.30). A female preponderance was observed. The majority (3/5; 60%) of the ulcers were observed in the fundus along the greater curvature of the stomach. Macroscopically, the ulcerations were fibrotic comparing to the surrounding gastric mucosa. A fibrotic border lining the ulcer could be seen in the gastric mucosa (Figure 4.48, A). In one cadaver (K16/10), gastric perforation was observed as a result of chronic ulceration. Histologically, the ulcerations were seen as a breach in the gastric mucosal lining with resultant necrosis, fibrosis and inflammatory cells (Figure 4.48, B). Loss of epithelium and extension into the muscular region of the stomach were noted and the ulcers were well-demarcated. None of the gastric ulcers showed signs of hemorrhage.

Table 4.30. Gastric ulcers in the cadaver cohort (n=127)

<i>Cadaver Ref. Nr.</i>	<i>Sex</i>	<i>Age</i>	<i>Anatomical Region</i>	<i>Size</i>
K16/10	Female	45	Fundus (greater curvature) (Fig. 4.48, A)	± 10mm
K75/11	Male	36	Fundus (greater curvature)	Small
K76/11	Female	*	Fundus (greater curvature)	Small (x2)
K124/11	Female	*	Pre-pyloric region	Small
K100/12	Female	46	Smaller curvature (Fig. 4.48, B)	25x10mm

* Age is unavailable

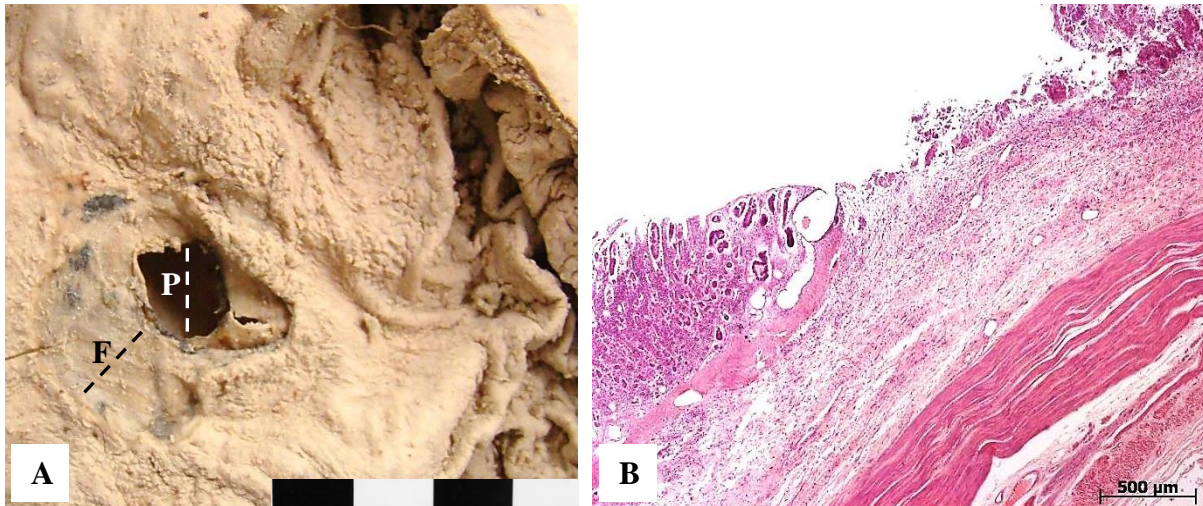


Figure 4.48. The morphology of gastric ulcers. A) a perforated gastric ulcer (P; \pm 10mm) with a surrounding fibrotic area (F) in the gastric fundus (K16/10); B) microscopic appearance of a gastric ulcer in cadaver K100/12, H&E (25x).

4.3.1.3 Gastritis

Dark patches suggestive of gastritis was observed in 11/127 (8.7%) cadavers (Table 4.31). The male to female ratio was 2.1:1 and the average age of the affected cadavers was 50.8 years. The majority of the gastric lesions were observed in the cardia of the stomach. Histologically, these cadavers presented with a mild, chronic superficial gastritis. Numerous chronic inflammatory cells, predominantly lymphocytes were scattered in the lamina propria (Figure 4.49). Mitotic figures at the base of the gastric pits indicated a rapid cell turnover. An acute inflammatory response was seen with a prominent polymorphonuclear infiltrate in the gastric lamina propria and glands. Atrophy of the mucosal glands was observed in some cadavers. No intestinal metaplasia was observed in any of the cadavers.

Table 4.31. Gastritis in the cadaver cohort (n=127)

<i>Cadaver Ref. Nr.</i>	<i>Sex</i>	<i>Age*</i>	<i>Anatomical Region</i>	<i>Microscopy</i>	<i>Type of Gastritis</i>
K81/09	Male	44	Fundus	Foci of chronic inflammatory cells	Chronic gastritis
K118/09	Male	*	Cardia	Chronic inflammatory cells distributed in gastric mucosa	Chronic gastritis
K47/10	Male	43	Fundus	Chronic inflammatory infiltrate	Chronic gastritis
K31/11	Male	53	Cardia	Foci of chronic inflammatory cells	Chronic gastritis
K63/11	Male	*	Cardia	Chronic inflammatory infiltrate (Fig. 4.49, A)	Chronic gastritis
K75/11	Male	36	Cardia	Foci of chronic inflammatory cells (Fig. 4.49, B)	Chronic gastritis
K124/11	Female	*	Cardia	Foci of chronic inflammatory cells	Chronic gastritis

<i>Cadaver Ref. Nr.</i>	<i>Sex</i>	<i>Age*</i>	<i>Anatomical Region</i>	<i>Microscopy</i>	<i>Type of Gastritis</i>
K138/11	Male	57	Cardia and fundus	Extensive chronic inflammatory infiltration	Chronic gastritis
K42/12	Female	*	Cardia	Foci of chronic inflammatory cells	Chronic gastritis
K43/12	Male	*	Cardia and fundus	Chronic inflammatory cells distributed in gastric mucosa	Chronic gastritis
K93/12	Male	72	Cardia	Extensive chronic inflammatory infiltration	Chronic gastritis

* Age is unavailable

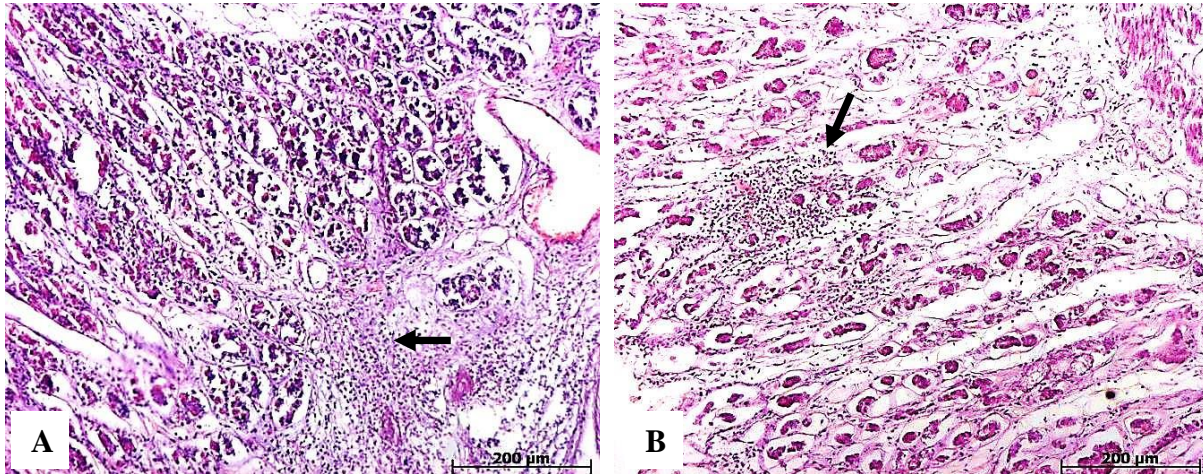


Figure 4.49. Microscopic appearance of chronic gastritis. A) Chronic inflammatory infiltrate in the cardia of cadaver K63/11, H&E (100x); B) chronic infiltrate in the gastric mucosa of cadaver K75/11, H&E (100x).

4.3.2 Diseases of the Intestines

4.3.2.1 Intestinal Tuberculosis

Tuberculous involvement of the intestines was observed in 2/127 (1.6%) cadavers (Table 4.32). The male to female ratio was 1:2.3 years and the average age of the affected cadavers was 32.5 years. Jejunal TB with a typical ulcerative pattern was observed in 1/127 (0.8%) cadaver (Figure 4.50, B). Cecal tuberculous involvement was observed in 1/127 (0.8%) cadaver. The cecal TB was of the hypertrophic type (Figure 4.50, A).

Table 4.32. Tuberculous involvement of the intestines in the cadaver cohort (n=127)

<i>Cadaver Ref. Nr.</i>	<i>Sex</i>	<i>Age*</i>	<i>Intestinal Involvement</i>	<i>Pulmonary Lesions</i>	<i>Extrapulmonary Lesions</i>
K55/11	Male	43	Tuberculous granulomas in the cecum	Bilateral PTB	Hepatic TB
K60/12	Female	22	Tuberculous granulomas in the jejunum	Bilateral PTB	None

* Age is unavailable

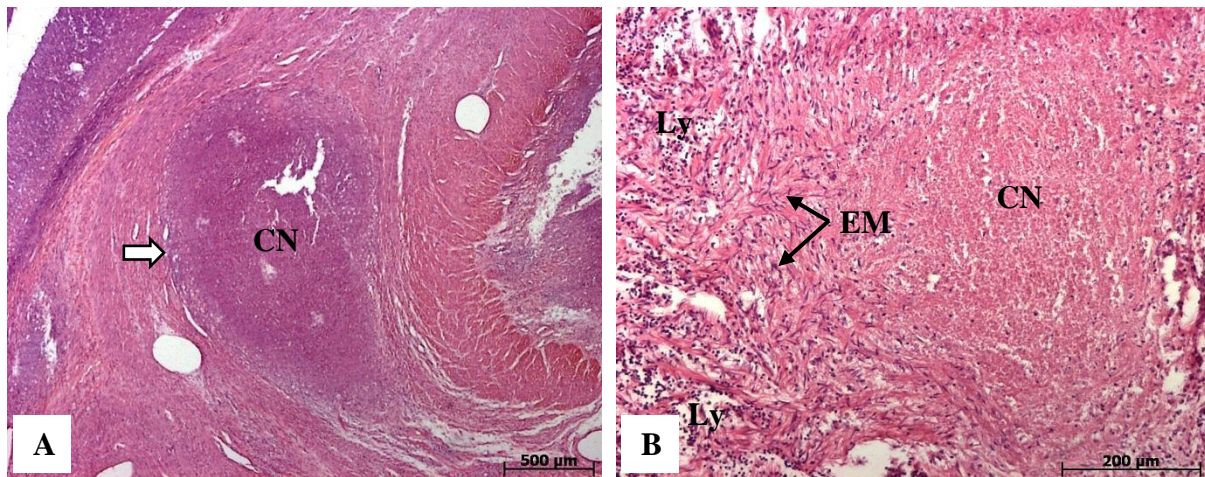


Figure 4.50. Microscopic appearance of intestinal TB. A) A granuloma (blocked arrow) with central caseation (CN) within the caecal wall of cadaver K55/11, H&E (25x); B granuloma with epithelioid macrophages (EM), scattered lymphocytes (Ly) and central caseation in the jejunal wall of cadaver K60/12, H&E (100x).

4.3.2.2 Benign Neoplastic Polyps of Intestinal Mucosa

Benign neoplastic polyps were observed in 6/127 (4.7%) cadavers. The cadavers with benign neoplastic polyps were all males with an average age of 52.2 years. A total of 3/6 (50.0%) were histologically classified as tubular adenoma. Tubular adenomas in the cadavers presented as pedunculated polypoid lesions (Figure 4.51, B). The adenomas were connected to the intestinal mucosa by a stalk of normal tissue (Figure 4.51, C and D). The adenomas observed in the cadavers were seen as solitary lesions with a bosselated appearance. Villous adenomas have a sessile polypoid appearance and was observed in 2/6 (33.3%) cadavers (Table 4.51, A). These adenomas were attached to a broad base and were composed of outgrowths of epithelial cells which were supported by a delicate connective tissue. A sessile serrated adenoma (SSA) was observed in 1/6 (16.7%) cadaver.

Table 4.33. Intestinal polyps and their anatomical locations in the cadaver cohort (n=127)

<i>Cadaver Ref. Nr.</i>	<i>Sex</i>	<i>Age</i>	<i>Anatomical Location</i>	<i>Type of Polyp</i>
K13/10	Male	47	Two small, sessile polyps in the distal colon	Villous adenoma (Fig. 4.51, A)
K52/11	Male	48	Distal colon	Tubular adenoma (Fig. 4.51, C)
K55/11	Male	43	Sessile polyps in the cecum	Sessile serrated adenoma (SSA)
K73/12	Male	72	Pedunculated polyp in the cecum	Tubular adenoma (Fig. 4.51, B)
K83/12	Male	59	Infiltrative nodule - jejunum	Villous adenoma
K106/12	Male	44	Pedunculated polyp in sigmoid colon	Tubular adenoma (Fig. 4.51, D)

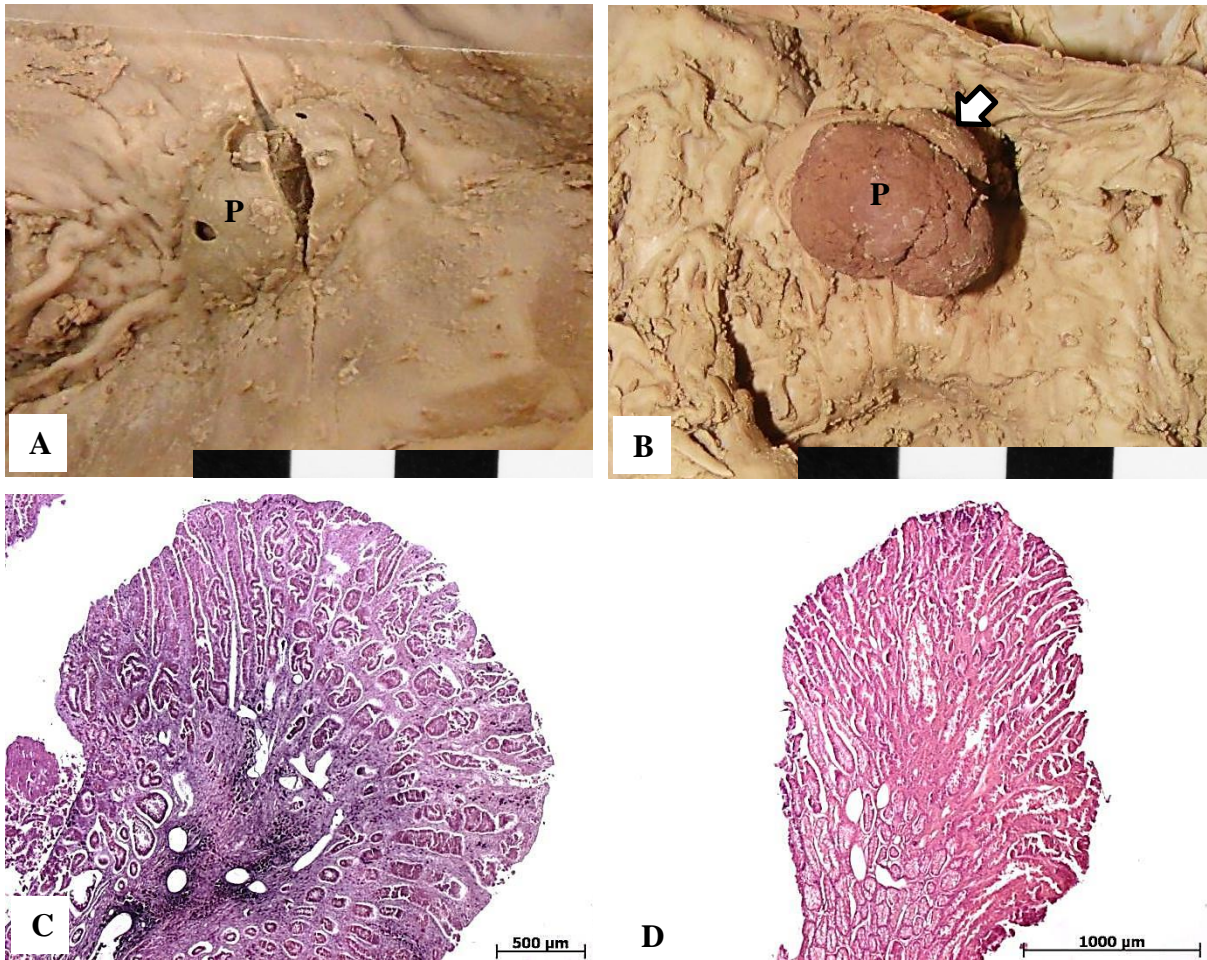


Figure 4.51. Benign neoplastic polyps in the cadaver cohort. A) a small, sessile polyp was observed in the duodenum of cadaver K13/10; B) a pedunculated polyp in the distal colon (K73/12); C) tubular adenoma in cadaver K52/11, H&E (25x); D) tubular adenoma in cadaver K106/12, H&E (25x); polyp (P), stalk (blocked arrow).

4.3.2.3 Intestinal Ulcers

Intestinal ulcers were observed in 5/127 (3.9%) cadavers (Table 4.34). The male to female ratio was 1:1.5. An average age of the affected cadavers was 41.6 years. The distal colon and jejunum were affected (Table 4.34). The area of intestinal ulceration had a darker, more fibrotic appearance during gross dissection (Figure 4.52, A). Histologically, inflammatory infiltrates consisting mostly of lymphocytes and plasma cells, were observed. One cadaver (K46/11) presented with ulcerative colitis (Figure 4.52, B). Three colonic ulcerations confined to the mucosa were seen in the distal colon. Granulomas were absent.

Table 4.34. Intestinal ulcers and their anatomical locations in the cadaver cohort (n=127)

<i>Cadaver Ref. Nr.</i>	<i>Sex</i>	<i>Age</i>	<i>Anatomical Location</i>
K81/09	Male	44	Ulceration in the intestinal mucosa (Fig. 4.52, A)
K46/11	Male	30	Distal colon (3 ulcers) – ulcerative colitis (Fig. 4.52, B)
K138/11	Male	57	Several ulcers - proximal jejunum
K60/12	Female	22	Infiltrative lesions - jejunum
K66/12	Female	55	Several ulcerations – distal colon

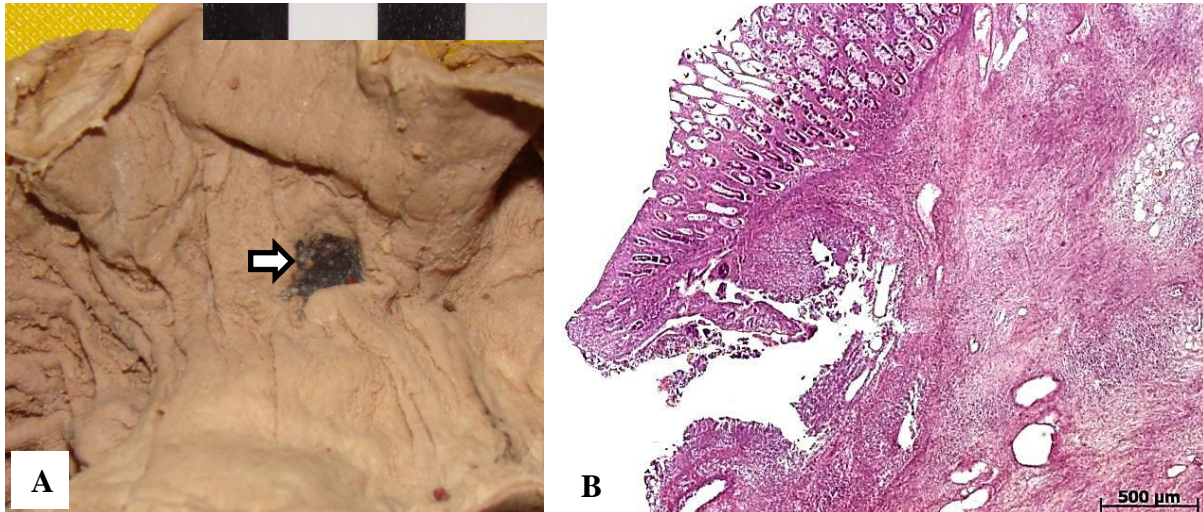


Figure 4.52. The microscopic appearance of intestinal ulcers. A) Intestinal ulceration with dark discoloration in the jejunum of cadaver K81/09 (blocked arrow); B) the border of a colonic ulcer of cadaver K46/11, H&E (25x).

4.3.2.4 Intestinal Neoplasms

4.3.2.4.1 Gastrointestinal Stromal Tumor (GIST)

Gastrointestinal stromal tumor (GIST) was observed in 1/127 (0.8%) cadaver (Table 4.35). It is a rare neoplasm arising from the intestinal mesenchymal cells. The GIST observed in cadaver K99/12 (male, 47 years), measured 27x25mm in maximum dimensions and was located externally to the proximal part of the jejunum (Figure 4.53, A). Histologically, the tumor cells had a spindle-shaped appearance and were arranged in short fascicles and whorls (Figure 4.53, B).

Table 4.35. Gastrointestinal stromal tumor (GIST) in the cadaver cohort (n=127)

<i>Cadaver Ref. Nr.</i>	<i>Sex</i>	<i>Age</i>	<i>Intestinal Involvement</i>	<i>Microscopic Appearance</i>
K99/12	Male	47	Proximal part of the jejunum	Spindle-shaped cells in short fascicles and whorls

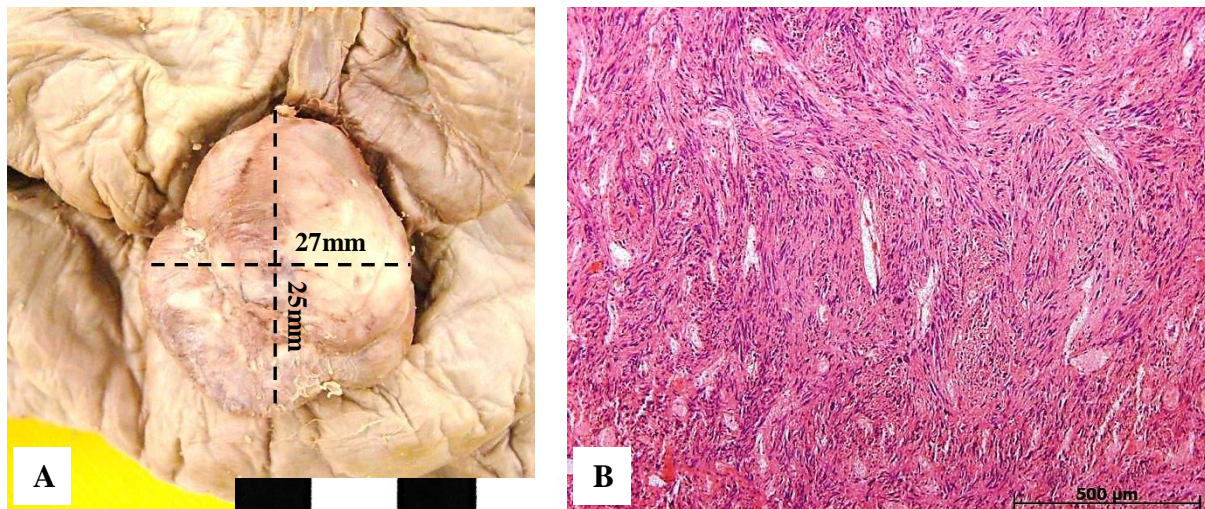


Figure 4.53. Gastrointestinal stromal tumor. A) A mesenchymal tumor was found outside the proximal part of the jejunum of cadaver K99/12. This nodule measured 27x25mm in diameter; B) histology of the nodule shows a typical spindle-shaped GIST, H&E (50x).

4.3.2.5 Diverticular Disease

Colonic diverticula were observed in 24/127 (18.9%) cadavers (Table 4.36). The average age of the cadavers with colonic diverticula was 54.1 years with a male to female ratio of 1:1.3. Diverticula which are acquired pouches of the colonic mucosa and submucosa were found within the sigmoid colon of 22/24 (91.7%) cadavers (Figure 4.54). The diverticula occurred in rows between the taenia coli, usually in the area where blood vessels penetrated the colonic wall. Diverticulitis implies inflamed diverticula. None of the colonic diverticula were inflamed. Histologically, thickening of the colonic muscular layer was observed. The pouches extruded through the thickened muscular layer via weakened areas within the colon (Figure 4.55).

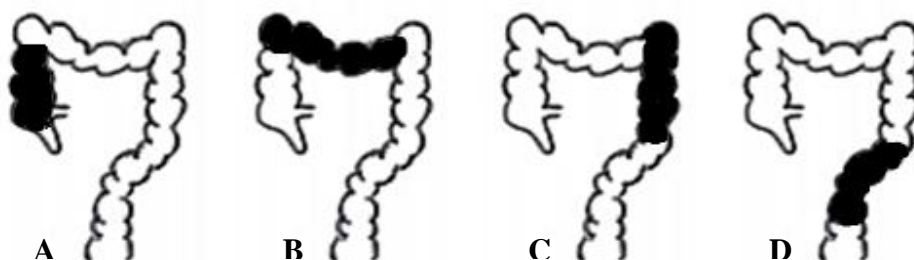


Figure 4.54. Distribution of colonic diverticula in the cadaver cohort. A) Diverticula in the ascending colon were seen in 1/24 (4.2%) cadaver; B) the transverse colon was affected in 1/24 (4.2%) cadaver; C) diverticula were seen in the descending colon in 6/24 (25.0%) cadavers; D) the sigmoid colon was affected in 22/24 (91.7%) cadavers.

Table 4.36. Colonic diverticula in the cadaver cohort (n=127)

<i>Cadaver Ref. Nr.</i>	<i>Sex</i>	<i>Age</i>	<i>Cadaver Nr</i>	<i>Sex</i>	<i>Age</i>
K112/09	Male	58	K28/12	Female	62
K115/09	Male	32	K50/12	Female	*
K19/10	Female	63	K51/12	Male	56
K30/10 (Fig. 4.55)	Male	*	K60/12	Female	22
K52/11	Male	48	K74/12	Female	52
K62/11	Male	83	K83/12	Male	59
K74/11	Male	70	K86/12	Female	24
K75/11	Male	36	K93/12	Male	72
K119/11	Male	*	K101/12	Male	58
K130/11	Female	81	K104/12	Female	61
K25/12	Male	39	K106/12	Male	44
K26/12	Male	*	K107/12	Female	62

* Age is unavailable

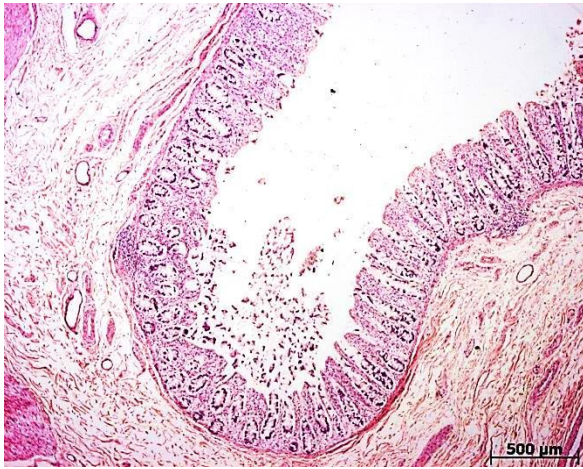


Figure 4.55. Microscopic appearance of diverticula. Diverticula in the colon of cadaver K30/10, H&E (25x).

4.3.2.6 Volvulus and Strangulation

A volvulus and strangulation was observed in 1/127 (0.8%) cadaver (Table 4.37). Cadaver K108/09 (male, 42 years) presented with intestinal obstruction as a result from a twist in the intestines. A segment of the bowel became trapped in the mesentery which compromised the intestinal blood supply (strangulation). The volvulus occurred around a band of fibrous tissue. It appeared as if the fibrous band was congenital in origin. Necrosis and hemorrhage was seen in the intestinal loops adjacent to the fibrous band (Figure 4.56).

Table 4.37. Intestinal volvulus in the cadaver cohort (n=127)

<i>Cadaver Ref. Nr.</i>	<i>Sex</i>	<i>Age</i>	<i>Intestinal Involvement</i>	<i>Morphology</i>
K108/09	Male	42	Jejunum	Necrosis and hemorrhage in adjacent intestinal loops

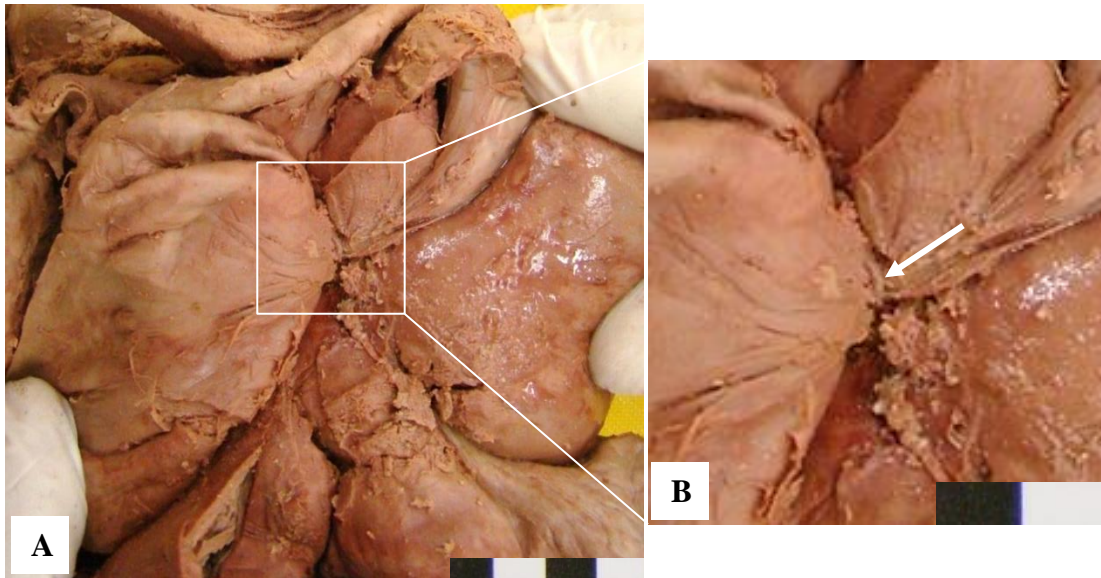


Figure 4.56. Intestinal volvulus. A) A volvulus was found in the intestines of cadaver K108/09. A fibrous band (indicated with an arrow in B), obstructed the intestinal lumen.

4.3.2.7 Parasitic Infestation

4.3.2.7.1 *Ascaris lumbricoides*

Ascaris lumbricoides was observed in 3/127 (2.4%) cadavers (Table 4.38). The male to female ratio was 1:4.5 and the average age of the affected cadavers was 58.5 years. These parasitic roundworms were found in the duodenum and proximal jejunum. No signs of ascariasis were noted in the infected cadavers. The worms were measured in order to determine the sex. Five of the six worms were male (Figure 4.57, A and B), as they measured not more than 170mm in length and 4mm in width. One worm (found in K28/12), appeared to have been female, with a width of more than 6mm (Figure 4.57, C). No other clinical implications were noted which was as a result of *A. lumbricoides*.

Table 4.38. *Ascaris lumbricoides* infestation of the intestines in the cadaver cohort (n=127)

<i>Cadaver Ref. Nr.</i>	<i>Sex</i>	<i>Age</i>	<i>Intestinal Involvement</i>	<i>Number of Roundworms</i>	<i>Sex of Roundworms</i>
K119/11	Male	*	Duodenum and proximal jejunum	Four	Male
K28/12	Female	62	Bend of the duodenum	One	Female
K66/12	Female	55	Proximal duodenum	One	Male

* Age is unavailable



Figure 4.57. *Ascaris lumbricoides*. A) One roundworm (89mm) found in the proximal duodenum of cadaver K66/12; B) four roundworms (from left to right; 169mm, 55mm, 38mm, 34mm) in the duodenum and proximal part of the jejunum of cadaver K119/11; C) one roundworm (153mm) in the bend of the duodenum of cadaver K28/12.

4.3.3 Diseases of the Pancreas

4.3.3.1 Pancreatic Tuberculosis

Tuberculous involvement of the pancreas was observed in 2/127 (1.6%) cadavers (Table 4.39). Both cadavers with pancreatic TB (PT) were males. Histologically, granulomatous inflammation was observed in the pancreatic parenchyma (Figure 4.58). Central necrosis with scattered lymphocytes and epithelioid macrophages were observed (Figure 4.58). Both cases were incidental findings during histologic examination.

Table 4.39. Pancreatic tuberculosis in the cadaver cohort (n=127)

<i>Cadaver Ref. Nr.</i>	<i>Macroscopic Appearance</i>	<i>Microscopic Findings</i>	<i>Pulmonary Lesions</i>	<i>Extrapulmonary Lesions</i>
K25/12	No obvious granulomas were noted in the pancreatic parenchyma	Small granuloma present (incidental finding) (Fig. 4.58, A)	Bilateral	Liver, spleen, both kidneys
K26/12	No granulomas noted in the pancreatic parenchyma	Small, focal granulomas present in parenchyma (incidental finding) (Fig. 4.58, B)	Bilateral	Liver, spleen, both kidneys

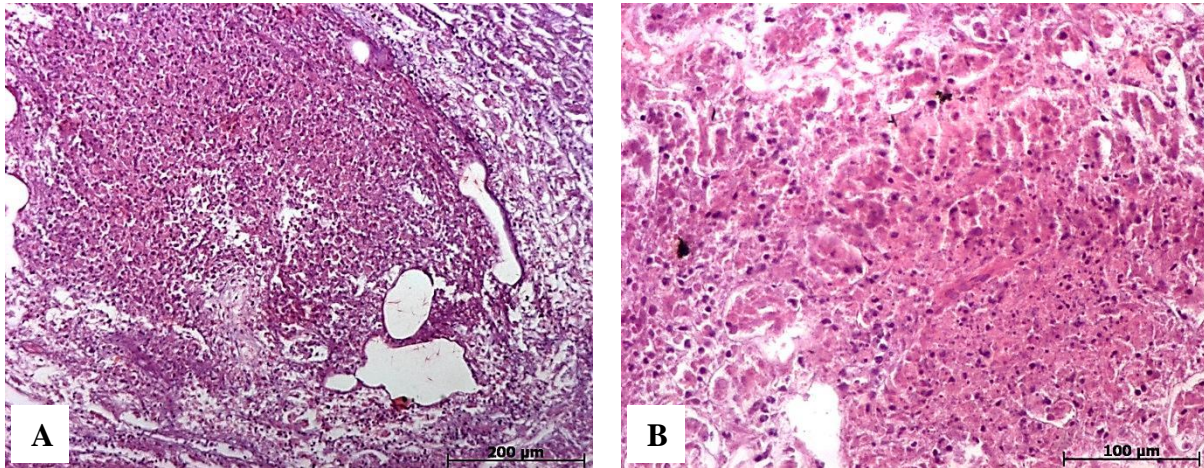


Figure 4.58. Microscopic appearance of pancreatic tuberculosis. A) Small, focal granuloma with scattered lymphocytes in the pancreas of cadaver K25/12, H&E (100x); B) granuloma with central necrosis within the pancreas of cadaver K26/12, H&E (200x).

4.3.3.2 Acute Pancreatitis

Acute pancreatitis (acute inflammation of the pancreas) was observed in 1/127 (0.8%) cadaver (Table 4.40). A hemorrhagic and swollen pancreas was observed. Extravasation of erythrocytes was seen as a result of enzymatic digestion of blood vessel walls (Figure 4.59, A). Fat necrosis was observed which gave the pancreas a chalky white appearance due to the digestion of peripancreatic fat. This occurred as a result of fat digestion by leaking lipases. Histologically, fibrosis and acute inflammatory cells were noted and hemosiderin was seen as a result of the extravasated erythrocytes (Figure 4.59, B).

Table 4.40. Acute pancreatitis in the cadaver cohort (n=127)

<i>Cadaver Ref. Nr.</i>	<i>Sex</i>	<i>Macroscopic Appearance</i>	<i>Microscopic Findings</i>
K70/11	Female	Hemorrhagic, hard and thickened	Hemorrhagic, fibrosis with hemosiderin pigment

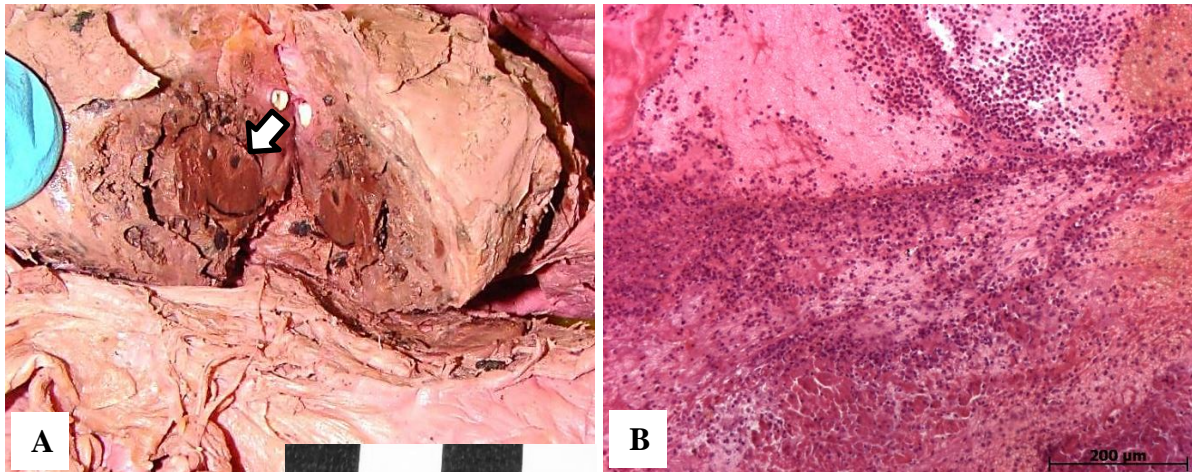


Figure 4.59. Acute pancreatitis. A) Gross appearance of a pancreas with an acute inflammation and hemorrhage (blocked arrow) in cadaver K70/11; B) hemorrhagic pancreas of cadaver K70/11 with fibrosis and acute inflammatory cells, H&E (25x).

4.3.3.3 Chronic Pancreatitis

Chronic pancreatitis is associated with recurrent episodes of acute pancreatitis and was observed in 5/127 (3.9%) cadavers (Table 4.41). The male to female ratio was 1:1.5 and the average age of the affected cadavers was 44.3 years. Extensive fibrosis gave the pancreas a firm and grayish appearance macroscopically (Figure 4.60, A). Pancreatic atrophy was also noted. Numerous areas of mineralization were noted and the ducts were cystically dilated. Some dilated ducts contained calculi. Histologically, substantial loss of acini with replacement by fibrosis was observed (Figure 4.60, B).

Table 4.41. Chronic pancreatitis in the cadaver cohort (n=127)

<i>Cadaver Ref. Nr.</i>	<i>Sex</i>	<i>Age*</i>	<i>Macroscopic Appearance</i>	<i>Microscopic Findings</i>
K104/09	Male	*	Hard and nodular with calcifications and cystic spaces	Fibrosis, cystic spaces (some with contents), calcification (Fig. 4.60, B)
K02/10	Male	31	Tail of the pancreas was hard and nodular on palpation	Lymphocytes, fibrosis, cystic spaces with eosinophilic contents, Kaposi's sarcoma lesions
K120/11	Female	53	Hard and nodular with calcifications and cystic spaces	Extensive fibrosis, cystic spaces (with contents), calcification
K148/11	Male	49	Extensive fibrotic, nodular and calcifications (Fig. 4.60, A)	Fibrosis, cystic spaces (some with contents), calcification
K50/12	Female	*	Small and cystic parenchyma	Lymphocytes, fibrosis, cystic spaces with eosinophilic contents

* Age is unavailable

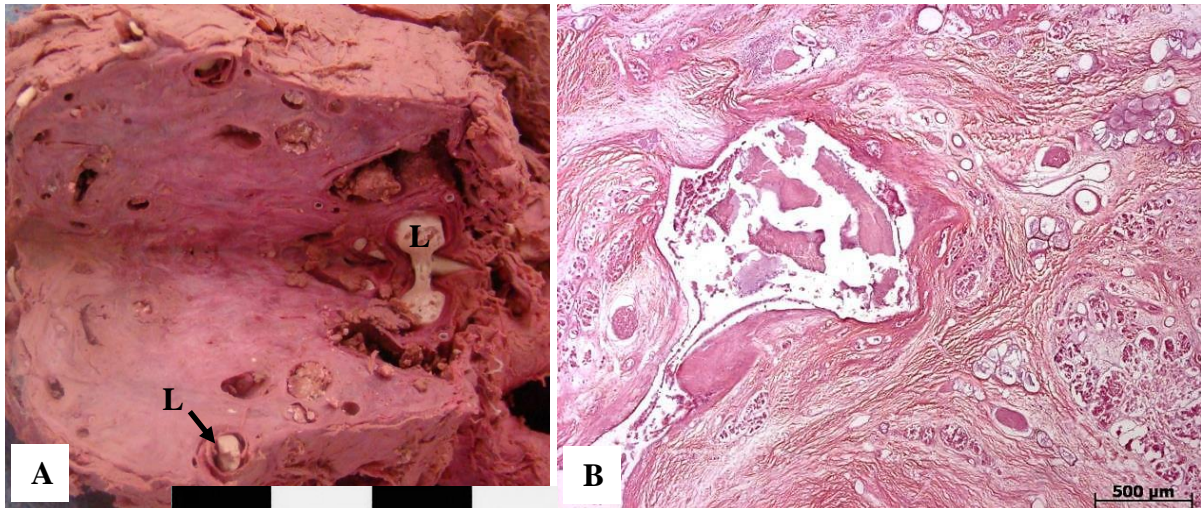


Figure 4.60. Chronic pancreatitis. A) Pancreas of cadaver K148/2 with extensive fibrosis and cystic areas (note the presence of latex (L) in the pancreatic arteries); B) pancreas of K104/09 with cystic space with contents and surrounding fibrosis, H&E (25x).

4.4 Hepatobiliary System

4.4.1 Hepatic Tuberculosis

Hepatic granulomas were observed in 15/127 (11.8%) cadavers (Table 4.42). The male to female ratio was 1.3:1 and the average age of the affected cadavers was 44.5 years. Macroscopically, hepatic tuberculous granulomas were well-circumscribed but coalesced in some cases. Histologically, the granulomas showed characteristic palisaded epithelioid macrophages, scattered lymphocytes and in some cases Langhans giant cells. No caseating necrosis in the granulomas was observed. Fibrosis was observed in 4/15 (26.7%) which gave a macroscopical cirrhotic appearance (Figure 4.61, A and B). The ZN stain in all of the cases revealed several acid-fast bacteria dispersed throughout the hepatocytes (Figure 4.61, C and D).

Table 4.42. Tuberculosis involvement of the liver in the cadaver cohort (n=127)

<i>Cadaver Ref. Nr.</i>	<i>Sex</i>	<i>Age *</i>	<i>Hepatic Involvement</i>	<i>Pulmonary TB Lesions</i>	<i>EPTB Involvement</i>	<i>Absolute Weight (g)</i>	<i>Adapted Weight (g)</i>
K87/09	Male	41	Entire liver	Bilateral PTB	Spleen, hilar	---	---
K45/10	Male	43	Focal granulomas	Bilateral PTB	Absent	---	---
K46/11	Male	30	Focal granulomas	Bilateral PTB	Spleen	1300.0	1352.0
K52/11	Male	48	Focal granulomas	Bilateral PTB	Hilar nodes	1040.0	1081.6
K55/11	Male	43	Focal granulomas	Bilateral PTB	Absent	1330.0	1383.2
K65/11	Female	52	Focal granulomas	Right PTB	Renal, hepatic, pancreatic, hilar	1040.0	1081.6
K119/11	Male	*	Focal granulomas	Bilateral PTB	Splenic, hilar	2080.0	2163.2
K121/11	Male	50	Small, focal granulomas	Bilateral PTB	Renal and spleen, pancreatic, hilar	2080.0	2163.2
K124/11	Female	*	Focal granuloma	Bilateral PTB	Spleen, hilar lymph nodes	1290.0	1341.6
K138/11	Male	57	Small, focal granuloma	Bilateral PTB	Absent	960.0	998.4
K140/11	Female	42	Focal granuloma	Bilateral PTB	Renal, spleen, duodenal lymph nodes	1400.0	1456.0
K25/12	Male	39	Focal granulomas	Bilateral PTB	Renal, spleen	2180.0	2267.2
K26/12	Male	*	Focal granulomas	Bilateral PTB	Renal, spleen	1330.0	1383.2
K42/12	Female	*	Entire liver	Bilateral PTB	Spleen	960.0	998.4
K49/12	Male	*	Focal granulomas	Bilateral PTB	Renal, spleen	1400.0	1456.0

* Mean percent change with formalin fixation = + 4.0% (according to Finkbeiner et al., 2004) --- Weight is unavailable

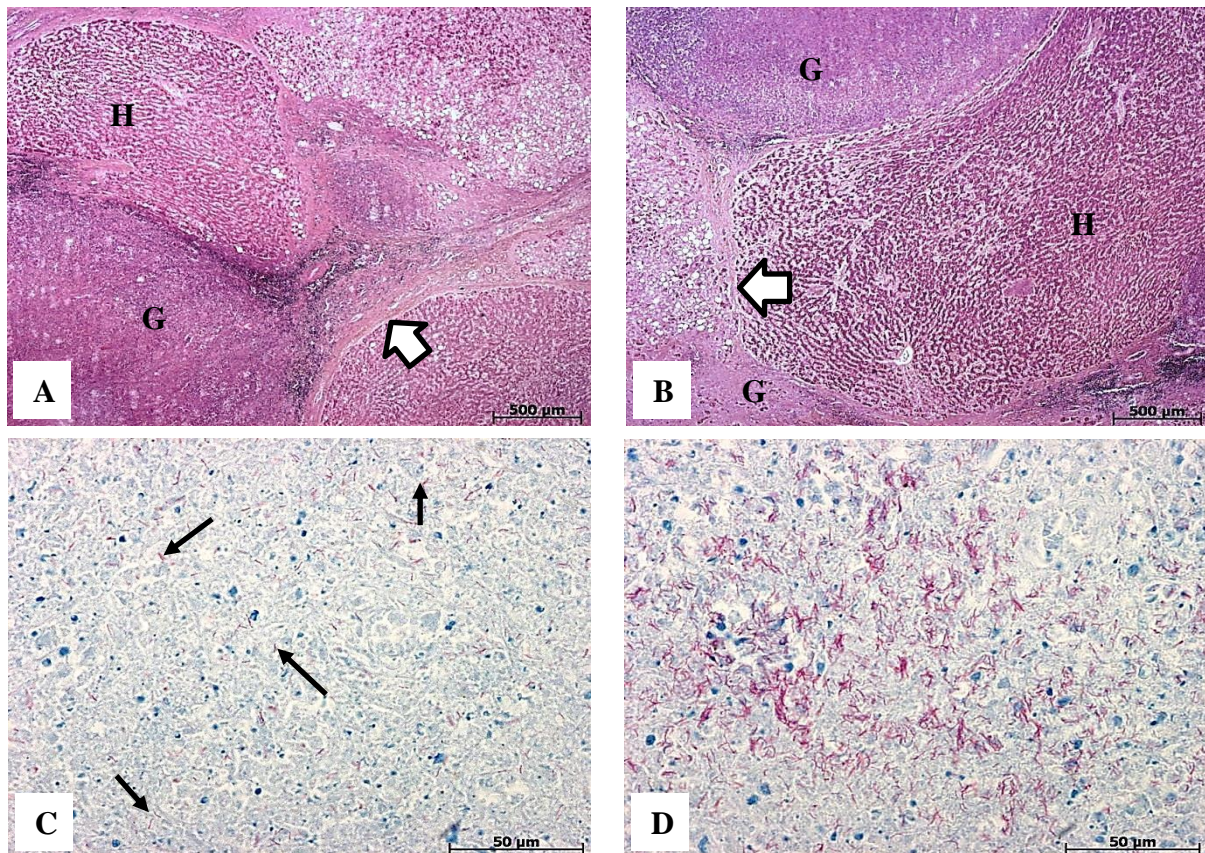


Figure 4.61. Hepatic tuberculosis. A) liver with granulomatous nodules in cadaver K87/09, H&E (25x); B) liver with granulomatous nodules in cadaver K87/09, H&E (25x); C) liver with acid-fast bacilli in cadaver K87/09, Ziehl-Neelsen (400x); D) liver with acid-fast bacilli (arrows), fibrosis (blocked arrows), granuloma (G), normal hepatocytes (H)

4.4.2 Acute Triaditis

Acute triaditis was observed in 2/127 (1.6%) cadavers (Table 4.43). Both cadavers with acute triaditis were males with an average age of 61.0 years. On gross inspection, the livers were relatively normal. Histologically, focal infiltration of acute inflammatory cells consisting mostly of polymorphonuclear cells, were observed within the portal triads (Figure 4.62).

Table 4.43. Acute triaditis in the cadaver cohort (n=127)

<i>Cadaver Ref. Nr.</i>	<i>Sex</i>	<i>Age</i>	<i>Microscopic Findings</i>	<i>Absolute Weight (g)</i>	<i>Adapted Weight (g)*</i>
K64/12	Male	50	Focal acute inflammatory cells (triaditis)	1630.0	1695.2
K93/12	Male	72	Focal acute inflammatory cells (triaditis)	990.0	1029.6

* Mean percent change with formalin fixation = + 4.0% (according to Finkbeiner et al., 2004)

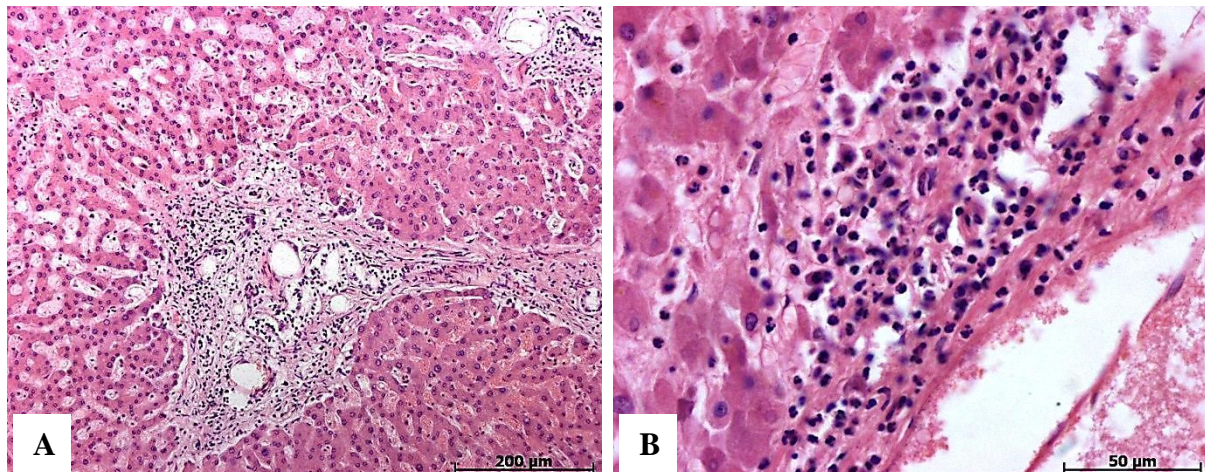


Figure 4.62. Microscopic appearance of acute triaditis. A) Acute inflammatory response within a portal triad of cadaver K93/12 which is extending to the adjacent triads, H&E (100x); B) magnification of a triad illustrates the acute inflammatory cells, cadaver K64/12, H&E (400x).

4.4.3 Alcoholic Hepatitis

Alcoholic hepatitis was observed in 1/127 (0.8%) cadaver (Table 4.44). Alcoholic hepatitis was diagnosed based on the microscopical findings and presented with hepatic steatosis, ballooning degeneration (swollen and vacuolated hepatocytes), and foci of acute inflammatory cells. Fibrosis was observed while inflammatory infiltration of the portal triads (triaditis) was seen (Figure 4.63). Hyaline bodies, known as Mallory bodies, were observed but were not a prominent feature (Figure 4.63, B).

Table 4.44. Alcoholic hepatitis in the cadaver cohort (n=127)

<i>Cadaver Ref. Nr.</i>	<i>Sex</i>	<i>Age</i>	<i>Microscopic Findings</i>	<i>Absolute Weight (g)</i>	<i>Adapted Weight (g)*</i>
K104/12	Female	61	Acute inflammatory cells, triaditis, hyaline bodies (Mallory) steatosis	600.0	624.0

* Mean percent change with formalin fixation = + 4.0% (according to Finkbeiner et al., 2004)

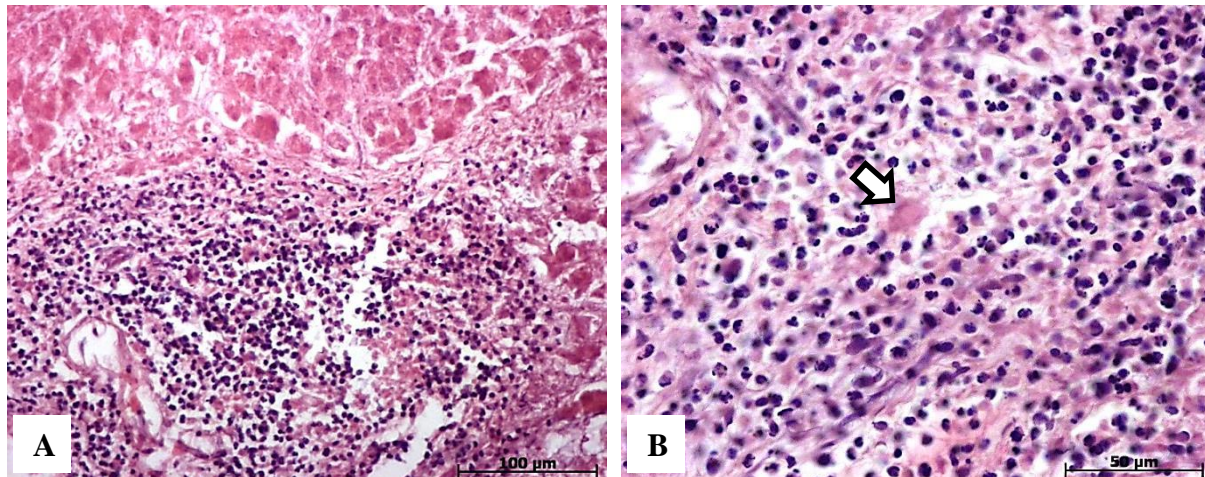


Figure 4.63. Microscopic appearance of alcoholic hepatitis. A) Acute inflammatory cells within the portal triads (triaditis) of cadaver K104/12 can be seen, H&E (200x); B) a hyaline body (Mallory body) can be seen amongst the inflammatory cells of cadaver K104/12, which is indicative of alcoholic hepatitis, H&E (400x); Mallory body (blocked arrow).

4.4.4 Chronic Hepatitis

Chronic hepatitis was observed in 11/124 (8.9%) cadavers (Table 4.45). The male to female ratio was 4.6:1 and the average age of the affected cadavers was 49.5 years. Histologically, the portal triads were infiltrated and expanded by a chronic inflammatory infiltrate, consisting of lymphocytes (Figure 4.64). The portal artery, vein and bile duct were easily identifiable within the affected portal tracts. In 4/11 (36.4%) cadavers, the portal tracts were disrupted with necrotic changes and is known as piecemeal necrosis, or “chronic active hepatitis”. The hepatic lobules were infiltrated by lymphocytes and were surrounded by apoptotic hepatocytes, which are known as spotty necrosis. Bridging necrosis were seen in 2/11 (18.2%) cadavers and occurred as a result of confluent areas of spotty and piecemeal necrosis. Chronic hepatocyte destruction may cause fibrosis which may lead to the development of hepatic cirrhosis.

Table 4.45. Chronic hepatitis in the cadaver cohort (n=127)

<i>Cadaver Ref. Nr.</i>	<i>Sex</i>	<i>Age*</i>	<i>Microscopic Findings</i>	<i>Absolute Weight (g)</i>	<i>Adapted Weight (g)**</i>
K80/09	Male	31	Accumulation of chronic inflammatory cells within portal triads	---	---
K81/09	Male	44	Focal infiltration of chronic inflammatory cells within the portal triads	---	---
K87/09	Male	*	Extensive infiltration of chronic inflammatory cells	---	---
K70/11	Female	*	Chronic inflammatory cells in portal triads	1250.0	1300.0
K74/11	Male	70	Accumulation of chronic inflammatory cells within portal triads (Fig. 4.64)	1440.0	1497.6
K25/12	Male	39	Several foci of chronic inflammatory cells within portal triads	2180.0	2267.2
K27/12	Male	66	Lymphocytic infiltration with fibrosis	1170.0	1216.8
K49/12	Male	*	Lymphocytic infiltration with fibrosis	1400.0	1456.0
K76/12	Male	*	Lymphocytes with bridging necrosis in hepatic parenchyma	1090.0	1133.6
K97/12	Male	*	Focal chronic inflammatory cells in portal triads	1850.0	1924.0
K99/12	Male	47	Chronic inflammatory cells with fibrosis in hepatic parenchyma	2170.0	2256.8

* Age is unavailable

** Mean percent change with formalin fixation = + 4.0% (according to Finkbeiner et al., 2004)

--- Weight is unavailable

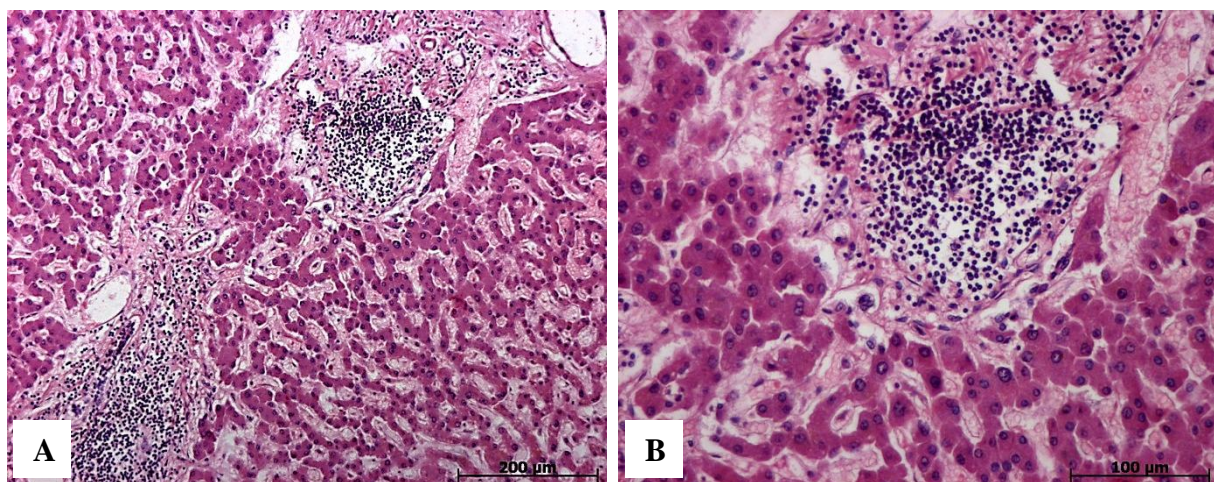


Figure 4.64. Microscopic appearance of chronic hepatitis. A) Hepatic parenchyma of cadaver K74/11 showing extensive inflammatory infiltration of the adjacent portal tracts, H&E (100x); B) on a higher magnification of the liver of cadaver K74/11, the inflammatory infiltrate consists of lymphocytes, which is consistent with a chronic hepatitis, H&E (200x).

4.4.5 Liver Cirrhosis

Liver cirrhosis was observed in 10/127 (7.9%) cadavers (Table 4.46). The male to female ratio was 1.8:1 and the average age of the affected cadaver was 46.7 years. Cirrhosis, the end result of chronic hepatic damage, leads to extensive disruption of the hepatic parenchyma with a nodular, bumpy appearance (Figure 4.65, A). The livers of the cadavers presenting

with cirrhosis were small and nodular on gross inspection. Histologically, dense and broad fibrotic bands extended from and connected to the portal triads (Figure 4.65, B). The neighboring hepatocytes contained fatty vacuoles in 8/10 (80.0%) cadavers which is consistent with alcoholic cirrhosis. In 2/10 (20.0%) cadavers, no signs of inflammation and fatty changes were seen, however dense bands of fibrous tissue were found disrupting the hepatic parenchyma.

Table 4.46. Cirrhosis in the cadaver population (n=127)

<i>Cadaver Ref. Nr.</i>	<i>Sex</i>	<i>Age*</i>	<i>Macroscopic Appearance</i>	<i>Microscopic Findings</i>	<i>Absolute Weight (g)</i>	<i>Adapted Weight (g)**</i>
K87/09	Male	*	Micronodular cirrhosis	Fibrosis within the hepatic parenchyma	---	---
K89/09	Male	41	Micronodular cirrhosis	Extensive fibrosis, hepatocytes arranged in nodules	---	---
K30/10	Male	*	Extensive micronodular cirrhosis (Fig. 4.65, A)	Micronodular cirrhosis with normal, regenerating hepatocytes (Fig. 4.65, A)	---	---
K31/11	Male	53	Extensive fibrosis,	Extensive fibrosis, micronodular cirrhosis	805.0	837.2
K43/11	Female	32	Micronodular cirrhosis	Fibrosis within the hepatic parenchyma	1490.0	1549.6
K70/11	Female	*	Micronodular cirrhosis	Extensive fibrosis, hepatocytes arranged in nodules	1250.0	1300.0
K121/11	Male	50	Slight discoloration of parenchyma with fibrosis	Micronodular cirrhosis with normal, regenerating hepatocytes	2080.0	2163.2
K49/12	Male	*	Micronodular cirrhosis	Fibrosis within the hepatic parenchyma	1400.0	1456.0
K61/12	Male	52	Fibrosis in hepatic parenchyma (micronodular)	Micronodular cirrhosis with normal, regenerating hepatocytes	1010.0	1050.4
K75/12	Male	52	Micronodular cirrhosis	Micronodular cirrhosis with normal, regenerating hepatocytes	1220.0	1268.8

* Age is unavailable

** Mean percent change with formalin fixation = + 4.0% (according to Finkbeiner et al., 2004)

--- Weight is unavailable

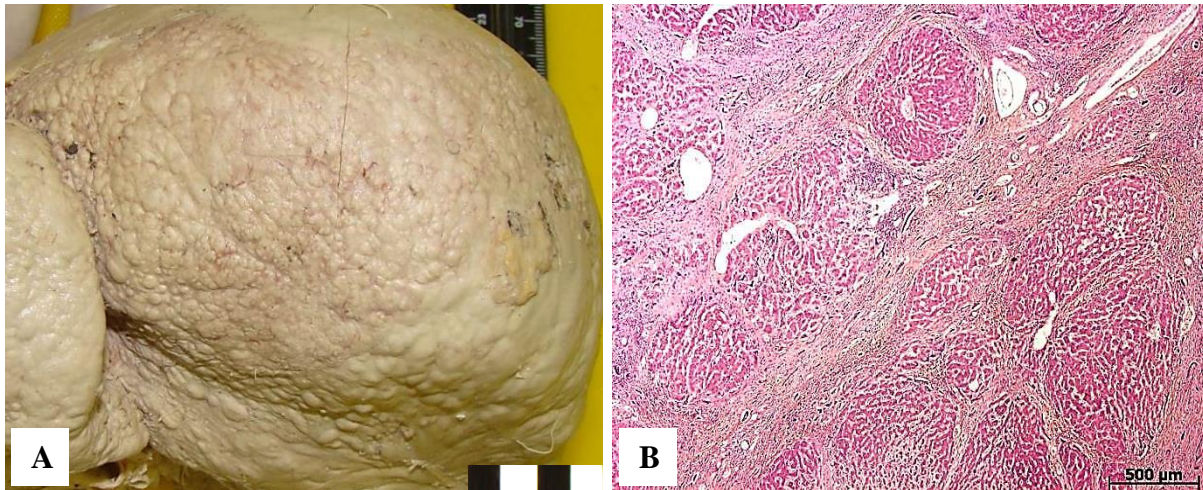


Figure 4.65. Morphology of liver cirrhosis. A) External surface of a cirrhotic liver with nodules measuring approximately 3mm in diameter (K30/10); B) the typical microscopic appearance of cirrhosis includes bands of fibrous tissue disrupting the hepatic parenchyma with absent inflammation and hepatic steatosis; cadaver K30/10, H&E (25x).

4.4.6 Hepatic Steatosis

Hepatic steatosis (fatty liver disease) was observed in 16/127 (12.6%) cadavers (Table 4.47).

The male to female ratio was 1:1.3 and average age of the affected cadavers was 41.2 years.

On gross inspection, the livers appeared pale with rounded edges. However, the final diagnosis was made after histological examination based on the distribution of fat vacuoles amongst the hepatocytes (Figure 4.66). The fat vacuoles in the hepatocytes observed in the cadaver cohort were large and the nuclei were displaced to the periphery (Figure 4.66, B).

Table 4.47. Hepatic steatosis in the cadaver cohort (n=127)

<i>Cadaver Ref. Nr.</i>	<i>Sex</i>	<i>Age*</i>	<i>Microscopic Findings</i>	<i>Degree of Steatosis**</i>	<i>Absolute Weight (g)</i>	<i>Adapted Weight (g)***</i>
K81/09	Male	44	Minimal fatty vacuoles in hepatocytes	Grade 1	---	---
K87/09	Male	*	Fatty vacuoles within hepatocytes	Grade 3	---	---
K104/09	Male	*	Extensive fatty vacuoles	Grade 4	---	---
K118/09	Male	*	Minimal fatty change	Grade 1	---	---
K45/10	Male	43	Fatty vacuoles within hepatocytes	Grade 2	---	---
K38/11	Male	68	Round edges, greasy	Grade 1	805.0	837.2
K44/11	Male	48	Extensive fatty change	Grade 4	2170.0	2256.8
K64/11	Female	48	Fatty vacuoles within hepatocytes	Grade 3	1020.0	1060.8
K116/11	Female	*	Extensive fatty change (Fig. 4.66)	Grade 4	1090.0	1133.6
K124/11	Female	*	Fatty vacuoles in hepatocytes	Grade 2	1290.0	1341.6
K140/11	Female	42	Minimal fatty change	Grade 1	1400.0	1456.0
K49/12	Male	*	Fat vacuoles within hepatocytes	Grade 1	1400.0	1456.0
K60/12	Female	22	Fat vacuoles in hepatocytes	Grade 3-4	910.0	946.4

<i>Cadaver Ref. Nr.</i>	<i>Sex</i>	<i>Age*</i>	<i>Microscopic Findings</i>	<i>Degree of Steatosis**</i>	<i>Absolute Weight (g)</i>	<i>Adapted Weight (g)***</i>
K86/12	Female	24	Extensive fatty change	Grade 4	1520.0	1580.8
K87/12	Male	24	Minimal fatty change	Grade 1	1500.0	1560.0

* Age is unavailable

** Grade 1: 0-25%; Grade 2: 25-50%; Grade 3: 50-75%; Grade 4: 75-100%

*** Mean percent change with formalin fixation = + 4.0% (according to Finkbeiner et al., 2004)

--- Weight is unavailable

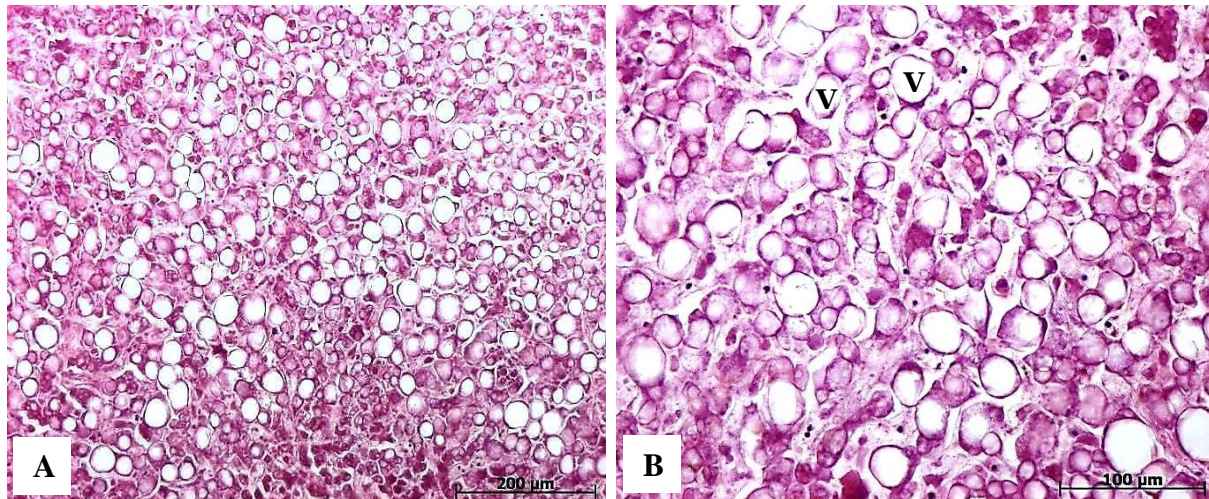


Figure 4.66. Microscopic appearance of hepatic steatosis. A) Hepatic parenchyma with fat droplets of cadaver K116/11, H&E (25x); B) fat vacuoles on a higher magnification within hepatic parenchyma of cadaver K116/11, H&E (200x); fat vacuoles (V).

4.4.7 Hepatic Neoplasms

Hepatic tumors were observed in 3/127 (2.4%) cadavers (Table 4.48). Of these, only 1/3 (33.3%) cadaver had a primary malignant neoplasm a hepatocellular carcinoma (HCC), while the remaining 2/3 (66.7%) cadavers had hepatic neoplasms of secondary origin. All of the affected cadavers were males and an average age of 59.5 years was observed.

Table 4.48. Hepatic neoplasms in the cadaver cohort (n=127)

<i>Cadaver Ref. Nr.</i>	<i>Sex</i>	<i>Age *</i>	<i>Macroscopic Appearance</i>	<i>Microscopic Findings</i>	<i>Absolute Weight (g)</i>	<i>Adapted Weight (g)**</i>	<i>Primary Lesion</i>
K30/10	Male	*	Well-circumscribed lesion situated adjacent to the capsule (Fig.4.67)	Cells with ample cytoplasm and round nuclei (Fig. 4.67)	---	---	HCC
K51/12	Male	56	Three round, well-circumscribed lesions (Fig. 4.68)	Well-circumscribed, sarcoma-like cells	1380.0	1435.2	Sarcomatoid Carcinoma
K82/12	Male	63	Several well-circumscribed nodules in the parenchyma	Necrotic, pleomorphic, hyperchromasia (Fig. 4.68)	2820.0	2932.8	ACA

* Age is unavailable

** Mean percent change with formalin fixation = + 4.0% (according to Finkbeiner et al., 2004)

--- Weight is unavailable

4.4.7.1 Hepatocellular Carcinoma

Hepatocellular carcinoma (HCC) was observed in 1/127 (0.8%) cadaver (Table 4.48). The HCC was seen as a well-circumscribed, oval-shaped lesion situated below the capsule (Figure 4.67, A). A fibrotic border lined the HCC. Bile was secreted, which is characteristic of a well-differentiated HCC. This gave the lesion a greenish appearance (Figure 4.67, A). Concomitant micronodular cirrhosis was observed. Histologically, bile-stained debris was observed in places. The neoplastic cells contained ample cytoplasm with round vesicular nuclei (Figure 4.67, B). A reticulin stain was performed and showed loss of normal reticulin surrounding the malignant hepatocytes, thereby confirming the diagnosis of a well-differentiated HCC (Figure 4.67, C and D).

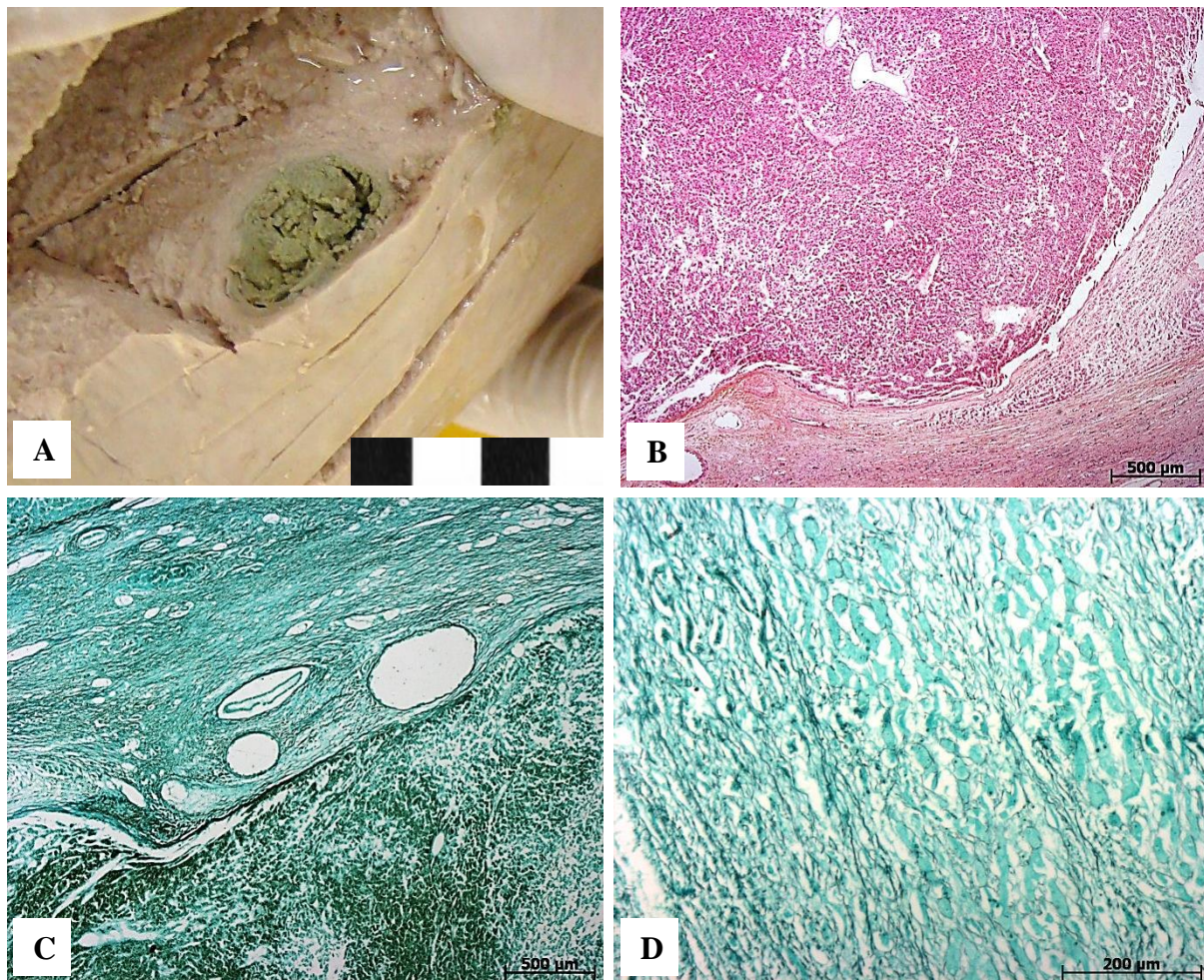


Figure 4.67. Morphology of hepatocellular carcinoma. A) Gross appearance of the greenish hepatocellular carcinoma within the hepatic parenchyma of cadaver K30/10; microscopic appearance of the hepatocellular carcinoma in cadaver K30/10, H&E (25x); C) reticulin stain revealed a well-defined HCC, reticulin stain (25x); D) surrounding the HCC, a framework of black reticulin fibers were observed adjacent to normal hepatocytes, reticulin stain (200x).

4.4.7.2 Metastatic Carcinomas

Hepatic metastases were observed in 2/127 (1.6%) cadavers (Table 4.48). Cadaver K51/12 (male, 56 years) presented with a solitary nodule measuring 9x11mm in maximum dimensions in the liver (Figure 4.68, A). Histology revealed islands with dark, spindle-shaped cells distributed throughout the sinusoids. Fibrotic bands were present within the nodules (Figure 4.68, B). A metastatic adenocarcinoma (ACA) from an unknown origin was observed in cadaver K82/12 (male, 63 years). The hepatic parenchyma contained several well-circumscribed nodules some of which appeared confluent (Figure 4.68, C). Histologically,

malignant, pleomorphic cells with hyperchromasia were observed (Figure 4.68, D). In addition, necrosis and fibrosis was observed.

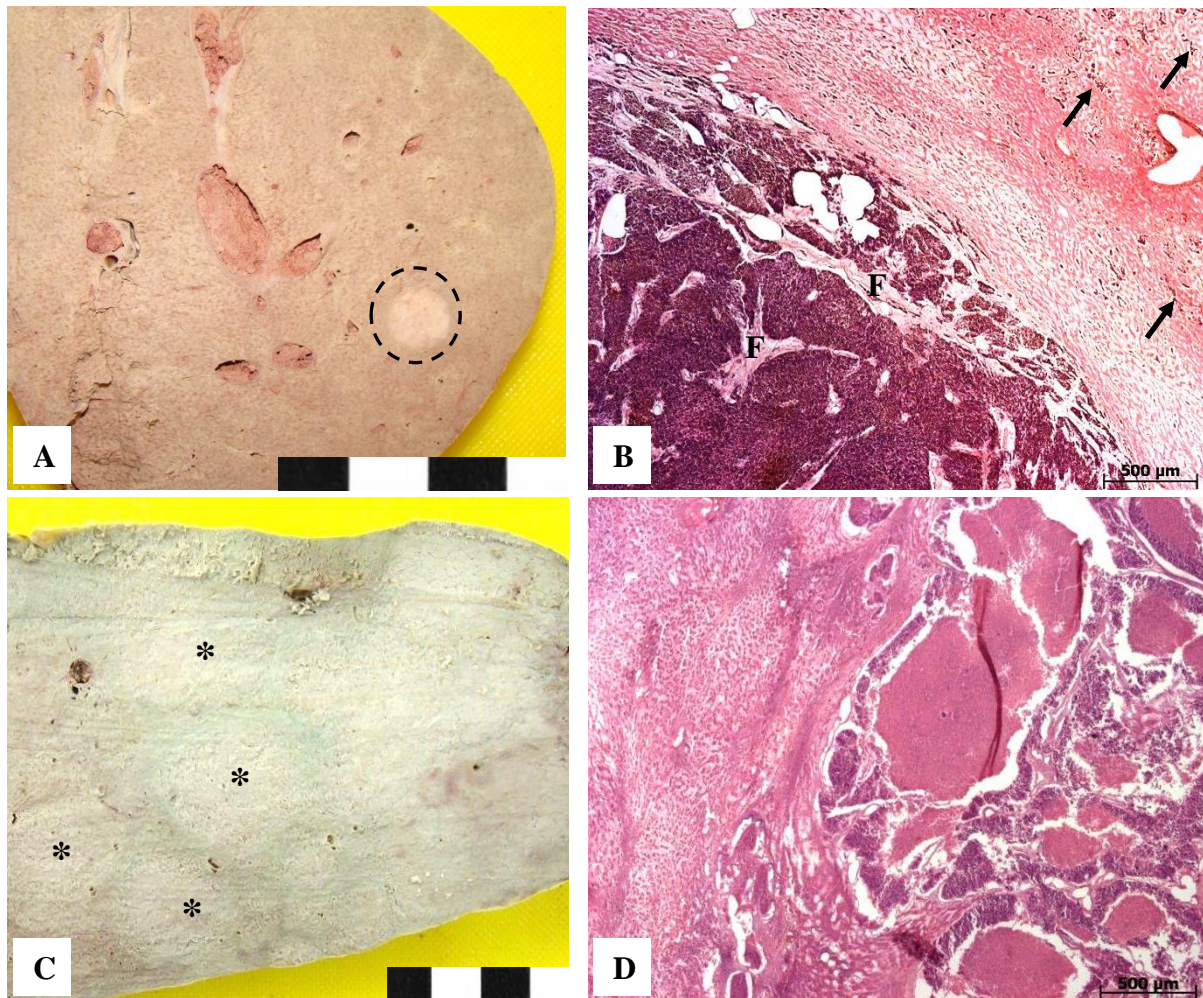


Figure 4.68. Hepatic metastases. A) A nodule measuring 9x11mm (circled area) was observed in the liver (K51/12); B) microscopical appearance of the nodule, H&E (25x); C) well-circumscribed nodules in the liver of cadaver K82/12; D) malignant, pleomorphic neoplasm with a necrotic appearance, H&E (25x); fibrosis (F), nodules (asterisks).

4.4.8 Tuberculosis of the Gallbladder

Gallbladder TB was observed in 1/127 (0.8%) cadaver. The gallbladder of cadaver K115/09 (male, 32 years) was small with a large, thin-walled diverticulum at the tip, measuring approximately 70mm in diameter (Figure 4.69, A and B). The semi-solid diverticular contents had a brownish appearance and within this fluid, several small, black pigment stones were observed. Histologically, this structure resembled a pedunculated abscess originating

from the gallbladder (Figure 4.69, C). Several multinucleated giant cells were observed as well as scattered lymphocytes, macrophages and necrosis (Figure 4.69, D). A ZN stain was performed on the tissue and revealed several acid-fast bacteria.

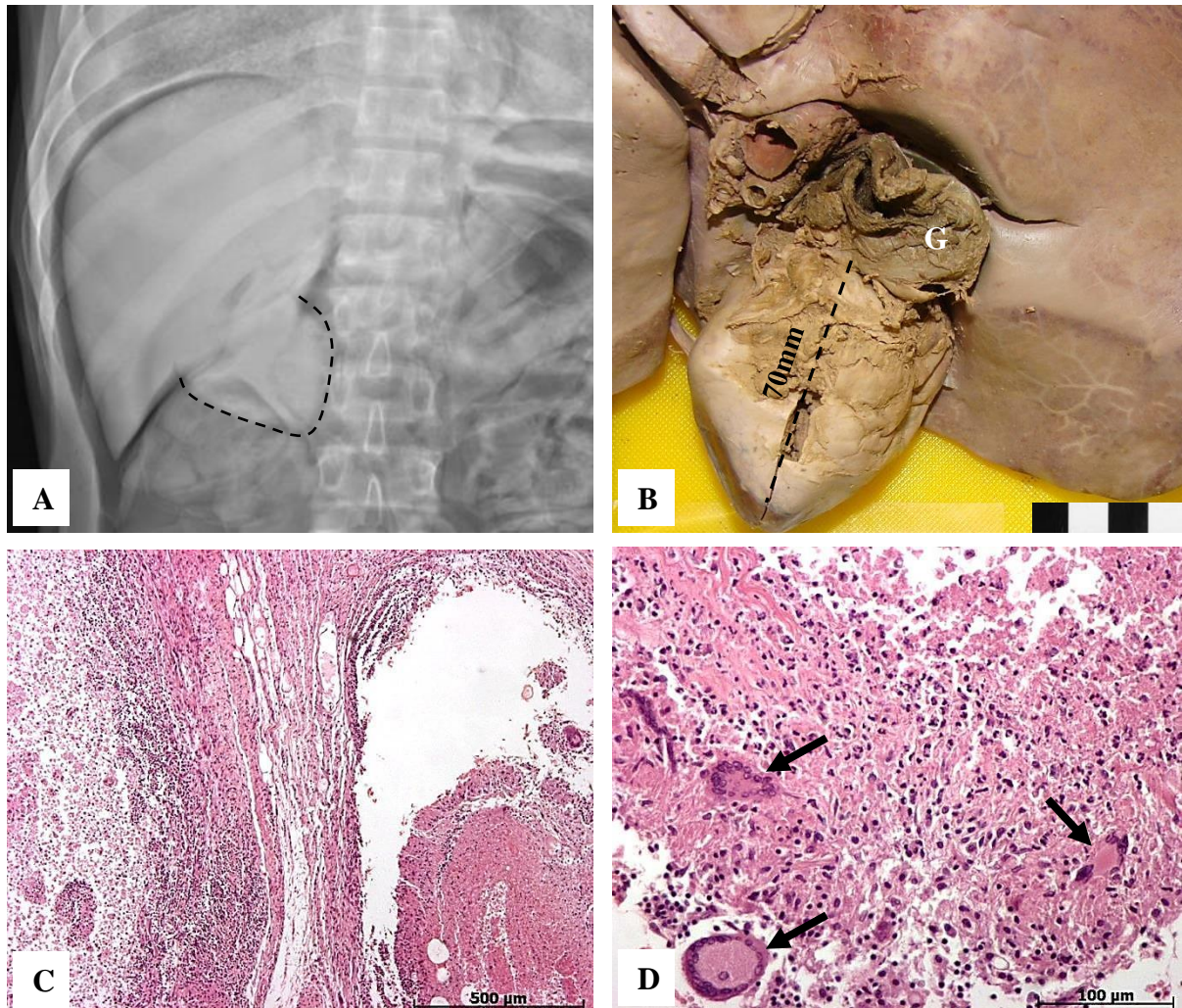


Figure 4.69. Tuberculosis of the gallbladder. A) X-ray of the liver of cadaver K115/09. The cyst could be visualized (dashed line); B) macroscopical appearance of a tuberculous cyst in the gallbladder; C) microscopical appearance of the cyst-like structure, H&E (50x); D) multinucleated giant cells in the wall of the cyst, H&E (200x); gallbladder (G); multinucleated giant cells (arrows).

4.4.9 Cholelithiasis

Cholelithiasis (gall stones) was observed in 7/127 (5.5%) cadavers. The male to female ratio was 2.8:1 and the average age of the cadavers with bile stones was 61.3 years. The two main types of gall stones were seen, namely cholesterol stones 1/7 (14.3%) and pigment stones 6/7

(85.7%). Pigment stones were small, dark and firm in texture (Figure 4.70, A) while the cholesterol stones were pale yellow to brown and round to oval in shape (Figure 4.70, B).

Table 4.49. Cholelithiasis in the cadaver cohort (n=127)

<i>Cadaver Ref. Nr.</i>	<i>Sex</i>	<i>Age</i>	<i>Macroscopic Appearance</i>	<i>Type of Gall Stone</i>
K83/09	Male	60	Very small stones mixed with bile	Pigment
K115/09	Male	32	Numerous, small, black stones within the diverticulum	Pigment
K30/10	Male	*	Few, small stones mixed with the bile	Pigment
K36/10	Male	82	Several stones ranging from light to dark in colour (Fig. 4.70, B)	Cholesterol
K130/11	Female	81	Three, small, black stones	Pigment
K51/12	Male	56	Five, black stones with varying sizes (Fig. 4.70, A)	Pigment
K52/12	Male	57	Several, small stones mixed with the bile	Pigment

* Age is unavailable

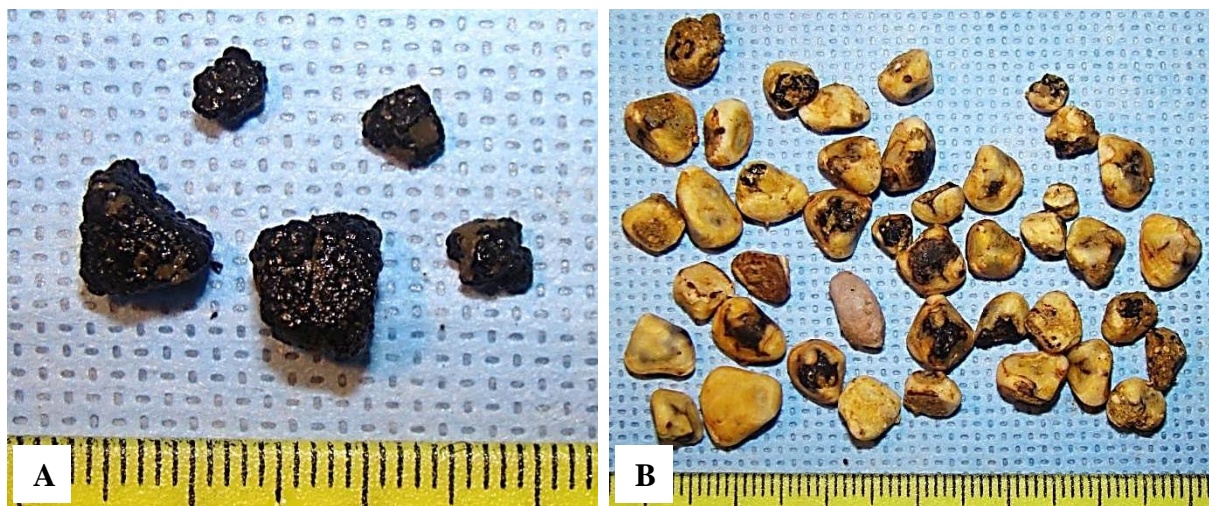


Figure 4.70. Cholelithiasis. A) Small, pigment stones in the gallbladder of cadaver K51/12; B) numerous cholesterol stones of varying sizes in the gallbladder of cadaver K36/10.

4.4.10 Benign Gallbladder Neoplasms

The gallbladder of cadaver K83/09 (male, 60 years) was affected by two different types of benign neoplasms (Table 4.50). At the tip of the fundus of the gallbladder, a sessile mass measuring approximately 30mm in diameter was present. It involved the wall of the gallbladder, had a soft consistency and was not encapsulated. Histologically, the mass involved the submucosal and muscular layers and was classified as an adenomyoma (Figure 4.71). Interlacing bundles of smooth muscle fibers were observed in the stroma which

separated the glandular structures (Figure 4.71). In some areas, the glandular structures were cystically dilated.

Table 4.50. Benign neoplasms of the gallbladder in the cadaver cohort (n=127)

<i>Cadaver Ref. Nr.</i>	<i>Sex</i>	<i>Age</i>	<i>Macroscopic Appearance</i>	<i>Type of Neoplasm</i>
K83/09	Male	60	Sessile mass at the tip of gallbladder fundus, mass in the body of the gallbladder	Adenomyoma, adenoma

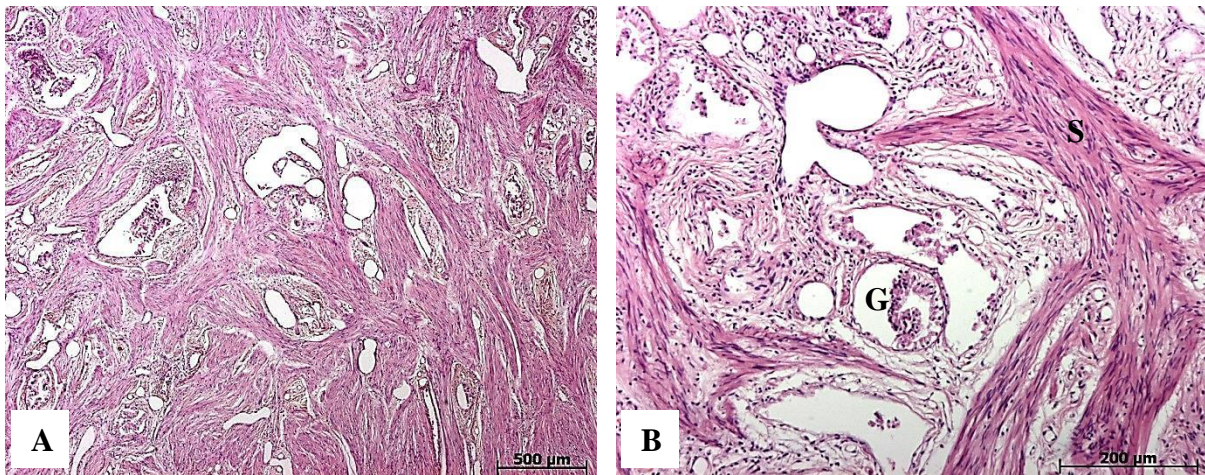


Figure 4.71. Adenomyoma of the gallbladder. A) Adenomyoma at the tip of the fundus of the gallbladder of cadaver K83/09, showing bundles of smooth muscle fibers, H&E (25x); B) a higher magnification of A illustrating a bundle of smooth muscle fibers (S) surrounding the glandular structures (G), H&E (100x).

In the body of the gallbladder, a more typical benign non-papillary or glandular adenoma was seen. The adenoma contained numerous glandular structures, some of which were extensively dilated. A stromal component separating the glandular structures was observed (Figure 4.72).

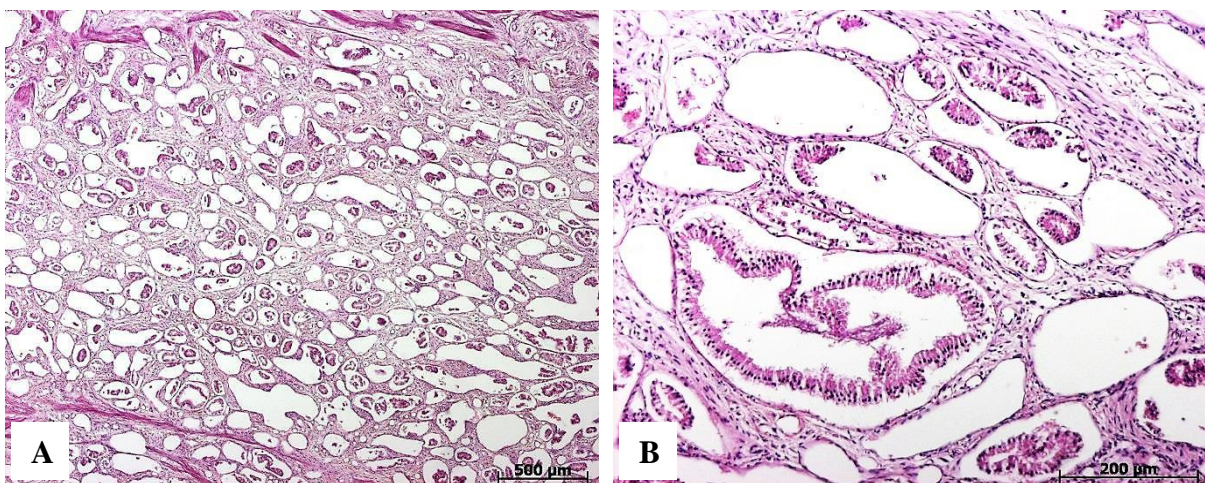


Figure 4.72. Adenoma of the gallbladder. A) Adenoma in the gallbladder lumen of cadaver K83/09, H&E (25x); B) magnification of the adenoma in the gallbladder lumen (K83/09), H&E (100x), note the majority of the glandular epithelium is washed out during processing.

4.4.11 Chronic Cholecystitis

Chronic cholecystitis was observed in 1/127 (0.8%) cadaver. The gallbladder of cadaver K83/09 (male, 60 years) contained Rokitansky-Aschoff diverticula within the wall of the gallbladder (Figure 4.73). These diverticula were herniations of the gallbladder epithelium into the smooth muscle layer. Remnants of gallbladder calculi were present within some of the diverticula (Figure 4.73, B).

Table 4.51. Cholecystitis in the cadaver cohort (n=127)

<i>Cadaver Ref. Nr.</i>	<i>Sex</i>	<i>Age</i>	<i>Microscopic Appearance</i>	<i>Type of Cholecystitis</i>
K83/09	Male	60	Rokitansky-Aschoff diverticula with calculi	Chronic cholecystitis

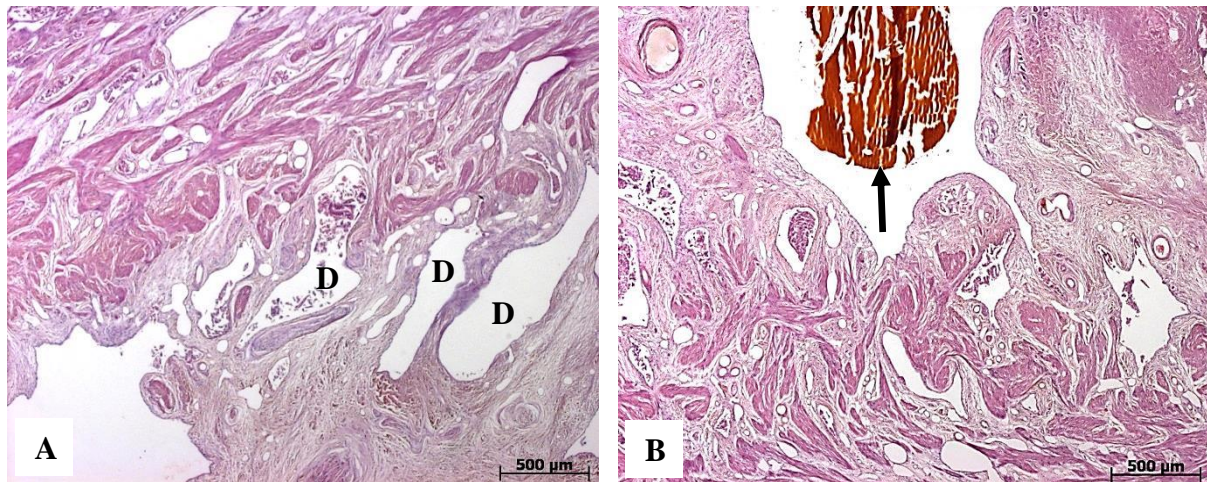


Figure 4.73. Microscopic appearance of chronic cholecystitis. A) Extensive diverticula (D) in the wall of the gallbladder (K83/09), H&E (25x); remnants of a calculus (arrow) within a Rokitansky-Aschoff diverticuli in the gallbladder of cadaver K83/09, H&E (25x).

4.5 Renal System

4.5.1 Renal Tuberculosis

Tuberculous involvement of the kidneys was observed in 13/127 (10.2%) cadavers (Table 4.52). The male to female ratio was 1:2.2 and the average age of the affected cadavers was 44.6 years. Bilateral pulmonary TB (PTB) was observed in 12/13 (92.3%) cadavers with renal TB. Both kidneys were affected by tuberculous lesions in (6/13) 46.2% cadavers, the right kidney in 4/13 (30.8%) and the left kidney in 3/12 (25.0%) cadavers. The tuberculous granulomas were unclear macroscopically except that the surfaces of the affected kidneys had an irregular appearance. Microscopically, renal tuberculosis had the typical TB granulomatous appearance within the renal parenchyma (Figure 4.74). Epithelioid macrophages, scattered lymphocytes a central area of caseation and surrounding fibrosis were observed (Figure 4.74).

Table 4.52. Renal tuberculosis in the cadaver cohort (n=127)

<i>Cadaver Ref. Nr.</i>	<i>Sex</i>	<i>Age *</i>	<i>Anatomical Involvement</i>	<i>Microscopic Findings</i>	<i>Pulmonary Lesions</i>	<i>Absolute Weight (g)</i>	<i>Adapted Weight (g)**</i>
K102/09	Female	28	Left kidney	Small, focal tuberculous granulomas	Bilateral PTB	---	---
K119/09	Female	50	Right kidney	Small, focal tuberculous granuloma	None	---	---
K42/10	Male	*	Right kidney	Tuberculous granuloma (focal) in parenchyma	Bilateral PTB	---	---
K15/11	Male	33	Left kidney	Tuberculous granulomas in renal parenchyma	Bilateral PTB	90.0	91.7
K64/11	Female	48	Left kidney	Tuberculous granulomas within renal parenchyma	Bilateral PTB	140.0	142.7
K65/11	Female	52	Right kidney	Tuberculous granuloma within renal capsule	Bilateral PTB	150.0	152.9
K121/11	Male	50	Both kidneys	Small, focal granulomas	Bilateral PTB	180.0; 220.0	183.4; 224.2
K140/11	Female	42	Both kidneys	Several granulomas with surrounding chronic inflammation	Bilateral PTB	180.0; 160.0	183.4; 163.0
K25/12	Male	39	Both kidneys	Chronic inflammatory cells and granulomas in renal parenchyma	Bilateral PTB	210.0; 240.0	214.0; 244.6
K26/12	Male	*	Both kidneys	Areas of granulomas with chronic inflammatory cells	Bilateral PTB	200.0, 200.0	203.8; 203.8
K49/12	Male	*	Both kidneys	Chronic inflammatory cells and granulomas	Bilateral PTB	180.0, 200.0	183.4; 203.8
K74/12	Female	52	Both kidneys	Granulomas, chronic inflammatory cells	Bilateral PTB	90.0, 100.0	91.7; 101.9

<i>Cadaver Ref. Nr.</i>	<i>Sex</i>	<i>Age *</i>	<i>Anatomical Involvement</i>	<i>Microscopic Findings</i>	<i>Pulmonary Lesions</i>	<i>Absolute Weight (g)</i>	<i>Adapted Weight (g)**</i>
K75/12	Male	52	Right kidney	Granulomatous nodules, lymphocytes (Fig. 4.74)	Bilateral PTB	180.0	183.4

* Age is unavailable,

** Mean percent change with formalin fixation = + 1.9% (according to Finkbeiner et al., 2004);

--- Weight is unavailable

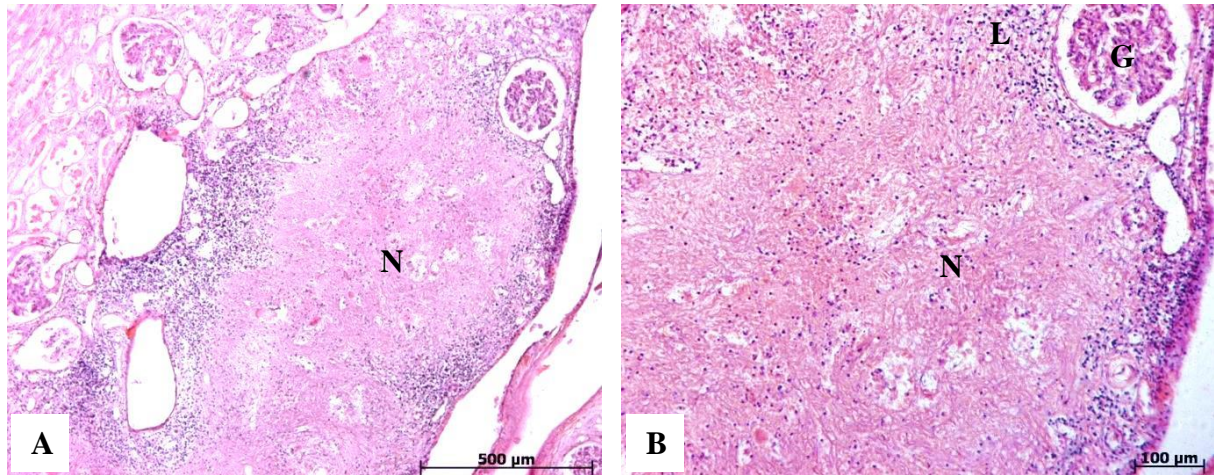


Figure 4.74. Microscopic appearance of renal tuberculosis. A) Right kidney of cadaver K75/12, H&E (50x); B) higher magnification of A, K75/12, H&E (100x); glomeruli (G), lymphocytic infiltrate (L), necrosis (N).

4.5.2 Glomerulosclerosis

Sclerosis of the glomeruli was observed in 27/127 (21.3%) cadavers (Table 4.53). The male to female ratio was 1.6:1. An average age of 48.4 years was noted. The right and left kidney was affected in 13/27 (48.2%) and 7/27 (25.9%) cadavers, respectively. Bilateral involvement was seen in 7/27 (25.9%) cadavers. Sclerotic glomeruli were diagnosed on microscopic level and were consistent with hypoxic injury to the renal parenchyma (Figure 4.75).

Table 4.53. Sclerosis of glomeruli in the cadaver cohort (n=127)

<i>Cadaver Ref. Nr.</i>	<i>Sex</i>	<i>Age*</i>	<i>Anatomical Involvement</i>	<i>Absolute Weight (g)</i>	<i>Adapted Weight (g)**</i>
K102/09	Female	28	Left kidney	---	---
K03/10	Male	34	Right kidney	---	---
K04/10	Female	39	Left kidney	---	---
K42/10	Male	*	Right kidney	---	---
K13/11	Female	47	Right kidney	170.0	173.2
K46/11	Male	30	Both kidneys	180.0; 170.0	183.4; 173.2
K53/11	Male	*	Right kidney	150.0	152.9
K64/11	Female	48	Right kidney	110.0	112.1
K75/11	Male	36	Both kidneys	240.0; 210.0	244.6; 214.0
K125/11	Male	39	Right kidney	200.0	203.8
K148/11	Male	49	Both kidneys	130.0; 110.0	132.5; 112.1

<i>Cadaver Ref. Nr.</i>	<i>Sex</i>	<i>Age*</i>	<i>Anatomical Involvement</i>	<i>Absolute Weight (g)</i>	<i>Adapted Weight (g)**</i>
K25/12	Male	39	Right kidney	210.0	214.0
K26/12	Male	*	Both kidneys	200.0; 200.0	203.8; 203.8
K27/12	Male	66	Right kidney	210.0	214.0
K28/12	Female	62	Left kidney	180.0	183.4
K43/12	Male	*	Right kidney	160.0	163.0
K46/12	Male	46	Both kidneys	100.0; 90.0	101.9; 91.7
K61/12	Male	52	Right kidney	210.0	214.0
K62/12	Female	73	Left kidney	260.0	264.9
K73/12	Male	72	Right kidney	90.0	91.7
K78/12	Male	61	Left kidney (Fig. 4.75, A)	130.0	132.5
K82/12	Male	63	Both kidneys	160.0, 160.0	163.0; 163.0
K83/12	Male	59	Right kidney (Fig. 4.75, B)	300.0	305.7
K87/12	Male	24	Left kidney	140.0	142.7
K98/12	Male	42	Right kidney	190.0	193.6
K99/12	Male	47	Left kidney	190.0	193.6
K101/12	Male	58	Both kidneys	80.0, 80.0	81.5; 81.5

* Age is unavailable

** Mean percent change with formalin fixation = + 1.9% (according to Finkbeiner et al., 2004)

--- Weight is unavailable

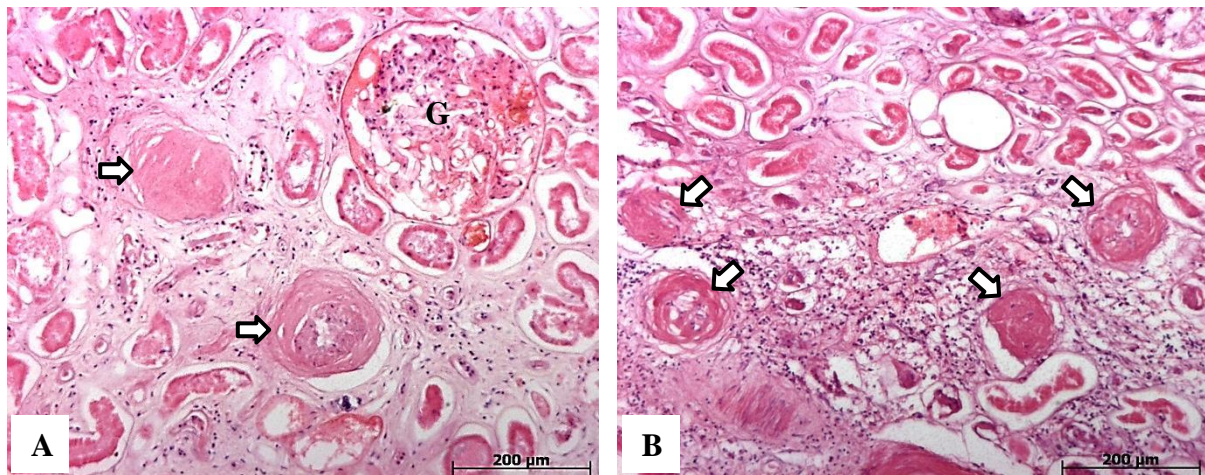


Figure 4.75. Microscopic appearance of sclerosis of glomeruli. A) Two glomeruli within the left kidney of cadaver K78/12 are entirely replaced with scarring tissue (blocked arrows), H&E (100x); note the relatively normal glomerulus (G); B) four scarred glomeruli (blocked arrows) adjacent to a chronic inflammatory process within the right kidney of cadaver K83/12, H&E (100x).

4.5.3 Acute Pyelonephritis

Acute pyelonephritis was observed in 3/127 (2.4%) cadavers (Table 4.54). The male to female ratio was 1:1.1 and the average age of the three affected cadavers was 59.0 years. During gross dissection, no visible signs of abscesses were noted when the capsule was stripped. Histologically, the tubules were affected, while the glomeruli in the renal cortex were spared (Figure 4.76, A). Neutrophils, lymphocytes and plasma cells have infiltrated the

renal interstitium and in severe cases, areas of suppuration were visible in the medulla as elongated foci (Figure 4.76, B).

Table 4.54. Acute pyelonephritis in the cadaver cohort (n=127)

<i>Cadaver Ref. Nr.</i>	<i>Sex</i>	<i>Age</i>	<i>Anatomical Involvement and Macroscopic Appearance</i>	<i>Microscopic Findings</i>	<i>Absolute Weight (g)</i>	<i>Adapted Weight (g)*</i>
K47/11	Male	64	Left kidney	Intense acute interstitial inflammatory response	150.0	152.9
K61/12	Male	52	Both kidneys (Fig. 4.76)	Fibrosis, glomerulosclerosis, inflammatory cells, necrosis	210.0; 230.0	214.0; 234.4
K104/12	Female	61	Both kidneys	Acute inflammatory cells, fibrosis	70.0; 80.0	71.3; 81.5

* Mean percent change with formalin fixation = + 1.9% (according to Finkbeiner et al., 2004)

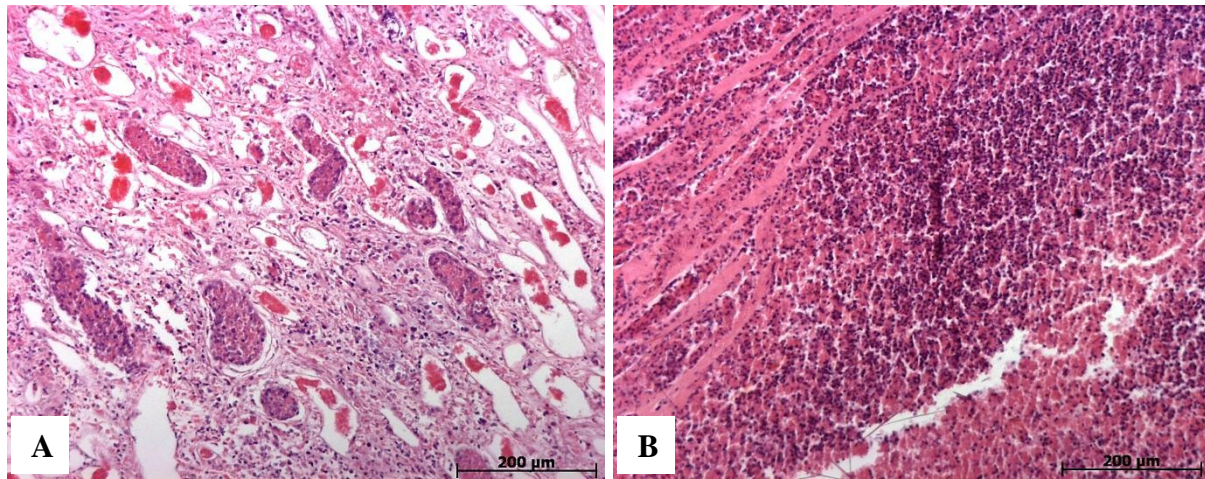


Figure 4.76. Microscopic appearance of acute pyelonephritis. A) An inflammatory infiltrate consisting mostly of neutrophils, lymphocytes and plasma cells have infiltrated the renal tubules of the left kidney of cadaver K61/12, H&E (100x); B) abscess formation (a localized area of suppuration) with acute inflammatory cells in the right kidney of the same cadaver as in A, H&E (100x).

4.5.4 Chronic Pyelonephritis

Chronic pyelonephritis was observed in 24/127 (18.9%) cadavers (Table 4.55). The male to female ratio was 1:1.1. An average age of the affected cadavers was 47.4 years. The right and left kidneys were affected in 8/24 (33.3%) and 7/24 (29.2%) cadavers, respectively. Bilateral involvement was seen in 9/24 (37.5%) cadavers. Macroscopically, the kidneys appeared small and scarred. A fibrous thickening was seen in the pelvis and calices where patchy areas of parenchymal destruction were observed. Histologically, the glomeruli appeared sclerosed and avascular (Figure 4.77, A). Tubular atrophy with dense eosinophilic casts was observed.

These tubules with casts had the appearance of thyroid follicles (“thyroidization”) (Figure 4.77). The interstitium was extensively infiltrated by lymphocytes and plasma cells.

Table 4.55. Chronic pyelonephritis in the cadaver cohort (n=127)

<i>Cadaver Ref. Nr.</i>	<i>Sex</i>	<i>Age*</i>	<i>Anatomical Involvement and Macroscopic Appearance</i>	<i>Microscopic Findings</i>	<i>Absolute Weight (g)</i>	<i>Adapted Weight (g)**</i>
K102/09	Female	28	Left kidney	Chronic inflammatory infiltrate within parenchyma	---	---
K119/09	Female	50	Right kidney	Chronic inflammatory infiltrate and fibrosis	---	---
K03/10	Male	34	Right kidney	Chronic inflammatory infiltrate, fibrosis	---	---
K12/10	Male	37	Left kidney	Fibrosis and chronic inflammatory infiltrate	---	---
K30/10	Male	*	Left kidney	Chronic inflammatory infiltrate with fibrosis	---	---
K10/11	Female	45	Right kidney	Fibrosis with chronic inflammatory infiltrate	140.0	142.7
K46/11	Male	30	Both kidneys	Fibrosis, chronic inflammatory infiltrate	180.0; 170.0	183.4; 173.2
K52/11	Male	48	Left kidney	Chronic inflammatory cellular infiltrate	160.0	163.0
K63/11	Male	*	Both kidneys	Chronic inflammatory cells, fibrosis	130.0; 170.0	132.5; 173.2
K65/11	Female	52	Left kidney	Chronic inflammatory cells, fibrosis	150.0	152.9
K70/11	Female	*	Right kidney	Chronic inflammatory cells, fibrosis	130.0	132.5
K116/11	Female	*	Right kidney	Chronic inflammatory infiltrate, fibrosis	130.0	132.5
K119/11	Male	*	Left kidney	Fibrosis, chronic inflammatory infiltrate	260.0	264.9
K140/11	Female	42	Both kidneys	Chronic inflammatory infiltrate, fibrosis	180.0; 160.0	183.4; 163.0
K58/12	Male	70	Both kidneys (Fig. 4.77, B)	Thyroidization, fibrosis, chronic inflammatory cells	120.0; 110.0	122.3; 112.1
K69/12	Male	*	Both kidneys	Chronic inflammatory cells, fibrosis	140.0; 140.0	142.7; 142.7
K82/12	Male	63	Right kidney (Fig. 4.77, A)	Chronic inflammatory cells, fibrosis	160.0	163.0
K83/12	Male	59	Both kidneys	Lymphocytes, fibrosis, thyroidization	300.0; 120.0	305.7; 122.3
K87/12	Male	24	Left kidney	Fibrosis, extensive infiltrate of lymphocytes	140.0; 140.0	142.7; 142.7
K93/12	Male	72	Both kidneys	Chronic inflammatory cells, fibrosis	100.0; 110.0	101.9; 112.1
K97/12	Male	*	Right kidney	Lymphocytes, fibrosis	180.0	183.4
K98/12	Male	42	Right kidney	Fibrosis, glomerulosclerosis, chronic inflammatory cells	190.0	193.6
K99/12	Male	47	Both kidneys	Fibrosis, chronic inflammatory cells, sclerotic glomeruli	150.0; 190.0	152.9; 193.6

<i>Cadaver Ref. Nr.</i>	<i>Sex</i>	<i>Age*</i>	<i>Anatomical Involvement and Macroscopic Appearance</i>	<i>Microscopic Findings</i>	<i>Absolute Weight (g)</i>	<i>Adapted Weight (g)**</i>
K107/12	Female	62	Both kidneys	Chronic inflammatory infiltrate, fibrosis	80.0; 90.0	81.5; 91.7

* Age is unavailable

** Mean percent change with formalin fixation = + 1.9% (according to Finkbeiner et al., 2004)

--- Weight is unavailable

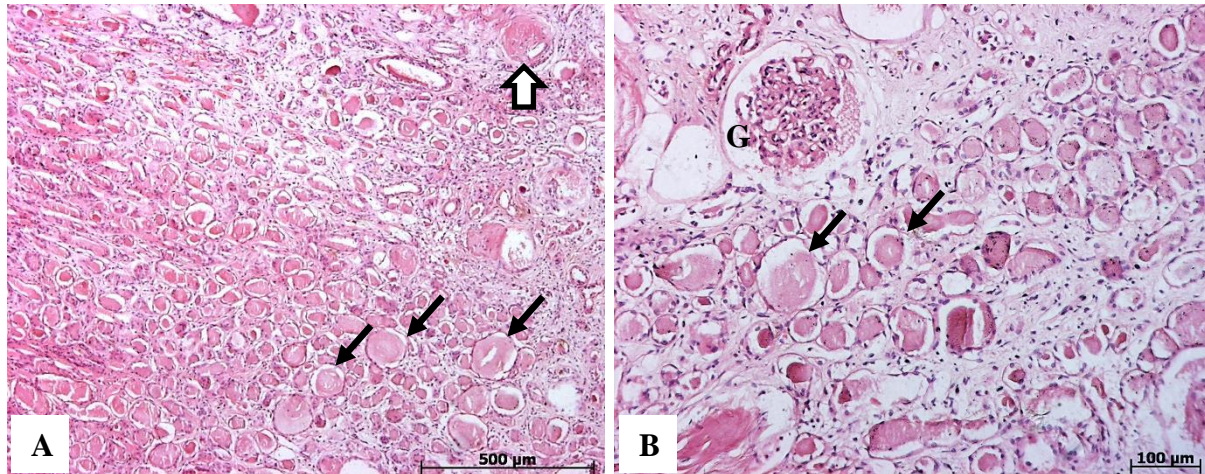


Figure 4.77. Microscopic appearance of chronic pyelonephritis. A) Thyroidization was observed in the right renal parenchyma of cadaver K82/12, H&E (50x); B) thyroidization in the right renal parenchyma of cadaver K58/12, H&E (100x), glomerulosclerosis (blocked arrow), glomerulus (G), thyroidization (small, black arrows).

4.5.5 Cystic Renal Disease

Simple cysts were seen in 18/127 (14.2%) cadavers (Table 4.56). The male to female ratio was 1.2:1. An average age of 58.5 years was noted. The simple cysts were generally seen as harmless lesions in the kidneys, either as solitary lesions 9/18 (50.0%) or as multiple lesions 9/18 (50.0%) of variable sizes. The right and left kidneys were affected in 7/18 (38.9%) and 9/18 (50.0%) cadavers, respectively. Bilateral involvement was noted in 2/18 (11.1%) cadavers. On gross inspection, the cysts were found to be lined by a smooth membrane and were mainly confined to the renal cortex (Figure 4.78). Massive cysts were encountered in 3/18 (16.7%) cadavers (Figure 4.78, A and C). Histologically, the membranes of the simple cysts were composed of a simple cuboidal epithelium (Figure 4.79).

Table 4.56. Simple renal cysts in the cadaver cohort (n=127)

<i>Cadaver Ref. Nr.</i>	<i>Sex</i>	<i>Age*</i>	<i>Solitary/ Multiple</i>	<i>Unilateral/ Bilateral</i>	<i>Renal Involvement</i>	<i>Absolute Weight (g)</i>	<i>Adapted Weight (g)**</i>
K83/09	Male	60	Solitary	Unilateral	Left kidney	---	---
K87/09	Male	*	Multiple	Unilateral	Right kidney	---	---
K106/09	Male	*	Multiple	Unilateral	Left kidney	---	---
K03/10	Male	34	Solitary	Unilateral	Right kidney	---	---
K12/10	Male	37	Multiple	Unilateral	Left kidney	---	---
K30/10	Male	*	Multiple	Bilateral	Both kidneys	---	---
K18/11	Female	76	Solitary	Unilateral	Left kidney	130.0	132.5
K47/11	Male	64	Solitary	Unilateral	Right kidney	150.0	152.9
K53/11	Male	*	Solitary	Unilateral	Right kidney	150.0	152.9
K69/11	Female	63	Multiple	Unilateral	Left kidney	80.0	81.5
K130/11	Female	81	Solitary	Unilateral	Left kidney	75.0	76.4
K27/12	Male	66	Solitary	Unilateral	Right kidney	210.0	214.0
K43/12	Male	*	Solitary	Unilateral	Right kidney	160.0	163.0
K46/12	Male	46	Multiple	Unilateral	Left kidney	90.0	91.7
K62/12	Female	73	Multiple	Bilateral	Both kidneys	120.0; 260.0	122.3; 264.9
K66/12	Female	55	Solitary	Unilateral	Left kidney	100.0	101.9
K82/12	Male	63	Multiple	Unilateral	Left kidney	160.0	163.0
K98/12	Male	42	Multiple	Unilateral	Right kidney	190.0	193.6

* Age is unavailable

** Mean percent change with formalin fixation = + 1.9% (according to Finkbeiner et al., 2004)

--- Weight is unavailable

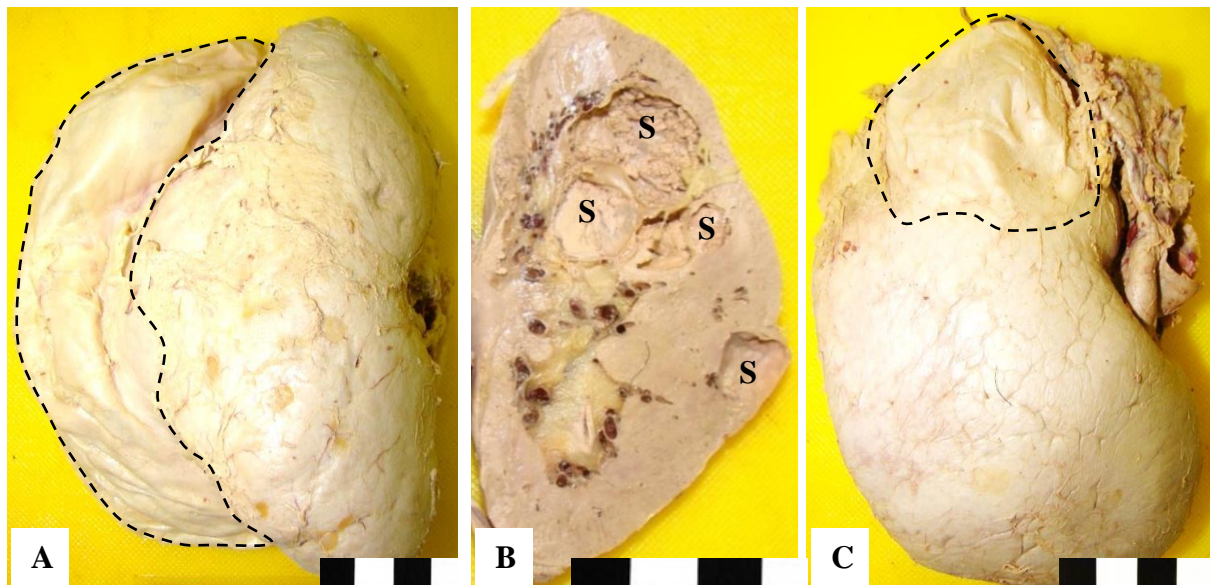


Figure 4.78. Macroscopic appearance of simple renal cysts. A) a large simple cyst (dashed lines) located in the right kidney of cadaver K62/12, anterior view; B) simple cysts in the parenchyma of the K82/12, longitudinal section, anterior view; C) simple cyst located superiorly in the right kidney of cadaver K27/12, anterior view.

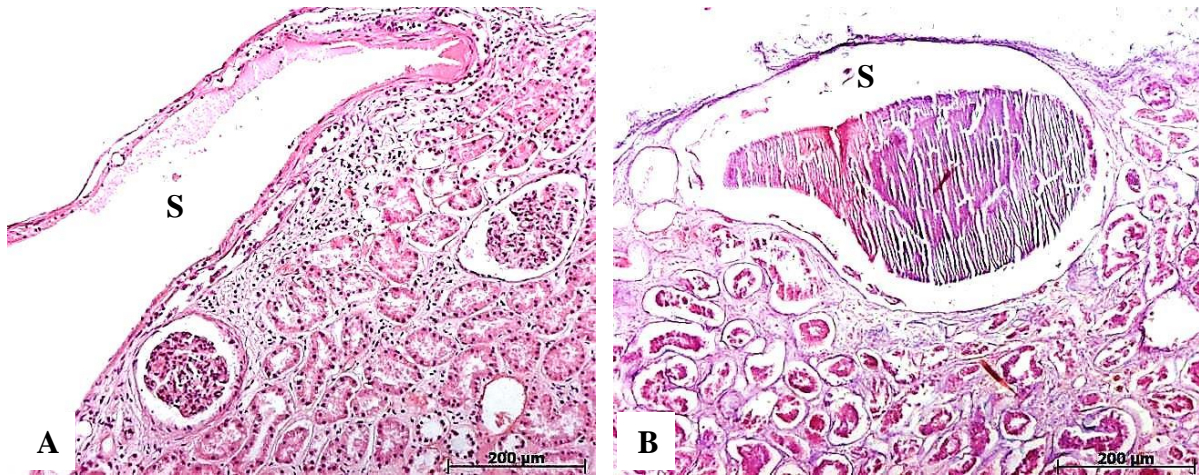


Figure 4.79. Microscopic appearance of simple renal cysts. A) Microscopic appearance of a simple cyst (K98/12), H&E (100x); B) simple cyst with contents in cadaver K62/11, H&E (100x); cyst (S).

4.5.6 Hypertensive Nephrosclerosis

Hypertensive nephrosclerosis was observed in 8/127 (6.3%) cadavers (Table 4.57). The male to female ratio was 3.2:1 and the average age of the affected cadavers was 61.1 years. Of these, 5/8 (62.5%) presented with benign (essential) nephrosclerosis, while malignant (accelerated) nephrosclerosis was observed in 3/8 (37.5%) cadavers. The average age of the affected cadavers was 60.8 years. Histologically, benign hypertension in the cadavers presented with marked thickening of the blood vessel walls of large- and medium-sized renal arteries within the renal parenchyma. Thickening of the arterial walls occurred as a result of a combination of medial hypertrophy and fibrous intimal thickening. The resultant decrease in the walls led to progressive sclerosis of the glomeruli. Malignant nephrosclerosis, characterized by a more severe and rapid form of hypertension, showed microscopic concentric intimal thickening of the large- and medium-sized renal arteries (Figure 4.80). This gave the arteries an “onion-skin” appearance due to the laminated, concentric intimal thickening (Figure 4.80).

Table 4.57. Hypertensive nephrosclerosis in the cadaver cohort (n=127)

<i>Cadaver Ref. Nr.</i>	<i>Sex</i>	<i>Age*</i>	<i>Anatomical Involvement and Microscopic Findings</i>	<i>Type of Hypertensive Nephrosclerosis</i>	<i>Absolute Weight (g)</i>	<i>Adapted Weight (g)*</i>
K18/11	Female	76	Left kidney	Malignant nephrosclerosis	130.0	132.5
K42/11	Male	*	Both kidneys	Benign nephrosclerosis	180.0; 140.0	183.4; 142.7
K46/12	Male	46	Right kidney	Benign nephrosclerosis	100.0	101.9
K58/12	Male	70	Right kidney	Malignant nephrosclerosis	90.0	91.7
K82/12	Male	63	Right kidney (Fig. 4.80)	Malignant nephrosclerosis	160.0	163.0
K83/12	Male	59	Both kidneys	Benign nephrosclerosis	300.0; 120.0	305.7; 122.3
K93/12	Male	72	Right kidney	Benign nephrosclerosis	100.0	101.9
K98/12	Male	42	Right kidney	Benign nephrosclerosis	190.0	193.6

* Mean percent change with formalin fixation = + 1.9% (according to Finkbeiner et al., 2004)

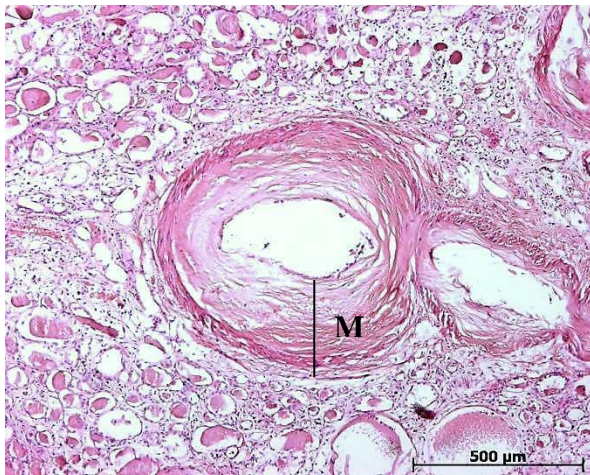


Figure 4.80. Microscopy of nephrosclerosis. Malignant arteriosclerosis (M) in the kidney parenchyma of cadaver K82/12, H&E (50x).

4.5.7 Healed Fibrotic Scars

Healed fibrotic renal scars was observed in 3/127 (2.4%) cadavers (Table 4.58). All of the cadavers affected were males. The average age of the affected cadavers was 56.7 years. Macroscopically, the scars had a wedge-shaped appearance and resembled an anemic infarct which occurred as a result of arterial occlusion in organs with end-arterial circulations. The margins of the scars had a hemorrhagic appearance (Figure 4.81, A). Histologically, the infarcted area had several sclerotic glomeruli as a result of hypoxia. Fibrosis was a prominent feature in the renal scars (Figure 4.81, B).

Table 4.58. Healed fibrotic renal scars in the cadaver cohort (n=127)

<i>Cadaver Ref. Nr.</i>	<i>Sex</i>	<i>Age</i>	<i>Anatomical Involvement and Macroscopic Appearance</i>	<i>Microscopic Findings</i>	<i>Absolute Weight (g)</i>	<i>Adapted Weight (g)*</i>
K03/10	Male	34	Right kidney	Wedge-shaped infarcted lesion with fibrosis	---	---
K47/11	Male	64	Right kidney (Fig. 4.81, A)	Large wedge-shaped lesion, fibrosis and glomerulosclerosis	150.0	152.9
K73/12	Male	72	Superior region of right kidney (Fig. 4.81, B)	Large wedge-shaped lesion with fibrosis	90.0	91.7

* Mean percent change with formalin fixation = + 1.9% (according to Finkbeiner et al., 2004)

--- Weight is unavailable

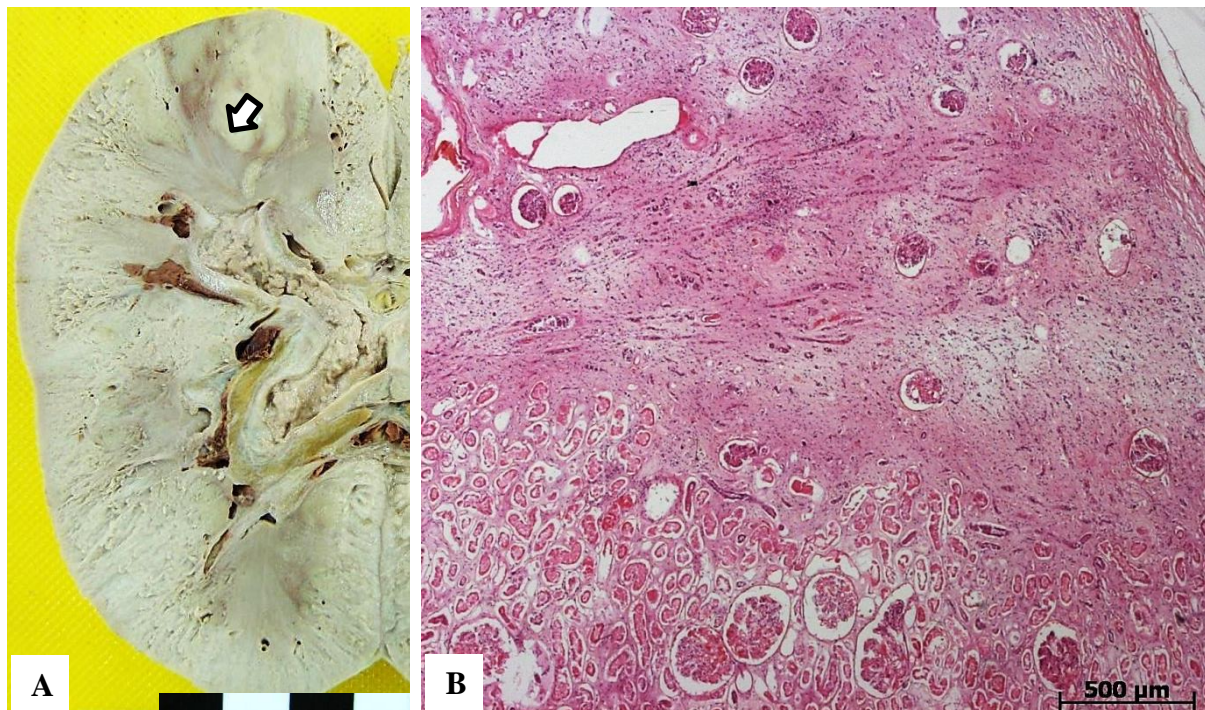


Figure 4.81. Healed fibrotic renal infarction. A) Right renal parenchyma of cadaver K47/11 shows a wedge-shaped scar (blocked arrow); longitudinal section, anterior view; B) fibrosis, sclerosis and an inflammatory infiltrate are the features of a healed fibrotic infarction, cadaver K73/12, H&E (25x).

4.5.8 Renal Neoplasms

Renal neoplasms were observed in 2/127 (1.6%) of the cadavers (Table 4.59). Both cadavers were males with an average of 52.0 years. Bilateral involvement was observed in both cadavers and both renal neoplasms were as a result of distant metastases from the lungs. Cadaver K94/12 presented with pale, fibrotic areas in the renal parenchyma (Figure 4.82, A). Histologically, the squamous cell carcinoma (SCC) tumor infiltrated the renal parenchyma of

both kidneys (Figure 4.83, A). Keratin pearls were absent and small areas of necrosis were visible (Figure 4.83, B). Tumor tissue completely replaced functional parenchyma in the left kidney of cadaver K106/12 (Figure 4.82, B), while a large, infiltrating neoplasm was observed superior to the right kidney (Figure 4.82, C). Histologically, fibrosis and necrosis was observed (Figure 4.83, B and C). Immunohistochemistry was applied to determine the origin and classification of the tumor in cadaver K106/12. Cytokeratin 7 (CK7) and cytokeratin 20 (CK20) markers were used. The result was CK7+/CK20- (Figure 4.84). A periodic acid-Schiff (PAS) stain was used to stain for the presence of mucins. The PAS stain was positive (Figure 4.85), which confirms the presence of an adenocarcinoma (ACA).

Table 4.59. Renal tumors in the cadaver cohort (n=127)

<i>Cadaver Ref. Nr.</i>	<i>Sex</i>	<i>Age</i>	<i>Macroscopic Appearance</i>	<i>Microscopic Findings</i>	<i>Absolute Weight (g)</i>	<i>Adapted Weight (g)*</i>
K94/12	Male	60	Both kidneys: pale, fibrotic areas within the renal parenchyma	Squamous cells in origin, keratin pearls absent, necrosis	220.0, 200.0	224.2; 203.8
K106/12	Male	44	Right: large, infiltrating growth superior to the kidney; Left: fibrotic growth infiltrated into renal parenchyma	Fibrosis, necrosis, dysplasia, pleomorphic and papillary appearance, ACA in origin	380.0, 410.0	387.2; 417.8

* Mean percent change with formalin fixation = + 1.9% (according to Finkbeiner et al., 2004)

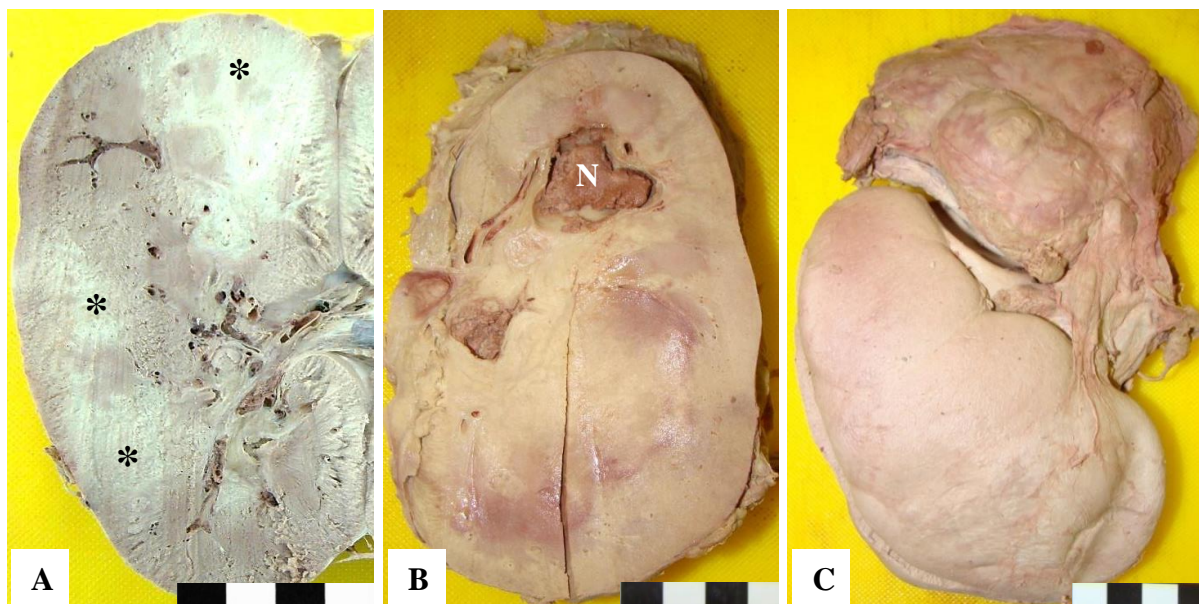


Figure 4.82. Macroscopic appearance of renal tumors in our cadaver cohort. A) Pale, fibrotic areas (asterisks) in the right kidney of cadaver K94/12, longitudinal section, anterior view; B) extensive fibrosis and necrosis in the left kidney of cadaver K106/12; longitudinal section, anterior view. The tumor tissue has entirely replaced the functional renal parenchyma; C) tumor tissue located superior to the right kidney of K106/12, anterior view.

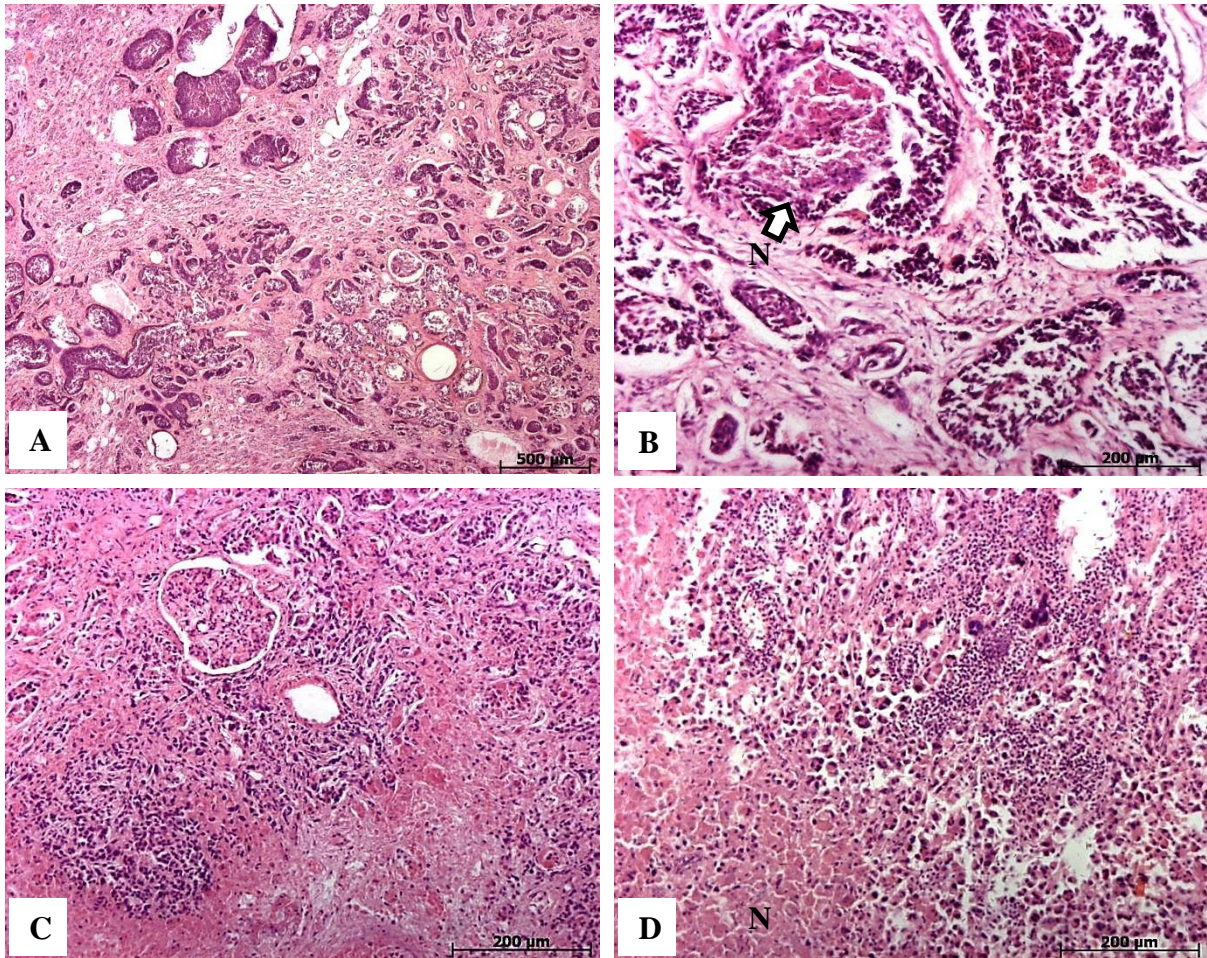


Figure 4.83. Microscopic appearance of renal tumors in our cadaver cohort. A) Squamous cell carcinoma (SCC) infiltrated the right kidney of cadaver K94/12, H&E (25x); B) small areas of necrosis (N) were present in the left kidney of cadaver K94/12, while keratin pearls were absent, H&E (100x); C) necrosis with dysplasia were observed in the left kidney of cadaver K106/12, H&E (100x); E) areas of necrosis (N) in the right kidney of cadaver K106/12, H&E (100x).

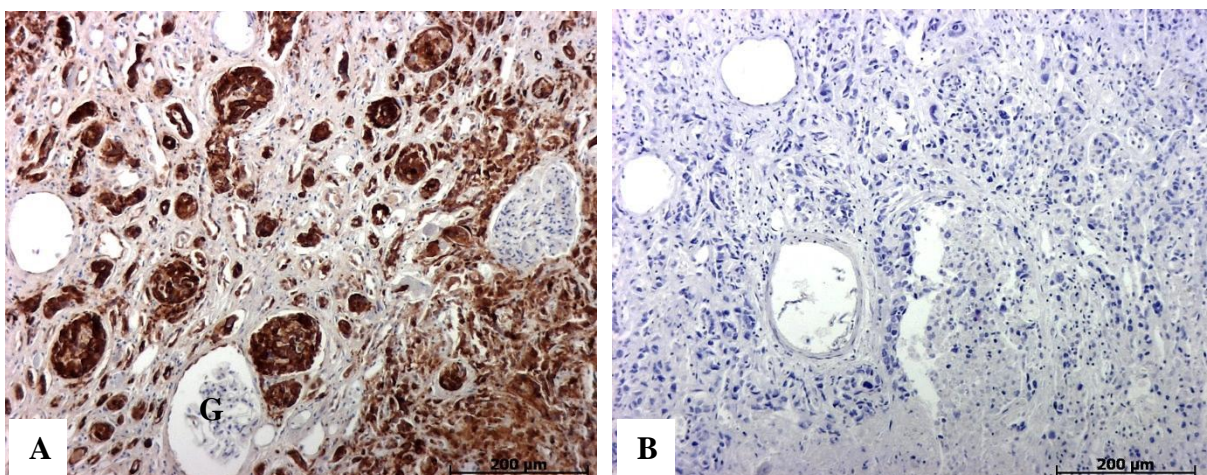


Figure 4.84. Immunohistochemistry of the renal tumor in cadaver K106/12. A) The tumor stained positively with the antibody to CK7, left kidney (100x); B) the tumor did not stain for the antibody to CK20, left kidney (100x); glomeruli (G).

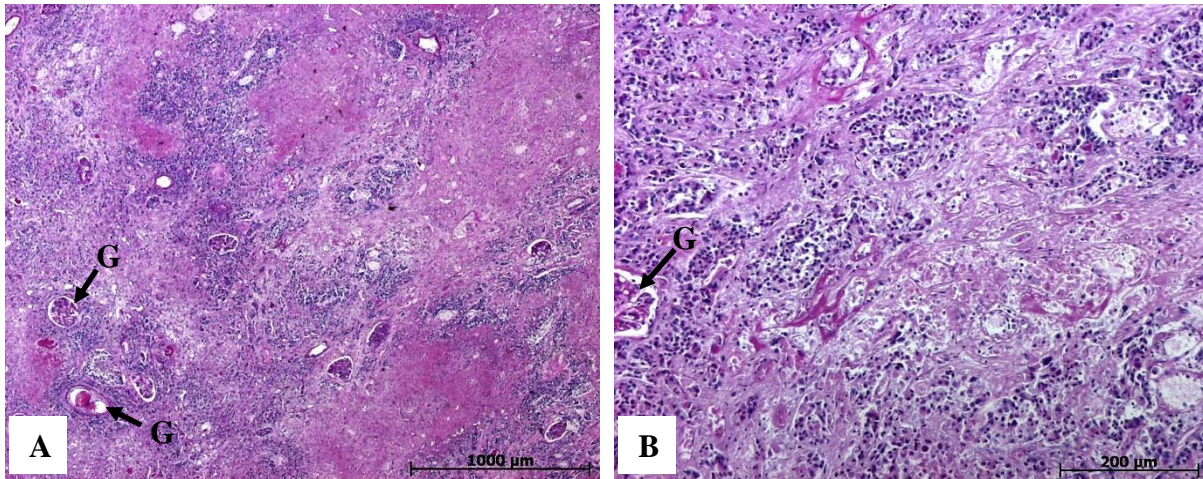


Figure 4.85. PAS stain of the tumor in cadaver K106/12. A) Mucins were illustrated in the left kidney, PAS (25x); B) magnification of A) showing the magenta-stained mucins in the left kidney, PAS stain (100x); glomeruli (G).

4.6 Male Genital System

4.6.1 Diseases of the Prostate

4.6.1.1 Benign Prostatic Hyperplasia (BPH)

Benign prostatic hyperplasia (BPH) or nodular hyperplasia was observed in 12/56 (21.4%) cadavers from the 2012 and 2013 cohorts (Table 4.60). The average age of the affected cadavers was 59.6 years. The prostate is generally enlarged; the nodules originate in the transitional zone and are of well-circumscribed that bulge from the surface. The nodules were solid in all of the cases with BPH (Figure 4.86, A). The urethra was compressed by the nodules. The peripheral prostatic glandular components were not involved and were compressed and atrophic. Histologically, the nodules contained proliferating glandular tissue and fibromuscular stroma. The proliferating glands were lined by columnar epithelium as well as a layer of basal cells (Figure 4.86, B). The hyperplastic nodules were observed in the para-urethral part of the gland and compressed the peripheral part. Occasionally, corpora amylacea were observed during histological examination (Figure 4.86, B).

Table 4.60. Benign prostatic hyperplasia in the cadaver cohort (n=56)

<i>Cadaver Ref. Nr.</i>	<i>Age*</i>	<i>Macroscopic Appearance</i>	<i>Microscopic Findings</i>
K15/11	33	Prostate slightly enlarged with prominent nodules in parenchyma	Areas of chronic inflammation dispersed through hyperplastic nodules
K42/11	*	Nodular and firm appearance	Hyperplastic nodules, fibrosis and corpora amylacea
K55/11	43	Nodules on the right side (in the transitional zone)	Hyperplastic nodules and fibrosis
K62/11	83	Nodular and firm appearance	Hyperplastic nodules, fibrosis and corpora amylacea
K74/11	70	Entire prostate has an extensively nodular appearance	Hyperplastic nodules with fibrosis
K129/11	65	Extensively nodular appearance	Hyperplastic nodules and fibrosis
K138/11	57	Nodules on the left side (in the transitional zone)	Hyperplastic nodules, fibrosis and corpora amylacea
K27/12	66	Nodules on both sides of the inner part of the transition zone (Fig. 4.86, A)	Hyperplastic nodules, fibrosis, corpora amylacea and ACA
K52/12	57	Nodular and firm appearance	Hyperplastic nodules and fibrosis
K78/12	61	Nodular and firm appearance	Hyperplastic nodules, fibrosis and corpora amylacea
K81/12	49	Nodular and firm appearance	Hyperplastic nodules and fibrosis (Fig. 4.86, B)
K93/12	72	Large nodules in prostatic transition zone	Areas of chronic inflammation dispersed through hyperplastic nodules, corpora amylacea

* Age is unavailable

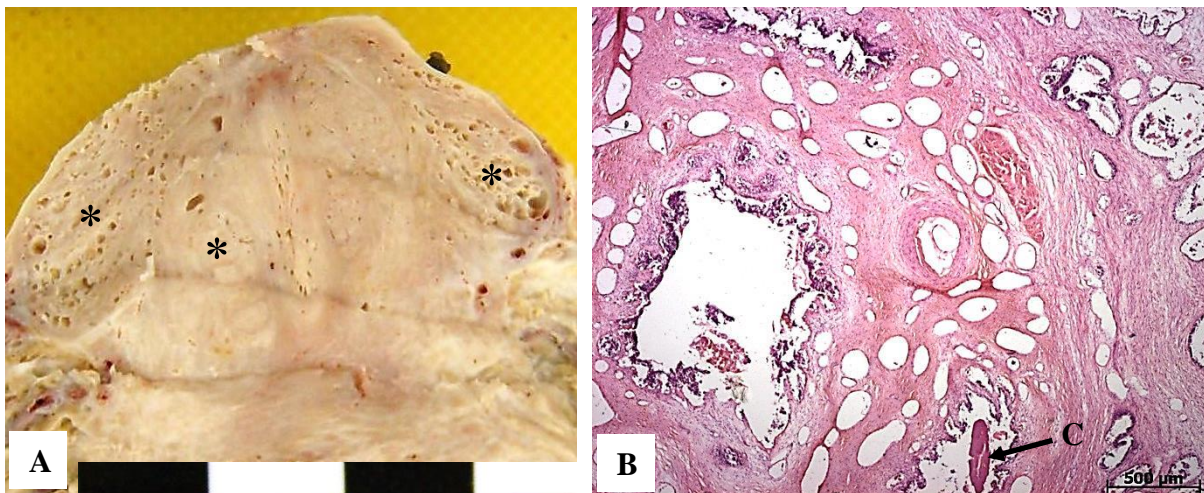


Figure 4.86. Benign prostatic hyperplasia (BPH). A) Prostate (K27/12) with a nodular appearance in the outer zone; B) round nodules of hyperplastic prostatic tissue in the prostate of cadaver K81/12, H&E (25x); nodules (asterisk), corpora amylacea (C).

4.6.1.2 Prostatic Adenocarcinoma

Adenocarcinoma (ACA) of the prostate was seen in 1/56 (1.8%) cadaver (Table 4.61). The cadaver was 66 years at time of death. The ACA was an incidental finding on histological examination for BPH (Figure 4.87). Incidental (latent) carcinomas of the prostate are

common incidental findings in old age. The ACA was a small tumor with no signs of metastases.

Table 4.61. Prostatic adenocarcinoma in the cadaver cohort (n=56)

<i>Cadaver Ref. Nr.</i>	<i>Age</i>	<i>Macroscopic Appearance</i>	<i>Microscopic Evaluation</i>
K27/12	66	No obvious macroscopic findings, benign prostatic hyperplasia, no metastases (Fig. 4.87, A)	Incidental finding, BPH, neoplastic glands, fibrous stroma (Fig. 4.87, B)

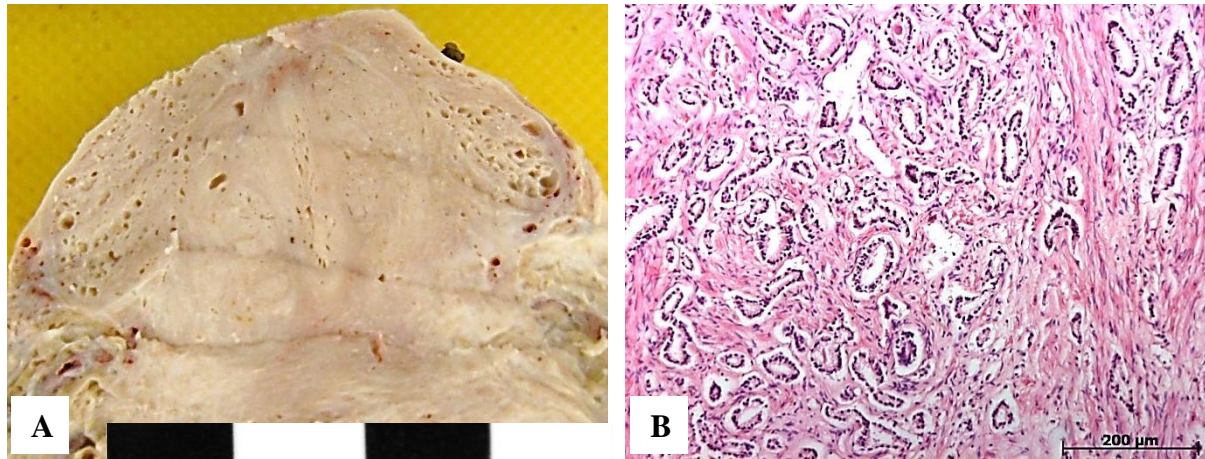


Figure 4.87. Prostatic adenocarcinoma. A) Prostate of cadaver K27/12 with extensive BPH in the periurethral zone and peripherally located carcinoma; B) prostatic adenocarcinoma consisting of neoplastic glands dispersed through and infiltrating a fibrous stroma.

4.6.1.3 Corpora Amylacea

Corpora amylacea was observed in 7/56 (12.5%) cadavers (Table 4.62). The average age of the cadaver with corpora was 66.0 years. The prostates with a hyperplastic appearance contained microcystic structures which represent dilated hyperplastic glands (Figure 4.88, A). The glandular epithelium contained inspissated proteinaceous material which was round to oval-shaped eosinophilic bodies in the glandular lumina (Figure 4.88, B).

Table 4.62. Corpora amylacea in the cadaver cohort (n=56)

<i>Cadaver Ref. Nr.</i>	<i>Age*</i>	<i>Macroscopic Appearance</i>	<i>Microscopic Findings</i>
K42/11	*	No obvious cystic spaces within prostatic parenchyma	Few, small proteinaceous concretions
K44/11	48	No obvious cystic spaces within prostatic parenchyma	Few, small proteinaceous concretions
K53/11	*	Small, cystic space containing black material	Small proteinaceous concretions
K62/11	83	No obvious cystic spaces within prostatic parenchyma	Few, small proteinaceous concretions

<i>Cadaver Ref. Nr.</i>	<i>Age*</i>	<i>Macroscopic Appearance</i>	<i>Microscopic Findings</i>
K27/12	66	No obvious cystic spaces were seen	Several, small, oval-shaped concretions were noted
K78/12	61	Three cystic spaces with small, black stones (Fig. 4.88, A)	Few, small, oval-shaped proteinaceous concretions (Fig. 4.88, B)
K93/12	72	Small, cystic space containing black material	Small proteinaceous concretions

* Age is unavailable

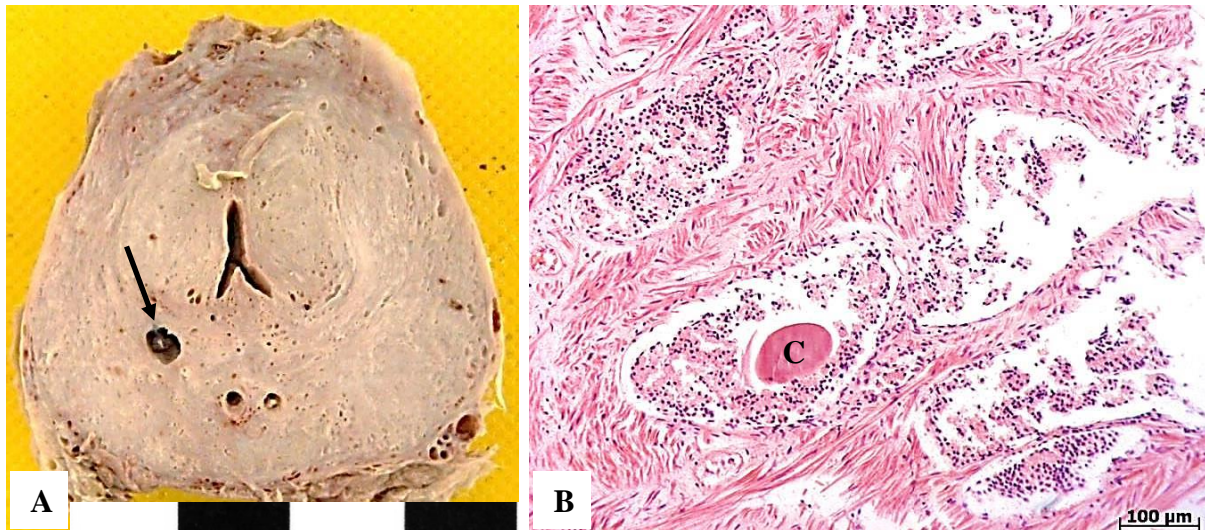


Figure 4.88. Corpora amylacea. A) Prostate (K78/12) with corpora amylacea within the outer zone (arrow); B) histology section (K78/12), H&E (100x), showing the location of the corpora amylacea within a gland; corpora amylacea (C).

4.6.1.4 Prostatitis

Prostatitis was observed in 3/56 (5.4%) cadavers (Table 4.63). Of these cases, 1/3 (33.3%) was classified as acute prostatitis and 2/3 (66.7%) chronic prostatitis. Histologically, small foci of inflammatory cells were observed within the prostatic parenchyma (Figure 4.89).

Table 4.63. Prostatitis in the cadaver cohort (n=56)

<i>Cadaver Ref. Nr.</i>	<i>Age</i>	<i>Macroscopic Appearance and Microscopic Findings</i>	<i>Diagnosis</i>
K15/11	33	Small foci of chronic inflammatory infiltrate within the prostatic parenchyma	Chronic prostatitis
K53/11	*	Foci of acute and chronic inflammatory infiltrate within prostatic stroma	Acute and chronic prostatitis
K93/12	72	Chronic inflammatory infiltrate in fibrotic stroma (Fig. 4.89)	Chronic prostatitis

* Age is unavailable

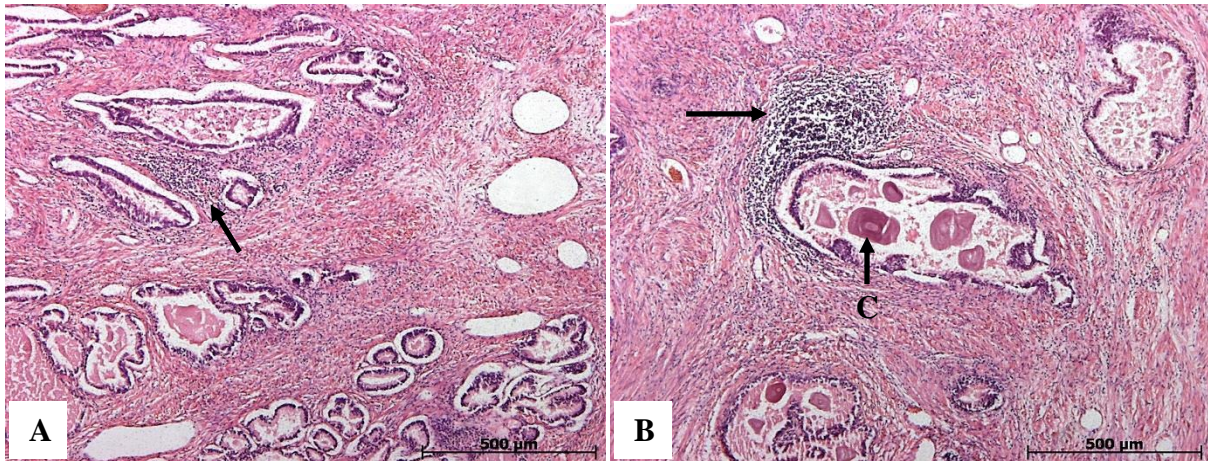


Figure 4.89. Microscopy of chronic prostatitis. A) Prostate of cadaver K93/12 showing inflammatory infiltrate within the prostatic parenchyma, H&E (50x); B) the same prostate as in (A) with lymphocytes and corpora amylacea within the glandular components, H&E (50x); corpora amylacea (C), lymphocytes (arrows).

4.6.2 Diseases of the Testis

4.6.2.1 Testicular Tuberculosis

Testicular TB was observed in 1/87 (1.1%) cadaver. The right testis of cadaver K15/11 was extensively enlarged with nodular fibrosis. Histologically, several granulomas with scattered lymphocytes were observed in the testicular parenchyma (Figure 4.90, B).

Table 4.64. Testicular TB in the cadaver cohort (n=56)

<i>Cadaver Ref. Nr.</i>	<i>Age</i>	<i>Involvement</i>	<i>Macroscopic Appearance</i>	<i>Microscopic Evaluation</i>
K15/11	33	Right (unilateral)	Enlarged	Tuberculous granulomas with scattered lymphocytes



Figure 4.90. Testicular TB. A) X-ray of the scrotal region of cadaver K15/11 with signs of enlargement; B) granulomatous reaction and scattered lymphocytes within the right testicular parenchyma, H&E (25x).

4.6.2.2 Hydrocele

A hydrocele was noted in 1/87 (1.1%) cadaver (Table 4.65). On gross inspection, the scrotum appeared enlarged (Figure 4.91, A). A hydrocele was noted as an accumulation of fluid within the sac of the tunica vaginalis, which is lined by a serosal membrane. The protein poor fluid (transudate) produced an enlarged testis (Figure 4.91, B).

Table 4.65. Hydrocele in the cadaver cohort (n=56)

<i>Cadaver Ref. Nr</i>	<i>Age</i>	<i>Involvement</i>	<i>Macroscopic Appearance</i>
K46/12	46	Right (unilateral)	Enlarged

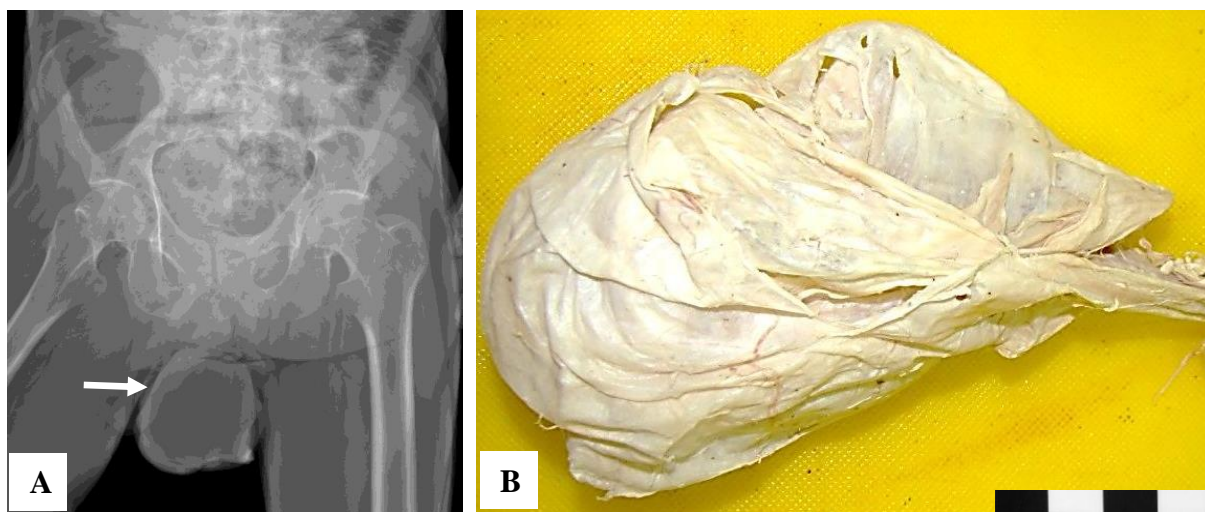


Figure 4.91. Hydrocele. A) X-ray of the cadaver K46/12 who presented with a unilateral hydrocele; B) on gross inspection, the right testis of cadaver K46/12 was greatly enlarged and appeared cyst-like with contents. The left testis was within normal limits.

4.6.2.3 Varicocele

Testicular varices, or varicocele, was observed in 1/87 (1.1%) cadaver (Table 4.66). A large number of blood vessels were found in the left testis of cadaver K95/09 while the right testis had a normal appearance. Histologically, the seminiferous tubules had an abnormal and irregular appearance (Figure 4.92).

Table 4.66. Varicocele in the cadaver cohort (n=56)

<i>Cadaver Ref. Nr</i>	<i>Involvement</i>	<i>Macroscopic Appearance</i>	<i>Microscopic Appearance</i>
K95/09	Left (unilateral)	Testicular atrophy	Blood vessels with abnormal parenchyma

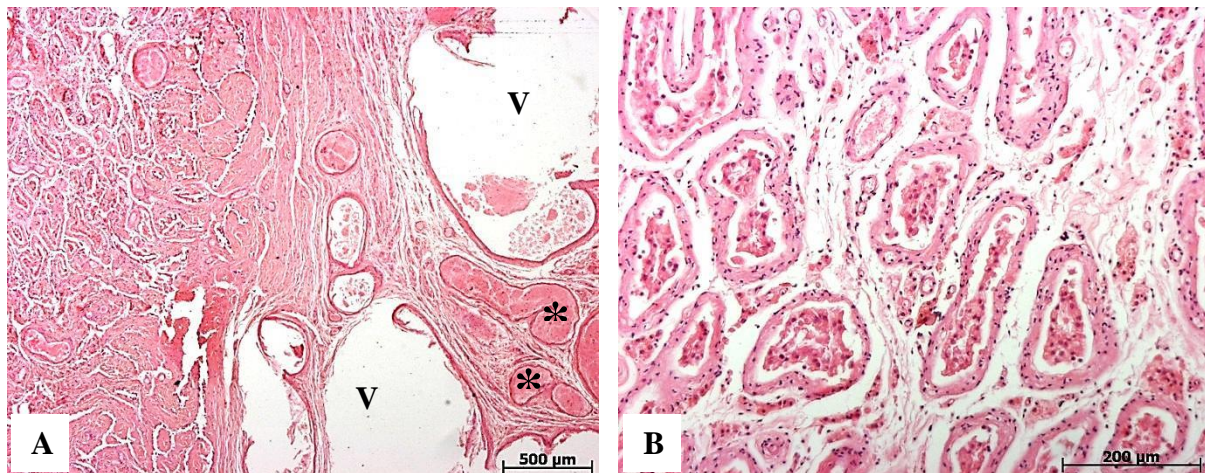


Figure 4.92. Microscopic appearance of varicocele. A) Several blood vessels (V), some filled with blood (*) were found in the left testis of cadaver K95/09, H&E (25x); B) magnification of the testicular parenchyma, revealed irregular and abnormal seminiferous tubules, H&E (100x).

4.7 Female Genital System

4.7.1 Uterine Fibroid Leiomyomas

Fibroid leiomyomas were observed in 4/40 (10.0%) cadavers (Table 4.67). The average age of the affected cadavers was 58.0 years. One cadaver (K100/12) presented with intramural leiomyomas, while cadavers K64/11 and K28/12 presented with both intra- and extramural leiomyomas (Figure 4.93, A). One cadaver showed signs of pedunculated growth in the uterine fundus. Histologically, the leiomyomas presented as well circumscribed lesions with a typical whirled pattern (Figure 4.93, B).

Table 4.67. Uterine leiomyomas in the cadaver cohort (n=40)

<i>Cadaver Ref. Nr.</i>	<i>Age</i>	<i>Macroscopic Appearance</i>	<i>Microscopic Findings</i>
K18/11	76	Pedunculated leiomyoma in the uterine fundus	Cells of the leiomyoma arranged in a whirly pattern
K64/11	48	Several intramural and extramural leiomyomas	Cells arranged in a whirled pattern (Fig. 4.93, B)
K28/12	62	Several intramural and extramural leiomyomas (large uterus – 260g) (Fig. 4.93, A)	Cells of the leiomyoma are arranged in a whirled pattern
K100/12	46	Two intramural leiomyomas	Cells arranged in a whirled pattern

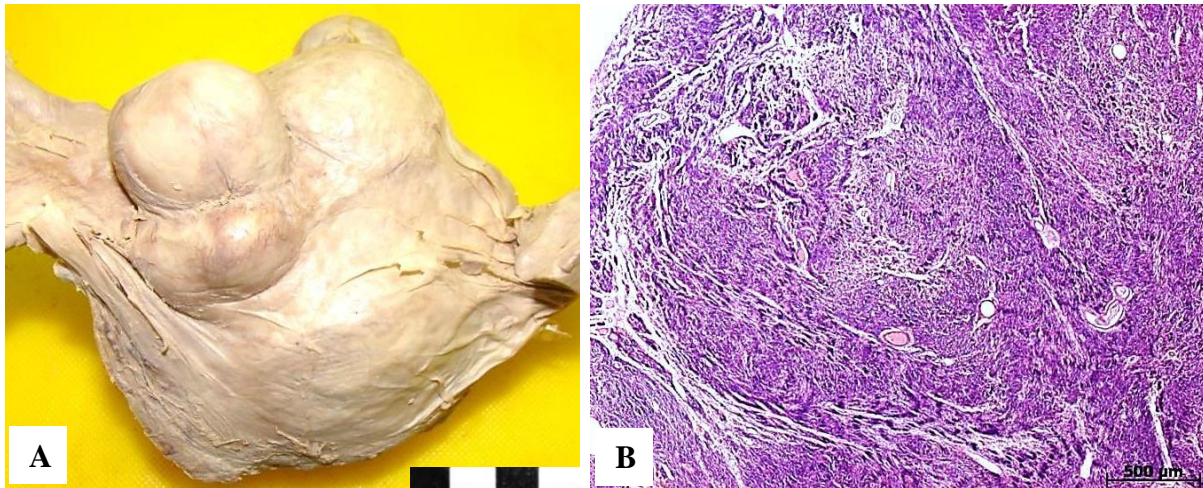


Figure 4.93. Uterine leiomyoma. A) Extensive fibroid leiomyomas are present in the uterus of cadaver K28/12; B) whirled pattern in the leiomyoma (K64/11), H&E (25x).

4.7.2 Cervical Intraepithelial Neoplasia (CIN)

Cervical intraepithelial neoplasia (CIN) was observed in 2/40 (5.0%) of the female cadavers from the 2012 and 2013 cohort (Table 4.68). Two of the three stages of CIN were observed in the cadavers. CIN I was seen in cadaver K13/11 (Figure 4.94, A). Histological, the cervical epithelium of this cadaver, dysplastic changes were seen in the lower third of the squamous epithelium. Koilocytotic change was seen in the superficial layers of the cervical epithelium (Figure 4.94, A). The cellular changes observed were consistent with a human papilloma virus (HPV) infection. Cadaver K10/11 on the other hand, showed microscopical signs significant of CIN, however, the grading of CIN was inconclusive as the cervical epithelium was sloughed off (Figure 4.94, B).

Table 4.68. Cervical intraepithelial neoplasia in the cadaver cohort (n=40)

<i>Cadaver Ref. Nr.</i>	<i>Age</i>	<i>Macroscopic Appearance</i>	<i>Microscopic Findings</i>	<i>Classification of CIN</i>
K10/11	45	Cervix appeared thickened	Koilocytotic atypia, dysplasia in lower third of epithelium	Inconclusive
K13/11	47	Cervix appeared thickened	Dysplastic changes in middle third of epithelium, koilocytotic changes	CIN I

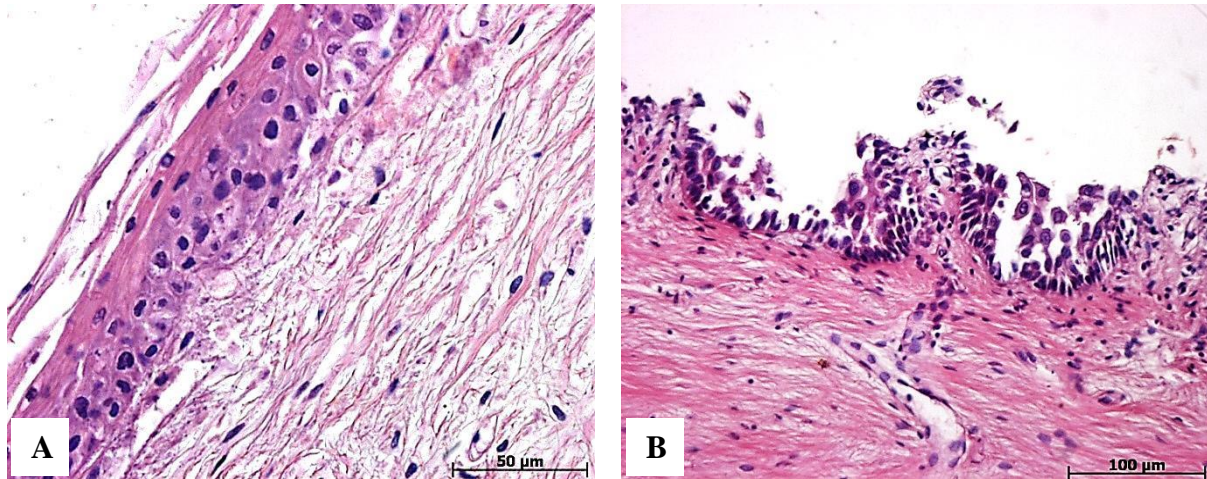


Figure 4.94. Microscopic appearance of cervical intraepithelial neoplasia (CIN). A) Mild dysplasia seen in the epithelium of the cervix of cadaver K13/11. The dysplastic epithelium contains enlarged, crowded cells with hyperchromasia, H&E (400x); B) the cervical epithelium of cadaver K10/11 was sloughed off resulting in an inconclusive grading of the CIN, H&E (200x).

4.8 Lymphoreticular System

4.8.1 Lymph Node Involvement

4.8.1.1 Tuberculous lymphadenitis

Tuberculous lymphadenitis was observed in 14/127 (11.0%) cadavers (Table 4.69), making it the most frequent manifestation of extrapulmonary tuberculosis in the cadaver population. The male to female ratio was 1:1.2 and the average age of the affected cadavers was 50.5 years. No signs of cervical lymph node involvement, also known as “scrofula”, were observed in the cadaver cohort. Enlargement of the mediastinal lymph nodes (lymphadenopathy) was mainly unilateral in 11/14 (78.6%) cadavers. These cadavers presented with no other concurrent extranodal involvement. A total of 4/14 (28.6%) cadavers presented with multifocal lymph nodal involvement. Macroscopically, the lymph nodes were enlarged with concomitant anthracotic pigmentation and caseation (Figure 4.95, A). Microscopically, the lymph nodes showed signs of a granulomatous reaction with central caseation (Figure 4.95, B). The affected lymph nodes generally contained more than one granuloma.

Table 4.69. Tuberculous lymphadenitis in the cadaver cohort (n=127)

<i>Cadaver Ref. Nr.</i>	<i>Sex</i>	<i>Age *</i>	<i>Lymph Nodal Involvement</i>	<i>Morphology</i>	<i>Pulmonary Lesions</i>	<i>Extrapulmonary Lesions</i>
K87/09	Male	*	Right and left hilar lymph nodes	Lymphadenopathy with anthracotic pigmentation and caseation (Fig. 4.95, A)	Bilateral PTB	Hepatic, splenic TB
K52/11	Male	48	Right hilar lymph nodes	Lymphadenopathy with anthracosis	Bilateral PTB	Hepatic, renal TB
K65/11	Female	52	Right hilar nodes, hepatic, pancreatic nodes	Caseating necrosis and anthracotic pigmentation	Right PTB	Hepatic, renal TB
K119/11	Male	*	Right and left hilar lymph nodes	Left side is more affected than right side with caseating necrosis	Bilateral PTB	Hepatic, splenic TB
K121/11	Male	50	Left hilar lymph nodes, pancreatic lymph nodes	Extensive lymphadenopathy, caseating necrosis	Bilateral PTB	Hepatic, splenic and renal TB
K124/11	Female	*	Right hilar lymph nodes	Anthracotic lymph nodes, caseating necrosis	Bilateral PTB	Hepatic, splenic TB
K140/11	Female	42	Duodenal lymph nodes, right inguinal nodes	Lymphadenopathy with caseating necrosis (Fig. 4.95, B)	Bilateral PTB	Hepatic, splenic and renal TB
K27/12	Male	66	Right hilar lymph nodes	Lymphadenopathy with caseating necrosis	Bilateral PTB	Absent
K61/12	Male	52	Right hilar lymph nodes	Lymphadenopathy with caseating necrosis	Bilateral PTB	Absent
K77/12	Female	32	Left hilar lymph nodes	Lymphadenopathy, caseation	Bilateral PTB	Absent
K81/12	Male	49	Right hilar lymph nodes	Anthracosis, caseating necrosis, granulomas	Right PTB	Absent
K93/12	Male	72	Right hilar lymph nodes	Lymphadenopathy	No PTB	Absent
K99/12	Male	47	Right hilar lymph nodes	Lymphadenopathy	Bilateral PTB	Absent
K100/12	Female	46	Right hilar lymph nodes, pancreatic lymph nodes	Lymphadenopathy, anthracosis, caseating necrosis, granulomas	Bilateral PTB	Absent

* Age is unavailable

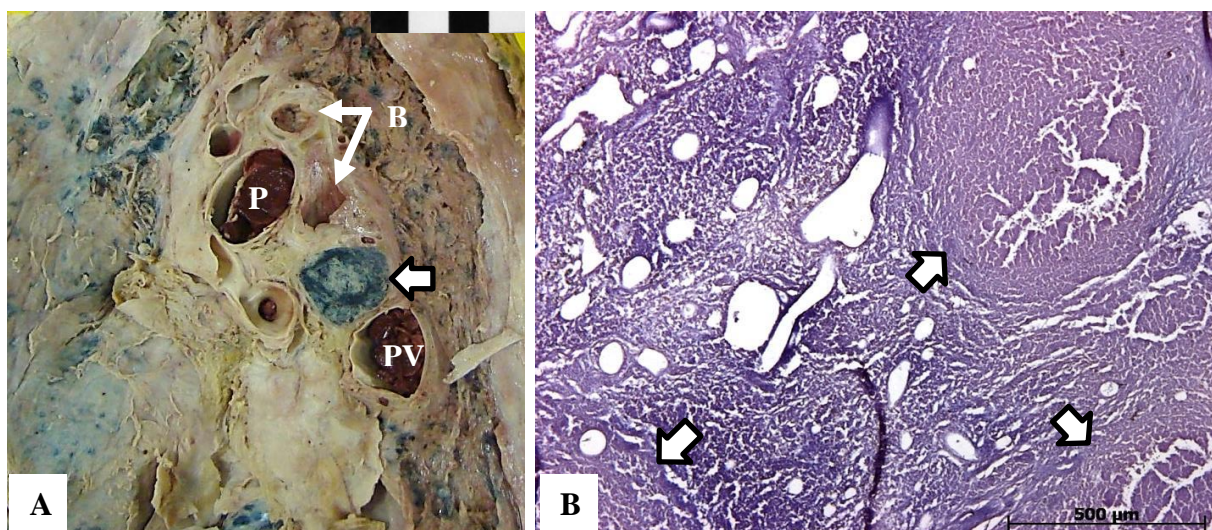


Figure 4.95. Morphologic appearance of tuberculous lymphadenitis. A) Right hilum of cadaver 27/12 shows lymphadenopathy with accompanying anthracosis and caseation (blocked arrows), medial view; B) several granulomatous lesions with central caseation can be seen in the duodenal lymph nodes of cadaver K140/11, H&E (50x); right bronchi (Br); pulmonary artery (PA); pulmonary vein (PV).

4.8.1.2 Lymphomatous Malignancy

Lymphomatous malignancy was seen in 1/127 (0.8%) cadaver (Table 4.70). The vermiform appendix of cadaver K124/12 was prominently enlarged with no signs of an acute appendicitis. Histologically, a very faint follicular organization of lymphoid cells was observed in several organs, namely the liver, spleen, kidneys and vermiform appendix (Figure 4.96).

Table 4.70. Lymphomatous malignancy in the cadaver cohort (n=127)

<i>Cadaver Ref. Nr.</i>	<i>Sex</i>	<i>Age</i>	<i>Macroscopic Appearance</i>	<i>Microscopic Evaluation</i>	<i>Organ Involvement</i>
K124/12	Male	55	Large vermiform appendix with no acute appendicitis	Follicular organization of lymphoid cells	Liver, spleen, both kidneys, appendix

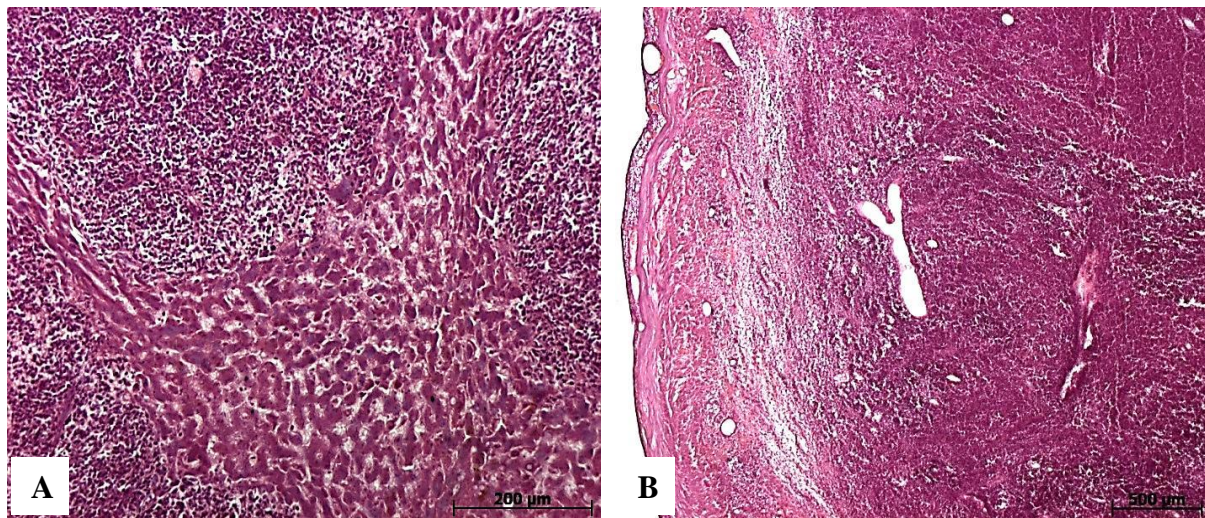


Figure 4.96. Microscopic appearance of lymphomatous malignancy. A) The hepatic parenchyma of cadaver K124/12 contained small, well-circumscribed nodules containing small lymphoid cells. A very faint follicular organization was noted and the cells appear malignant in origin, H&E (100x); B) the prominent lymphoid follicles found in a normal appendix was absent in the appendix of cadaver K124/12. Instead, the appendix presented with abundant lymphoid cells uniformly distributed within the lamina propria and submucosa, H&E (25x).

4.8.2 Spleen

4.8.2.1 Splenic Tuberculosis

Tuberculous involvement of the spleen was observed in 21/127 (16.5%) cadavers (Table 4.71). The male to female ratio was 1:2.4 and the average age of the affected cadavers was 43.2 years. Focal granulomatous involvement was observed in 13/21 (61.9%), while the entire spleen was affected in 8/21 (38.1%) cadavers (Figure 4.97, A and C). Isolated splenic

involvement in the absence of pulmonary TB was observed in 4/21 (19.0%) cadavers, while splenic involvement with pulmonary TB and extrapulmonary TB was seen in 17/21 (81.0%) cadavers. Microscopically, several granulomas of differing sizes were observed (Figure 4.97, B). Caseating necrosis was a common feature with the splenic granulomas (Figure 4.97, D)

Table 4.71. Tuberculosis involvement of the spleen in the cadaver cohort (n=127)

<i>Cadaver Ref. Nr.</i>	<i>Sex</i>	<i>Age *</i>	<i>Splenic Involvement</i>	<i>Absolute Weight (g)</i>	<i>Adapted Weight (g)**</i>	<i>Pulmonary Lesions</i>	<i>Extrapulmonary Lesions</i>
K87/09	Male	*	Entire spleen (Fig. 4.97, B, D)	---	---	PTB in both lungs	Liver
K108/09	Male	42	Entire spleen	---	---	None	None
K13/11	Female	47	Focal granulomas	60.0	61.3	PTB in both lungs	None
K46/11	Male	30	Focal granulomas	240.0	245.0	PTB in both lungs	None
K64/11	Female	48	Entire spleen	60.0	61.3	PTB in both lungs	Left kidney
K72/11	Male	*	Focal granulomas	290.0	296.1	None	None
K116/11	Female	*	Focal granulomas	90.0	91.9	PTB in both lungs	None
K119/11	Male	*	Focal granulomas	220.0	224.6	PTB in both lungs	Liver
K120/11	Female	53	Focal granulomas	120.0	122.5	PTB in both lungs	None
K121/11	Male	50	Entire spleen	420.0	428.8	PTB in both lungs	Liver, both kidneys
K124/11	Female	*	Entire spleen	240.0	245.0	PTB in left lung	Liver
K140/11	Female	42	Entire spleen	440.0	449.2	PTB in both lungs	Liver, both kidneys
K25/12	Male	39	Focal granulomas	450.0	459.5	PTB in both lungs	Liver, pancreas, both kidneys
K26/12	Male	*	Focal granulomas	160.0	163.4	PTB in both lungs	Liver, pancreas, both kidneys
K42/12	Female	*	Entire spleen (Fig. 4.97, A)	610.0	622.8	PTB in both lungs	Liver
K49/12	Male	*	Entire spleen (Fig. 4.97, C)	600.0	612.6	PTB in both lungs	Both kidneys
K60/12	Female	22	Focal granulomas	240.0	245.0	PTB in both lungs	None
K74/12	Female	52	Focal granulomas	180.0	183.8	PTB in both lungs	Both kidneys
K75/12	Male	52	Focal granulomas	290.0	296.1	PTB in both lungs	None
K86/12	Female	24	Periphery	120.0	122.5	None	None
K104/12	Female	61	Focal granulomas	150.0	153.2	None	None

* Age is unavailable

** Mean percent change with formalin fixation = + 2.1% (according to Finkbeiner et al., 2004)

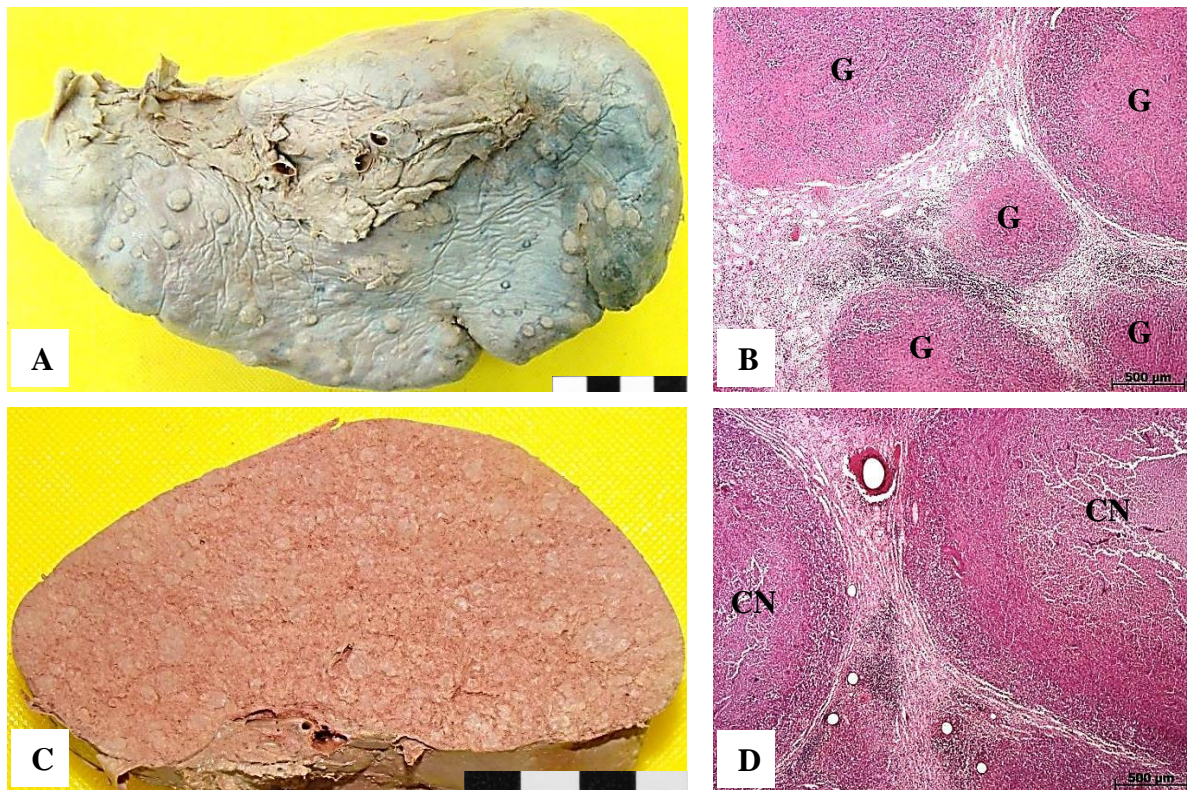


Figure 4.97. Splenic TB. A) Several nodules were found on the entire spleen (K42/12); B) spleen (K87/09), H&E (25x); C) splenic parenchyma showing lighter tuberculous granulomas in the entire spleen (K49/12); D) spleen (K87/09), H&E (25x); caseating necrosis (CN), granulomas (G).

4.9 Brain

The brains of the cadavers from the 2012 and 2013 cohorts (n=87) were evaluated for pathological lesions. The brains were extensively decomposed in 7/87 (8.0%) cadavers, which made evaluation impossible. The remaining 80 brains were evaluated and the following pathological observations were made.

4.9.1 Tuberculosis of the Brain

Tuberculosis of the brain, either in the form of tuberculous meningitis (TBM) or intraparenchymal tuberculomas, was absent in the cadaver cohort.

4.9.2 Hydrocephalus

Hydrocephalus was observed in 2/80 (2.5%) cadavers with a male to female ratio of 1:1.8 (Table 4.72). Cadaver K79/12 presented with unilateral hydrocephalus in the right lateral ventricle. A soft area measuring 30x10mm in maximum dimension was seen on the surface of the parietal and part of the temporal lobes. This was consistent with the enlarged lateral ventricle. Bilateral involvement was observed in cadaver K93/12 who showed signs of intraparenchymal tuberculomas. Gliosis was noted and the possibility exists that the tuberculomas obstructed and altered the flow and absorption of cerebrospinal fluid (CSF).

Table 4.72. Hydrocephalus in the cadaver population (n=80)

<i>Cadaver Ref. Nr.</i>	<i>Sex</i>	<i>Age</i>	<i>Involvement</i>	<i>Underlying Cause</i>
K79/12	Female	49	Right lateral ventricle (unilateral involvement)	Hydrocephalus <i>ex vacuo</i>
K93/12	Male	72	Bilateral involvement	Inconclusive

4.9.3 Cerebrovascular Disease

4.9.3.1 Cerebral Infarction

Cerebral infarctions were observed in 2/80 (2.5%) cadavers with a male to female ratio of 1:1.8 (Table 4.73). Macroscopic evaluation revealed pale, poorly circumscribed areas within the cerebral parenchyma (Figure 4.98, A). Histologically, a chronic inflammatory infiltrate consisting of lymphocytes and plasma cells were seen within the areas of cerebral infarctions (Figure 4.98, B). No acute inflammatory infiltrate was seen in any of the cerebral infarcts, suggesting that the age of the infarcts was more than two days old.

Table 4.73. Cerebral infarctions in the cadaver cohort (n=80)

<i>Cadaver Ref. Nr.</i>	<i>Sex</i>	<i>Age</i>	<i>Macroscopical Appearance</i>	<i>Microscopical Findings</i>	<i>Underlying Cause</i>
K40/11	Female	*	Dura and arachnoid in left temporo-parietal region appears fibrotic (focal)	Plasma cells and lymphocytes, hemosiderin	Arteriosclerosis
K80/11	Male	38	Right hemisphere, parietal lobe	Wedge-shaped pyramidal cells	Impaired blood flow

* Age is unavailable

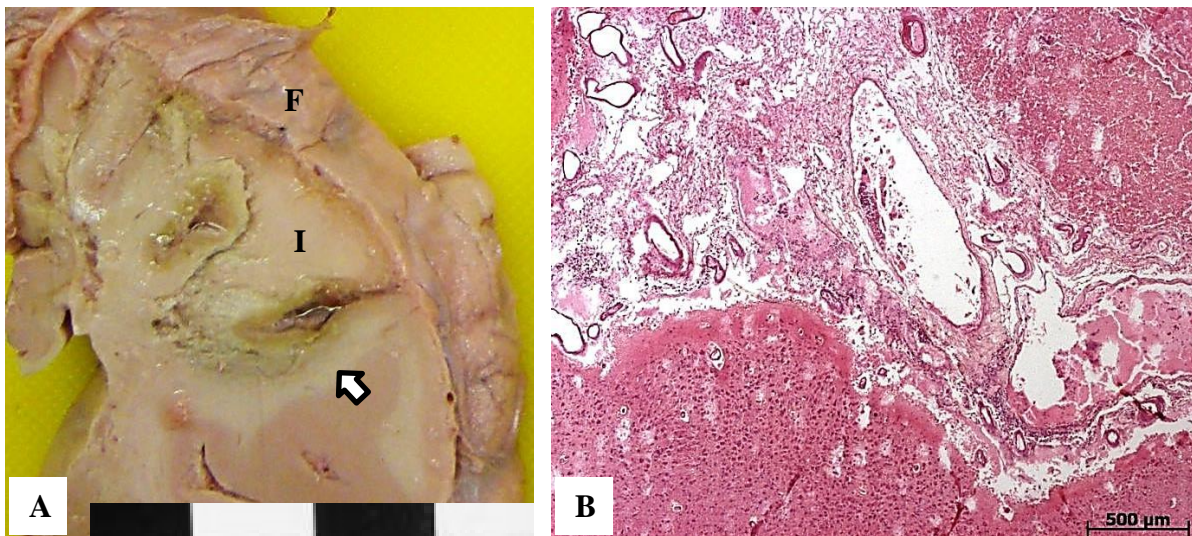


Figure 4.98. Cerebral infarction. A) Area of an “old” (fibrotic) localized infarction in the left tempo-parietal lobe of cadaver K40/11; fibrotic arachnoid (F); infarction (I), border of infarction (blocked arrow).

4.9.4 Bacterial Infections

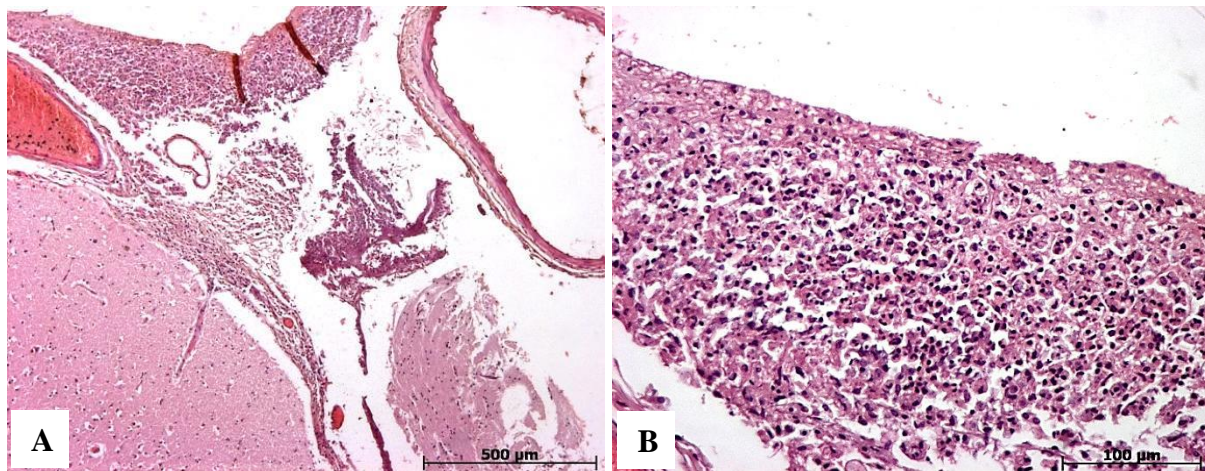
4.9.4.1 Bacterial Meningitis

Bacterial meningitis was observed in 4/80 (5.0%) cadavers. The male to female ratio was 1:1.7 and the average age of the affected cadavers was 64.3 years. Acute bacterial meningitis was observed in cadaver K42/11. A primary acute choroid plexitis was the origin of the meningeal infection from where the infection was hematogenously disseminated to the meninges. Opacified or “cloudy” leptomeninges (arachnoid and pia mater collectively) were seen in the left hemispheres of the affected cadavers. Microscopically, large numbers of inflammatory cells (consisting mostly of polymorphs) were observed in the leptomeningeal spaces (Figure 4.99). No signs of cerebral abscesses were observed in the affected cadavers. A mixed inflammatory infiltrate was observed in 1/4 (25.0%) cadavers, suggesting the presence of an early resolution phase. Table 4.74 gives a summary of the cadavers affected by bacterial meningitis.

Table 4.74. Bacterial meningitis in the cadaver cohort (n=80)

<i>Cadaver Ref. Nr.</i>	<i>Sex</i>	<i>Age</i>	<i>Macroscopical Appearance</i>	<i>Microscopical Findings</i>
K42/11	Male	*	At the base of the hippocampus	Acute inflammatory cells, fibropurulent exudate (Fig. 4.99)
K74/11	Male	70	Arachnoid of left temporal lobe appear fibrotic	Mixed inflammatory cells
K28/12	Female	62	Arachnoid of the left parietal lobe appears opacified/"cloudy"	Acute inflammatory cells
K78/12	Male	61	Arachnoid of the left hemisphere appear opacified/"cloudy"	Acute inflammatory cells

* Age is unavailable

**Figure 4.99. Purulent leptomeningitis.** A) Microscopic appearance of a purulent leptomeningitis in cadaver K42/11, H&E (50x); B) magnification of A, showing an acute inflammatory infiltrate consisting mostly of polymorphonuclear neutrophils, within the leptomeninges, H&E (200x).

4.10 Breast

4.10.1 Fibrocystic Change

Fibrocystic change of the female breast was observed in 2/40 (5.0%) cadavers (Table 4.75).

The average age of the cadavers with fibrocystic change was 52.5 years. Macroscopically, a dense fibrous tissue was present in the superior medial quadrant of the right breast on both cadavers (Figure 4.100, A). Histologically, dilation of the mammary ducts to form cystic spaces was seen (Figure 4.100, B). Variable amounts of fibrosis were seen within the breast stroma (Figure 4.100, B).

Table 4.75. Fibrocystic change in the female cadaver cohort (n=40)

<i>Cadaver Ref. Nr.</i>	<i>Age</i>	<i>Mammary Involvement</i>	<i>Microscopic Findings</i>
K06/10	53	Right breast	Irregular, cystically dilated ducts, stromal fibrosis, cuboidal epithelium
K65/11	52	Right breast	Irregular, cystically dilated ducts, stromal fibrosis, cuboidal epithelium

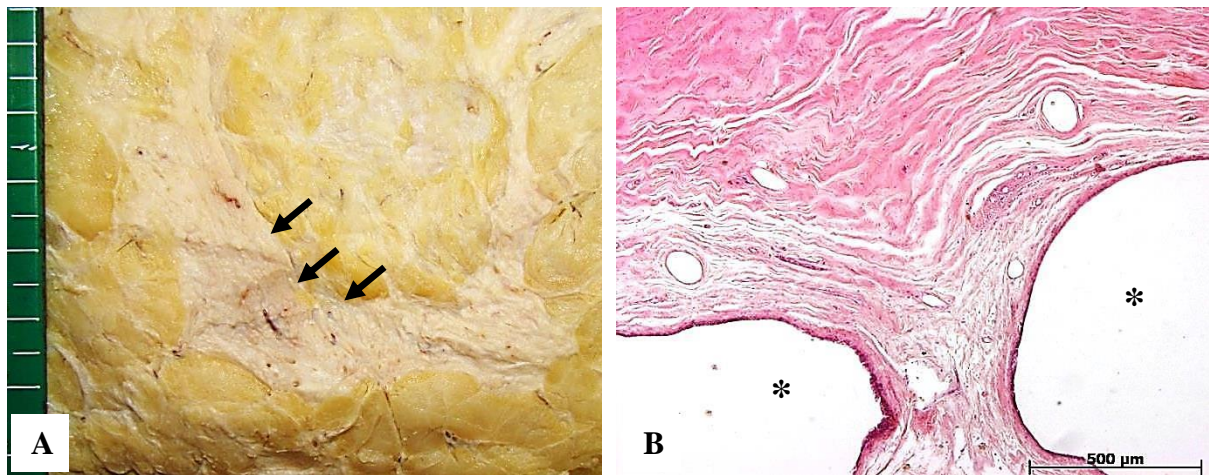


Figure 4.100. Fibrocystic change of the female breast. A) Macroscopic appearance of fibrosis in the right breast (K65/11); B) fibrocystic changes with fibrosis and dilated mammary glands, H&E (50x); dilated glands (asterisks) fibrosis (arrows).

4.10.2 Fibroadenoma

Fibroadenoma, a benign neoplasm of the breast, was observed in 1/40 (2.5%) cadaver (Table 4.76). Cadaver K13/11 (47 years) presented with discrete nodules with a firm consistency in the left breast. On cut section, fibrosis was observed directly posterior to the areola of the left breast (Figure 4.101, A). Histologically, the fibroadenoma had a biphasic appearance. Fibroblastic stroma and duct-like epithelium-lined glands of varying sizes were observed (Figure 4.101, B).

Table 4.76. Fibroadenoma in the female cadaver cohort (n=40)

<i>Cadaver Ref. Nr.</i>	<i>Age</i>	<i>Mammary Involvement</i>	<i>Morphological Appearance</i>
K13/11	47	Left breast	Dense fibrosis posterior to the areola with a microscopic biphasic appearance

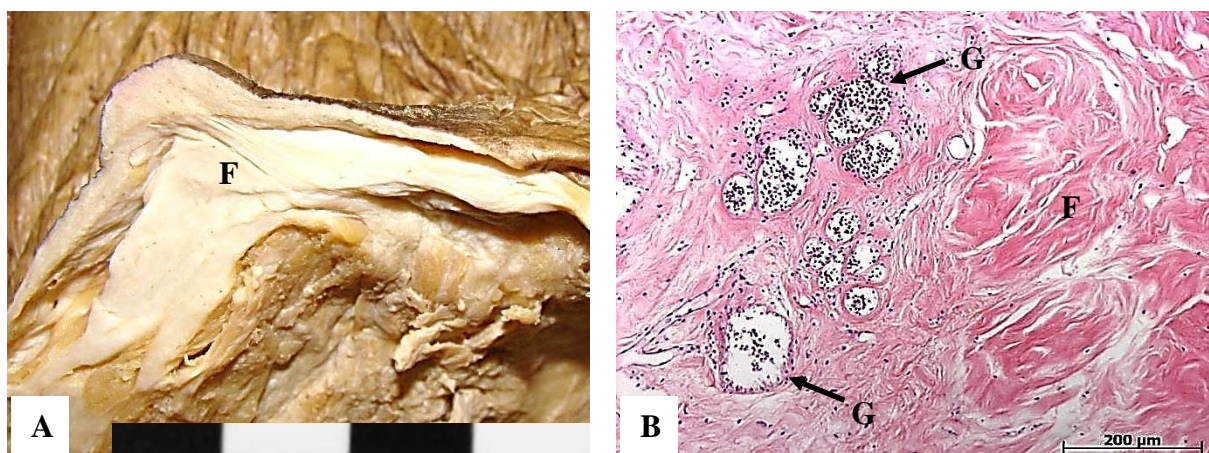


Figure 4.101. Fibroadenoma of the female breast. A) A fibrous nodule below the areola in the left breast of cadaver K13/11; B) fibrous and glandular tissue in the left breast of cadaver K13/11, H&E (100x), fibrosis (F); glandular tissue (G).

4.11 Skeletal System

4.11.1 Study Subjects

For this part of the study, 124 complete skeletal remains of the total cadaver cohort was investigated and analysed for skeletal pathology. Cadavers K96/09, K04/10 and K138/11 were not included in the study population due to technical problems.

4.11.2 Skull

4.11.2.1 Maxillofacial Fractures

Healed facial fractures were observed in 37/124 (29.6%) cadavers (Table 4.77). The male to female ratio of the affected cadavers was 1.1:1 and the average age was 52.2 years. A total of 16/124 (12.9%) cadavers presented with healed zygomatic arch fractures of which 68% were fractures to the temporal process (Figure 4.102, A), 25.0% to the maxillary process and 6.2% to the frontal process of the zygomatic bone. A total of 22/124 (17.7%) cadavers presented with fractures to the nasal bones of which 36.4% were to the left nasal bone, 9.1% to the right nasal bone and 54.5% to both nasal bones (Figure 4.102, B). The majority of the maxillofacial fractures were to the left side of the face. This finding analysed with the McNemar's test and revealed a statistically significant difference between left- and right-sided maxillofacial fractures (chi-square $p = 0.01902$; $p < 0.05$). Calvarium trauma was seen in 14/124 (11.3%) cadavers. Two cadavers (1.6%) presented with small glass fragments, presumably from a glass bottle, in the right parietal bone lateral to the sagittal suture (Figure 4.102, C) and left lateral part of the coronal suture (Figure 4.102, F), respectively. Depressed fractures of the dome of the skull was seen in 9/124 (7.3%) cadavers (Figure 4.102, D) A surgical fracture repair was seen in 1/124 (0.8%) cadaver (Figure 4.102, E).

Table 4.77. Maxillofacial trauma in the cadaver cohort (n=124)

<i>Cadaver Ref. Nr.</i>	<i>Sex</i>	<i>Age</i> *	<i>Skull Involvement</i>
K81/09	Male	44	Healed fracture of maxillary process of the left zygomatic arch
K83/09	Male	60	Healed fracture of frontal process of zygomatic bone
K89/09	Male	41	Healed fracture of right zygomatic arch
K95/09	Male	*	Healed superior nasal bone fracture
K101/09	Male	48	Depressed maxillary and temporal process of left zygomatic bone; depressed fracture in the right frontal bone
K104/09	Male	*	Healed fractures of both nasal bones
K108/09	Male	42	Healed fracture of the superior part of the right nasal bone
K10/10	Male	36	Decompressed fracture in superior left eye orbit, healed right nasal bone fracture, healed malaligned fracture of the maxillary process of the right zygomatic bone
K36/10	Male	82	Healed fractures of both nasal bones
K47/10	Male	43	Remnants of glass in the left coronal suture (4x5mm)
K05/11	Female	41	Healed left nasal bone fracture; healed left superior eye orbit fracture
K10/11	Female	45	Healed fracture of the superior part of nasal bone
K13/11	Female	47	Healed fracture (left superior nasal bone), indent right parietal bone (15x15mm)
K31/11	Male	53	Healed fracture of the left superior nasal bone
K38/11	Male	68	Indents in the right part of the frontal bone and left part of occipital bone
K43/11	Female	32	Healed fracture along the length of right temporal and parietal bones
K47/11	Male	64	Healed fracture (left nasal bone), depressed fracture (superior part of left eye orbit), malaligned healed fracture of the temporal and maxillary processes of the right zygomatic bone
K64/11	Female	48	Antimortem fracture (right parietal bone); right temporal depression
K70/11	Female	*	Healed fracture of the left superior part of the nasal bone
K72/11	Male	*	Healed fracture in the temporal process of the left zygomatic arch
K101/11	Male	50	Healed fracture superior to the left maxillary sinus
K124/11	Female	*	Healed fracture in the temporal process of the left zygomatic bone
K126/11	Male	45	Healed left nasal bone fracture
K26/12	Male	*	Depressed fracture in the right side of the calvarium
K28/12	Female	62	Healed right nasal bone fracture
K43/12	Male	*	Healed right and left nasal fractures
K49/12	Male	*	Depressed fracture superior to the right eye orbit (30x13mm)
K50/12	Female	*	Healed fractures of the temporal process of left zygomatic bone, both nasal bones
K51/12	Male	56	Depressed healed fracture of the temporal process of the left zygomatic bone
K58/12	Male	70	Depressed temporal process of the right zygomatic bone
K61/12	Male	52	Healed fracture (both nasal bones); glass right parietal bone (5x5mm); indent - inner view of skull
K66/12	Female	55	Depressed fracture lateral to the mid-sagittal suture (8x9mm)
K73/12	Male	72	Healed fracture (both nasal bones); healed fracture temporal process of the right zygomatic bone
K74/12	Female	52	Depressed healed fracture of the temporal process of the left zygomatic bone
K76/12	Male	*	Healed fractures of both nasal bones, depressed fracture (25x9mm) in the right occipital bone
K83/12	Male	59	Healed fracture (left nasal bone)
K98/12	Male	42	Depressed fracture in frontal bone (17x9mm), healed indents (3 right parietal and 2 left parietal bones)

* Age is unavailable

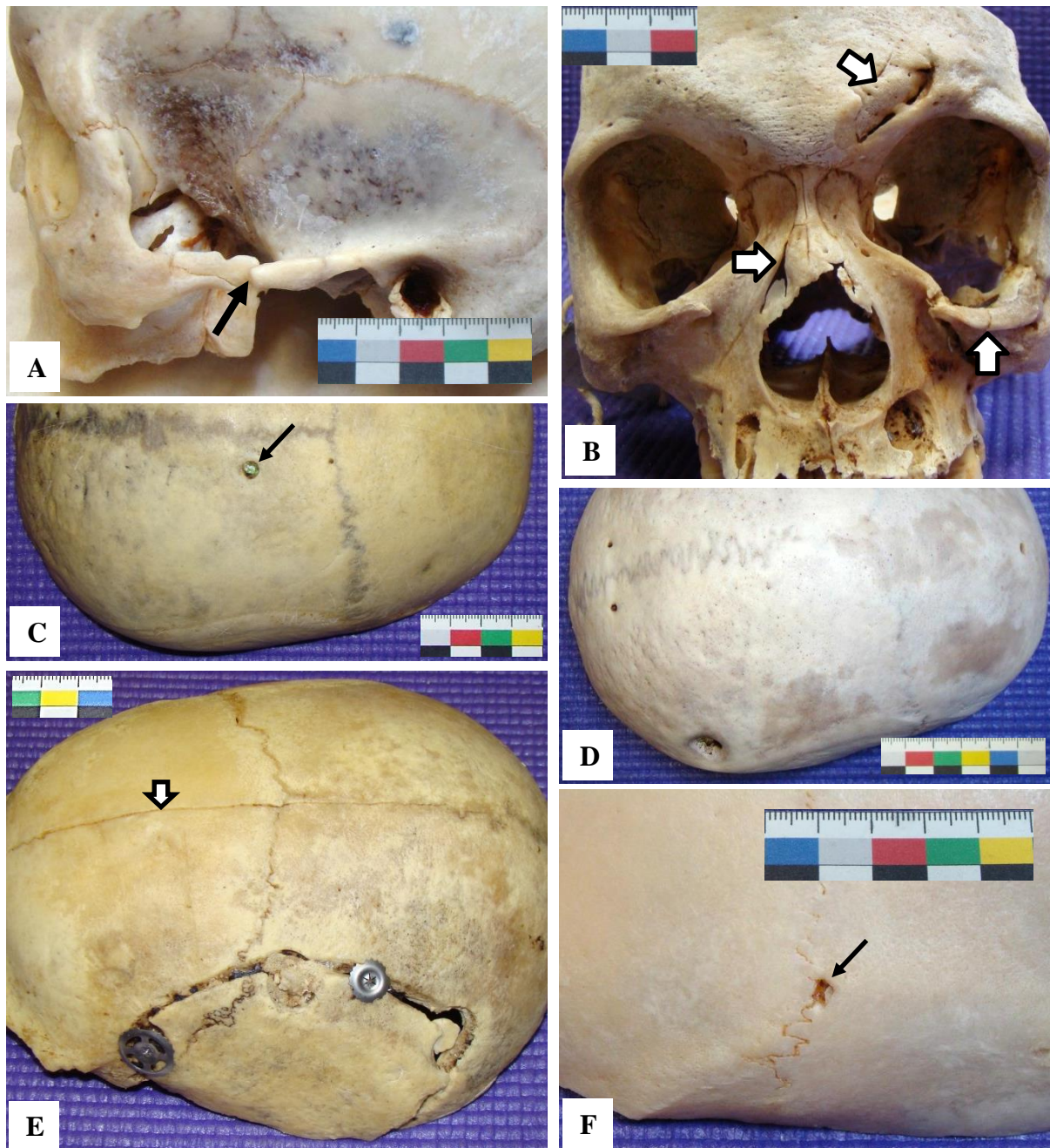


Figure 4.102. Healed maxillofacial trauma. A) Malaligned healed fracture of the temporal part of the left zygomatic process of cadaver K50/12; B) healed maxillofacial trauma (blocked arrows) to the left side of cadaver K10/10; C) remnants of glass (arrow) in the dome of the skull of cadaver K61/12, lateral to the sagittal suture and posterior to the coronal suture; D) depressed fracture on the right side of the temporal bone of cadaver K13/11; E) healed repair of the left side of the dome of the skull of cadaver K26/12, lateral view. Note the metopic suture (blocked arrow); F) a small glass fragment within the fibrous joint of the left coronal suture of cadaver K47/10.

4.11.2.2 Maxillary and Mandibular Apical Periodontal Cysts

Maxillary apical periodontal cysts were observed in 6/125 (4.8%) cadavers (Table 4.78, Figure 4.103), while mandibular apical periodontal cysts were seen in 1/125 (0.8%) cadavers.

Males were affected and the average age was 46.1 years. Periodontitis was seen with accompanying interalveolar atrophy and bony pitting. Partial remodelling was observed in the areas,

Table 4.78. Maxillary and mandibular apical periodontal cysts in the cadaver cohort (n=124)

<i>Cadaver Ref. Nr.</i>	<i>Sex</i>	<i>Age</i>	<i>Maxillary Involvement</i>
K03/10	Male	34	Bilateral maxillary apical periodontal cysts (Fig. 4.103, B)
K10/10	Male	36	Apical periodontal cyst in left part of the maxilla (Fig. 4.103, A)
K101/11	Male	50	Signs of antemortal maxillary sinus infection
K126/11	Male	45	Right maxillary molar apical periodontal cyst
K75/12	Male	52	Two apical periodontal cysts in the left and right maxilla
K83/12	Male	59	Apical periodontal cysts on both sides of the mandible below the molars
K99/12	Male	47	Two apical periodontal cysts in the superior left and right parts of the maxilla

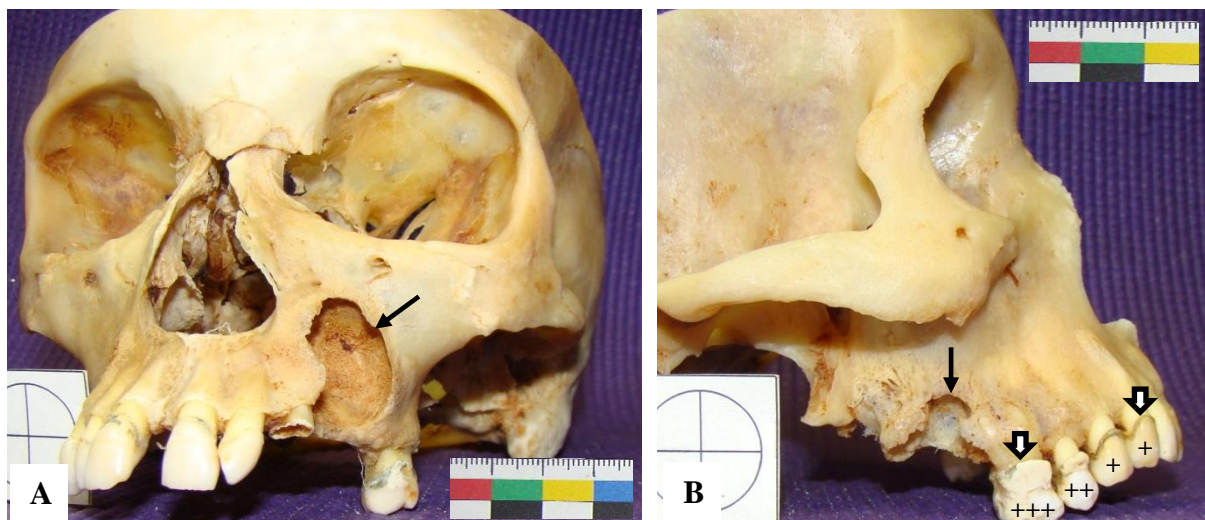


Figure 4.103. Maxillary apical periodontal cysts. A) A massive antemortal apical periodontal cyst (black arrow) with adjacent areas of remodelling in the left maxilla of cadaver K10/10, antero-lateral view; B) apical periodontal cyst (black arrow) in the right maxilla of cadaver K03/10, lateral view. Note the presence of calculi along the alveolar line (blocked arrows, slight (+), medium (++) , considerable (+++)) according to Brothwell, 1981).

4.11.2.3 Mandibular Trauma

Mandibular trauma was observed in 2/124 cadavers (1.6%) (Table 4.79). The male to female ratio was 1:2.2. One cadaver K50/12, presented with an oblique healed fracture of the left mandibular ramus (Figure 4.103, A), while cadaver K10/10 presented with a malaligned

healed fracture of the left part of the mandibular body, inferior to the mental foramen (Figure 4.103, B and C).

Table 4.79. Mandibular trauma in the cadaver cohort (n=124)

<i>Cadaver Ref. Nr.</i>	<i>Sex</i>	<i>Age*</i>	<i>Morphology</i>
K10/10	Male	36	Malaligned healed fracture of the left part of the mandibular body, inferior to the mental foramen
K50/12	Female	*	Oblique healed fracture in the left mandibular ramus

* Age is unavailable

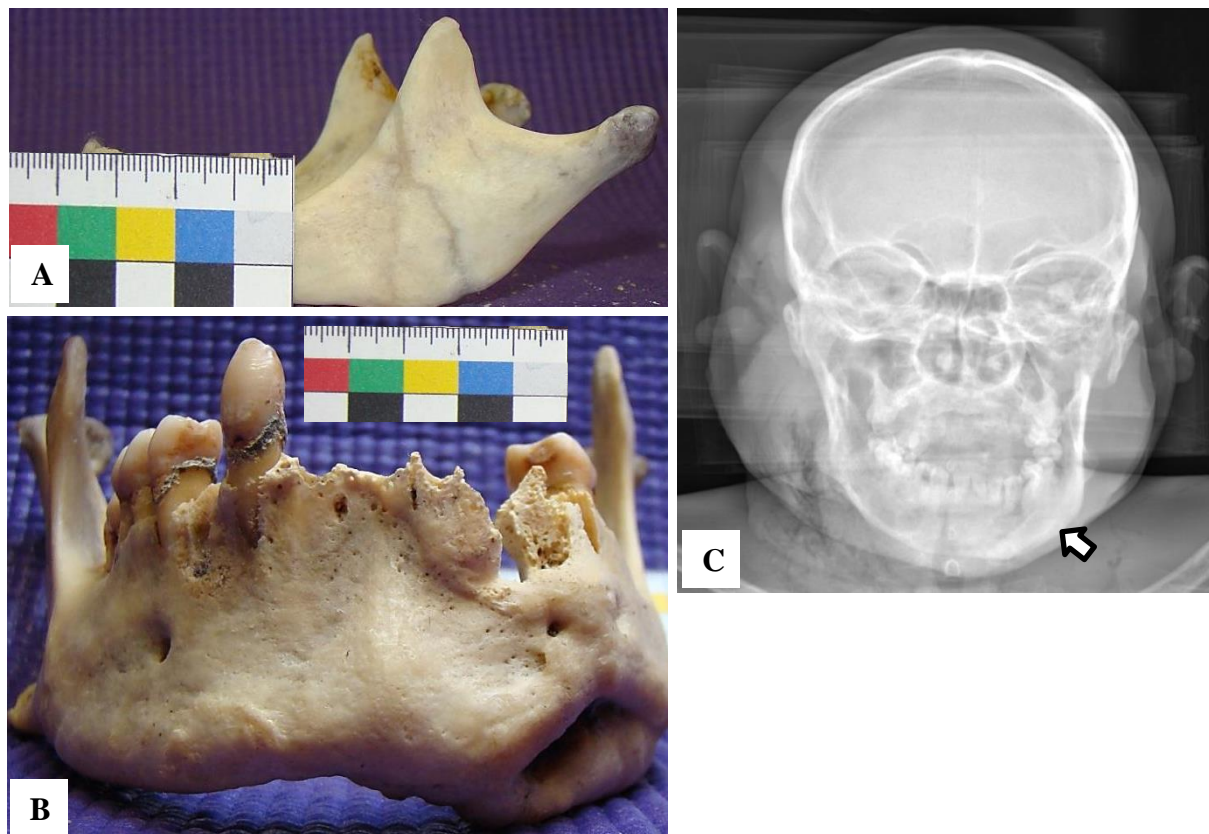


Figure 4.104. Healed mandibular fractures. A) Oblique healed fracture of the left mandibular ramus of cadaver K50/12, lateral view; B) malaligned healed fracture of the left part of the mandibular body, inferior to the left mental foramen; C) X-ray of cadaver K10/10 showing a dense area (blocked area) corresponding with the healed malaligned fracture in B.

4.11.2.4 Mandibular Implants

Mandibular implants were observed in 2/124 cadavers (1.6%) (Table 4.80). The male to female ratio was 1:2.2 and the average age of the affected cadavers was 76.5 years. Both cadavers presented with fixed mandibular prostheses which differed in appearance. The

prosthesis of cadaver K99/09 contained the mandibular teeth (Figure 4.105, A), while cadaver K62/11 presented with steel mandibular prosthesis (Figure 4.105, B).

Table 4.80. Mandibular implants in the cadaver cohort (n=124)

<i>Cadaver Ref. Nr.</i>	<i>Sex</i>	<i>Age</i>	<i>Type of Prosthesis</i>
K99/09	Female	70	Fixed mandibular prosthesis with four screws placed in mandibular body
K62/11	Male	83	Fixed mandibular prosthesis with two screws placed perpendicular within the mandibular body

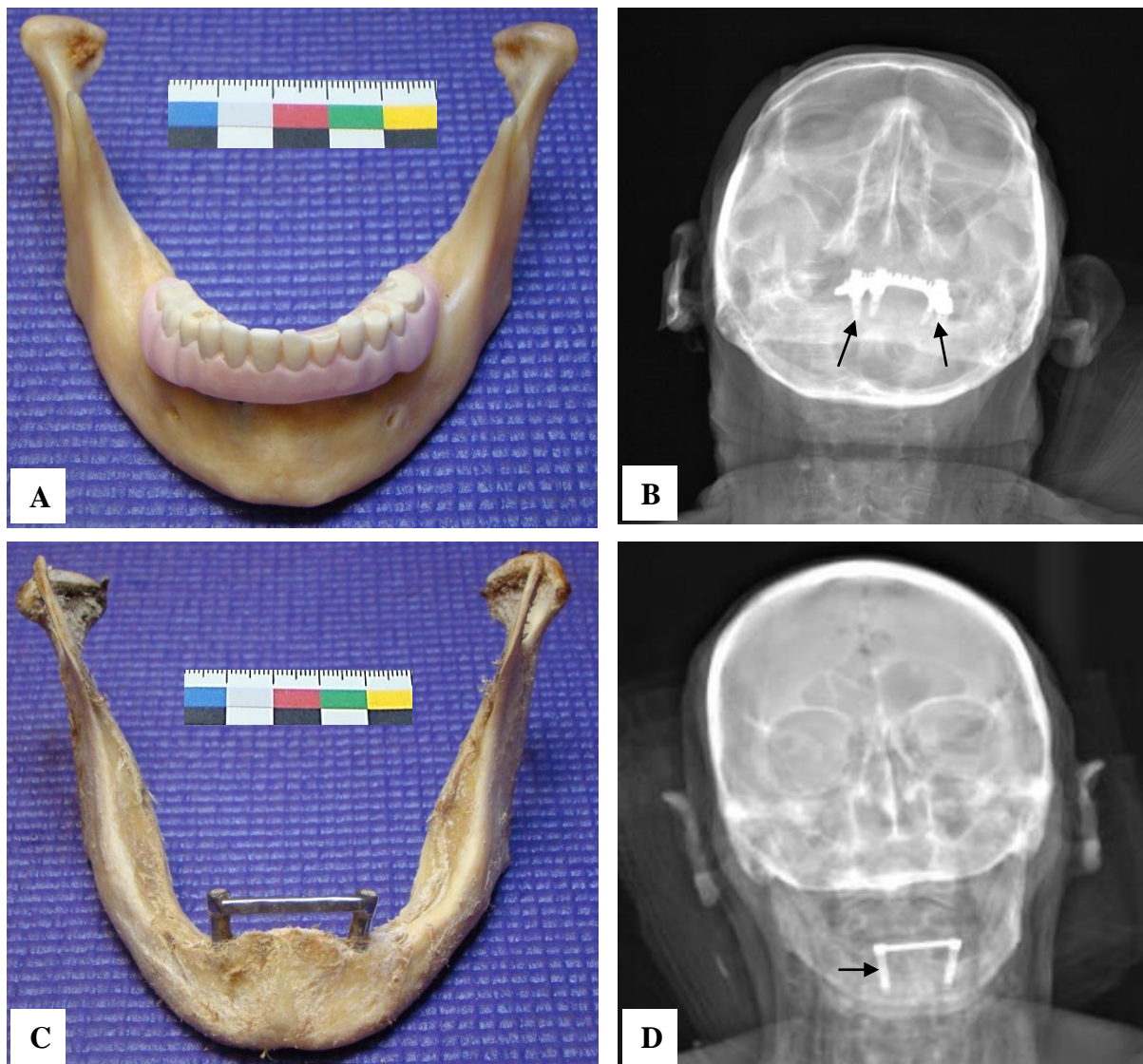


Figure 4.105. Fixed mandibular prosthesis. A) Fixed mandibular prosthesis in cadaver K99/09, antero-superior view; B) X-ray of the face showing the fixed prosthesis with four screws (arrows) penetrating the mandible (note the head is tilted); C) fixed mandibular prosthesis in cadaver K62/11, antero-superior view; D) facial X-ray indicating the position of the prosthesis within the mandible. Two screws were found penetrating the mandible.

4.11.3 Spine

4.11.3.1 Vertebral Tuberculosis

Vertebral TB, also known as Pott's disease, was seen in 1/124 (0.8%) cadavers. Cadaver K19/10 (female, 63 years) presented with Pott's disease of thoracic vertebra T7 and T8. The vertebral bodies of T7 and T8 were collapsed, sclerotic and anteriorly wedged (Figure 4.106). Caseation was absent within the vertebral bodies and no signs of a soft tissue abscess was noted. The left thoracic anterior longitudinal ligament was ossified. This finding is associated with diffuse idiopathic skeletal hyperostosis (DISH).

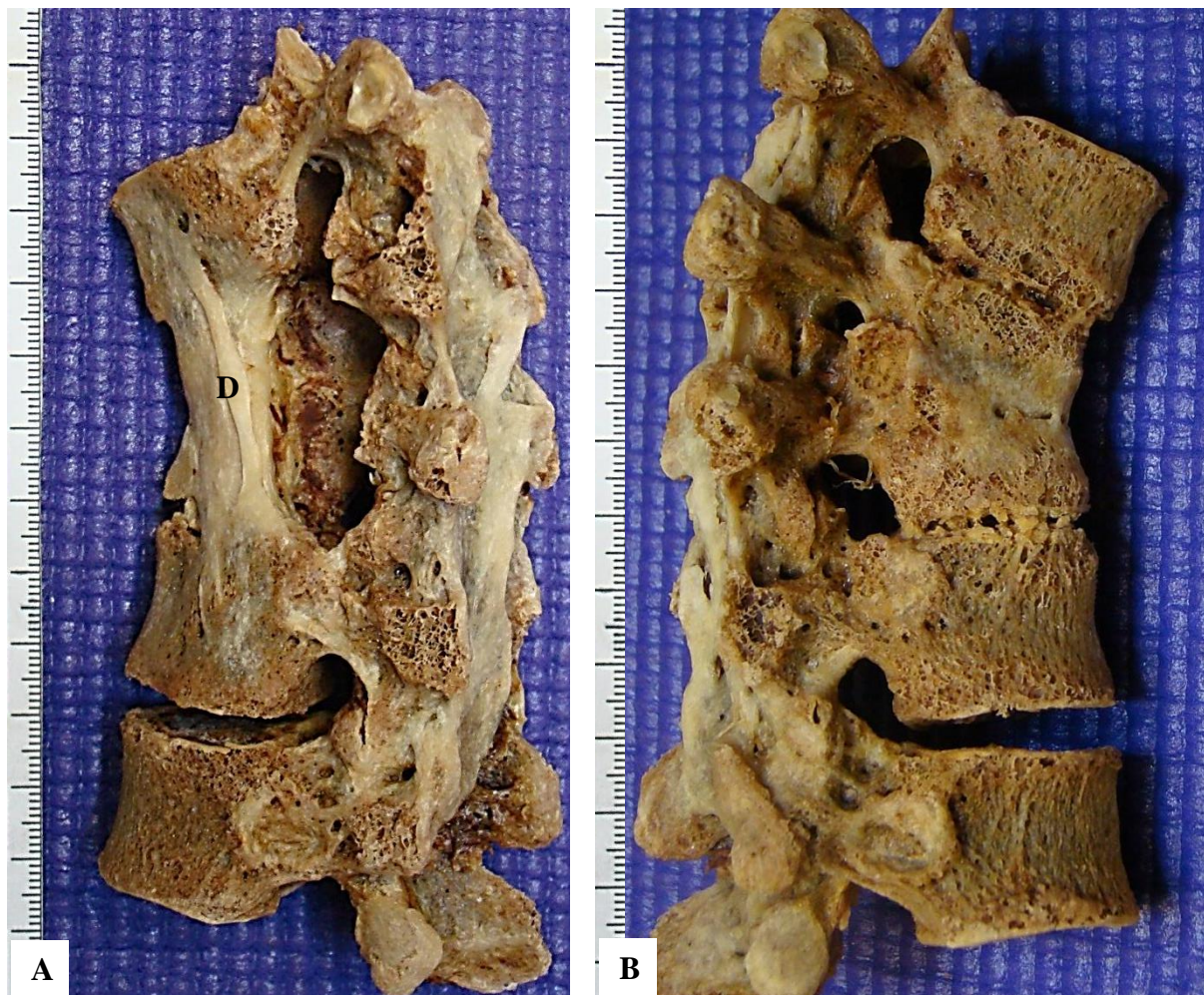


Figure 4.106. Vertebral tuberculosis (Pott's disease). A) Severe bone destruction and ossification of the left thoracic anterior longitudinal ligament (DISH) of the thoracic vertebrae T6-T9 of cadaver K19/10, left lateral view; B) the bodies of T7 and T8 are collapsed, anteriorly wedged and sclerotic, right lateral view; DISH (D).

4.11.3.2 Surgical Fusion

Cervical spinal fusion (arthrodesis) was observed in 1/124 (0.8%) cadaver. A cervical plate designed for anterior vertebral body fixation, was located on the anterior aspect of the vertebral bodies of C5 and C6 of cadaver K118/09 (Figure 4.107). Signs of a cervical discectomy and bony fusion were observed in the area surrounding the cervical plate (Figure 4.107, B).

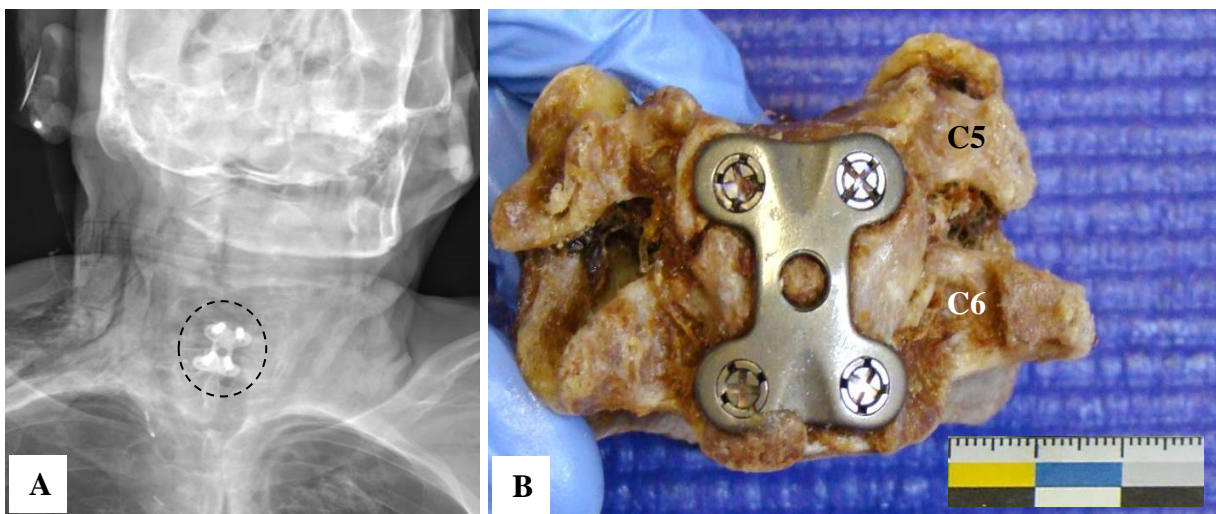


Figure 4.107. Anterior cervical fixation. A) Lodox[®] X-ray image of the cervical fixation plate (circled area) on the anterior aspect of the vertebral bodies of C5 and C6; B) anterior view of C5 and C6

4.11.3.3 Diffuse Idiopathic Skeletal Hyperostosis (DISH)

Diffuse idiopathic skeletal hyperostosis (DISH) was observed in 12/124 (9.7%) cadavers (Table 4.81). The male to female ratio was 2.3:1 and the average age of the affected cadavers was 60.5 years. The main feature of DISH is ossification of the right thoracic anterior longitudinal ligament (Figure 4.108). These ossifications resemble a typical “candle wax” appearance. The cervical region was involved in 4/12 (33.3%) cadavers, the thoracic region in 9/12 (75.0%) cadavers and the lumbar region in 4/12 (33.3%) cadavers. Of the 12 cadavers with DISH, four cadavers had involvement of more than one vertebral region (Figure 4.109).

Table 4.81. DISH in the cadaver cohort (n=124)

<i>Cadaver Ref. Nr.</i>	<i>Sex</i>	<i>Age</i>	<i>Vertebral Involvement</i>
K104/09	Male	*	Fusion of T8-L1
K118/09	Male	*	Fusion of T1-T2
K19/10	Female	63	Fusion of T7-T8 (See vertebral TB)
K42/11	Male	*	Fusion of C4-C5
K53/11	Male	*	Fusion of C6-C7; T4-T8; T9-T12; L1-L2
K62/11	Male	83	Fusion of C3-C7; T1-T2; T3-T12 (Fig. 4.109)
K72/11	Male	*	Fusion of T2-T3; T4-T6; T7-T9; T11-T12 (Fig. 4.108, A, C)
K101/11	Male	50	Fusion of T7-T8 (Fig. 4.108, B)
K26/12	Male	*	Fusion of T7-T10
K28/12	Female	62	Fusion of L1-L2
K46/12	Male	46	Fusion of C2-C3
K83/12	Male	59	Fusion of T3-T10; T12-L3

* Age is unavailable

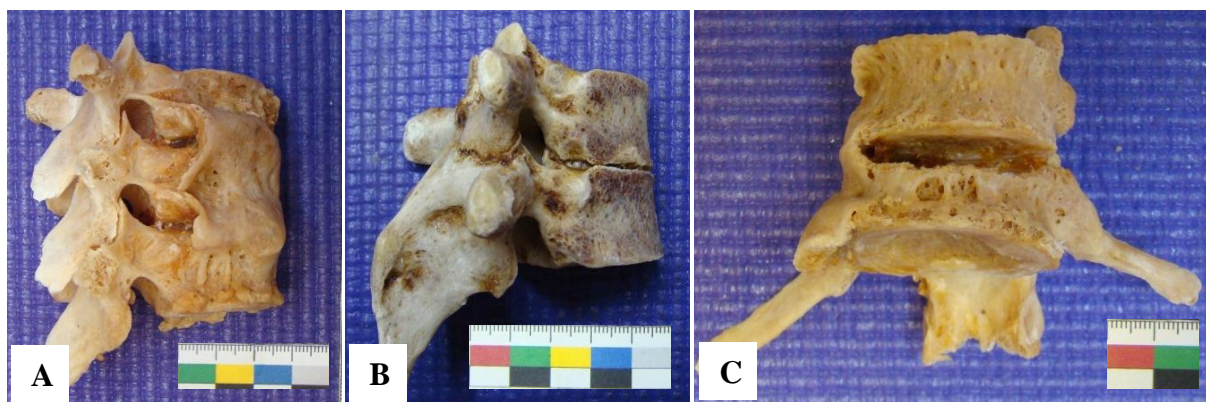


Figure 4.108. Diffuse idiopathic skeletal hyperostosis (DISH). A) fusion of the ventral bodies of thoracic vertebrae T4-T6 of cadaver K72/11, lateral view; B) fusion of the spinous processes of thoracic vertebrae T7-T8 of cadaver K101/11, lateral view; C) fusion on the lateral aspects of the ventral bodies of thoracic vertebrae T11-T12 of cadaver K72/11, anterior view. Note the fusion of the ribs to the transverse processes of the corresponding vertebrae.

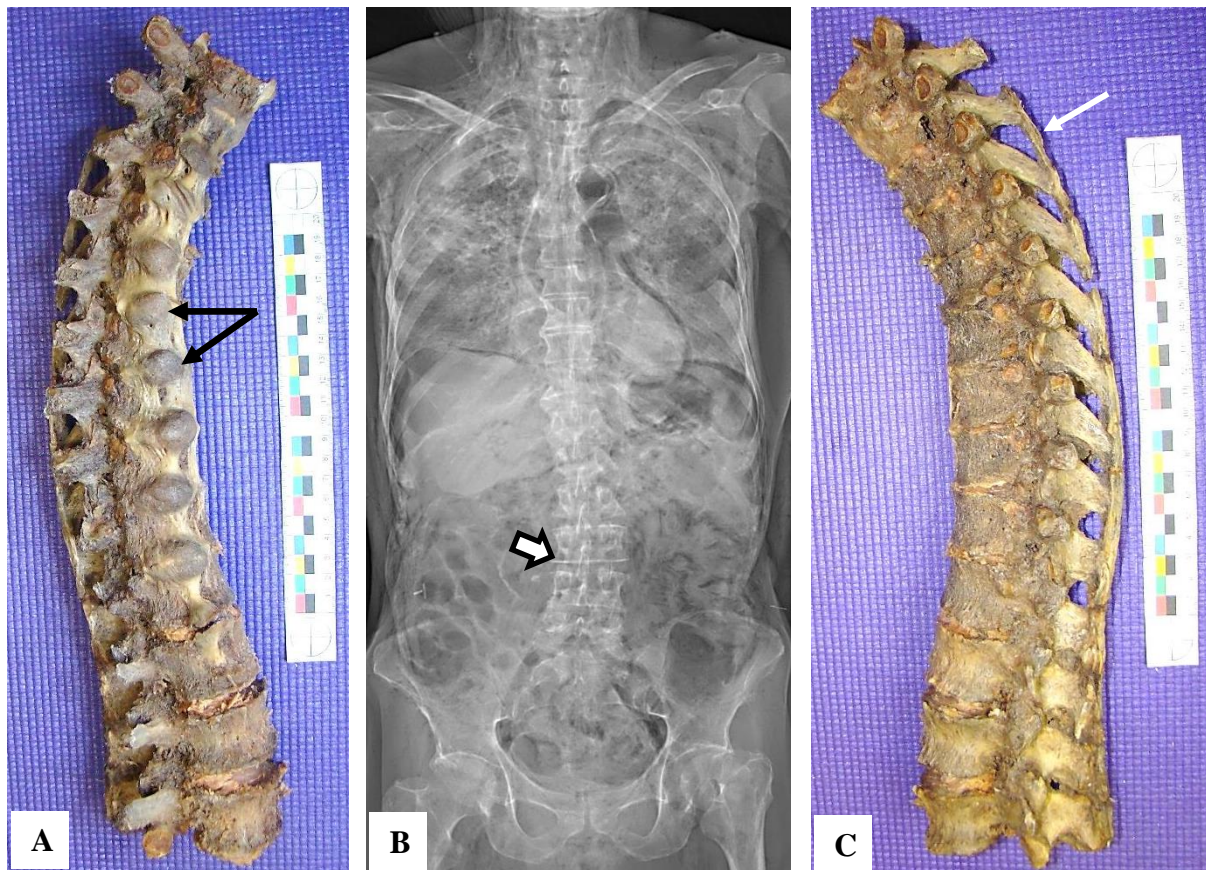


Figure 4.109. Spinal fusion as a result of DISH in cadaver K62/11. A) Fusion of the majority of the thoracic vertebrae with ossification of the intervertebral disks (black arrows), right lateral view; B) Lodox[®] X-ray of the cadaver showing a bend in the lumbar region (blocked arrow); C) fusion of the vertebrae with little to no intervertebral disks present in the thoracic region, left lateral view. Note the spinous processes are fused as a result of ossified longitudinal ligaments (white arrow).

4.11.3.4 Spina Bifida (Rachischisis)

Spina bifida, the most common form of spinal congenital defects, was noted in 2/124 (1.6%) cadavers (Table 4.82). Both cadavers with spina bifida were males and both were of unknown age. Spina bifida occulta (SBO) occurs when partial midline skeletal closure of one or more of the posterior neural arches takes place. The atlas (C1) (Figure 4.110, A) and thoracic vertebrae T1 and T2 were involved in one cadaver (K87/09), while lumbar involvement of L4 and L5 (Figure 4.110, B) was seen in cadaver K118/09. No protruding meningeal or neural structures in the area of SBO was observed.

Table 4.82. Spina bifida in the cadaver cohort (n=124)

<i>Cadaver Ref. Nr.</i>	<i>Sex</i>	<i>Vertebral Involvement</i>
K87/09	Male	Cervical spina bifida (C1), thoracic vertebrae (T1-T2) (Fig. 4.110, A)
K118/09	Male	Lumbar spina bifida (L4 and L5) (Fig. 4.110, B)

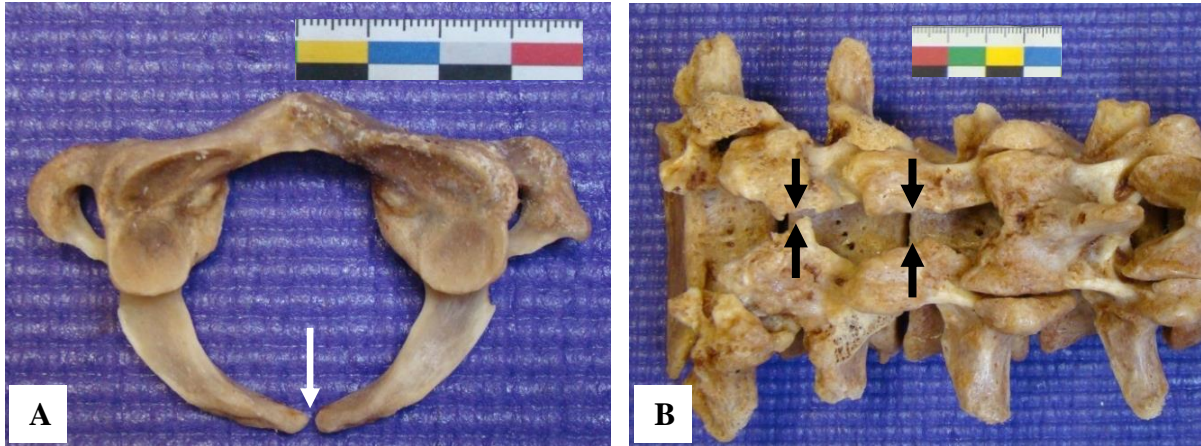


Figure 4.110. Spina bifida. A) spina bifida of the anterior bony rim of the atlas (C1) of cadaver K87/09; C) unfused neural arches with absent spinous processes of lumbar vertebrae L4 and L5 (arrows) of cadaver K118/09.

4.11.3.5 Vertebral Osteophytes

Vertebral osteophytes, a common age associated features, was seen in 70/124 (56.5%) cadavers (Table 4.83). The male to female ratio was 1.1:1 and the average age of the affected cadavers was 54.1 years. Of the 70 cadavers, cervical vertebral osteophytes were seen in 49/70 (70.0%) cadavers, thoracic vertebral osteophytes in 44/70 (62.9%) cadavers and lumbar vertebral osteophytes in 65/70 (92.9%) cadavers. Degeneration of the solid fibro-cartilaginous joints, such as the intervertebral disks, allows for the vertebrae to be closer to each other which may cause irritation and consequently lead to marginal bone formation, or marginal osteophytes. Generally, synostosis (fusion) of the “kissing” marginal osteophytes is absent, as long of there is still movement along the joints.

Table 4.83. Vertebral osteophytosis in the cadaver cohort (n=124)

<i>Cadaver Ref. Nr.</i>	<i>Sex</i>	<i>Age</i>	<i>Vertebral Involvement</i>
K81/09	Male	44	Cervical C3-C7; thoracic T1, T7-T9; lumbar L2-L5
K82/09	Male	47	Cervical C5-C7; thoracic T8-T9, T10-T12; lumbar L1-L5

<i>Cadaver Ref. Nr.</i>	<i>Sex</i>	<i>Age</i>	<i>Vertebral Involvement</i>
K83/09	Male	60	Lumbar L1-L5
K89/09	Male	41	Lumbar L1 and L5
K95/09	Male	*	Numerous osteophytes on all of the vertebrae
K99/09	Female	70	Numerous osteophytes on all of the vertebrae
K104/09	Male	*	Cervical C3-C7; thoracic T1-T12; lumbar L1-L5
K106/09	Male	*	Cervical C3-C7; thoracic T2-T7, T8-T12; lumbar L1-L5
K108/09	Male	42	Thoracic T6-T11; lumbar L4
K112/09	Male	58	Cervical C3-C4; lumbar L3-L5
K119/09	Female	50	Thoracic T4-T12; lumbar L1, L3-L5
K01/10	Male	53	Cervical C5; thoracic T7, T8; lumbar L2-L5
K03/10	Male	34	Cervical C5-C6
K06/10	Female	53	Cervical C4-C7; thoracic T2-T12; lumbar L1-L4
K16/10	Female	45	Lumbar L3-L5
K18/10	Female	32	Cervical C4-C7; lumbar L5
K19/10	Female	63	Cervical C4-C7; lumbar L3
K30/10	Male	*	Cervical C4-C5; thoracic T5, T7 – T8; lumbar L1-L5
K36/10	Male	82	Cervical C5, thoracic T12; lumbar L1-L5
K40/10	Male	47	Cervical C4, C7; lumbar L3-L5
K42/10	Male	*	Thoracic T10-T11; lumbar L3-L5
K45/10	Male	43	Cervical C4-C6; lumbar L4
K47/10	Male	43	Thoracic T11-T12; lumbar L1-L4
K10/11	Female	45	Lumbar L2-L4
K13/11	Female	47	Lumbar L2
K31/11	Male	53	Lumbar L3-L5
K38/11	Male	68	Cervical C3-C5; lumbar L5 (extensive)
K40/11	Female	*	Cervical C3-C6; thoracic T7-T11; lumbar L2-L5
K42/11	Male	*	Cervical C3, C6-C7; thoracic T2-T6, T9-T12; lumbar L1-L5
K44/11	Male	48	Thoracic T4-T6, T7-T11; lumbar L1-L5
K47/11	Male	64	Cervical C4-C5; lumbar L3-L5
K53/11	Male	*	Cervical C1-C2, C4-C7; thoracic T1-T3, T4-T8, T9-T12; lumbar L1-L2, L3-L6
K62/11	Male	83	Lumbar L4-L5
K64/11	Female	48	Thoracic T11-T12; lumbar L1-L4
K65/11	Female	52	Cervical C7; thoracic T1-T9
K74/11	Male	70	Cervical C5-C6, thoracic T10-T11; lumbar L2-L4
K76/11	Female	*	Cervical C4; lumbar L4 (Fig. 4.111, B)
K82/11	Female	39	Cervical C5; lumbar L5
K101/11	Male	50	Cervical C4-C6
K120/11	Female	53	Thoracic T8-T9, T11-T12; lumbar L1-L2
K121/11	Male	50	Cervical C3-C6; T2-T3, T10-T12; lumbar L4-L5
K126/11	Male	45	Cervical C3-C5; lumbar L2-L5
K129/11	Male	65	Cervical C3-C7; thoracic T11; lumbar L3-L4
K130/11	Female	81	Cervical C3-C7; thoracic T12; lumbar L2-L6
K140/11	Female	42	Thoracic T3-T9, T10-T12; lumbar L1, L4-L5
K26/12	Male	*	Cervical C3-C7; thoracic T1, T5-T6
K27/12	Male	66	Cervical C2-C4; thoracic T10-T11; lumbar L4-L5
K28/12	Female	62	Cervical C1-C2, C3-C4; thoracic T4-T5, T7-T10, T11-12; lumbar L4-L5
K31/12	Male	45	Cervical C6; lumbar L4-L5
K43/12	Male	*	Cervical C5-C7; lumbar L3-L5
K46/12	Male	46	Thoracic T7-T9; T10-T12; lumbar L2-L4
K50/12	Female	*	Cervical C3-C6; thoracic T9; lumbar L3 (Fig. 4.111, A)
K51/12	Male	56	Cervical C5, C7; thoracic T1-T9, T10-T12; lumbar L2-L3
K52/12	Male	57	Cervical C3-C4; thoracic T10-T12
K57/12	Male	51	Cervical C3-C7; thoracic T4, T11-T12; lumbar L1-L5
K58/12	Male	70	Cervical C4-C7; lumbar L2-L5
K61/12	Male	52	Cervical C2-C6; thoracic T11-T12; lumbar L1-L2
K64/12	Male	50	Cervical C3-C7; thoracic T11-T12; lumbar L1-L5
K73/12	Male	72	Lumbar L4-L5
K75/12	Male	52	Cervical C3-C7; lumbar L2-L5

<i>Cadaver Ref. Nr.</i>	<i>Sex</i>	<i>Age</i>	<i>Vertebral Involvement</i>
K76/12	Male	*	Thoracic T2; lumbar L5
K78/12	Male	61	Cervical C4; thoracic T10, T12; lumbar L1-L5
K79/12	Female	49	Cervical C3-C7; thoracic T10-T11; lumbar L3-L5
K82/12	Male	63	Cervical C3; thoracic T6-T7; lumbar L2-L4
K83/12	Male	59	Cervical C3-C7; thoracic T2-T12; lumbar L3-L5
K94/12	Male	60	Cervical C4-C5; lumbar L4-L5
K98/12	Male	42	Cervical C2-C5; thoracic T4-T9, T11; lumbar L1-L5
K100/12	Female	46	Thoracic T4-T5, T7-T9; lumbar L2-L4
K107/12	Female	62	Lumbar L5
K124/12	Male	55	Thoracic T6-T8; lumbar L2

* Age is unavailable

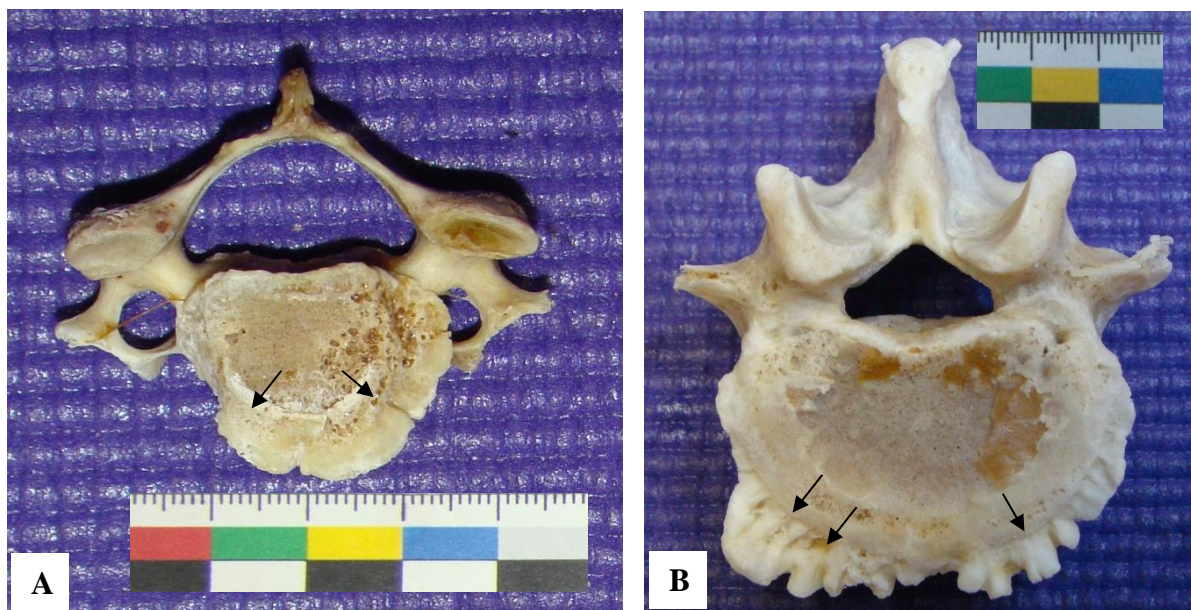


Figure 4.111. Osteophytic changes. A) Marginal osteophytes on the anterior aspects of the ventral body (arrows) of the cervical vertebra C3 of cadaver K50/12, superior view; B) marginal osteophytes on the supero-anterior aspects of the ventral body (arrows) of lumbar vertebrae L4 of cadaver K76/11, superior view.

4.11.3.6 Spondylolysis

Spondylolysis, defined as the failure of union between the partes interarticulares of the vertebrae, was seen in 2/124 (1.6%) cadavers (Table 4.84). The lumbar vertebrae of both male cadavers were affected. The result is a vertebra with two distinct parts.

Table 4.84. Spondylolysis in the cadaver cohort (n=124)

<i>Cadaver Ref. Nr.</i>	<i>Sex</i>	<i>Age</i>	<i>Vertebral Involvement</i>
K57/12	Male	51	Lumbar vertebra L5 (Fig. 4.112, A)
K69/12	Male	*	Lumbar vertebra L3 (Fig. 4.112, B)

* Age is unavailable

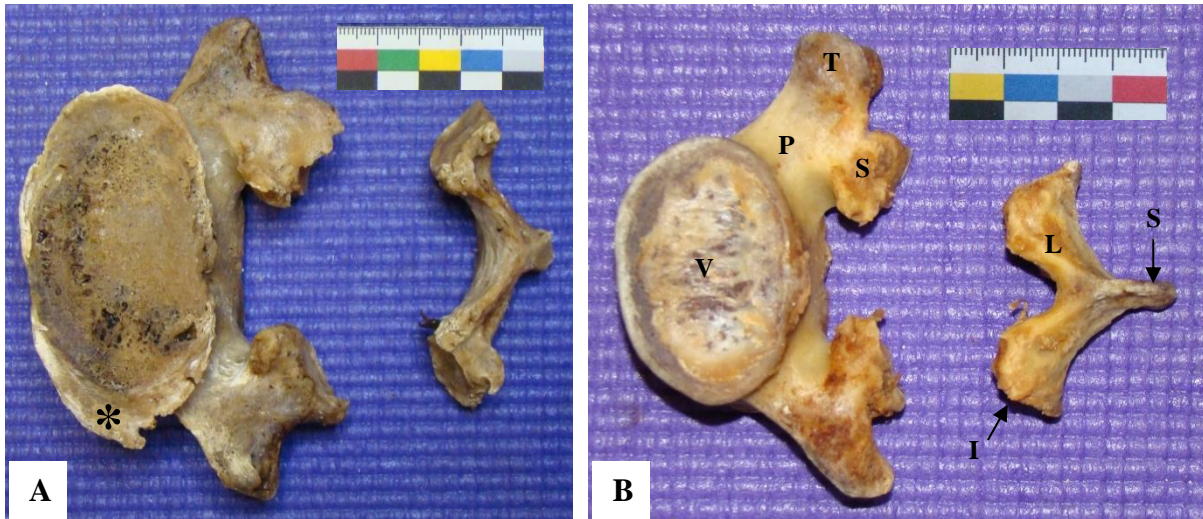


Figure 4.112. Spondylolysis. A) Neural arch separation of lumbar vertebrae L5 of cadaver K57/12. The vertebra is separated into two parts; B) neural arch separation of lumbar vertebra L3 of cadaver K69/12, superior view, the ventral (anterior) part consists of the ventral body (V), pedicles (P), superior articular process (S) and transverse process (T) and the dorsal (posterior) part consists of the laminae (L), spinous process (S) and inferior articular process (I), osteophytes (asterisk).

4.11.3.7 Sacral Trauma

Sacral trauma was seen in 1/124 (0.8%) cadavers. Cadaver K50/12 presented with a healed sacral fracture (Figure 4.113, A). The right superior sacral part as well as the right ala was malaligned as a result of healing. As a result, the anterior sacral foramina were deformed and oval in shape (Figure 4.113, A). The right auricular surface (for the sacroiliac joint) was deformed which resulted in a malaligned attachment of the right os coxa (Figure 4.113, B).

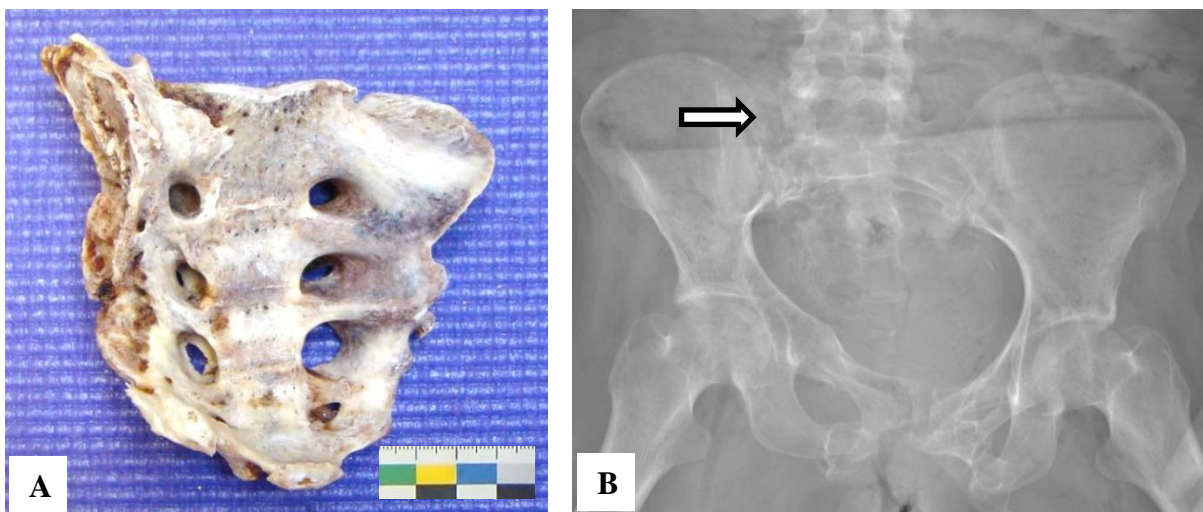


Figure 4.113. Fracture of the sacrum. A) The right lateral part of the sacrum was fractured and malaligned in cadaver K50/12, antero-lateral view; B) iodox[®] X-ray of the pelvic region of cadaver K50/12 showing the malalignment of the sacrum in relation to the right os coxa (arrow).

4.11.3.8 Transitional Vertebrae at the Lumbosacral Level

Lumbosacral transitional vertebrae (LSTV) were observed in 9/124 (7.3%) cadavers (Table 4.85). The male to female ratio was 1:2.7 and the average age of the affected cadavers was 42.0 years. Lumbarisation was seen in 2/9 (22.2%) cadavers, while sacralisation was seen in 7/9 (77.8%) cadavers. Different types of lumbarisation and sacralisation was observed in the cadaver cohort. Sacralisation type II and type III were observed in five and two cadavers, respectively. Sacralisation type II (incomplete sacralisation) occurs as a result of formation of a diarthrodial joint between the sacrum and transverse process. Sacralisation type III (complete sacralisation) was the most common form of lumbosacral transitional vertebrae (LSTV) observed in the cadavers (Figure 4.113, A). These cadavers presented with complete fusion of the fifth lumbar vertebra to the sacral basis. The end result is four vertebrae and six sacral vertebrae. Two cadavers presented with a type I and type III lumbarisation, respectively. Lumbarisation type I is characterised by well-formed facet joints on the first sacral vertebra that are similar to lumbar facet joints. Lumbarisation type III (complete lumbarisation) occurs when complete separation between S1 and the sacrum occurs (Figure 4.113, B). The result was six lumbar vertebrae and four sacral vertebrae.

Table 4.85. Lumbarisation and sacralisation in the cadaver cohort (n=124)

<i>Cadaver Ref. Nr.</i>	<i>Sex</i>	<i>Age*</i>	<i>Sacral Involvement</i>	<i>Type</i>	<i>Unilateral/Bilateral</i>
K80/09	Male	31	Lumbarisation of S1	Type I	Unilateral
K102/09	Female	28	Sacralisation of L5 (Fig. 4.113, A)	Type III	Bilateral
K108/09	Male	42	Sacralisation of L5	Type III	Bilateral
K06/10	Female	53	Sacralisation of L5	Type III	Bilateral
K47/10	Male	43	Lumbarisation of S1 (Fig. 4.113, B)	Type III	Unilateral
K10/11	Female	45	Sacralisation of L5	Type III	Bilateral
K64/11	Female	48	Sacralisation of L5	Type III	Bilateral
K72/11	Male	*	Sacralisation of L5	Type II	Bilateral
K100/12	Female	46	Sacralisation of L5	Type II	Unilateral

* Age is unavailable

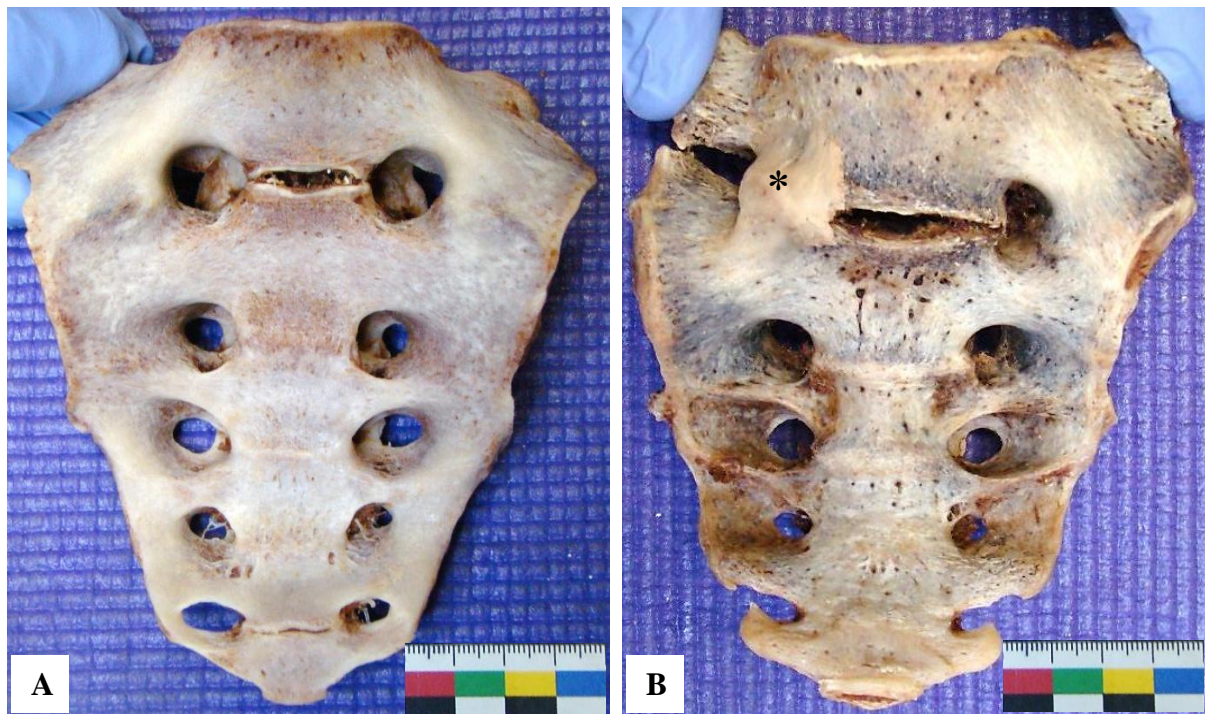


Figure 4.113. Sacralisation and lumbarisation. A) Complete sacralisation of S1 of cadaver K102/09, anterior view; B) complete lumbarisation of L5 of cadaver K47/10, anterior view; osteophytic changes (asterisk).

4.11.4 Thorax

4.11.4.1 Rib Lesions

Rib lesions were seen in 35/124 (28.2%) cadavers (Table 4.86). The male to female ratio was 1.8:1 and the average age of the affected cadavers was 50.4 years. The right side of the rib cage was affected unilaterally in 4/35 (11.4%) cadavers, the left side was unilaterally affected in 6/35 (17.1%) cadavers and bilateral involvement was seen in 25/35 (71.5%) cadavers.

Table 4.86. Rib lesions in the cadaver cohort (n=124)

<i>Cadaver Ref. Nr.</i>	<i>Sex</i>	<i>Age*</i>	<i>Rib Involvement</i>	<i>Anatomical Position</i>	<i>Pulmonary Infection</i>	<i>Pleuritis</i>
K81/09	Male	44	R = 6; L = 7	Rib shafts, visceral surface	Bilateral PTB	Present
K83/09	Male	60	R = 5; L = 6	Rib shafts, visceral surface	Bilateral PTB, lung tumour, bronchiectasis	Present
K102/09	Female	28	R = 4; L = 4	Rib shafts, visceral surface	Bilateral PTB, bronchiectasis	Present
K104/09	Male	*	R = 4	Rib shafts and vertebral necks, visceral surface	Bilateral PTB, pneumonia	Present
K112/09	Male	58	R = 3; L = 4	Rib shafts, visceral surface	Bilateral PTB, pneumonia	Present
K30/10	Male	*	R = 1	Rib shaft, visceral surface	Bilateral PTB	Present

<i>Cadaver Ref. Nr.</i>	<i>Sex</i>	<i>Age*</i>	<i>Rib Involvement</i>	<i>Anatomical Position</i>	<i>Pulmonary Infection</i>	<i>Pleuritis</i>
K40/10	Male	47	L = 9	Rib shafts and vertebral necks, visceral surface	Bilateral PTB	Present
K47/10	Male	43	R = 9; L = 11	Rib shafts and vertebral necks, visceral surface	PTB absent, parenchymal fibrosis	Absent
K05/11	Female	41	R = 4; L = 5	Rib shafts and vertebral necks, visceral surface	PTB absent, L pneumonectomy	Present
K38/11	Male	68	R = 1; L = 1	Rib shafts, visceral surface	Bilateral PTB, bronchiectasis	Present
K44/11	Male	48	R = 2; L = 5	Rib shafts and vertebral necks, visceral surface	PTB absent	Absent
K52/11	Male	48	R = 3; L = 3	Shafts (right), vertebral necks (left)	Bilateral PTB, parenchymal fibrosis	Present
K62/11	Male	83	L = 1	Rib shaft, visceral surface	Bilateral PTB, pneumonia	Present
K65/11	Female	52	R = 6; L = 1	Rib shafts and vertebral necks, visceral surface	Unilateral PTB	Present
K74/11	Male	70	L = 3	Rib shafts, visceral surface	PTB absent	Absent
K75/11	Male	36	R = 3; L = 8	Rib shafts, visceral surface	Bilateral PTB, parenchymal fibrosis	Present
K126/11	Male	45	R = 2; L = 3	Rib shafts, visceral surface	Bilateral PTB, pneumonia	Present
K130/11	Female	81	L = 1	Rib shaft, visceral surface	PTB absent	Absent
K148/11	Male	49	R = 1	Rib shafts and vertebral necks, visceral surface	Bilateral PTB, parenchymal fibrosis	Present
K25/12	Male	39	R = 4; L = 4	Rib shafts and vertebral necks, visceral surface	Bilateral PTB, bronchiectasis	Present
K26/12	Male	*	R = 9; L = 4	Rib shafts and vertebral necks, visceral surface	Bilateral PTB, bronchiectasis	Present
K27/12	Male	66	R = 8; L = 7	Rib shafts and vertebral necks and costal part, visceral surface	Bilateral PTB, bronchiectasis	Present
K31/12	Male	45	L = 3	Rib shafts, visceral surface	Bilateral PTB	Absent
K43/12	Male	*	R = 2; L = 8	Rib shafts and vertebral necks, visceral surface	Bilateral PTB, pneumonia	Present
K46/12	Male	46	R = 5; L = 6	Rib shafts, visceral surface	Bilateral PTB, bronchiectasis	Absent
K51/12	Male	56	R = 3	Rib shafts, visceral surface	Bilateral PTB, bronchiectasis, lung tumor	Present
K57/12	Male	51	R = 6; L = 7	Rib shafts and vertebral necks, visceral surface	Unilateral PTB, bronchiectasis (right)	Present
K60/12	Female	22	R = 4; L = 6	Rib shafts and vertebral necks, visceral surface	Bilateral PTB, pneumonia	Present
K61/12	Male	52	R = 2, L = 3	Rib shafts, visceral surface	Bilateral PTB, broncho-pneumonia	Present
K77/12	Female	32	R = 3; L = 5	Rib shafts, visceral surface	Bilateral PTB, pneumonia	
K79/12	Female	49	R = 5; L = 5	Rib shafts and vertebral necks, visceral surface	Bilateral PTB	
K81/12	Male	49	R = 6; L = 11	Rib shafts and vertebral necks, visceral surface	Bilateral PTB	

<i>Cadaver Ref. Nr.</i>	<i>Sex</i>	<i>Age*</i>	<i>Rib Involvement</i>	<i>Anatomical Position</i>	<i>Pulmonary Infection</i>	<i>Pleuritis</i>
K82/12	Male	63	R = 7; L = 7	Rib shafts and vertebral necks, visceral surface	Bilateral PTB	
K97/12	Male	*	R = 8; L = 3	Rib shafts, visceral surface	Bilateral PTB, pneumonia	Absent
K98/12	Male	42	L = 5	Rib shafts, visceral surface	Bilateral PTB	Absent

4.11.4.1.1 Prevalence and Distribution of Rib Lesions

The appearance of the lesions ranged from proliferative lesions to plaque-like lesions located on the visceral surface. Proliferative lesions were seen in the ribs of all 35 cadavers affected with lesions, while plaque-like lesions were observed in only 1/35 (2.9%) cadaver. The lesions were all observed on the visceral surface in the area in close association with the parietal pleura (Figure 4.115).

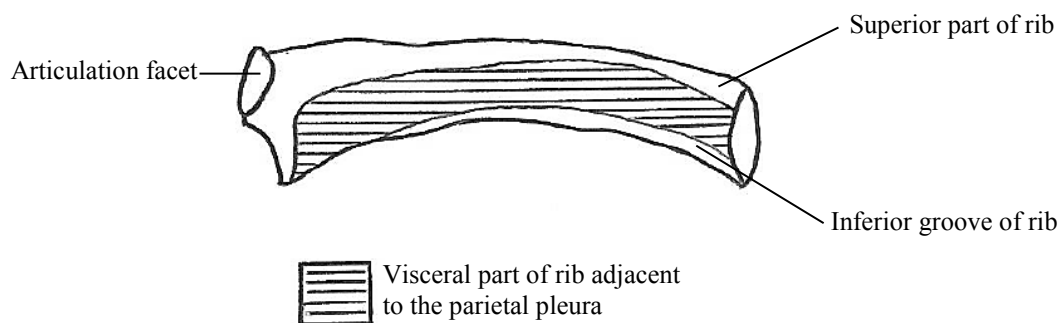


Figure 4.115. Parietal pleural attachment. A diagram to illustrate the attachment of the pleura to the visceral surface of the adjacent rib (Diagram adapted from Roberts et al., 1994).

The distribution of periostotic on each individual rib was determined and their location was divided into three regions, A, B or C depending on their distribution (Figure 4.116). In the diagram below, A represents the area between the head and the tubercle of the rib, B the angle of the rib and C the body of the rib.

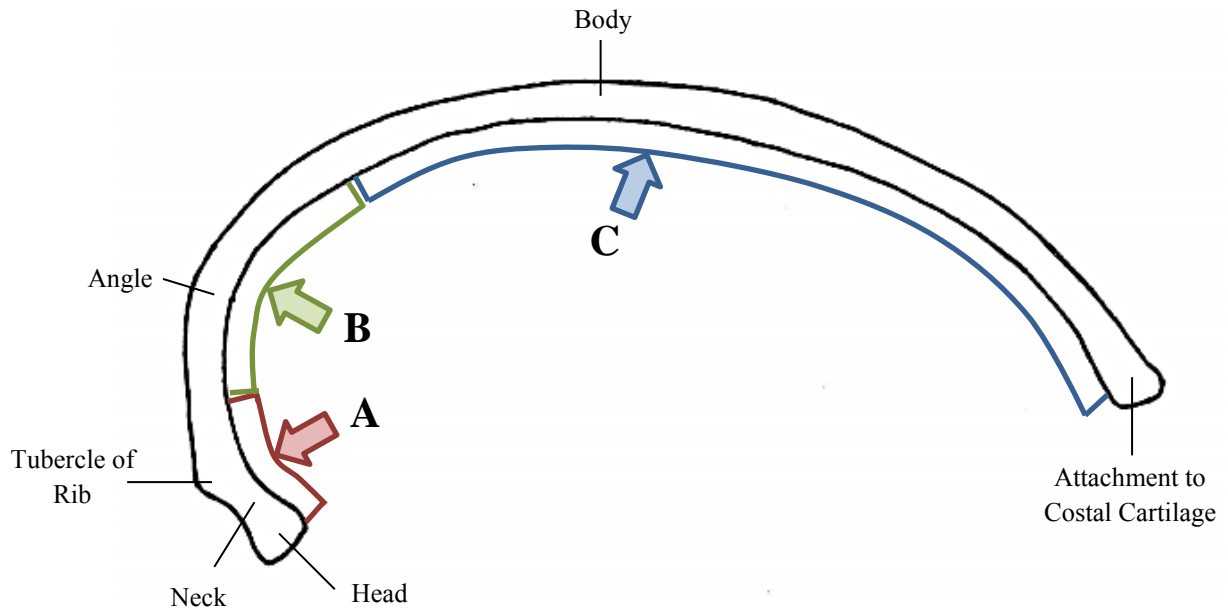
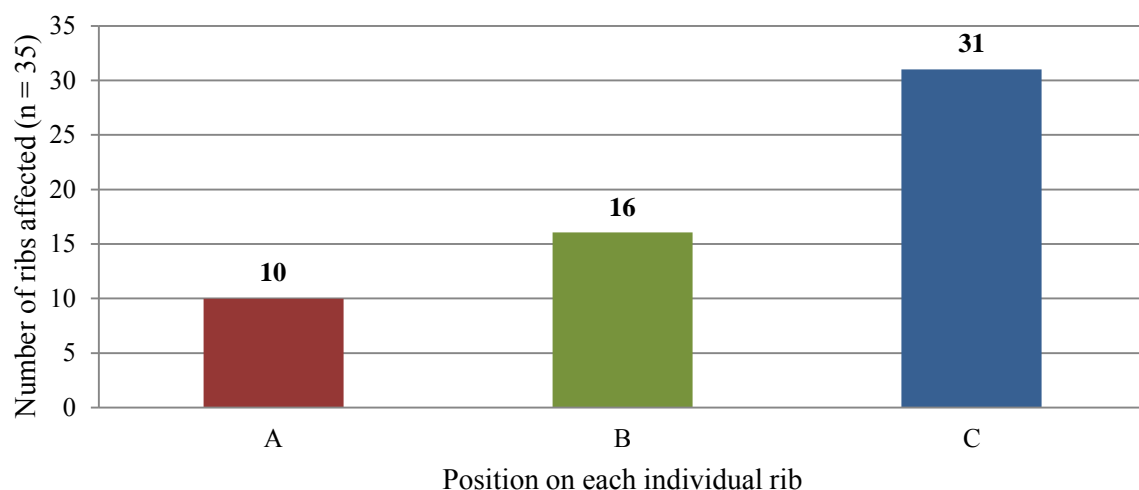


Figure 4.116. Position of periostotic lesions on each individual rib. For the purpose of this study, each individual rib was divided into three regions; A, B and C; area between the head and the tubercle of the rib (A), angle of the rib (B) and body of the rib (C).

In the graph below, the position of the periostotic lesions on each of the ribs are illustrated.

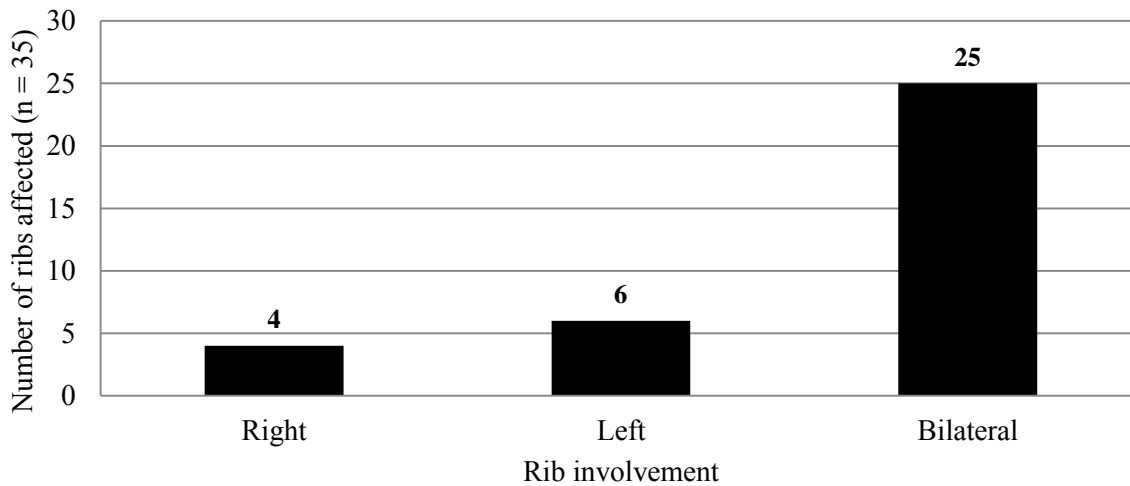
As can be seen in Figure 4.117, the body of the rib was more commonly affected than the angle and neck of the ribs, respectively.

Figure 4.117. The number and position of periostotic lesions on each individual rib. Area between the head and the tubercle of the rib (A), angle of the rib (B) and body of the rib (C).



Periostotic rib lesions were more commonly observed bilaterally, while a slight predilection for the left ribs were observed compared to the right ribs when they were unilaterally affected (Figure 4.118).

Figure 4.118. The number of rib lesions affecting the right and left side, unilaterally, as well as the number of bilateral involvement.



4.11.4.1.2 Morphology of the Rib Lesions

A variety of morphologic different periostotic lesions presented on the visceral sides of the ribs. These lesions ranged from subperiosteal growth (Figure 4.119) to proliferative rib lesions representing distinct nodules (Figures 4.120 and 4.121) to plaque formation on the sternal end of the ribs (Figure 4.122).

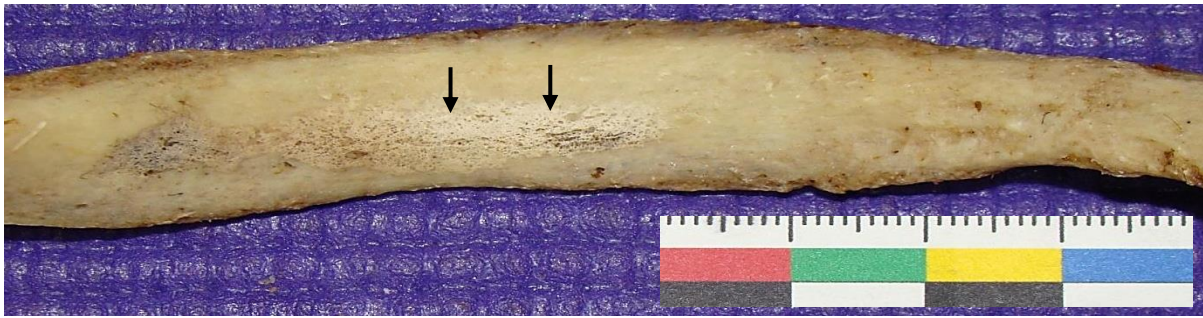


Figure 4.119. Subperiosteal rib lesions. The visceral surface of the right rib 11 of cadaver K25/12 contained subperiosteal growth, postero-lateral view.

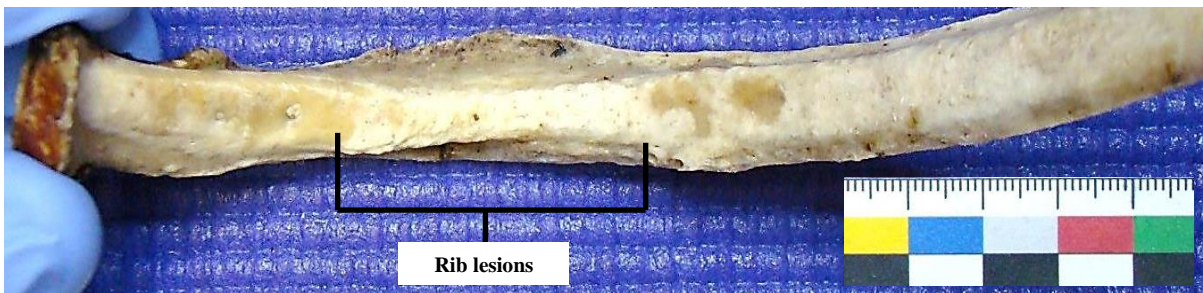


Figure 4.120. Proliferative rib lesions. Rib lesions can be seen on the posterior aspect of the left rib of cadaver K51/12, postero-lateral view.



Figure 4.121. Proliferative rib lesions. The visceral surface of the fifth left rib of cadaver K75/11 contained proliferative lesions on the neck and shaft of the rib, postero-lateral view.



Figure 4.122. Plaque-like rib lesion. The sternal end of the left rib 8 of cadaver K27/12 contained a white plaque-like lesion on the visceral surface, posterior view.

4.11.4.2 Rib Trauma

Healed rib fractures were seen in 46/124 (37.1%) cadavers (unilateral on the right side 3/46 (6.5%), unilateral on the left side 15/46 (32.6%) and bilateral 28/46 (60.9%) (Table 4.87). In 9/46 (19.6%) cadavers more than one healed fracture was seen per rib as opposed to 37/46 (80.4%) of the cadavers who presented with only one healed fracture per rib. Posterior healed fractures were seen in 20/46 (43.5%) cadavers while the remaining fractures were observed on the lateral aspects of the ribs and areas close to the sternal ends. Callus formation was characteristic of healed fractures (Figure 4.123). The male to female ratio was 1:1.1 and the average age of the affected cadavers was 52.6 years.

Table 4.87. Rib trauma in the cadaver cohort (n=124)

<i>Cadaver Ref. Nr.</i>	<i>Sex</i>	<i>Age*</i>	<i>Rib Involvement</i>	<i>Number of Healed Fractures Per Rib</i>	<i>Location of Fracture</i>
K81/09	Male	44	Healed right and left rib fractures	One	Posterior on the shaft close to the neck
K82/09	Male	47	Healed right and left rib fractures	One	Posterior on the shaft close to the neck
K83/09	Male	60	Healed left rib fracture	One	On the shaft (lateral)
K95/09	Male	*	Healed right and left rib fractures	One	On the shafts (lateral)
K104/09	Male	*	Healed rib fractures (Right = 2; Left = 6)	Multiple	Posterior on the shaft close to the neck
K108/09	Male	42	Healed left rib fractures	One	Posterior on the shaft close to the neck
K110/09	Female	49	Healed rib fractures (Right = 6; Left = 6)	One	Posterior on the shaft close to the neck
K112/09	Male	58	Healed right rib fractures	Multiple	Posterior on the shaft close to the neck
K113/09	Male	40	Healed left rib fracture	One	On the shafts (lateral)
K01/10	Male	53	Healed rib fractures (Right = 3; Left = 2)	One	On the shafts (lateral)
K30/10	Male	*	Healed rib fractures (Right = 5)	One	Posterior on the shaft close to the neck
K45/10	Male	43	Healed right and left rib fractures	One	Posterior on the shaft close to the neck
K47/10	Male	43	Healed right rib fractures	One	On the shafts (lateral)
K10/11	Female	45	Healed right and left rib fractures	One	Posterior on the shaft close to the neck
K13/11	Female	47	Healed right and left rib fractures	One	Posterior on the shaft close to the neck
K38/11	Male	68	Healed rib fractures (Right = 6; Left = 5)	One	On the shafts (lateral side) and close to the sternal ends
K40/11	Female	*	Healed left rib fractures (Left = 2)	One	On the shafts (lateral)
K42/11	Male	*	Healed left rib fractures (Left = 4)	One	On the shafts (lateral)

<i>Cadaver Ref. Nr.</i>	<i>Sex</i>	<i>Age</i>	<i>Rib Involvement</i>	<i>Number of Healed Fractures Per Rib</i>	<i>Location of Fracture</i>
K44/11	Male	48	Healed rib fractures (Right = 1; Left = 2)	One	On the shafts (lateral)
K47/11	Male	64	Healed left rib fractures (Left = 3)	One	Posterior on the shaft close to the neck
K65/11	Female	52	Healed rib fractures (Right = 6; Left = 1)	One	Posterior on the shaft close to the neck
K69/11	Female	63	Healed left rib fractures (Left = 2)	One	On the shafts (lateral)
K70/11	Female	*	Healed right and left rib fractures	One	On the shafts (lateral)
K74/11	Male	70	Healed rib fractures (Right = 3; Left = 1)	One	On the shafts (lateral)
K75/11	Male	36	Healed left rib fractures (Left = 1)	One	On the shafts (lateral side) and close to the sternal ends
K76/11	Female	*	Healed right and left rib fractures	One	Posterior on the shaft close to the neck
K82/11	Female	39	Healed right and left rib fractures	One	On the shafts (lateral)
K121/11	Male	50	Healed rib fractures (Right = 6; Left = 6)	Multiple	Posterior (left side); shaft and sternal ends (right side)
K124/11	Female	*	Healed left rib fracture (Left = 1)	One	On the shaft (lateral)
K126/11	Male	45	Healed left rib fracture (Left = 1)	One	On the shaft (lateral)
K140/11	Female	42	Healed left rib fractures (Left = 2)	One	Shaft (one fracture), sternal end (one fracture)
K148/11	Male	49	Healed left rib fractures (Left = 6)	One	On the shafts (lateral)
K26/12	Male	*	Healed rib fractures (Right = 9; Left = 7)	Multiple	Posterior (left side); shaft and sternal ends (right side)
K27/12	Male	66	Healed left rib fracture (Left = 2)	One	Posterior on the shaft close to the neck
K28/12	Female	62	Healed rib fractures (Right = 4; Left = 1)	One	On the shafts (lateral)
K43/12	Male	*	Healed rib fractures (Right = 3; Left = 5)	One	On the shafts (lateral)
K46/12	Male	46	Healed rib fractures (Right = 1; Left = 2)	One	On the shafts (lateral)
K50/12	Female	*	Healed right and left rib fractures	Multiple	Posterior on the shaft close to the neck
K58/12	Male	70	Healed rib fractures (Right = 3; Left = 3)	One	Posterior on the shaft close to the neck
K61/12	Male	52	Healed rib fractures (Right = 6; Left = 6)	Multiple (Fig. 4.123)	On the shafts (lateral)
K62/12	Female	73	Healed left rib fracture (Left = 1)	One	On the shaft (lateral)
K73/12	Male	72	Healed rib fractures (Right = 4; Left = 6)	Multiple	Posterior on the shaft close to the neck
K74/12	Female	52	Healed rib fractures (Right = 2; Left = 2)	Multiple	Posterior on the shaft close to the neck
K78/12	Male	61	Healed left rib fractures (Left = 2)	Multiple	Posterior on the shaft close to the neck
K99/12	Male	47	Healed right and left rib fractures	One	On the shafts (lateral)
K106/12	Male	44	Healed right and left rib fractures	One	On the shafts (lateral)

* Age is unavailable



Figure 4.123. Healed rib trauma. Multiple healed fractures with remodelling can be seen on four of the left ribs of cadaver K61/12, superior view, healed fractures (asterisks).

4.11.4.3 Sternum

4.11.4.3.1 Pectus Carinatum (Pigeon Breast)

Pectus carinatum (pigeon breast) was observed in 3/124 (2.4%) cadavers (Table 4.88) and occurs as a result of a vitamin D deficiency, particularly during childhood. The male to female ratio was 1:1.1. The ages of the male cadavers were unavailable. The corpus sterni showed an outward bend (towards the anterior aspect) with the manubrium and xiphoid process (if present) located more posteriorly (Figure 4.124). The pigeon breast deformities were not observable on the chest X-rays.

Table 4.88. Pectus carinatum in the cadaver cohort (n=124)

<i>Cadaver Ref. Nr.</i>	<i>Sex</i>	<i>Age*</i>	<i>Sternal Involvement</i>
K118/09	Male	*	Corpus sterni has a severe outward bend along the width in the area of the fourth costal notch (Fig. 4.124)
K30/10	Male	*	Sternum has a bend in the area of the third costal notch
K69/11	Female	63	Sternum has a severe bend in the area of the fourth notch

* Age is unavailable

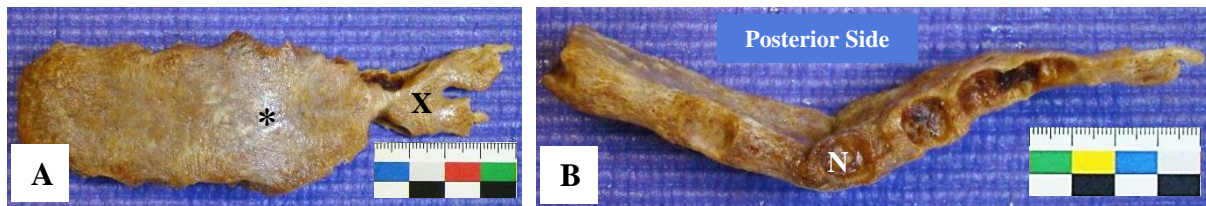


Figure 4.124. Pectus carinatum. A) Corpus sterni with fused xiphoid process (X) of cadaver K118/09 is showing the outward bend (asterisk), anterior view; B) the left lateral side of the same sternum as in (A) showing severe outward bending leading to the pigeon breast appearance, lateral view; fourth costal notch (N).

4.11.4.4 Clavicle

4.11.4.4.1 Clavicular Trauma

Clavicular trauma was seen in 3/124 (2.4%) cadavers (Table 4.89). All the cadavers affected were males. The average age of the cadavers with signs of clavicular trauma was 55.5 years. Two of the three clavicular fractures in the cadavers were observed along the clavicular shaft (Figure 4.125). The acromial (lateral) end was affected in one cadaver while the sternal (medial) ends of all three clavicles in question were spared of trauma.

Table 4.89. Clavicular trauma in the cadaver cohort (n=124)

<i>Cadaver Ref. Nr.</i>	<i>Sex</i>	<i>Age*</i>	<i>Clavicular Involvement</i>
K121/11	Male	50	Healed fracture in the lateral end of right clavicle
K51/12	Male	*	Healed fracture in the shaft of right clavicle
K78/12	Male	61	Healed fracture in the shaft of right clavicle

* Age is unavailable

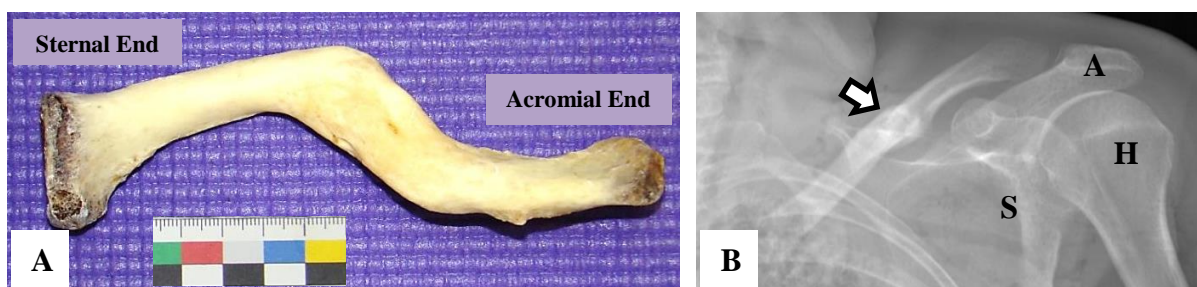


Figure 4.125. Clavicular trauma. A) Healed fracture can be seen in the shaft of the left clavicle of cadaver K51/12, superior view; B) corresponding X-ray showing the fractured left clavicle (arrow); acromion (A), humerus (H), scapula (S).

4.11.5 Upper Limb

4.11.5.1 Healed Trauma of the Upper Limb

Upper limb fractures were noted in 22/124 (17.7%) cadavers. The male to female ratio was 1:1.5 and the average age of the affected cadavers was 49.4 years. The humerus was involved in 3/22 (13.6%) cadavers, the ulna in 20/22 (90.9%) cadavers and the radius in 5/22 (22.7%) cadavers. Unilateral involvement of the left side was seen in 13/22 (59.1%) cadavers, unilateral involvement of the right side was observed in 4/22 (18.2%) cadavers, while bilateral involvement was observed in 5/22 (22.7%) cadavers. Of these upper limb fractures, 4/22 (18.2%) were repaired and fixed with orthopedic wires, nails and plates. Table 4.90 gives a brief overview of the observed upper limb fractures.

Table 4.90. Upper limb fractures in the cadaver cohort (n=124)

<i>Cadaver Ref. Nr.</i>	<i>Sex</i>	<i>Age*</i>	<i>Upper Limb Involvement</i>	<i>Implantation Present</i>
K82/09	Male	47	Healed fracture in the shaft of left ulna and proximal region of right ulna	None
K95/09	Male	*	Remodelling and healing of fracture in left humeral shaft	None
K110/09	Female	49	Healed fracture of the proximal part of right ulna	None
K115/09	Male	32	Healed fracture of the head of left ulna	None
K01/10	Male	53	Proximal part of left ulna (Fig. 4.127, A, B)	Orthopaedic wires
K19/10	Female	63	Healed fracture in the shaft of left ulna	None
K45/10	Male	43	Healed fractures in shaft of left ulna and left radius	None
K05/11	Female	41	Healed fracture in shaft of left ulna	None
K06/11	Male	37	Healed fracture in shaft of right ulna	None
K13/11	Female	47	Healed fracture in the left ulna	None
K38/11	Male	68	Healed fracture in distal part of left ulna	None
K64/11	Female	48	Healed fracture of distal part left ulna; healed fracture of proximal part of right ulna	Orthopaedic wires (right olecranon)
K70/11	Female	*	Healed fracture of right distal ulna	None
K76/11	Female	*	Healed fracture of distal part of left humerus and proximal part of left ulna (Fig. 4.127, C, D)	Orthopaedic wires, plates and nails
K26/12	Male	*	Healed fractures in distal region of both ulnae	None
K28/12	Female	62	Healed left radial fracture in distal region (malaligned)	None
K31/12	Male	45	Healed left radial fracture in the shaft	None
K50/12	Female	*	Healed fracture of the proximal region of left ulna and shaft of right radius; healed fracture of shaft of right humerus (Fig. 4.126)	None
K58/12	Male	70	Healed fractures in distal regions of both ulnae	None
K61/12	Male	52	Healed fracture in the distal part of left ulna	None
K87/12	Male	24	Healed fracture of the shaft of left ulna; bony fusion with the left radius (Fig. 4.127, E, F)	Orthopaedic plate and screws
K101/12	Male	58	Healed fracture in the shaft of right ulna	None

* Age is unavailable



Figure 4.126. Healed upper limb fractures. A) callus formation as a result of healing in the proximal part of the left ulnar shaft of cadaver K50/12, posterior view; B) malaligned healed fracture of the shaft of the right radius of cadaver K50/12, posterior view.

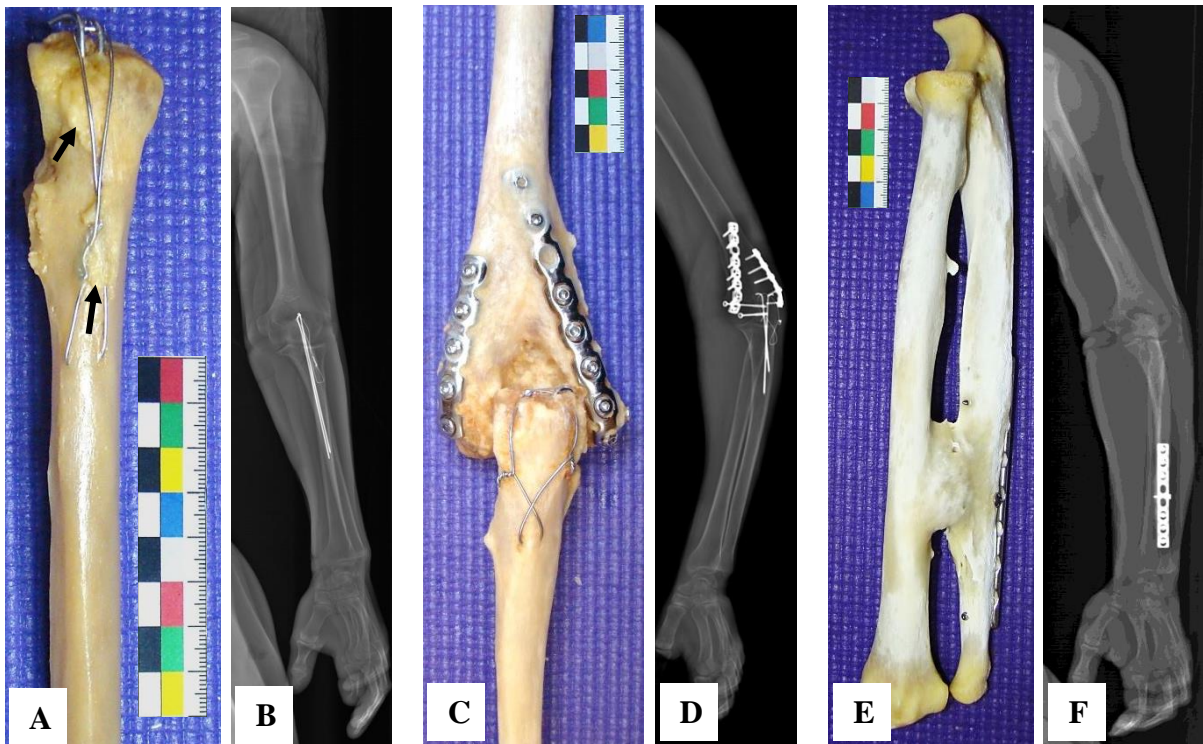


Figure 4.127. Upper limb fractures and repair. A) Orthopaedic wires in the olecranon of left ulna of cadaver K01/10 with accompanying remodelling (arrows), posterior view; B) X-ray of the left upper limb of cadaver K01/10 showing the wire extending into medullary canal of left ulna; C) fracture repair of the distal part of the left humerus and proximal part (olecranon) of the left ulna of cadaver K76/11, posterior view; D) X-ray of the left upper limb of cadaver K76/11 showing extensive orthopaedic repair; E) healed fracture and remodelling of the shaft of left ulna and bony fusion with the left radius of cadaver K87/12, posterior view; F) X-ray of cadaver K87/12, indicating the orthopaedic plate along the shaft of left ulna.

4.11.5.2 Scapula

4.11.5.2.1 Scapular Trauma

Scapular trauma was seen in 5/124 (4.0%) cadavers. The male to female ratio was 1:3.2. The healed fractures were observed on the posterior aspect of the scapula, including the scapular spine (Figure 4.128). Table 4.91 gives a brief overview of the observed healed fractures on the scapula.

Table 4.91. Scapular fractures in the cadaver cohort (n=124)

<i>Cadaver Ref. Nr.</i>	<i>Sex</i>	<i>Age*</i>	<i>Scapular Involvement</i>
K59/11	Male	34	Healed fracture of the right acromion
K64/11	Female	48	Healed fracture of the left scapula inferior to the glenoid cavity on the lateral border (Fig. 4.128)
K70/11	Female	*	Healed fracture of the right scapular spine; healed fracture left acromion and healed fracture of the left scapular spine
K119/11	Male	*	Healed fracture of the right scapula (Fig. 4.128)
K50/12	Female	*	Healed fracture of the right scapula inferior to the scapular spine

* Age is unavailable

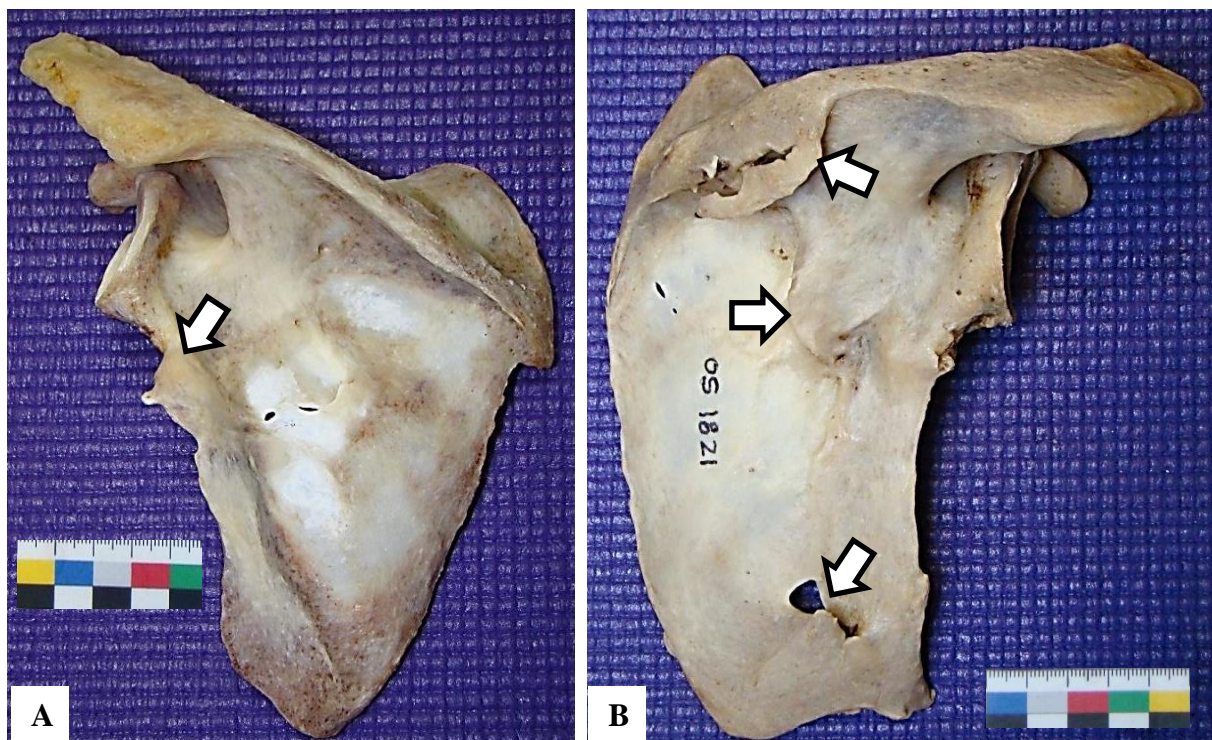


Figure 4.128. Healed scapular fractures. A) Healed fracture (arrow) of the left scapula of cadaver K64/11 inferior to the glenoid cavity on the lateral border, posterior view; B) healed fractures (arrows) of the right scapula of cadaver K119/11, posterior view.

4.11.5.2.2 Dislocation in the Shoulder Joint

Dislocation of the shoulder joint was seen in 1/124 (0.8%) cadaver. The right shoulder of cadaver K12/10 was dislocated a time prior to death and was never completely repaired. The head of the humerus showed degenerative changes (Figure 4.129, A). Over time, remodelling occurred on the anterior aspect of the scapula, medial to the glenoid cavity (Figure 4.129, B). These changes corresponded with the new location of the humeral head anterior to the glenoid cavity (Figure 4.129, C). The presence of a Bankart lesion, as a result of continuous anterior shoulder dislocations, could not be confirmed as the glenoid labrum (glenoid ligament) has been removed during the boiling process.

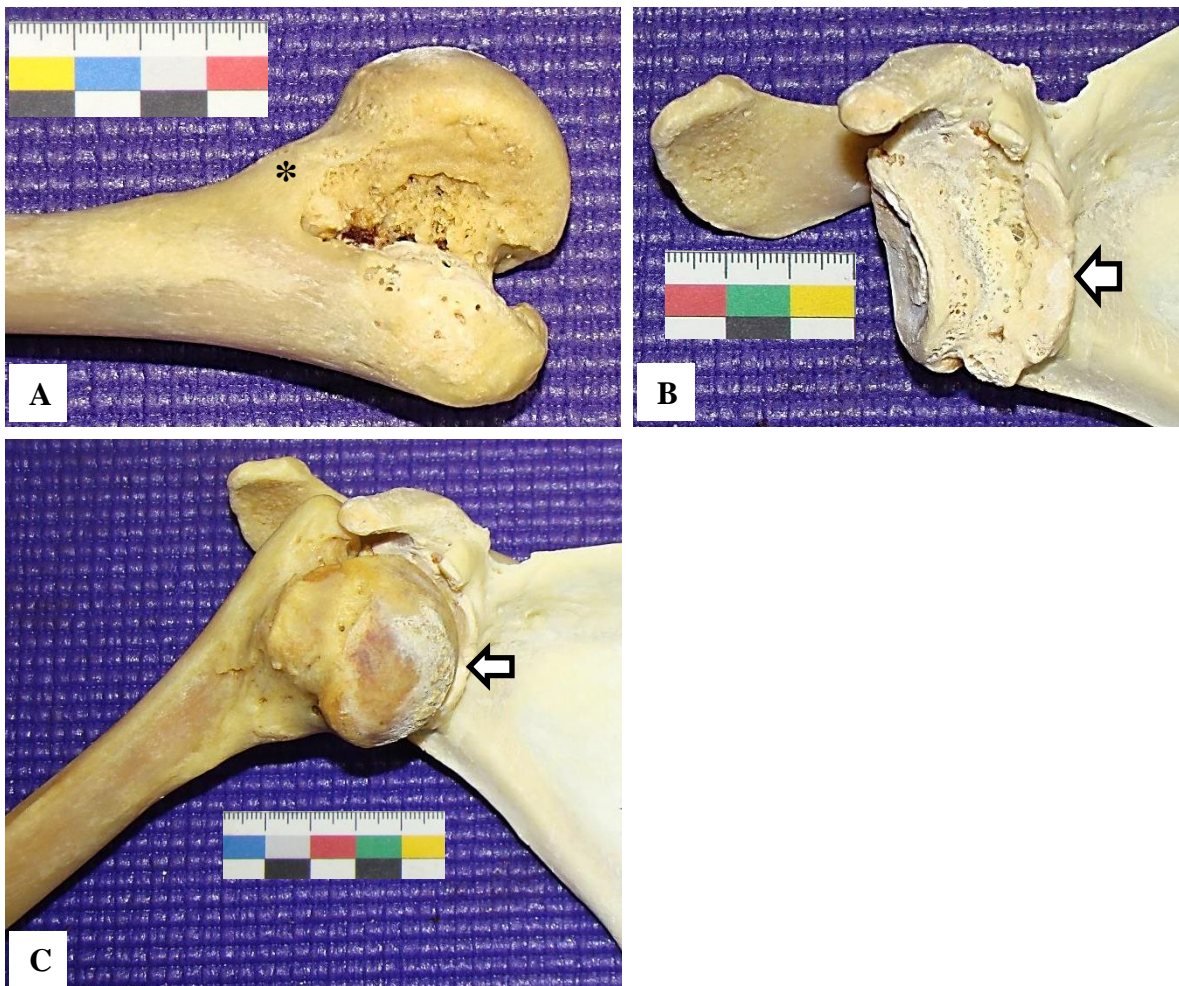


Figure 4.129. Permanent shoulder dislocation. A) Right humeral head degeneration of cadaver K12/10, posterior view. Note the area where bone is added to the humeral head as a result of degeneration (asterisk); B) remodelling (blocked arrow) medial to the glenoid cavity of the scapula, anterior view; C) position of the humeral head in the glenoid cavity, anterior view.

4.11.5.2.3 Degenerative Joint Disease of the Upper Limb

Degenerative joint disease (DJD) in the joints of the upper limb were observed in 17/124 (13.7%) cadavers. The male to female ratio was 2.1:1 and the average age of the affected cadavers was 51.7 years. Osteoarthritic changes were seen in the shoulder joint, including the glenoid fossa (31.3%) and humeral anatomical necks (25.0%). The arthritic changes in the elbow joint were observed in the ulnar trochlear notch (93.8%) and radial articular fovea (12.5%). Arthritic changes of the wrist joint were observed in the radial lunate and scaphoid articular facets (18.8%) and ulnar articular facet (6.3%). Table 4.92 gives a brief overview of the cadavers with degeneration of the joints of the upper limbs.

Table 4.92. Degeneration of the upper limb in the cadaver cohort (n=124)

<i>Cadaver Ref. Nr.</i>	<i>Sex</i>	<i>Age*</i>	<i>Upper Limb Involvement</i>
K104/09	Male	*	Degeneration of both glenoid fossae, bilateral ulnar trochlear notch degeneration
K106/09	Male	*	Degeneration of both humeral anatomical necks and trochlear notches of both ulnae
K13/11	Female	47	Osteoarthritic changes in trochlear notch of right ulna and articular fovea of the right radius (Fig. 4.130, A)
K38/11	Male	68	Degeneration of both glenoid fossae and humeral anatomical necks, bilateral ulnar trochlear notch degeneration and lunate and scaphoid facet degeneration (of both radii)
K40/11	Female	*	Degeneration of trochlear notches of both ulnae
K42/11	Male	*	Degeneration of both glenoid fossae and right humeral anatomical neck, right ulnar trochlear notch degeneration
K53/11	Male	*	Degeneration of right glenoid fossa, bilateral ulnar trochlear notch degeneration, bilateral articular foveae
K119/11	Male	*	Degeneration of the right proximal and distal humerus
K120/11	Female	53	Bilateral degeneration of ulnar trochlear notches
K126/11	Male	45	Degeneration of both lunate and scaphoid facets of both radii
K148/11	Male	49	Bilateral degeneration of ulnar trochlear notches
K43/12	Male	*	Bilateral degeneration of ulnar trochlear notches
K57/12	Male	51	Degeneration of right ulnar trochlear notch
K58/12	Male	70	Bilateral degeneration of ulnar trochlear notches, distal articular facet of right ulna (Fig. 4.130, B)
K73/12	Male	72	Bilateral degeneration of ulnar trochlear notches
K93/12	Male	72	Degeneration of both glenoid fossae and humeral anatomical necks, bilateral ulnar trochlear notch degeneration and lunate and scaphoid facet degeneration of right radius
K98/12	Male	42	Degeneration of both humeral anatomical necks and both ulnar trochlear notches

* Age is unavailable

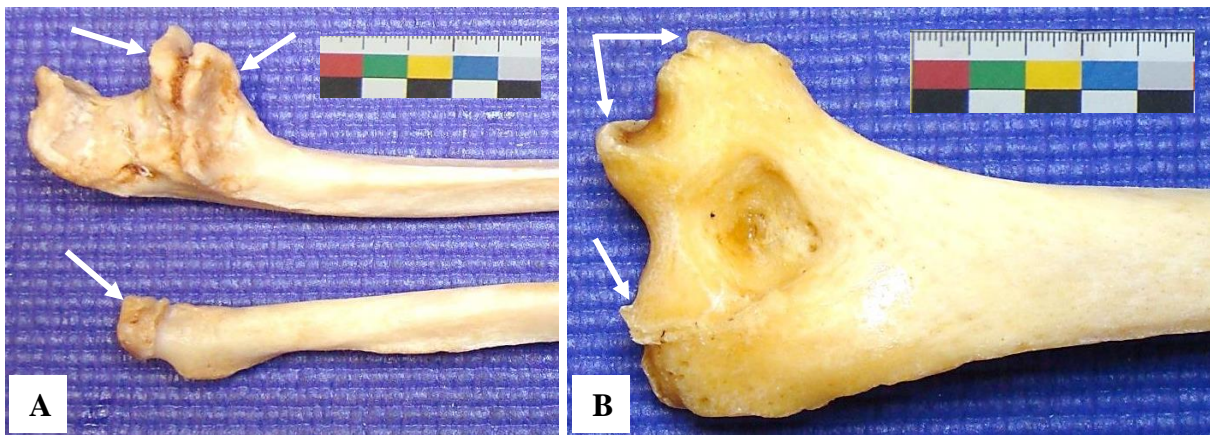


Figure 4.130. Osteoarthritis in the upper limb. A) Joint degeneration (arrows) can be seen in the proximal part of the right ulna and radius of cadaver K13/11, anterior view; B) degeneration (arrows) in the area of the right humeral trochlea and capitulum of cadaver K58/12, posterior view.

4.11.6 Lower Limb

4.11.6.1 Healed Trauma of the Lower Limb

Lower limb fractures were noted in 23/124 (18.5%) cadavers (Table 4.93). The male to female ratio was 1:1.2 and the average age of the affected cadavers was 48.7 years. No femoral fractures were observed in the cadavers. Tibial and fibular fractures were seen in 12/23 (52.2%) and 16/23 (69.9%) cadavers, respectively. Unilateral involvement of the right side was seen in 11/23 (47.8%) cadavers, unilateral involvement of the left side was seen in 9/23 (39.1%) cadavers while bilateral involvement was seen in 4/23 (17.4%) cadavers. Of the lower limb fractures, 3/23 (13.0%) were repaired fixed with orthopaedic screws and/or nails (Figure 4.131).

Table 4.93. Lower limb fractures in the cadaver cohort (n=124)

<i>Cadaver Ref. Nr.</i>	<i>Sex</i>	<i>Age*</i>	<i>Lower Limb Involvement</i>	<i>Implantation Present</i>
K110/09	Female	49	Healed fracture in the proximal region of right tibia	None
K10/10	Male	36	Distal part of the left tibia and fibula (Fig. 4.131, A and B)	Orthopaedic screws
K13/10	Male	47	Bony fusion between the distal region of left tibia and fibula following a fracture	None
K30/10	Male	*	Healed fracture of the right medial malleolus	None
K42/10	Male	*	Carpals of right foot	Orthopaedic screws
K45/10	Male	43	Fractures in both distal areas in the area of the fibular triangular subcutaneous areas	None

<i>Cadaver Ref. Nr.</i>	<i>Sex</i>	<i>Age*</i>	<i>Lower Limb Involvement</i>	<i>Implantation Present</i>
K47/10	Male	43	Healed fracture in the shaft of the right tibia	None
K05/11	Female	41	Healed fracture in the area inferior to the left fibular head	None
K10/11	Female	45	Healed fractures in the left medial malleolus	None
K31/11	Male	53	Bony fusion the distal region of right tibia and fibula following a fracture (Fig. 4.131, C and D)	None
K38/11	Male	68	Healed fracture in the shaft of the right tibia, healed fracture of the lateral malleolus of left fibula	None
K44/11	Male	48	Malaligned healed fractures of the shafts of both the left tibia and fibula	None
K59/11	Male	34	Healed fracture in the area inferior to the left fibular head	None
K64/11	Female	48	Bilateral healed fractures in the fibular lateral malleoli	None
K70/11	Female	*	Healed fracture in the right fibular lateral malleolus	None
K76/11	Female	*	Healed fracture in the area inferior to the right fibular head	None
K124/11	Female	*	Malaligned bony fusion between the distal region of left tibia and fibula following a fracture	None
K26/12	Male	*	Bony fusion the distal region of right tibia and fibula following a fracture, healed fracture in the area inferior to the left fibular head	None
K43/12	Male	*	Healed fracture in the area inferior to the right fibular head	None
K50/12	Female	*	Healed fracture of the proximal part of the right tibia	None
K61/12	Male	52	Healed fracture of the shaft of the left fibula	None
K73/12	Male	72	Healed fracture of the proximal region of the right tibia	None
K75/12	Male	52	Healed fracture in the distal regions of both the left tibia and fibula (Fig. 4.131, E and F)	Orthopaedic screws

* Age is unavailable

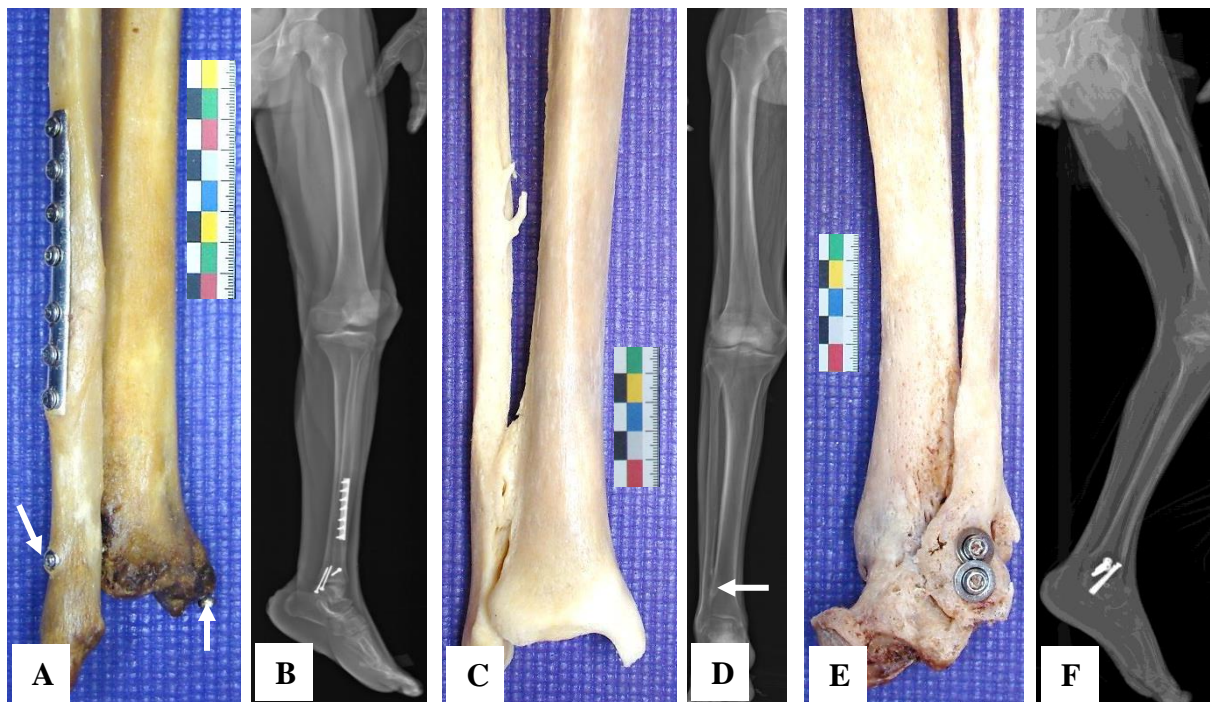


Figure 4.131. Tibial and fibular repair. A) orthopaedic screws and plate in the distal left fibula and tibia of cadaver K10/10, anterior view; B) X-ray of cadaver K10/10 showing the orthopaedic implants within the left tibia and fibula; C) bony fusion between the right tibia and fibula of cadaver K31/11, anterior view; D) X-ray of cadaver K31/11 showing the bony fusion (arrow); E) orthopaedic implants in the distal parts of the left tibia and fibula of cadaver K75/12, postero-lateral view; F) the orthopaedic implants were visible on the X-ray of cadaver K75/12.

4.11.6.2 Patellar Fractures

Patellar fractures were observed in 2/124 (1.6%) cadavers. Both cadavers were males and the average age was 69.0 years. Bilateral involvement was observed in cadaver K27/12 (Figure 4.132, A), while unilateral involvement occurred in the right patella of cadaver K73/12 (Figure 4.132, B). All the fractures were seen on the posterior aspect of the patellae. Table 4.94 gives an overview of the cadavers with patellar fractures.

Table 4.94. Patellar fractures in the cadaver cohort (n=124)

<i>Cadaver Ref. Nr.</i>	<i>Sex</i>	<i>Age*</i>	<i>Patellar Involvement</i>
K27/12	Male	66	Bilateral involvement
K73/12	Male	72	Unilateral involvement of the right patella

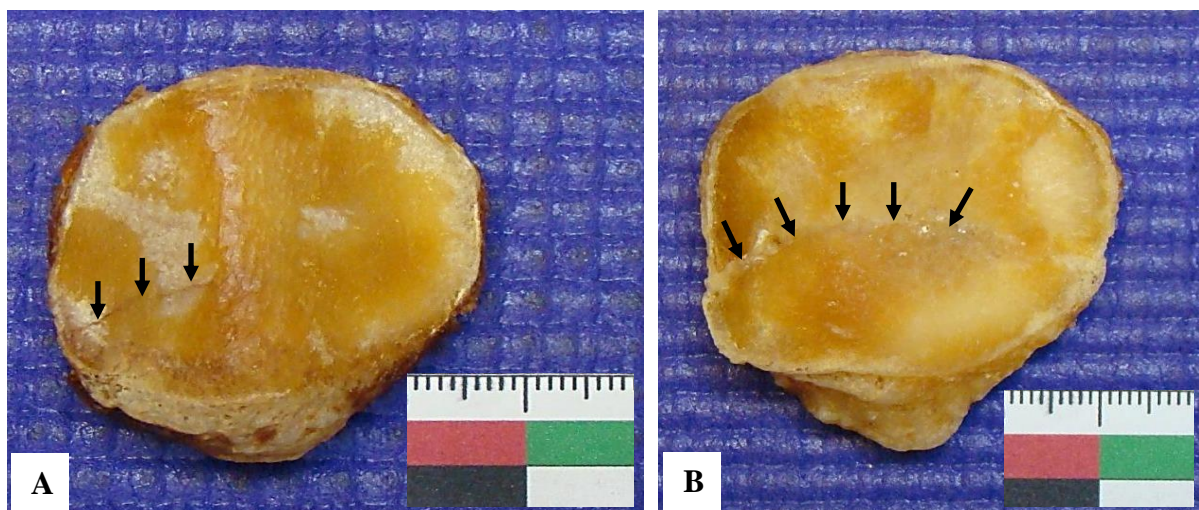


Figure 4.132. Patellar fractures. A) Left patella of cadaver K66/12 showing a healed fracture (arrows) of the medial articular facet, posterior view; B) right patella of cadaver K73/12 showing a healed fracture (arrows) involving the medial and lateral articular facets, posterior view.

4.11.6.3 Degenerative Joint Disease of the Hip Joint

Degenerative joint disease (DJD) of the hip joint was seen in 24/124 (19.4%) cadavers (Table 4.95). The male to female ratio was 1.4:1 and an average age of 61.8 years. Acetabular osteophytes were a common feature in the cadavers with DJD.

Table 4.95. Pelvic osteoarthritis in the cadaver cohort (n=124)

<i>Cadaver Ref. Nr.</i>	<i>Sex</i>	<i>Age*</i>	<i>Pelvic Involvement</i>
K104/09	Male	*	Degeneration of both acetabula, osteophytic changes
K106/09	Male	*	Degeneration of both acetabula (implant in left acetabulum)
K112/09	Male	58	Degeneration of both acetabula
K01/10	Male	53	Degeneration of both acetabula
K19/10	Female	63	Degeneration of both acetabula
K30/10	Male	*	Degeneration of both acetabula
K36/10	Male	82	Degeneration of the right acetabulum
K38/11	Male	68	Degeneration of both acetabula, osteophytic change
K40/11	Female	*	Degeneration of both acetabula
K42/11	Male	*	Degeneration of both acetabula and pubic symphysis
K44/11	Male	48	Degeneration of both acetabula, osteophytic change
K47/11	Male	64	Degeneration of both acetabula
K53/11	Male	*	Degeneration of both acetabula, osteophytic change
K62/11	Male	83	Degeneration of both acetabula
K65/11	Female	52	Degeneration of both acetabula, osteophytic changes superior to acetabula
K69/11	Female	63	Degeneration of both acetabula
K74/11	Male	70	Degeneration of both acetabula, osteophytic change
K130/11	Female	81	Degeneration of both acetabula
K25/12	Male	39	Degeneration of both acetabula, osteophytic change
K28/12	Female	62	Degeneration of both acetabula, osteophytic change
K43/12	Male	*	Degeneration of both acetabula, osteophytic change
K57/12	Male	51	Degeneration of both acetabula
K93/12	Male	72	Degeneration of both acetabula, osteophytic change
K98/12	Male	42	Degeneration of both acetabula, osteophytic change

* Age is unavailable

4.11.6.4 Bilateral Total Hip Arthroplasty (THA)

Bilateral hip replacements were observed in 1/124 (0.8%) cadaver. This male cadaver (K106/09) presented with bilateral total hip arthroplasty (THA).

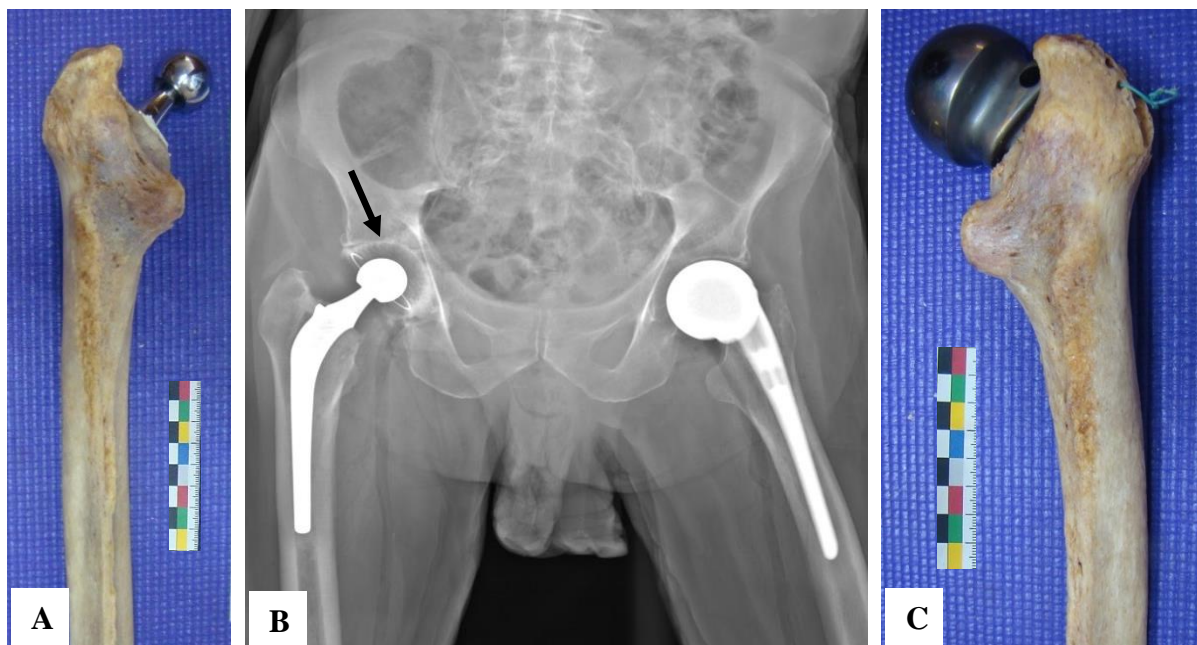


Figure 4.133. Bilateral total hip arthroplasty (K106/09). A) The right head of the femur was replaced with a smaller prosthetic head; B) the Lodox[®] image demonstrating the replacements. A prosthetic acetabulum was placed in the right os coxa (arrow); C) the left femur head was replaced with a larger prosthetic head.

4.11.6.5 Pelvic Trauma

Pelvic trauma was seen in 2/124 (1.6%) cadavers (Table 4.96). The male to female ratio of the cadavers with signs of pelvic trauma was 1:2.2. Cadaver (K82/11) presented with an implantation in the region of the pubic symphysis (Figure 4.134, A and B). The left iliac spine, along the iliac fossa, of cadaver K118/09 showed extensive signs of trauma and healing (Figure 4.134, C-E).

Table 4.96. Pelvic trauma in the cadaver cohort (n=124)

<i>Cadaver Ref. Nr.</i>	<i>Sex</i>	<i>Age*</i>	<i>Pelvic Involvement</i>
K118/09	Male	*	Malaligned healed fracture of the left iliac spine
K82/11	Female	39	Implantation in the area of the pubic symphysis

* Age is unavailable

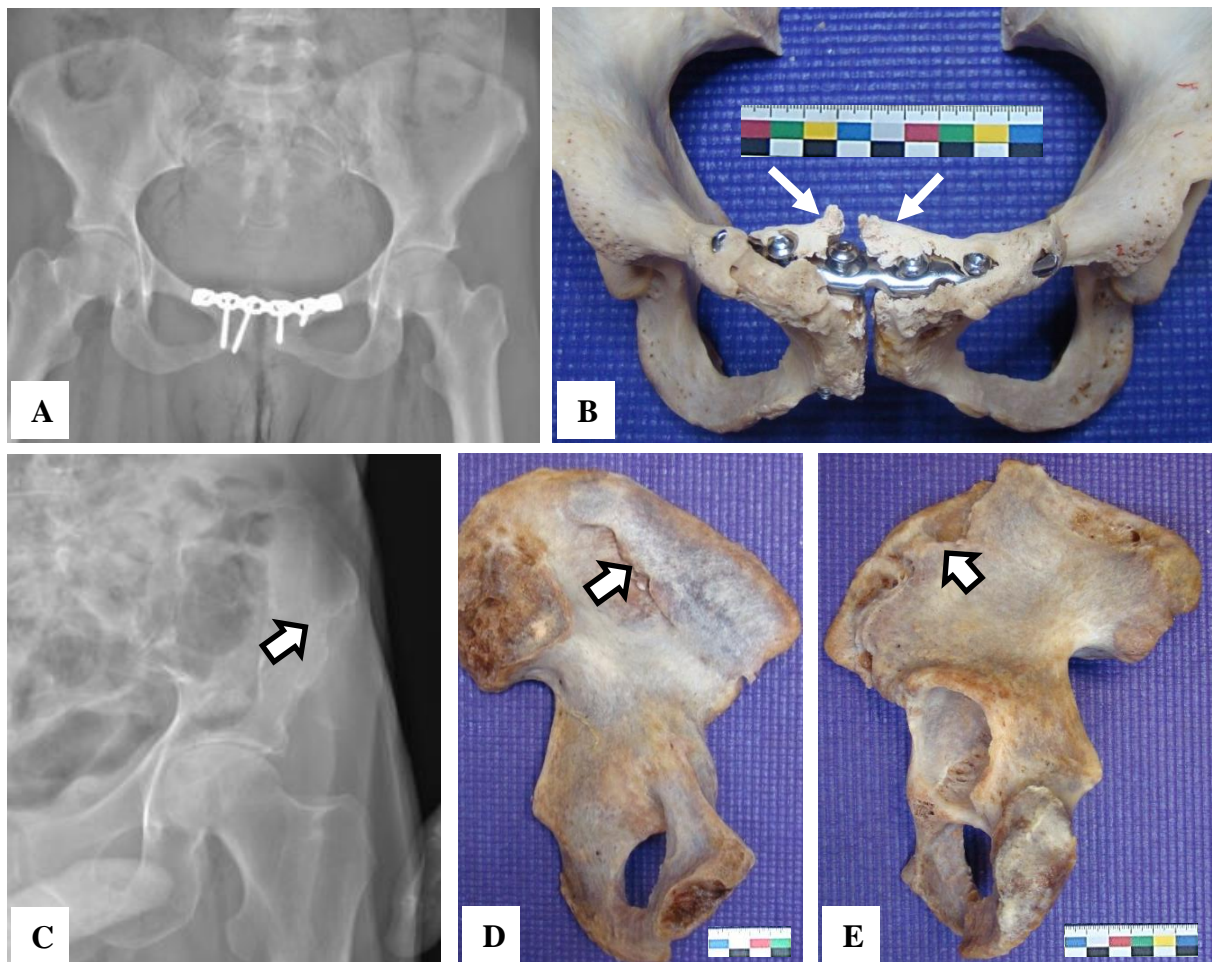


Figure 4.134. Pelvic trauma. A) X-ray image of the pelvis of cadaver K82/11 showing orthopaedic implants within the pubic symphysis; B) orthopaedic implant with remodelling (arrows) to repair a pubic symphysis fracture, antero-superior view; C) X-ray of cadaver K118/09 illustrating a healed fracture (arrow) in the iliac fossa of the right os coxae; D) left os coxae with a malaligned healed iliac fracture (arrow), antero-medial view; E) healed fracture (arrow) of the left os coxae of cadaver K118/09, postero-lateral view.

4.11.6.6 Sacroiliac Joint (SIJ) Fusion

Fusion of the sacroiliac joint (SIJ) to the os coxae was seen in 9/124 (7.3%) cadavers (Table, 4.97, Figure 4.135). All of the cadavers with SIJ fusion were males with an average age of 57.9 years. Unilateral involvement 6/9 (66.7%) was seen on the right and left side in 3/6 (50.0%) and 3/6 (50.0%) cadavers, respectively. Bilateral involvement was seen in 3/9 (33.3%) cadavers (Figure 4.135, B). Diffuse idiopathic skeletal hyperostosis (DISH) was absent in 8/9 (88.9%) cadavers.

Table 4.97. Sacral fusion to os coxae in the cadaver cohort (n=124)

<i>Cadaver Ref. Nr.</i>	<i>Sex</i>	<i>Age*</i>	<i>Pelvic Involvement</i>	<i>Vertebral Fusion</i>
K119/11	Male	*	Unilateral involvement (left)	Diffuse idiopathic skeletal hyperostosis absent
K51/12	Male	56	Unilateral involvement (right)	Diffuse idiopathic skeletal hyperostosis absent
K57/12	Male	51	Bilateral involvement	Diffuse idiopathic skeletal hyperostosis absent
K64/12	Male	50	Unilateral involvement (left)	Diffuse idiopathic skeletal hyperostosis absent
K73/12	Male	72	Unilateral involvement (left)	Diffuse idiopathic skeletal hyperostosis absent
K78/12	Male	61	Bilateral involvement	Diffuse idiopathic skeletal hyperostosis absent
K83/12	Male	59	Bilateral involvement	Diffuse idiopathic skeletal hyperostosis present
K93/12	Male	72	Unilateral involvement (right)	Diffuse idiopathic skeletal hyperostosis absent
K98/12	Male	42	Unilateral involvement (right)	Diffuse idiopathic skeletal hyperostosis absent

* Age is unavailable

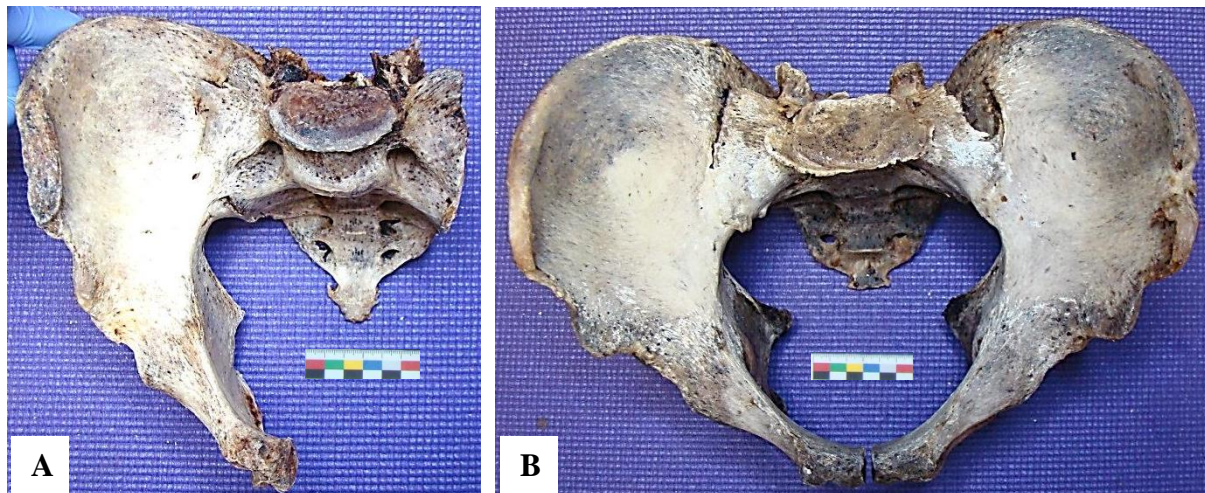


Figure 4.135. Fusion of sacrum to os coxae. A) Right os coxa was fused to the sacrum of cadaver K51/12, superior view; B) bilateral fusion of both os coxae to sacrum of cadaver K57/12; superior view.

4.11.6.7 Degenerative Joint Disease of the Knee Joint

Degenerative joint disease (DJD) in the knee joint were observed in 9/124 (7.3%) cadavers (Table 4.98). The male to female ratio of the affected cadavers was 1.6:1 and the average age was 62.1 years. The arthritic changes in the knee joint included the femoral medial and lateral condyles 6/9 (66.7%) (Figure 4.136), patellar articular surfaces 4/9 (44.4%) and tibial medial and lateral condyles 5/9 (55.6%) cadavers. Unilateral involvement of the left side was seen in 1/9 (11.1%) cadavers while no unilateral involvement of the right side was observed. Bilateral involvement of the knee joint was seen in 8/9 (88.9%) cadavers.

Table 4.98. Degeneration of the knee joint in the cadaver cohort (n=124)

<i>Cadaver Ref. Nr.</i>	<i>Sex</i>	<i>Age</i>	<i>Lower Limb Involvement</i>
K104/09	Male	*	Degeneration of articular surfaces of lateral and medial condyles of both tibia
K106/09	Male	*	Degeneration of lateral and medial condyles of both femurs, and bilateral patellar articular facet degeneration (Fig. 4.136, A)
K113/09	Male	40	Degeneration of the articular surfaces of the left tibial lateral and medial condyles
K19/10	Female	63	Degeneration of articular surfaces of lateral and medial condyles of both tibia
K62/11	Male	83	Degeneration of bilateral femoral condylar articular surfaces, and bilateral patellar articular facet degeneration
K121/11	Male	50	Degeneration of bilateral femoral condylar articular surfaces
K51/12	Male	56	Degeneration of bilateral femoral condylar articular surfaces, bilateral patellar articular facet degeneration, both tibial condylar degeneration (Fig. 4.136, B)
K58/12	Male	70	Degeneration of bilateral femoral condylar articular surfaces, bilateral patellar articular facet degeneration, both tibial condylar degeneration
K69/12	Female	73	Degeneration of lateral and medial condyles of both femurs

* Age is unavailable

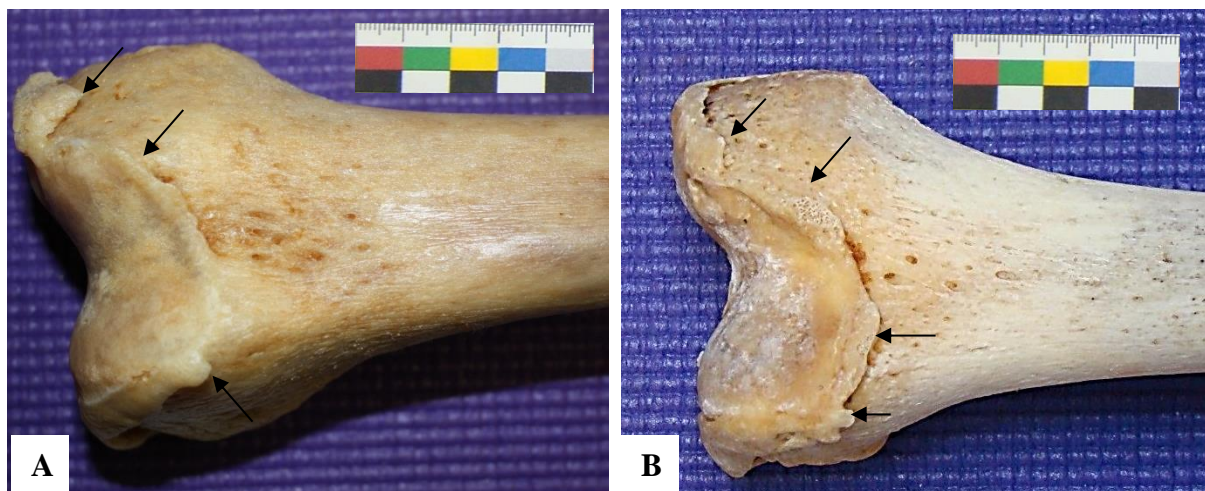


Figure 4.136. Osteoarthritis in the knee joint. A) Distal end of the right femur of cadaver K106/09 with extensive lipping as a result of degenerative joint disease (DJD), anterior view; B) distal end of right femur with extensive osteoarthritis in the condylar area as well as the patellar lip of cadaver K51/12, anterior view.

4.11.7 Infectious Diseases

4.11.7.1 Osteomyelitis

Osteomyelitis, inflammation of bone (osteitis) and bone marrow (myelitis), was seen in 3/124 (2.4%) cadavers (Table 4.99). Extensive bone destruction and reactive, irregular new bone formation results in a sequestrum and involucrum, respectively and are common features of osteomyelitis (Figure 4.137).

Table 4.99. Osteomyelitis of the skeleton in the cadaver cohort (n=124)

<i>Cadaver Ref. Nr.</i>	<i>Sex</i>	<i>Age*</i>	<i>Skeletal Involvement</i>
K36/10	Male	82	Distal part of medial malleolus of right tibia
K101/11	Male	50	Right distal part of humerus
K50/12	Female	*	Shaft of left humerus (secondary to fracture)

* Age is unavailable

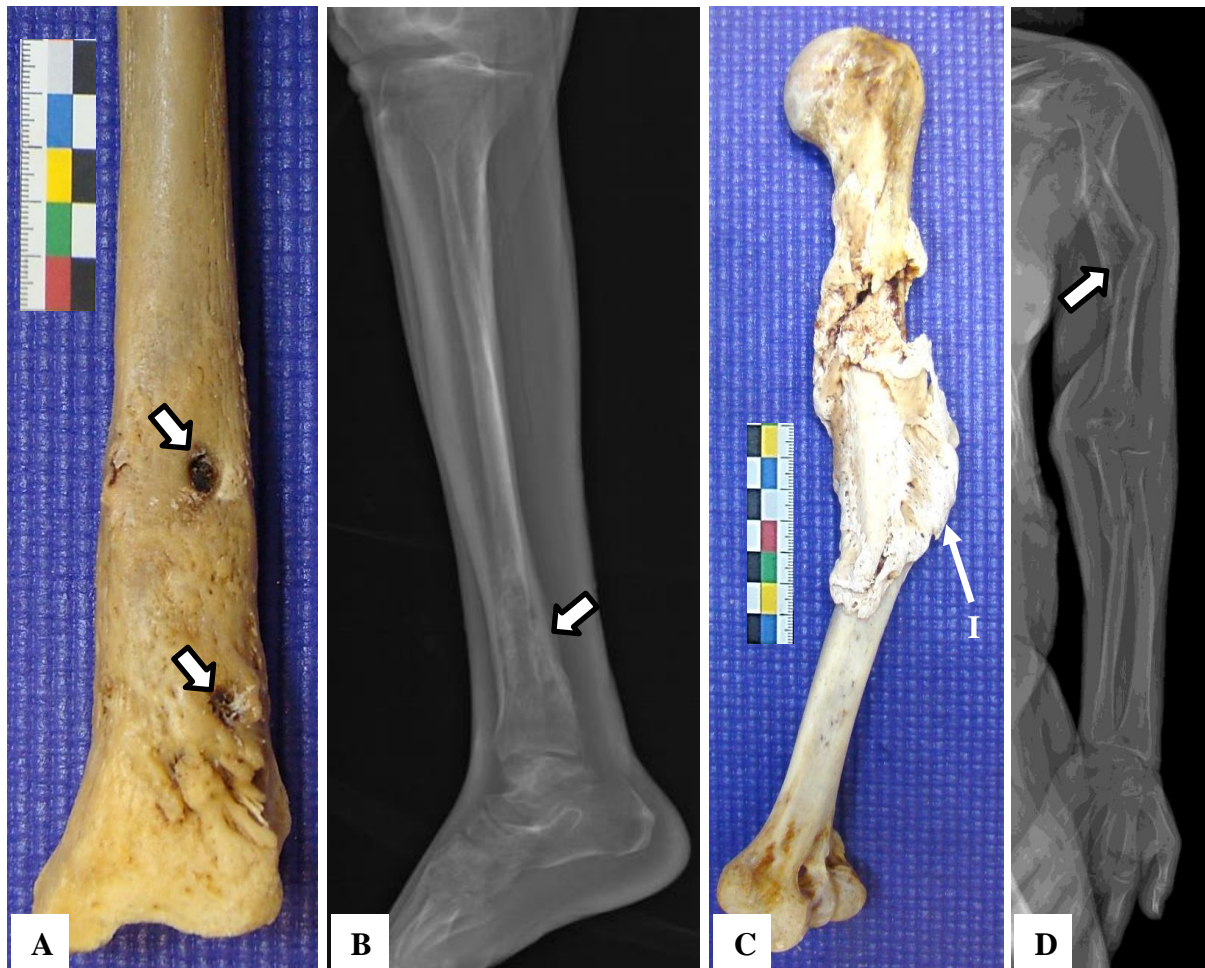


Figure 4.137. Osteomyelitis. A) Osteomyelitis superior to the medial malleolus of the right tibia of cadaver K36/10 with cloaca, posterior view; B) X-ray of the right leg of cadaver K36/10 with changes evident on the distal part of the tibia (blocked arrow); C) osteomyelitis secondary to a rotational fracture in the shaft of the left humerus of cadaver K50/12, antero-medial view; D) X-ray of the left arm of cadaver K50/12, note healing in the proximal left ulna, Involucrum (I).

4.11.8 Circulatory Disorders

4.11.8.1 Hypertrophic (Pulmonary) Osteoarthropathy (HPOA)

Hypertrophic (pulmonary) osteoarthropathy (HPOA), a clinical syndrome which includes clubbing of the fingers and toes as well as periostitis of tubular bones, was seen in 15/124 (12.1%) of the cadavers (Table 4.100). The male to female ratio was 1.3:1 and the average age of the affected cadavers was 45.2 years. The triad of periostitis, clubbing and arthritis was observed in combination or separately in the cadavers. Clubbing of the fingers was observed in 2/15 (13.3%) cadavers (Figure 4.139, A and B). In all of the cadavers with HPOA, non-specific periostitis was observed on the tubular bones, including the femur, tibia, fibula, humerus, radius, ulna and in some cases the pelvis (Figure 4.139, C). Extensive involvement of the entire skeleton, excluding the skull was observed in one cadaver (K83/09, male 60 years) (Figure 4.138). The ribs and vertebrae showed non-specific periostitis in 2/15 (13.3%) and 1/15 (6.7%), respectively. Pulmonary TB was observed in 12/15 (80.0%) of the cadavers with HPOA.

Table 4.100. Hypertrophic (pulmonary) osteoarthropathy in the cadaver cohort (n=124)

<i>Cadaver Ref. Nr.</i>	<i>Sex</i>	<i>Age*</i>	<i>Skeletal Involvement</i>	<i>Underlying Systemic Disease</i>
K83/09	Male	60	Dome of skull, clavicles, scapulae, posterior right humerus, both ulnae, both radii, os coxae, anterior parts of both femurs, both tibia, both fibulae (Fig. 4.138)	Pulmonary TB, pulmonary and gallbladder neoplasms
K102/09	Female	28	Four left ribs, posterior and distal regions of both tibia	Pulmonary TB
K18/10	Female	32	5 th lumbar vertebral body, right posterior humerus, both ulnae, both radii, os coxae, anterior parts of both femurs, both tibia, right fibula	Pulmonary TB
K06/11	Male	37	Anterior and proximal parts of both tibia	Emphysema
K65/11	Female	52	Shaft and distal part of left ulna, anterior superior to both femoral condyles, lateral malleolus of right fibula	Pulmonary and extrapulmonary TB
K75/11	Male	36	Shafts of both ulnae, distal parts of both radii, superior to both acetabula, anterior shaft of right femur, shafts of both tibia, shaft of left fibula, shaft and lateral malleolus of right fibula, clubbing of the fingers (Fig. 4.139, C)	Pulmonary TB; bronchiectasis
K148/11	Male	49	Anterior, medial and proximal areas of both tibia, shafts of both fibulae	Pulmonary TB and pneumonia
K25/12	Male	39	Bilateral rib lesions, left clavicle, distal parts of both humeri, shafts of both ulnae, distal parts of both radii, anterior shafts of both femurs, posterior of both medial malleoli, proximal anterior part of right tibia	Pulmonary and extrapulmonary TB

<i>Cadaver Ref. Nr.</i>	<i>Sex</i>	<i>Age*</i>	<i>Skeletal Involvement</i>	<i>Underlying Systemic Disease</i>
K27/12	Male	66	Area inferior to coracoid process and medial to glenoid fossa of right scapula, shaft of left ulna, distal part of left radius, both shafts of femurs, shafts of both tibias, shafts of both fibulae	Pulmonary and liver disease
K43/12	Male	*	Distal part of left radius, both medial malleoli, lateral side of left tibia, proximal part of right fibula	Pulmonary TB
K46/12	Male	46	Clubbing of the fingers (Fig. 4.139, A and B), shafts of both tibia and fibula	Pulmonary TB; bronchiectasis
K60/12	Female	22	Both shafts of femurs, inferior to the left tibial head, shafts of both fibulae	Pulmonary and extrapulmonary TB
K81/12	Male	49	Superior and anterior to the medial and lateral femoral condyles	Pulmonary TB
K93/12	Male	72	Superior to both medial malleoli, both lateral malleoli	Liver and gastrointestinal disease
K97/12	Male	*	Medial malleolus of right tibia	Pulmonary TB

* Age is unavailable

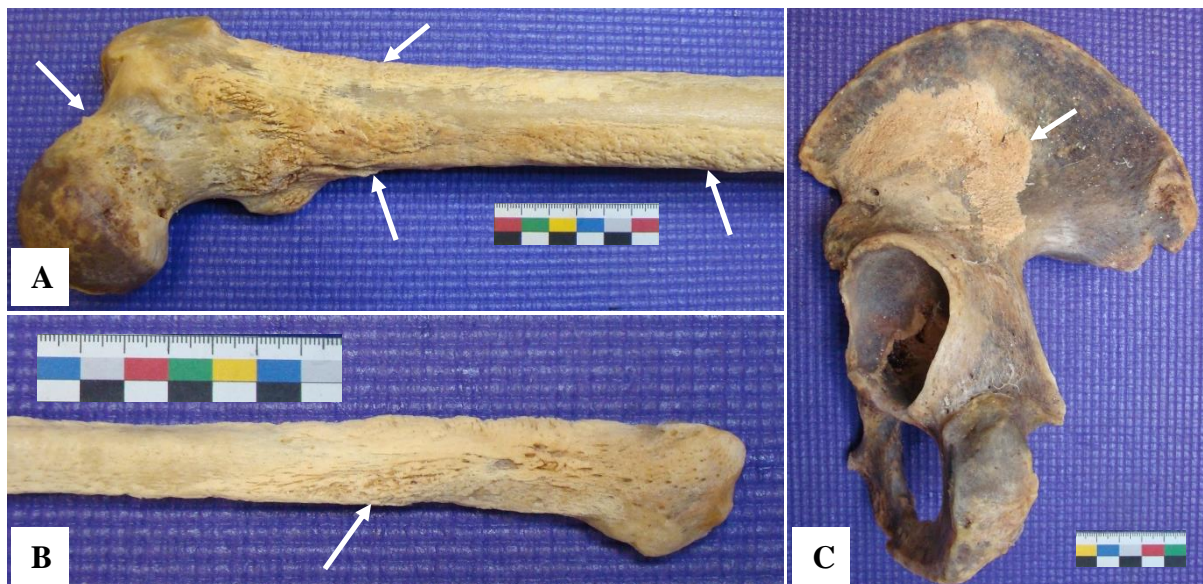


Figure 4.138. Hypertrophic pulmonary osteoarthropathy (HPOA) in cadaver K83/09. A) Both femurs were affected by a widespread deposition of subperiosteal bone of an individual possible affected by scurvy, proximal part of left femur, anterior view; B) deposition of subperiosteal bone in the proximal part of the right fibula, anterior view; C) deposition of subperiosteal bone on the iliac superior to the acetabulum left os coxa, postero-lateral view.

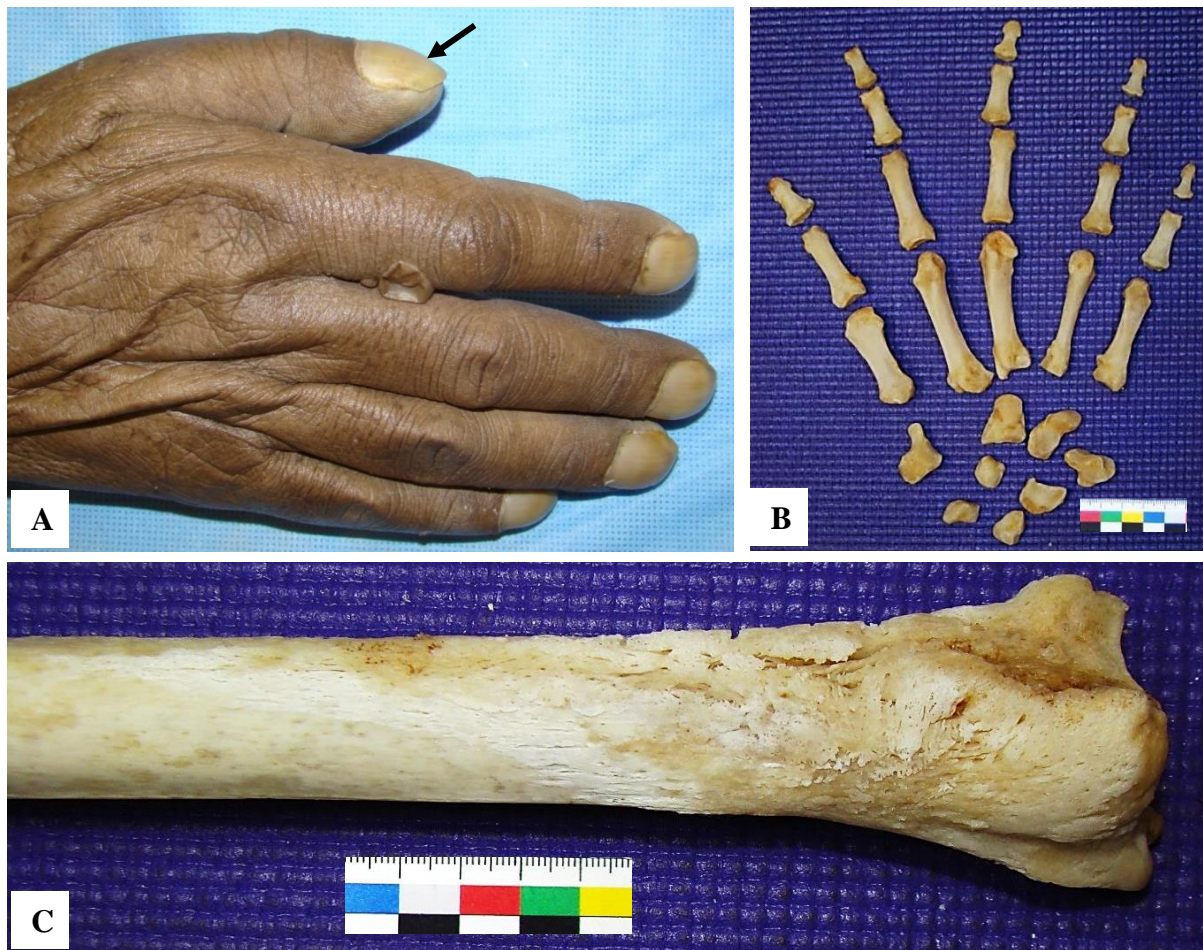


Figure 4.139. Hypertrophic (pulmonary) osteoarthropathy (HPOA). A) Right hand of cadaver K46/12, dorsal view; B) skeletal remains of the right hand (K46/12) showing little to no macroscopic signs of HPOA; C) right tibia of cadaver K75/11 showing non-specific periostitis, postero-medial view.

4.11.9 Hematological Disorders

4.11.9.1 Cribra Orbitalia (CO)

Cribra orbitalia (CO) was seen in 6/124 (4.8%) cadavers (Table 4.101). All the affected cadavers were males and the average age was 46.0 years. Small pores in the antero-lateral part of the superior orbital roof were present in the cadavers with CO (Figure 4.140). Bilateral involvement was seen in all of the cadavers with CO.

Table 4.101. Cribra orbitalia (CO) in the cadaver cohort (n=124)

<i>Cadaver Ref. Nr.</i>	<i>Sex</i>	<i>Age*</i>	<i>Orbit Involvement</i>
K95/09	Male	*	Minimal bilateral involvement in the superior orbital roofs
K113/09	Male	40	Bilateral involvement in the superior orbital roofs
K38/11	Male	68	Bilateral involvement of the antero-lateral part of the superior orbit roofs

<i>Cadaver Ref. Nr.</i>	<i>Sex</i>	<i>Age*</i>	<i>Orbit Involvement</i>
K44/11	Male	48	Bilateral involvement of the antero-lateral part of the superior orbit roofs (Fig. 4.140, A)
K64/12	Male	50	Bilateral involvement of the antero-lateral part of the superior orbit roofs (Fig. 4.140, B)
K87/12	Male	24	Minimal bilateral involvement in the superior orbital roofs

* Age is unavailable

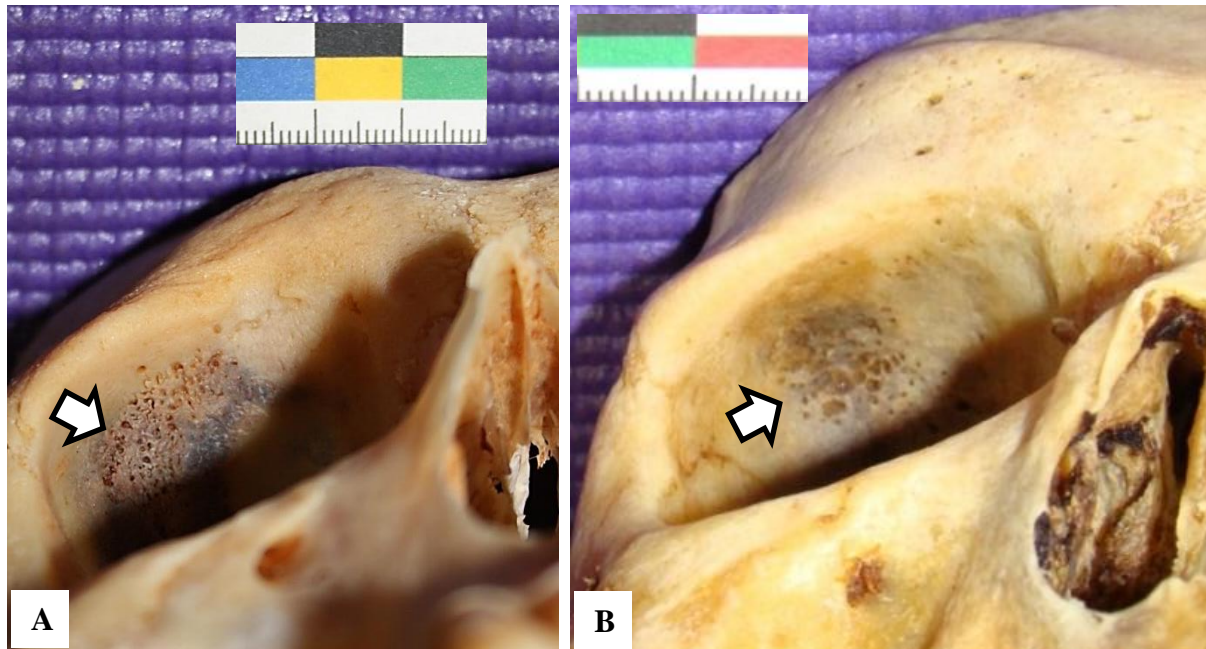


Figure 4.140. Cribra orbitalia in the cadaver cohort. A) Antero-lateral region of the superior orbital roof of cadaver K44/11 with a sieve-like appearance (arrow), inferior view; B) antero-lateral region of both superior orbital roofs of cadaver K64/12 contained small pores (arrow), inferior view.

4.11.10 Miscellaneous Bone Conditions

4.11.10.1 Paget's Disease of the Bone (Osteitis Deformans)

Paget's disease of the bone (osteitis deformans) was seen in 1/127 (0.8%) cadaver (K79/12, 49 years). This chronic inflammatory condition resulted in the proliferation of the bone of the skull, coracoid process of the left scapula, scapular (lateral) side of the left clavicle and the distal and proximal parts of the left humerus and left ulna, respectively (Figure 4.141). The bones of the skull that was affected included the following; petrous and squamous part of temporal bone and the greater and lesser wings of sphenoid bone.

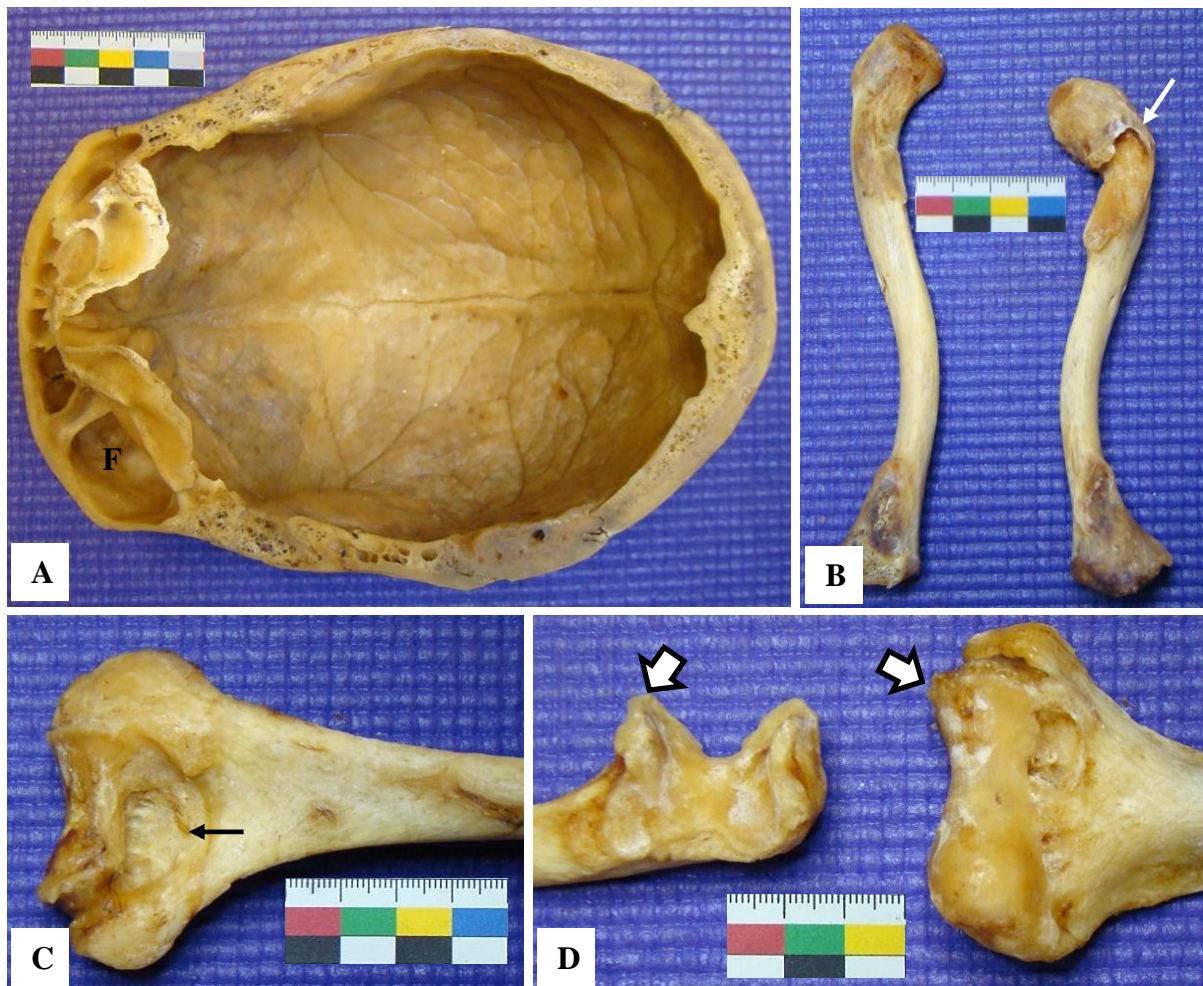


Figure 4.141. Paget's Disease (Osteitis deformans). A) The skull of cadaver K79/12 showing extensive thickening of the cranial vault, inferior view. The skull was 14mm in maximum width; B) the lateral side of the left clavicle had a deformed appearance (white arrow), inferior view; C) the olecranon fossa of the left humerus had appeared deformed and osteoarthritic (black arrow), posterior view; D) osteoarthritic changes (blocked arrows) in the distal and proximal parts of the left humerus and left ulna, respectively; frontal sinus (F).

4.11.10.2 Internal Frontal Hyperostosis (IFH)

Internal frontal hyperostosis (IFH) was seen in 2/124 (1.6%) cadavers (Table 4.102). Both affected cadavers were females with an average age of 67.5 years. Sieve-like holes were found symmetrically on the frontal bones. No occipital and parietal involvement was seen in either of the cadavers. Vault thickness and expanded diploic veins were prominent in the area of the frontal bones (Figure 4.142). The vault thickness resulted in a direct visualisation of the trabeculae of the spongy bone.

Table 4.102. Internal frontal hyperostosis (IFH) in the cadaver cohort (n=124)

<i>Cadaver Ref. Nr.</i>	<i>Sex</i>	<i>Age*</i>	<i>Skeletal Involvement</i>
K28/12	Female	62	Symmetric diploic venous enlargement resulting in a thickened skull (Fig. 4.142)
K62/12	Female	73	Diploic venous enlargement (symmetric)

* Age is unavailable

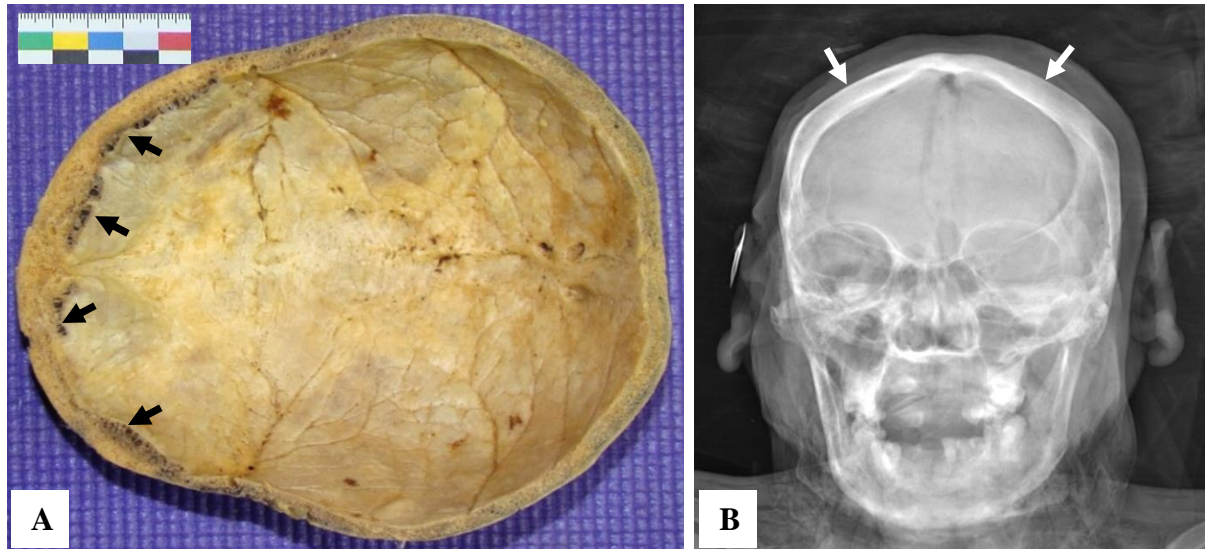


Figure 4.142. Internal frontal hyperostosis. Symmetrical sieve-like holes in the frontal and parietal bones with accompanying vault thickness in the dome of the skull of cadaver K28/12, inferior view; B) X-ray of cadaver K28/12 showing the increased thickness in the dome of the skull (arrows).

4.11.12 Distribution of Skeletal Pathology in the Cadaver Cohort

The diagram below is a summary of the skeletal pathology observed in the cadaver cohort.

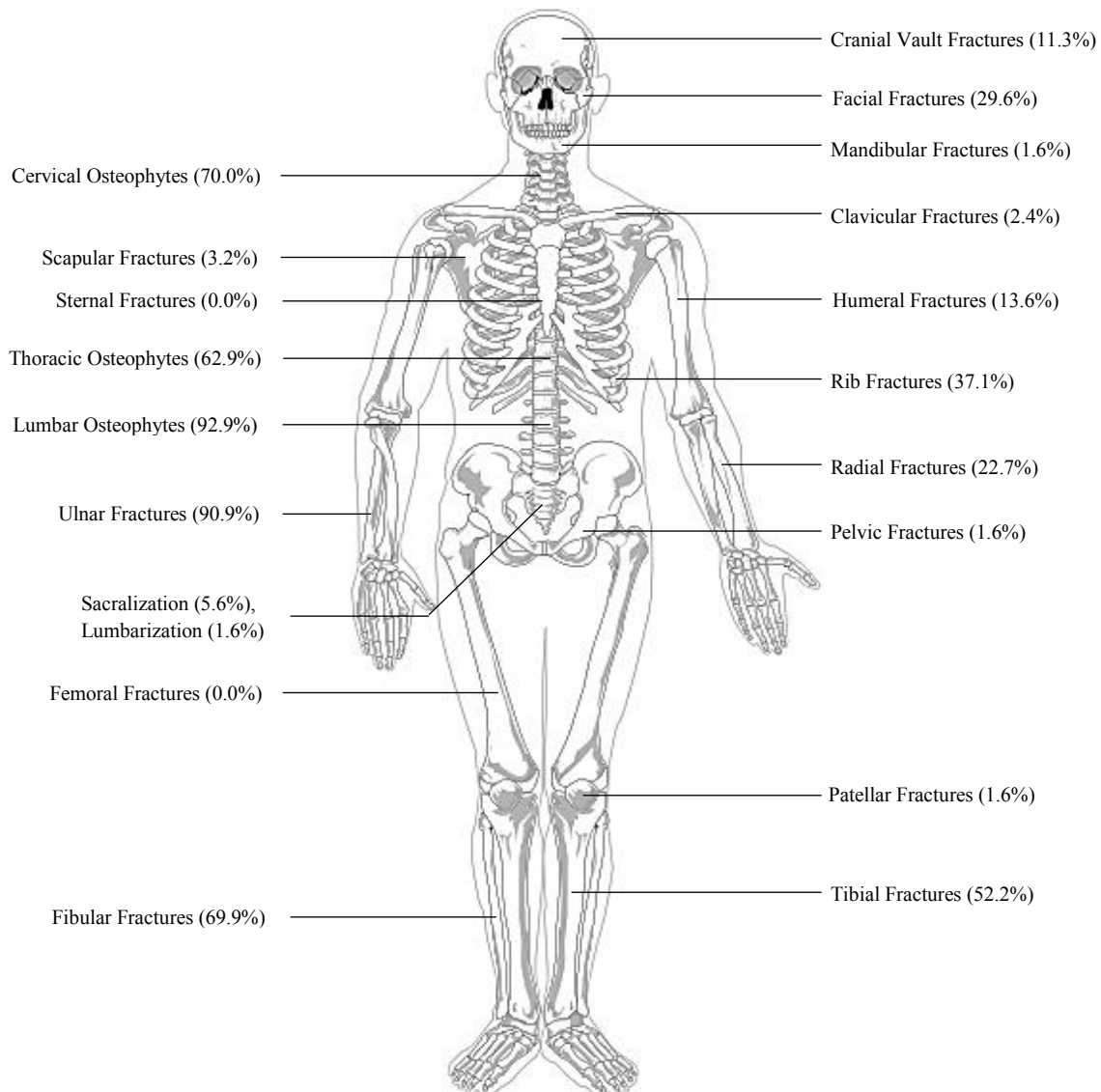


Figure 4.143. Summary of skeletal pathology. The majority of fractures were seen in the craniofacial region, with the inferior limbs being less affected with fractures than the superior limbs (adapted from a diagram obtained from: <http://www.paradoja7.com/skeleton-in-human-body-2/>).

4.12 Statistical Analysis

Statistical analysis was performed using Statistica[®] Version 12.0 (StatSoft Inc. 2014, USA). A contingency table (cross-tabulation) analysis was done to determine associations between the prevalence of systemic disease and pulmonary tuberculosis. The chi-square statistic (χ^2) was used to determine whether the variables were statistically associated or independent from each other. The Fisher exact test was used as an alternative to the chi-square statistic to describe the degree to which the values from one variable could determine those of the other variable. A statistical p-value of less than 0.05 was considered to be statistically significant. Finally, correspondence analyses, a statistical technique which provides a graphical representation of the cross-tabulations, were used to visualize disease associations with pulmonary TB on a 2D plot.

4.12.1 Risk Factors for Tuberculosis

4.12.1.1 Sex

4.12.1.1.1 Association between Sex Disparity and Pulmonary TB

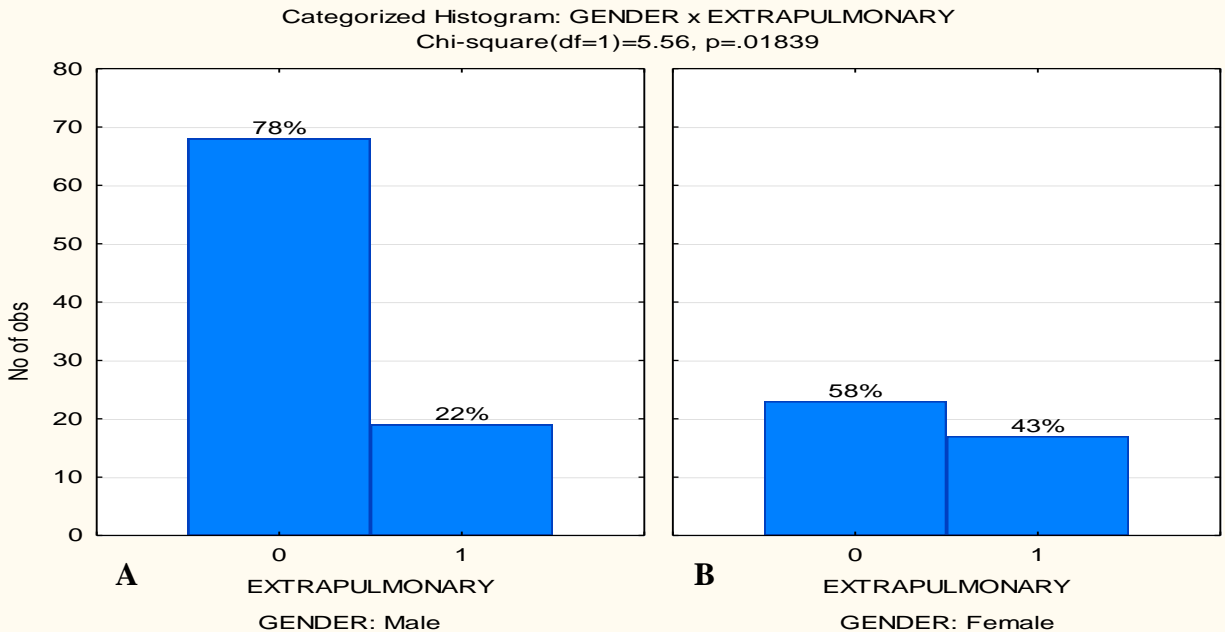
The prevalence of pulmonary TB in the total male population (n=87) and total female population (n=40) was compared to determine a statistical relationship between pulmonary TB in males and females. Although the p-value (p=0.56623; p>0.05) was more than 0.05, a statistically significant association was observed, suggesting that males were significantly more commonly affected than females.

4.12.1.1.2 Association between Sex Disparity and Extrapulmonary TB

The prevalence of extrapulmonary TB in the total male population (n=87) and total female population (n=40) was statistically compared. A clear statistical significance in the prevalence of

extrapulmonary TB between males and females exists (Chi-squared $p = 0.01839$; $p < 0.05$). A total of 22% of male cadavers presented with extrapulmonary TB involvement (Figure 4.144, A), while 43% of the females showed signs of extrapulmonary TB involvement (Figure 4.144, B).

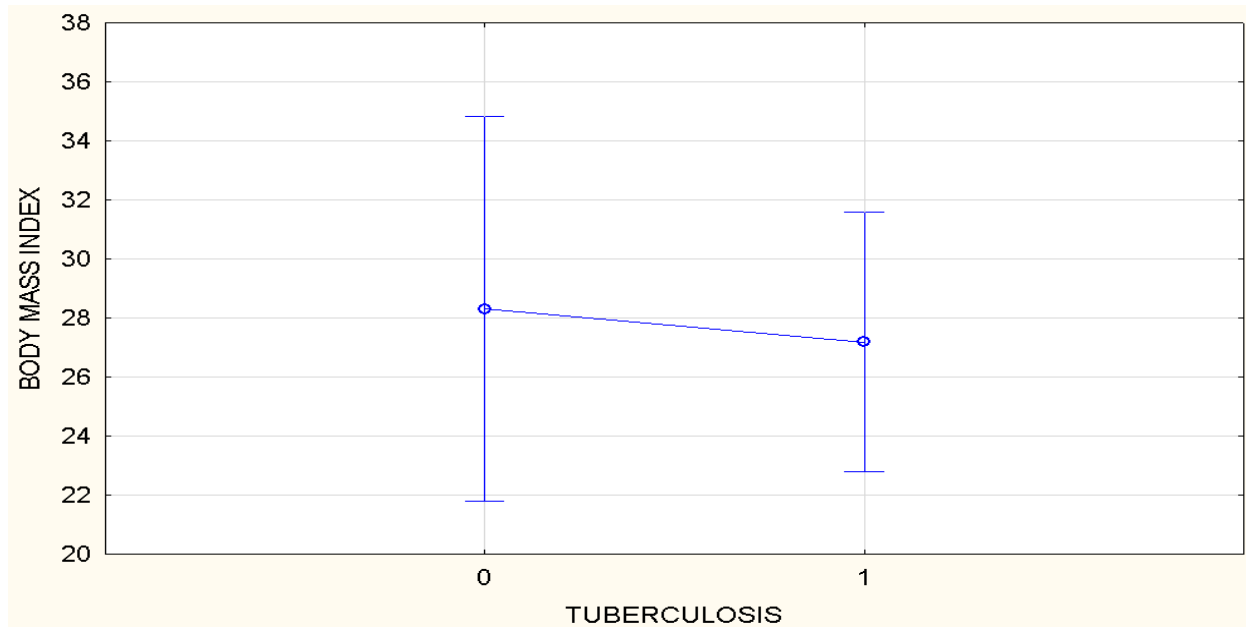
Figure 4.144. Association between sex and prevalence of extrapulmonary TB. A) Prevalence of extrapulmonary TB in males; B) prevalence of extrapulmonary TB in females; Chi-squared n



4.12.1.2 Body Mass Index (BMI)

The body mass index (BMI) of the total cadaver population ranged from 6.2 to 42.3 (average 16.5). The average BMI of the cadavers with PTB was 16.2. The analysis of variance (ANOVA) statistical test was performed to determine whether a relationship exists between PTB and BMI. Although a lower BMI was observed in the cadavers with PTB (Figure 4.145), no statistically significant relationship was observed (Chi-squared $p = 0.78$; Mann-Whitney U $p = 0.96$; $p > 0.05$).

Figure 4.145. Association between body mass index (BMI) and prevalence of pulmonary TB. Chi-squared $p = 0.78$; Mann-Whitney U $p = 0.96$; absent (0); present (1).

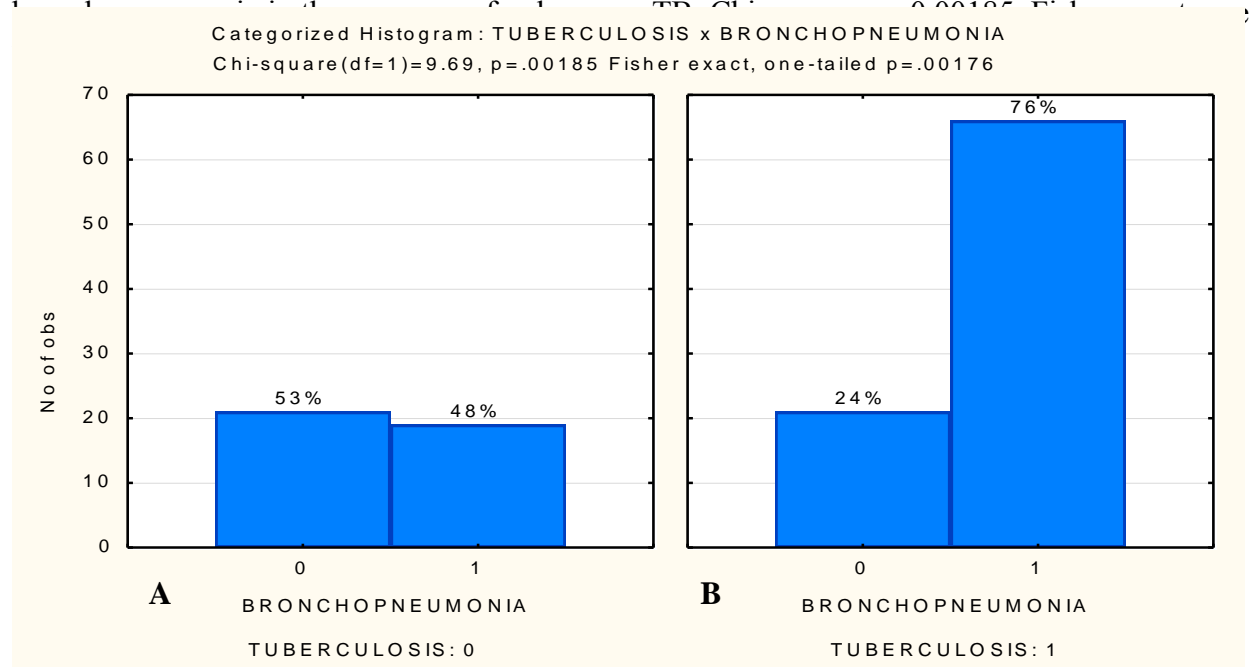


4.12.2 Pulmonary TB versus Pulmonary Disease

4.12.2.1 Association between Pulmonary TB and Bronchopneumonia

A strong statistically significant association was observed between the prevalence of pulmonary TB and bronchopneumonia in our cadaver cohort (Chi-squared $p = 0.00185$; Fisher exact $p = 0.00176$; $p < 0.05$). Figure 4.146 (A), illustrates that when pulmonary TB was absent, 48% of the cadavers showed macroscopic signs of bronchopneumonia, while when pulmonary TB was present in the cadaver population, 76% of the cadavers were positive for bronchopneumonia (Figure 4.146, B).

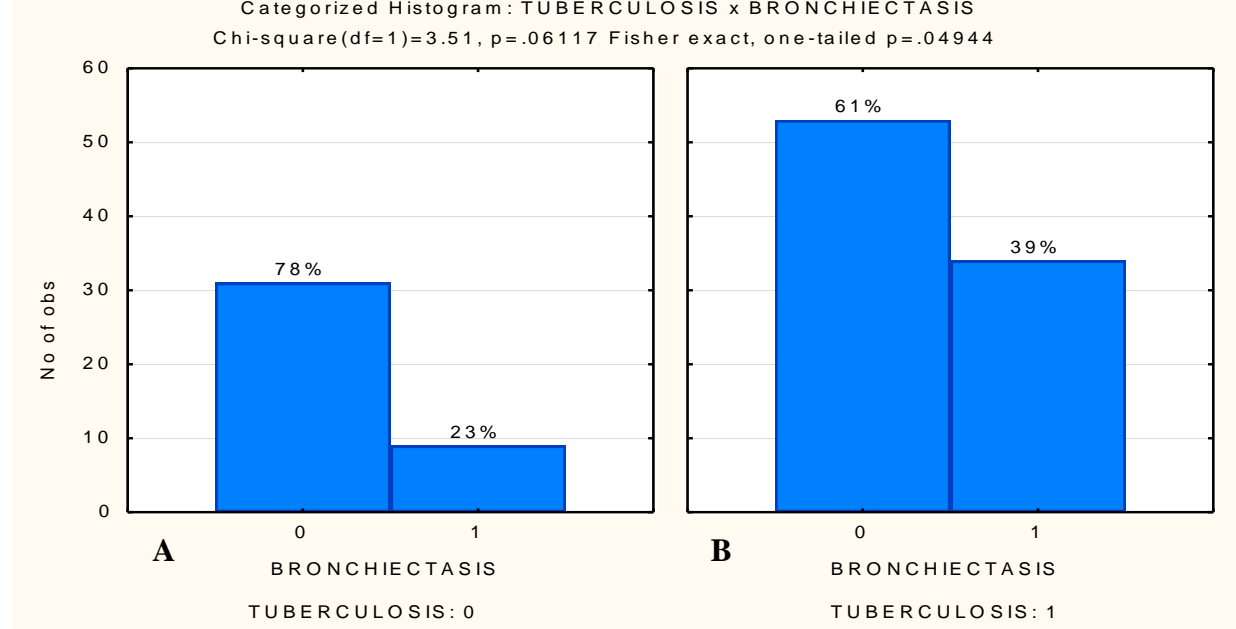
Figure 4.146. Association between pulmonary TB and bronchopneumonia. A) Number of observations of bronchopneumonia in the absence of pulmonary TB; B) observations of



4.12.2.2 Association between Pulmonary TB and Bronchiectasis

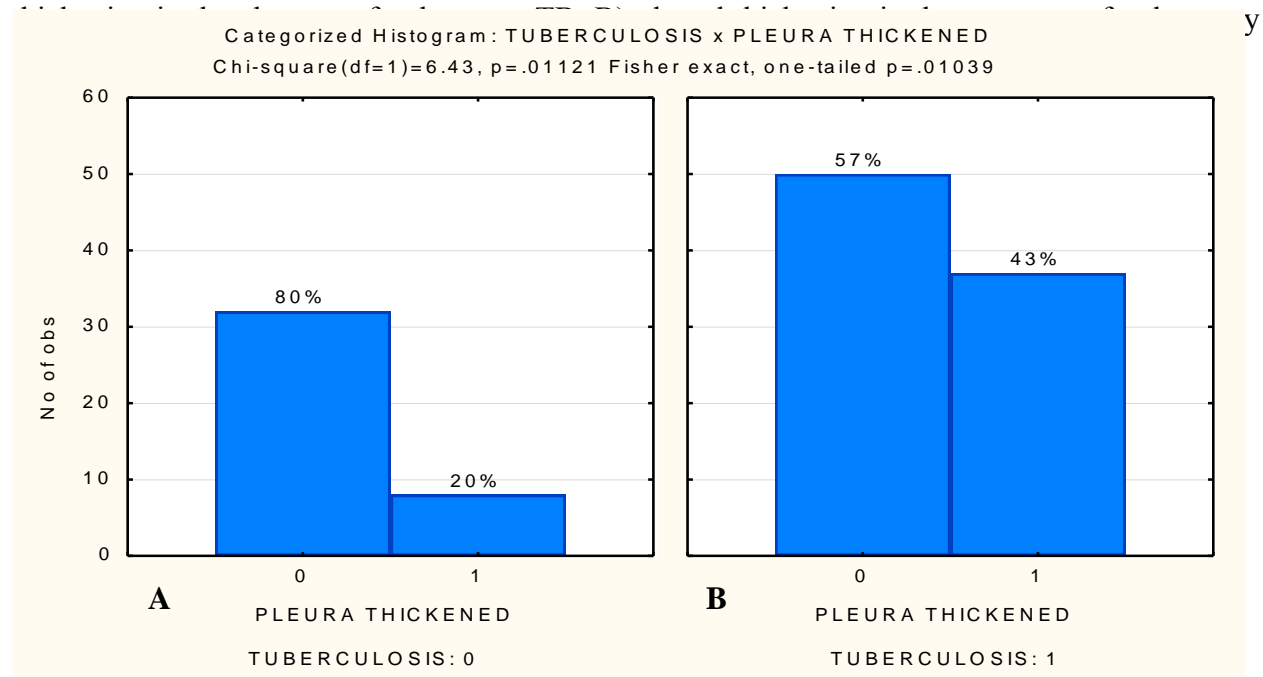
When the relationship between pulmonary TB and bronchiectasis was statistically correlated, a significant correlation was observed (Chi-squared $p = 0.06117$; Fisher exact $p = 0.04944$; $p < 0.05$). Figure 4.147, A illustrates that bronchiectasis was present in 23% of the cadavers without PTB, while in Figure 4.147, B, 39% of the cadavers with bronchiectasis had concomitant PTB.

Figure 4.147. Association between pulmonary TB and bronchiectasis. A) Bronchiectasis in the absence of pulmonary TB; B) bronchiectasis in the presence of pulmonary TB. Chi-square p



4.12.2.3 Association between Pulmonary TB and Pleural Thickening

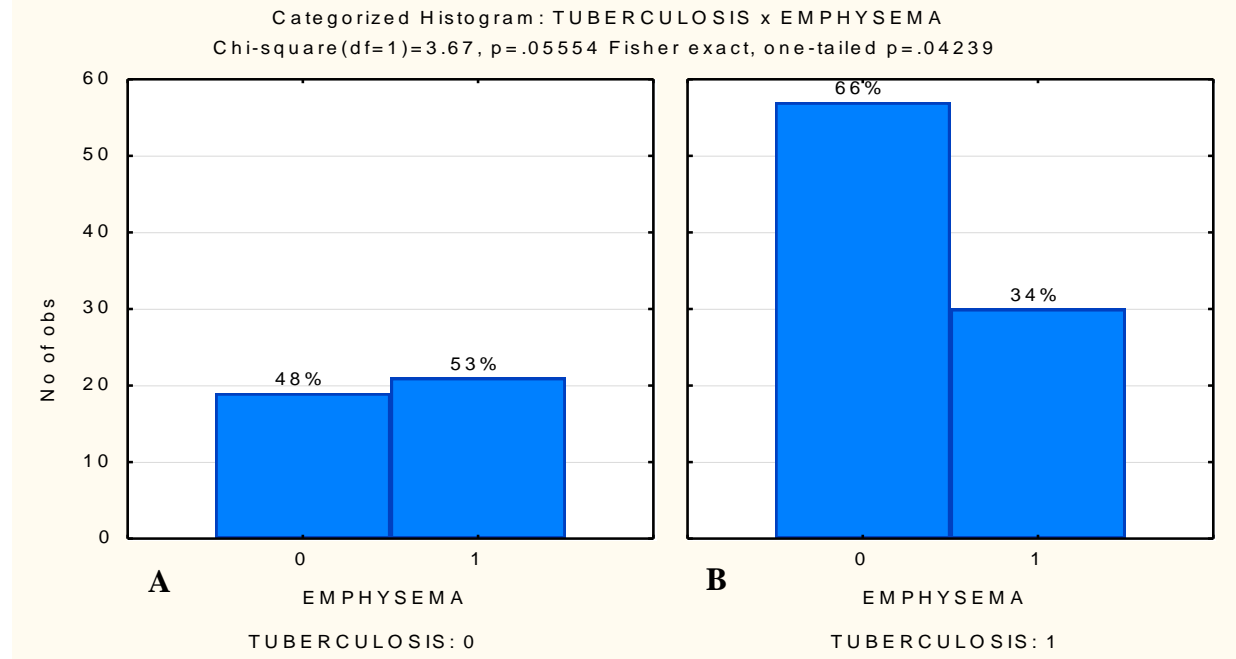
A statistically significant association was observed between pulmonary TB and pleural thickening (Chi-squared $p = 0.01121$; Fisher exact $p = 0.01039$). When pulmonary TB was absent in our cadaver population, 20% of the cadavers showed macroscopic signs of pleural thickening (Figure 4.148, A). A total of 43% of the cadavers were positive for pleural thickening when pulmonary TB was present (Figure 4.148, B).

Figure 4.148. Association between pulmonary TB and pleural thickening. A) Pleural

4.12.2.4 Association between Pulmonary TB and Emphysema

When TB was absent in the cadavers, 53% showed macroscopical signs of emphysema (Figure 4.149, A). In the TB-positive cadavers, 34% were positive for emphysema (Figure 4.149, B). There was therefore a decrease in the prevalence of emphysema associated with pulmonary TB. The cross-tabulation analysis revealed a negative statistical correlation between pulmonary TB and emphysema (Chi-squared $p = 0.05554$; Fisher exact $p = 0.04239$). The chi-squared p -value was more than 0.05; however, the Fisher exact value was less than 0.05. This indicates that the presence of pulmonary TB is likely to be diagnosed in the absence of emphysema.

Figure 4.149. Association between pulmonary TB and emphysema. A) Number of observations of emphysema in the absence of pulmonary TB; B) number of observations of emphysema in the presence of pulmonary TB. Chi-square $p = 0.02061$. Fisher exact, one-tailed $p = 0.04239$.



4.12.3 Statistically Independent Pulmonary Findings in the Cadaver Cohort

The cross-tabulation analysis was performed to determine an association between pulmonary TB and adhesions, anthracosis, bronchiectasis, lung tumours and pleural effusions, respectively. All of these associations were found not to be statistically significant as the chi-squared p-value was more than 0.05 (Table 4.103).

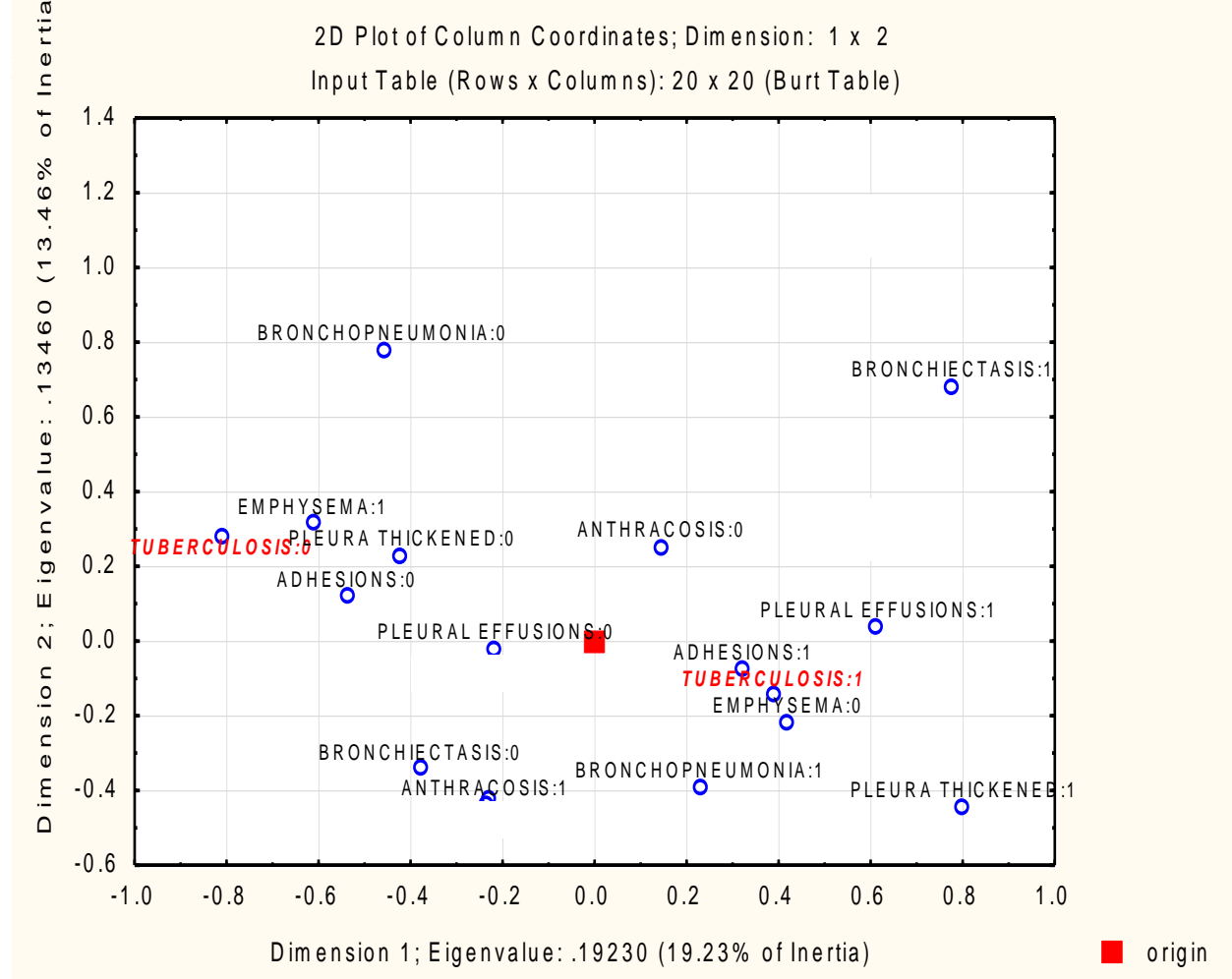
Table 4.103. Pulmonary findings that were statistically independent from pulmonary TB

<i>Pulmonary Finding</i>	<i>Chi-Squared Value</i>	<i>Fisher Exact Value</i>
Adhesions	0.83901	0.49539
Anthracosis	0.46009	0.29178
Lung Tumours	0.52213	0.41801
Pleural Effusions	0.23424	0.17068

4.12.4 Correspondence Analysis

A correspondence analysis was performed to provide a graphical representation of the pulmonary findings in association with pulmonary TB in a 2D plot (Figure 4.150).

Figure 4.150. A graphical representation of the association between pulmonary TB and



In Figure 4.150, the absence and presence of a finding was indicated with a 0 and 1, respectively. The pulmonary findings that were associated with pulmonary TB (*TUBERCULOSIS: 1*) included pulmonary adhesions, pleural effusions, pleural thickening and bronchopneumonia (Figure 4.150). These findings were all grouped together and were located on the right side of the origin.

Also on the right side of the origin, bronchiectasis was associated with tuberculosis, however, these points were further apart, making them less statistically dependent. A close negative correlation between emphysema and pulmonary TB was also illustrated by the 2D plot (Figure 4.150). The point of absence of emphysema was located on the right side of the origin and was close to the point of tuberculosis. On the left side of the origin, at the side where tuberculosis was absent, the points indicating the absence of pulmonary adhesions, pleural effusions, pleural thickening and bronchopneumonia were all closely located to each other (Figure 4.150). The point indicating the presence of anthracosis was located on the left side of the origin, showing an association between the absence of TB and the presence of anthracosis. However, these associations were not statistically significant.

4.12.5 Association between Pulmonary TB and Rib Lesions

The occurrence of periostotic rib lesions were determined in the cadaver population and compared to the presence of pulmonary TB. In the TB-negative cadavers, 20% presented with periostotic lesions on the visceral aspects of the ribs, while in TB-positive cadavers, 32% presented with rib lesions on the visceral rib aspects (Figure 4.151). There was no statistical association between the prevalence of pulmonary and the prevalence of rib lesions ($p>0.05$).

Figure 4.151. Association between pulmonary TB and rib lesions. A) Number of observations of rib lesions in the absence of pulmonary TB; B) number of observations of rib lesions in the

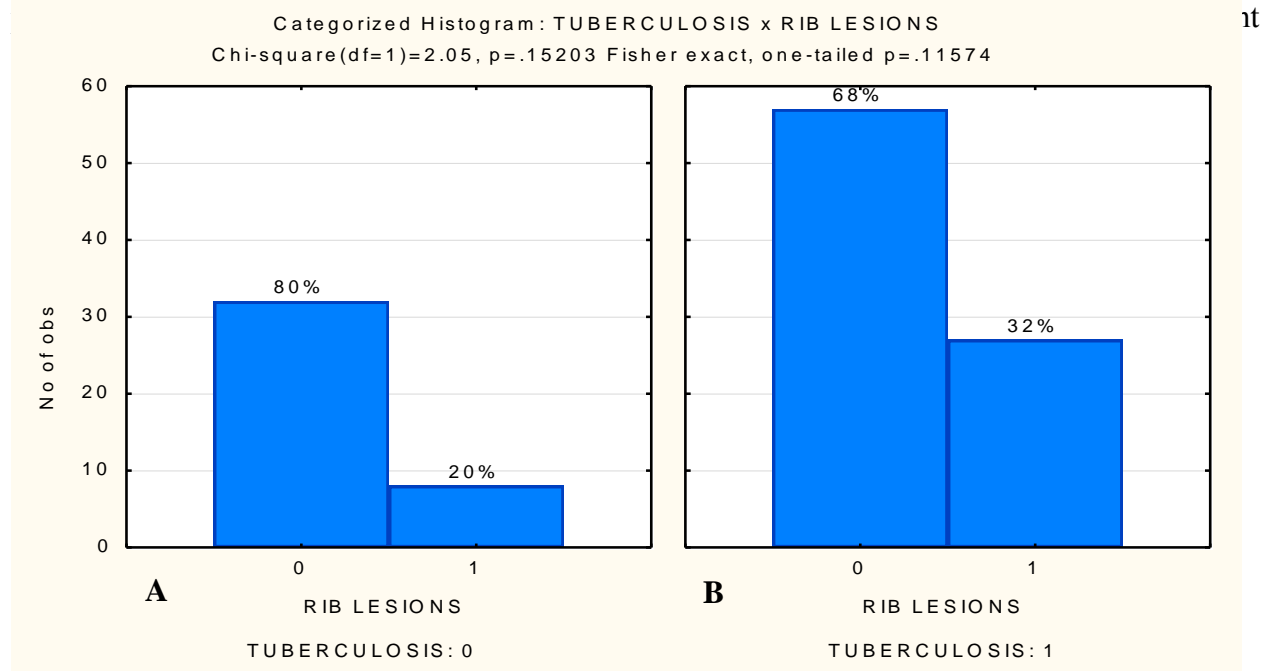
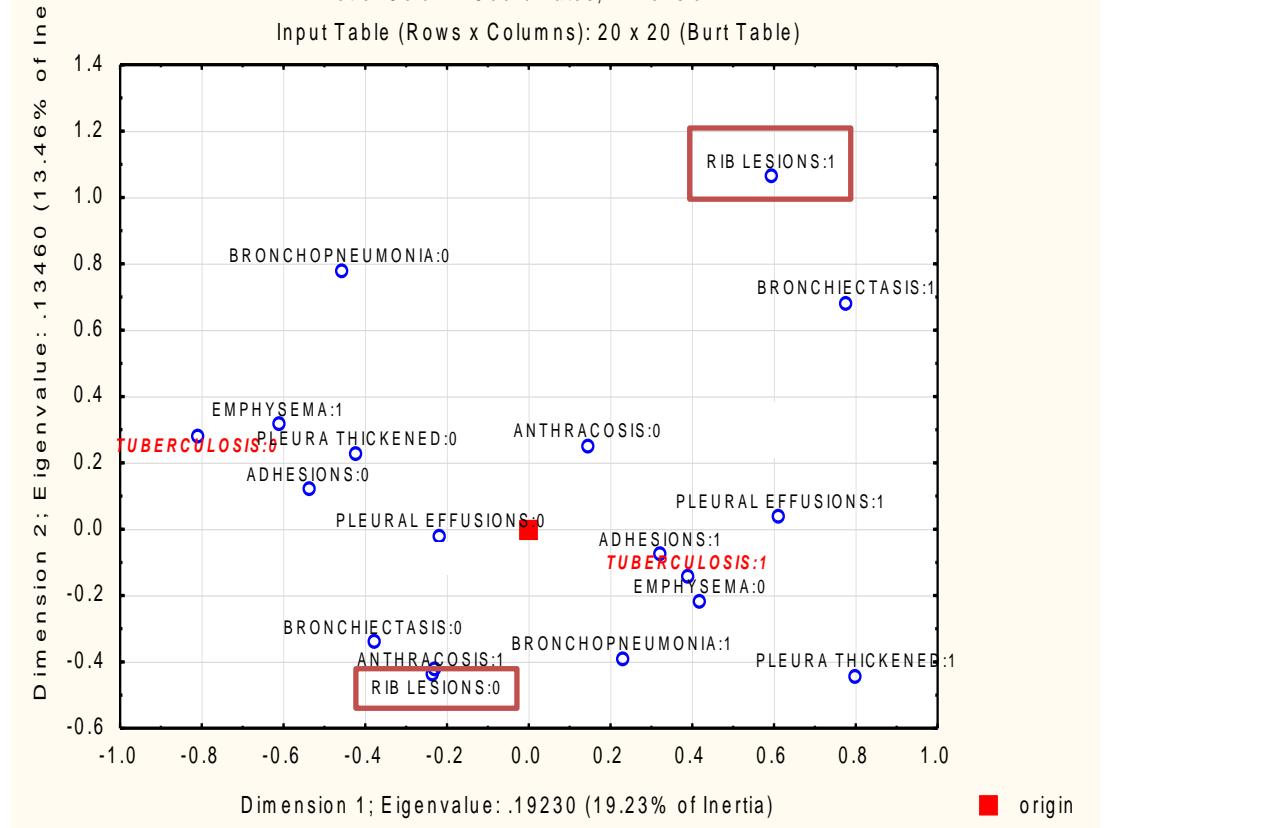


Figure 4.152. A graphical representation of the association between pulmonary TB and rib lesions. The red

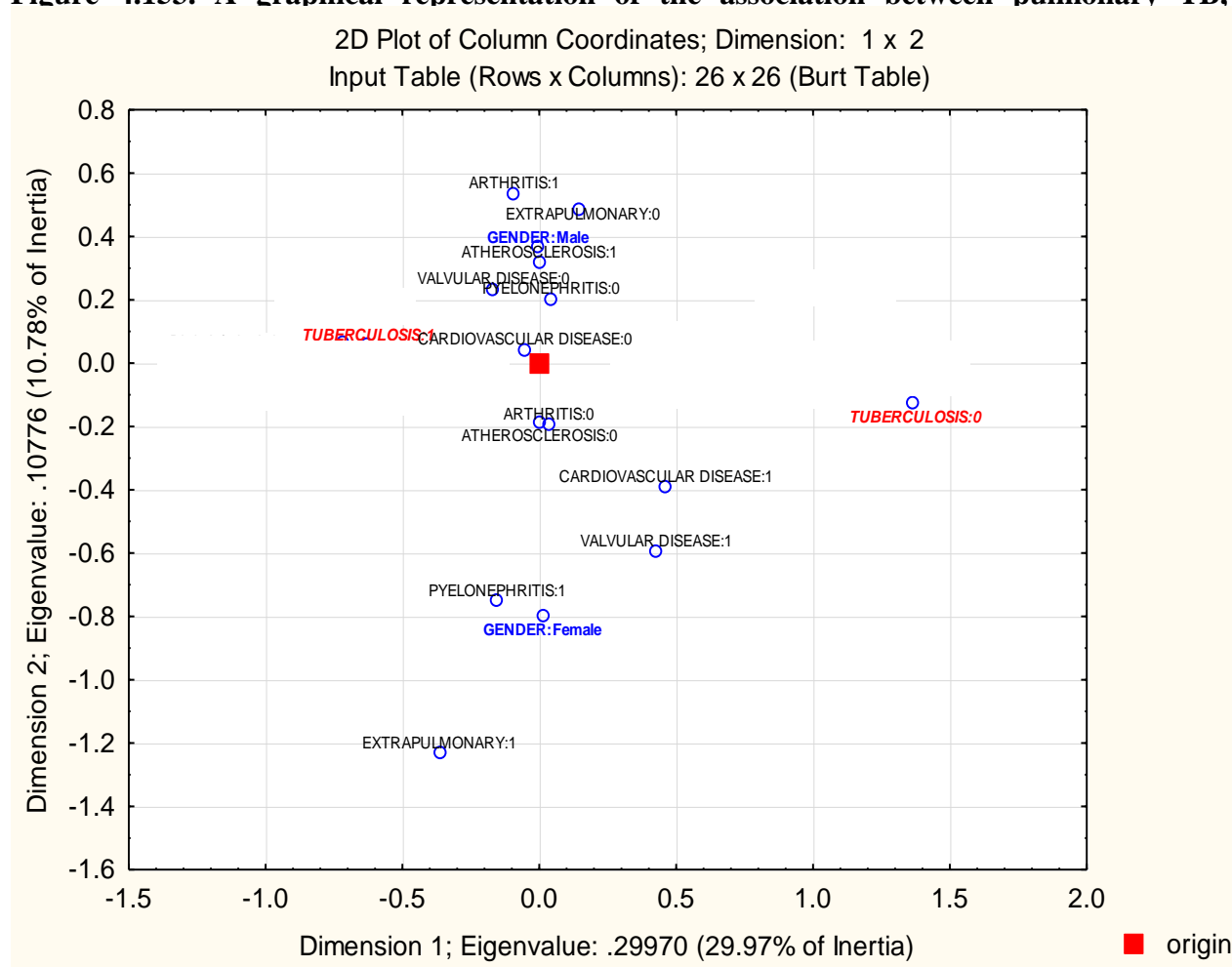


As can be seen in figure 4.152, the point to indicate the presence of rib lesions is located on the right side of the origin, suggesting an association between the prevalence of rib lesions and pulmonary TB (Figure 4.152).

4.12.6 Correspondence Analysis

4.12.6.1 Association between the prevalence of pulmonary and extrapulmonary TB, sex and risk factors

The correspondence analysis was used to graphically visualize the associations between pulmonary TB, extrapulmonary TB, sex and risk factors for the development of TB (Figure 4.153). From this analysis, it is evident that the prevalence of extrapulmonary TB is more commonly associated with females than males in our cadaver cohort (Figure 4.153). The risk factors associated with an increased prevalence of pulmonary TB includes arthritis, atherosclerosis, cardiovascular disease (CVD), pyelonephritis and cardiac valvular disease and was visualized on the 2D plot (Figure 4.153). It is evident that arthritis and atherosclerosis are closely associated with the male population in our study as these findings were located above the point of origin. Pyelonephritis, CVD and valvular disease were all located below the point of origin, suggesting a close association with the female population from our study (Figure 4.153).

Figure 4.153. A graphical representation of the association between pulmonary TB,

4.13 Molecular Analysis

Of the five extraction methods, all was successful in extracting mycobacterial nucleic acids from our cadaver population; however, with variable success (Table 4.104).

4.13.1 Quantitation of nucleic acids.

The quantitation of nucleic acid of each of the extracted samples was done using a NanoDrop® spectrophotometer (ND-1000, V3.7.1).

Table 4.104. A summary of the extraction methods used in this study

Extraction Method	Number of Samples	Range of Concentration (ng/ μ l)	Range of A_{260}/A_{280} ratio	Reference
NucliSens [®] miniMag [®]	50	18.3 – 312.6	1.2 – 1.6	Manufacturer's instructions
Qiagen [®] QIAamp [®] FFPE	60	35.6 – 235.9	1.7 – 2.3	Dedhia <i>et al.</i> , 2007
Salting out method	80	68.9 – 996.3	1.4 – 1.9	Miller <i>et al.</i> , 1988
HAIN [®] Genotype [®] DNA isolation	30	9.8 – 229.5	1.7 – 2.1	Manufacturer's instructions
Phenol/Chloroform	34	11.0 – 441.8	1.0 – 1.7	Ausubel <i>et al.</i> , 1995

The concentration of nucleic acids extracted ranged between 10ng/ μ l to 1000ng/ μ l (Table 4.104). The A_{260}/A_{280} ratio of the extracted nucleic acids was determined and values of between 1.1 and 2.3 were obtained. The A_{260}/A_{280} ratio gave an indication of the amount of organic material such as protein, present in relation to the amount of nucleic acids. Nucleic acids and proteins are visualised at 260nm and 280nm, respectively. An A_{260}/A_{280} ratio of 2.0 is considered a good value, as it indicates a higher concentration of nucleic acids comparing to organic material. The concentrations of nucleic acids obtained with the salting out method were the highest among the five extraction methods (Table 4.104). Even though different nucleic acid concentrations and A_{260}/A_{280} ratios were obtained with the five extraction methods, the resultant nucleic acids were still viable for PCR applications.

4.13.2 Molecular Techniques to Demonstrate *M. tuberculosis*

4.13.2.1 HAIN[®] MTBDRplus[®] DNA kit (ver. 2.0)

A total of 253 extracted samples from the 127 cadavers were analysed by the HAIN[®] MTBDRplus[®] DNA kit (version 2.0). Although the intensities of the different hybridization bands varied, the presence of the *Mycobacterium tuberculosis* complex (MTBC) could be

determined in 88/97 (90.7%) cadavers macroscopically positive for TB. The presence of MTBC was confirmed with the presence of the TUB band (Figures 4.154 and 4.155).

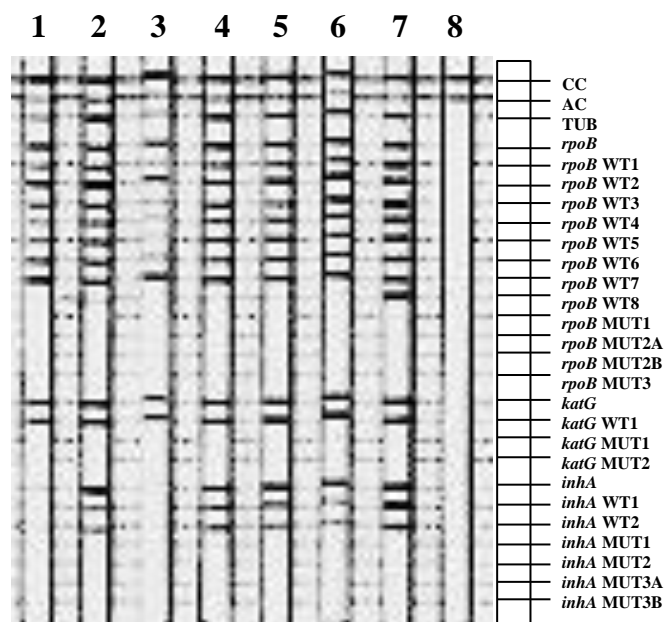


Figure 4.154. HAIN® MTBDRplus® DNA kit results. The MTBDRplus results from 10 cadaver pulmonary samples. Lane 1, K57/12 (R); lane 2, K52/12 (R); lane3, K50/12 (R); lane 4, K50/12 (L); lane 5, K49/12 (L); lane 6, K43/12 (L); lane 7, K40/11 (R); lane 8, K38/11 (R); lane 9, K38/11 (L) and lane 10, K47/10 (L).

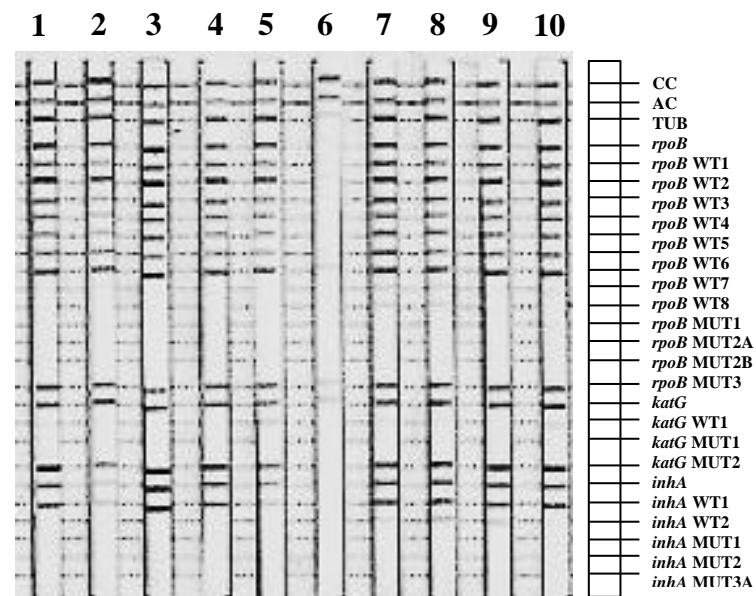


Figure 4.155. HAIN® MTBDRplus® DNA kit results. The MTBDRplus results from eight pulmonary samples. Lane 1, K108/09 (R); lane 2, K112/09 (R); lane3, K118/09 (L); lane 4, K03/10 (L); lane 5, K06/10 (R); lane 6, K13/10 (R); lane 7, H37Rv; lane 8, blank.

One of the advantages of the HAIN[®] MTBDRplus[®] DNA kit (version 2.0) is to determine resistance to first-line drugs, including rifampicin (RIF) and isoniazid (INH). In our study, however, resistance to RIF could not be determined in the pulmonary samples due to the absence of the wild type 8 (*rpoB*WT8) band in 79/97 (81.4%) samples (Figures 4.154 and 4.155). In addition, the *katG* and *inhA* bands were infrequently absent in the samples. Resistance to RIF and INH were therefore difficult to determine. The sensitivity of the MTBDRplus (2.0) kit was not determined.

4.13.2.2 IS6110 PCR

The IS6110 insertion sequence is not only a highly conserved sequence (Donoghue *et al.*, 2004), but it is found within the genome of the MTBC and occurs in several copies which are distributed throughout the entire genome (Fang and Forbes, 1997; Donoghue *et al.*, 2004).

Amplification of 123bp of the IS6110 insertion sequence was used to identify *Mycobacterium tuberculosis*. Extracted DNA isolates from 60 cadavers which were macroscopically positive for PTB were amplified and the amplified DNA products were visualised with gel electrophoresis, using a 1% agarose gel. The IS6110 PCR was positive in 40.0% (24/60) of the confirmed pulmonary TB samples.

Figure 4.156 shows the 123bp amplification products of the IS6110 sequence of *M. tuberculosis*.

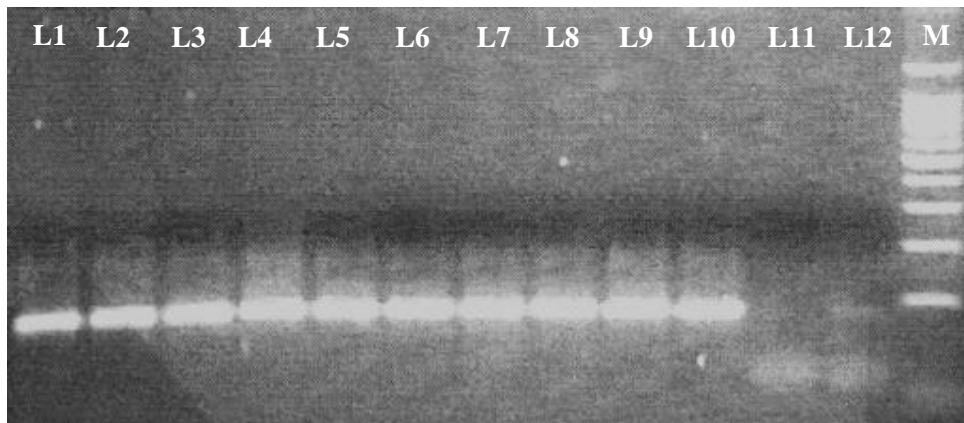


Figure 4.156. IS6110 PCR gel electrophoresis. This figure shows the 123bp amplification products of the IS6110 region within the *M. tuberculosis* genome extracted from the cadaver population. Lane 1, K05/11 (R); lane 2, K06/11 (R); lane 3, K06/11 (L); lane 4, K10/11 (R); lane 5, K10/11 (L); lane 6, K13/11 (R); lane 7, K15/11 (R); lane 8, K15/11 (L); lane 9, K18/11 (R); lane 10, K18/11 (L); lane 11, blank (R); lane 12, blank (L); M, DNA ladder.

4.13.3 Molecular Techniques for Typing of *M. tuberculosis*

4.13.3.1 Spoligotyping

Spoligotyping (“spacer oligotyping”) is currently the most commonly used PCR-based reverse-hybridization technique (Brudey *et al.*, 2006) to differentiate between strains (Goyal *et al.*, 1997). It is a simple and fast method to simultaneously detect and type *M. tuberculosis*, based on hybridization of 43 spacer oligonucleotides (Kamerbeek *et al.*, 1997).

Extracted samples from 50 cadavers were analysed by spoligotyping. No distinct patterns could be identified from the extracted samples. A typical Beijing spoligotyping pattern will show hybridization of spacer 35 to 43 together with no hybridization of spacers 1 to 34 (Anh *et al.*, 2000; Streicher *et al.*, 2004; Cox *et al.*, 2005). The BCG positive control spoligotyping pattern demonstrate the absence of spacers 3, 9, 16 and 39-43, while the H37Rv positive control is characterised by the absence of spacers 20-21 and 33-36 (Streicher *et al.*, 2004). The majority of our extracted samples showed hybridization of spacers 35-43 (Figure 4.157). Spacers 33-34 were

rarely hybridized (Figure 4.157) while spacers 1-32 showed hybridization in an irregular and unidentifiable manner.

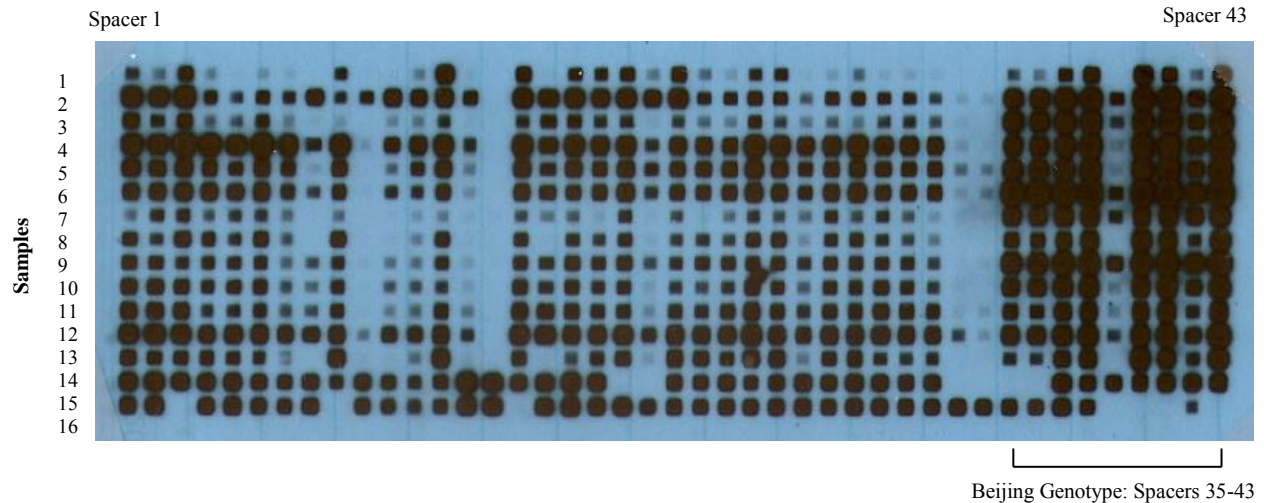


Figure 4.157. Spoligotyping patterns of some of the isolates analysed in the present study. The PCR products were hybridized to 43 spacer sequences observed between the direct regions (DRs) in the mycobacterial genome. A black dot is indicative of the presence of a spacer, while the blank spaces indicate the absence of the particular spacer. This figure shows the spoligotypes of 13 cadaver samples (lanes 1-13), one H37Rv sample (lane 14), one BCG sample (lane 15) and one blank sample (lane 16).

The spoligotyping method was not repeated on the remaining of the pulmonary samples due to the poor results obtained from the samples.

4.13.3.2 RD105 and Mtub02/RD105 PCR

Large sequence polymorphisms (LSPs) have been used previously to describe organisms belonging to the *Mycobacterium tuberculosis* complex (MTBC) (Tsolaki *et al.*, 2005). One such LSP, the RD105 genomic deletion of 3,467bp, is a prominent marker for the Beijing family of strains (Tsolaki *et al.*, 2005; Hanekom *et al.*, 2007; Rindi *et al.*, 2009).

Amplification of the RD105 deletion in the genome of *M. tuberculosis* was done using extracted nucleic acids from 40 cadavers with PTB. The protocol followed was previously applied by

Tsolaki *et al.* (2005) A total of 8/40 (20.0%) cadavers showed successful amplification of the region. The RD105 PCR was non-specific with a very low sensitivity. The PCR was repeated and different results were obtained suggesting this PCR was non-repeatable. Due to the limited success of the RD105 PCR with the cadaver samples, several primers with differing sizes were designed in and around the RD105 region. This was done without any success in differentiating the mycobacterial species.

The Mtub02 locus, a mycobacterial interspersed repetitive-unit – variable number tandem-repeat (MIRU-VNTR), was used in combination with the RD105 PCR in order to differentiate between Beijing and non-Beijing family isolates.

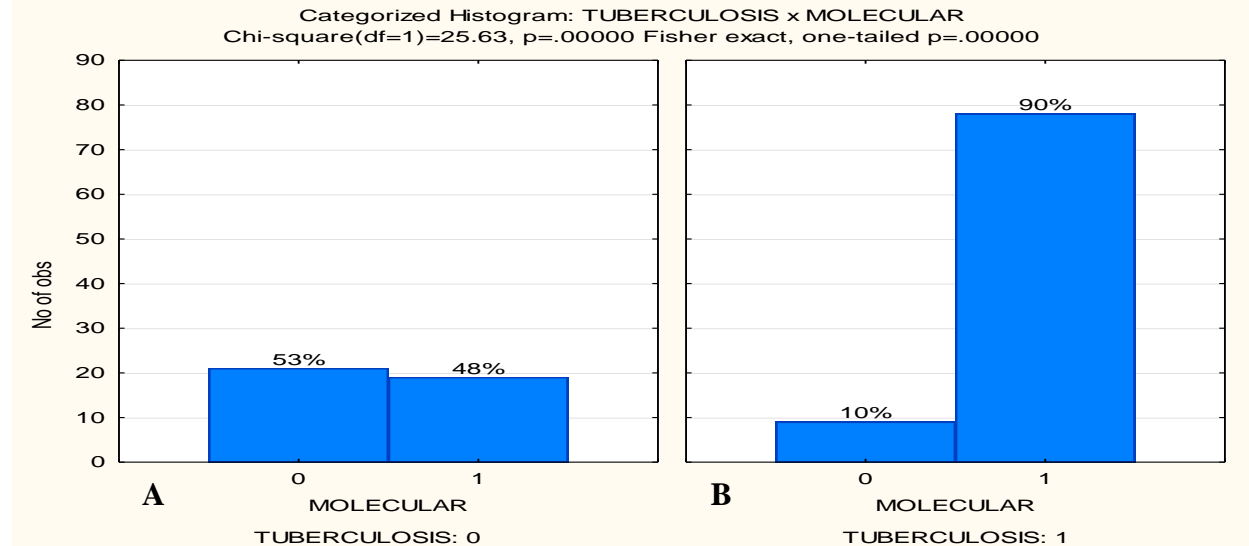
Amplification of the Mtub02/RD105 regions in the genome of *M. tuberculosis* was done using extracted nucleic acids from 50 cadavers with PTB. Successful amplification was observed in a total of 10/50 (20.0%) cadavers. Like the RD105 PCR, limited success was achieved with this PCR. According to Liu *et al.* (2011), the Mtub02 PCR is a good alternative to the spoligotyping. While only 4/50 (8.0%) cadavers samples were successfully amplified, both the Beijing and non-Beijing bands were visualized, suggesting that these PCRs were not specific. Therefore, due to the limited success, differentiation between the Beijing and non-Beijing isolates could not be achieved in our study.

4.13.4 Overall Combination of Macroscopic and Molecular Results

A cross-tabulation test was performed to determine the efficacy with which mycobacterial DNA could be detected using molecular applications. These findings were compared with the

pathology findings during gross dissection and revealed a statistical significance ($p < 0.05$). Mycobacterial DNA was extracted and amplified in 90% of the cadavers with pulmonary TB (Figure 4.158).

Figure 4.158. Cross-tabulation to determine the statistical significance between the molecular and pathology results A) Molecular results were positive in the absence of pulmonary TB; B) molecular results were positive in



4.14 Radiological Analysis: Chest X-Ray Evaluation

4.14.1 Pulmonary Analysis

4.14.1.1 Pulmonary Cavitation

Pulmonary cavitation as a result of pulmonary TB, was observed in 27/40 (67.5%) of the cadavers from the first cadaver cohort (n=40). The cavitations presented as uni- or bilateral, thin-walled spaces in the pulmonary parenchyma (Figure 4.159) and were as a result of secondary PTB. Cavitation due to a pulmonary neoplasm or abscess was not observed in the cadavers.

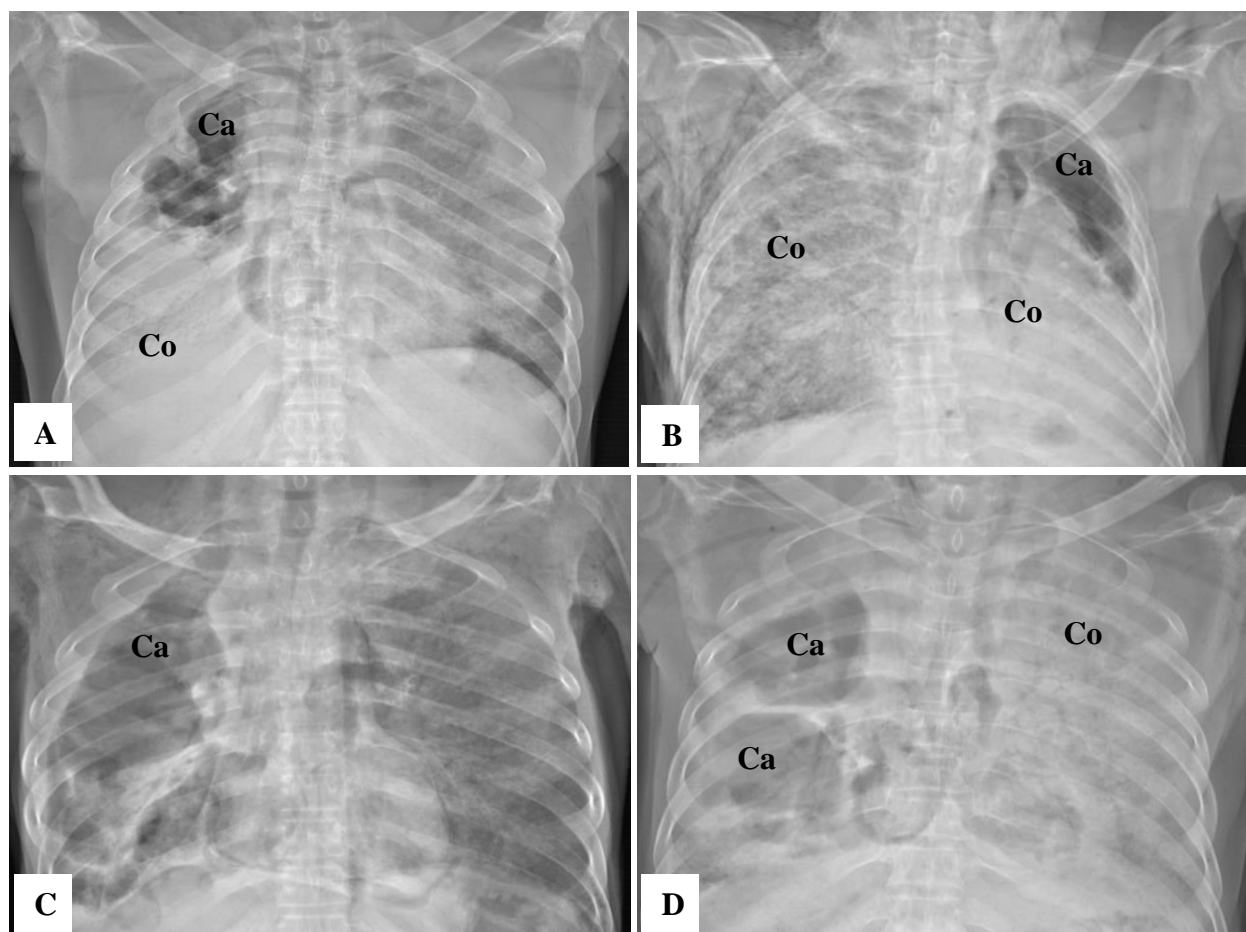


Figure 4.159. Pulmonary cavitation on the chest X-ray of the first cadaver cohort (n=40). A) Cavitation in the left superior lobe and consolidation in the right lung of cadaver K01/10, PA view; B) cavitation in the right superior lobe with opacification in the right inferior lobe of cadaver K12/10, PA view; C) cavitation in the right lung of cadaver K42/10, PA view; D) two large cavities in the right lung of cadaver K96/09, PA view; cavity (Ca), consolidation (Co).

4.14.1.2 Emphysematous Appearance

Large, voluminous lungs consistent of emphysema were observed in 5/40 (12.5%) cadavers. The lungs looked larger than usual and blood vessels were more difficult to identify (Figure 4.160). Signs of pneumothorax were observed in one cadaver with emphysema (Figure 4.160, A).

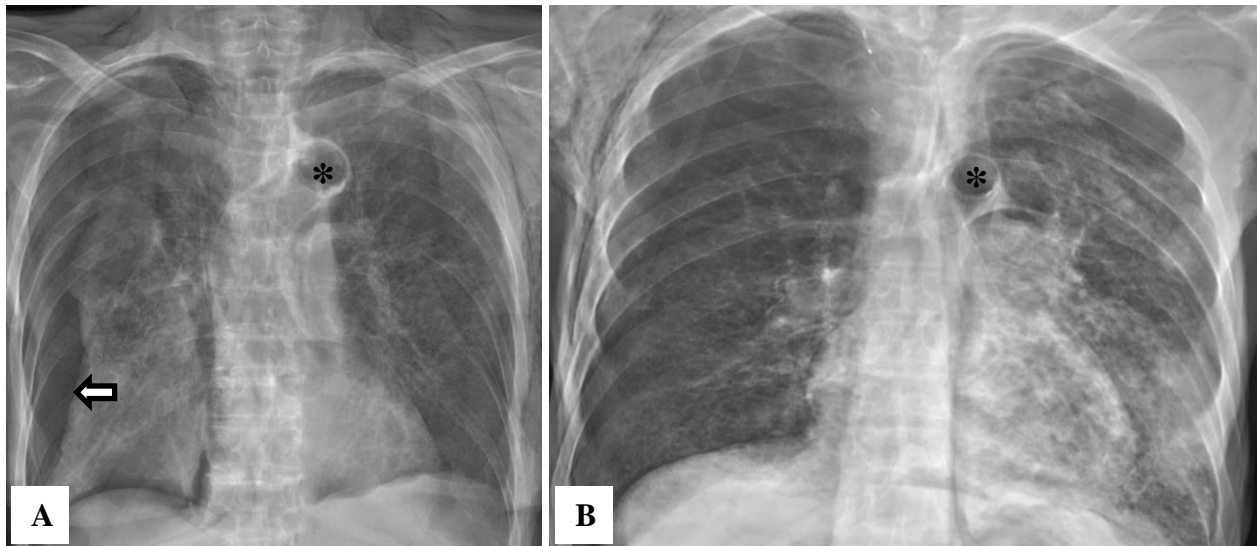


Figure 4.160. Emphysema on the chest X-ray of the first cadaver cohort (n=40). A) Large and voluminous lungs characteristic of emphysema, cadaver K99/09, PA view. Note the unilateral pneumothorax (blocked arrow); B) emphysematous lungs of cadaver K118/09, PA view; aortic arch (asterisk).

4.14.1.3 Consolidation

Consolidation was frequently observed on the CXRs of the cadavers (Figure 4.161). Opacification occurred as a result of a variety of conditions including neoplastic growth, fibrosis, both lobar and bronchopneumonia and pleural effusions and presented as an opacification on the CXRs of the cadavers.

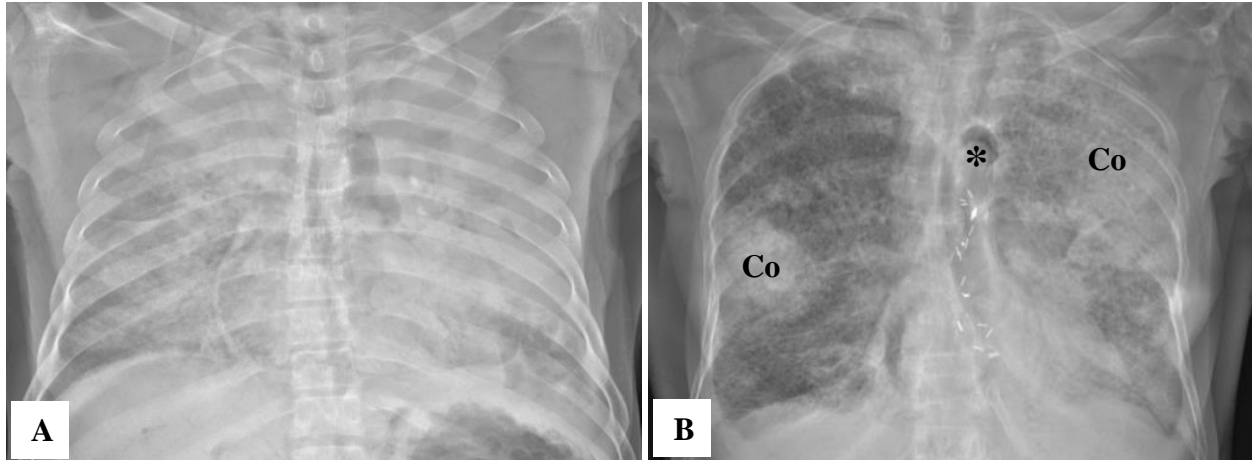


Figure 4.161. Consolidation on the chest X-ray of the first cadaver cohort (n=40). A) Extensive bilateral consolidation in cadavers K10/10, PA view; B) areas of consolidation in both lobes of cadaver K19/10, PA view; Aortic arch (asterisk), consolidation (Co).

4.14.1.4 Pneumothorax

For this study, pneumothorax was diagnosed when the edge of the lung was visible and were observed in 5/40 (12.5%) cadavers and (Figure 4.162).

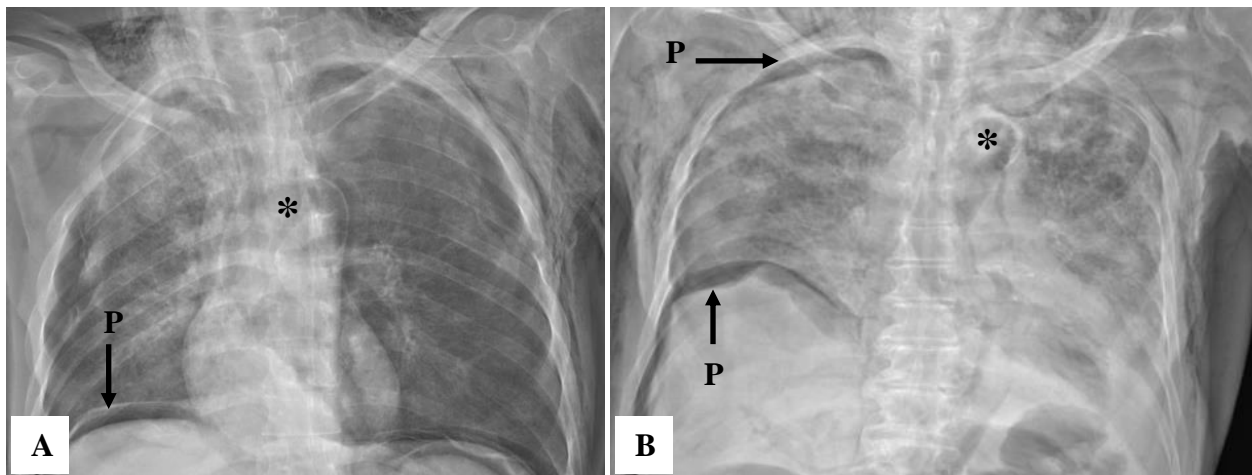


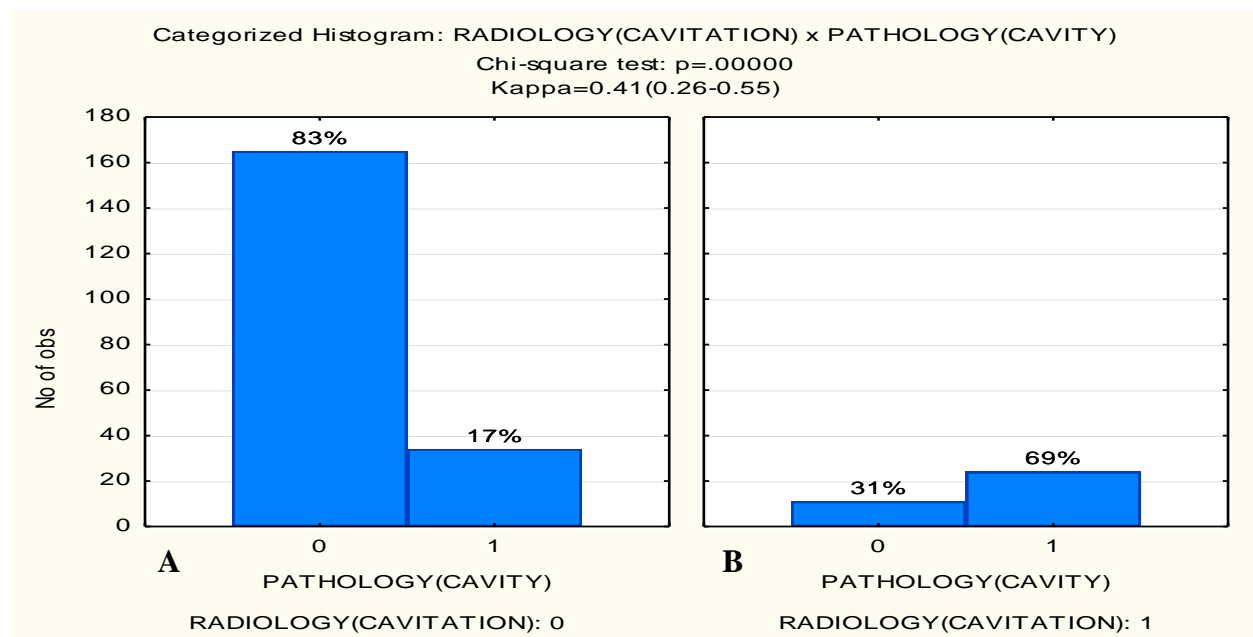
Figure 4.162. Pneumothorax on the chest X-ray of the first cadaver cohort (n=40). A) Pneumothorax B) signs of a pneumothorax in the right superior lobe of cadaver K106/09, PA view; Aortic arch (asterisk), pneumothorax (P).

4.14.2 Statistical Findings

Statistical analysis was done using Statistica[®] Version 12. The cross-tabulation test was done to correlate radiology and pathology in the cadaver samples.

4.14.2.1 Radiology versus Pathology: Segments 1-6

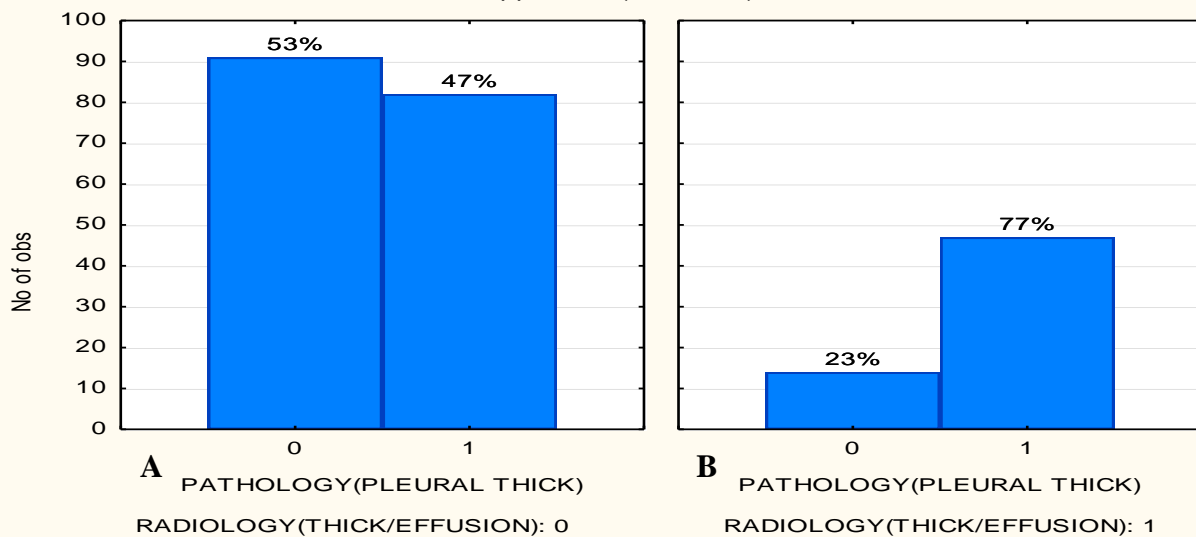
A cross-tabulation test used to evaluate the six lung segments revealed that pulmonary cavitation ($p < 0.05$; Kappa factor 0.41) and pleural thickening ($p < 0.05$; Kappa factor 0.22) were the only pulmonary findings that could be positively correlated in the first cadaver cohort ($n = 40$). Pulmonary cavitation was not positively diagnosed using radiology, when cavitation was present in 17% of the cadavers during gross dissection (Figure 4.163, A). However, pulmonary cavitation was positively correlated in 69% of the cadavers when radiological and pathological findings were compared (Figure 4.163, B).



Pleural thickening was observed during gross dissection in 47% of the cadavers which could not be positively correlated with the radiological findings (Figure 4.164, A). However, pleural thickening was positively diagnosed using pathologic and radiologic findings in 77% of the cadavers (Figure 4.164, B).

Figure 4.164. Association between radiology and pathology: pleural thickening. A cross-

Categorized Histogram: RADIOLOGY(THICK/EFFUSION) x PATHOLOGY(PLEURAL THICK)
Chi-square test: $p=.00004$
Kappa=0.22(0.12-0.32)



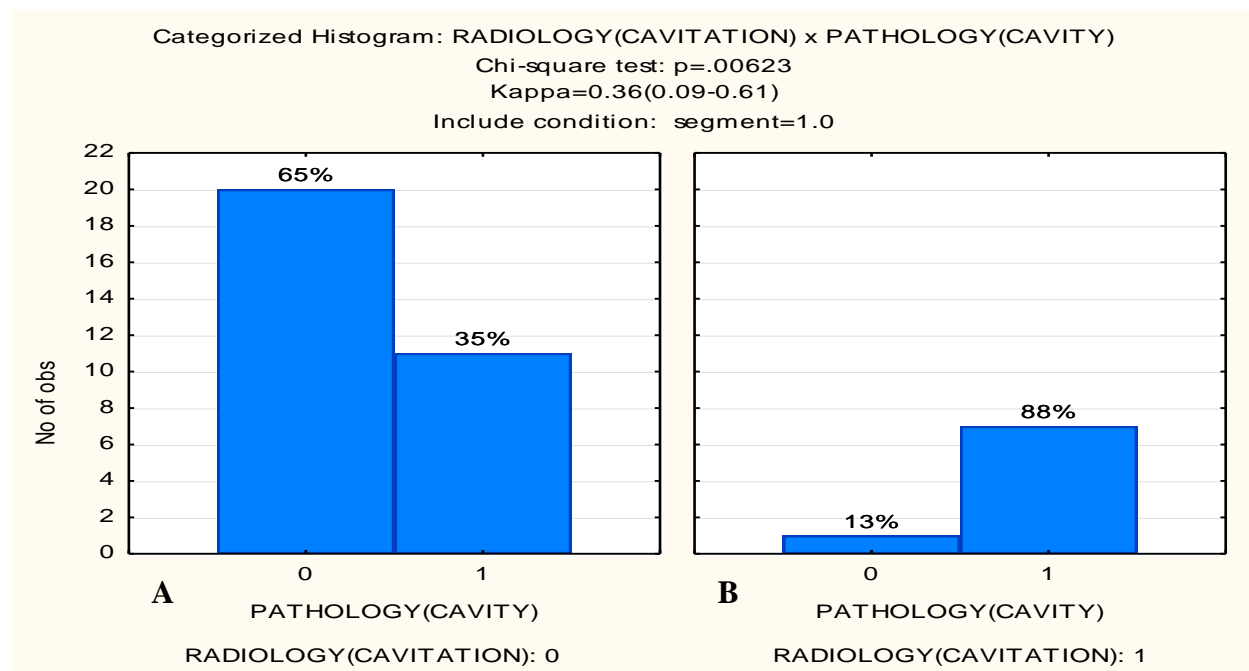
Nodules, opacification, collapse, bronchiectasis and tumor masses were not positively correlated between the pathological and radiological findings (Table 4.105).

Table 4.105. Observed frequencies in all of the segments in the first cadaver cohort (n=40)

<i>Finding/Feature (Radiology/Pathology)</i>	<i>Chi-Squared Value</i>	<i>Statistically Significant ($p>0.05$)</i>	<i>Kappa Coefficeance Factor</i>
Nodules/Nodules	0.26648	No	0.08
Opacification/Consolidation	0.91729	No	0.00
Opacification/Nodules	0.23966	No	0.03
Opacification/Hematoma	0.39873	No	0.00
Collapse/Collapse	0.85268	No	0.01
Bronchiectasis/Bronchiectasis	0.66916	No	0.02
Mass/Mass	0.71797	No	0.02

4.14.2.2 Radiology versus Pathology: Segment 1

The first segment represented the superior part of the right lung. Cavitation ($p < 0.05$; Kappa factor 0.36) and pleural thickening ($p < 0.05$; Kappa factor 0.27) were the only findings that could be positively correlated between radiology and pathology (Table 4.106, Figure 4.165, A). The cross-tabulation test revealed that the pathological and radiological findings in the right superior lobe (first segment) were positively correlated in 88% of the cadavers (Chi-square $p = 0.00523$, $p < 0.05$) (Figure 4.165, B).



Pleural thickening was positively correlated in 92% of the cadavers when the cross-tabulation test was applied (Chi-square $p = 0.01728$, $p < 0.05$) (Table 4.106, Figure 4.166).

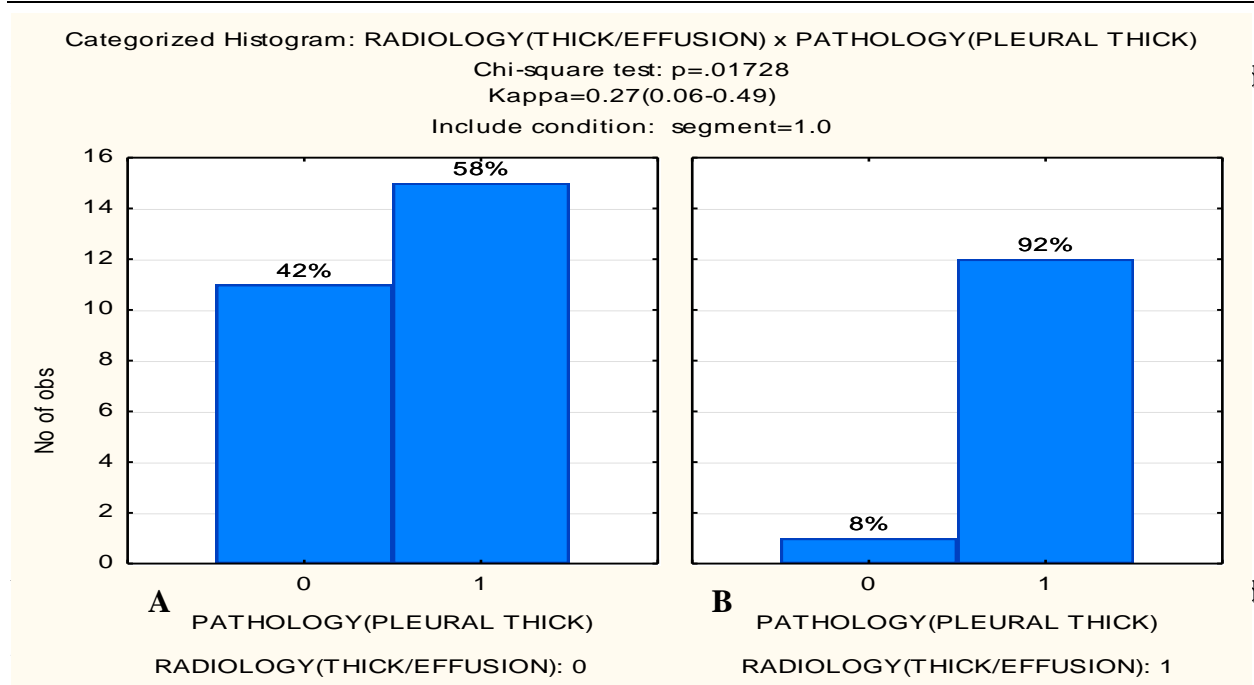


Table 4.106. Observed frequencies in the first segment in the first cadaver cohort (n=40)

<i>Finding/Feature (Radiology/Pathology)</i>	<i>Chi-Squared Value</i>	<i>Statistically Significant (p>0.05)</i>	<i>Kappa Coefficiencie Factor</i>
Nodules/Nodules	0.33333	No	*
Opacification/Consolidation	0.67610	No	*
Opacification/Hematoma	0.46553	No	*
Collapse/Collapse	1.00000	No	*
Bronchiectasis/Bronchiectasis	0.88630	No	*
Mass/Mass	1.00000	No	*
Cavitation/Cavity	0.00623	Yes	0.36
Pleural thickening or Effusion/Pleural thickening	0.01728	Yes	0.27

* Kappa Coefficiencie factor was not determined as the Chi-squared value was not significant

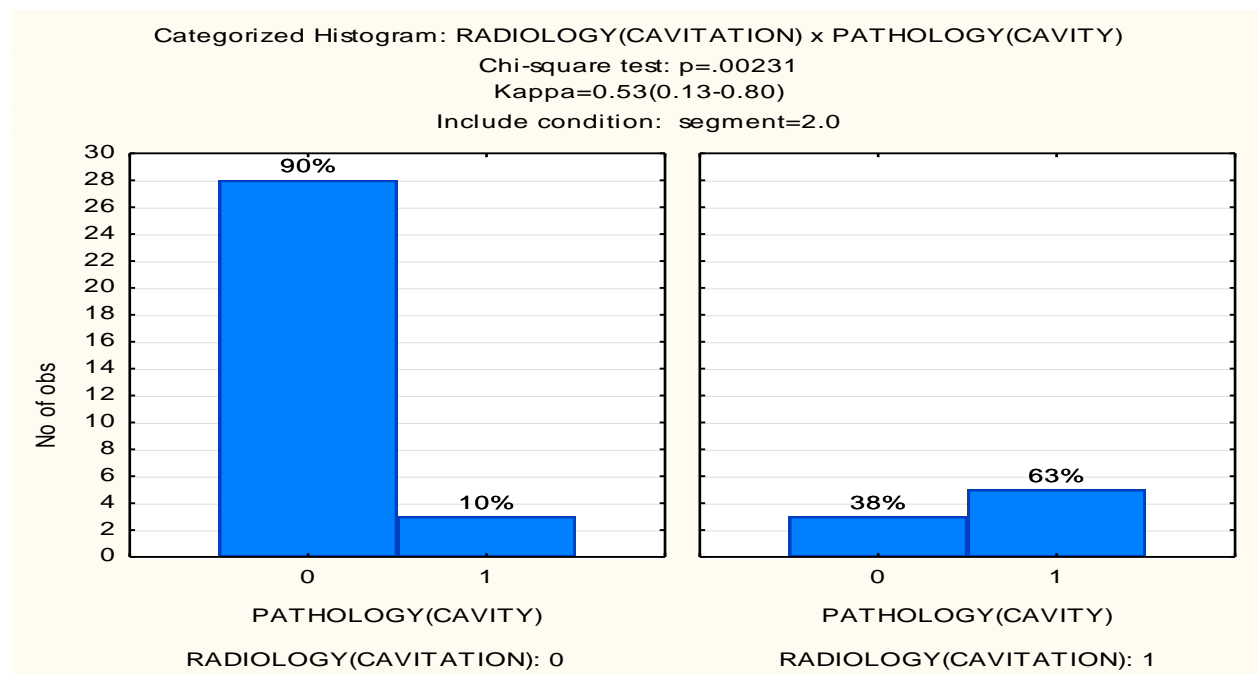
4.14.2.3 Radiology versus Pathology: Segment 2

The second segment was representative of the inferior part of the right superior lobe and superior part of the right inferior lobe. The only finding that could be positively correlated between radiology and pathology was cavitation ($p<0.05$; Kappa factor 0.53) within the lung (Table 4.107, Figure 4.167)

Table 4.107. Observed frequencies in the second segment in the first cadaver cohort (n=40)

<i>Finding/Feature (Radiology/Pathology)</i>	<i>Chi-Squared Value</i>	<i>Statistically Significant (p>0.05)</i>	<i>Kappa Coefficiene Factor</i>
Nodules/Nodules	0.36553	No	*
Opacification/Consolidation	0.15945	No	*
Opacification/Hematoma	0.56049	No	*
Collapse/Collapse	1.00000	No	*
Bronchiectasis/Bronchiectasis	0.84799	No	*
Mass/Mass	1.00000	No	*
Cavitation/Cavity	0.00231	Yes	0.53
Pleural thickening or Effusion/Pleural thickening	0.16660	No	*

* Kappa Coefficiene factor was not determined as the Chi-squared value was not significant



4.14.2.4 Radiology versus Pathology: Segment 3

The third segment was representative of the right inferior lobe of the lung. None of the findings could be positively correlated between radiology and pathology features in the inferior lobe of the right lung (Table 4.108).

Table 4.108. Observed frequencies in the third segment in the first cadaver cohort (n=40)

<i>Finding/Feature (Radiology/Pathology)</i>	<i>Chi-Squared Value</i>	<i>Statistically Significant (p>0.05)</i>
Nodules/Nodules	0.41056	No
Opacification/Consolidation	0.11790	No
Opacification/Hematoma	1.00000	No
Collapse/Collapse	1.00000	No
Bronchiectasis/Bronchiectasis	0.70215	No
Mass/Mass	1.00000	No
Cavitation/Cavity	0.64186	No
Pleural thickening or Effusion/Pleural thickening	0.50558	No

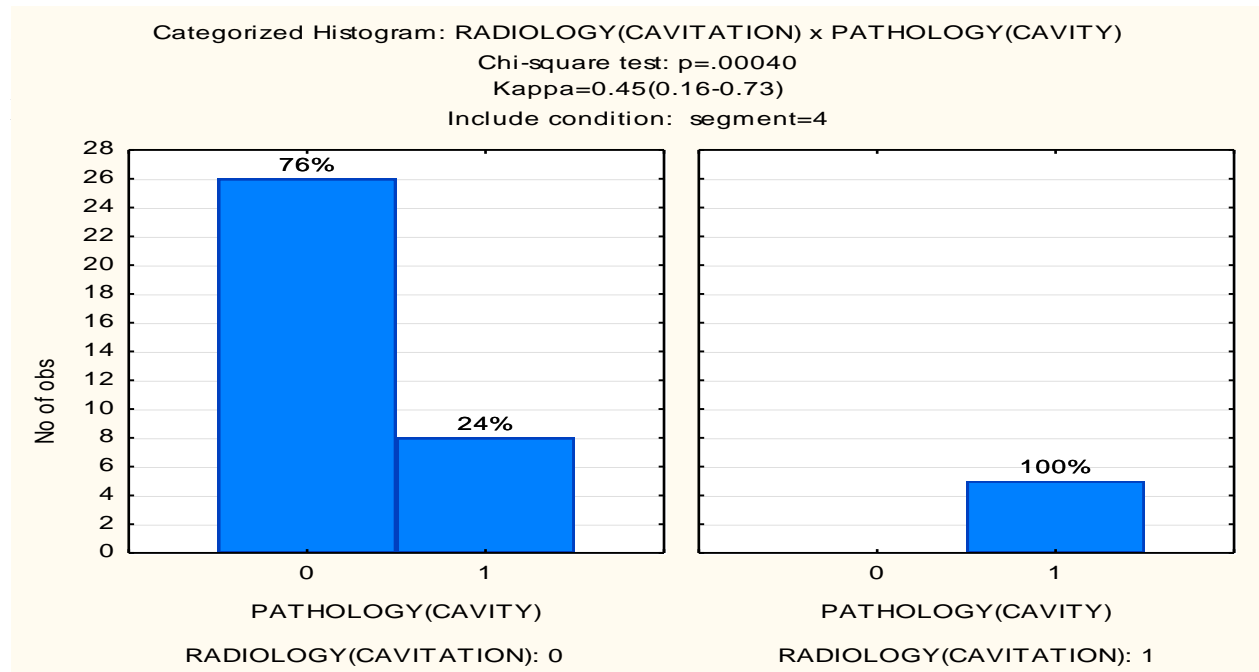
4.14.2.5 Radiology versus Pathology: Segment 4

The fourth segment represented the superior part of the left lung. Pulmonary cavitation was the only positive finding that could be positively correlated ($p < 0.05$; Kappa factor 0.45) between radiology and pathology (Table 4.109, Figure 4.168)

Table 4.109. Observed frequencies in the fourth segment in the first cadaver cohort (n=40)

<i>Finding/Feature (Radiology/Pathology)</i>	<i>Chi-Squared Value</i>	<i>Statistically Significant (p>0.05)</i>	<i>Kappa Coefficiencie Factor</i>
Nodules/Nodules	0.35398	No	*
Opacification/Consolidation	0.77544	No	*
Opacification/Hematoma	1.00000	No	*
Collapse/Collapse	1.00000	No	*
Bronchiectasis/Bronchiectasis	0.16223	No	*
Mass/Mass	1.00000	No	*
Cavitation/Cavity	0.00040	Yes	0.45
Pleural thickening or Effusion/Pleural thickening	0.07157	No	*

* Kappa Coefficiencie factor was not determined as the Chi-squared value was not significant



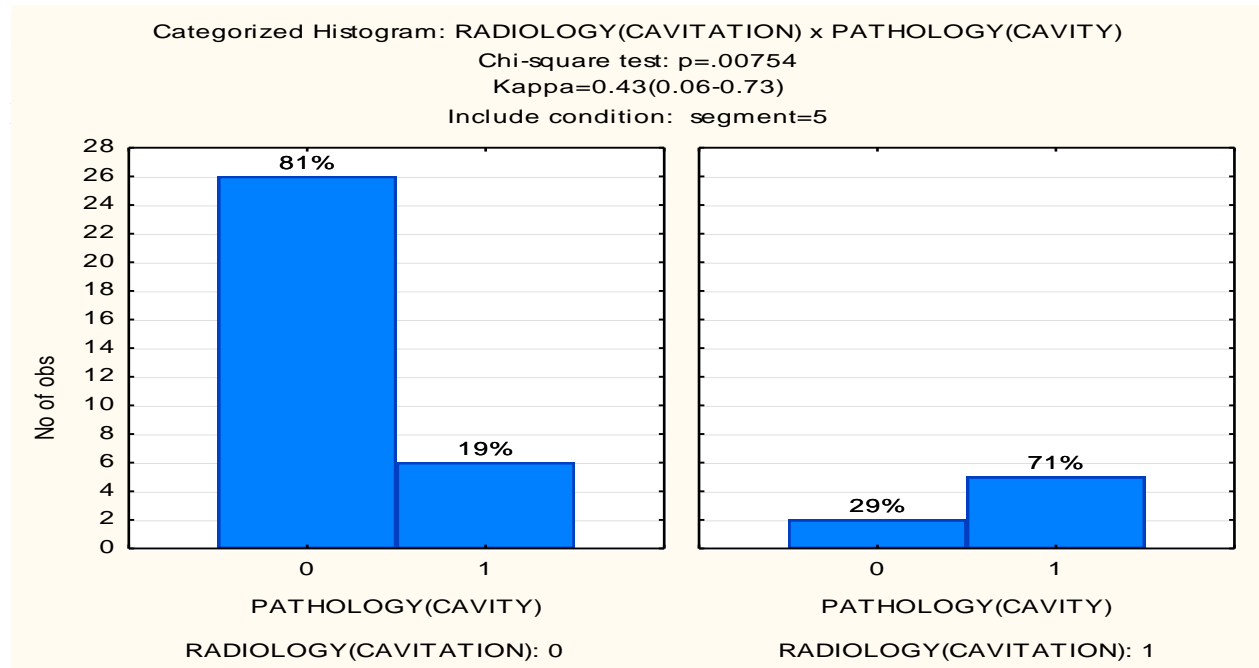
4.14.2.6 Radiology versus Pathology: Segment 5

The fifth segment was representative of the inferior part of the superior left lung and superior part of the inferior left lung. Only one finding, pulmonary cavitation ($p < 0.05$; Kappa factor 0.43) could be positively correlated between radiology and pathology (Table 4.110, Figure 4.169).

Table 4.110. Observed frequencies in the fifth segment in the first cadaver cohort (n=40)

<i>Finding/Feature (Radiology/Pathology)</i>	<i>Chi-Squared Value</i>	<i>Statistically Significant (p>0.05)</i>	<i>Kappa Coefficiency Factor</i>
Nodules/Nodules	0.23536	No	*
Opacification/Consolidation	0.16269	No	*
Opacification/Hematoma	1.00000	No	*
Collapse/Collapse	1.00000	No	*
Bronchiectasis/Bronchiectasis	0.13917	No	*
Mass/Mass	1.00000	No	*
Cavitation/Cavity	0.00754	Yes	0.43
Pleural thickening or Effusion/Pleural thickening	0.16872	No	*

* Kappa Coefficiency factor was not determined as the Chi-squared value was not significant



4.14.2.7 Radiology versus Pathology: Segment 6

The sixth segment represented the inferior part of the left lung. Pulmonary pleural thickening was the only finding that could be positively correlated ($p < 0.05$; Kappa factor 0.29) between radiology and pathology (Table 4.111, Figure 4.170).

Table 4.111. Observed frequencies in the sixth segment in the first cadaver cohort (n=40)

<i>Finding/Feature (Radiology/Pathology)</i>	<i>Chi-Squared Value</i>	<i>Statistically Significant (p>0.05)</i>	<i>Kappa Coefficiency Factor</i>
Nodules/Nodules	0.48152	No	*
Opacification/Consolidation	1.00000	No	*
Opacification/Hematoma	1.00000	No	*
Collapse/Collapse	1.00000	No	*
Bronchiectasis/Bronchiectasis	0.40812	No	*
Mass/Mass	1.00000	No	*
Cavitation/Cavity	0.14475	No	*
Pleural thickening or Effusion/Pleural thickening	0.01561	Yes	0.29

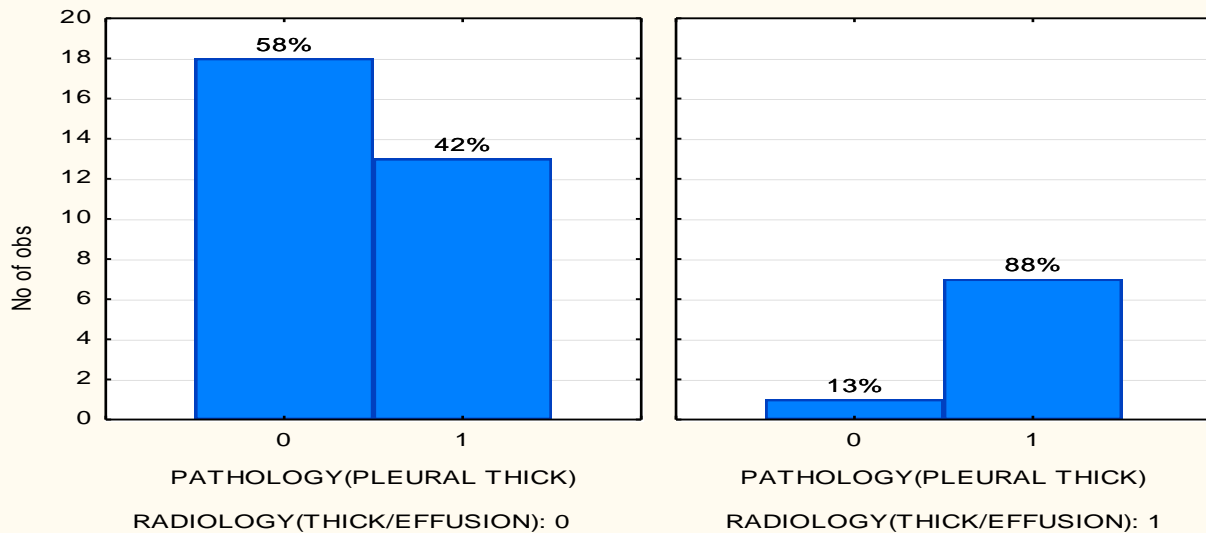
* Kappa Coefficiency factor was not determined as the Chi-squared value was not significant

Categorized Histogram: RADIOLOGY(THICK/EFFUSION) x PATHOLOGY(PLEURAL THICK)

Chi-square test: p=.01561

Kappa=0.29(0.07-0.54)

Include condition: segment=6



4.14.3 Evaluation: Cardiovascular Findings

4.14.3.1 Cardiomegaly

For the purpose of this part of the study, cardiomegaly was diagnosed on the chest X-ray (CXR) when the transverse diameter of the cardiac silhouette on the CXR was more than 50% of the transthoracic diameter. Cardiomegaly was observed on 30/127 (23.6%) cadaver CXRs (Figure 4.171). The heart appeared within normal limits on 43/127 (33.9%) CXRs (Figure 4.171), while 54/127 (42.5%) heart borders could not be distinguished from the pulmonary parenchyma.

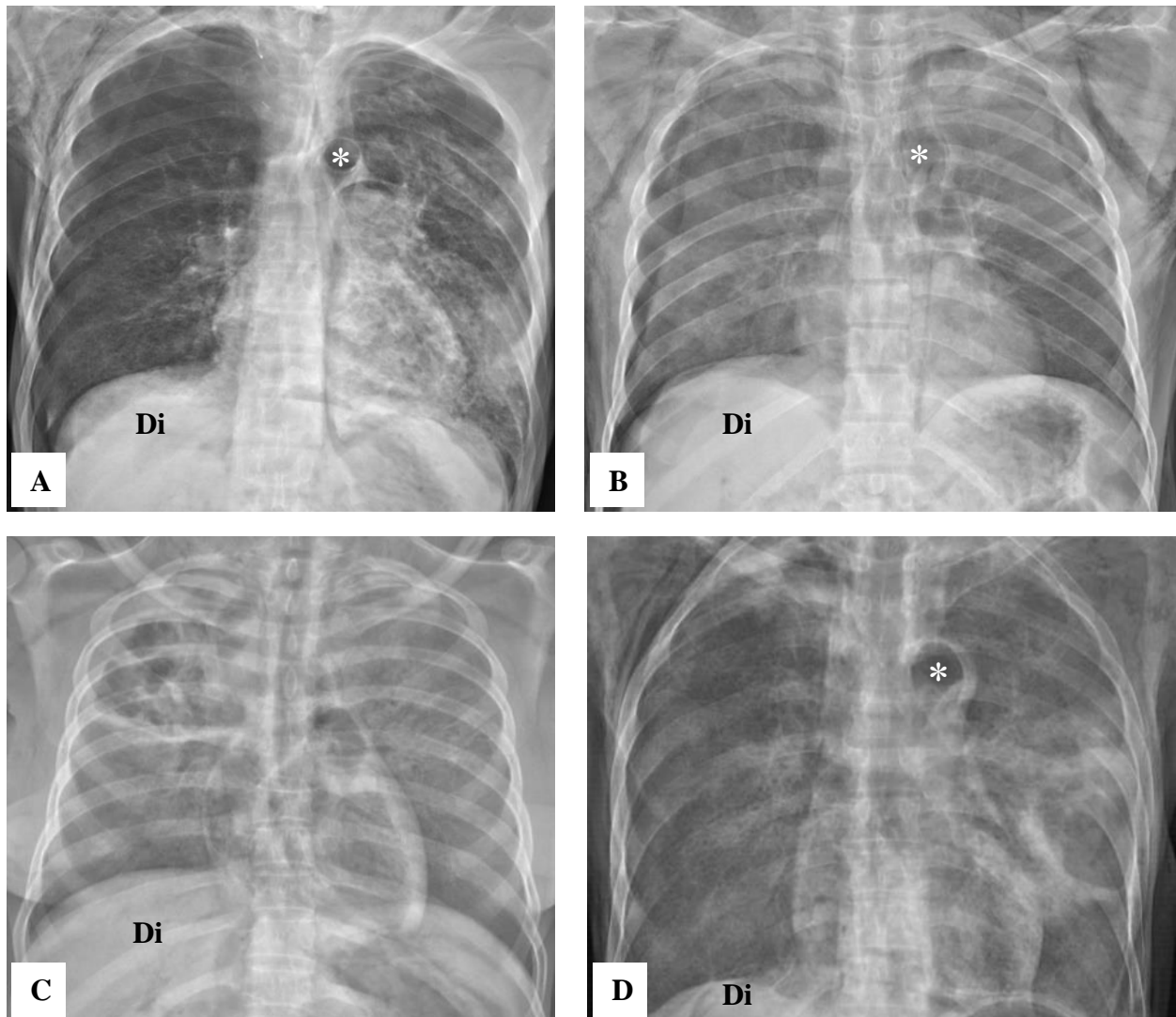


Figure 4.171. Cardiac features on the cadaver CXR. A) Enlargement of the heart in the cadaver K118/09, PA view; B) the heart of cadaver K05/10 was within normal limits, PA view; C) cadaver K04/10 presented with a normal sized heart, PA view; D) the heart of cadaver K112/09 presented with a heart with normal limits; aortic arch (asterisk), diaphragm (D).

4.14.3.2 Hyperattenuation of Aortas

Enlarged, well-demarcated aortas with clear aortic walls were observed in 43/127 (33.9%) cadavers when the Lodox[®] full-body digital X-rays were analyzed (Figure 4.172).

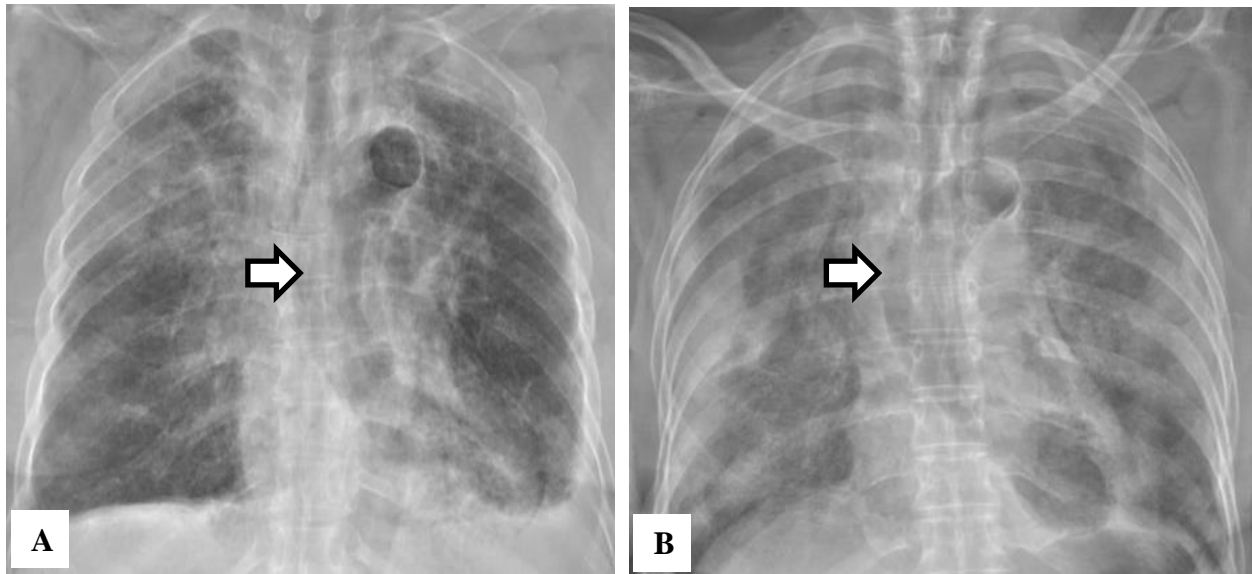


Figure 4.172. Hyperattenuation of the aortas on the CXR. A) CXR of cadaver K18/11 showing the prominent and enlarged ascending aorta (blocked arrow); B) CXR of cadaver K130/11 showing ascending aorta (blocked arrow) extending into the left ventricle.

Discussion

“To be healthy is to race death successfully”

L. Angel, 1984

5.1 Main Findings: Morphological Analysis

In this study, a morphological assessment was done to determine the health status of a cadaver population (n=127) at the FMHS, SU. Special reference was given to TB lesion morphology and distribution.

5.1.1 Pulmonary Tuberculosis

Pulmonary tuberculosis (PTB) was a common occurrence (76.4%) in the cadavers in our study cohort with 22.8% presenting with extrapulmonary TB (EPTB). This was expected as almost all cadavers originated from the high TB burdened Western Cape Province of South Africa. Furthermore, the concurrent increased HIV incidence in the past three decades exacerbated TB incidence rates immensely (Lawn *et al.*, 2006; Wood *et al.*, 2010). In our study, the average age of cadavers with PTB was 47.1 years (range 22 to 83 years). The majority of cadavers with PTB fell within the 40-49 age group. The 30-39 and 50-59 year age groups were the second and third most commonly affected ages, respectively. This is in accordance with Lawn *et al.* (2006) and Wood *et al.* (2010) who stated that TB in South Africa currently tends to develop at a much younger age comparing to previous years. This is due to an extremely high burden of latent TB infection (LTBI) in children and adolescents in impoverished Townships in Cape Town, South Africa. These findings, regarding TB prevalence, correlate with data from other studies (Lanjewar and Duggal, 2001; Corbett *et al.*, 2007; Den Boon *et al.*, 2007; Van't Hoog *et al.*, 2011); however, all of these studies included human immunodeficiency virus (HIV) infection as a predisposing risk factor which influences the PTB prevalence. One limitation of this study is that the HIV status, smear and culture findings of the cadavers are unknown. As this is not an epidemiological study, we were able to investigate the prevalence and morphological appearance

of PTB and EPTB within a small cadaver cohort from low socio-economic backgrounds in South Africa.

Although no statistically significant difference was noted in the manifestation of pulmonary TB between the right and left lung ($p > 0.05$), the right lung showed a slight predilection for pulmonary TB. According to a review by Garay *et al.* (1996), a somewhat higher percentage of right pulmonary involvement was seen in patients from the 20th century. This finding was ascribed to the anatomy of the right primary bronchus, which is wider, shorter and more vertical than the left primary bronchus. Woodring *et al.* (1986), conversely, observed equal involvement of both lungs in their study subjects. Research has shown that the site for the development of primary pulmonary TB is the region of the lung with the greatest ventilation. The most common sites for infection are therefore the middle or inferior regions of the lung as well as the anterior segment of the superior lobes (Woodring *et al.*, 1986).

5.1.2 Systemic (Extrapulmonary) Tuberculosis

For the purpose of this discussion, systemic (extrapulmonary) TB involvement will be discussed in the order from most to least commonly involved sites of infection.

Lymphadenitis is the most prevalent form of EPTB in adults, especially in countries with a high burden of TB (Polesky *et al.*, 2005; Reuter and Wood, 2009). According to the literature lymphadenitis is more prevalent in young females, although any age or race may be affected (Chen *et al.*, 1992; Artenstein *et al.*, 1995; Geldmacher *et al.*, 2002; Ebdrup *et al.*, 2003; Polesky *et al.*, 2005; Reuter and Wood, 2009). In our study, 35.7% of the cadavers with TB

lymphadenitis were females with an average age of 43.0 years. Cervical lymph nodes are said to be the most common site for EPTB involvement (Dandapat *et al.*, 1990; Memish *et al.*, 2000), however, in our study no cervical lymph nodes were noted to be affected in the cadavers. The mediastinal, mesenteric and inguinal lymph nodes were affected with mediastinal involvement (92.9%) being the most prevalent followed by mesenteric (28.6%) and inguinal (7.1%) involvement. Mediastinal or hilar tuberculous lymphadenitis is a common manifestation of primary tuberculosis (Agrons *et al.*, 1993; Moon *et al.*, 1998; Reuter and Wood, 2009). In a study done in Kigali, Rwanda, up to 80% of HIV-infected patients with PTB showed mediastinal lymphadenopathy (Batungwanayo *et al.*, 1992). In our study, 13/127 (10.2%) cadavers presented with enlarged, caseating tuberculous lymphadenitis in the mediastinal lymph nodes. The HIV status of the cadavers could not be established, thus making it impossible to determine the effect of HIV on lymphadenitis in the cadaver cohort. Isolated tuberculous mesenteric lymphadenopathy in HIV-negative patients is rare (Reuter and Wood, 2009). From our results, the cadavers with mesenteric tuberculous involvement did not have abdominal solid organ involvement, peritonitis or bowel involvement. This, in accordance with the literature, is a very rare finding (Reuter and Wood, 2009). The cadavers with mesenteric involvement however, had concomitant mediastinal lymph node involvement, indicating a diffuse lymph node involvement which may suggest a compromised immune system.

Isolated splenic involvement is an extremely rare form of extrapulmonary TB (Sheen-Chen *et al.*, 1995; Sharma *et al.*, 2007; Fooladi *et al.*, 2009; Zhan *et al.*, 2010). Fooladi *et al.* (2009) noted two forms of splenic TB, of which the first occurred as a result of disseminated TB, usually in those with compromised immune systems. This form of TB is common and the spleen

is the third most common organ to be involved with disseminated TB. From the findings from the present study, 21/127 (16.9%) cadavers had splenic involvement. Of those affected, 17/21 (81.0%) cadavers showed splenic involvement as a result of disseminated TB which is therefore consistent with the literature. The second form of TB described by Fooladi *et al.* (2009) is an unusual form and includes isolated involvement of the spleen in the absence of dissemination. This form of splenic TB was observed in 4/21 (19.0%) cadavers from our study cohort. The majority of research on the latter form of splenic TB is in the form of case reports (Sheen-Chen *et al.*, 1995; Fooladi *et al.*, 2009; Zhan *et al.*, 2010). From 1997 to 2003, 23 patients were hospitalized with isolated splenic TB in India (Sharma *et al.*, 2007). This amounts to approximately 3.3 patients per year at the particular institution in India, which is also a high burden country with regard to TB and HIV. Over a three year period in which the present study was performed, four cadavers presented with isolated splenic TB. This amounts to 1.3 cadavers per year. Although the prevalence of isolated splenic TB is relatively low in high burden countries compared to disseminated TB, the clinician's differential diagnosis of nodules or granulomas on the spleen, should include isolated splenic TB, even in the absence of disseminated TB.

Miliary hepatic TB is one of the most common manifestations in persons with pulmonary TB (Alvarez, 2006). Males have twice the risk for developing hepatobiliary TB compared to females (Alvarez, 2006). The reason for this is currently unknown. We found a slight male predilection with regard to hepatobiliary TB was observed (male to female ratio = 1.3:1). In regions where pulmonary TB occurs frequently, abdominal TB is common too, particularly in developing countries (Saluja *et al.*, 2007). From our results, one cadaver (0.8%) with hepatic TB presented

with intestinal TB, while splenic, renal and abdominal lymph nodal involvement was observed in 66.7%, 40.0% and 20.0% of the cadavers with hepatic TB, respectively. In the present study, hepatic granulomas were noted during gross dissection in 11/15 (73.3%) of the dissected livers, while 4/15 (26.7%) cases were diagnosed on microscopic level. Desai *et al.* (2006) stated that histopathological examination of hepatic tissue should not be the gold standard for TB diagnosis, as only one of their 76 subjects had caseating granulomas. Instead, the authors noted the importance of demonstrating acid-fast bacilli (AFB) within the granulomas as hepatic epithelioid cell granulomas can occur in primary biliary cirrhosis, chronic hepatitis, sarcoidosis and Crohn's disease (McCluggage and Sloan, 1994; Desai *et al.*, 2006). The interpretation of hepatic granulomas is therefore dependent on the clinical appearance as well as biopsy results (Dourakis *et al.*, 2007). In the present study, AFB was demonstrated in 9/15 (60.0%) of the cadaver's liver sections. The lack of AFB in the remaining livers could be due to three possible reasons. Firstly, it is possible that the samples were taken at an area in the liver with a low frequency of AFB. Secondly, the Ziehl-Nielsen (ZN) stain is not as sensitive to demonstrate AFB in formalin-fixed paraffin-embedded (FFPE) tissues (Hermans *et al.*, 1990; Berk *et al.*, 1993) compared to molecular techniques, such as polymerase chain reaction (PCR). And thirdly, it is possible that the AFB were missed during sectioning of the sampled tissues. It should furthermore be noted that the liver may be infected with *Mycobacterium avium-intracellulare* (MAI), especially in individuals with compromised immune systems. MAI infection produces AFB-positive granulomas within the hepatic parenchyma (Farhi *et al.*, 1986; Alvarez, 2006). In our study, differentiation between infections caused by MAI or MTBC could not be accurately determined, making it impossible to ascertain the causative agent in each of the cadavers.

Renal TB has a male predilection, usually occurs bilaterally in the renal medullae and occurs in patients between 20 and 40 years of age (Chun and Hale, 2004). The worldwide prevalence of renal and genital TB is unknown, especially in impoverished regions, as the majority of cases go clinically undetected. In this study, tuberculous granulomas were noted within the renal parenchyma of 13/127 (10.2%) of cadavers. An average age of 44.6 years (range 28-52 years) was observed which is only slightly higher than what is reported by Chun and Hale (2004). A female preponderance (1:1.9) was observed which is in contrast with the study by Chun and Hale (2004). To our knowledge, the present study is the first of its kind in the Western Cape and little is known about the distribution and sex disparity in renal TB in the Western Cape population. Females on average are more likely to develop lower urinary tract infection (UTI) compared to males (Harrington and Hooton, 2000). However, renal TB is almost always acquired as a result of hematogenous dissemination from the lung or other site (Eastwood and Corbishley, 2009). The female preponderance in our study can therefore not be ascribed to UTI, as none of the cadavers with renal TB exhibited signs of UTI. The initial renal granulomas are more commonly observed in the glomeruli of the renal cortex due to the increased blood flow and high oxygen tension in this area (Eastwood and Corbishley, 2009). This was the case in our cadavers with all the renal granulomas located within the renal cortex. Invasion into the loops of Henle was absent. Chronic renal failure (CRF) and end-stage renal disease (ESRD) are both clinical entities that are associated with and caused by TB (Eastwood and Corbishley, 2009), but are mainly diagnosed by urine and/or blood tests. Two of the most common causes of CRF include chronic pyelonephritis and renal hypertension. In our cadavers, CRF and ESRD could not be determined as we did not have knowledge of and access to urine and/or blood tests performed prior to death. We could however, observe and diagnose renal signs of hypertension, chronic pyelonephritis and

glomerulosclerosis in the cadaver cohort. Statistically significant associations were observed between renal TB and chronic pyelonephritis and renal TB and glomerulosclerosis in our cadaver cohort ($p < 0.05$), suggesting the presence of renal TB is associated with the presence of these conditions.

Ileocaecal tuberculosis is the most prevalent form of abdominal TB (Pereira *et al.*, 2005; Sharma and Ahuja, 2009). This increased prevalence of ileocaecal TB was observed in studies in Hong Kong (n=58 patients) (Leung *et al.*, 2006) and the UK (n=59 patients) (Singhal *et al.* 2005). In 18-36% of the subjects with abdominal TB in the Hong Kong and UK studies showed concomitant PTB infection (Singhal *et al.*, 2005; Leung *et al.*, 2006; Sharma and Ahuja, 2009). One of the two cadavers in the present study with gastrointestinal involvement, presented with TB in the ileocaecal region. Concomitant active pulmonary TB was observed in this cadaver. Tuberculous involvement of the jejunum is relatively uncommon and is usually associated with peritonitis (Pereira *et al.*, 2005). In our study, only 1/127 (0.8%) cadaver presented with jejunal TB without peritonitis. Non-specific mucosal ulcers were observed in the same cadaver and are consistent with findings from the study by Pereira *et al.* (2005). Both cadavers with jejunal and ileocaecal involvement showed extensive cavitory pulmonary TB which may explain the presence of gastrointestinal involvement as a result of dissemination. A direct association between cavitory pulmonary disease and gastrointestinal involvement has been shown in affected patients. This is consistent with continued exposure to infected swallowed material (Reuter *et al.*, 2009) Studies done in the US and South Africa, revealed that between 25% to 28% of subjects showed both gastrointestinal involvement and extensive cavitation in the lung (Bogen *et al.*,

1950; Pettengell *et al.*, 1990). These studies, together with the findings from the present study, illustrate the association between pulmonary cavitation and gastrointestinal involvement.

Pancreatic tuberculosis (PT) or peripancreatic lymph node tuberculous involvement is an extremely rare entity with only a few cases reported in the literature (Bhansali, 1977; Pombo *et al.*, 1998; Demir *et al.*, 2001; Akhan and Pringot, 2002; Chaudhary *et al.*, 2002; Xia *et al.*, 2003). The overall incidence of PT, even in the presence of splenic and hepatic tuberculous involvement, has been shown in the literature to be between 0% and 4.7% (Bhansali, 1977; Chaudhary *et al.*, 2002). Two cadavers (1.6%) in our study presented with PT in the pancreatic heads, which is according to Akhan and Pringot (2002) the most common site for PT lesions. Chaudhary *et al.* (2002) demonstrated the need for histopathology in the diagnosis of PT. In the two cadavers, PT was an incidental finding during histologic evaluation, thus also illustrating the need for histopathology in diagnosing PT. Concomitant active PTB as well as splenic and hepatic tuberculous involvement were observed in both cadavers with PT. Calcification, a common associated finding (Denton and Hossain, 1993; Akhan and Pringot, 2002), was absent in both cadavers. Pancreatic TB generally occurs in two subsets of patients; those who reside in areas where TB is endemic and those with compromised immune systems (Bhansali, 1977; Desai *et al.*, 1991; Evans *et al.*, 2000; Chaudhary *et al.*, 2002). Both cadavers with PT from our study, originated primarily from a high TB burden area.

The gallbladder is an unlikely organ to be affected by primary TB due to the inhibitory effects of bile on mycobacterial growth (Kumar *et al.*, 2000; Vanhoenacker *et al.*, 2004; Ramia *et al.*, 2006; Ramesh *et al.*, 2008). The incidence of gallbladder TB (GT) has been shown to coincide

with severe abdominal tuberculosis and generally presents as miliary TB affecting the peritoneum, mesentery and lymph nodes (Kumar *et al.*, 2000; Vanhoenacker *et al.*, 2004). Cholelithiasis and duct obstruction are regarded as essential for the development of GT (Ramia *et al.*, 2006; Xu *et al.*, 2011). In our study, one cadaver (0.8%) had GT with pulmonary TB and no concomitant EPTB involvement, which is in contrast with findings from other studies. Cholelithiasis was observed in this cadaver and a ZN stain revealed several AFB. A large, thick-walled mass containing an unspecified brown-colored fluid with small pigment stones was observed which has been described by Vanhoenacker *et al.* (2004) as characteristic of GT.

In developing countries, genitourinary TB is another common form of EPTB (Çek, 2009). Testicular TB occurs less frequently compared to prostatic or epididymal TB (Gorse and Belshe, 1985; Çek, 2009). In our study, one cadaver presented with solitary testicular TB, while no female genital TB was observed. Concomitant renal TB was observed in the cadaver with testicular TB. In studies done by Christensen (1974) and Simon *et al.* (1977), concomitant renal TB was a common finding in the subjects with genital TB.

Tuberculous myocarditis is extremely rare and lethal form of TB (Ilgazli *et al.*, 2004; Mayosi, 2009). Tuberculous pericarditis on the other hand, is a more common form of cardiac TB in developing countries and in particular those with a high burden of TB (Ilgazli *et al.*, 2004). This is in contrast with our findings as no cardiac TB was observed in our cadavers who originated mainly from the Western Cape, a high TB burden province in South Africa.

Central nervous system (CNS) TB may present in all age groups, however, the majority of patients are generally below the age of 20 years (Bernaerts *et al.*, 2003). Of all the EPTB manifestations, tuberculous meningitis (TBM) is clinically the most severe form (Brancusi *et al.*, 2012). HIV-negative individuals with TBM have a mortality of 25% compared to the 67% mortality in HIV-positive individuals with TBM (Thwaites *et al.*, 2004; Török *et al.*, 2011; Brancusi *et al.*, 2012). In our study, neither TBM nor parenchymal tuberculomas were observed in the brains of the cadaver cohort.

Only 1/124 (0.8%) cadaver showed macroscopic signs of skeletal TB (spinal TB). This may be due to a number of reasons. A total of 76.4% of the cadaver cohort presented with pulmonary TB of which the majority had extensive granulomatous lesions with necrosis. It may be that the immune system of the individuals was unable to effectively control the mycobacterial invader. The individuals therefore succumbed to their illness prior to dissemination to the skeletal system. According to a study done by Zink *et al.* (2001), osseous tuberculous involvement was observed in less than 10% of the patients suffering from chronic tuberculosis. The authors described the osseous involvement as a result of hematogenous dissemination from pulmonary and intestinal TB as being a “rare event” (Zink *et al.*, 2001). This may explain the absence of skeletal TB involvement in our cadaver cohort.

According to the literature, men have a predilection to develop TB in developing countries compared to women (Caracta, 2003; Austin *et al.*, 2004; Balasubramanian *et al.*, 2004, Neyrolles and Quintana-Murci, 2009). The increased prevalence of TB-positive males is seen in all regions of the world and is not necessarily restricted to developing countries (Neyrolles and Quintana-

Murci, 2009). Prevalence studies have revealed that females have a higher progression rate from infection to disease, particularly in women of childbearing age between 15 and 40 years (Caracta, 2003; Austin *et al.*, 2004; Crampin *et al.*, 2004). Yet, there is a concern that females with TB may go unnoticed due to several socio-cultural factors, including reduced access to healthcare and stigmatization (Caracta, 2003; Austin *et al.*, 2004; Balasubramanian *et al.*, 2004). In a study by Balasubramanian *et al.* (2004), a decrease in the prevalence of TB was observed among females from South India due to increased access to healthcare and success in treatment, therefore disproving the notion that female TB-positive patients were under-notified. Differences in immune responses between males and females may account for the sex disparities in the prevalence of TB. Female gonadal steroid hormones, such as estrogen, may play a subtle role in the symptoms and outcomes of pulmonary TB (Caracta, 2003). Recent studies have shown that estradiol enhances activation of macrophages (Neyrolles and Quintana-Murci, 2009). Furthermore, females less than 45 years of age may have an increased access to healthcare, as they usually take their children to clinics and public hospitals for immunizations (Balasubramanian *et al.*, 2004). It is believed that heavy alcohol consumption and smoking contribute to the sex disparity (Chan-Yeung *et al.*, 2002). In a survey study to investigate alcohol consumption trends in South Africa, males were shown to consume on average, more alcohol compared to females (Peltzer and Ramlagan, 2009). We did not have information on the alcohol and smoking history of the cadavers in this study, however, in the Western Cape, the proportion of males abusing alcohol and smoking is likely higher than females. In our cadaver cohort, no statistical significant difference in the prevalence of pulmonary TB between males and females was noted ($p > 0.05$). In addition to the small population number ($n=127$), the male to female

ratio of our cadaver cohort was 1.1:1 and could explain the absence of a sex disparity in our cadavers.

Despite the global sex disparity in tuberculosis rates, little research has focused on the association between EPTB and sex. In a cross-sectional study done in Hong Kong in 2002, EPTB occurred more commonly in females compared to men (Noertjojo *et al.*, 2002). Similarly, a hospital-based, retrospective study performed in Nepal, revealed a higher predilection for EPTB involvement in female patients (Sreeramareddy *et al.*, 2008). A statistically significant association was observed between the prevalence of EPTB and sex in our cadaver population ($p < 0.05$). Females showed an increased predilection for EPTB involvement. The sex disparity observed with EPTB suggests that female responses may facilitate the development of EPTB (Musellim *et al.*, 2005).

In our study, the spleen, liver and lymph nodes were the most common sites of EPTB. A number of studies in different regions of the world revealed a variable localization of EPTB among the different populations. The genitourinary system and skin were most commonly affected by EPTB in Hong Kong (Noertjojo *et al.*, 2002), whereas bone and joint involvement were common in the United States (Yang *et al.*, 2004) and Taiwan (Lin *et al.*, 2009). The results from the present study are comparable to studies from Turkey (Musellim *et al.*, 2005), Nepal (Sreeramareddy *et al.*, 2008) and Germany (Geldmacher *et al.*, 2002). Noertjojo and coworkers observed a difference in the site of organ involvement in EPTB between HIV-positive and – negative patients as well as between males and females (Noertjojo *et al.*, 2002). It was observed that HIV-positive patients tended to present more often with miliary TB compared to HIV-

negative patients. In addition, females had a tendency to develop lymph node disease, whereas males had pleural disease (Noertjojo *et al.*, 2002).

5.1.3 Risk Factors for Tuberculosis

It has been shown that certain ethnic groups are more susceptible to *M. tuberculosis* infection, compared to others (Stead *et al.*, 1990; Thwaites *et al.*, 2000). Studies suggest that underweight black individuals are more prone to *M. tuberculosis* infection compared to white individuals (Stead *et al.*, 1990; Thwaites *et al.*, 2000). It has been proposed that the human genetic makeup may influence susceptibility to mycobacterial infection. This has been confirmed when polymorphisms in the human *NRAMP1* gene resulted in increased susceptibility to *Mtb.* infection, particularly in the West African population (Bellamy *et al.*, 1998; Thwaites *et al.*, 2000). Differences between ethnic groups have been observed in the clinical course and pathologic features of PTB (Rich, 1951; Stead *et al.*, 1990). Black individuals had a more rapid clinical course with caseating necrosis (Rich, 1951).

The association between pulmonary TB and body habitus has been widely reviewed for years (Davies, 2005). Numerous studies have shown that thin, underweight individuals have a significantly higher risk of developing TB compared to individuals with a body mass index (BMI) within normal limits (Tverdal, 1986; Davies, 2005; Lönnroth *et al.*, 2010). Obesity on the contrary, has been linked with a significantly decreased risk of active pulmonary TB, particularly in the elderly (Leung *et al.*, 2007). Malnutrition has long been regarded as a connection between body mass and TB, but this does not clarify the decreased risk associated with obesity (Leung *et al.*, 2007). The effect of body mass is observed in adults of all ages (Leung *et al.*, 2007). The

phenomenon of an increased BMI with a concomitant decreased risk of active disease is only observed with regards to PTB. EPTB on the other hand, does not conform to the risk-lowering effect of a high BMI. Usually, EPTB is associated with compromised immunity, which could explain this finding (Leung *et al.*, 2007). The average weight and BMI of the cadavers from our study were 45.3kg and 16.5, respectively. This suggests that the cadavers from the present study were generally underweight. Three possible factors may explain the relatively low average weight and BMI. Firstly and perhaps the most important factor, the cadavers in the present study were typically malnourished as the majority originated from communities with a low socio-economic status (SES) and were in some cases homeless. The association between SES and health status of a population has been established in the past (Adler *et al.*, 1994; Davies, 2005). Poverty, defined in financial terms as a low income per capita, has been linked to an increased susceptibility to pulmonary TB and HIV infection (Bates *et al.*, 2004; Harling *et al.*, 2008). A low per capita income together with a high rate of population growth will result in insufficient provision of public health services (Labuschagne and Mathey, 2000). Poor housing, overcrowding, poor hygiene and water supplies, can lead to decreased nutrition and consequently reduced immunity (Darbyshire, 1995; Moss *et al.*, 2000; Govender *et al.*, 2011). Homelessness has been reported as a major risk factor of pulmonary TB (Moss *et al.*, 2000). Houses in informal settlements generally have poor structural integrity with damp interiors which together with overcrowding is favorable for the spread of *M. tuberculosis* (Govender *et al.*, 2011). People residing in impoverished areas frequently fail to manage chronic diseases as they lack preventative healthcare (Govender *et al.*, 2010). An improved SES, on the other hand, has been linked to a decline of tuberculosis (Leung *et al.*, 2007). As approximately 90% of our cadavers are unclaimed individuals with no medical history available, the possibility exists that the

majority of these cadavers were socio-economically deprived and homeless which put them at an increased risk of developing TB.

In addition to housing and SES, Williamson *et al.* (1987) and Addolorato *et al.* (1998) observed a reduced body weight in individuals with a daily heavy intake of alcohol, particularly in chronic alcoholics. The connection between heavy alcohol consumption and TB has been shown in several studies in the past (Davies, 2005). Increased rates of alcohol use in communities with low SES have led to increased additional burdens on previously under-resourced public services (London *et al.*, 1998). Alcohol consumption has been associated with an increased risk of pulmonary TB (Rehm *et al.*, 2010). Poor nutrition and excessive alcohol consumption go hand in hand and has been shown to impair immune status (Davies, 2005). In our cadaver cohort, a statistically significant association was observed between the prevalence of TB and liver disease associated with heavy consumption of alcohol ($p < 0.05$). In addition to alcohol abuse, smoking has been implicated as an independent cause of reduced body weights (Williamson *et al.*, 1987). Smoking and alcohol abuse either in isolation or in combination with each other, may explain the findings from our study. A strong statistically significant association exists between smoking and tuberculosis (Davies, 2005). Numerous studies have confirmed this notion, particularly in China (Yu *et al.*, 1988) and India (Gajalakshmi *et al.*, 2003). The potential importance of the association between tenacious smoking and PTB could not be investigated in our cadaver population as the smoking history in our cadavers could not be determined.

PTB is a common wasting disease and is responsible for weight loss and deficiencies of macro- and micronutrients of the infected individual (Cegielski and McMurray, 2004; Lönnroth *et al.*,

2010). It is possible that the low body weights are due to the presence of PTB in our cadavers. To our knowledge little is known about dead versus live body weight measurements in humans. There is a possibility that the postmortem weights may differ slightly from antimortem measurements. A statistically significant association between TB incidence and a low BMI has been demonstrated (Bates *et al.*, 2004; Cegielski and McMurray, 2004; Lönnroth *et al.*, 2010). In our study, a lower BMI was reported with the presence of TB; however, this was not statistically significant ($p > 0.05$). One possible explanation exists for this finding. The total skeletal height (TSH) was estimated for each cadaver by using the left femur length. The equations to determine TSH in Negroid and Caucasian populations were developed by Lundy and Feldesman (1987) and Dayal (2003), respectively. To our knowledge, no equation has been developed to estimate TSH in mixed race populations, however, for this study, the equation by Lundy and Feldesman (1987) was used to determine the TSH in mixed race individuals. This was confirmed by Prof. Maryna Steyn, forensic anthropologist, Pretoria University (Personal interview, June 2, 2014). It is therefore possible, however, that the calculated BMI values from the weights after death and femur lengths differed slightly from the BMI values of the cadavers prior to death.

Since the beginning of the HIV/AIDS epidemic in the early 1980's, a strong association between TB and HIV became apparent (McShane, 2005; Lawn and Churchyard, 2009). This co-epidemic is extremely common in the Sub-Saharan countries (Lawn and Churchyard, 2009). Patients infected with HIV and TB has an increased mortality risk (McShane, 2005). In addition, differences in mortality risks between sexes have been observed, with a 1.6% higher mortality risk in females compared to males (Lawn and Churchyard, 2009).

5.1.4 Systemic Pathology

5.1.4.1 Pulmonary System

Pneumonias have been classified into lobar pneumonia, bronchopneumonia and interstitial pneumonia (Fraser *et al.*, 1994; Reittner *et al.*, 2003). Broncho- and lobar pneumonias are commonly confined to the alveolar spaces, while interstitial pneumonias are commonly associated with a parenchymal distribution (Fraser *et al.*, 1994; Reittner *et al.*, 2003). An impaired immune system and subsequent increased susceptibility to infections has been associated with heavy alcohol consumption (Rehm *et al.*, 2009). In a study by Samokhvalov *et al.* (2010), a strong statistical association was observed between alcohol consumption and community-acquired pneumonia (CAP) and nosocomial pneumonia. In our study, information on patterns of alcohol consumption prior to death was not known. We did, however, observe liver disease associated with heavy alcohol consumption, such as cirrhosis and hepatic steatosis. When comparing alcoholic liver disease with the prevalence of pneumonia in our cadaver cohort, a statistically significant association was observed between these two conditions ($p < 0.05$). While an atypical CAP is commonly caused by bacterium (i.e. *Mycoplasma spp.*) or viruses (i.e. Influenza-virus) and has a similar appearance to lymphocytic interstitial pneumonitis (LIP), some differences do occur. Lymphocytic interstitial pneumonitis is a benign lymphoproliferative disorder commonly found in individuals with compromised immune systems, such as those with autoimmune disorders or HIV/AIDS (Sharland *et al.*, 1997; Jikhoh *et al.*, 2000). In addition to this, LIP is much more common in HIV-positive children; however adults may also be affected. In this study, two cadavers presented with signs typically seen in LIP. Although information regarding the etiologies of the pneumonitis/pneumonia is not known, we postulate that the observable findings may suggest a LIP infection.

The critically ill are at increased risk for aspiration pneumonia (Marik, 2001). The three cadavers in our study with aspiration pneumonia were all males with signs of extensive PTB. One cadaver presented with acute lung injury (ALI) and pneumocystis pneumonia (PCP), one with chronic bronchitis and fat embolism amongst others and the other cadaver with PTB only. In all of these cadavers, the conditions or diseases were severe, suggesting these cadavers were critically ill prior to death. Aspiration pneumonia is usually associated with increased age, but the average age of the cadavers in our study was 40.5 years. However, the fact that the cadavers showed signs of severe systemic disease during gross dissection and histopathology, may explain the younger age in our cadaver population with ALI/ARDS.

A male predisposition for emphysema has been reported (Dransfield *et al.*, 2007; Martinez *et al.*, 2007; Grydeland *et al.*, 2009). The sex disparity in our cadaver study is consistent with these studies. One possible explanation for the male preponderance for emphysema in the general population and in our study is that males are more exposed to occupational airborne agents as well as passive smoking, particularly in the first decade of life (Grydeland *et al.*, 2009). This is due to increased exposure to parental smoking as boys are more likely to be surrounded by adult male smokers, compared to girls of the same age (Grydeland *et al.*, 2009). It has furthermore been shown that an increase in age results in an increased prevalence of emphysema (Gevenois *et al.*, 1996; Grydeland *et al.*, 2009). The average age of cadavers with emphysema was 52.7 years (30-80 years). A total of 41.1% of the cadavers with emphysema was 50 years and older.

Chronic bronchitis, another condition grouped under chronic obstructive pulmonary disorder (COPD), was observed in our cadaver cohort with a male preponderance (3.5:1). The male

predilection was in accordance with the literature (Ferris and Anderson, 1962; Menezes *et al.*, 1994; Albalak *et al.*, 1999), however, in a study by Pandey (1984), males and females were affected equally by chronic bronchitis. An increase in the prevalence of chronic bronchitis above the age of 40 years has previously been reported (Menezes *et al.*, 1994) and in support of this the average age of cadavers with chronic bronchitis in this study was 49.0 years (range 39-72 years). No signs of chronic bronchitis were found in cadavers younger than 39 years.

Bronchiectasis (BE), described as permanent and abnormal dilation of bronchi and bronchioles, is usually associated with chronic pulmonary inflammation (Cohen and Sahn, 1999; Karakoc *et al.*, 2001; Weycker *et al.*, 2005; O'Donnell, 2008; Seitz *et al.*, 2010; Kumar *et al.*, 2013). The incidence of BE in developed countries has declined due to vaccination and effective treatment against major viral and bacterial pulmonary illnesses (Karakoc *et al.*, 2001). BE, however, remains a major problem and complication of chronic pulmonary inflammation in developing countries (Nikolaizik and Warner, 1994; Karakoc *et al.*, 2001). A statistically significant association was seen between BE and pneumonia in our cadaver cohort ($p < 0.05$). Although our findings were in accordance with findings from other studies (Nicotra *et al.*, 1995; Cohen and Sahn, 1999; Pasteur *et al.*, 2000; Karakoc *et al.*, 2001), little is known about the prevalence of BE in a Western Cape population with a high burden of TB. The present study therefore fills this void. BE is more prevalent amongst women when compared to men as well as in older individuals (Nicotra *et al.*, 1995; O'Donnell *et al.*, 1998; Pasteur *et al.*, 2000; Weycker *et al.*, 2005). This was in contrast with findings from our study. The male to female ratio of our cadaver cohort was 2.3:1, meaning that males were twice as common affected by BE than females. The fact that the majority of our cadaver cohort was males, could explain this sex disparity amongst

our study subjects. The average age of our cadavers affected by BE was 53.7 years. According to Weycker *et al.* (2005), an increase in prevalence is noted after 45 years of age (range 22 – 72 years) and it further increases exponentially with an increase in age. In our study, 57.1% of the cadavers with BE were older than 45 years supporting the notion that BE is more prevalent with increasing age. On the other hand, BE was observed in 26.5% cadavers under the age of 45 years. A statistically significant association was observed between BE and PTB ($p < 0.05$). This suggests that due to the presence of PTB in younger individuals in our cadaver cohort, BE is likely to occur in conjunction with PTB in younger individuals in our cadaver cohort.

Acute lung injury (ALI) and its severe form acute respiratory distress syndrome (ARDS) have a direct effect on the lungs and are generally found in the critically ill (MacCallum and Evans, 2005). There is a lack of epidemiological and population-based evidence in developing countries with regards to ALI. The present study therefore is the first to report the prevalence of ALI and ARDS in a high burden TB community from a developing country. In the present study, males were more commonly affected by ALI/ARDS than females. This appears to be consistent with studies conducted in developed countries, such as the US (Moss and Mannino, 2002). In addition, black individuals were shown to be more commonly affected by ALI/ARDS together with an overall higher mortality rate (Moss and Mannino., 2002; Rubinfeld and Herridge, 2007; Erickson *et al.*, 2009). In our study, no white cadavers presented with ALI/ARDS, while ALI/ARDS were found in the majority of mixed race cadavers. Two possible explanations may be given for the observed ethnic disparity. Firstly, differences in SES may determine the severity of the disease in the different ethnicities. This phenomenon was also reported by Moss and Mannino (2002) and Erickson *et al.* (2009). And secondly, the mixed race cadavers constituted

the majority of cadavers in our cadaver cohort. This may explain the preponderance of mixed race cadavers affected by BE in our study.

Cytomegalovirus (CMV) infection has been associated with ALI/ARDS in the past (Simmons *et al.*, 1979; Fowler *et al.*, 1983). Females, particularly of child-bearing age, are more prone to CMV infection which in addition contributes to vertical transmission to unborn fetuses (Staras *et al.*, 2006). In our study, two cadavers which were both females presented with CMV infection. Furthermore, a low SES has also been linked to increased risk for CMV infection (Staras *et al.*, 2006). Our cadavers are mainly from low socio-economic backgrounds, which is most likely a predisposing factor in our cadaver cohort. In a study by Morgello *et al.* (2002), CMV was the most common infection in a HIV-infected population over a period of 20 years, thus suggesting that CMV infection is a common AIDS-defining disease. Sepkowitz (2002) reported a 12% incidence of CMV infection as an AIDS-associated infection in individuals without highly active antiretroviral therapy (HAART), while severe CMV infections were rare in immune competent individuals (Sepkowitz, 2002). We can only speculate about the role of HIV in CMV infections in our cadaver cohort as the HIV statuses of the cadavers were unknown. A common fungal infection resulting in ALI/ARDS is *Pneumocystis jiroveci* (formerly referred to as *Pneumocystis carinii*). Morgello *et al.* (2002) reported that 29.0% of their reviewed autopsy cases (n=394) were infected with pneumocystis pneumonia (PCP) with an observed male preponderance. We found similar results as 3.9% cadavers in our study presented with PCP with an observed male predominance.

Lung carcinoma is one of the most common malignancies and accounts for just under 20% of all deaths related to carcinomas (Pomplun, 2007). The incidence of lung cancer has been shown to be associated with population-related smoking behavior (Lopez-Abente *et al.*, 1995; Pomplun, 2007). Squamous cell carcinoma (SCC) has the strongest relationship with tobacco smoke inhalation followed by adenocarcinoma (ACA). Adenocarcinoma *in situ* (AIS) has a relatively low incidence in most published reports (Sider, 1990; Bonomo *et al.*, 1998). No association with AIS and smoking has been determined (Stull *et al.*, 1990; Bonomo *et al.*, 1998). Doll and Hill proposed two possible causes for the increase in pulmonary carcinomas: 1) general atmospheric pollution, especially in urban areas as a result of fumes emitted from motor vehicles, industrial plants and open fires and 2) tobacco smoke inhalation (Doll and Hill, 1950). Small cell carcinomas and SCC's are most likely caused by heavy smoking, while ACA may be encountered in lighter smoking (Sridhar and Raub, 1992; Travis *et al.*, 1996). For this study, a history of smoking was unavailable and it is therefore not known whether the individual was a smoker prior to death.

Pulmonary hypertension (PH) occurs as a result of advanced chronic pulmonary disease (Rich *et al.*, 1989; Beiderlinden *et al.*, 2006). Patients with ARDS frequently manifest with PH (Tomashefski *et al.*, 1983; Squara *et al.*, 1998; Beiderlinden *et al.*, 2006), however the severity of ARDS has not been correlated with the prevalence of PH. Generally, PH is determined by measuring the mean pulmonary artery pressure (≤ 25 mmHg), pulmonary artery trunk (≥ 29 mm) and the finding of right ventricular failure (Beiderlinden *et al.*, 2006). In our cadavers, however, longstanding or chronic PH most probably contributed to the morphologic changes observed in the pulmonary parenchyma. These changes were visualized with the Verhoeff's stain and

included hypertrophy of the arterial tunica media. Regarding sex and age, more males were affected than females in our study (1.4:1) and the average age of the affected cadavers was 47.7 years (36-60 years). Rich *et al.* (1989) noted that males are more likely to develop PH and the prevalence increases after the age of 34 years (Rich *et al.*, 1989). Our findings are therefore in accordance with the findings by Rich *et al.* (1989). To our knowledge, little if any, has been reported on the frequency of right or left lung involvement in PH. The majority of research focuses on the vasculature involved rather than pulmonary site. In our study, unilateral involvement of the right lung was seen in all of the cadavers affected by PH. This suggests that the right lung may have a slight tendency for the development of PH compared to the left lung in our cadavers.

Bone marrow (fat) emboli are common complications of orthopedic procedures and long bone fractures (Glazer and Onion, 2001; Mellor and Soni, 2001; Gupta and Reilly, 2007). The prevalence of fat embolism syndrome (FES), a condition described by hypoxia, change in mental status and bilateral pulmonary infiltration, is generally between 0.25% and 1.25% in fracture patients (Peltier, 1969; Glazer and Onion, 2001; Mellor and Soni, 2001). Due to the lack of a medical history of the cadaver, the presence of FES could not be determined. What we do know however, was that a solitary fracture of the right sixth rib was present and that unilateral involvement of the right lung was observed, making the probability of FES prior to death unlikely.

5.1.4.2 Cardiovascular System

Enlargement of the heart, or cardiomegaly, is a common sign of ventricular dysfunction (Kannel, 2000). In living patients, chest X-ray (CXR) is the gold standard in determining cardiomegaly and it is diagnosed when the heart measures more than 50% of the transthoracic diameter (Levy *et al.*, 1988; Geokas *et al.*, 1990; Frishman *et al.*, 1992; Corne and Pointon, 2010). When the Lodox[®] full-body digital X-rays of the cadavers were evaluated, the hearts of 30/127 (23.6%) cadavers measured more than 50% of the transthoracic diameter. When the hearts were inspected during gross dissection, only two hearts weighed more than 500g and were classified as being enlarged. The large discrepancy may be due to the fact that the cadavers were in the supine position when the X-rays were taken and because an inspiration-effort from the cadavers was absent. This may have resulted in the heart appearing larger than usual (Corne and Pointon, 2010). The 23.6% of the cadavers with signs of cardiomegaly was therefore an over-estimation when both the limitations were taken into account and the true prevalence of cardiomegaly could therefore not be determined using this approach.

Two autopsy studies revealed a patent foramen ovale (PFO) incidence of 27.3% (n=965) and 29.0% (n=1100) (Thompson and Evans, 1930; Hagen *et al.*, 1984). The size of the PFO in both studies ranged from 1.0mm to 20.0mm. The PFO in our study measured an area of 20x30mm. These measurements were made in embalmed tissue and may be less than what is expected should the hearts not been embalmed. Hagen *et al.* (1984) observed a decrease in the fibro-elasticity of the heart as a result of formalin-fixation. An increase in the average size of PFO has been associated with an increase in age (Hagen *et al.* (1984). Unfortunately, the age of the cadaver with the PFO in our study was not available.

A St. Jude mechanical valve prosthesis (St. Jude Medical Inc., St. Paul, Minnesota) was observed in one male cadaver in our study. Fibrotic growth was noted on the lateral disc of the mechanical prosthesis. In a retrospective study to determine the occurrence of structural dysfunction of the St. Jude valve, no dysfunction or measurable wear and tear was observed in 1112 patients with this particular valve (Baudet *et al.*, 1995). An increased risk for thromboembolism exists with patients with St. Jude mechanical valve prosthesis (Emery *et al.*, 2005).

Degenerative aortic valvular disease, defined as increased leaflet thickness, stiffening and calcification of the aortic valve, is a common finding in the elderly (Boon *et al.*, 1997; Stewart *et al.*, 1997). Virmani *et al.* (1991) and Lindroos *et al.* (1993) noted an increase in the aortic circumference with age. Similarly, Singh *et al.* (1999) reported age as an influential factor on the prevalence of valvular disease. The average age of the cadavers with aortic valvular disease in our study was 57.0 years (range 32-73 years) and 83.3% of all cadavers were older than 50 years, supporting the observations made by Virmani *et al.* (1991) and Lindroos *et al.* (1993). Apart from aging, smoking and hypertension were confirmed to be risk factors for calcific aortic stenosis (Virmani *et al.*, 1991; Stewart *et al.*, 1997). As mentioned earlier, information of the smoking habits of the cadavers prior to death was unavailable. Little can therefore be said regarding the effects of smoking on the degree and prevalence of valvular disease in our cadaver cohort. In terms of valvular circumference measurements, this study has three limitations to consider. Firstly, the valvular circumferential measurements were obtained from the 2012 and 2013 cadaver cohort (n=87). The 2011 cadaver cohort formed part of the pilot study and these measurements were not taken in this cohort. We could therefore only ascertain valvular disease

in two cadaver cohorts. Secondly, cadavers who presented with valvular abnormalities with unknown age were excluded from this part of the study. This was done to determine stenosis based on sex and age and to be able to compare the measurements with data from Sunderman and Boerner (1949) and Kitzman *et al.* (1988). Lastly, the cadavers were formalin-fixed and the effects of formalin on the measurements of the heart and its structures are unknown. Hagen *et al.* (1984) previously noticed shrinkage in the fibro-elasticity of the heart as a result of formalin-fixation. The effects of formalin on the cardiac valves, however, remain unclear.

Although the effects of formalin-fixation on the structures of the heart remain unclear, we compared our findings with autopsy measurements by Sunderman and Boerner (1949) and Kitzman *et al.* (1988). Mitral stenosis was observed in 24/87 (27.6%) cadavers. Mitral valve stenosis is believed to be initiated by a rheumatic insult following a streptococcal infection (Selzer and Cohn, 1972). Roberts (1983) observed mitral stenosis in 434 patients and all were rheumatic in origin. One cadaver presented with macroscopic signs of rheumatic valvular disease (RVD). Mitral annulus calcification which is a frequent occurrence in the elderly (Boon *et al.*, 1997) was absent in our cadavers. The possibility still remains that formalin-fixation may cause a postmortem contraction of the mitral valvular ring and thereby artificially inducing mitral valvular stenosis in the cadavers.

Coronary heart disease (CHD) is uncommon in premenopausal females compared to males of similar age (Williams *et al.*, 1990; Roeters van Lennep *et al.*, 2002). Ovarian estrogen and its role in modulating impaired endothelium-mediated dilation of atherosclerotic coronary arteries have been implicated in reducing the risk for CHD (Williams *et al.*, 1990; Roeters van Lennep *et*

al., 2002). In our study, the male to female ratio for CHD was 1.2:1. The average age of the females affected by occlusive coronary artery disease (CAD) in our study was 51.5 years (range 28-73 years). The one female cadaver of 28 years with 30% luminal occlusion in the left anterior descending (LAD) coronary artery was the exception with regard to age. The average age of the males affected was 55.7 years. Our findings are therefore in agreement with the findings from the literature which suggests that females of premenopausal age are less likely to develop CHD as a result of CAD compared to males of a similar age.

Calcification of the coronary arteries occurs almost entirely in atherosclerotic plaques (Sangiorgi *et al.*, 1998). As a function of sex and age, the prevalence of calcification ranged from 14% in young adults to 70% in the elderly (Goel *et al.*, 1992; Janowitz *et al.*, 1993; Sangiorgi *et al.*, 1998). Coronary arterial calcification was observed in 18/42 (42.9%) cadavers in our study. Males were more commonly affected (77.8%) compared to females (22.2%). This male preponderance in our study is in agreement with the study from Goel *et al.* (1992) who observed a male predisposition for coronary artery calcification in 597 patients. In a large study by Hoff *et al.* (2001) to investigate coronary artery calcium in 35 246 adults, it was uncommon for males younger than 40 years and females younger than 50 years to be affected by coronary arterial calcification. In our study all the males with coronary artery calcification were older than 40 years and the females older than 50 years, with the exception of one female. Bosma *et al.* (2005) observed an increased prevalence of smoking and hypertension among individuals from a low SES and suggested that individuals from low SES have a higher risk of coronary heart disease. The prevalence of CHD in our cadaver cohort therefore confirms this notion as most cadavers

are of low SES. Roeters van Lennep *et al.* (2002) and Khot *et al.* (2003) confirmed smoking and hypertension as risk factors for CHD.

Myocarditis, inflammation of the myocardial wall, often goes clinically silent and a microscopic evaluation is needed for a final diagnosis (Passarino *et al.*, 1997). Myocarditis is therefore not easily detected in the clinical setting and the majority of myocarditis research is based on autopsy studies. Passarino *et al.*, (1997) reported very similar frequencies of myocarditis in men and women. Three males and one female had microscopic signs of myocarditis in this study. The sex bias seen in our study is possibly attributed to the low number (4 of the 127) of cadavers affected by myocarditis. The average age of the cadavers affected was 47.0 years, which is in accordance with incidence studies from Finland. In this population-based study by Kytö *et al.* (2007), the range of ages at which the most deaths as a result of myocarditis occurred, was between 35 and 54 years.

Lipofuscin, the pigment commonly found in aged organs such as the heart and brain, is a remnant of indigestible intralysosomal material (Terman and Brunk, 2004). There are strong indications that lipofuscin pigment deposition within organs promotes age-related pathology such as heart failure (Terman and Brunk, 2004). In fact, several pathological conditions, malnutrition and tumors are associated with increased pigment deposition (Brunk and Terman, 2002). In our study, lipofuscin deposition was observed in 10.2% cadavers. In the majority of the cadavers, cardiac involvement was observed with no lipofuscin deposition observed in the brains. The cadaver brains were at a more advanced stage of decomposition at the time of macroscopic dissection and this was particularly evident when the histology was evaluated. The

decomposition made it less likely to observed age-related pathology such as lipofuscin deposition.

Hypertrophic obstructive cardiomyopathy (HOCM) is an idiopathic condition characterized by septal and left ventricular hypertrophy without dilation and obstruction of the left ventricular outflow tract (Shapiro and McKenna *et al.*, 1983; Heric *et al.*, 1995). HOCM is not only a disease of the young and middle-aged, but has also been implicated in the elderly (Davies *et al.*, 1974; Pomerance and Davies, 1975). In fact, mild myocardial hypertrophy without dilation is one of the effects of the normal ageing heart (Levy *et al.*, 1988; Geokas *et al.*, 1990; Frishman *et al.*, 1992). In our study, the average age of cadavers with signs of HOCM was 35.5 years. This is in accordance with the literature and suggests that the HOCM in our cadavers were not as a result of normal ageing, but rather other causes, such as underlying valvular disease. HOCM has been shown to be relatively rare as the prevalence has been reported to be 0.2% (1:500) (Maron, 2002). In our study, 3/127 cadavers presented with signs of HOCM, making the prevalence 2.4%, which is higher than reported. In terms of wall thickness, in the cadavers with HOCM, hypertrophy of the left ventricle and septum were observed. In all the cadavers investigated, the left ventricular and septal wall thickness measured more than 14mm and 13mm in maximum width, respectively. Similar findings were observed by Shapiro and McKenna (1983) who observed an increased thickness in the left ventricular and septal walls. When our findings were compared with results from Sunderman and Boerner (1949) and Kitzman *et al.* (1988), it was evident that our cadavers with HOCM had ventricular wall measurements above the normal spectrum, thus illustrating ventricular wall hypertrophy in all of our cadavers with HOCM. Aronow *et al.* (1997) observed no statistically significant difference in prevalence of HOCM

between males and females. In addition, it should be noted that dilatation and hypertrophy are common findings in hearts examined post mortally (Murphy *et al.*, 1988). Therefore, the hypertrophic hearts in our study may possibly be as a result of post mortal changes.

In a population-based study done by Singh *et al.* (2001) to assess the prevalence and risk factors for abdominal aortic aneurysm (AAA), it was reported that smoking, age, hypercholesterolemia and hypertension were the common risk factors associated with AAA. Similar findings were observed by Simoni *et al.* (1995), Lederle *et al.* (1997), Naydeck *et al.* (1999) and Wilmink *et al.* (1999). Wilmink *et al.* (1999) suggested that smoking enhances elastin degradation within arterial walls. Sex differences have been noted, with men affected nearly four times more frequently than women (Singh *et al.*, 2001). This finding is consistent with our study where the majority of the cadavers with AAA were male (male to female ratio = 1.6:1). We observed higher frequencies of small AAAs than large AAAs and this is in agreement with other studies where the increased prevalence of smaller AAAs has been reported (Simoni *et al.*, 1995; Lederle *et al.*, 1997; Naydeck *et al.*, 1999).

Aortic dissections have been shown to be more common in males between 50 and 60 years and in females older than 60 years (Anagnostopoulos *et al.*, 1972). Under the age of 40 years no sex disparity has been observed (Dow *et al.*, 1966; Anagnostopoulos *et al.*, 1972). In our study, only one male cadaver was affected and in this case, the external iliac artery was involved, instead of the aorta. Aortic dissections have been associated with hypertension and Marfan syndrome in the literature (Larson and Edwards, 1984; Hagan *et al.*, 2000; Erbel *et al.*, 2001). No signs of

systemic hypertension or Marfan syndrome were observed in the cadaver with the aortic dissection.

A primary popliteal venous aneurysm (PVA) is a very rare occurrence and is defined as a focal dilatation of the popliteal vein within the popliteal fossa (Bergqvist *et al.*, 2006). Their prevalence is difficult to ascertain as the literature lacks population-based studies (Bergqvist *et al.*, 2006). A PVA is usually asymptomatic, however an increased associated risk of pulmonary embolism does exist (Bergqvist *et al.*, 2006). The cadaver with bilateral PVA in this cadaver cohort (K82/09; male, 47 years) did not show any signs of a pulmonary thromboembolism which may indicate the likelihood of asymptomatic PVA which was not related to the terminal cause of death in this individual.

5.1.4.3 Gastrointestinal Tract System

Although gastric ulcers are commonly found in the gastrointestinal tract, a multifactorial pathogenesis exists for their development (Eastwood, 1997; Maity *et al.*, 2003). Several studies have demonstrated a direct association between cigarette smoking and gastroduodenal ulceration, as smokers are more likely to develop ulcers (Debas *et al.*, 1971; Kurata *et al.*, 1987; Eastwood, 1997; Maity *et al.*, 2003; Thomas *et al.*, 2005). The effect of smoking on the prevalence of gastric ulcers in our study could not be confirmed as the smoking history was unavailable. In addition to smoking, a corpus-predominant gastritis has been linked to the development of gastric ulcers (Chan and Leung, 2002). In our study, a concomitant chronic gastritis was observed in 2/5 (40.0%) cadavers with gastric ulcers. The link between gastritis and gastric ulcers in our study could not be confirmed due to the small sample size and due to the small

degree of gastritis which possibly did not contribute to the development of gastric ulcers. Apart from gastritis and smoking as etiological agents for gastric ulcers, *Helicobacter pylori* infection and non-steroidal anti-inflammatory drugs (NSAIDs) have been implicated as risk factors for development of gastric ulcers. The gastric epithelial-lining of the cadavers was sloughed off and autolytic as a result of decomposition. We could therefore not determine whether *H. pylori* infection caused gastric ulcers in our cadaver cohort. As the medical history was unavailable we do not know if any of these individuals used NSAIDs and if its use contributed to gastric ulcer formation prior to death. Estrogens have been used in the past to successfully treat gastric ulceration, as estrogen and progestogens have been shown to increase gastric mucus secretion (Parbhoo and Johnston, 1966; Collier and Pain, 1985). Postmenopausal females are therefore at a higher risk for gastric ulceration compared to premenopausal females (Parbhoo and Johnston, 1966; Collier and Pain, 1985). In our study, the age of two of the females with gastric ulcers was unavailable, however, the remaining were 45 years and older, suggesting that decreased sex hormones in postmenopausal females may play a role in the pathogenesis of gastric ulcers.

Superficial and chronic atrophic gastritis are both common findings in chronic alcoholics, as high levels of alcohol consumption have been shown to damage the gastric mucosa by increasing gastric acid secretion (Bujanda, 2000; Maity *et al.*, 2003; Choi *et al.*, 2006). Similarly, cigarette smoking was shown to be harmful to the gastric mucosa particularly in patients with gastric ulcers (Debas *et al.*, 1971; Maity *et al.*, 2003). A predilection for males have been observed in the literature, as males tend to be subjected to more dangerous social factors such as alcohol consumption and smoking (Choi *et al.*, 2006). In our study, twice as many males were affected by gastritis compared to females. A *H. pylori* infection usually leads to chronic, non-atrophic

gastritis (Sipponen *et al.*, 1994). We could not determine the contributory role of *H. pylori* in the cadavers with gastritis in our study as a result of sloughed off gastric epithelium.

An extensive morphological classification of benign intestinal polyps was described by Ekelund and Lindström (Ekelund and Lindström, 1974). The authors noted that intestinal adenomas ranged from simple adenomas (adenomatous polyps) to adenomatous polyps with villous surfaces (adenovillous polyp) to villous papillomatous adenomas (adenovillous papilloma) (Ekelund and Lindström, 1974). The same classification was adopted for the present study. A predilection for males to develop intestinal polyps compared to females was reported by several authors (Rider *et al.*, 1954; Ekelund and Lindström, 1974). From the present study the cadavers who presented with benign intestinal polyps (6/127; 4.7%), were all males with an average age of 52.5 years. To our knowledge, little is available on the sex disparity observed with benign intestinal polyps in the Western Cape population. The present study therefore illustrates a male preponderance which may be ascribed to an underlying genetic role in the development of benign intestinal polyps.

Gastrointestinal stromal tumor (GIST) is a common neoplasm of the mesenchymal cells of the gastrointestinal tract (GIT) (Strickland *et al.*, 2001; Rubin *et al.*, 2007; Gupta *et al.*, 2008; Stamatakos *et al.*, 2009; Liegl-Atzwanger *et al.*, 2010). It can occur at any location within the GIT, with 25-40% of the GIST cases occurring in the small intestinal segment (Rubin *et al.*, 2007; Stamatakos *et al.*, 2009; Liegl-Atzwanger *et al.*, 2010). Strickland *et al.* (2001) noted only 1-2% of small bowel involvement. If the GIST occurs in the jejunum or ileum, the indication of malignancy is when the tumor size is larger than 50mm in diameter (Strickland *et al.*, 2001). In

our study, the maximum dimensions of the GIST were 27x25mm, which suggests that the GIST was benign. These tumors have no predilection for age and sex (Rubin *et al.*, 2007; Gupta *et al.*, 2008; Stamatakos *et al.*, 2009). The male cadaver in our study with a GIST was 47 years of age. This was an incidental finding during gross dissection. Rubin *et al.* (2007) observed intestinal ulceration as a complication of GIST. Intestinal ulceration was absent in the affected cadaver.

Colonic diverticula are a common health problem in developed countries but rarely observed in developing countries (Hughes, 1969; Stollman and Raskin, 2004) with a definite racial bias (Hughes, 1969). The true incidence and prevalence of colonic diverticulosis are difficult to estimate as the majority of the patients are asymptomatic (Stollman and Raskin, 2004). Colonic diverticula were observed in 24/127 (18.9%) cadavers and the average age of the affected cadavers was 54.1 years. Our findings correlate with findings from studies by Hughes, (1969); Parks, (1969); Simpson *et al.*, (2002) and Stollman and Raskin, (2004) who observed an increase in colonic diverticula in the second half of life. The male to female ratio of the affected cadavers was 1:1.3. This slight female preponderance in our study is in contrast with studies by Stollman and Raskin (2004) and Jacobs (2007) in which they noted no sex difference among their subjects. In a study by McConnell *et al.* (2003) females tend to, on average, present five years later with diverticula and complications thereof compared to males. This notion may explain our findings with regard to observed sex differences. The descending and sigmoid colon were the most common anatomical sites of colonic diverticula amongst our cadavers. Hughes (1969) and Stollman and Raskin (1999) noted similar findings. Similarly to Hughes (1969), caecal and ascending colonic involvement were rare in our cadavers. Our findings are in contrast with findings from Asian populations. In Singapore and Hong Kong, a strikingly high frequency of

the right hemi-colon involvement was observed (Lee, 1986; Chan *et al.*, 1998). None of the affected cadavers in our study showed signs of colonic diverticulitis. Possible etiological agents were correlated with the incidence of colonic diverticula in a study done by Hughes (1969). Colonic diverticula were negatively correlated with colonic length, cholelithiasis and hypertension. Atheromatous changes in the aorta were however positively correlated with colonic diverticula (Hughes, 1969). This correlation can possibly be as an effect of age on both diseases (Hughes, 1969). In our study, however, no statistically significant association was found between atheromatous changes in the aorta and colonic diverticula ($p > 0.05$). Keeley (1958) noted no colonic diverticula in the 2367 necropsies from Baragwanath Hospital in Johannesburg, South Africa. Colonic diverticula were described by Bremner and Ackerman (1970) as being extremely rare in the black population in South Africa. This picture did not change over the past few decades. From the present study, the ratio of colonic diverticula between mixed race, white and black cadavers was 16:5:3, suggesting that colonic diverticula are more common in the mixed race and white population compared to blacks. Two possibilities may explain the racial variation. Firstly, a genetic component may play a role and secondly, a low dietary intake of fiber can explain the differences in incidence and pathogenesis of colonic diverticula (Simpson *et al.*, 2002; Commane *et al.*, 2009).

Torsion of a loop of the small intestine is an extremely rare occurrence and may affect any age (Moretz and Morton, 1949). The fact that only one cadaver (K108/09; male, 42 years) presented with acute volvulus and subsequent strangulation and necrosis, confirm this as a rare finding. By comparing the findings in the literature, the stomach seems to be the most common site for volvulus and strangulation to occur, followed by colonic volvulus, in particular the sigmoid

colon (Ballantyne *et al.*, 1985; Muang and Saing, 1995; Godshall *et al.*, 1999). Intestinal volvulus is relatively common in children, especially those infected with *Ascaris lumbricoides* (Muang and Saing, 1995). In our study, 3/127 (2.4%) cadavers were infected with *A. lumbricoides* but showed no sign of intestinal volvulus. No signs of the nematode infection were observed in the cadaver with the acute volvulus.

Infection with *Ascaris lumbricoides* has been shown to influence the nutritional status of the host (O’Lorcain and Holland, 2000; Jardim-Botelho *et al.*, 2008). This may be as a result of reduced intestinal absorption and luminal obstruction (Smith *et al.*, 2001; Jardim-Botelho *et al.*, 2008). Several factors have been proposed for helminthic infections, including poor SES, overcrowding, personal and food hygiene, social class and sex (O’Lorcain and Holland, 2000; Smith *et al.*, 2001). Infection with *A. lumbricoides* has no sex predilection (Smith *et al.*, 2001). This is in contrast with findings from our study, as a female predominance was observed (male to female ratio = 1:4.5). The male cadaver in our study with *A. lumbricoides*, however, had a more severe infection with more helminthes observed in the intestinal segment compared to the infected females. No sign of ascariasis, the disease associated with *A. lumbricoides* infection, was observed in any of the infected cadavers.

Recent data suggests the incidence of acute pancreatitis (AP) varies noticeably throughout the world (Appelros and Borgström, 1999; Banks, 2002). The two most common causes of acute pancreatitis are heavy alcohol consumption and cholelithiasis (Banks, 2002). In a study done by Trapnell and Duncan, significantly more females were affected by AP caused by cholelithiasis compared to males. Males, on the other hand, with a history of chronic alcohol consumption,

were more commonly affected by AP (Trapnell and Duncan, 1975). The female cadaver with AP from our study (K70/11) was the only cadaver with AP in our study. Cholelithiasis was absent in the cadaver and without a medical history or knowledge regarding alcohol consumption prior to death, the etiology of the AP in this cadaver could not be established.

Several population-based studies regarding the epidemiology of chronic pancreatitis (CP) revealed an increase in the incidence of CP in almost every nation (Jupp *et al.*, 2010), in particular developed countries where high levels of alcohol are consumed (Steer *et al.* 1995). Cholelithiasis was absent in all of the cadavers with CP in our study. Four types of chronic pancreatitis exist, of which chronic calcifying pancreatitis is the most common form (Kumar and Clark, 1998). All of the cadavers showed signs of calcification within the pancreatic parenchyma and no obstructive lesions were noted within the main pancreatic duct. This suggests that CP in our cadavers was most likely caused by chronic alcohol consumption prior to their death. No sex difference was observed in the cadaver population. This is in contrast with findings from studies from Europe and Asia (Lin *et al.*, 2000; Frulloni *et al.*, 2009; Jupp *et al.*, 2010). They showed a clear sex difference in chronic pancreatitis with a male predominance (Lin *et al.*, 2000; Frulloni *et al.*, 2009; Jupp *et al.*, 2010). Our study sample is too small to make a definitive statement regarding sex differences among our cadaver population and may explain the contrasting findings compared to the studies by Lin *et al.* (2000); Frulloni *et al.* (2009) and Jupp *et al.* (2010).

5.1.4.4 Hepatobiliary System

A low SES is linked with excessive alcohol use, which is a risk factor for various chronic diseases, such as cardiovascular and liver diseases (Wiles *et al.*, 2007).

In a study done on a population group from Japan, Ohnishi *et al.*, (1982) observed an accelerated development of hepatic cirrhosis in individuals with a usual intake of more than 25ml of ethanol per day. Mortality as a result of cirrhosis is almost twice as high in males compared to females (Mann *et al.*, 2009). In our study, the male to female ratio was similar (1.8:1). Females on the other hand, have been shown to have a higher chance of developing cirrhosis compared to males (Tuyns and Pequignot, 1984; Saunders and Latt, 1993; Mann *et al.*, 2003). Two possibilities exist for the sex disparity. Firstly, females tend to have a higher level of blood alcohol compared to men as the concentration of the alcohol dehydrogenase enzyme has been shown to be lower in the female stomach (Frezza *et al.*, 1990; Mann *et al.*, 2003). Secondly, estrogen has been shown to increase the susceptibility of the liver to alcohol (Ikejima *et al.*, 1998; Mann *et al.*, 2003). Ethnic differences in cirrhosis rates have been observed with blacks being more commonly affected than whites (Mann *et al.*, 2003). In our study, however, there was a tendency for white individuals to be more commonly affected compared to black and mixed race individuals. Several factors have been proposed for the ethnic differences including, age, income, education, family history of drinking and stress (Jones-Webb, 1998; Mann *et al.*, 2003).

Hepatic steatosis (fatty liver disease) is a common histological finding which can be ascribed to high rates of alcohol consumption, metabolic syndrome and drug use (Saunders and Latt, 1993; Day and James, 1998, Bellentani *et al.*, 2000; Browning *et al.*, 2004). The literature has

demonstrated that hepatic steatosis can either coincide with or lead to steatohepatitis and consequently fibrosis (Day and James, 1998). In a study done by Browning *et al.* (2004) on the prevalence of hepatic steatosis in an urban population in the United States, twice as many white men were found to be affected by hepatic steatosis white women. The Hispanic and Negroid ethnic groups did not show a statistically significant sex difference in their study subjects. The sex difference in the white ethnic group may be a result of excess alcohol intake per day in men compared to women (Browning *et al.*, 2004). Hepatic steatosis was observed in 16/127 (12.6%) cadavers from our study of which 10/16 (62.5%) of the affected cadavers were males. We found no statistically significant difference between males and females with hepatic steatosis ($p > 0.05$). The study by Browning *et al.* (2004) was done on the American population with different population dynamics compared to the South African population and may suggest the difference in the findings between their study and ours.

Non-alcoholic fatty liver disease (NAFLD) is an acquired metabolic liver disease that is commonly associated with obesity and insulin resistance (Fan and Farrell, 2009). The worldwide incidence of NAFLD remains unknown as little prospective studies have been performed and some of the disease stages, observed specifically during NAFLD, have not clearly been defined (Fan and Farrell, 2009). Non-alcoholic steatohepatitis (NASH), steatosis and cirrhosis are common findings observed with NAFLD and may mimic the entire spectrum of liver conditions associated with alcohol abuse (Fan and Farrell, 2009; Kumar *et al.*, 2013). Information on the alcohol use of the cadavers was unavailable. Even though steatohepatitis, steatosis and cirrhosis were observed in the cadaver cohort, the cause of these conditions remains speculative.

Alcoholic hepatitis shares common histologic findings with NASH and NAFLD; however the severity of these histologic findings is typically greater in alcoholic hepatitis (Lucey *et al.*, 2009). The cadaver with alcoholic hepatitis in our study was a 61 year old female. This is consistent with the literature, as the female sex is a risk factor and the typical age of presentation of alcoholic hepatitis is between 40 and 60 years.

Liver hemangiomas (LH) is one of the most common benign liver neoplasms and are frequently observed in young females (Yoon *et al.*, 2003; Herman *et al.*, 2005; Giannitrapani *et al.*, 2006; Kim *et al.*, 2006). In 70% of the patients with LH, multiple lesions are observed (Giannitrapani *et al.*, 2006). The female preponderance in the literature has been linked to the role of estrogen in the pathogenesis of LH (Giannitrapani *et al.*, 2006). The LH lesions are usually an incidental finding (Herman *et al.*, 2005), which was the case in our cadaver with LH. In contrast to the findings from the literature, the cadaver in our study was a 39-year old male.

An increased rate of hepatocellular carcinoma (HCC) development has been observed with a habitual alcohol intake (Ohnishi *et al.*, 1982; Saunders and Latt, 1993). Similarly, cirrhosis is considered a premalignant condition as it has been found to predispose individuals to develop HCC (Fattovich *et al.*, 2004). In our study, one male cadaver with unavailable age and extensive cirrhosis presented with a solitary HCC lesion. Multiple HCC nodules were found in the absence of cirrhosis in a 62-year old male cadaver. Elderly males have been found in several studies to be associated with an increased risk of HCC development among individuals with cirrhosis (Zaman *et al.*, 1985; Fattovich *et al.*, 2004; Sangiovanni *et al.*, 2004; Sherman, 2010). Likewise, in the

absence of cirrhosis, males are more frequently affected by HCC compared to females (Kew *et al.*, 2002).

Christensen and Ishak (1970) proposed a classification of benign and pseudo-tumors of the gallbladder. In this simplified classification, an adenoma is regarded as a benign neoplasm of the gallbladder, while an adenomyoma is classified as a benign pseudo-tumor. In our study, we found two different benign primary gallbladder neoplasms in one cadaver (K83/09; male, 60 years). An adenoma was found within and obstructed the lumen of the gallbladder, while the adenomyoma was located within the wall of the gallbladder. In an extensive review by Lee *et al.* (2004), the prevalence of polypoid lesions of the gallbladder ranged from 4.3% to 4.6% in a Danish population (Jorgensen and Jensen, 1990), 3.5% to 6.3% in a Japanese population (Segawa *et al.*, 1992) and 6.9% in a Chinese population (Chen *et al.*, 1997). From the Danish and Japanese studies, it is apparent that males are more likely to be affected by benign gallbladder neoplasms (Jorgensen and Jensen, 1990; Segawa *et al.*, 1992), while a higher prevalence of gallbladder carcinoma has been reported in females (Randi *et al.*, 2006). The sex disparity can either be ascribed to the possible role of sex hormones, obesity or a family history of gallbladder neoplasms (Randi *et al.*, 2006). In our study, only one male cadaver presented with benign growth of the gallbladder. Little could therefore be said about the prevalence and sex disparity of gallbladder neoplasms in our study due to the small sample size.

The prevalence of gallstones increases with age in all the ethnic groups (Shaffer, 2006). The average age of our cadavers was 61.3 years. A female predilection for gallstones has previously been described (Rhomberg *et al.*, 1984; Miquel *et al.*, 1998; Everhart *et al.*, 1999; Acalovschi,

2001; Singh *et al.*, 2001; Shaffer, 2006). The female sex hormones, especially estrogen, have been proposed as the reason for the sex disparity (Shaffer, 2006). In our study, however, a male to female ratio of 2.8:1 was observed. Our findings are in contrast with the literature as only one female cadaver presented with cholelithiasis compared to six male cadavers.

5.1.4.5 Renal System

Glomerulosclerosis is a common finding in the aging kidney (Silva, 2005). In a study done by Kasiske, a direct association was observed between the numbers of sclerotic glomeruli versus age (Kasiske, 1987). The average age of the affected cadavers in our study was 48.4 years (range 24–73 years). Glomerulosclerosis was most commonly observed in the cadavers in their fourth and fifth decade of life. In addition to age, direct statistical correlations were observed between glomerulosclerosis and aortic atherosclerosis ($p < 0.05$) and glomerulosclerosis and arterial hypertension ($p < 0.05$). This is consistent with findings from the studies by Kasiske (1987) and Silva (2005). A male preponderance was observed in our cadaver cohort. This sex difference observed in our study is comparable to findings from an in-depth review by Silbiger and Neugarten (1995) in which a predilection for glomerulosclerosis in males was observed. It has been proposed that estrogen may play a protective role in the development of glomerulosclerosis in females (Silbiger and Neugarten, 1995) and may therefore explain the sex disparity in our study.

In our study females were slightly more commonly affected by acute and chronic pyelonephritis, compared to males (male to female ratio = 1:1.1). This is in accordance with studies in the literature (Freedman, 1967; Ki *et al.*, 2004; Czaja *et al.*, 2007). No sex difference however is

observed in patients older than 60 years (Ki *et al.*, 2004). The average age of the cadavers with acute pyelonephritis was 59.0 years, while an average age of the cadavers with chronic pyelonephritis was 47.4 years. Two possibilities exist for the observed sex differences in our cadavers. Firstly, the average age of the cadavers with acute and chronic pyelonephritis is both below 60 years. And secondly, the sample size affected by pyelonephritis, in particular acute pyelonephritis, is relatively small and accurate sex differences can therefore not be determined. A direct statistically significant association was observed between the prevalence of acute and chronic pyelonephritis in our cadavers and arterial hypertension ($p < 0.05$). This finding is consistent with findings by Butler (1937) and Pfau and Rosenmann (1978). Hypertensive nephrosclerosis is regarded as a frequent cause of end-stage renal disease (ESRD) (Marcantoni *et al.*, 2002).

Renal cysts are thought to be acquired lesions from diverticula in the distal convoluted tubules (Carrim and Murchison, 2003; Terada *et al.*, 2008; Zhou *et al.*, 2008). It is believed that the development of simple renal cysts occurs as a result of age and consequently weakening of the tubular basement membranes (Carrim and Murchison, 2003; Terada *et al.*, 2008; Zhou *et al.*, 2008). The aging kidney is therefore prone to cystic development and this may present as solitary or multiple cysts. The ages of the affected cadavers from the present study ranged from 34 to 81 with an average age of 58.5 years. The results from our study confirm a steady increase in the prevalence of simple renal cysts with age. Our findings are in accordance with findings from other studies (Hale and Morgan, 1969; Carrim and Murchison, 2003; Terada *et al.*, 2008). The majority of renal cysts in a study by Hale and Morgan (1969) presented in the fifth decade of their subjects. In our study, male were to some extent more commonly affected with simple renal

cysts compared to females (male to female ratio = 1.2:1). This higher prevalence of renal cysts in males has been consistently observed in other studies (Caglioti *et al.*, 1993; Carrim and Murchison, 2003). It has been proposed that urinary obstruction and renal arteriosclerosis may be responsible for renal cysts (Gardner, 1988; Carrim and Murchison, 2003). Urinary obstruction is more prominent in older men as a result of enlarged prostates and may explain the male predominance in renal cysts (Gardner, 1988).

Secondary renal neoplasms are the most commonly encountered renal malignancy during autopsies (Bailey *et al.*, 1998). Abrams *et al.* (1950) reviewed 1000 consecutive postmortem findings of patients with malignant epithelial neoplasms and reported a renal metastases prevalence of 12.6%, while Klinger (1951) observed a prevalence of renal metastases in only 2.4% of 5000 autopsies. In our study, a prevalence of 1.6% (2/127) was observed. To our knowledge, little, if any exists in the literature on the prevalence of metastases to the kidneys in the South African population, and in particular the Western Cape population. Our study therefore fills this void by reporting the prevalence of renal metastases in a population from low socio-economic backgrounds. In addition to the prevalence, the most common primary origin has been shown to be the pulmonary system, which is in accordance with our study as both cadavers presented with a primary pulmonary neoplasm. However, the small study sample may influence these findings. A larger study sample is therefore needed to determine the most common primary origin in a South African population.

5.1.4.6 Genital System

Benign prostatic hyperplasia (BPH) results in a diffuse enlargement of the prostatic transitional zone due to the presence of nodules (Simpson, 1997). More than 50% of men over the age of 60 years have benign prostatic hyperplasia while up to 30% of these men present with lower urinary tract symptoms (LUTS) (Thorpe and Neal, 2003). This is consistent with findings from our study, as 6/12 (50%) males over the age of 60.0 years presented with BPH. Potential risk factors for the development of BPH include alcohol, diet, genetic factors, age and a previous history of urogenital tuberculosis (Sidney *et al.*, 1991; Thorpe and Neal, 2003). Only one cadaver with BPH had both renal TB and testicular TB.

The pathogenesis of BPH is associated with the presence of corpora amylacea and prostatic calculi (Briganti *et al.*, 2009). Corpora amylacea have in addition been shown to contribute to prostatitis and prostate carcinogenesis (Sciarra *et al.*, 2007). In our study, 41.7% cadavers with BPH had concomitant corpora amylacea within the prostatic parenchyma. Our findings indicate no statistical significance between BPH and corpora amylacea. We believed the lack in statistical power between BPH and corpora amylacea was due to our small male cohort.

Prostatitis is regarded as the most common urologic disease in men younger than 50 years of age (Collins *et al.*, 1998). It has been shown that prostatitis affects men of all ages and is more common in the elderly (Roberts *et al.*, 1998; McNaughton Collins *et al.*, 1999; Nickel, 2007). Prostatitis was shown to be strongly associated with the pathogenesis of BPH (Nickel, 2007; Briganti *et al.*, 2009). We found that 66.7% of the cadavers with prostatitis had concomitant BPH and a statistically significant association between the presence of BPH and prostatitis

($p < 0.05$) was observed. This finding is expected as both diseases are prevalent in the elderly (Nickel, 2007). Benign prostatic hyperplasia has been linked to prostatic carcinogenesis (Bostwick *et al.*, 1992; Guess, 2001). One cadaver presented with BPH, corpora amylacea and prostatic ACA. Unfortunately the cohort size was too small to determine a true correlation between prostatic carcinoma and BPH, corpora amylacea and prostatitis in our cadaver cohort.

A collection of serous fluid in the tunica vaginalis or patent processus vaginalis is known as a hydrocele which is idiopathic in the majority of cases (Dogra *et al.*, 2003; Agbakwuru *et al.*, 2008). Testicular torsion, testicular tumors or trauma are known secondary causes for hydrocele (Ku *et al.*, 2001; Dogra *et al.*, 2003; Agbakwuru *et al.*, 2008). In a study by Agbakwuru *et al.* (2008), 80% of the patients ($n=50$) with hydrocele was older than 50 years. Only one male cadaver, in our study, had unilateral hydrocele and was 46 years old. A large, scrotal swelling is however also characteristic of a hydrocele (Dogra *et al.*, 2003; Agbakwuru *et al.*, 2008) and was this typical presentation visible in this particular cadaver.

Varicoceles are found in approximately 11% to 15% of adolescent males (Oster, 1971; Yerokin, 1979; Witt and Lipshultz, 1993; Skoog *et al.*, 1997; Misseri *et al.*, 2001; Paduch and Skoog, 2001; Dogra *et al.*, 2003; Canales *et al.*, 2005), however in the infertile male population, 25.4% of males have been found to be affected by varicoceles (Akbay *et al.*, 2000). Males with varicoceles are likely to have significantly smaller testis on the affected side (Lipshultz and Corriere, 1977). In addition to size, Dubin and Amelar (1978) observed a preponderance of left-sided involvement with more than 90% ($n=986$) of their patients presenting with unilateral varicocele. Similar findings were observed by Paduch and Skoog (2001), Dogra *et al.* (2003) and

Canales *et al.* (2005). Findings from our study support the evidence, as left-sided testicular varicocele with concomitant testicular atrophy was observed. Numerous reasons have been proposed as to why left-sided involvement predominates. The majority of studies suggest the long left testicular vein and its drainage into the left renal vein at a 90° angle as a possible reason for left-sided predominance (Skoog *et al.*, 1997; Paduch and Skoog, 2001; Dogra *et al.*, 2003). Several authors have suggested increasing age as a risk factor for development of varicoceles and consequently testicular failure (Akbay *et al.*, 2000; Canales *et al.*, 2005). In our study, the effects of age on testicular varicoceles and failure could not be determined as the sample size was too small and the age of the affected cadaver was unavailable.

Uterine leiomyomas, also referred to as fibroid tumors, have been found to be more common in women from black ethnicity than white women (Marshall *et al.*, 1997; Vollenhoven, 1998; Stewart, 2001; Baird *et al.*, 2002; Flake *et al.*, 2003). The reason for the ethnic differences are unknown, however environmental factors, stress and diet have been proposed as possible reasons (Baird *et al.*, 2002). In our study, one black female cadaver, one mixed race cadaver and one cadaver with unknown ethnicity presented with uterine leiomyomas. Extensive uterine involvement with accompanying uterine enlargement was seen in the black female cadaver and cadaver with unknown ethnicity. Our study sample was too small to determine true racial differences in the prevalence of uterine leiomyomas. In addition to race, an increase in age has been shown to directly correlate with the prevalence of leiomyomas (Stewart, 2001; Flake 2003). According to the literature, the majority of women were in their 40's when the leiomyomas become symptomatic (Stewart, 2001). The three cadavers from our cohort with leiomyomas were also above the age of 40 years, with an average age of 52.0 years.

In the late 80's and early 90's, asymptomatic genital warts, also referred to as condylomata acuminata, were diagnosed in approximately 20% of the overall South African female population, irrespective of race (Cooper *et al.*, 1991). The highest incidence (66.0%) was been reported in black females (Markowitz *et al.*, 1986). More than 15 years later, cervical cancer as a result of human papillomavirus (HPV) remains a major problem with the highest incidence amongst black females (Kay *et al.*, 2003).

5.1.4.7 Lymphoreticular System

Non-Hodgkin lymphoma (NHL) of the appendix is rare and when present, usually infiltrates and involves the entire appendix (Pickhardt *et al.*, 2003; O'Donnell *et al.*, 2007). The most common manifestation of appendiceal lymphoma is acute appendicitis (Müller *et al.*, 1997; Pickhardt *et al.*, 2002; Pickhardt *et al.*, 2003; O'Donnell *et al.*, 2007). The appendix of cadaver K124/12 (male, 55 years) was diffusely enlarged but still kept the original vermiform appearance. This is consistent with what is described in the literature regarding appendiceal lymphomas. Generally, lymphoma of the GIT is seen in individuals with compromised immune systems, usually as a result of HIV and AIDS (Pickhardt *et al.*, 2002), however, the GIT overall is the most common extranodal site for NHL development (Pasquale *et al.*, 1994; Pickhardt *et al.*, 2002; O'Donnell *et al.*, 2007). Metastases from the appendix to the liver, spleen and kidneys were observed in the cadaver.

5.1.4.8 Brain

Hydrocephalus is a common finding in developing countries, particularly in East Africa (Warf, 2005). Infectious and congenital causes have been linked to the high incidence of hydrocephalus in Central African countries, including Zambia, Malawi and Zimbabwe (Adeloya, 2001; Warf, 2005). The focus of the majority of studies concerning hydrocephalus was infantile hydrocephalus and treatment thereof. Hydrocephalus in the adult life may develop either as a result of neoplasms of the brainstem, posterior fossa and choroid plexus, or as a consequence of head injury, such as subarachnoid hemorrhage (SAH) (Kumar and Clarke, 1999). In addition, an infectious disease, such as tuberculous meningitis (TBM), has been linked to the development of hydrocephalus (Kumar and Clarke, 1999; Chan *et al.*, 2003). In our study, however, one female cadaver presented with unilateral involvement as a result of what appears to be hydrocephalus *ex vacuo* which is normally caused by brain atrophy (Jha *et al.*, 2010; Venkataramana, 2011). Ageing, hypoxia, severe infection or head trauma have all been implicated as causes of hydrocephalus *ex vacuo*. This cadaver did not present with obvious brain abnormalities. In addition, Paget's disease (osteitis deformans) was observed with an extensively thickened skull vault. It is believed that excessive bone resorption on the internal aspect of the skull with concomitant stenosis of the foramen magnum and increased intracranial pressure resulted in obstruction of and impaired CSF resorption. The underlying cause of the bilateral hydrocephalic involvement in the male cadaver from our study was inconclusive. This cadaver was a 72-year old male and it is most likely that hydrocephalus *ex vacuo* as a result of age led to the bilateral hydrocephalus. Males have a slightly higher predilection for congenital hydrocephalus development as a result of X-chromosomal-linked aqueductal stenosis; however, this is mainly applied to infantile hydrocephalus (Venkataramana, 2011). The lack of epidemiological studies

of adult hydrocephalus and sex disparities makes it difficult to determine the effect of sex on the prevalence and outcome of hydrocephalus.

Cerebral infarction is more common in males than females, while an increase in incidence and mortality in females occurs with an increase in age (Bramlett and Dietrich, 2004). It has been proposed that hormonal differences between males and females affect the incidence and outcome of brain ischemia, as premenopausal females have a significantly lower risk of cerebral infarction (Sadoshima *et al.*, 1988; Alkayed *et al.*, 1998; Zhang *et al.*, 1998; Bramlett and Dietrich, 2004). Estrogen and progesterone has been implicated as neuroprotective hormones (Sadoshima *et al.*, 1988; Alkayed *et al.*, 1998; Zhang *et al.*, 1998; Bramlett and Dietrich, 2004). The age of the female cadaver in our study with signs of a cerebral infarction, was unknown. The cadaver, however, had extensive atherosclerotic involvement of both thoracic and abdominal aorta and three coronary arteries were 50% or more occluded. The right coronary artery (RCA) was 90% occluded. As she had extensive atherosclerosis in several blood vessels, it can be assumed that this female was postmenopausal. In addition the possibility exists that the cerebral infarction could be as a result of restricted blood flow due to atherosclerotic involvement of the cerebral arteries. We did not observe obvious signs of arterial occlusion, however this cannot be excluded.

Acute bacterial meningitis is less common in adults (Beers *et al.*, 2003). Males have a higher predilection for the development of bacterial meningitis (BM) (Wenger *et al.*, 1990; Pérez *et al.*, 2010). In addition, infants and the elderly are at a higher risk for developing BM (Tang *et al.*, 1999; Gurley *et al.*, 2009; Pérez *et al.*, 2010). In our study, three males were affected compared

to one female. The average age of the cadavers with BM in our study, was 64.3 years (range: 61-70 years). The burden of BM is higher in impoverished areas, mainly as a consequence of malnutrition, poor living conditions and poor access to public health services (Stephens *et al.*, 2007; Gurley *et al.*, 2009). Meningitis has a profound impact on the underlying cerebral parenchyma (Jan *et al.*, 2003), with cerebral infarcts being the most common cerebral complication of meningitis (Friede, 1973). In our study, cerebral infarcts were absent in the cadavers with BM. It should be noted that the focus of the study by Friede (1973) and Jan *et al.* (2003) were both on BM during infancy and it could differ from complications observed in adults. The left hemisphere was involved in all of our cadavers. To our knowledge, little information is available on the brain hemisphere BM is prone to develop. Anatomical variations and anomalies in the Circle of Willis (CoW) have been extensively described (Kayembe *et al.*, 1984; Eftekhar *et al.*, 2006; Cilliers, 2013). It is possible that hypoplastic or stenotic right middle and posterior cerebral arteries could have contributed to the predominantly left-sided appearance of BM; however, it is less likely that this was the case in all of our cadavers with BM that we identified. In 2013, the anatomical variation in the CoW was investigated in the 2013 cadaver cohort. No remarkable variations and anomalies were found in those cadavers with BM (Cilliers, 2013). It is therefore less likely that the arterial anatomy played a role in the left-sided predominance in our study.

It should be noted that the brains in our study were decomposed, some to such an extent that brain matter could not be distinguished and a diagnosis therefore impossible to make. For future research on embalmed brain material, it is proposed that during the embalming procedure, the brains should be removed as soon as possible and placed in containers with 10% buffered neutral

formalin (BNF) and not only once the students are dissecting the cadavers which often is 6 months after embalming.

5.1.4.9 Breast

Fibrocystic change of the breast is regarded as a benign change in the female breast, usually bilateral with a peak incidence between 41 and 45 years (Murad and Von Haam, 1968). Both cadavers in our study with fibrocystic changes in the breast had unilateral involvement and the average age was 52.5 years. Fibroadenoma (FA), on the other hand, is a common, well-defined benign fibroepithelial tumor (Cole-Beuglet *et al.*, 1982; Dupont *et al.*, 1994; El-Wakeel and Umpleby, 2003). It has been reported in the literature that women with fibroadenomas have a three-time higher risk of developing breast cancer (Dupont *et al.*, 1994). Fibroadenomas are more commonly seen in women younger than 25 and generally present as small, well-circumscribed nodules (Cole-Beuglet *et al.*, 1982). The female cadaver in our study with morphologic features of a fibroadenoma was 47 years of age. No significant signs of malignancy were noted in this cadaver.

5.1.4.10 Skeletal System

Two of the most common causes of craniofacial trauma are motor vehicle accidents (MVAs) and blunt assault (BA) (Shapiro *et al.*, 2001; Shahim *et al.*, 2006; Bakardjiev and Pechalova, 2007). Some researchers have shown that MVAs tend to be the primary cause for craniofacial features; however recent studies have suggested craniofacial fractures are as a result of an increase in the incidence of BA (Afzelius and Rosen, 1980; Haug *et al.*, 1990; Shapiro *et al.*, 2001; Brasileiro and Passeri, 2006). A strong association between alcohol and facial fractures has been

documented in the literature (McDade *et al.*, 1982; Hill *et al.*, 1984; Shapiro *et al.*, 2001). The data from the present study suggests that high rates of alcohol consumption may be an important factor in the incidence of craniofacial fractures. In our study, the use and outcomes of alcohol prior to the cadavers' demise could not be determined. We can however speculate, particularly if liver disease associated with heavy alcohol consumption is involved. In our study, a strong statistical association was observed between the prevalence of maxillofacial fractures and liver disease consistent with alcohol abuse ($p < 0.05$). The presence of remnants of glass presumably from glass bottles containing alcohol, in the external skull vault of two cadavers from our study, can certainly corroborate this statement.

The left side of the face was more commonly involved with maxillofacial trauma than the right side. This was statistically confirmed using the MacNemar statistical test ($p = 0.02$; $p < 0.05$). In terms of facial involvement, healed fractures of the zygomatic and nasal bones most commonly observed in the cadaver cohort. Mandibular fractures were less commonly observed (1.6%). The left side of the face being more involved can be explained in part (but not exclusively) by the assault injury pattern. The right arm of the attacker landing on the left side of the victim's face may explain the majority of left-sided involvement in the cadavers. Ellis *et al.* (1985) noted similar findings in their study: a predominance of left-sided injuries and a male to female ratio of 4:1. Zygomatic and maxillary processes of the zygomatic bone are the most prevalent location for fractures resulting from interpersonal violence (Brasileiro and Passeri, 2006). Scarfe (2005) noted a predilection for mandibular fractures compared to maxillary fractures when maxillofacial trauma was investigated. We found, however, that the maxilla was the most common site for fractures in the cadavers. The male to female ratio of the cadavers with maxillofacial trauma in

our cohort was 2.4:1. This sex difference with a male preponderance has been observed in other studies and can possibly be explained by the fact that males are more likely to encounter in interpersonal violence (Afzelius and Rosen, 1980; Khalil and Shaladi, 1981; Hill *et al.*, 1984; Ellis *et al.*, 1985; Adi *et al.*, 1990; Gassner *et al.*, 2003; Motamedi, 2003; Bakardjiev and Pechalova, 2007).

Although the global prevalence and geographical distribution of periodontal apical cysts are currently unknown, it remains the most common of all mandibular and maxillary cysts (Ramachandran Nair, 2003). Reported prevalence has ranged from 7.8% (Ledesma-Montes *et al.*, 2000; Avelar *et al.*, 2009) to 55.0% (Ramachandran Nair, 2003). Apical cysts are found in the tooth-bearing jaw with the maxilla being more commonly affected compared to the mandible (Ramachandran Nair, 2003). Periodontal apical cysts are more common in the 30 to 39 age group, with a male predilection (Bhaskar, 1966; Avelar *et al.*, 2009). In our study, a prevalence of 5.6% was observed which is slightly less than the reported prevalence by Ledesma-Montes *et al.* (2000) and Avelar *et al.* (2009). Furthermore, all of the affected cadavers in our study were males which are in accordance with the findings by Bhaskar, (1966) and Avelar *et al.* (2009). To our knowledge, little exists on the prevalence of periodontal apical cysts in the Western Cape population. Our study therefore gives an insight into the prevalence of periodontal cysts in persons from low socio-economic backgrounds in the Western Cape.

Anterior cervical plates are beneficial, as it provide immediate stability and restoration of the normal lordotic curve (Park *et al.*, 2005). Nonetheless, long-term adjacent-level degenerative changes have been reported, in particular anterior osteophyte development and anterior

longitudinal ligament ossification (Braunstein *et al.*, 1980; Hilibrand *et al.*, 1999; Hilibrand and Robbins, 2004; Park *et al.*, 2005). In our study, anterior marginal osteophyte formation in the adjacent vertebrae was observed in the cadaver who presented with arthrodesis. However, complete bridging of the adjacent disc space as well as ossification of the anterior longitudinal ligament, was absent. The signs and symptoms of radiculopathy, myelopathy and cervical instability, are common pathologic conditions which result from arthrodesis (Hilibrand *et al.*, 1999; Park *et al.*, 2005), could not be determined in our cadaver. The spinal canal and both the anterior and posterior tubercles of the transverse processes on either side of both vertebrae appeared normal. We can therefore assume that the spinal cord posterior to and spinal nerves running from C5 and C6 were intact and unharmed, making it less likely for radiculopathy and myelopathy to have occurred prior to death.

Diffuse idiopathic skeletal hyperostosis (DISH) is a common skeletal condition of unknown etiology (Weinfeld *et al.*, 1997; Kim *et al.*, 2004; Sarzi-Puttini and Atzeni, 2004; Westerfeld *et al.*, 2008). With DISH, longitudinal ligaments and entheses in the spinal column become ossified consequently leading to decreased mobility (Weinfeld *et al.*, 1997; Kim *et al.*, 2004; Sarzi-Puttini and Atzeni, 2004; Westerfeld *et al.*, 2008). In a review by Utsinger (1985) on racial and ethnic disparity in the prevalence of DISH, a wide-ranging prevalence was observed in different geographic regions worldwide. A predisposition for males exists (Utsinger, 1985; Westerfeld *et al.*, 2008; Aufderheide and Rodríguez-Martín, 2011) and it is believed to be more common among white individuals compared to black individuals (Utsinger, 1985; Aufderheide and Rodríguez-Martín, 2011). This was in agreement with findings from our study as a male

preponderance was observed (male to female ratio = 2.3:1). With regard to ethnicity in our study, mixed race individuals were more commonly affected by DISH, followed by whites. Less black individuals were affected (mixed race: white: black = 1.7:1.5:1). DISH generally presents after the fourth decade of life (Aufderheide and Rodríguez-Martín, 2011). Our findings support this impression as the average age of the affected cadavers was 60.5 years. Trauma, occupational stress, endocrine abnormalities and genetic factors are among the factors that have been proposed as possible causes of DISH, however, the etiology still remains unknown (Weinfeld *et al.*, 1997; Kim *et al.*, 2004; Sarzi-Puttini and Atzeni, 2004). The portion of the spine commonly affected by DISH is the thoracic spine (Kim *et al.*, 2004; Sarzi-Puttini and Atzeni, 2004). This is in accordance with findings from the present study as the thoracic spine was the most common segment involved (75.0%) followed by the cervical spine (33.3%) and lumbar spine (16.7%).

Spina bifida (rachischisis) is one of most common spinal congenital defects (Aufderheide and Rodríguez-Martín, 2011). The prevalence of spina bifida occulta (SBO) in the lumbosacral segments is relatively high, ranging between 5-25% of cases (Wynne-Davies, 1975; Aufderheide and Rodríguez-Martín, 2011). This is particularly prevalent at the 5th lumbar and 1st sacral level. This condition, however, should be distinguished from the more serious spina bifida cystica. None of our cadavers presented with the latter. Incomplete fusion of the posterior vertebral neural arch was observed in 1.6% of the cadaver cohort. Two cadavers presented with incomplete fusion at the 4th and 5th lumbar level and atlas, respectively. The incidence of SBO has been shown to be higher in individuals below 40 years (Boone *et al.*, 1985). As part of aging, new bone formation or calcification may occur in the connective tissue located in the posterior arch defect (Boone *et al.*, 1985), which may explain the decreased incidence of SBO over the age

of 40 years. Some studies have indicated progressive closure of spinal defects below the age of 18 years (Boone *et al.*, 1985). The ages of both affected cadavers in our study were unknown.

Osteoarthritis (OA), a common finding in the elderly, is typically associated with marginal osteophyte formation on the anterior aspects of the vertebral bodies (Klaassen *et al.*, 2011). Vertebral osteophytes have been implicated as a response to erect posture during bipedal movement rather than differences in occupational stress (Knusel *et al.*, 1997; Klaassen *et al.*, 2011). This may suggest the absence of disparities with regard to sex, ethnicity and social class (Klaassen *et al.*, 2011). Vertebral osteophytes were a common feature in our study as 56.5% of cadavers were affected. No sex disparity was observed and the average age of the affected cadavers was 54.1 years (range 32-83 years). Vertebral osteophytes are uncommon under the age of 30 years and have an increased occurrence with an increase in age (Aufderheide and Rodríguez-Martín, 2011). Despite the fact that vertebral osteophytes may develop on all of the cervical vertebrae, the lower cervical vertebrae have an increased tendency to be affected which is ascribed to their mobility (Yoskovitch and Kantor, 2001; Klaassen *et al.*, 2011). In our study, cervical vertebrae C3 to C7 were the most commonly affected. Atlas and axis involvement in combination with the lower cervical vertebrae were affected in 5/70 (7.1%) cadavers with osteophytes. O'Neill *et al.* (1999) showed a predilection for T9 and T10 osteophytic development in 1180 subjects with thoracic spinal involvement. This was in agreement with findings from our study as 24/70 (34.3%) cadavers had T9 and T10 involvement. Overall, the lower thoracic vertebrae (T7-T12) were more commonly affected (57.1%) compared to the upper thoracic vertebrae (T1-T6) (27.1%). The disparity between upper and lower thoracic vertebrae can be explained by the load-bearing nature, particularly in the lower vertebrae (Klaassen *et al.*,

2011). Lumbar vertebrae are, like their thoracic counterparts, common sites for the formation of osteophytes (Klaassen *et al.*, 2011). This is in agreement with our study as lumbar involvement was observed in (65/70) 92.9% of the cadavers with vertebral osteophytes. Mechanical factors and heavy physical activity are the causes for development of lumbar vertebral osteophytes (O'Neill *et al.*, 1999). Karasik *et al.* (2006) associated lumbar vertebral osteophytes with cardiovascular complications in the Framingham Heart Study. In the study by Karasik *et al.* (2006), a correlation was observed between anterior lumbar vertebral osteophytes and abdominal aortic atherosclerosis in 2018 subjects. Our findings support this finding as a statistically significant association ($p < 0.05$) was observed between anterior lumbar vertebral osteophytes and abdominal aortic atherosclerosis in the cadavers. Although several studies have focused on the epidemiological prevalence of osteoarthritis and vertebral osteophytes, little has been published to our knowledge on the prevalence and incidence of osteoarthritis in the Western Cape population.

The average prevalence of spondylolysis in the literature ranges from 3.5% to 7.0% (Eisenstein, 1978; Soler and Calderón, 2000; Kalichman *et al.*, 2009). A predilection for males exists (Kalichman *et al.*, 2009; Aufderheide and Rodríguez-Martín, 2011). In our study, spondylolysis was observed in 1.6% of the cadavers. Both of the cadavers in our study with spondylolysis were males; one black individual and one individual with mixed ancestry. Black individuals are less likely to be affected compared to white individuals (Aufderheide and Rodríguez-Martín, 2011). For many years the natural history of spondylolysis has been under debate since the fetal incidence has been shown to be zero (Newman and Stone, 1963; Beutler *et al.*, 2003). Rosenberg *et al.* (1981) investigated the prevalence of spondylolysis and spondylolisthesis in 143 non-

ambulatory adults. The authors noted no pars defects on obtained radiographs. These findings, as well as a study by Frederickson *et al.*, (1984), gave the impression that pars lesions occur as a result of continuous stress to the lower lumbar region (Standaert and Herring, 2000). The presence of spondylolysis is therefore indicative of a history of strenuous work by the individual which may result in lower lumbar pars lesions. This was confirmed by Prof. George Maat, a forensic anthropologist at Leiden University in the Netherlands (Personal Communication, May 12, 2014). The cadavers from low socio-economic backgrounds were most likely forced by circumstances to do hard labor to earn an income, which may explain the presence of spondylolysis in the small study cohort.

Lumbosacral transitional vertebrae (LSTV) are congenital spinal anomalies which are commonly seen in between 4 and 30% of the general population (Hsieh *et al.*, 2000; Konin and Walz, 2010). Of these anomalies, sacralisation (transition of L5 to a sacral configuration) is more commonly observed than lumbarisation (assimilation of S1 to the lumbar vertebrae) (Bron *et al.*, 2007). Sacralisation has been described in a study done by Dharati and coworkers and was seen in about 3.6% to 18% of the study subjects, usually occurring bilaterally (Dharati *et al.*, 2012). In addition, the authors noted a male predominance of sacralisation within their study subjects (Dharati *et al.*, 2012).

Trauma to the thoracic area encompasses 10-15% of all traumas (Sirmali *et al.*, 2003). The most common ribs fractured, as a result of blunt force trauma, are ribs 4 to 9 (Sirmali *et al.*, 2003). Our findings support this observation as the majority of the rib fractures were observed on multiple ribs with more fracture occurring on the left side (32.6%) when compared to the right side

(6.5%). Even though the time and cause of the rib fractures in our study could not be confirmed, it is likely that the fractures were as a result of MVAs, falls or blunt force trauma (BFT). All of the rib fractures observed in our cadavers showed callus formation, suggesting that they did not occur shortly before death, and therefore is not the cause of death. Sirmali *et al.* (2003) suggested rib fractures are indicative of severe trauma and an increase in morbidity and mortality is observed with an increase in the number of involved ribs. No signs of concomitant liver or splenic trauma were observed with lower rib fractures in our cadavers. The occurrence of liver or splenic trauma as a consequence of lower rib fractures were described by Bulger *et al.* (2000); Wicky *et al.* (2000) and Sirmali *et al.* (2003).

Pectus carinatum (“pigeon breast”) is regarded as one of the most common congenital abnormalities of the anterior thoracic wall; however it is still less frequently observed than pectus excavatum (Goretsky *et al.*, 2004; Lamrani *et al.*, 2010; Van der Merwe *et al.*, 2013). Pectus carinatum has a male predilection with up to 80% of affected cases involving males (Goretsky *et al.*, 2004). In our study, 2/3 (66.7%) cadavers with pectus carinatum were males. None of the cadavers in our study presented with pectus excavatum.

Females are more commonly affected by peripheral fractures compared to males (Donaldson *et al.*, 1990; Baron *et al.*, 1996; Baron *et al.*, 1996). Trabecular bone has been shown to be more susceptible to osteoporosis, especially in postmenopausal women (Mazess, 1983; Donaldson *et al.*, 1990). This explains the female preponderance in the literature as the majority of the studies include older subjects in their study samples. A slight male preponderance for peripheral fractures was observed in our study with a male to female ratio of 1.6:1. Two possible

explanations exist for this finding. Firstly, the fact that our cadavers are mostly from low socio-economic backgrounds where alcohol is consumed on a daily basis and increased interpersonal violence (IPV) is observed, can explain the male preponderance in our study sample. Secondly, the average age of the cadavers with peripheral fractures was 49.2 years, which is relatively young compared to subjects in the literature. Since osteoporosis is regarded as a disease of the elderly, it was less likely that the fractures observed in the cadavers were as a result of decreased bone density. With reference to the site of peripheral fractures, the most proximal and distal ends of the bones have the highest incidence (Baron *et al.*, 1996).

Patellar fractures have a low incidence and no sex disparity (Baron *et al.*, 1996). In our cohort, two cadavers presented with patellar fractures and both were males. Males and black individuals have a lower risk for pelvic fractures compared to females and whites (De Smet and Neff, 1985; Griffin *et al.*, 1992; Baron *et al.*, 1996). The male to female ratio of the cadavers with pelvic fractures in our study was 1:2.3 and the ethnicity was mixed race and black. No posterior lesions were observed in the sacral region of the cadaver with the open book pelvic fracture, suggesting the disruption of the pubic symphysis was less than 2.5cm (Tile, 1988). One female cadaver presented with healed sacral trauma. Generally, sacral fractures are associated with other fractures of the pelvic ring (Tile, 1988). The sacral fracture occurred as an isolated fracture as this cadaver did not have signs of any other fractures in her pelvic ring. This cadaver, however, had multiple healed fractures of the appendicular and axial skeleton, suggesting a history of either involvement in a MVA or several episodes of BA. A predilection for elderly males exists for clavicular and scapular fractures (Baron *et al.*, 1996). With regard to clavicular fractures, all of the cadavers with signs of clavicular trauma were males over the age of 50 years. This was

consistent with studies by Knowelden *et al.* (1964); Donaldson *et al.* (1990); Griffin *et al.* (1992) and Baron *et al.* (1996). In terms of the scapular fractures, 60% of the cadavers from our study were females which are in contrast with what has been shown (Knowelden *et al.*, 1964; Donaldson *et al.*, 1990; Griffin *et al.*, 1992; Baron *et al.*, 1996). Although the female preponderance observed in our study is in contrast with other studies, it may be ascribed to increased domestic violence as scapular fractures are characteristic of physical abuse (Hornor, 2005).

Erosion or compression of the glenoid fossa during glenoid instability and shoulder dislocation resulted in changes in the glenoid rim morphology (Sugaya *et al.*, 2003). Failure to treat the shoulder dislocation in one cadaver resulted in osseous changes in the glenoid fossa, antero-medial part of scapula and humeral head which showed extensive degeneration as a result of continuous friction against the anterior rim of the glenoid fossa. A Bankart lesion is a common finding in repeated shoulder dislocations and occurs when a part of the antero-inferior labrum detaches from the glenoid (Sugaya *et al.*, 2003). A bony Bankart lesion was observed in the cadaver with the dislocation in our study, which is consistent with repeated or permanent anterior shoulder dislocation. A low incidence of less than 2% of shoulder dislocations in different population groups has been reported by several authors (Nordqvist and Petersson, 1995; Edelson, 1996). In our study, one male cadaver was affected, and even though a male preponderance has previously been observed (Hovelius *et al.*, 1983), the true incidence of shoulder dislocations in our study cannot be determined due to the small sample size.

Although degenerative joint disease (DJD) is the most common type of joint disease, the true prevalence remains uncertain due to the large number of asymptomatic cases (Salter, 2002). Radiological studies have suggested that over 80% of people older than 55 years have DJD. DJD is not caused by old age; however the prevalence of DJD increases as one gets older (Salter, 2002). The average age of the cadavers with DJD in our study was 59.5 years (range: 39-83 years) with 58.8% of the affected cadavers being older than 50 years. Mechanical stress as a result of “wear and tear” is regarded as one of the main causes of DJD (Salter *et al.*, 2002). Obesity has been associated with an increased incidence of DJD, not only due to biomechanical factors but also as a result of lipid metabolism (Aspden *et al.*, 2001). The average body mass index (BMI) of the cadavers in our study was 16.5, which suggests that the cadavers were on average underweight. In our study, DJD was observed in 34 cadavers, with only 3/34 (8.8%) cadavers being overweight, suggesting that obesity did not play a role in DJD in our cadavers but rather factors such as strenuous physical activity. Degenerative changes to the joints appear to not be sex-specific (Bachmann *et al.*, 1999; Bonsell *et al.*, 2000). In our study, no statistically significant difference ($p > 0.05$) was observed between males and females, therefore supporting the notion by Bonsell *et al.* (2000). Bilateral total hip arthroplasty (THA) was observed in one cadaver (male, unknown age). The THA in this cadaver appeared to have been performed during two different hospitalizations as the two prostheses differed in size and appearance. The acetabular component of both prostheses was cemented onto the bone. Although the use of cemented THA is still a common procedure today, uncemented THA is increasingly common in Europe and North America (Hailer *et al.*, 2010).

Sacroiliac joint (SIJ) fusion is a common occurrence within the older adult population with a dominant male prevalence (Stewart, 1984; Waldron and Rogers, 1990; Dar *et al.*, 2005; Dar *et al.*, 2008). Our findings confirm this as 6.5% of our cadavers had SIJ fusion and all were males with an average age of 57.9 years (range 42-72 years). Fusion typically occurs on the superior aspects of the sacroiliac joint (Dar *et al.*, 2008), as was the case in our study. Stewart (1984) noted a slight predilection of right-sided involvement when SIJ fusion was unilateral, and is in agreement with our findings. Although unilateral involvement was observed, bilateral involvement was still more common in our study. Ankylosing spondylitis (AS), a condition of unknown etiology is commonly associated with bilateral SIJ involvement (Braun *et al.*, 2002; Aufderheide and Rodríguez-Martín, 2011). Incomplete or complete bony fusion of the SIJ is a *sine qua non* finding in AS (Braun *et al.*, 2002; Aufderheide and Rodríguez-Martín, 2011). DISH, on the other hand, has been implicated in bony fusion of the SIJ, however in the presence of DISH; intra-articular bony ankylosis is absent (Aufderheide and Rodríguez-Martín, 2011). In our study, DISH was absent in 7/8 (87.5%) of the cadavers with SIJ fusion, suggesting AS is the cause for bony SIJ fusion in these cadavers. Bilateral bony bridges were observed in the cadaver with DISH. In this cadaver it is therefore unlikely that AS played a role in SIJ fusion.

Osteomyelitis, a bacterial inflammatory reaction with concomitant bone destruction (Lew and Waldvogel, 2004; Underwood, 2004), has no sex or age preference and may affect any portion of bone (Lew and Waldvogel, 2004). Osteomyelitis is common in children and the elderly (Underwood, 2004). The average age of the cadavers with osteomyelitis was 66.0 years (range: 50-82 years). The bones mostly affected by osteomyelitis, in our study, were the humerus and tibia. These sites are in accordance with findings from other studies in which the tibia, femur and

humerus have been shown to be the most common sites of osteomyelitis (Agaja and Ayorinde, 2008; Beckles *et al.*, 2010). Signs of direct contamination from external contamination were present in one cadaver with osteomyelitis (this was as a result of a compound fracture). Hematogenous dissemination was the most likely route of infection in the remaining cadavers with osteomyelitis. To our knowledge the majority of research on osteomyelitis has focused on the burden, morphology and treatment of osteomyelitis in children (Blyth *et al.*, 2001; Museru and Mcharo, 2001; Kucukkaya *et al.*, 2002; Beckles *et al.*, 2010; Wynn Jones *et al.*, 2011) and very little is known about adult osteomyelitis. Our study therefore gives an insight into the prevalence of osteomyelitis in a Western Cape population with a high TB burden and low SES.

Cortical bone reacts to insults by periosteal reaction (Rana *et al.*, 2009). Bilateral periosteal new bone formation is characteristic of hypertrophic (pulmonary) osteoarthropathy (HPOA). HPOA, defined as a triad of tubular bone periostitis, digital clubbing and arthritis, has been associated with several diseases, such as pulmonary neoplasms and infections (Ali *et al.*, 1980; Vigorita, 1999; Yao *et al.*, 2009; Ito *et al.*, 2010). Even though digital clubbing is associated with HPOA, it is not a constant finding in individuals with HPOA (Morgan *et al.*, 1996). This was in agreement with findings from our study as digital clubbing was observed in only 2/15 cadavers (13.3%). The tibia was mostly affected by non-specific periostitis (13/15; 86.7%), followed by the fibula (9/15; 60.0%) and femur (7/15; 46.7%). HPOA is typically associated with pulmonary neoplasms (Vigorita, 1999; Ito *et al.*, 2010) and were described by Ito *et al.* (2010) as being a paraneoplastic condition. One cadaver which had signs of HPOA presented with a concomitant primary pulmonary neoplasm (adenocarcinoma). In addition to pulmonary neoplasms, bronchiectasis has been implicated to cause HPOA (Vigorita, 1999). In our study, bronchiectasis

was observed in 10/15 (66.7%) cadavers with HPOA. This association was proven to be statistically significant ($p < 0.05$) in our cadaver cohort. Liver disease on the other hand, was only observed in 6/15 cadavers (40.0%). The link between liver disease and HPOA in our study was statistically insignificant ($p > 0.05$), suggesting the HPOA was not a complication of liver disease in our cadavers.

Cribriform orbitalia (CO) has been associated with several conditions, including acquired or congenital anemia (Bergman, 1993; Wapler *et al.*, 2004; Aufderheide and Rodrigues-Martin, 2011), nutritional deficiencies, particularly magnesium ions (Mg^{2+}), chloride ions (Cl^-), iron (Fe^{3+}) and folic acids or by helminthiasis or malaria (Bergman, 1993). In our study, no signs of CO were observed in the cadavers with *Ascaris lumbricoides* infection, suggesting that the duration of the *A. lumbricoides* infection was not long enough to result in CO. In addition to helminthic infections, an increased susceptibility to anemia is associated with certain gastrointestinal disease (Blom *et al.*, 2005). Gastrointestinal diseases, including gastric and intestinal ulcers were absent in the cadavers with CO. Females are more prone to anemia during menstruation, pregnancy and lactation (Bharati and Basu, 1990). In our study, however, no females were affected by CO, proposing that CO in the males were most probably acquired during childhood years. Some bacterial pathogens, including *M. tuberculosis* have been shown to thrive at high levels of iron (Walter *et al.*, 1997; Lounis *et al.*, 2001; Blom *et al.*, 2005). PTB was observed in 4/6 (66.7%) cadavers with CO. It is most likely that PTB played a role in acquired iron deficiency which resulted in CO; however, this association could not be confirmed in the present study.

Paget's disease of bone (osteitis deformans) is commonly observed in white individuals from European descent; however, black individuals may also be affected (Barker, 1981; Gennari *et al.*, 2005). In our study, the cadaver (K79/12) affected with Paget's disease was of mixed ancestry (female, 49 years). Little is known about the prevalence disparity between white and black individuals compared to individuals of mixed ancestry. Due to the small sample size in our study, we are not able to address the prevalence of Paget's disease in our cohort. Gennari *et al.* (2005) observed 1% prevalence among 1778 subjects from Italy, which was comparable to the 1% prevalence among 4528 subjects from Spain (Guañabens *et al.*, 2008). Poór *et al.* (2006) observed an even lower prevalence (0.3%) in 6935 individuals from different parts in Europe. This illustrates that even though Paget's disease is a relatively common finding in white individuals from Europe, it still remains a rare skeletal condition. Isolated hyperphosphatasia has been regarded as the biochemical characteristic for Paget's disease (Doyle *et al.*, 2002; Gennari *et al.*, 2005). Individuals with Paget's disease exclusively affecting one or two bones are likely to have a plasma alkaline phosphatase (ALP) activity of less than 150U/L (Doyle *et al.*, 2002). Although information of the plasma ALP levels of this cadaver is unknown, it may explain the unilateral involvement of four bones.

Internal frontal hyperostosis (IFH), defined as bone deposition exclusively to the inner table of the frontal and occasionally parietal bones, has been reported to be a common phenomenon in postmenopausal females (Verdy *et al.*, 1978; Barber *et al.*, 1997; She and Szakacs, 2004). This is in agreement with findings from our study as two female cadavers aged 62 and 73 years, respectively, presented with thickening of the frontal and parietal bones. Although Hershkovitz *et al.* (1999), observed a female preponderance, males also presented with IFH. In our study,

both cadavers with IFH were females. Even though several conditions, including diabetes, obesity and acromegaly, have been observed in combination with IFH, the aetiology remains unknown (She and Szakacs, 2004). It is believed that prolonged estrogen stimulation is linked to IFH (She and Szakacs, 2004), which may explain the increased prevalence in postmenopausal females.

5.1.5 Statistically Significant Trends Observed in the Present Study

The present study illustrates a downward trend in the anatomical distribution of PTB over the three cadaver cohorts (years). One possible explanation may clarify this observation: according to the Centre for Social Science Research (CSSR), more South Africans are currently on highly active antiretroviral therapy (HAART) compared to the year 2005. A linear increase has been observed since 2005 with more than 800,000 individuals receiving HAART in 2010 (Nattrass, 2006). Keeping this in mind, it is possible that the individuals from the last cohort (2013) have received therapy and this may therefore explain the downward trend in PTB lesions compared to the 2011 and 2012 cohorts. On the other hand, as the dynamic of each cohort is different, the observable findings may just be an accidental coincidence.

Pneumonia is regarded as one of the most common infectious diseases responsible for a high morbidity and mortality worldwide (Franquet, 2001). Acute bronchopneumonia was observed in 62/127 (48.8%) cadavers, occasionally in conjunction with TB (27/97; 27.8%). A statistically significant association ($p < 0.05$) was observed between the prevalence of pulmonary TB and bronchopneumonia in our cadaver cohort, suggesting that an underlying bronchopneumonia in the cadavers resulted in the lungs being more susceptible for a TB infection and *vice versa*.

Several precipitating risk factors for pneumonia have been proposed by Kumar and Clarke (1999), including cigarette smoking, heavy consumption of alcohol, bronchiectasis and immunosuppression as a result of HIV/AIDS with a resultant PCP, MAI or CMV infection. In our cadavers, these risk factors most likely contributed to and explain the high prevalence of underlying pneumonia. The focus of the majority of pneumonia-related research in South Africa, to our knowledge, is on specific etiological agents responsible for pneumonia, particularly in the pediatric population. Furthermore, research has focused on the incidence of pneumonia in immune-compromised individuals in South Africa. To our knowledge, little is known about the prevalence of bronchopneumonia in a Western Cape population, particularly a population with a high prevalence *M. tuberculosis* infection. This study may therefore give an insight into the prevalence of pneumonia in association with PTB in a Western Cape based population.

Nontuberculous mycobacteria (NTM) are ubiquitous environmental microorganisms that have been shown to cause disease, especially in immune-compromised individuals (Khor et al., 2001; Kim et al., 2008). An underlying chronic lung disease, such as chronic obstructive pulmonary disorder (COPD), in middle-aged men was previously recognized as a risk factor for nontuberculous mycobacterial infections (Kim et al., 2008). *Mycobacterium avium* complex (MAC), a common NTM, has been responsible for mycobacterial infection in individuals affected with HIV and AIDS (Khor et al., 2001). Prince et al. (1989) and others observed an increase in the number of NTM infections in elderly white female patients without preexisting lung disease (Huang et al., 1999; Sepkowitz, 2002 Kim et al., 2008). It has been proposed that NTM infection in HIV-negative, elderly white women may be the result of an immune defect (Kim et al., 2008). However, the morphologic characteristics of these NTM-infected, HIV-

negative individuals include skeletal abnormalities such as scoliosis and pectus excavatum, as well as mitral valve prolapse and a thin body habitus (Kim *et al.*, 2008; Reves and Schluger, 2014). A limitation of our study, however, was that the presence of NTM could not be distinguished from the MTBC infection. It was therefore impossible to tell if the mycobacterial infection in each cadaver with TB was a mixed infection with NTM involvement.

The deposition of carbon pigment within the pulmonary parenchyma is known as anthracosis (Emamhadi *et al.*, 2012; Kumar *et al.*, 2013). In this study, only two types of pneumoconiosis were observed in the cadaver cohort; asymptomatic anthracosis and simple coal workers pneumoconiosis (CWP). The main difference between these two conditions is that cadavers with simple CWP typically presented with carbon-laden macrophages, while this feature was absent in the asymptomatic cases. Progressive massive fibrosis (PMF) is associated with the third form of pneumoconiosis; namely complicated CWP (Kumar *et al.* 2007). The pulmonary cavitations observed in cadavers with anthracosis were most probably due to pulmonary pathology other than CWP and PMF. In more severe cases, bronchial anthracofibrosis (BAF) may lead to stenosis of the bronchial airways (Emamhadi *et al.*, 2012). In a study to determine the relationship between BAF and PTB, a statistically significant association ($p < 0.05$) was observed (Emamhadi *et al.* 2012). The cadavers from our study did not show morphologic signs of BAF and a correlation between BAF and PTB could therefore not be determined. With regard to pulmonary anthracosis in our cadavers, no statistical significant association was observed with pulmonary TB ($p > 0.05$). This is in contrast with findings from other studies (Chung *et al.*, 1998; Kim *et al.*, 2009; Ghanei *et al.*, 2011). One possible explanation exists for the difference in findings. The average age of the affected cadavers was 49.8 years. Pazoki *et al.* (2012) observed

an average age of 72.3 years among their 150 subjects. Both Ghanei *et al.* (2011) and Pazoki *et al.* (2012) reported an increased prevalence of pulmonary anthracosis among the elderly. Ghanei *et al.* (2011) stated that an increase in age leads to a 1.07% increased risk of developing anthracosis. The relative young age of our cadavers compared to subjects from other studies, may explain the absence of a statistical association between anthracosis and PTB. According to the literature, females tend to have a predilection for the development of pulmonary anthracosis (Chung *et al.*, 1998; Kim *et al.*, 2009; Fekri *et al.*, 2010; Ghanei *et al.*, 2011) and the affected male to female ratio of affected cadavers was 1:1.2. This is therefore in agreement with the literature.

Pulmonary TB and chronic obstructive pulmonary disease (COPD) are both pulmonary diseases with major mortality and morbidity worldwide (Chakrabarti *et al.*, 2007; Inghammar *et al.*, 2010). Pulmonary TB and COPD have certain risk factors in common, including smoking and low SES (Inghammar *et al.*, 2010). Emphysema, bronchiectasis, chronic bronchitis and asthma are all conditions collectively grouped under COPD.

In our study, a negative statistically significant correlation between emphysema and PTB was observed ($p < 0.05$). This correlation suggests that when emphysema was present PTB was absent and *vice versa*. Usually, irregular emphysema is diagnosed when respiratory bronchioles, alveolar ducts and alveolar sacs are affected by large airspaces (bullae) in a haphazard manner (Heppleston and Leopold, 1961). Pulmonary TB, whether treated or untreated, has been shown to result in airflow obstruction (Hnizdo *et al.*, 2000). Although the majority of the cadavers showed signs of PTB with extensive cavitation and fibrosis, the findings from our study suggests

that pulmonary emphysema in our study were most likely as a result of smoking or inhalation of airborne pollutants (i.e. wood fires and passive smoke inhalation), rather than PTB.

Bronchiectasis is an uncommon disease with a variety of causes (Barker, 2002). A statistically significant association was observed between bronchiectasis and pulmonary TB in our cadavers ($p < 0.05$). This was in accordance with the literature (Jordan *et al.*, 2010). Swensen *et al.* (1994) implicated *Mycobacterium avium* complex (MAC) as the primary cause of bronchiectasis in patients infected with MAC. Barker (2002) noted that a primary MAC infection is particularly common in elderly white females and can lead to the development of bronchiectasis. A chronic and persistent cough, small pulmonary nodules and middle-lobe involvement are common features of a MAC infection (Huang *et al.*, 1999; Barker, 2002; Sepkowitz, 2002; Kim *et al.*, 2008). The association between a MAC infection and bronchiectasis may be explained by the fact that a chronic cough concomitant with continuous production of mucus predisposes the lung to develop mucus plugging and chronic obstructions, which is a risk factor for the development of bronchiectasis. Mannino and Buist (2007) reported the highest frequency of COPD in the South African male population. This study was compared to 16 countries, including China, Philippines and Mexico. Although bronchiectasis is grouped under COPD, the true prevalence of bronchiectasis remains unknown in the Western Cape population. The present study can therefore fill this void and report a prevalence of 39.0% in the cadavers from low socio-economic backgrounds with a high prevalence of PTB.

Pleural effusions found in our cadavers can be ascribed to one of the following causes. During the embalming process, constant pressures are maintained to permit flow of embalming fluid

through the cadaver. These pressures may lead to an artefactual pleural effusion (Chew *et al.*, 2006). The presence of the pleural effusions may be a result of an inflammatory process within the pulmonary parenchyma, such as the chronic inflammatory response associated with TB. A statistically significant association was observed between the radiological and pathological findings of pleural effusions in the first cadaver cohort ($p < 0.05$). However, when the pleural effusions were correlated with pulmonary TB, no statistical significant association was observed ($p > 0.05$) making it more probable that pleural effusion resulted from the embalming process and was thus an artifactual finding.

Although pleural thickening is typically observed in patients with TB and tuberculous pleurisy, it remains unclear why some patients do not develop pleural thickening (Ferrer, 1997). In our study, however, a statistically significant association was observed between pulmonary TB and pleural thickening in our cadaver cohort ($p < 0.05$). While pleural thickening is commonly diagnosed on the standard CXR (Aktogu *et al.*, 1996), the full-body digital X-rays used in the present study were used to successfully demonstrate pleural thickening in the cadavers. The prevalence of pleural thickening with underlying PTB disease in the Western Cape is currently unknown. This study can therefore contribute to the understanding of the prevalence of pleural thickening in association with PTB in this cadaver cohort originating from the Western Cape.

Tuberculous involvement of the ribs as a result of hematogenous dissemination, is an uncommon feature, however, direct spread from an active tuberculous pleuritis may be more common (Roberts *et al.*, 1994; Santos *et al.*, 2006). Proliferative inflammatory lesions are the common manifestation of tuberculous rib involvement, rather than osteolytic changes resulting from

hematogenous dissemination. According to Santos *et al.* (2006), tuberculous involvement of the ribs is usually seen concomitant with tuberculous involvement of the spine, also known as Pott's disease. In the total cadaver cohort used for our study, 1/124 (0.8%) cadaver with spinal TB was seen and proliferative rib lesions were observed in 35/124 (28.2%) cadavers. If the statement by Santos *et al.* (2006) mentioned above is to be believed, none of the proliferative rib lesions in our cadavers were therefore the result of an active TB pleuritis. In the present study, tuberculous involvement of the pulmonary system is the more common manifestation of this disease, which may explain the decreased prevalence of spinal involvement in the cadaver cohort. When pleural involvement was compared with pulmonary TB findings in our cadaver cohort, a statistically significant association ($p < 0.05$) was observed. The presence of rib lesions and pulmonary TB, on the other hand, showed no statistically significant association ($p > 0.05$). This suggests that the proliferative rib lesions we have observed were not related to TB, but possibly the result of a bacterial pleuritis, which also corresponds to the statement by Santos *et al.* (2006). In addition, Mays *et al.* (2002) observed no correlation between visceral surface rib lesions and tuberculous infection within their study cohort. They noted that it would be injudicious to assume that rib involvement is indicative of TB infection, especially for the purposes of paleopathology.

Spinal TB, as a result of hematogenous dissemination to the anteriorly located vertebral body, is regarded as one of the most common manifestations of skeletal TB (Pertuiset *et al.*, 1999; Turgut, 2001; Abou-Raya and Abou-Raya, 2006; Cormican *et al.*, 2006). The adult intervertebral disks are avascular, making primary tuberculous discitis impossible (Pertuiset *et al.*, 1999). One of our cadavers presented with spinal tuberculous involvement. Spinal fusion occurred as a result of contact between adjacent vertebrae. This is a common finding when spinal TB is observed

(Holloway *et al.*, 2013). Steyn *et al.* (2013) observed a decrease in the overall frequencies of spinal lesions, which they ascribed to different host genetics and variations in strain lineages. The authors also proposed that an increased life expectancy may result in an increased incidence of skeletal involvement (Steyn *et al.*, 2013). HIV remains a major problem in individuals from low socio-economic backgrounds and co-infection with TB may result in a decrease in skeletal involvement as the individuals have a decreased life expectancy. The same understanding can be applied to our cadaver cohort and may explain the decreased skeletal TB involvement.

Pulmonary TB has been implicated in the development of lung cancer (Liang *et al.*, 2009). The chronic inflammation is followed by a high level of fibroblastic activity which is responsible for the development of a fibrous scar (Liang *et al.* 2009). Dheda *et al.* (2005) suggested that interleukin-3 (IL-3), IL-4 and tumor necrosis factor (TNF), the inflammatory cytokines produced during TB, play an important role in the development of a fibrous wall and the scar may contribute to the pathogenesis of a lung tumor. In our cadaver study, no significant association was observed ($p>0.05$), suggesting that in this small cohort, the presence of pulmonary TB is not associated with an increased risk of pulmonary neoplasms.

During chronic inflammation, such as PTB, several immune-modulatory cytokines like IL-1, IL-4 and IL-6, are produced by the antigen presenting cells (APCs) (Turken *et al.*, 2002; Lee and Hirani, 2006; Kumar *et al.*, 2013). High levels of IL-4, a pleiotropic cytokine is found in the serum of patients with chronic inflammatory diseases (Lee and Hirani, 2006). Alexandersen *et al.* (2006) suggested a direct relationship between atherosclerosis and chronic inflammation. Elevated levels of IL-4 have also been detected in the atherosclerotic plaques (Lee and Hirani,

2006). Furthermore, hemostatic changes observed in patients with severe PTB may lead to the development of hypercoagulable states (Turken *et al.*, 2002).

The incidence of cardiovascular disease, in particular atherosclerosis, differs considerably between males and females. This is mainly due to hormone differences (Epstein *et al.*, 1999). Recent studies showed that estrogen had athero-protective effects against the development of atherosclerosis in females (Epstein *et al.*, 1999). Estrogen has been shown to alter serum lipid concentration, affects coagulation and fibrinolysis and plays a role in the production of vasoactive molecules, such as nitric oxide and prostaglandins. As a result, estrogen promotes vasodilation and inhibits atherogenesis (Epstein *et al.*, 1999), which may explain the slight male preponderance with regards to atherosclerosis in the present study.

5.2 Main Findings: Molecular Analysis

Mycobacterial cell walls are virtually not permeable, which contributes to their resistance and persistence within the host. The perseverance of acid-fast bacilli within calcified lung lesions has previously been described in the literature (Pap *et al.*, 1999; Bartos *et al.*, 2006). Furthermore, mycobacteria have been shown to survive in their hosts after death and may be found in tissues subjected to long-term storage (Gerston *et al.*, 1998; Barnes *et al.* 2000; Demiryürek *et al.*, 2002; Gerston *et al.*, 2004; Nolte, 2005). Fletcher *et al.* (2003) were able to extract and amplify mycobacterial DNA of up to 200bp from clinical samples showing macroscopic signs of TB. A positive Ziehl-Neelsen (ZN) result indicated the presence of acid-fast bacteria within the granulomas of our cadaver cohort. However, a number of the negative ZN samples from our study were shown to be positive for mycobacterial DNA when molecular amplification was

applied. This might be due to the possibility that viable mycobacteria are in fact present within the embalmed cadavers; despite the negative ZN and microscopic findings and that that tissue sampling was not extensive enough to represent the entire lung. Another reason might be that direct microscopy and ZN staining of the FFPE pulmonary samples lack sensitivity and specificity (Hermans *et al.*, 1990; Berk *et al.*, 1993) While bacterial culturing is the gold standard for detection of *M. tuberculosis*, it is a time-consuming procedure which may take up to a few months to obtain a positive result (Hermans *et al.*, 1990). Fortunately, a more rapid and sensitive technique compared to AFB staining has been developed for the detection of *M. tuberculosis*. The IS6110 PCR amplifies the high copy numbers of the IS6110 sequence which may increase the sensitivity in the detection of *M. tuberculosis* particularly in paucibacillary tissues (Hermans *et al.*, 1990; Berk *et al.*, 1993; Bartos *et al.*, 2006). This indicates that molecular amplification of mycobacterial DNA is much more specific than ZN staining and could explain why the majority of our samples were positive for mycobacterial DNA in the absence of a positive ZN stain. In the cases where TB was diagnosed with the microscopic findings but negative PCR results were observed, the possibility exists that either very low levels of mycobacteria were present or that viable mycobacteria were completely degraded.

An inverse relationship between positive PCR results and target size of archival DNA has previously been described in the literature (Hagelberg *et al.*, 1989; Höss *et al.*, 1996; Fletcher *et al.*, 2003). This is thought to be as a result of DNA fragmentation over time, which is typical of older DNA (Fletcher *et al.*, 2003). Tissue samples which were subjected to 10% buffered neutral formalin fixation prior to extraction of nucleic acids have been shown to undergo a degree of fragmentation (An and Fleming, 1991; Srinivasan *et al.*, 2002). Our cadavers were embalmed

prior to dissection and kept at temperatures of approximately 18°C for a minimum of 6 months to one year. This means that the human and mycobacterial DNA were subjected to high concentrations of phenol, formaldehyde, ethanol and other chemicals for a long period of time after embalming was completed. During dissections, medical students are instructed to prevent the cadavers from drying out by wetting the organs with 10% buffered neutral formalin (BNF). This further contributes to the hostile environment causing DNA degradation within the cadavers. When the samples were removed, they were placed in labeled specimen bottles containing 10% BNF, which is standard procedure for histology fixation. The majority of studies in the literature focused on DNA extraction from FFPE tissues from biopsy material taken directly from the patient (Jackson *et al.*, 1990; An and Fleming, 1991; Ben-Ezra *et al.*, 1991; Frank *et al.*, 1996; Howe *et al.*, 1997; Marchetti *et al.*, 1998; Chan *et al.*, 2001; Farrugia *et al.*, 2010). As far as we know, Bartos *et al.* (2006) were the only other authors who examined tissue samples from embalmed cadavers for PCR amplification of mycobacterial DNA. Their findings were similar to ours; however, they used only four cadavers. They were successful in obtaining a positive PCR result, yet they were unsuccessful in culturing the mycobacteria. Even though formalin has tuberculocidal effects the embalming fluid cannot successfully penetrate granulomas within the organ parenchyma (Best *et al.*, 1990; Demiryürek *et al.*, 2002; Nemeč *et al.*, 2013; Correia *et al.*, 2014). Correia *et al.* (2014) noted that *Mtb.* may remain viable up to 36 days after embalming. The embalming formulation that is used at the department of Basic Medical Sciences at the University of Free State (UFS), where that study was undertaken, is similar to the embalming method used at our institution (US). The authors at UFS noted that the embalming method was effective in bringing into being non-infectious mycobacteria in TB-positive cadavers (Correia *et al.*, 2014). By the time the cadavers were dissected by medical

students and researchers, the mycobacteria were regarded as non-viable and could therefore not be cultured; however degraded DNA was illustrated with molecular applications.

Zink *et al.* (2001) examined remains from ancient Egyptian tissue samples for morphological and molecular signs of TB. From their samples it was evident that even though the remains showed typical morphological signs of TB, only 66% of the cases were confirmed to contain mycobacterial DNA with molecular studies. The authors noted the limitation of using ancient DNA for molecular analysis (Zink *et al.*, 2001). Similarly, from our results, nucleic acids could be successfully extracted, amplified and analyzed in 107/127 (84.3%). There are three possible explanations for these results. Firstly, the methodologies used for nucleic acid extraction may not have been effective in recovering DNA from FFPE tissue. This is however unlikely as five different nucleic acid extraction protocols were employed to extract DNA from the cadaver samples. In addition, a variety of PCR primers for mycobacterial DNA were used in the present study, each of the primers optimized to achieve a maximum sensitivity. The target amplified product sizes varied from approximately 80bp to more than 500bp. Secondly, there is a possibility that the mycobacterial DNA could not be amplified during the PCR. Nucleotide modification may be the reason for this. In a study done by Srinivasan *et al.* (2002), formaldehyde, a major component of embalming fluid, was found to react with nucleic acids. The *Taq* polymerase enzyme used during the PCR amplification is known for not being able to recognize chemical modifications of the nucleic acids. Therefore, it would not be possible to achieve extension of DNA chains, which is the function of the *Taq* polymerase enzyme (Pääbo, 1989; Barnes *et al.*, 2000). Finally, the absence of DNA in the pulmonary samples could be a result of nucleic acid degradation. This is the most likely scenario as the cadavers used for this

study was obtained between 2009 and 2012. They were embalmed with a combination of phenol, ethanol and formaldehyde and stored in conditions not suitable for the conservation of DNA. Furthermore, the pulmonary samples from the embalmed cadavers were treated and fixed with 10% BNF and embedded in paraffin wax. This in turn would generate protein cross-link in the nucleic acids. All of these changes are not conducive for PCR amplification.

The insertion sequence *IS6110* was the only PCR method to yield valuable data from archival DNA compared to amplification of direct repeat (DR) regions (Donoghue *et al.*, 2004). The amplification of the DR spacers is highly dependent on the preservation of the samples (Donoghue *et al.*, 2004). A positive spoligotyping result has previously been achieved when performed on archival and ancient DNA (aDNA) (Zink *et al.*, 2001; Fletcher *et al.*, 2003; Donoghue *et al.*, 2004). Spoligotyping on our cadaver pulmonary samples, on the other hand, was ineffective in determining and establishing the mycobacterial genotypes as no distinct pattern was observed. It should be noted that particular patterns may be the result of an accumulation of mixed infections (Donoghue *et al.*, 2004). The spoligotypes from our cadavers however, showed no distinct pattern to possibly distinguish mixed infections. According to Taylor *et al.* (1999), care must be taken when drawing conclusions from the spoligotyping patterns from archival and aDNA as they may be altered due to degradation. Degradation of mycobacterial DNA was most likely the reason for the unidentifiable spoligotypes in our cadaver cohort.

A major limitation of this study was that different mycobacterial species could not be differentiated and confirmed. Similar results were observed when the bactericidal properties of

formalin were inspected on mycobacteria from formalin-fixed lungs (Gerston *et al.*, 2004; Correia *et al.*, 2014). Differentiating MTBC from other mycobacterial families will result in a correct diagnosis and appropriate treatment regimen. Accompanied by appropriate and effective public health measures could prevent horizontal transmission between patients. Furthermore, differentiation and characterization of mycobacteria may provide important epidemiological knowledge in a given population (Sen Gupta *et al.*, 2003). Differentiation of mycobacterial DNA has been shown to be successful in peripheral blood (Condos *et al.*, 1996), sputum samples (Godfrey-Fausset, 1995) and even in ancient mummified remains (Zink *et al.*, 2003). The success of differentiation of mycobacterial DNA, is dependent on bacterial load and sample size (Heinmöller *et al.*, 2001; Sen Gupta *et al.*, 2003). We therefore adapted a PCR protocol to enhance the sensitivity of PCR detection as proposed by Sen Gupta *et al.* (2003). The adapted PCR protocols in our study, however, still produced a percentage of false-negative results and the rate of false-positive results may even be higher than expected. This agrees with results from other studies (Cabras *et al.*, 2000; Heinmöller *et al.*, 2001). *In situ* hybridization (ISH) has been shown to be successful (100% sensitivity) in differentiating mycobacterial species from FFPE tissue but the preferred sample for this technique was mycobacterial cultures (Zerbi *et al.*, 2001). It is believed that the embalming fluid together with the storage period prior to the cadaver dissection could interfere with the ISH and this process was therefore not included in the present study. On a morphological level, both caseating and non-caseating granulomas may develop as a result of NTM infection and one can therefore not distinguish between MTBC and NTM based on the presence or absence of necrosis (Schulz *et al.*, 2005). Schulz *et al.* (2005) has shown that the 65kDa heat-shock protein gene is an effective tool for the identification of mycobacterial species. As the majority of our cadavers were most probably infected with mycobacterial species

belonging to MTBC, we chose to differentiate between MTBC and NTM infection within our cadaver cohort. The HAIN[®] MTBDR_{plus}[®] DNA kit (version 2.0), a line probe assay used to determine resistance to rifampicin (RIF) and isoniazid (INH), was found to be successful in determining the presence of mycobacterial species belonging to the MTBC. The resistance to the first-line drugs, such as RIF and INH, however, could not be determined successfully. There are two reasons for this. To begin with, the *rpoB* wild-type (WT) 8 probe was absent in approximately 90% of our samples. Under normal conditions, an absent *rpoB* WT8 probe in the presence of an *rpoB* MUT 3 probe is suggestive of RIF resistance. In the majority of our samples, however, both the *rpoB* WT8 and *rpoB* MUT 3 probes were absent. When HAIN[®] Head Office in Germany was consulted; they proposed the Genotype DNA isolation kit as extraction method for the DNA. The Genotype DNA isolation kit, together with the other four extraction kits all revealed the same line probe assay (LPA) result; absent *rpoB* WT8 and *rpoB* MUT 3 probes. The resistance patterns could therefore not be accurately analysed. Finally, it is believed that one or more of the ingredients of the embalming fluid together with the storage period prior to the cadaver dissection interfered with the HAIN[®] MTBDR_{plus}[®] DNA kit and prevented effective binding to the different *rpoB*, *katG* and *inhA* probes. On the other hand, the TUB probe was present and could therefore confirm the presence of MTBC in our cadaver samples. The presence of MTBC with the HAIN[®] MTBDR_{plus}[®] DNA kit correlated with the macroscopic and microscopic findings in the cadavers. It should also be noted that only the probe band with an intensity as strong as the amplification control (AC) probe was considered as positive (Rienthong *et al.*, 2009).

Cross-contamination is a major problem when working with TB samples in histology laboratories (Gerston *et al.*, 2004). Precautions were taken to prevent cross-contamination between the cadaver pulmonary samples. The samples were handled separately and the cutting blade of the microtome was properly cleaned prior to and after each block was sectioned. It can be said with some certainty that the molecular results obtained from our cadavers are not due to cross-contamination.

After reviewing the literature and evaluating the results, three possible reasons exist for a negative TB-PCR result in our cadaver study. Firstly, tissue sampling errors may have given rise to false-negative results (Hermans *et al.*, 1990). Tissue sampling errors include the use of small tissue samples, selection of areas without mycobacteria and an irregular distribution of mycobacteria within the tissue samples. Secondly, mycobacterial DNA may be damaged due to the fixation process, may be lost during the extraction process or the mycobacterial bacilli may be missed during sectioning. And finally, Hermans *et al.* (1990) noted that tissue with signs of necrosis may inhibit the detection of Mtb. The majority of the cadavers in our cohort presented with extensive necrosis in the pulmonary parenchyma and may explain the number of false-negative cases.

5.3 Main Findings: Radiological Analysis

The chest X-ray (CXR) is the gold standard for diagnosing PTB (Cahn *et al.*, 2003). The typical chest radiograph of PTB in infected patients shows apical and superior lobe involvement, particularly cavity formation (Matsuoka *et al.*, 2004). Studies have shown that the appearance of PTB in the immune-compromised, especially those infected with HIV, is different from the usual

PTB pattern (Aderaye *et al.*, 2003). Pulmonary TB in patients infected with HIV, usually manifests with a decreased number of cavities and an increased involvement of the hilar lymph nodes. Interstitial infiltrates and pleural effusions are also particularly common (Aderaye *et al.*, 2003).

5.4 Postmortem Changes Mimicking Disease

Postmortem changes can cause specific problems when using imaging for diagnostic purposes (Roberts *et al.*, 2012). During embalming at the Division Anatomy and Histology, Stellenbosch University, the carotid artery is used to introduce the embalming fluid to the arterial tree. Consequently the majority of remaining systemic blood is pushed to the venous side during infusion. As a result, postmortem venous thrombosis is a common feature in embalmed cadavers. Shiotani and coworkers described the presence of a high density fluid within the cardiac chambers and blood vessels (Shiotani *et al.*, 2002; Shiotani *et al.*, 2006). In addition to blood, the cadavers also had air in the blood vessels, particularly the arterial tree. Both findings can be presumed to have been as a result of embalming (Chew *et al.*, 2006).

Pleural effusions were extremely common in our embalmed cadavers. Retrospective correlation after gross dissection revealed that some of the cadavers had signs of pleural pathology. A statistical significance ($p < 0.05$; Kappa factor 0.22) was found between the gross and radiologic appearance of pleural effusions in the cadavers. In the cadavers with no obvious signs of gross pleural pathology, a clear fluid was observed within the hemithoraces when the anterior chest wall was reflected and the lungs removed. Even though the clear fluid was not analyzed, we can safely assume it was embalming fluid. Chew *et al.* (2006) noted similar findings on postmortem

computed tomography on embalmed cadavers. The authors stated that the pleural effusions in the absence of pleural pathology, was most likely influenced by the embalming procedure and storage interval of cadavers.

Edematous changes and hypostasis within the pulmonary system after death is a common observation during autopsies and gross dissections (Shiotani *et al.*, 2011). A study was done by Shiotani *et al.* (2011) to determine the differences in appearance of pulmonary edema between immediate and delayed computed tomography in deceased individuals. They found that after death, the lungs tended to have an opacified, consolidated appearance on postmortem computed tomography (PMCT) which is consistent with congestive pulmonary edema. It should be noted that pulmonary edema is a characteristic finding in cardiac-related pathology, including left-sided heart failure. All of the subjects in the study done by Shiotani *et al.* (2011) died of cardiac-related illnesses and the amount of fluid infusion in their cases was not known. Durlacher *et al.* (1950) noted pulmonary congestion and edema in their subjects (rabbits) and suggested two factors responsible for this finding. Firstly, pulmonary congestion and edema resulted from a pressure gradient between the pulmonary vasculature and alveoli. Secondly, changes in the permeability of the capillaries occurred (Durlacher *et al.*, 1950). These factors can certainly be applied to our cadaver cohort, as they were initially subjected to increased intravascular pressures during embalming which may force proteinaceous substances into the alveolar spaces, and secondly, alterations in the permeability of the capillaries may lead to the appearance of pulmonary edema. Shiotani *et al.* (2011) noted that a delay between the time of death and the time at which imaging was acquired may cause two diagnostic problems. Firstly, opacification and consolidation of the lungs as a postmortem effect may disguise pre-existing pulmonary

pathology, including pneumonia. Secondly, when pulmonary edema is present directly after death, autopsy or gross dissection may overemphasize the severity. The authors concluded that the postmortem findings of the lungs are not fixed and will change as time progresses after death (Shiotani *et al.*, 2011). The critically ill, such as those with ALI or ARDS, commonly presents with pulmonary edema (Monnet *et al.*, 2007). In our study, 95/127 (74.8%) cadavers showed microscopic signs of pulmonary edema, while 25/127 (19.7%) presented with diffuse alveolar damage (DAD) as a result of ALI/ARDS. It is imperative in the clinical setting to differentiate between hydrostatic pulmonary edema and ALI/ARDS as the etiology and subsequent treatment differ (Monnet *et al.*, 2007). Clinically, the left atrial pressure is normal in ALI and ARDS cases, while an increased left atrial pressure is observed in the cases with hydrostatic pulmonary edema (Monnet *et al.*, 2007). In our study, information regarding cardiac output is unknown and therefore the true etiology of pulmonary edema could not be determined in our cadavers, except those with signs of ALI/ARDS. However, the effect of the embalming is thought to play a definitive role in the cadaver study sample as the majority of cadavers presented with pulmonary edema.

An increase in the diameter of the heart together with hyperattenuation of the aortic wall on PMCT has been described to occur as a result of postmortem change (Shiotani *et al.*, 2002; Shiotani *et al.*, 2003). During the embalming procedure at the Division of Anatomy and Histology, large amounts of embalming fluid are introduced into the arterial tree. In addition, the mean circulatory pressure of the venous system increases, as the blood in the arterial system is pushed into the venous system. This should be considered as a reason for an increased cardiac diameter after embalming. After death, the shape of the heart should adopt the shape observed

during the diastolic phase (Shiotani *et al.*, 2003). A non-negligible percentage of our cadavers (30/127; 23.6%) presented with apparently dilated hearts and it is therefore possible that the embalming procedure can cause an artifactual dilation of the heart which may be misdiagnosed as a dilated cardiomyopathy. Concerning the thoracic aortas, Shiotani *et al.* (2002) observed hyperattenuation of the aortic walls on PMCT. We did not apply PMCT in our study, however, enlarged, well-demarcated aortas with clear aortic walls were observed in 43/127 (33.9%) cadavers when the Lodox[®] full-body digital X-rays were analysed. Hyperattenuation of the aortas in our cadavers can be seen as a result of embalming fluid entering the thoracic aorta and clearing it of remaining blood. This makes the aortas clearly visible on the CXRs of embalmed cadavers.

Scholing *et al.*, (2009) determined the role of PMCT as an alternative to standard autopsy in determining cause of death (COD). The authors noted that some solid organ pathology was commonly missed when PMCT was applied. These lesions included hematomas, emphysema, brain contusions and superficial lesions of the organs. Similar to their findings, pathology in our cadaver cohort was frequently missed when the Lodox[®] full-body digital X-rays were evaluated. We were unable to make a statistically significant pathologic-radiologic correlation between the majorities of pulmonary pathology observed, except pulmonary cavitation and pleural thickening. During the radiological evaluation of the cadaver chest X-rays, the lung fields of a large number of cadavers appeared opacified, making it difficult to observe and diagnose intrathoracic pathology. One of the advantages of the Lodox[®] Statscan[®] lies in its ability to easily detect foreign objects and obvious fractures within the human body. However, myocardial infarctions and abdominal pathology cannot be diagnosed with X-ray imaging systems. With

regards to traumatic injury to the thoracic wall, the Lodox[®] Statscan[®] missed rib fractures in the majority of the cadavers. Pneumonia presents as consolidation on a CXR (Corne and Pointon, 2010). Consolidation has been previously diagnosed with the Lodox[®] full-body digital X-rays (Daya *et al.*, 2009), suggesting the Lodox[®] imaging system is capable of diagnosing pneumonia in live patients. In our cadaver, however, pneumonia could not be diagnosed. There are two possible explanations for this. Firstly, the consolidated appearance was masked by a non-specific opacification which occurred most likely as a result of embalming and lack of inspiration. Secondly, the degree of pneumonia varied for each cadaver affected by pneumonia. This suggests that consolidation and consequently pneumonia could not be visualized on the CXR of the cadavers with the least severe degree of pneumonia.

5.5 Impact of the Study

In the present study an increase tendency for individuals with a low SES to present with disseminated (miliary) TB was observed. This was mainly attributed to their impaired immune systems, poor nutrition, improper housing and substance abuse such as alcohol and cigarettes. These factors are well-known in the literature to cause a decrease in an individual's immunity (Davies, 2005). In the Cape Town metropole, particularly in the Northern suburbs, community health centers (CHC), in areas such as Elsiesriver, Eerste Rivier, Mitchell's Plain, Vanguard, Delft and Mfuleni, constantly receive and treat patients with TB, either as isolated pulmonary TB (PTB) or the disseminated form. In addition to the CHCs, public hospitals, including Tygerberg Hospital and Karl Bremer Hospital are also experiencing a profound increase in TB-positive patients. This study showed that it is more likely for individuals from low SES communities, to present with PTB or miliary TB, with the latter being significantly high among these

communities. By disseminating this valuable information to the CHCs and public hospitals not only to our local health community but also to the scientific community (by means of peer-reviewed articles), health personnel can obtain the knowledge to take into account the probability of miliary TB among these individuals and adjust the treatment of these individuals accordingly. In addition to this major finding, this study also confirmed that PTB was more common among the male population compared to females of child-bearing age. Similarly, cardiovascular diseases, such as atherosclerosis and consequently ischemic heart disease (IHD), are uncommon in females of the same age. This study confirmed statistically that being a female (with significant levels of estrogen) somehow plays a role in “preventing” PTB and IHD. The literature confirmed that the “protective” effects of estrogen have been demonstrated, however, the subjects of vast majority of the research were rat models. This study is unique in that both the TB status and cardiovascular disease status of the individuals are known.

If the study by Labuschagne and Mathey (2000) is considered, the profile of the cadavers at our institution differs significantly from the cadavers during 1956 to 1996. We have observed an increase in TB, particularly PTB and HIV/AIDS-related diseases in the current cadaver population. This information gives us an idea of the changing face of diseases in a population with low SES over the past six decades. With this concurrent increase in pulmonary pathology in the cadavers, the students can use this to their advantage and observe and learn the pathology while dissecting.

The use of gross macroscopic autopsy as a tool for determining cause of death has previously been recognized (Goldman et al, 1983; Bernardi *et al.*, 2005). Bernardi *et al.* (2005) raised the

question whether or not macroscopic autopsy was complete without systemic histological analysis and therefore aimed to determine the need for microscopy during autopsy. They revealed that histological analysis had a major impact on gross diagnosis and that most diagnostic discrepancies between autopsy and histological examination were noted in the lungs, liver and kidneys. Histological analysis is therefore essential in determining the cause of death (Bernardi *et al.*, 2005). Similar findings were noted in a review by Roulson *et al.* (2005) where microscopic analysis was essential in confirming the diagnosis made on macroscopic level, especially when discrepancies in the main diagnosis, particularly pulmonary-related pathology, was noted. These authors furthermore noted that they were able to diagnose ARDS and carcinoma with histology, which was originally misdiagnosed as lobar and bronchopneumonia, respectively during macroscopic evaluation. Similarly, we experienced discrepancies in macroscopic and microscopic diagnosis. The embalming process resulted in discoloration of organs, in particular the liver and spleen. Furthermore, the consistency of the organs often changed markedly, with some organs becoming extremely hard. In the thorax, embalming-induced pleural effusions were commonly encountered in our cadaver study sample. If the diagnosis could not be confirmed on macroscopic level, a differential diagnosis was made, which was correlated with the histological findings. A section was taken from all the organs of each cadaver for standard evaluation and in a large number of cases, the histological findings were seen as incidental findings. This illustrates the necessity for histological examination during autopsy to accurately confirm the main diagnosis and prevent misdiagnosis on macroscopic level.

The value of combining anatomy, radiology and pathology during medical dissections has previously been recognized (Gunderman and Wilson, 2005; Gregory *et al.*, 2009). Kotzé *et al.* (2012) investigated the efficacy of full-body digital X-rays during medical dissections. These X-rays allowed the students to visualize internal structures prior to as well as during dissections. In addition, abnormalities, specifically pulmonary and skeletal pathology could be observed while dissections were ongoing. The study by Kotzé *et al.* (2012) was performed on the first cadaver cohort used for the present study in 2011. Full-body digital X-rays mounted to the walls of the dissection halls at the Faculty of Medicine and Health Sciences, University of Stellenbosch (FMHS, SU) have shown to be beneficial to medical students. In addition to normal surface and internal organ anatomy, the students were made aware of the pathology while they were dissecting the cadavers. In South Africa and other developing countries, it is imperative for medical students to be exposed to AIDS-defining diseases in their pre-clinical years as they will frequently encounter them when they are clinical practitioners. At the FMHS, SU, the integrated systems-based curriculum is used where students are exposed to systemic anatomy and pathology within weeks of each other. They can therefore be made aware of systemic pathology while they are dissecting the cadavers shortly before dealing with the theory on systemic pathology.

5.6 Limitations of the Study

As would be expected from a study on cadavers used for medical training, several limitations were experienced. Decomposition due to sometimes varying periods of time between death and fixation was problematic. As a result, the brains were severely compromised. In 5/127 (3.9%)

cadavers, the level of decomposition made diagnosis almost impossible both on macroscopic and microscopic level.

Another limitation of this study was that no medical history was available to the researcher including a clinical background, history of smoking, HIV-status and COD. The fact that approximately 90% of our study cohort was unclaimed bodies from low socio-economic backgrounds explained the absence of medical histories. It is an extremely costly process to determine HIV-status in embalmed cadavers with no guarantees of success and regrettably the cost implication was prohibitive in post fixation determination of the 127 cadaver HIV statuses. Furthermore, the National Health Act No 61 of 2003 prevents researchers to publish, even in anonymous studies such as the present one, the terminal cause of death. In our study we therefore aimed to determine the underlying cause of death of each cadaver. Demographic data, such as age, sex and ethnicity was included in the study as far as it was available to the researcher.

A further limitation was the degree of denatured human and mycobacterial DNA. Several different extraction methods were used to obtain the best possible quality DNA. The salting out method was found to be the most suitable and cost-effective method. Several PCR applications with different *Taq* polymerase enzymes were used to analyze the DNA. Several difficulties were experienced as the DNA appeared to be more degraded than originally expected. We introduced the HAIN[®] MTBDR_{plus}[®] (ver. 2.0) kit. Species belonging to the MTBC could be successfully determined. Their resistance to first-line drugs could however not be accurately established. Even though TB was confirmed primarily by means of the morphological appearance of the lung

parenchyma, this technique contributed greatly in the confirmation of our macroscopic and histological diagnosis.

Full-body digital X-rays were obtained from the cadavers after they were embalmed as we are not permitted, by law, to transport unfixed cadavers once they have reached our facility. During the embalming procedure, the upper and lower limbs tended to pull up towards the body. Measures were taken to prevent this during embalming; however, we were unable to avoid this completely. It was therefore very difficult to maintain the cadavers in the anatomical position. The images of the hands and feet were therefore distorted in the majority of the full-body digital X-rays. In addition we were unable to evaluate the joint spaces due to the position of the cadavers.

5.7 Future Research

The following future research may be an outflow from the present study:

The prevalence of osteological TB lesions can be correlated with molecular genotyping of the respective lesions. Several studies have shown skeletal remains to be the ideal site for extraction of mycobacterial DNA (Donoghue *et al.*, 1998; Taylor *et al.*, 1999; Gernaey *et al.*, 2001; Zink *et al.*, 2003; Donoghue *et al.* 2004). By incorporating molecular genotyping in paleopathology, disease patterns and epidemiology, particularly of TB, can be determined.

A complete dental analysis can be performed on the cadaver cohort to establish certain living conditions during childhood. The presence of enamel hypoplasia can tell a great deal about the individual's health. The presence of maxillary and mandibular abscesses, together with

periodontitis and calculus deposition may give insights into dental hygiene and risk factors for dental disease.

Computed tomography (CT) of a cadaver cohort, prior to dissection, can reveal more than just anatomy. A comparison can be done on the morphologic appearance between unembalmed and embalmed cadavers using PMCT. The effects of embalming fluid on the human body and organs can be more accurately established with transverse CT imaging.

The prevalence and distribution of emphysema in the cadaver cohort can be determined by making longitudinal sections instead of transverse sections. The longitudinal section of the lung can then be embedded in paraffin wax and sectioned to visualize the site of emphysematous bullae in the length of the lung.

Formalin-embalmed cadavers undergo profound changes with regard to the colour and strength of the organs. By applying embalming methods with reduced formalin content, the colour and consistency of the organs can be well preserved. The efficacy of the Lodox[®] Statscan[®] Imaging System in diagnosing pulmonary pathology can be evaluated on these cadavers and the results can be compared to the findings from the present study.

5.8 Conclusion

The present study provides a comprehensive pathology report of six organ systems including the skeletal system of 127 cadavers used for medical dissection at the FMHS, SU. The hypothesis of this study states that as these cadavers are mostly unclaimed cadavers from the Western Cape, South Africa, the majority would be expected to be infected with TB. This study shows that pulmonary TB (PTB) was indeed a common manifestation (76.4%) in the cadaver cohort, with males being more commonly affected than females. Secondary PTB typically results in extensive pulmonary cavitations and that was also true for the cadaver population in the present study. A predilection for superior lobe involvement with TB was observed compared to the inferior lobes. This is in contrast with studies that showed an increased tendency of the middle and inferior lobes to be affected by PTB. With regards to EPTB, females were more commonly affected in the present study. This female predilection for EPTB involvement was also previously reported, which suggests that the female sex hormones may either play a protective role against the development of PTB, or they may facilitate the development of EPTB. EPTB was observed in 22.8% of cadavers, with the spleen, liver and lymph nodes the most common sites of infection. Although these sites were also identified by epidemiological studies from other developing countries with a high TB prevalence, in these studies the lymph nodes were the most common EPTB sites.

Although a lower body mass index (BMI) has been implicated as a risk factor for TB (Lönnroth *et al.*, 2010), little is known about the relationship between a very low BMI and TB. In this study, no statistically significant association was observed between a lower BMI and PTB. As the majority of the cadavers in this study had very low BMI (BMI < 16.0), it is likely that very

low BMI values may play a role in TB infection, whether as a risk factor or as the outcome of this disease. Further research, however, is needed to determine the biological role of very low BMI with regards to TB as seen in the cadavers.

In addition to PTB lesions, this health assessment study gives a detailed holistic view of the health status of the cadavers from low socio-economic backgrounds. When TB was investigated in association with systemic pathology, significant trends were observed. One such trend, and perhaps the most striking, was the negative correlation between pulmonary emphysema and PTB in the cadaver cohort. In addition to pulmonary emphysema and contrary to the literature, pulmonary anthracosis, adhesions and pleural effusions were not statistically associated with PTB, including pleural TB, in this study, suggesting that these conditions resulted from pulmonary diseases other than PTB.

The present study furthermore emphasizes the important role of histological examination in determining the diagnosis in the cadaver population. The need for histopathology was illustrated particularly in the pulmonary, cardiovascular and renal system. Incidental findings with histopathology were often encountered in the present study, particularly with regard to pancreatic- and renal TB.

Molecular techniques have been applied to formalin-fixed paraffin-embedded (FFPE) biopsied material in the past. However, little research has focused on the efficiency of molecular techniques, such as nucleic acid extraction methods, line probe assays (LPA) and polymerase chain reactions (PCR) on previously embalmed formalin-fixed paraffin-embedded samples. To

our knowledge, this study is one of the first to apply these techniques to extract and amplify mycobacterial DNA from embalmed cadavers. Although five different nucleic acid extraction methods were applied and tested, the standard salting-out method, which is routinely used in molecular laboratories worldwide, was shown to be the most effective method in extracting nucleic acids from previously embalmed, FFPE tissue. From the variety of molecular applications used to detect and differentiate mycobacterial species, the HAIN[®] MTBDR^{plus}[®] DNA kit (version 2.0), a line probe assay (LPA), was the most effective in determining the presence of *M. tuberculosis* and species belonging to the MTBC in embalmed cadavers. It was found that the larger the fragment size to be amplified, the higher the possibility that a positive PCR result would occur. This was in addition dependent on bacterial load and sample size. The IS6110 PCR was the most successful PCR in amplifying mycobacterial DNA compared to the RD105 and MTUB02/RD105 PCR. Although the cadavers with PTB were infected with species belonging to the MTBC, the genotypes could not be differentiated. We could therefore not determine nor exclude the presence of NTM in the cadaver cohort. Nonetheless, the HAIN[®] MTBDR^{plus}[®] DNA kit (version 2.0), remains the method of choice to demonstrate the presence of species belonging to the MTBC in embalmed cadavers.

The chest X-ray (CXR) is the gold standard for diagnosing PTB in living subjects. Digital imaging systems have several technical and practical benefits and are currently the gold standard in radiography (De Crop *et al.*, 2012). To our knowledge, the focus of the majority of studies which incorporated the Lodox[®] Statscan[®] Imaging System was either to evaluate the status of trauma patients in trauma centers in developed countries, or to assist in the field of forensic

pathology. The present study incorporated the X-rays of embalmed cadavers and determined that it was useful in observing cavitations and pleural thickening in the embalmed cadavers.

In developing countries, such as South Africa, it is crucial for medical students to be exposed to diseases, particularly AIDS-associated diseases, in their pre-clinical years as they will encounter it frequently in their years as a clinical practitioner. Currently, medical students at SU are exposed to a number of pathology during dissection of embalmed cadavers. At the FMHS, SU, the integrated systems based module curriculum is being used where systemic anatomy and pathology are taught within weeks of each other. Students can therefore be made aware of the pathology while they are dissecting the cadavers shortly before dealing with the pathology of the system. This study gives an insight into commonly observed pathology in the dissected cadaver and can therefore be used for student teaching at the FMHS, SU.

In this study, a morphological assessment of the health status of a cadaver cohort originating from the Western Cape, South Africa, was investigated. To our knowledge, this is the first study of its kind to investigate TB and systemic pathology using several molecular techniques and postmortem radiology, in cadavers from low socio-economic backgrounds, primarily from a high TB burden province. The epidemiological prevalence in this population, CXR findings with regards to PTB using full-body digital X-rays and molecular results from previously embalmed, FFPE tissue are therefore novel observations. While there is a good understanding of TB epidemiology, etiology, biochemistry and morphology in humans, the effects of concomitant systemic pathology associated with TB, remains unclear. By incorporating diagnostic molecular

techniques and radiology into the anatomical setting to diagnose TB in cadavers, it could be a step forward in a more complete and thorough diagnostic and therapeutic approach.

REFERENCE LIST

Aalto ML. 1986. Mucosubstances in classification of serous and mucinous ovarian tumors: a morphometrical study. *European Journal of Obstetrics & Gynecology and Reproductive Biology* 22:139-144.

Abou-Raya S, Abou-Raya A. 2006. Spinal tuberculosis: overlooked? *Journal of Internal Medicine* 260: 160-163.

Abrams HL, Spiro R, Goldstein N. 1950. Metastases in carcinoma. Analysis of 1000 autopsied cases. *Cancer* 3:74-85.

Acalovschi M. 2001. Cholesterol gallstones: from epidemiology to prevention. *Postgraduate Medical Journal* 77:221-229.

Adeloye A. 2001. Management of infantile hydrocephalus in Central Africa. *Tropical Doctor* 31:67-70.

Aderaye G, Bruchfeld J, Assefa G, Feleke D, Källenius G, Baat M, Lindquist L. 2003. The relationship between disease pattern and disease burden by chest radiography, *M. tuberculosis* load, and HIV status in patients with pulmonary tuberculosis in Addis Ababa. *Infection* 32:333-338.

Adi M, Ogden GR, Crisholm DM. 1990. An analysis of mandibular fractures in Dundee, Scotland (1977-1985). *British Journal of Oral and Maxillofacial Surgery* 28:194-199.

Adler NE, Boyce T, Chesney MA, Cohen S, Folkman S, Kahn RL, Syme SL. 1994. Socioeconomic status and health. *American Psychologist* 49:15-24.

Addolorato G, Capristo E, Greco AV, Stefanini GF, Gasbarrini G. 1998. Influence of chronic alcohol abuse on body weight and energy metabolism: is excess ethanol consumption a risk factor for obesity or malnutrition? *Journal of Internal Medicine* 244:387-395.

Afzelius L, Rosen C. 1980. Facial fractures: a review of 368 cases. *International Journal of Oral Surgery* 9:25-32.

Agaja SB, Ayorinde RO. 2008. Chronic osteomyelitis in Ilorin, Nigeria. *South African Journal of Surgery* 46:116-118.

Agbakwuru EA, Salako AA, Olajide AO, Takure AO, Eziyi AK. 2008. Hydrocelectomy under local anaesthesia in a Nigerian adult population. *African Health Sciences* 8:160-162.

- Agrons GA, Markowitz RI, Kramer SS.** 1993. Pulmonary tuberculosis in children. *Seminars in Roentgenology* 27:158-172.
- Akbay E, Cayan S, Doruk E, Duce MN, Bozlu M.** 2000. The prevalence of Varicocele and Varicocele-related testicular atrophy in Turkish children and adolescents. *BJU International* 86:490-493.
- Akhan O, Pringot J.** 2002. Imaging of abdominal tuberculosis. *European Radiology* 12:312-323.
- Aktogu S, Yorgancioglu A, Çirak K, Köse T, Dereli SM.** 1996. Clinical spectrum of pulmonary and pleural tuberculosis: a report of 5,480 cases. *European Respiratory Journal* 9:2031-2035.
- Albalak R, Frisancho AR, Keeler GJ.** 1999. Domestic biomass fuel combustion and chronic bronchitis in two rural Bolivian villages. *Thorax* 54:1004-1008.
- Alexandersen P, Tankó LB, Bagger YZ, Jespersen J, Skouby SO, Christiansen C.** 2006. Associations between aortic calcification and components of body composition in elderly men. *Obesity* 14:1571-1578.
- Ali A, Tetalman MR, Fordham EW, Turner DA, Chiles JT, Patel SL, Schmidt KD.** 1980. Distribution of hypertrophic pulmonary osteoarthropathy. *American Journal of Radiology* 134:771-780.
- Alkayed NK, Harukuni I, Kimes AS, London ED, Traystman RJ, Hurn PD.** 1998. Sex-linked brain injury in experimental stroke. *Stroke A Journal of Cerebral Circulation* 29:159-165.
- Alvarez SZ.** 2006. Hepatobiliary tuberculosis. *Phil J Gastroenterol* 2:1-10.
- American Thoracic Society.** 1990. Diagnostic standards and classification of tuberculosis. *American Review of Respiratory Disease* 142:725-735.
- Amirlak B, Zakhary B, Weichman K, Ahluwalia H, Forse AR, Gaines RD.** 2009. Novel use of Lodox® Statscan® in a level one trauma center. *Turkish Journal of Trauma & Emergency Surgery* 15:521-528. (Review)
- Anh DD, Borgdorff MW, Van LN, Lan NTN, Van Gorkom T, Kremer K, Van Soolingen D.** 2000. *Mycobacterium tuberculosis* Beijing genotype emerging in Vietnam. *Emerging Infectious Diseases* 6:302-305.

An SF, Fleming KA. 1991. Removal of inhibitor(s) of the polymerase chain reaction from formalin fixed, paraffin wax embedded tissues. *Journal of Clinical Pathology* 44:924-927.

Anagnostopoulos CE, Prabhakar MJS, Kittle CF. 1972. Aortic dissections and dissecting aneurysms. *The American Journal of Cardiology* 30:263-273.

Andiman WA, Martin K, Rubinstein A, Pahwa S, Eastman R, Katz BZ, Pitt J, Miller G. 1985. Opportunistic lymphoproliferations associated with Epstein-Barr viral DNA in infants and children with AIDS. *Lancet* 21:1390-1393.

Andrews JR, Shah NS, Gandhi N, Moll T, Friedland G. 2007. Multidrug-resistant and extensively drug-resistant tuberculosis: Implications for the HIV epidemic and antiretroviral therapy rollout in South Africa. *The Journal of Infectious Diseases* 196:482-490.

Andronikou S, Wieselthaler N. 2009. Imaging for tuberculosis in children. In HS Schaaf & A Zumla (eds.), *Tuberculosis. A comprehensive clinical reference*, pp. 262-396, Saunders Elsevier, Philadelphia.

Annals of Thoracic Medicine. 2006. Figure 25: Primary Mycobacterium tuberculosis. [Internet]. Available: http://www.thoracicmedicine.org/viewimage.asp?img=AnnThoracMed_2010_5_4_201_69106_f28.jpg. (Accessed: 22 February 2013)

Annals of Thoracic Medicine. 2006. Figure 26: Primary Mycobacterium tuberculosis. [Internet]. Available: http://www.thoracicmedicine.org/viewimage.asp?img=AnnThoracMed_2010_5_4_201_69106_f29.jpg. (Accessed: 22 February 2013)

Appelros S, Borgström A. 1999. Incidence, aetiology and mortality rate of acute pancreatitis over 10 years in a defined urban population in Sweden. *British Journal of Surgery* 86:465-470.

Aronow WS, Ahn C, Kronzon I. 1997. Prevalence of echocardiographic findings in 554 men and in 1243 women aged > 60 years in a long-term health care facility. *American Journal of Cardiology* 79:379-80.

Artenstein AW, Kim JH, Williams WJ, Chung RCY. 1995. Isolated peripheral tuberculous lymphadenitis in adults: current clinical and diagnostic issues. *Clinical Infectious Diseases* 20:876-882.

Aspden RM, Scheven BAA, Hutchinson JD. 2001. Osteoarthritis as a systemic disorder including stromal cell differentiation and lipid metabolism. *Lancet* 357:1118-1120.

Aston NO, Chir M. 1997. Abdominal tuberculosis. *World Journal of Surgery* 21:492-499.

Aufderheide AC, Rodríguez-Martín C. 2011. The Cambridge Encyclopedia of Human Paleopathology. 1st ed. Cambridge University Press, Cambridge.

Austin JF, Dick JM, Zwarenstein M. 2004. Sex disparity amongst TB suspects and new TB patients according to data recorded at the South African Institute of Medical Research laboratory for the Western Cape region of South Africa. *International Journal of Tuberculosis and Lung Disease* 8:435-439.

Ausubel F, Brent R, Kingston R, Moore D, Seidman JG, Smith J, Struhl K. 1995. Short protocols in molecular biology. 3rd ed, unit 2.1, pp 2-3, Wiley, New Jersey.

Avelar RL, Antunes AA, Carvalho RWF, Bezerra PGCF, Neto PJO, Andrade ESS. 2009. Odontogenic cysts: a clinicopathological study of 507 cases. *Journal of Oral Science* 51:581-586.

Bachmann GF, Basad E, Rauber K, Damian MS, Rau WS. 1999. Degenerative joint disease on MRI and physical activity: a clinical study of the knee joint in 320 patients. *European Radiology* 9:145-152.

Bailey JE, Roubidoux MA, Dunnich NR. 1998. Secondary renal neoplasms. *Abdominal Imaging* 23:266-274.

Baird DD, Dunson DB, Hill MC, Cousins D, Schectman JM. 2002. High cumulative incidence of uterine leiomyoma in black and white women: ultrasound evidence. *American Journal of Obstetrics and Gynecology* 188:100-107.

Balasubramanian R, Garg R, Santha T, Gopi PG, Subramani R, Chandrasekaran V, Thomas A, Rajeswari R, Anandakrishan R, Perumal M, Niruparani C, Sudha G, Jaggarajamma K, Frieden TR, Narayanan PR. 2004. Sex disparities in tuberculosis: report from a rural DOTS program in south India. *International Journal of Tuberculosis and Lung Disease* 8:323-332.

Bali HK, Wahi S, Sharma BK, et al. 1990. Myocardial tuberculosis presenting as restrictive cardiomyopathy. *American Heart Journal* 120:703-706.

- Ballantyne GH, Brandner MD, Beart RW, Ilstrup DM.** 1985. Volvulus of the colon. *Annals of Surgery* 202:83-92.
- Ball CG, Nicol AJ, Beningfield SJ, Navsaria PH.** 2007. Emergency room arteriography: an updated digital technology. *Scandinavian Journal of Surgery* 96:67-71.
- Bamjee Y, Lownie JF, Cleaton-Jones PE, Lownie MA.** 1996. Maxillofacial injuries in a group of South Africans under 18 years of age. *British Journal of Oral and Maxillofacial Surgery* 34:298-302.
- Bancroft JD, Gamble M.** 2011. Theory and practice of histological techniques. Sixth Edition, pp. 121-324, Churchill Livingstone, Elsevier, Philadelphia.
- Banks PA.** 2002. Epidemiology, natural history, and predictors of disease outcome in acute and chronic pancreatitis. *Gastrointestinal Endoscopy* 56:S226-S230.
- Bakardjiev A, Pechalova P.** 2007. Maxillofacial fractures in southern Bulgaria – a retrospective study of 1706 cases. *Journal of Cranio-Maxillofacial Surgery* 35:147-150.
- Barbad CSV, Cukier A, De VARvalho CRR, BarbasHilho JV, Light RW.** 1991. The relationship between pleural fluid findings and the development of pleural thickening in patients with pleural thickening. *Chest* 100:1264-1267.
- Barber G, Watt I, Rogers J.** 1997. A comparison of radiological and palaeopathological diagnostic criteria for hyperostosis frontalis interna. *International Journal of Osteoarchaeology* 7:157-164.
- Barker AF.** 2002. Bronchiectasis. *New England Journal of Medicine* 346:1383-1393.
- Barker DJP.** 1981. The epidemiology of Paget's disease. *Metabolic Bone Disease and Related Research* 4&5:231-234.
- Barnes I, Holton J, Vaira D, Spigelman M, Thomas MG.** 2000. An assessment of the long-term preservation of the DNA of a bacterial pathogen in ethanol-preserved archival material. *Journal of Pathology* 192:554-559.
- Baron JA, Barrett JA, Karagas MR.** 1996. The epidemiology of peripheral fractures. *Bone* 18:209S-213S.

- Baron JA, Karagas M, Barrett J, Kniffin W, Malenka D, Mayor M, Keller RB.** 1996. Basic epidemiology of fractures of the upper and lower limb among Americans over 65 years of age. *Epidemiology* 7:612-618.
- Bartos M, Pavlikova H, Dvorska L, Horvath R, Dendis M, Flodr P, Kolar Z, Weston RT, Pac L, Matlova L, Pavlik I.** 2006. Risk assessment of mycobacterial infections (human tuberculosis and avian mycobacteriosis) during anatomical dissection of cadavers. *Veterinarni Medicina* 51:311-319.
- Bascuñana CB and Belák K.** 1996. Detection and identification of mycobacteria in formalin-fixed, paraffin-embedded tissues by nested PCR and restriction enzyme analysis. *Journal of Clinical Microbiology* 34:2351-2355.
- Bates I, Fenton C, Gruber J, Lalloo D, Lara AM, Squire SB, Theobald S, Thomson R, Tolhurst R.** 2004. Vulnerability to malaria, tuberculosis, and HIV/AIDS infection and disease. Part 1: determinants operating at individual and household level. *Lancet Infectious Diseases* 4:267-277.
- Batungwanayo J, Taelman H, Dhote R, Bogaerts J, Allen S, Van De Perre P.** 1992. Pulmonary tuberculosis in Kigali, Rwanda. Impact of human immunodeficiency virus infection on clinical and radiographic presentation. *American Review of Respiratory Disease* 146:53-56.
- Baudet EM, Puel V, McBride JT, Grimaud JP, Roques F, Clerc F, Roques X, Laborde N.** 1995. Long-term results of valve replacement with the St. Jude medical prosthesis. *The Journal of Thoracic and Cardiovascular Surgery* 109:858-870.
- Beckles VLL, Wynn Jones H, Harrison WJ.** 2010. Chronic haematogenous osteomyelitis in children. A retrospective review of 167 patients in Malawi. *Journal of Bone and Joint Surgery* 92B:1138-1143.
- Beers MH, Fletcher AJ, Jones TV, Porter R, Berkwits M, Kaplan JL.** 2003. The Merck manual of medical information. 2nd ed. Pocket Books, New York.
- Behr MA, Small PM.** 1997. Molecular fingerprinting of *Mycobacterium tuberculosis*: how can it help the clinician? *Clinical Infectious Diseases* 25:806-810.
- Beiderlinden M, Kuehl H, Boes T, Peters J.** 2006. Prevalence of pulmonary hypertension associated with severe acute respiratory distress syndrome: predictive value of computed tomography. *Intensive Care Medicine* 32:852-857.

- Bellamy R, Ruwende C, Corrah T, McAdam KPWJ, Whittle HC, Hill AVS.** 1998. Variations in the *NRAMP1* gene and susceptibility to tuberculosis in West Africans. *The New England Journal of Medicine* 338:640-644.
- Bellentani S, Saccoccio G, masutti F, Croc  LS, Brandi G, Sasso F, Cristanini G, Tiribelli C.** 2000. Prevalence of and risk factors for hepatic steatosis in Northern Italy. *Annals of Internal Medicine* 132:112-117.
- Ben-Ezra J, Johnson DA, Rossi J, Cook N, Wu A.** 1991. Effect of fixation on the amplification of nucleic acids from paraffin-embedded material by the polymerase chain reaction. *The Journal of Histochemistry and Cytochemistry* 39:351-354.
- Berg KM, Kunins HV, Jackson JL, Nahvi S, Chaudry A, Harris KA, Malik R, Arnsten JH.** 2008. Association between alcohol consumption and both osteoporotic fracture and bone density. *The American Journal of Medicine* 121:406-418.
- Bergman P.** 1993. The occurrence of selected non-metrical traits of the skull in relation to *cibra orbitalia* and grave equipment. *Variability and Evolution* 2/3:63-75.
- Bergqvist D, Bj rk M, Ljungman C.** 2006. Popliteal venous aneurysm – a systemic review. *World Journal of Surgery* 30:273-279.
- Berk RH, Yazici M, Atabey N, Ozdamar OS, Pabuccuoglu U, Alici E.** 1996. Detection of *Mycobacterium tuberculosis* in formaldehyde solution-fixed, paraffin-embedded tissue by polymerase chain reaction in Pott's disease. *Spine* 21:1991-1995.
- Bernaerts A, Vanhoenacker FM, Parizel PM, Van Goethem JWM, Van Altena R, Laridon A, De Roeck J, Coeman V, De Schepper AM.** 2003. Tuberculosis of the central nervous system: overview of neuroradiological findings. *European Radiology* 13:1876-1890.
- Bernardi FDC, Saldiva PHN, Mauad T.** 2005. Histological examination has a major impact on macroscopic necropsy diagnoses. *Journal of Clinical Pathology* 58:1261-1264.
- Best M, Sattar SA, Springthorpe VS, Kennedy ME.** 1990. Efficacies of selected disinfectants against *Mycobacterium tuberculosis*. *Journal of Clinical Microbiology* 28:2234-2239.
- Beutler WJ, Fredrickson BE, Murtland A, Sweeney CA, Grant WD, Baker D.** 2003. The natural history of spondylolysis and spondylolisthesis. 45-year follow-up evaluation. *Spine* 28:1027-1035.

- Bezuidenhout J, Schneider JW.** 2009. Pathology and pathogenesis of tuberculosis. In HS Schaaf & A Zumla (eds.), *Tuberculosis. A comprehensive clinical reference*, pp. 117-128, Saunders Elsevier, Philadelphia.
- Bhansali SK.** 1977. Abdominal tuberculosis. Experiences with 300 cases. *American Journal of Gastroenterology* 67:324-337.
- Bharati P, Basu A.** 1990. Fertility, mortality and maternal anaemic status in a village population of West Bengal, India. *Annals of Human Biology* 17:331-335.
- Bhaskar SN.** 1966. Oral surgery – oral pathology conference no. 17, Walter Reed Army Medical Center: periapical lesions-types, incidence and clinical features. *Oral Surgery, Oral Medicine, Oral Pathology* 21:657-671.
- Blom DE, Buikstra JE, Keng L, Tomczak PD, Shoreman E, Stevens-Tuttle D.** 2005. Anemia and childhood mortality: latitudinal patterning along the coast of Pre-Columbian Peru. *American Journal of Physical Anthropology* 127:152-169.
- Blyth MJG, Kincaid R, Craigen MAC, Bennet GC.** 2001. The changing epidemiology of acute and subacute haematogenous osteomyelitis in children. *Journal of Bone and Joint Surgery* 83B:99-102.
- Bogen E, Butt EM, Djang AH, Aijian HS.** 1950. Frequency of tuberculous lesions discovered at autopsy at Los Angeles County General Hospital, 1918-1948. *California Medicine* 73:566-569.
- Bonsell S, Pearsall AW, Heitman RJ, Helms CA, Major NM, Speer KP.** 2000. The relationship of age, sex and degenerative changes observed on radiographs of the shoulder in asymptomatic individuals. *Journal of Bone and Joint Surgery* 82B: 1135-1139.
- Boon A, Cheriex E, Lodder J, Kessels F.** 1997. Cardiac valve calcification: characteristics of patients with calcification of the mitral annulus or aortic valve. *Heart* 78:472-474.
- Boone D, Parsons D, Lachmann SM, Sherwood T.** 1985. Spina bifida occulta: lesion or anomaly? *Clinical Radiology* 36:159-161.
- Bosma H, Van Jaarsveld CHM, Tuinstra J, Sanderman R, Ranchor AV, Van EijkJThM, Kempen GIJM.** 2005. Low control beliefs, classical coronary risk factors, and socio-economic differences in heart disease in older persons. *Social Science & Medicine* 60:737-745.

- Bostwick DG, Cooner WH, Denis L, Jones GW, Scardino PT, Murphy GP.** 1992. The association of benign prostatic hyperplasia and cancer of the prostate. *Cancer Supplement* 70:291-301.
- Botha MH, Van der Merwe FH.** 2009. Female genital tuberculosis. In HS Schaaf & A Zumla (eds.), *Tuberculosis. A comprehensive clinical reference*, pp. 457-462, Saunders Elsevier, Philadelphia.
- Braber S, Verheijden KAT, Henricks PAJ, Kraneveld AD, Folkerts G.** 2010. A comparison of fixation methods on lung morphology in a murine model of emphysema. *American Journal of Physiology – Lung Cellular and Molecular Physiology* 299:L843-L851.
- Bramlett HM, Dietrich WD.** 2004. Pathophysiology of cerebral ischemia and brain trauma: similarities and differences. *Journal of Cerebral Blood Flow & Metabolism* 24:133-150.
- Brancusi F, Farrar J, Heemskerk D.** 2012. Tuberculous meningitis in adults: a review of a decade of developments focusing on prognostic factors for outcome. *Future Microbiology* 7:1101-1116.
- Braun J, Golder W, Bollow M, Sieper J, Van Der Heijde D.** 2002. Imaging and scoring in ankylosing spondylitis. *Clinical and Experimental Rheumatology* 20:S178-S184.
- Braunstein EM, Hunter LY, Bailey RW.** 1980. Long term radiographic changes following anterior cervical fusion. *Clinical Radiology* 31:201-203.
- Brasileiro BF, Passeri LA.** 2006. Epidemiological analysis of maxillofacial fractures in Brazil: A 5-year prospective study. *Oral Surgery, Oral Medicine, Oral Pathology, Oral Radiology, and Endodontics* 102:28-34.
- Briganti A, Capitanio U, Suardi N, Gallina A, Salonia A, Bianchi M, Tutolo M, Di Girolamo V, Guazzoni G, Rigatti P, Montorsi F.** 2009. Benign prostatic hyperplasia and its aetiologies. *European Urology Supplements* 8:865-871.
- Bron JL, Van Royen BJ, Wuisman PIJM.** 2007. The clinical significance of lumbosacral transitional anomalies. *Acta Orthopaedica Belgica* 73:687-695.
- Brothwell DR.** 1981. Digging up bones: the excavation, treatment and study of human skeletal remains. Cornell University Press, New York, pp. 51-54.

- Browning JD, Szczepaniak LS, Dobbins R, Nuremberg P, Horton JD, Cohen JC, Grundy SM, Hobbs HH.** 2004. Prevalence of hepatic steatosis in an urban population in the United States: impact of ethnicity. *Hepatology* 40:1387-1395.
- Brudey K, Driscoll JR, Rigouts L, Prodinger WM, Gori A, Al-Hajoj SA et al.** 2006. *Mycobacterium tuberculosis* complex genetic diversity: mining the fourth international spoligotyping database (SpolDB4) for classification, population genetics and epidemiology. *BMC Microbiology* 6:23.
- Brunk UT, Terman A.** 2002. Lipofuscin: mechanisms of age-related accumulation and influence on cell function. *Free Radical Biology and Medicine* 33:611-619.
- Bujanda L.** 2000. The effects of alcohol consumption upon the gastrointestinal tract. *The American Journal of Gastroenterology* 95:3374-3382.
- Bulger EM, Arneson MA, Mock CN, Jurkovich GJ.** 2000. Rib fractures in the elderly. *The Journal of Trauma: Injury, infection and critical care* 48:1040-1046.
- Burkitt HG, Stevens A, Lowe JS, Young B.** 1996. Wheater's Basic Histopathology. A colour atlas and text. Third Edition, pp. 86-100; 110-121, Churchill Livingstone, New York.
- Butler AM.** 1937. Chronic pyelonephritis and arterial hypertension. *Journal of Clinical Investigation* 16:889-897.
- Cabras AD, Kremer M, Schulz S, Werner M, Hummel M, Komminoth P, Höfler G, Höfler H.** 2000. Quality assessment in diagnostic molecular pathology: experience from a German-Austrian-Swiss multicenter trial. *Virchows Archiv* 437:46-51.
- Caglioti A, Esposito C, Fuiano G, Buzio C, Postorino M, Rampino T, Conte G, Dal Canton A.** 1993. Prevalence of symptoms in patients with simple renal cysts. *British Medical Journal* 306:430-431.
- Cahn P, Perez H, Ben G, Ochoa C.** 2003. Tuberculosis and HIV: a partnership against the most vulnerable. *Journal of the International Association of Providers of AIDS Care* 2:106-123.
- Canales BK, Zapzalka DM, Ercole CJ, Carey P, Haus E, Aeppli D, Pryor JL.** 2005. Prevalence and effect of varicoceles in an elderly population. *Urology* 66:627-631.
- Caracta CF.** 2003. Sex differences in pulmonary disease. *The Mount Sinai Journal of Medicine* 70:215-224.

- Carrim ZI, Murchison JT.** 2003. The prevalence of simple renal and hepatic cysts detected by spiral computed tomography. *Clinical Radiology* 58:626-629.
- Cegielski JP, McMurray DN.** 2004. The relationship between malnutrition and tuberculosis: evidence from studies in humans and experimental animals. *International Journal of Tuberculosis and Lung Disease* 8:286-298.
- Çek M.** 2009. Male genital tuberculosis. In HS Schaaf & A Zumla (eds.), *Tuberculosis. A comprehensive clinical reference*, pp. 450-456, Saunders Elsevier, Philadelphia.
- Chakrabarti B, Calverley PMA, Davies PDO.** 2007. Tuberculosis and its incidence, special nature, and relationship with chronic obstructive pulmonary disease. *International Journal of COPD*. 2:263-272.
- Chan KH, Cheung RTF, Fong CY, Tsang KL, Mak W, Ho SL.** 2003. Clinical relevance of hydrocephalus as a presenting feature of tuberculous meningitis. *Q J Med* 96:643-648.
- Chan PKS, Chan DPC, To KF, Yu MY, Cheung JLK, Cheng AF.** 2001. Evaluation of extraction methods from paraffin wax embedded tissues for PCR amplification of human and viral DNA. *Journal of Clinical Pathology* 54:401-403.
- Chan-Yeung M, Noertjojo K, Chan SL, Tam CM.** 2002. Sex differences in tuberculosis in Hong Kong. *International Journal of Tuberculosis and Lung Disease* 6:11-18.
- Chatzicostas C, Koutroubakis IE, Tzardi M, Roussomoustakaki M, Prassopoulos P, Kouroumalis EA.** 2002. Colonic tuberculosis mimicking Crohn's disease: case report. *BMC Gastroenterology* 2:10
- Chaudhary A, Negi SS, Sachdev AK, Gondal R.** 2002. Pancreatic tuberculosis: still a histopathological diagnosis. *Digestive Surgery* 19:389-392.
- Chan CC, Lo KKL, Chung ECH, Lo SS, Hon TYW.** 1998. Colonic diverticulosis in Hong Kong: distribution pattern and clinical significance. *Clinical Radiology* 53:842-844.
- Chan FKL, Leung WK.** 2002. Peptic-ulcer disease. *Lancet* 360:933-941.
- Chen CY, Lu CL, Chang FY, Lee SD.** 1997. Risk factors for gallbladder polyps in the Chinese population. *American Journal of Gastroenterology* 92:2066-2068.

- Chen RJ, Fu CY, Wu SC, Wang YC, Chung PK, Huang HC, Huang JC, Lu CW.** 2010. Diagnostic accuracy, biohazard safety, and cost effectiveness – The Lodox/Statscan provides a beneficial alternative for the primary evaluation of patients with multiple injuries. *Journal of Trauma* 69:826-830.
- Chen YM, Lee PY, Su WJ, Perng RP.** 1992. Lymph node tuberculosis: 7-year experience in Veterans General Hospital, Taipei, Taiwan. *Tubercle and Lung Disease* 73:368-371.
- Chew FS, Relyea-Chew A, Ochoa ER.** 2006. Postmortem computed tomography of cadavers embalmed for use in teaching gross anatomy. *Journal of Computer Assisted Tomography* 30:949-954.
- Chien RN, Lin EY, Liaw YE.** 1995. Hepatic tuberculosis: comparison of miliary and local form. *Infection* 23:5-8.
- Choi S, Lim YJ, Park SK.** 2006. Risk factor analysis for metaplastic gastritis in Koreans. *World Journal of Gastroenterology* 12:2584-2587.
- Christensen AH, Ishak KG.** 1970. Benign tumors and pseudotumors of the gallbladder. Report of 180 cases. *Archives of Pathology* 90:423-432.
- Christensen WI.** 1974. Genitourinary tuberculosis: review of 102 cases. *Medicine (Baltimore)* 53:377-390.
- Chung MP, Lee KS, Han J, Kim H, Rhee CH, Han YC, Kwon OJ.** 1998. Bronchial stenosis due to anthracofibrosis. *Chest* 113:344-350.
- Chun HM, Hale B.** 2004. Renal tuberculosis. Three cases and a review of the literature. *Infectious Diseases in Clinical Practice* 12:117-122.
- Churg AM, Myers JL, Tazelaar HD, Wright JL.** 2005. Thurlbeck's Pathology of the Lung. Thieme. New York.
- Cilliers K.** 2013. The anatomical variation of the Circle of Willis in a cadaver cohort representing the population dynamics of the Western Cape. Unpublished HonsBSc. Thesis, Stellenbosch University.
- Clark ML, Kumar PJ.** 1998. Liver, biliary tract and pancreatic diseases. In PJ Kumar & ML Clark (eds.), *Clinical medicine*, fourth edition, pp. 346-350, Saunders, Philadelphia.

- Cohen M, Sahn SA.** 1999. Bronchiectasis in systemic diseases. *Chest* 116:1063-1074.
- Cole ST, Brosch R, Parkhill J et al.** 1998. Deciphering the biology of *Mycobacterium tuberculosis* from the complete genome sequence. *Nature* 393:537-544.
- Cole-Beuglet C, Soriano RZ, Kurtz AB, Goldberg BB.** 1982. Fibroadenoma of the breast: sonomammography correlated with pathology in 122. *American Journal of Roentgenology* 140:369-375.
- Collier DSTJ, Pain JA.** 1985. Non-steroidal anti-inflammatory drugs and peptic ulcer perforation. *Gut* 26:359-363.
- Comas I, Homolka S, Niemann S, Gacneux S.** 2009. Genotyping of genetically monomorphic bacteria: DNA sequencing in *Mycobacterium tuberculosis* highlights the limitations of current methodologies. *PlosONE* 4:e7815.
- Commane DM, Arasaradnam RP, Mills S, Mathers JC, Bradburn M.** 2009. Diet, ageing and genetic factors in the pathogenesis of diverticular disease. *World Journal of Gastroenterology* 15:2479-2488.
- Condos R, McClune A, Rom WN, Schluger NW.** 1996. Peripheral-blood-based PCR assay to identify patients with active pulmonary tuberculosis. *Lancet* 347:1082-1085.
- Cooper K, Herrington CS, Graham AK, Evans MF, McGee JO'D.** 1991. *In situ* human papillomavirus (HPV) genotyping of cervical intraepithelial neoplasia in South African and British patients: evidence for putative HPV integration *in vivo*. *Journal of Clinical Pathology* 44:400-405.
- Corbett EL, Bandason T, Cheung YB, Munyati S, Godfrey-Faussett P, Hayes R, Churchyard G, Butterworth A, Mason P.** 2007. Epidemiology of tuberculosis in a high HIV prevalence population provided with enhanced diagnosis of symptomatic disease. *PLoS Medicine* 4:e22.
- Cormican L, Hammal R, Messenger J, Milburn HJ.** 2006. Current difficulties in the diagnosis and management of spinal tuberculosis. *Postgraduate Medical Journal* 82:46-51.
- Corne J, Pointon K.** 2010. How to look at a chest X-ray. In J Corne & K Pointon (eds.), *Chest X-rays made easy*, 3rd ed., pp. 2-13, Churchill Livingstone, Edinburgh.

- Cox HS, Kubica T, Doshetov D, Kebede Y, Rüsç-Gerdess S, Niemann S.** 2005. The Beijing genotype and drug resistant tuberculosis in the Aral Sea region of Central Asia. *Respiratory Research* 6:134-142.
- Crampin AC, Glynn JR, Floyd S, Malema SS, Mwinuka VK, Ngwira BMM, Mwaungulu FD, Warndorff DK, Fine PEM.** 2004. Tuberculosis and sex: exploring the patterns in a case control study in Malawi. *International Journal of Tuberculosis and Lung Disease* 8:194-203.
- Czaja CA, Scholes D, Hooton TM, Stamm WE.** 2007. Population-based epidemiologic analysis of acute pyelonephritis. *Clinical Infectious Diseases* 45:273-280.
- Daley CL, Gotway M.** 2009. Imaging of tuberculosis in adults. In HS Schaaf & A Zumla (eds.), *Tuberculosis. A comprehensive clinical reference*, pp. 237-261, Saunders Elsevier, Philadelphia.
- Dandapat MC, Mishra BM, Dash SP, Kar PK.** 1990. Peripheral lymph node tuberculosis: a review of 80 cases. *British Journal of Surgery* 77:911-912.
- Daniel TM.** 2009. The history of tuberculosis. Past, present, and challenges for the future. In HS Schaaf & A Zumla (eds.), *Tuberculosis. A comprehensive clinical reference*, pp. 1-7, Saunders Elsevier, Philadelphia.
- Darbyshire JH.** 1995. Tuberculosis: old reasons for a new increase? *British Medical Journal* 310:954-955.
- Dar G, Khamis S, Peleg S, Masharawi Y, Steinberg N, Peled N, Latimer B, Hershkovitz I.** 2008. Sacroiliac joint fusion and the implications for manual therapy diagnosis and treatment. *Manual Therapy* 13:155-158.
- Dar G, Peleg S, Masharawi Y, Steinberg N, Rothschild BM, Peled N, Hershkovitz I.** 2005. Sacroiliac joint bridging: demographical and anatomical aspects. *Spine* 30:E429-E432.
- Davidson PT, Horowitz I.** 1970. Skeletal Tuberculosis. A review with patient presentations and discussion. *The American Journal of Medicine* 48:77-84. (Review)
- Davies MJ, Pomerance A, Teare RD.** 1974. Pathological features of hypertrophic obstructive cardiomyopathy. *Journal of Clinical Pathology* 27:529-535.
- Davies, PDO.** 2005. Risk factors for tuberculosis. *Monaldi Archives for Chest Disease* 63:37-46.

- Dayal MR.** 2003. Stature estimates from the long bones of South African whites using regression formulae. University of the Witwatersrand: Unpublished MSc thesis.
- Daya RB, Kibel MA, Pitcher RD, Workman L, Douglas TS, Sanders V.** 2009. A pilot study evaluating erect chest imaging in children, using the Lodox Statscan digital X-ray machine. *South African Journal of Radiology* 13:80-85.
- Day CP, James OFW.** 1998. Hepatic steatosis: innocent bystander or guilty party? *Hepatology* 27:1463-1466.
- Debas HT, Cohen MM, Holubitsky IB, Harrison RC.** 1971. Effect of cigarette smoking on human gastric secretory responses. *Gut* 12:93-96.
- De Crop A, Bacher K, Van Hoof T, Smeets PV, Smet BS, Vergauwen M, Kiendys U, Duyck P, Verstraete K, D'Herde K, Thierens H.** 2012. Correlation of contrast-detail analysis and clinical image quality assessment in chest radiography with a human cadaver study. *Radiology* 262:298-304.
- Demir K, Kaymakoglu S, Besisik F, Durakoglu Z, Ozdil S, Kaplan Y, Boztas G, Cakaloglu Y, Okten A.** 2001. Solitary pancreatic tuberculosis in immunocompetent patients mimicking pancreatic carcinoma. *Journal of Gastroenterology and Hepatology* 16:1071-1074.
- Demiryürek D, Bayramoğlu A, Ustaçelebi Ş.** 2002. Infective agents in fixed human cadavers: a brief review and suggested guidelines. *The Anatomical Record (New Anat.)* 269:194-197.
- Den Boon S, Van Lill SWP, Borgdorff MW, Enarson DA, Verver S, Bateman ED, Irusen E, Lombard CJ, White NW, de Villiers C, Beyers N.** 2007. High prevalence of tuberculosis in previously treated patients, Cape Town, South Africa. *Emerging Infectious Diseases* 13:1189-1194.
- Denton T, Hossain J.** 1993. A radiological study of abdominal tuberculosis in a Saudi population, with special reference to ultrasound and computed tomography. *Clinical Radiology* 47:409-414.
- Desai CS, Joshi AG, Abraham P, Desai DC, Deshpande RB, Bhaduri A, Shah SR.** 2006. Hepatic tuberculosis in absence of disseminated abdominal tuberculosis. *Annals of Hepatology* 5:41-43.
- Desai DC, Swaroop VS, Mohandas KM, Borges A, Dhir V, Nagral A, Jagannath P, Sharma OP.** 1991. Tuberculosis of the pancreas. *American Journal of Gastroenterology* 86:761-763.

- De Smet AA, Neff JR.** 1985. Pubic and sacral insufficiency fractures: clinical course and radiologic findings. *American Journal of Roentgenology* 145:601-606.
- Deyle S, Wagner A, Benneker LM, Jeger V, Eggli S, Bonel HM, Zimmermann H, Exadaktylos AK.** 2009. Could full-body digital X-ray (LODOX-Statscan) screening in trauma challenge conventional radiography? *The Journal of Trauma* 66:418-422.
- Dharati K, Nagar SK, Ojaswini M, Dipali T, Paras S, Sucheta P.** 2012. A study of sacralisation of fifth lumbar vertebra in Gujarat. *National Journal of Medical Research* 2:211-213.
- Dhedia P, Tarale S, Dhongde G, Khadapkar R, Das B.** 2007. Evaluation of DNA extraction methods and real-time PCR optimization on formalin-fixed paraffin-embedded tissues. *Asian Pacific Journal of Cancer Prevention* 8:55-59.
- Dogra VS, Gottlieb RH, Oka M, Rubens DJ.** 2003. Sonography of the scrotum. *Radiology* 227:18-36.
- Doll R, Hill AB.** 1999. Smoking and carcinoma of the lung. *Bulletin of the World Health Organization* 77:84-93.
- Donaldson LJ, Cook A, Thomson RG.** 1990. Incidence of fractures in a geographically defined population. *Journal of Epidemiology and Community Health* 44:241-245.
- Donoghue HD, Spigelman M, Greenblatt CL, Lev-Maor G, Bar-Gal GK, Matheson C, Vernon K, Nerlich AG, Zink AR.** 2004. Tuberculosis: from prehistory to Robert Koch, as revealed by ancient DNA. *Lancet Infectious Diseases*. 4:584-592. Review.
- Donoghue HD, Spigelman M, Zias J, Germaey-Child AM, Minnikin DE.** 1998. *Mycobacterium tuberculosis* complex DNA in calcified pleura from remains 1400 years old. *Letters in Applied Microbiology* 27:265-269.
- Dourakis SP, Saramadou R, Alexopoulou A, Kafiri G, Deutsch M, Koskinasa J, Archimandritis AJ.** 2007. Hepatic granulomas: a 6-year experience in a single center in Greece. *European Journal of Gastroenterology & Hepatology* 19:101-104.
- Dow J, Roebuck EJ, Cole F.** 1966. Dissecting aneurysms of the aorta. *British Journal of Radiology* 39:915-927.

- Doyle T, Gunn J, Anderson G, Gill M, Cundy T.** 2002. Paget's disease in New Zealand: evidence for declining prevalence. *Bone* 31:616-619.
- Dransfield MT, Washko GR, Foreman MG, Estepar RSJ, Reilly J, Bailey WC.** 2007. Sex differences in the severity of CT emphysema in COPD. *Chest* 132:464-470.
- Drobniewski F, Khanna P.** 2009. Multidrug-resistant tuberculosis in adults. In HS Schaaf & A Zumla (eds.), *Tuberculosis. A comprehensive clinical reference*, pp. 539-550, Saunders Elsevier, Philadelphia.
- Dubin L, Amelar D.** 1978. Varicocele. *Urologic Clinics of North America* 5:563-564.
- Dupont WD, Page DL, Parl FF, Vnencak-Jones CL, Plummer WD, Rados MS, Schuyler PA.** 1994. Long-term risk of breast cancer in women with fibroadenoma. *The New England Journal of Medicine* 331:10-15.
- Durlacher SH, Banfield WG, Bergner AD.** 1950. Post-mortem pulmonary edema. *Yale Journal of Biology and Medicine* 22:565-572.
- Eastwood GL.** 1997. Is smoking still important in the pathogenesis of peptic ulcer disease? *Journal of Clinical Gastroenterology* 25:S1-S7.
- Eastwood JB, Corbishley CM.** 2009. Tuberculosis of the kidney and urinary tract. In HS Schaaf & A Zumla (eds.), *Tuberculosis. A comprehensive clinical reference*, pp. 438-449, Saunders Elsevier, Philadelphia.
- Ebdrup L, Storgaard M, Jensen-Fangel S, Obel N.** 2003. Ten years of extrapulmonary tuberculosis in a Danish University Clinic. *Scandinavian Journal of Infectious Diseases* 35:244-246.
- Edelson JG.** 1996. Bony changes of the glenoid as a consequence of shoulder instability. *Journal of Shoulder and Elbow Surgery* 5:293-298.
- Eftekhar B, Dadmehr M, Ansari S, Ghodsi M, Nazparvar B, Ketabchi E.** 2006. Are the distributions of variations of circle of Willis different in different populations? – Results of an anatomical study and review of literature. *BMC Neuroradiology* 6:22-30.
- Eisenstein S.** 1978. Spondylolysis: a skeletal investigation of two population groups. *Journal of Bone and Joint Surgery* 60B:488-494.

- Ekelund G, Lindström C.** 1974. Histopathological analysis of benign polyps in patients with carcinoma of the colon and rectum. *Gut* 15:654-663.
- Ellis E, El-Attar A, Moos KF.** 1985. An analysis of 2067 cases of zygomatico-orbital fracture. *Journal of Oral and Maxillofacial Surgery* 43:417-428.
- ElTayeb A, ElTayeb A, Ibrahim N, Essa A, Abdu F.** 2008. Extra pulmonary childhood tuberculosis. *Egyptian Journal of Surgery* 27:185-190.
- El-Wakeel H, Umpleby HC.** 2003. Systemic review of fibroadenoma as a risk factor for breast cancer. *The Breast* 12:302-307.
- Emamhadi M, Mostafazadeh B, Masjedi M, Bahadori M, Shafiee G.** 2012. Relationship between bronchial anthracofibrosis and pulmonary tuberculosis: autopsy findings. *International Journal of Occupational Hygiene* 5:35-38.
- Emery RW, Krogh CC, Arom KV, Emery AM, Benyo-Albrecht K, Joyce LD, Nicoloff DM.** 2005. The St. Jude medical cardiac valve prosthesis: a 25-year experience with single valve replacement. *Annals of Thoracic Surgery* 79:776-783.
- Engin G, Acunaş B, Acunaş G, Tunaci M.** 2000. Imaging of extrapulmonary tuberculosis. *RadioGraphics* 20:471-488.
- Erbel R, Alfonso F, Boileau C, Dirsch O, Eber B, Haverich A, Rakowski H, Struyven J, Radegran K, Sechtem U, Taylor J, Zollikofer C.** 2001. Diagnosis and management of aortic dissection. Recommendations of the Task Force on Aortic Dissection, European Society of Cardiology. *European Heart Journal* 22:1642-1681.
- Erickson SE, Shlipak MG, Martin GS, Wheeler AP, Ancukiewicz M, Matthay MA, Eisner MD.** 2009. Racial and ethnic disparities in mortality from acute lung injury. *Critical Care Medicine* 37:1-6.
- Epstein FH, Mendelsohn ME, Karas RH.** 1999. The protective effects of estrogen on the cardiovascular system. *The New England Journal of Medicine* 340:1801-1811.
- Evangelopoulos DS, Deyle S, Zimmermann H, Exadaktylos K.** 2010. Full-body radiography (LODOX Statscan) in trauma and emergency medicine: a report from the first European installation site. *Trauma* 0:1-11.

- Evans JD, Hamanaka Y, Olliff SP, Neoptolemos JP.** 2000. Tuberculosis of the pancreas presenting as metastatic pancreatic carcinoma. A case report and review of the literature. *Digestive Surgery* 17:183-187.
- Everhart JE, Khare M, Hill M, Maurer KR.** 1999. Prevalence and ethnic differences in gallbladder disease in the United States. *Gastroenterology* 117:632-639.
- Fang Z, Forbes KJ.** 1997. A *Mycobacterium tuberculosis* IS6110 preferential locus (*ipl*) for insertion into the genome. *Journal of Clinical Microbiology* 35:479-481.
- Fan JG, Farrell GC.** 2009. Epidemiology of non-alcoholic fatty liver disease in China. *Journal of Hepatology* 50:204-210.
- Farhi DC, Mason UG, Horsburgh CR.** 1986. Pathologic findings in disseminated *Mycobacterium avium-intracellulare* infection. A report of 11 cases. *American Journal of Clinical Pathology* 85:67-72.
- Farrugia A, Keyser C, Ludes B.** 2010. Efficiency evaluation of a DNA extraction and purification protocol on archival formalin-fixed and paraffin-embedded tissue. *Forensic Science International* 194:e25-e28.
- Fattovich G, Stroffolini T, Zagni I, Donato F.** 2004. Hepatocellular carcinoma in cirrhosis: incidence and risk factors. *Gastroenterology* 127:S35-S50.
- Fekri MS, Lashkarizadeh MR, Kardoost AH, Shokoohi M.** 2010. Bronchial anthracosis and pulmonary tuberculosis. *Tanaffos* 9:21-25.
- Ferrer J.** 1997. Pleural tuberculosis. *European Respiratory Journal* 10:942-947.
- Ferris BG, Anderson DO.** 1962. The prevalence of chronic respiratory disease in a New Hampshire town. *American Review of Respiratory Disease* 86:165-177.
- Finkbeiner WE, Ursell PC, Davis RL.** 2004. Autopsy pathology: a manual and atlas. First Edition, pp. 41-65, Churchill Livingstone, Philadelphia.
- Flake GP, Andersen J, Dixon D.** 2003. Etiology and pathogenesis of uterine leiomyomas: a review. *Environmental Health Perspectives* 111:1037-1054.

- Fletcher HA, Donoghue HD, Holton J, Pap I, Spigelman M.** 2003. Widespread occurrence of *Mycobacterium tuberculosis* DNA from 18th- 19th century Hungarians. *American Journal of Physical Anthropology* 120:144-152.
- Flores L, Van T, Narayanan S, DeRiemer K, Kato-Maeda M, Gagneux S.** 2007. Large sequence polymorphisms classify *Mycobacterium tuberculosis* strains with ancestral spoligotyping patterns. *Journal of Clinical Microbiology* 45:3393-3395.
- Foo FJ, Verbeke CS, Guthrie JA, Ala A, Menon KV.** 2007. Pancreatic and peripancreatic tuberculosis mimicking malignancy. *Journal of the Pancreas* 8:201-205.
- Fooladi AAI, Hosseini MJ, Azizi Y.** 2009. Splenic tuberculosis: a case report. *International Journal of Infectious Diseases* 13:e273-e275.
- Fourie B.** 2011. The burden of tuberculosis in South Africa. [Internet]. Available: <http://www.sahealthinfo.org/tb/tburden.htm>. [August 5, 2011].
- Fowler AA, Hamman RF, Good JT, Benson KN, Baird M, Eberle DJ, Petty TL, Hyers TM.** 1983. Adult respiratory distress syndrome: risk with common predispositions. *Annals of Internal Medicine* 99:593-597.
- Frank TS, Svoboda-Newman SM, His ED.** 1996. Comparison of methods for extracting DNA from formalin-fixed paraffin sections for nonisotopic PCR. *Diagnostic Molecular Pathology* 5:220-224.
- Franquet T.** 2001. Imaging of pneumonia: trends and algorithms. *European Respiratory Journal* 18:196-208.
- Fraser RS, Pare PJ, Fraser RG, Pare PD.** 1994. Synopsis of diseases of the chest. Second edition, pp. 287-395. Saunders, Philadelphia.
- Frederickson BE, Baker D, McHolick WJ, Yuan HA, Lubicky JP.** 1984. The natural history of spondylolysis and spondylolisthesis. *Journal of Bone and Joint Surgery* 66:699-707.
- Freedman BI, Iskandar SS, Appel RG.** 1995. The link between hypertension and nephrosclerosis. *American Journal of Kidney Diseases* 25:207-221.
- Freedman LR.** 1967. Chronic pyelonephritis at autopsy. *Annals of Internal Medicine* 66:697-710.

- Frezza M, Di Padova C, Pozzato G, Terpin M, Baraona E, Lieber CS.** 1990. High blood alcohol levels in women. The role of decreased gastric alcohol dehydrogenase activity and first-pass metabolism. *New England Journal of Medicine* 322:95-99.
- Friede RL.** 1973. Cerebral infarcts complicating neonatal leptomeningitis. *Acta Neuropathologica* 23:245-253.
- Frishman WH, Nadelmann J, Ooi WL, Greenberg S, Heiman M, Kahn S, Guzik H, Lazar EJ, Aronson M.** 1992. Cardiomegaly on chest x-ray: prognostic implications from a ten-year cohort study of elderly subjects: a report from the Bronx Longitudinal Aging study. *American Heart Journal* 124:1026-1029.
- Frothingham R, Meeker-O'Connell, WA.** 1998. Genetic diversity in the *Mycobacterium tuberculosis* complex based on variable numbers of tandem DNA repeats. *Microbiology* 144:1189-1196.
- Frulloni L, Gabbrielli A, Pezzilli R, Zerbi A, Cavestro GM, Marotta F, Falconi M, Gaia E, Uomo G, Maringhini A, Mutignani M, Maisonneuve P, Di Carlo V, Cavallini G, PanCroInfAISP Study Group.** 2009. Chronic pancreatitis: report from a multicenter Italian survey (PanCroInfAISP) on 893 patients. *Digestive and Liver Disease* 41:311-317.
- Gajalakshmi V, Peto R, Kanaka TS, Jha P.** 2003. Smoking and mortality from tuberculosis and other diseases in India: retrospective study of 43000 adult male deaths and 35000 controls. *Lancet* 362:507-515.
- Gandy M.** 2003. Life without germs: contested episodes in the history of tuberculosis. In M Gandy & A Zumla (eds.), *The return of the white plaque*, pp.15-38, Verso, London.
- Gardner JR.** 1988. Cystic kidneys. *Kidney International* 33:610-621.
- Geake TM, Spitaels JM, Moshal MG, Simjee AE.** 1981. Peritoneoscopy in the diagnosis of tuberculous peritonitis. *Gastrointestinal Endoscopy* 27:66-68.
- Gassner R, Tuli T, Hächl O, Rudish A, Ulmer H.** 2003. Cranio-maxillofacial trauma: a 10 year review of 9543 cases with 21 067 injuries. *Journal of Cranio-Maxillofacial Surgery* 31:51-61.
- Geldmacher H, Taube C, Kroeger C, Magnussen H, Kirsten DK.** 2002. Assessment of lymph node tuberculosis in Northern Germany: a clinical review. *Chest* 121:1177-1182.

- Gennari L, Di Stefano M, Merlotti D, Giordano N, Martini G, Tamone C, Zatterri R, De Lucchi R, Baldi C, Vattimo A, Capoccia S, Burrioni L, Geraci S, De Paola V, Calabro A, Avanzati A, Isaia G, Nuti R.** 2005. Prevalence of Paget's disease of bone in Italy. *Journal of Bone and Mineral Research* 20:1845-1850.
- Geokas MC, Lakatta EG, Makinodan T, Timiras PS.** 1990. The aging process. *Annals of Internal Medicine* 113:455-466.
- Gernaey AM, Minnikin DE, Copley MS, Dixon RA, Middleton JC, Roberts CA.** 2001. Mycolic acids and ancient DNA confirm an osteological diagnosis of tuberculosis. *Tuberculosis* 81:259-265.
- Gerston KF, Blumberg L, Tshabalala VA, Murray J.** 2004. Viability of mycobacteria in formalin-fixed lungs. *Human Pathology* 35:571-575.
- Gerston KF, Blumberg L, Gafoor H.** 1998. Viability of mycobacteria in formalin-fixed tissues. *International Journal of Tuberculosis and Lung Disease* 2:521-523.
- Gevenois PA, Scillia P, de Maertelaer V, Michils A, De Vuyst P, Yernault JC.** 1996. The effects of age, sex, lung size, and hyperinflation on CT lung densitometry. *American Journal of Roentgenology* 167:1169-1173.
- Ghanei M, Aslani J, Peyman M, Asl MA, Pirnazar O.** 2011. Bronchial anthracosis: a potent clue for diagnosis of pulmonary tuberculosis. *Oman Medical Journal* 26:19-22.
- Giannitrapani L, Soresi M, La Spada E, Cervello M, D'Alessandro N, Montalto G.** 2006. Sex hormones and risk of liver tumor. *Annals New York Academy of Sciences* 1089:228-236.
- Glazer JL, Onion DK.** 2001. Fat embolism syndrome in a surgical patient. *Journal of the American Board of Family Practice* 14:310-313.
- Glickman MS, Jacobs WR.** 2001. Microbial pathogenesis of *Mycobacterium tuberculosis*: dawn of a discipline. *Cell* 104:477-485. (Review).
- Godfrey-Faussett P.** 1995. Molecular diagnosis of tuberculosis the need for new diagnostic tools. *Thorax* 50:709-711.
- Godshall D, Mossallam U, Rosenbaum R.** 1999. Gastric volvulus: case report and review of the literature. *The Journal of Emergency Medicine* 17:837-840.

- Goel M, Wong ND, Eisenberg H, Hagar J, Kelly K, Tobis JM.** 1992. Risk factor correlates of coronary calcium as evaluated by ultrafast computed tomography. *American Journal of Cardiology* 70:977-980.
- Golden MP, Vikram HR.** 2005. Extrapulmonary tuberculosis: an overview. *American Family Physician* 72:1761-1768.
- Goretsky MJ, Kelly RE, Croitoru D, Nuss D.** 2004. Chest wall anomalies: pectus excavatum and pectus carinatum. *Adolescent Medicine* 15:455-471.
- Gori A, Bandera A, Marchetti G, Esposti AD, Catozzi L, Nardi GP, Gazzola L, Ferrario G, Van Embden JDA, Van Soolingen D, Moroni M, Franzetti F.** 2005. Spoligotyping and *Mycobacterium tuberculosis*. *Emerging Infectious Diseases* 11:1242-1248.
- Gorse GJ, Belshe RB.** 1985. Male genital tuberculosis: a review of the literature with instructive case reports. *Reviews of Infectious Diseases* 7:511-524.
- Goussard P, Kling S, Gie RP.** 2009. Management of complicated intrathoracic and upper airway tuberculosis in children. In HS Schaaf & A Zumla (eds.), *Tuberculosis. A comprehensive clinical reference*, pp. 364-376, Saunders Elsevier, Philadelphia.
- Govender T, Barnes JM, Pieper CH.** 2010. Living in low-cost housing settlements in Cape Town, South Africa – the epidemiological characteristics associated with increased health vulnerability. *Journal of Urban Health* 87:899-911.
- Govender T, Barnes JM, Pieper CH.** 2011. Housing conditions, sanitation status and associated health risks in selected subsidized low-cost housing settlements in Cape Town, South Africa. *Habitat International* 35:335-342.
- Goyal M, Saunders NA, Van Embden JDA, Young DB, Shaw RJ.** 1997. Differentiation of *Mycobacterium tuberculosis* isolates by spoligotyping and IS6110 restriction fragment length polymorphism. *Journal of Clinical Microbiology* 35:647-651.
- Graham SM, Marais BJ, Gie RP.** 2009. Clinical features and index of suspicion of tuberculosis in children. In HS Schaaf & A Zumla (eds.), *Tuberculosis. A comprehensive clinical reference*, pp. 154-163, Saunders Elsevier, Philadelphia.
- Gregory JK, Lachman N, Camp CL, Chen LP, Pawlina W.** 2009. Restructuring a basic science course for core competencies: an example from anatomy teaching. *Medical Teacher* 31:855-861.

- Griffin MR, Ray WA, Fought RL, Melton LJ.** 1992. Black-white differences in fracture rates. *American Journal of Epidemiology* 136:1378-1385.
- Grydeland TB, Dirksen A, Coxson HO, Pillai SG, Sharma S, Eide GE, Gulsvik A, Bakke PS.** 2009. Quantitative computed tomography: emphysema and airway wall thickness by sex, age and smoking. *European Respiratory Journal* 34:858-865.
- Guañabens N, Garrido J, Gobbo M, Piga AM, Del Pino J, Torrijos A, Descalzo MA, Garcia FJB, Cros JRR, Carbonell J, Pérez MR, Tomero J, Carmona L.** 2008. Prevalence of Paget's disease of bone in Spain. *Bone* 43:1006-1009.
- Guess HA.** 2001. Benign prostatic hyperplasia and prostatic cancer. *Epidemiologic Reviews* 23:152-158.
- Gunderman RB, Wilson PK.** 2005. Exploring the human interior: the roles of cadaver dissection and radiologic imaging in teaching anatomy. *Academic Medicine* 80:745-749.
- Gupta A, Reilly CS.** 2007. Fat embolism. *Continuing Education in Anaesthesia, Critical Care & Pain* 7:148-151.
- Gupta P, Tewari M, Shukla HS.** 2008. Gastrointestinal stromal tumor. *Surgical Oncology* 17:129-138.
- Gupta SK, Jain AK, Gupta JP, et al.** 1988. Duodenal tuberculosis. *Clinical Radiology* 39:159-161.
- Gurley ES, Hossain MJ, Montgomery SP, Petersen LR, Sejvar JJ, Mayer LW, Whitney A, Dull P, Nahar N, Uddin AKMR, Rahman ME, Ekram ARMS, Luby SP, Breiman RF.** 2009. Etiologies of bacterial meningitis in Bangladesh: results from a hospital-based study. *The American Journal of Tropical Medicine and Hygiene* 81:475-483.
- Hagelberg E, Sykes B, Hedges R.** 1989. Ancient bone DNA amplified. *Nature* 342:485.
- Hale JE, Morgan MN.** 1969. Simple renal cysts. *Postgraduate Medical Journal* 45:767-772.
- Hagan PG, Nienaber CA, Isselbacher EM, Bruckman D, Karavite DJ, Russman PL, Evangelista A, Fattori R, Suzuki T, Oh JK, Moore AG, Malouf JF, Pape LA, Gaca C, Sechtem U, Lenferink S, Deutsch HJ, Diedrichs H, Robles JM, Llovet A, Gilon D, Das SK, Armstrong WF, Deeb GM, Eagle KA.** 2000. The International registry of acute aortic

dissection (IRAD). New insights into an old disease. *Journal of the American Medical Association* 283:897-903.

Hagen PT, Scholz DG, Edwards WD. 1984. Incidence and size of patent foramen ovale during the first 10 decades of life: an autopsy study of 965 normal hearts. *Mayo Clinic Proceedings* 59:17-20

Hailer NP, Garellick G, Kärrholm J. 2010. Uncemented and cemented primary total hip arthroplasty in the Swedish Hip Arthroplasty Register. Evaluation of 170,413 operations. *Acta Orthopaedica* 81:34-41.

Hanekom M, Van Der Spuy GD, Streicher E, Ndabambi SL, McEvoy CRE, Kidd M, Beyers N, Victor TC, Van Helden PD, Warren RM. 2007. A recently evolved sublineage of the *Mycobacterium tuberculosis* Beijing strain family is associated with an increased ability to spread and cause disease. *Journal of Clinical Microbiology* 45:1483-1490.

Harling G, Ehrlich R, Myer L. 2008. The social epidemiology of tuberculosis in South Africa: A multilevel analysis. *Social Science & Medicine* 66:492-505.

Harrington RD, Hooton TM. 2000. Urinary tract infection risk factors and sex. *The Journal of Sex-specific Medicine* 3:27-34.

Hawley PR, Wolfe HRI, Fullerton JM. 1968. Hypertrophic tuberculosis of the rectum. *Gut* 9:461-465.

Health24.com. S.a. SA scanner stars in Grey's Anatomy. [Internet]. Available: <http://www.health24.com/Lifestyle/Man/Multimedia/Lodox-scanner-stars-in-Greys-Anatomy-20130611> (Accessed: 25 July 2014).

Heinmöller E, Renke B, Beyser K, Dietmaier W, Langner C, Rüschoff J. 2001. Pitfalls in diagnostic molecular pathology – significance of sampling error. *Virchows Archiv* 439:504-511.

Heppleston AG, Leopold JG. 1961. Chronic pulmonary emphysema. Anatomy and pathogenesis. *The American Journal of Medicine* 31:279-291.

Heric B, Lytle BW, Miller DP, Rosenkranz ER, Lever HM, Cosgrove DM. 1995. Surgical management of hypertrophic obstructive cardiomyopathy. Early and late results. *Journal of Thoracic and Cardiovascular Surgery* 110:195-208.

- Herman P, Costa MLV, Machado MAC, Pugliese V, D’Albuquerque LAC, Machado MCC, Gama-Rodrigues JJ, Saad WA.** 2005. Management of hepatic hemangiomas: a 14-year experience. *Journal of Gastrointestinal Surgery* 9:853-859.
- Hermans PWM, Schuitema ARJ, Van Soolingen D, Verstynen CP, Bik EM, Thole JE, Kolk AH, Van Embden JD.** 1990. Specific detection of *Mycobacterium tuberculosis* complex strains by polymerase chain reaction. *Journal of Clinical Microbiology* 28:1204-1213.
- Hershkovitz I, Greenwald C, Rothschild BM, Latimer B, Dutour O, Jellema LM, Wish-Baratz.** 1999. Hyperostosis frontalis interna: an anthropological perspective. *American Journal of Physical Anthropology* 109:303-325.
- Hesseling AC, Schaaf HS, Gie RP, Starke JR, Beyers N.** 2002. A critical review of diagnostic approaches used in the diagnosis of childhood tuberculosis. *International Journal of Tuberculosis and Lung Disease* 6:1038-1045.
- Heyderman RS, Makunike R, Muza T, Odwee M, Kadzirange G, Manyemba J, Muchedzi C, Ndemera B, Gomo ZAR, Gwanzura LKZ, Mason PR.** 1998. Pleural tuberculosis in Harare, Zimbabwe: the relationship between human immunodeficiency virus, CD4 lymphocyte count, granuloma formation and disseminated disease. *Tropical Medicine and International Health* 3:14-20.
- Hilibrand AS, Carlson GD, Palumbo MA, Jones PK, Bohlman HH.** 1999. Radiculopathy and myelopathy at segments adjacent to the site of a previous anterior cervical arthrodesis. *The Journal of Bone & Joint Surgery* 81A:519-528.
- Hilibrand AS, Robbins M.** 2004. Adjacent segment degeneration and adjacent segment disease: the consequences of spinal fusion? *The Spine Journal* 4:190S-194S.
- Hill CM, Crosher RF, Carroll MJ, Mason DA.** 1984. Facial fractures – the results of a prospective four-year study. *Journal of Maxillofacial Surgery* 12:267-270.
- Hnizdo E, Singh T, Churhyard G.** 2000. Chronic pulmonary function impairment caused by initial and recurrent pulmonary tuberculosis following treatment. *Thorax* 55:32-38.
- Ho TS, Wang SM, Shen CF, Lee KH, Liu CC.** 2011. Clinical perspectives of childhood tuberculosis in Taiwan. *Journal of the Formosan Medical Association* 110: 737-743.

- Hoff JA, Chomka EV, Krainik AJ, Daviglius M, Rich S, Kondos GT.** 2001. Age and sex distributions of coronary artery calcium detected by electron beam tomography in 35246 adults. *American Journal of Cardiology* 87:1335-1339.
- Hoffmann CJ, Churchyard GJ.** 2009. Pulmonary tuberculosis in adults. In HS Schaaf & A Zumla (eds.), *Tuberculosis. A comprehensive clinical reference*, pp. 332-341, Saunders Elsevier, Philadelphia.
- Holbrook TL, Barrett-Connor E.** 1993. A prospective study of alcohol consumption and bone mineral density. *British Medical Journal* 306:1506-1509.
- Holloway KL, Link K, Rühli F, Henneberg M.** 2013. Skeletal lesions in human tuberculosis may sometimes heal: an aid to palaeopathological diagnoses. *PLoS ONE* 8:e62798
- Hoon JR, Dockerty MB, Pemberton J.** 1950. Ileocaecal tuberculosis including a comparison of this disease with nono-specific regional enterocolitis and noncaseous tuberculated enterocolitis. *International Abstracts of Surgery* 91:417-440.
- Hornor G.** 2005. Physical abuse: recognition and reporting. *Journal of Pediatric Health Care* 19:4-11.
- Höss M, Jaruga P, Zastowny TH, Dizdaroglu M, Pääbo S.** 1996. DNA damage and DNA sequence retrieval from ancient tissues. *Nucleic Acids Research* 24:1304-1307.
- Hovellius L, Eriksson K, Fredin H, Hagberg G, Hussenius A, Lind B, Thorling J, Weckstrom J.** 1983. Recurrences after initial dislocation of the shoulder. Results of a prospective study of treatment. *Journal of Bone and Joint Surgery* 65:343-349.
- Howe JR, Klimstra DS, Cordon-Cardo C.** 1997. DNA extraction from paraffin-embedded tissues using a salting-out procedure: a reliable method for PCR amplification of archival material. *Histology and Histopathology* 12:595-601.
- Hsieh CJ, Vanderford JD, Moreau SR, Prong T.** 2000. Lumbosacral transitional segments: classification, prevalence, and effect on disk height. *Journal of Manipulative and Physiological Therapeutics* 23:483-489.
- Huang JH, Kao PN, Adi V, Ruoss SJ.** 1999. *Mycobacterium avium-intracellulare* pulmonary infections in HIV-negative patients without preexisting lung disease. *Chest* 115:1033-1040.
- Hughes LE.** 1969. Postmortem survey of diverticular disease of the colon. *Gut* 10:336-351.

- Human Skeleton.** S.a. [Internet]. Available: <http://www.paradoja7.com/skeleton-in-human-body-2/>. (06 April 2014).
- Hunt CR, Benbow EW, Knox WF, McMahon RFT, McWilliam LJ.** 1995. Can histopathologists diagnose bronchopneumonia? *Journal of Clinical Pathology* 48:120-123.
- Ilgazli A, Bayaci H, Basyigit I, Yildiz F.** 2004. Extrapulmonary tuberculosis: clinical and epidemiologic spectrum of 636 cases. *Archives of Medical Research* 35:435-441.
- Ikejima K, Enomoto N, Iimuro Y, Ikejima A, Fang D, Xu J, Forman DT, Brenner DA, Thurman RG.** 1998. Estrogen increases sensitivity of hepatic Kupffer cells to endotoxin. *American Journal of Physiology – Gastrointestinal and Liver Physiology* 274:G669-G676.
- Ilyas SE, Chen FF, Hodgson TA, Speight PM, Lacey CJN, Porter SR.** 2002. Labial tuberculosis: a unique cause of lip swelling complicating HIV infection. *HIV Medicine* 3:283:286.
- Inghammar M, Ekbohm A, Engström G, Ljungberg B, Romanus V, Löfdahl C, Egesten A.** 2010. COPD and the risk of tuberculosis – a population-based cohort study. *PLoS ONE* 5:e10138.
- Ioachim HL.** 1983. Pathology of Granulomas. First Edition. Raven Press. New York.
- Ito T, Goto K, Yoh K, Niho S, Ohmatsu H, Kubota K, Nagai K, Miyazaki E, Kumamoto T, Nishiwaki Y.** 2010. Hypertrophic pulmonary osteoarthropathy as a paraneoplastic manifestation of lung cancer. *Journal of Thoracic Oncology* 5:976-980.
- Jackson DP, Lewis FA, Taylor GR, Boylston AW, Quirke P.** 1990. Tissue extraction of DNA and RNA and analysis by the polymerase chain reaction. *Journal of Clinical Pathology* 43:499-504.
- Jacobs DO.** 2007. Diverticulitis. *New England Journal of Medicine* 357:2057-2066.
- Janowitz WR, Agatston AS, Kaplan G, Viamonte M.** 1993. Differences in prevalence and extent of coronary artery calcium detected by ultrafast computed tomography in asymptomatic men and women. *The American Journal of Cardiology* 72:247-254.
- Jan W, Zimmerman RA, Bilaniuk LT, Hunter JV, Simon EM, Haselgrove J.** 2003. Diffusion-weighted imaging in acute bacterial meningitis in infancy. *Neuroradiology* 45: 634-639.

- Jardim-Botelho A, Brooker S, Geiger SM, Fleming F, Lopes ACS, Diemert DJ, Corrêa-Oliviera R, Bethony JM.** 2008. Age patterns in undernutrition and helminth infection in a rural area of Brazil: associations with ascariasis and hookworm. *Tropical Medicine and International Health* 13:458-467.
- Jeong YJ, Lee KS.** 2008. Pulmonary tuberculosis: up-to-date imaging and management. *American Journal of Roentgenology* 191:834-844.
- Jha R, Khadka N, Kumar P.** 2010. Management of hydrocephalus – our experience. *Postgraduate Medical Journal of NAMS* 10:68-70.
- Johkoh T, Ichikado K, Akira M, Honda O, Tomiyama N, Mihara N, Kozuka T, Koyama M, Hamada S, Nakamura H.** 2000. Lymphocytic interstitial pneumonia. Follow-up CT findings in 14 patients. *Journal of Thoracic Imaging* 15:162-167.
- Jones-Webb R.** 1998. Drinking patterns and problems among African-Americans: recent findings. *Alcohol Health & Research World* 22:260-264.
- Jordan TS, Spencer EM, Davies P.** 2010. Tuberculosis, bronchiectasis and chronic airflow obstruction. *Respirology* 15:623-628.
- Jorgensen T, Jensen KH.** 1990. Polyps in the gallbladder: a prevalence study. *Scandinavian Journal of Gastroenterology* 25:281-286.
- Jupp J, Fine D, Johnson CD.** 2010. The epidemiology and socioeconomic impact of chronic pancreatitis. *Best Practice & Research Clinical Gastroenterology* 24:219-231.
- Kahn R, Abid S, Jafri W, Abbas Z, Hameed K, Ahmad Z.** 2006. Diagnostic dilemma of abdominal tuberculosis in non-HIV patient: an ongoing challenge for physicians. *World Journal of Gastroenterology* 12:6371-6375.
- Kalichman L, Kim DH, Li L, Guermazi A, Berkin V, Hunter DJ.** 2009. Spondylolysis and spondylolisthesis: prevalence and association with low back pain in the adult community-based population. *Spine* 34:199-205.
- Kasiske BL.** 1987. Relationship between vascular disease and age-associated changes in the human kidney. *Kidney International* 31:1153-1159.
- Kayembe KNT, Sasahara M, Hazama F.** 1984. Cerebral aneurysms and variations in the circle of Willis. *Stroke* 15:846-850.

- Kay P, Soeters R, Nevin J, Denny L, Dehaeck CMC, Williamson AL.** 2003. High prevalence of HPV 16 in South African women with cancer of the cervix and cervical intraepithelial neoplasia. *Journal of Medical Virology* 71:265-273.
- Kamerbeek J, Schouls L, Kolk A, Van Agterveld M, Van Soolingen D, Kuijper S, Bunschoten A, Molhuizen H, Shaw R, Goyal M, Van Embden J.** 1997. Simultaneous detection and strain differentiation of *Mycobacterium tuberculosis* for diagnosis and epidemiology. *Journal of Clinical Microbiology* 35:907-914.
- Karakoc GB, Yilmaz M, Altintas DU, Kendirli SG.** 2001. Bronchiectasis: still a problem. *Pediatric Pulmonology* 32:175-178.
- Karasik D, Kiel DP, Kiely DK, Cupples LA, Wilson PWF, O'Donnell JO, Felson DT.** 2006. Abdominal aortic calcification and exostoses at the hand and lumbar spine: the Framingham Study. *Calcified Tissue International* 78:1-8.
- Karim SSA, Churchyard GJ, Karim QA, Lawn SD.** 2009. HIV infection and tuberculosis in South Africa: an urgent need to escalate the public health response. *Lancet* 374:921-933.
- Kew MC.** 2002. Epidemiology of hepatocellular carcinoma. *Toxicology* 181-182:35-38.
- Khalil F, Shaladi OA.** 1981. Fractures of the facial bones in the eastern region of Libya. *British Journal of Oral Surgery* 19:300-304.
- Khoor A, Leslie KO, Tazelaar HD, Helmers RA, Colby TV.** 2001. Diffuse pulmonary disease caused by nontuberculous mycobacteria in immunocompetent people (hot tub lung). *American Journal of Clinical Pathology* 115:755-762.
- Khot UN, Khot MB, Bajzer CT, Sapp SK, Ohman EM, Brener SJ, Ellis SG, Lincoff AM, Topol EJ.** 2003. Prevalence of conventional risk factors in patients with coronary heart disease. *Journal of the American Medical Association* 290:898-904.
- Kim GE, Thung SN, Tsui WMS, Ferrell LD.** 2006. Hepatic cavernous hemangioma: underrecognized associated histologic features. *Liver International* 26:334-338.
- Ki M, Park T, Choi B, Foxman B.** 2004. The epidemiology of acute pyelonephritis in South Korea, 1997-1999. *American Journal of Epidemiology* 160:985-993
- Kim RD, Greenberg DE, Ehrmantraut ME, Guide SV, Ding L, Shea Y, Brown MR, Chernick M, Steagall WK, Glasgow CG, Lin J, Jolley C, Sorbara L, Raffeld M, Hill S,**

- Avila N, Sachdev V, Barnhart LA, Anderson VL, Claypool R, Hilligoss DM, Garofalo M, Fitzgerald A, Anaya-O'Brien S, Darnell D, DeCastro R, Menning HM, Ricklefs SM, Porcella SF, Olivier KN, Moss J, Holland SM.** 2008. Pulmonary nontuberculous mycobacterial disease. *American Journal of Respiratory and Critical Care Medicine* 178:1066-1074.
- Kim SK, Choi BR, Kim CG, Chung SH, Choe JY, Joo KB, Bae SC, Yoo DH, Jun JB.** 2004. The prevalence of diffuse idiopathic skeletal hyperostosis in Korea. *Journal of Rheumatology* 31:2032-2035.
- Kim YJ, Jung CY, Shin HW, Lee BK.** 2009. Biomass smoke induced bronchial anthracofibrosis: presenting features and clinical course. *Respiratory Medicine* 103:757-765.
- Kitzman DW, Scholz DG, Hagen PT, Ilstrup DM, Edwards WD.** 1988. Age-related changes in normal human hearts. Part II: (Maturity): a quantitative anatomic study of 765 specimens from subjects 20 to 99 years old. *Mayo Clinic Proceedings* 63:137-146.
- Klaassen Z, Tubbs RS, Apaydin N, Hage R, Jordan R, Loukas M.** 2011. Vertebral spinal osteophytes. *Anatomical Science International* 86:1-9.
- Klinger ME.** 1951. Secondary tumors of the genitourinary tract. *Journal of Urology* 65:144-153.
- Knowelden J, Buhr AJ, Dunbar O.** 1964. Incidence of fractures in persons over 35 years of age. *British Journal of Preventative & Social Medicine* 18:130-141.
- Knüsel CJ, Göggel S, Lucy D.** 1997. Comparative degeneration joint disease of the vertebral column in the Medieval Monastic cemetery of the Gilbertine Priory of St. Andrew, Fishergate, York, England. *American Journal of Physical Anthropology* 103:481-495.
- Konin GP, Walz DM.** 2010. Lumbosacral transitional vertebrae: classification, imaging findings, and clinical relevance. *American Journal of Neuroradiology* 31:1778-1786.
- Kotzé SH, Mole CG, Greyling LM.** 2012. The translucent cadaver: an evaluation of the use of full body digital X-ray images and drawings in surface anatomy education. *Anatomical Sciences Education* 5:287-294.
- Kremer K, Glynn JR, Lillebaek T, Niemann S, Kurepina NE, Kreiswirth BN, Bifani PJ, Van Soolingen D.** 2004. Definition of the Beijing/W lineage of *Mycobacterium tuberculosis* on the basis of genetic markers. *Journal of Clinical Microbiology* 42:4040-4049.

- Ku HJ, Kim ME, Lee NK, Park YH.** 2001. The excisional, placcation and internal drainage techniques: a comparison of the results for idiopathic hydrocele. *BJU International* 87:82-84.
- Kucukkaya M, Kabukcuoglu Y, Tezer M, Kuzgun U.** 2002. Management of childhood chronic tibial osteomyelitis with the Ilizarov method. *Journal of Pediatric Orthopaedics* 22:632-637.
- Kumar K, Ayub M, Kumar M, Keswani NK, Shukla HS.** 2000. Tuberculosis of the gallbladder. *HPB Surgery* 11:401-404.
- Kumar P, Clarke M.** 1999. *Clinical Medicine*, 4th ed. W. B. Saunders, Edinburgh, pp. 1081.
- Kumar V, Abbas AK, Aster JC.** 2013. *Robbins Basic Pathology*, 9th ed. Elsevier, Philadelphia, pp. 475.
- Kumar V, Abbas AK, Fausto N, Mitchell RN.** 2007. *Robbins Basic Pathology*. Eighth Edition. Saunders, Elsevier. Philadelphia.
- Kurata JH, Elashoff JD, Nogawa AN, Haile BM.** 1986. Sex and smoking differences in duodenal ulcer mortality. *American Journal of Public Health* 76:700-702.
- Kytö V, Saraste A, Voipio-Pulkki L, Saukko P.** 2007. Incidence of fatal myocarditis: a population-based study in Finland. *American Journal of Epidemiology* 165:570-574.
- Labuschagne BCJ, Mathey B.** 2000. Cadaver profile at University of Stellenbosch Medical School, South Africa, 1956-1996. *Clinical Anatomy* 13:88-93.
- Lamrani YA, Houssaini NS, Kamaoui I, Maârroufi M, Tizniti S.** 2010. Congenital superior sternal cleft – an unusual age of diagnosis with review of the literature. *European Journal of Radiology Extra* 73:e33-e35
- Lanjewar DN, Duggal R.** 2001. Pulmonary pathology in patients with AIDS: an autopsy study from Mumbai. *HIV Medicine* 2:266-271.
- Larson EW, Edwards WD.** 1984. Risk factors for aortic dissection: a necropsy study of 161 cases. *American Journal of Cardiology* 53:849-855.
- Lawn SD, Bekker L, Middelkoop K, Myer L, Wood R.** 2006. Impact of HIV infection on the epidemiology of tuberculosis in a peri-urban community in South Africa: the need for age-specific interventions. *Clinical Infectious Diseases* 42:1040-1047.

- Lawn SD, Churchyard G.** 2009. Epidemiology of HIV-associated tuberculosis. *Current Opinion in HIV and AIDS* 4:325-333.
- Lederle FA, Johnson GR, Wilson SE, Chute EP, Littooy FN, Bandyk D, Krupski WC, Barone GW, Acher CW, Ballard DJ.** 1997. Prevalence and associations of abdominal aortic aneurysm detected through screening. *Annals of Internal Medicine* 126:441-449.
- Ledesma-Montes C, Hernandez-Guerrero JC, Garces-Ortiz M.** 2000. Clinico-pathologic study of odontogenic cysts in a Mexican sample population. *Archives of Medical Research* 31:373-376.
- Lee KF, Wong J, Li JCM, Lai PBS.** 2004. Polypoid lesions of the gallbladder. *The American Journal of Surgery* 188:186-190.
- Lee YS.** 1986. Diverticular disease of the large bowel in Singapore: an autopsy study. *Diseases of the Colon and Rectum* 29:330-335.
- Lee YW, Hirani AA.** 2006. Role of interleukin-4 in atherosclerosis. *Archives of Pharmacal Research* 29:1-15.
- Lemma E, Zimhony O, Greenblatt CL, Koltunov V, Zylber MI, Vernon K, Spigelman M.** 2007. Attempts to revive *Mycobacterium tuberculosis* from 300-year-old human mummies. *FEMS Microbiology Letters* 283:54-61.
- Leong FJ, Eum S, Via LE, Barry CE.** 2011. Pathology of tuberculosis in the human lung. In FJ Leong, V Dartois, T Dick (eds.), *A color atlas of comparative pathology of pulmonary tuberculosis*, pp. 53-82, CRC Press.
- Leslie KO, Wick MR.** 2005. *Practical Pulmonary Pathology. A Diagnostic Approach*. First Edition. Churchill Livingstone. China.
- Leung AN.** 1999. Pulmonary tuberculosis: the essentials. *Radiology* 201:307-322.
- Leung CC, Lam TH, Chan WM, Yew WW, Ho KS, Leung G, Law WS, Tam CM, Chan CK, Chang KC.** 2007. Lower risk of tuberculosis in obesity. *Archives of Internal Medicine* 167:1297-1304.
- Leung VKS, Law ST, Lam CW, Luk ISC, Chau TN, Loke TKL, Chan WH, Lam SH.** 2006. Intestinal tuberculosis in a regional hospital in Hong Kong: a 10-year experience. *Hong Kong Medical Journal* 12:264-271.

- Levy D, Anderson KM, Savage DD, Kannel WB, Christiansen JC, Castelli WP.** 1988. Echocardiographically detected left ventricular hypertrophy: prevalence and risk factors. *Annals of Internal Medicine* 108:7-13.
- Lew DP, Waldvogel FA.** 2004. Osteomyelitis. *Lancet* 364:369-379.
- Liegl-Atzwanger B, Fletcher JA, Fletcher CDM.** 2010. Gastrointestinal stromal tumors. *Virchows Archiv* 456:111-127.
- Lindroos M, Kupari M, Heikkilä J, Tilvis R.** 1993. Prevalence of aortic valve abnormalities in the elderly: an echocardiographic study of a random population sample. *Journal of the American College of Surgeons* 21:1220-1225.
- Lin JN, Lai CH, Chen YH, Lee SSJ, Tsai SS, Huang CK, Chung HC, Liang SH, Lin HH.** 2009. Risk factors for extra-pulmonary tuberculosis compared to pulmonary tuberculosis. *International Journal of Tuberculosis and Lung Disease* 13:620-625.
- Lin Y, Tamakoshi A, Matsuno S, Takeda K, Hayakawa T, Kitagawa M, Naruse S, Kawamura T, Wakai K, Aoki R, Kojima M, Ohno Y.** 2000. Nationwide epidemiological survey of chronic pancreatitis in Japan. *Journal of Gastroenterology* 35:136-141.
- Lipshultz LI, Corriere JN.** 1977. Progressive testicular atrophy in the varicocele patient. *Journal of Urology* 117:175-176.
- Liu R, Xing L, Peng Z, Zhang Y, Zhu C, Yang Z.** 2011. Usefulness of mycobacterial interspersed repetitive-unit locus PCR amplification in rapid diagnosis of Beijing lineage strain infection among pediatric tuberculosis patients. *Journal of Clinical Microbiology* 49:712-714.
- Lodox Systems.** 2012. Lodox critical imaging technology. [Internet] Available: www.lodox.com. (Accessed: 18 March 2013)
- London L, Nell V, Thompson M-L, Myers JE.** 1998. Health status among farm workers in the Western Cape – collateral evidence from a study of occupational hazards. *South African Medical Journal* 88:1096-1101.
- Lönnroth K, Williams BG, Cegielski P, Dye C.** 2010. A consistent log-linear relationship between tuberculosis incidence and body mass index. *International Journal of Epidemiology* 39:149-155.

- Lopez-Abente G, Pollan M, de la Iglesia P, Ruiz M.** 1995. Characterization of the lung cancer epidemic in the European Union (1970-1990). *Cancer Epidemiology, Biomarkers and Prevention* 4:813-820.
- López Gude MJ, Pérez de la Sota E, Romero JMC, Delgado JF, Sánchez MAG, Aguado JM, Sánchez JJR.** 2006. An Unusual Indication for Cardiac Transplantation: Isolated Myocardial Tuberculosis. *The Journal of Heart and Lung Transplantation* 25:128-130.
- Lorell BH.** 1997. Pericardial diseases. In: Braunwald E (ed.). *Heart Disease: A textbook of cardiovascular medicine*, fifth edition, pp. 1479-1534. Saunders, Philadelphia.
- Lounis N, Truffot-Pernot C, Grosset J, Gordeuk VR, Boelaert JR.** 2001. Iron and *Mycobacterium tuberculosis* infection. *Journal of Clinical Virology* 20:123-126.
- Lin JN, Lai CH, Chen YH, Lee SSJ, Tsai SS, Huang CK, Chung HC, Liang SH, Lin HH.** 2009. Risk factors for extra-pulmonary tuberculosis compared to pulmonary tuberculosis. *International Journal of Tuberculosis and Lung Disease* 13:620-625.
- Luo T, Yang C, Gao Q.** 2011. Mycobacterial interspersed repetitive-unit locus PCR amplification and Beijing strains of *Mycobacterium tuberculosis*. *Journal of Clinical Microbiology* 49:4026-4027.
- Lundy JK, Feldesman MR.** 1987. Revised equations for estimating living stature from the long bones of the South African Negro. *South African Journal of Science* 83:54-55.
- Lucey MR, Mathurin P, Morgan TR.** 2009. Alcoholic hepatitis. *The New England Journal of Medicine* 360:2758-2769.
- MacCallum NS, Evans TW.** 2005. Epidemiology of acute lung injury. *Current Opinion in Critical Care* 11:43-49.
- Maity P, Biswas K, Roy S, Banerjee RK, Bandyopadhyay U.** 2003. Smoking and the pathogenesis of gastroduodenal ulcer – recent mechanistic update. *Molecular and Cellular Biochemistry* 253:329-338.
- Mann RE, Smart RG, Govoni R.** 2003. The epidemiology of alcoholic liver disease. *Alcohol Research & Health* 27:209-219.
- Mannino DM, Buist AS.** 2007. Global burden of COPD: risk factors, prevalence, and future trends. *Lancet* 370:765-773.

- Marais BJ, Gie RP, Schaaf HS, Hesselning AC, Enarson DA, Beyers N.** 2006. The spectrum of disease in children treated for tuberculosis in a highly endemic area. *Int J Tuberc Lung Dis* 10:732-738.
- Marais BJ, Schaaf HS, Donald PR.** 2009. Management algorithms for pediatric tuberculosis. In HS Schaaf & A Zumla (eds.), *Tuberculosis. A comprehensive clinical reference*, pp. 323-331, Saunders Elsevier, Philadelphia.
- Marcantoni C, Ma L, Federspiel C, Fogo AB.** 2002. Hypertensive nephrosclerosis in African Americans versus Caucasians. *Kidney International* 62:172-180.
- Marchetti G, Gori A, Catozzi L, Vago L, Nebuloni M, Rossi MC, Esposti AD, Bandera A, Franzetti F.** 1998. Evaluation of PCR in detection of *Mycobacterium tuberculosis* from formalin-fixed, paraffin-embedded tissues: comparison of four amplification assays. *Journal of Clinical Microbiology* 36:1512-1517.
- Marik PE.** 2001. Aspiration pneumonitis and aspiration pneumonia. *New England Journal of Medicine* 344:665-671.
- Markowitz S, Leiman G, Margolis KA.** 1986. Human papillomavirus and cervical intraepithelial neoplasia in an African population. *South African Journal of Epidemiology and Infection* 1:65-69.
- Maron BJ.** 2002. Hypertrophic cardiomyopathy. A systemic review. *Journal of the American Medical Association* 287:1308-1320.
- Marshall LM, Spiegelman D, Barbieri RL, Goldman MB, Manson JE, Colditz GA, Willett WC, Hunter DJ.** 1997. Variation in the incidence of uterine leiomyoma among premenopausal women by age and race. *Obstetrics & Gynecology* 90:967-973.
- Martinez FJ, Curtis JL, Sciruba F, Mumford J, Giardino ND, Weinmann G, Kazerooni E, Murray S, Criner GJ, Sin DD, Hogg J, Ries AL, Han M, Fishman AP, Make B, Hoffman EA, Mohsenifar Z, Wise R.** 2007. Sex differences in severe pulmonary emphysema. *American Journal of Respiratory and Critical Care Medicine* 176:243-252.
- Matos V, Santos AL.** 2006. On the trail of pulmonary tuberculosis based on rib lesions: results from human identified skeletal collection from MuseuBocage (Lisbon, Portugal). *American Journal of Physical Anthropology* 130: 190-200.

- Matsuoka S, Uchiyama K, Shima H, Suzuki K, Shimura A, Sasaki Y, Yamagishi F.** 2004. Relationship between CT findings of pulmonary tuberculosis and the number of acid-fast bacilli on sputum smears. *Journal of Clinical Imaging* 28:119-123.
- Mayosi BM, Burgess LJ, Doubell AF.** 2005. Tuberculous pericarditis. *Circulation* 112:3608-3616.
- Mayosi BM.** 2009. Tuberculous pericarditis and myocarditis in adults and children. In HS Schaaf & A Zumla (eds.), *Tuberculosis. A comprehensive clinical reference*, pp. 351-360, Saunders Elsevier, Philadelphia.
- Mays S, Fysh E, Taylor GM.** 2002. Investigation of the link between visceral surface rib lesions and tuberculosis in a medieval skeletal series from England using ancient DNA. *American Journal of Physical Anthropology* 119:27-36.
- Mazess RB.** 1983. Noninvasive methods for quantitating trabecular bone. In LV Avioli (ed.), *The osteoporotic syndrome*, pp. 85-114, Grune and Stratton.
- McAdams HP, Erasmus J, Winter JA.** 1995. Radiologic manifestations of pulmonary tuberculosis. *Radiologic Clinics of North America* 33:655-678.
- McCluggage WG, Sloan JM.** 1994. Hepatic granulomas in Northern Ireland: a thirteen year review. *Histopathology* 25:219-228.
- McConnell EJ, Tessier DJ, Wolff BG.** 2003. Population-based incidence of complicated diverticular disease of the sigmoid colon based on sex and age. *Diseases of the Colon and Rectum* 46:1110-1114.
- McDade AM, McNicol RD, Ward-Booth P, Chesworth J, Moos KF.** 1982. The aetiology of maxillo-facial injuries, with special reference to the abuse of alcohol. *International Journal of Oral Surgery* 11:152-155.
- McEvoy CRE, Warren RM, Van Helden PD.** 2009. Molecular methods and their application in tuberculosis epidemiology. In HS Schaaf & A Zumla (eds.), *Tuberculosis. A comprehensive clinical reference*, pp. 28-37, Saunders Elsevier, Philadelphia.
- McNaughton Collins M, Stafford RS, O'Leary MP, Barry MJ.** 1999. Distinguishing chronic prostatitis and benign prostatic hyperplasia symptoms: results of a national survey of physician visits. *Urology* 53:921-925.

- McSane H.** 2005. Co-infection with HIV and TB: double trouble. *International Journal of STD and AIDS* 16:95-101.
- Mellor A, Soni N.** 2001. Fat embolism. *Anaesthesia* 56:145-154.
- Memish ZA, Mah MW, Al Mahmood S, Bannatyne RM, Khan MY.** 2000. Clinico-diagnostic experience with tuberculous lymphadenitis in Saudi Arabia. *Clinical Microbiology and Infection* 6:137-141.
- Menezes AMB, Victora CG, Rigatto M.** 1994. Prevalence and risk factors for chronic bronchitis in Pelotas, RS, Brazil: a population-based study. *Thorax* 49:1217-1221.
- Miles KA.** 2005. Diagnostic imaging in undergraduate medical education: an expanding role. *Clinical Radiology* 60:742-745. (Review)
- Miller S, Dykes D, Polesky H.** 1988. A simple salting out procedure for extracting DNA from human nucleated cells. *Nucleic Acids Research* 16:1215
- Miquel JF, Covarrubias C, Villaroel L, Mingrone G, Greco AV, Puglielli L, Carvalho P, Marshall G, Del Pino G, Nervi F.** 1998. Genetic epidemiology of cholesterol cholelithiasis among Chilean Hispanics, Amerindians, and Maoris. *Gastroenterology* 115:937-946.
- Misseri R, Gershbein AB, Horowitz M, Glassberg KI.** 2001. The adolescent varicocele. II: the incidence of hydrocele and delayed recurrent varicocele after varicocelectomy in a long-term follow-up. *BJU International* 87:494-498.
- Modjarrad K, Zulu I, Redden DT, Njobvu L, Freedman DO, Vermund SH.** 2005. Prevalence and predictors of intestinal helminth infections among human immunodeficiency virus type 1-infected adults in an urban African setting. *American Journal of Tropical Medicine and Hygiene* 73:777-782.
- Moll AP, Friedland G, Gandhi NR, Sarita Shah N.** 2009. Extensively drug-resistant tuberculosis (XDR-TB). In HS Schaaf & A Zumla (eds.), *Tuberculosis. A comprehensive clinical reference*, pp. 551-559, Saunders Elsevier, Philadelphia.
- Monnet X, Anguel N, Osman D, Hamzaoui O, Richard C, Teboul JL.** 2007. Assessing pulmonary permeability by transpulmonary thermodilution allows differentiation of hydrostatic pulmonary edema from ALI/ARDS. *Intensive Care Medicine* 33:448-453.

- Moon WK, Im J, Yeon KM, Han MC.** 1998. Mediastinal tuberculous lymphadenitis: CT findings of active and inactive disease. *American Journal of Roentgenology* 170:715-718.
- Morgan B, Coakley F, Finlay DB, Belton I.** 1996. Hypertrophic osteoarthropathy in staging skeletal scintigraphy for lung cancer. *Clinical Radiology* 51:694-697.
- Morgello S, Mahboob R, Yakoushina T, Khan S, Hague K.** 2002. Autopsy findings in a human immunodeficiency virus-infected population over 2 decades. *Archives of Pathology & Laboratory Medicine* 126:182-190.
- Moss AR, Hahn JA, Tulskey JP, Daley CL, Small PM, Hopewell PC.** 2000. Tuberculosis in the homeless. *American Journal of Respiratory and Critical Care Medicine* 162:460-464.
- Moss M, Mannino DM.** 2002. Race and sex differences in acute respiratory distress syndrome deaths in the United States: an analysis of multiple-cause mortality data (1979-1996). *Critical Care Medicine* 30:1679-1685.
- Motamedi MHK.** 2003. An assessment of maxillofacial fractures: a 5-year study of 237 patients. *Journal of Oral and Maxillofacial Surgery* 61:61-64.
- Muang M, Saing H.** 1995. Intestinal volvulus: an experience in a developing country. *Journal of Pediatric Surgery* 30:679-681.
- Müller G, Dargent JL, Duwel V, D'Olne D, Vanvuchelen J, Haot J, Hustin J.** 1997. Leukaemia and lymphoma of the appendix presenting as acute appendicitis or acute abdomen. *Journal of Cancer Research and Clinical Oncology* 123:560-564.
- Mulligan ME, Flye CW.** 2006. Initial experience with Lodox Statscan imaging system for detecting injuries of the pelvis and appendicular skeleton. *Emergency Radiology* 13:129-133.
- Murad TM, Von Haam E.** 1968. The ultrastructure of fibrocystic disease of the breast. *Cancer* 22:587-600.
- Musellim B, Erturan S, Sonmez Duman E, Ongen G.** 2005. Comparison of extra-pulmonary and pulmonary tuberculosis cases: factors influencing the site of reactivation. *International Journal of Tuberculosis and Lung Disease* 9:1220-1223.
- Museru LM, Mcharo CN.** 2001. Chronic osteomyelitis: a continuing orthopaedic challenge in developing countries. *International Orthopaedics* 25:127-131.

Muttarak M, Wilfred C, Peh G, Lojanapiwat B, Chaiwun B. 2001. Tuberculous epididymitis and epididymorchitis: sonographic appearances. *American Journal of Roentgenology* 176:1459-1466.

National Health Act No 61 of 2003.

Nattrass N. 2006. South Africa's "rollout" of highly active antiretroviral therapy: a critical assessment. *Journal of Acquired Immune Deficiency Syndrome* 43:618-623.

Naydeck BL, Sutton-Tyrrell K, Schiller KD, Newman AB, Kuller LH. 1999. Prevalence and risk factors for abdominal aortic aneurysms in older adults with and without isolated systolic hypertension. *American Journal of Cardiology* 83:759-764.

Nemec SF, Bankier AA, Eisenberg RL. 2013. Upper lobe – predominant diseases of the lung. *American Journal of Roentgenology* 200:W222-W237.

Newman PH, Stone KH. 1963. The etiology of spondylolisthesis. *Journal of Bone and Joint Surgery* 45B:39-59.

Neyrolles O, Quintana-Murci L. 2009. Sexual inequality in tuberculosis. *PLoS Medicine* 6:e1000199.

Nickel JC. 2007. Inflammation and benign prostatic hyperplasia. *Urology Clinics of North America* 35:109-115.

Nicotra MB, Rivera M, Dale AM, Shepherd R, Carter R. 1995. Clinical, pathophysiologic, and microbiologic characterization of bronchiectasis in an aging cohort. *Chest* 108:955-961.

Nikolaizik WH, Warner JO. 1994. Aetiology of chronic suppurative lung disease. *Archives of Disease in Childhood* 70:141-142.

Nogales-Ortiz F, Tarancon I, Nogales FF. 1979. The pathology of female genital tuberculosis. A 31-year study of 1436 cases. *Obstetrics & Gynecology* 53:422-428.

Nordqvist A, Petersson CJ. 1995. Incidence and causes of shoulder girdle injuries in an urban population. *Journal of Shoulder and Elbow Surgery* 4:107-112.

O'Donnell AE. 2008. Bronchiectasis. *Chest* 134:815-823.

- O'Donnell AE, Barker AF, Ilowite JS, Fick RB, rhDNase Study Group.** 1998. Treatment of idiopathic bronchiectasis with aerosolized recombinant human DNase I. *Chest* 113:1329-1334.
- O'Donnell ME, Badger SA, Beattie GC, Carson J, Garstin WIH.** 2007. Malignant neoplasms of the appendix. *International Journal of Colorectal Disease* 22:1239-1248.
- Ohnishi K, Iida J, Iwama S, Goto N, Nomura F, Takashi M, Mishima A, Kono K, Kimura K, Musha H, Kotota K, Okuda K.** 1982. The effect of chronic habitual alcohol intake on the development of liver cirrhosis and hepatocellular carcinoma. *Cancer* 49:672-677.
- O'Lorcain P, Holland CV.** 2000. The public health importance of *Ascaris lumbricoides*. *Parasitology* 121:S51-S71.
- O'Neill TW, McCloskey EV, Kanis JA, Bhalla AK, Reeve J, Reid DM, Todd C, Woolf AD, Silman AJ.** 1999. The distribution, determinants and clinical correlates of vertebral osteoporosis: a population based survey. *The Journal of Rheumatology* 26:842-848.
- Oster J.** 1971. Varicocele in children and adolescents. An investigation of the incidence among Danish school children. *Scandinavian Journal of Urology and Nephrology* 5:27-32.
- Pääbo S.** 1989. Ancient DNA: extraction, characterization, molecular cloning and enzymatic amplification. *Proceedings of the National Academy of Sciences* 86:1939-1943.
- Paduch DA, Skoog SJ.** 2001. Current management of adolescent varicocele. *Reviews in Urology* 3:120-133.
- Pandey MR.** 1984. Prevalence of chronic bronchitis in a rural community of the Hill region of Nepal. *Thorax* 39:331-336.
- Pap I, Józsa L, Repa I, Bajzik G, Lakhani SR, Donoghue HD, Spigelman M.** 1999. 18 – 19th century tuberculosis in naturally mummified individuals (Vác, Hungary). In: Pálfi G, Dutour O, Deák J, Hutás I, editors. Tuberculosis past and present. Budapest: Golden Books/Tuberculosis Foundation. pp. 421-428.
- Parbhoo SP, Johnston IDA.** 1966. Effects of oestrogens and progestogens on gastric secretion in patients with duodenal ulcer. *Gut* 7:612-618.
- Park JB, Cho YS, Riew KD.** 2005. Development of adjacent-level ossification in patients with an anterior cervical plate. *The Journal of Bone & Joint Surgery* 87A:558-563

- Parks TG.** 1969. Natural history of diverticular disease of the colon. A review of 521 cases. *British Medical Journal* 4:639-645.
- Parwati I, Van Crevel R, Van Soolingen D.** 2010. Possible underlying mechanisms for successful emergence of the *Mycobacterium tuberculosis* Beijing genotype strains. *Lancet Infectious Diseases* 10:103-111. [Review]
- Pasquale MD, Shabahang M, Bitterman P, Lack EE, Evans SRT.** 1994. Primary lymphoma of the appendix. Case report and review of the literature. *Surgical Oncology* 3:243-248.
- Passarino G, Burlo P, Ciccone G, Comino A, Cravello M, Iannicelli P, Mollo F.** 1997. Prevalence of myocarditis at autopsy in Turin, Italy. *Archives of Pathology & Laboratory Medicine* 121:619-622.
- Pasteur MC, Helliwell SM, Houghton SJ, Webb SC, Foweraker JE, Coulden RA, Flower CD, Bilton D, Keogan MT.** 2000. An investigation into causative factors in patients with bronchiectasis. *American Journal of Respiratory and Critical Care Medicine* 162:1277-1284.
- Pastores SM, Naidich DP, Aranda CP, et al.** 1993. Intrathoracic adenopathy associated with pulmonary tuberculosis in patients with human immunodeficiency virus infection. *Chest* 103:1433-1437.
- Paustian FF.** 1964. Tuberculosis of the intestine. In HL Bockus (ed.), *Gastroenterology*, 2nd ed., pp. 311, Saunders, Philadelphia.
- Pazoki M, Goodarzi HM, Taheri AH, Seifirad S, Nematollahi N, Paknejad O.** 2012. Prevalence of tuberculosis in patients with anthracosis: study on 150 subjects. *Archives of Iranian Medicine* 15:128-130.
- Peltier LF.** 1969. Fat embolism: a current concept. *Clinical Orthopaedics & Related Research* 66:241-253.
- Peltzer K, Ramlagan S.** 2009. Alcohol use trends in South Africa. *Journal of Social Sciences* 18:1-12.
- Pereira JM, Madureira AJ, Vieira A, Ramos I.** 2005. Abdominal tuberculosis: imaging features. *European Journal of Radiology* 55:173-180.

- Pérez AE, Dickinson FO, Rodriquez M.** 2010. Community acquired bacterial meningitis in Cuba: a follow-up of a decade. *BMC Infectious Diseases* 10:130-138.
- Pertuiset E, Beaudreuil J, Loité F, Horusitzky A, Kemiche F, Richette P, Clerc-Wyel D, Cerf-Payrastre I, Dorfmann H, Glowinski J, Crouzet J, Bardin T, Meyer O, Dryll A, Ziza J, Khan M, Kuntz D.** 1999. Spinal tuberculosis in adults. A study of 103 cases in a developed country, 1980-1994. *Medicine* 78:309-320.
- Pettengell KE, Larsen C, Garb M, Mayet FGH, Simjee AF, Pirie D.** 1990. Gastrointestinal tuberculosis in patients with pulmonary tuberculosis. *QJM: An International Journal of Medicine* 74:303-308.
- Pfau A, Rosenmann E.** 1978. Unilateral chronic pyelonephritis and hypertension: coincidental or causal relationship? *The American Journal of Medicine* 65:499-506.
- Pickhardt PJ, Levy AD, Rohrnamm CA, Abbondanzo SL, Kende AI.** 2002. Non-Hodgkin's lymphoma of the appendix: clinical and CT findings with pathologic correlation. *American Journal of Roentgenology* 178:1123-1127.
- Pickhardt PJ, Levy AD, Rohrnamm CA, Kende AI.** 2003. Primary neoplasm of the appendix: radiologic spectrum of disease with pathologic correlation. *RadioGraphics* 23:645-662.
- Polesky A, Grove W, Bhatia G.** 2005. Peripheral tuberculous lymphadenitis. Epidemiology, diagnosis, treatment and outcome. *Medicine (Baltimore)* 84:350-362.
- Pombo F, DíazCandamio MJ, Rodriquez E, Pombo S.** 1998. Pancreatic tuberculosis: CT findings. *Abdominal Imaging* 23:394-397.
- Pomerance A, Davies MJ.** 1975. Pathologic features of hypertrophic obstructive cardiomyopathy (HOCM) in the elderly. *British Heart Journal* 37:305-312.
- Pomplun S.** 2007. Pathology of lung cancer. In SR Desai, R Reznick, J Husband (eds.), *Lung Cancer*, pp. 12-26, Cambridge.
- Poór G, Donáth J, Fornet B, Cooper C.** 2006. Epidemiology of Paget's disease in Europe: the prevalence is decreasing. *Journal of Bone and Mineral Research* 21:1545-1549.
- Porcel JM, Leung CC, Restrepo MI, Lee P.** 2012. Year in review 2011: respiratory infections, tuberculosis, pleural diseases, bronchoscopic intervention and imaging. *Respirology* 17:573-582.

Prince DS, Peterson DD, Steiner RM, Gottlieb JE, Scott R, Israel HL, Figueroa WG, Fish JE. 1989. Infection with *Mycobacterium avium* complex in patients without predisposing conditions. *The New England Journal of Medicine* 321:863-868.

Radiopaedia.org. 2013. Miliary tuberculosis. [Internet] Available: <http://radiopaedia.org/cases/miliary-tuberculosis-2>. (Accessed: 20 February 2013).

Radiopaedia.org. 2013. Ranke complex. [Internet] Available: <http://radiopaedia.org/images/831487>. (Accessed: 20 February 2013).

Ramachandran Nair PN. 2003. Non-microbial etiology: periapical cysts sustain post-treatment apical periodontitis. *Endodontic Topics* 6:96-113.

Ramesh J, Banait GS, Ormerod LP. 2008. Abdominal tuberculosis in a district general hospital: a retrospective review of 86 cases. *QJM: An International Journal of Medicine* 101:189-195.

Ramia JM, Muffak K, Fernández A, Villar J, Garrote D, Ferron JA. 2006. Gallbladder tuberculosis: false-positive PET diagnosis of gallbladder cancer. *World Journal of Gastroenterology* 12:6559-6560.

Rana RS, Wu JS, Eisenberg RL. 2009. Periosteal reaction. *American Journal of Roentgenology* 193:W259-W272.

Randi G, Franceschi S, La Vecchia C. 2006. Gallbladder cancer worldwide: geographical distribution and risk factors. *International Journal of Cancer* 118:1591-1602.

Rattan A, Kalia A, Ahmad N. 1998. Multidrug-Resistant *Mycobacterium tuberculosis*: molecular perspectives. *Emerging Infectious Diseases* 4:195-209.

Rehm J, Baliunas D, Borges GLG, Graham K, Irving H, Kehoe T, Parry CD, Patra J, Popova S, Poznyak V, Roerecke M, Room R, Samokhvalov AV, Taylor B. 2010. The relation between different dimensions of alcohol consumption and burden of disease: an overview. *Addiction* 105:817-843.

Rehm J, Samokhvalov A, Neuman MG, Room R, Parry C, Lönnroth K, Patra J, Poznyak V, Popova S. 2009. The association between alcohol use, alcohol use disorders and tuberculosis (TB). A systematic review. *BMC Public Health* 9:450-461

- Reittner P, Ward S, Heyneman L, Johkoh T, Müller NL.** 2003. Pneumonia: high-resolution CT findings in 114 patients. *European Radiology* 13:515-521.
- Reuter H, Burgess LJ, Doubell AF.** 2005. Epidemiology of pericardial effusions at a large academic hospital in South Africa. *Epidemiology & Infection* 133:393-399.
- Reuter H, Wood R.** 2009. Tuberculosis of lymph nodes and the reticuloendothelial system in adults. In HS Schaaf & A Zumla (eds.), *Tuberculosis. A comprehensive clinical reference*, pp. 397-400, Saunders Elsevier, Philadelphia.
- Reuter H, Wood R, Schaaf HS, Donald PR.** 2009. Overview of extrapulmonary tuberculosis in adults and children. In HS Schaaf & A Zumla (eds.), *Tuberculosis. A comprehensive clinical reference*, pp. 377-390, Saunders Elsevier, Philadelphia.
- Reves R, Schluger NW.** 2014. Update in tuberculosis and nontuberculous mycobacterial infections 2013. *American Journal of Respiratory and Critical Care Medicine* 189:894-898.
- Rhomberg HP, Judmair G, Lochs A.** 1984. How common are gallstones? (letter) *British Medical Journal* 13:1002.
- Rich AR.** 1951. The pathogenesis of tuberculosis, 2nd ed., pp. 131-148, CC Thomas, Springfield.
- Rich S, Chomka E, Hasara L, Hart K, Drizd T, Joo E, Levy PS.** 1989. The prevalence of pulmonary hypertension in the United States. Adult population estimates obtained from measurements of chest roentgenograms from the NHANES II survey. *Chest* 96:236-241.
- Rider JA, Kirsner JB, Moeller HC, Palmer WL.** 1954. Polyps of the colon and rectum. Their incidence and relationship to carcinoma. *The American Journal of Medicine* 16:555-564.
- Rieder HL, Snider DE, Cauthen GM.** 1990. Extrapulmonary tuberculosis in the United States. *American Review of Respiratory Disease* 141:347-351.
- Rienthong D, Rienthong S, Boonin C, Woraswad S, Kasetjaroen Y.** 2009. Rapid detection for early appearance of rifampicin and isoniazid resistance in *Mycobacterium tuberculosis*. *Sriraj Medical Journal* 61:49-55.
- Rindi L, Lari N, Cuccu B, Garzelli C.** 2009. Evolutionary pathway of the Beijing lineage of *Mycobacterium tuberculosis* based on genomic deletions and *mutT* genes polymorphisms. *Infection, Genetics and Evolution* 9:48-53.

- Roberts ISD, Benamore RE, Benbow EW, Lee SH, Harris JN, Jackson A, Mallet S, Patankar T, Peebles C, Roobottom C, Traill ZC.** 2012. Post-mortem imaging as an alternative to autopsy in the diagnosis of adult deaths: a validation study. *Lancet* 379:136-142.
- Roberts CA, Boylston A, Buckley L, Chamberlain AC, Murphy EM.** 1998. Rib lesions and tuberculosis: the palaeopathological evidence. *Tubercle and Lung Disease* 79:55-60.
- Roberts C, Lucy D, Manchester K.** 1994. Inflammatory lesions of ribs: an analysis of the Terry Collection. *American Journal of Physical Anthropology* 95:169-182.
- Roberts RO, Lieber MM, Rhodes T, Girman CJ, Bostwick DG, Jacobsen SJ.** 1998. Prevalence of a physician-assigned diagnosis of prostatitis: the Olmsted County study of urinary symptoms and health status among men. *Urology* 51:578-584.
- Roberts WC.** 1983. Morphologic features of the normal and abnormal mitral valve. *The American Journal of Cardiology* 51:1005-1028.
- Roeters van Lennep JE, Westerveld HT, Erkelens DW, van der Wall EE.** 2002. Risk factors for coronary heart disease: implications of sex. *Cardiovascular Research* 53:538-549.
- Rosenberg NJ, Bargar WL, Friedman B.** 1981. The incidence of spondylolysis and spondylolisthesis in nonambulatory patients. *Spine* 6:35-38.
- Roulson J, Benbow EW, Hasleton PS.** 2005. Discrepancies between clinical and autopsy diagnosis and the value of post mortem histology; a meta-analysis and review. *Histopathology* 47:551-559.
- Rubinfeld GD, Herridge MS.** 2007. Epidemiology and outcomes of acute lung injury. *Chest* 131:554-562.
- Rubin BP, Heinrich MC, Corless CL.** 2007. Gastrointestinal stromal tumour. *Lancet* 369:1731-1741.
- Sadoshima S, Nakatomi Y, Fujii K, Ooboshi H, Ishitsuka T, Ogata J, Fujishlma M.** 1988. Mortality and histological findings of the brain during and after cerebral ischemia in male and female spontaneously hypertensive rats. *Brain Research* 454:238-243.
- Salter DM.** 2002. Degenerative joint disease. *Current Diagnostic Pathology* 8:11-18.

- Saluja SS, Ray S, Pal S, Kukeraja M, Srivastava DN, Sahni P, Chattopadhyay TK.** 2007. Hepatobiliary and pancreatic tuberculosis: a two decade experience. *BMC Surgery* 7:10.
- Samokhvalov AV, Irving HM, Rehm J.** 2010. Alcohol consumption as a risk factor for pneumonia: a systematic review and meta-analysis. *Epidemiology & Infection* 138:1789-1795.
- Sangiovanni A, Del Ninno E, Fasani P, De Fazio C, Ronchi G, Romeo R, Morabito A, de Franchis R, Colombo M.** 2004. Increased survival of cirrhotic patients with a hepatocellular carcinoma detected during surveillance. *Gastroenterology* 126:1005-1014.
- Santos AL, Roberts CA.** 2006. Anatomy of a serial killer: differential diagnosis of tuberculosis based on rib lesions of adult individuals from the Coimbra identified skeletal collection, Portugal. *American Journal of Physical Anthropology* 130:38-49.
- Saracoglu OF, Mungan T, Tanzer F.** 1991. Pelvic tuberculosis. *International Journal of Gynecology and Obstetrics* 31:115-120.
- Sarzi-Puttini P, Atzeni F.** 2004. New developments in our understanding of DISH (diffuse idiopathic skeletal hyperostosis). *Current Opinion in Rheumatology* 16:287-292.
- Sato S, Yao K, Yao T, Schlemper RJ, Matsui T, Sakurai T, Iwashita A.** 2004. Colonoscopy in the diagnosis of intestinal tuberculosis in asymptomatic patients. *Gastrointestinal Endoscopy* 59:362-368.
- Scarfe WC.** 2005. Imaging of maxillofacial trauma: evolutions and emerging revolutions. *Oral Surgery, Oral Medicine, Oral Pathology, Oral Radiology, and Endodontics* 100:S75-S96.
- Schaaf HS, Reuter H.** 2009. Practical approaches to ordering diagnostic tests. In HS Schaaf & A Zumla (eds.), *Tuberculosis. A comprehensive clinical reference*, pp. 397-400, Saunders Elsevier, Philadelphia.
- Schmidt GD, Roberts LS.** 1989. *Foundations of parasitology*. 4th ed., pp. 451-455. Times Mirror/Mosby College Publishing, St. Louis.
- Schoeman JH, Westaway MS, Neethling A.** 1991. The relationship between socioeconomic factors and pulmonary tuberculosis. *International Journal of Epidemiology* 20:435-440.
- Scholing M, Saltzherr TP, Fung Kon Jin PHP, Ponsen KJ, Reitsma JB, Lameris JS, Goslings JC.** 2009. The value of postmortem computed tomography as an alternative for autopsy in trauma victims: a systemic review. *European Radiology* 19:2333-2341.

- Schulz S, Cabras AD, Kremer M, Weirich G, Miethke T, Bösmüller H, Höfler H, Werner M, Fend F.** 2005. Species identification of mycobacteria in paraffin-embedded tissues: frequent detection of nontuberculous mycobacteria. *Modern Pathology* 18:274-282.
- Sciarra A, Di Silverio F, Salciccia S, Gomez AMA, Gentilucci A, Gentile V.** 2007. Inflammation and chronic prostatic diseases: evidence for a link? *European Urology* 52:964-972.
- Segawa K, Arisawa T, Niwa Y, Suzuki T, Tsukamoto Y, Goto H, Hamajima E, Shimodaira M, Ohmiya N.** 1992. Prevalence of gallbladder polyps among apparently healthy Japanese: ultrasonographic study. *American Journal of Gastroenterology* 87:630-633.
- Seitz AE, Olivier KN, Steiner CA, Montes de Oca R, Holland SM, Prevots DR.** 2010. Trends and burden of bronchiectasis-associated hospitalizations in the United States, 1993-2006. *Chest* 138:944-949.
- Selzer A, Cohn KE.** 1972. Natural history of mitral stenosis. A review. *Circulation* 45:878-890.
- Sen Gupta R, Hillemann D, Kubica T, Zissel G, Müller-Quernheim J, Galle J, Vollmer E, Goldmann T.** 2003. HOPE-fixation enables improved PCR-based detection and differentiation of *Mycobacterium tuberculosis* complex in paraffin-embedded tissues. *Pathology – Research and Practice* 199:619-623.
- Sepkowitz KA.** 2002. Opportunistic infections in patients with and patients without acquired immunodeficiency syndrome. *Clinical Infectious Diseases* 34:1098-1107.
- Shafer RW, Kim DS, Wiess JP, et al.** 1991. Extrapulmonary tuberculosis in patients with human immunodeficiency virus infection. *Medicine (Baltimore)* 70:384-397.
- Shaffer EA.** 2006. Epidemiology of gallbladder stone disease. *Best Practice & Research Clinical Gastroenterology* 20:981-996.
- Shahim FN, Cameron P, McNeil JJ.** 2006. Maxillofacial trauma in major trauma patients. *Australian Dental Journal* 51:225-230.
- Shapiro AJ, Johnson RM, Miller SF, McCarthy MC.** 2001. Facial fractures in a level I trauma centre: the importance of protective devices and alcohol abuse. *Injury-International Journal of the Care of the Injured (Injury)* 32:353-356.

- Shapiro LM, McKenna WJ.** 1983. Distribution of left ventricular hypertrophy in hypertrophic cardiomyopathy: a two-dimensional echocardiographic study. *Journal of the American College of Cardiology* 2:437-444.
- Sharland M, Gibb DM, Holland F.** 1997. Respiratory morbidity from lymphocytic interstitial pneumonitis (LIP) in vertically acquired HIV infection. *Archives of Disease in Childhood* 76:334-336.
- Sharma MP, Ahuja V.** 2009. Abdominal (gastrointestinal tract) tuberculosis in adults. In HS Schaaf & A Zumla (eds.), *Tuberculosis. A comprehensive clinical reference*, pp. 424-431, Saunders Elsevier, Philadelphia.
- Sharma MP, Bhatia V.** 2004. Abdominal tuberculosis. *Indian Journal of Medical Research* 120:305-315. (Review)
- Sharma SK, Smith-Rohrberg D, Tahir M, Mohan A, Seith A.** 2007. Radiological manifestations of splenic tuberculosis: a 23-patient case series from India. *Indian Journal of Medical Research* 125:669-678.
- Sheen-Chen SM, Chou FF, Wan YL, Eng HL.** 1995. Tuberculosis presenting as a solitary splenic tumour. *Tubercle and Lung Disease* 76:80-83.
- Sherman M.** 2010. Epidemiology of hepatocellular carcinoma. *Oncology* 78:7-10.
- She R, Szakacs J.** 2004. Hyperostosis frontalis interna: case report and review of literature. *Annals of Clinical and Laboratory Science* 34:206-208.
- Shiotani S, Kobayashi T, Hayakawa H, Kikuchi K, Kohno M.** 2011. Postmortem pulmonary edema: a comparison between immediate and delayed postmortem computed tomography. *Legal Medicine* 13:151-155.
- Shiotani S, Kohno M, Ohashi N, Yamazaki K, Itai Y.** 2002. Postmortem intravascular high-density fluid level (hypostasis): CT findings. *Journal of Computer Assisted Tomography* 26:892-893.
- Shiotani S, Kohno M, Ohashi N, Yamazaki K, Nakayama H, Ito Y, Kaga K, Ebashi T, Itai Y.** 2002. Hyperattenuating aortic wall on postmortem computed tomography (PMCT). *Radiation Medicine* 20:201-206.

- Shiotani S, Kohno M, Ohashi N, Yamazaki K, Nakayama H, Watanabe K, Itai Y.** 2003. Dilatation of the heart on postmortem computed tomography (PMCT): comparison with live CT. *Radiation Medicine* 21:29-35.
- Shiotani S, Kohno M, Ohashi N, Yamazaki K, Nakayama H, Watanabe K, Oyake Y, Itai Y.** 2004. Non-traumatic postmortem computed tomographic (PMCT) findings of the lung. *Forensic Science International* 139:39-48.
- Sider L.** 1990. Radiographic manifestation of primary bronchogenic carcinoma. *Radiologic Clinics of North America*. 28:583-597.
- Sidney S, Quesenberry C, Sadler MC, Lydick EG, Guess HA, Cattolica EV.** 1991. Risk factors for surgically treated benign prostatic hyperplasia in a prepaid health care plan. *Urology* 38: 13-19 (supplement)
- Silbiger SR, Neugarten J.** 1995. The impact of sex on the progression of chronic renal disease. *American Journal of Kidney Diseases* 25:515-533.
- Silva FG.** 2005. The aging kidney: a review – part I. *International Urology and Nephrology* 37:185-205.
- Simmons DH, Nash G, Brigham KL, Tierney DF.** 1979. Adult respiratory distress syndrome. *Western Journal of Medicine* 130:218-235.
- Simon HB, Weinstein AJ, Pasternak MS, Swartz MN, Kunz LJ.** 1977. Genitourinary tuberculosis. Clinical features in a general hospital population. *The American Journal of Medicine* 63:410-420.
- Simoni G, Pastorino C, Perrone R, Ardia A, Gianrossi R, Decian F, Cittadini G, Baiardi A, Bachi V.** 1995. Screening for abdominal aortic aneurysms and associated risk factors in a general population. *European Journal of Vascular and Endovascular Surgery* 10:207-210.
- Simpson J, Scholefield JH, Spiller RC.** 2002. Pathogenesis of colonic diverticula. *British Journal of Surgery* 89:546-554.
- Simpson RJ.** 1997. Benign prostatic hyperplasia. *British Journal of General Practice* 47:235-240.

- Singh JP, Evans JC, Levy D, Larson MG, Freed LA, Fuller DL, Lehman B, Benjamin EJ.** 1999. Prevalence and clinical determinants of mitral, tricuspid, and aortic regurgitation (the Framingham Heart Study). *American Journal of Cardiology* 83:897-902.
- Singh K, Bona KH, Jacobsen BK, Bjork L, Solberg S.** 2001. Prevalence of and risk factors for abdominal aortic aneurysms in a population-based study. *American Journal of Epidemiology* 154:236-244.
- Singh V, Trikha B, Nain C, Singh K, Bose S.** 2001. Epidemiology of gallstone disease in Chandigarh: a community-based study. *Journal of Gastroenterology and Hepatology* 16:560-563.
- Singhal A, Gulati A, Frizell R, Manning AP.** 2005. Abdominal tuberculosis in Bradford, UK: 1992-2002. *European Journal of Gastroenterology and Hepatology* 17:967-971.
- Sipponen P, Helske T, Järvinen P, Hyvärinen H, Seppälä K, Siurala M.** 1994. Fall in the prevalence of chronic gastritis over 15 years: analysis of outpatient series in Finland from 1977, 1985, and 1992. *Gut* 35:1167-1171.
- Sirmali M, TürütH, Topçu S, Gülhan E, Ülkü Y, Kaya S, Taştepe I.** 2003. A comprehensive analysis of traumatic rib fractures: morbidity, mortality and management. *European Journal of Cardio-Thoracic Surgery* 24:133-138.
- Sitas F, Urban M, Bradshaw D, Kielkowski D, Bah S, Peto R.** 2004. Tobacco attributable deaths in South Africa. *Tobacco Control* 13:396-399.
- Skoog SJ, Roberts KP, Goldstein M, Pryor JL.** 1997. The adolescent varicocele: what's new with an old problem in young patients? *Pediatrics* 100:112-122.
- Smith HM, DeKaminsky RG, Niwas S, Soto RJ, Jolly PE.** 2001. Prevalence and intensity of infections of *Ascaris lumbricoides* and *Trichuris trichiura* and associated socio-demographic variables in four rural Honduran communities. *Memórias do Instituto Oswaldo Cruz* 96:303-314.
- Soler T, Calderón C.** 2000. The prevalence of spondylolysis in the Spanish elite athlete. *The American Journal of Sports Medicine* 28:57-62.
- Souhami RL, Moxham J.** 1990. Musculoskeletal and connective tissue disease. In RL Souhami & J Moxham (eds.), *Textbook of Medicine*, pp. 975-1038, Churchill Livingstone.

South African Provincial Map. S.a. [Internet]. Available: <http://home.global.co.za/~mercon/map.htm>. [2014, 3 May]

Spigelman M, Lemma E. 1993. The use of the polymerase chain reaction (PCR) to detect *Mycobacterium tuberculosis* in ancient skeletons. *International Journal of Osteoarchaeology* 3:137-143.

Squara P, Dhainaut JFA, Artigas A, Carlet J, European Collaborative ARDS Working Group. 1998. Hemodynamic profile in severe ARDS: results of the European Collaborative ARDS study. *Intensive Care Medicine* 24:1018-1028.

Sreeramareddy CT, Panduru KV, Verma SC, Joshi HS, Bates MN. 2008. Comparison of pulmonary and extrapulmonary tuberculosis in Nepal – a hospital-based retrospective study. *BMC Infectious Diseases* 8:8.

Sreevatsan S, Pan X, Stockbauer KE, Connell ND, Kreiswirth BN, Whittam TS, Musser JM. 1997. Restricted structural gene polymorphism in the *Mycobacterium tuberculosis* complex indicates evolutionary recent global dissemination. *Proceedings of the National Academy of Sciences* 94:9869-9874.

Sridhar KS, Raub WA Jr. 1992. Present and past smoking history and other predisposing factors in 100 lung cancer patients. *Chest* 101:19-25.

Srinivasan M, Sedmak D, Jewell S. 2002. Effect of fixatives and tissue processing on the content and integrity of nucleic acids. *American Journal of Pathology* 161:1961-1971.

Stamatakis M, Douzinas E, Stefanaki C, Safioleas P, Polyzou E, Levidou G, Safioleas M. 2009. Gastrointestinal stromal tumor. *World Journal of Surgical Oncology* 7:61-70.

Standaert CJ, Herring SA. 2000. Spondylolysis: a critical review. *British Journal of Sports Medicine* 34:415-422.

Staras SAS, Dollard SC, Radford KW, Flanders WD, Pass RF, Cannon MJ. 2006. Seroprevalence of cytomegalovirus infection in the United States, 1988-1994. *Clinical Infectious Diseases* 43:1143-1151.

Statistics South Africa. 2010 Mortality and causes of death in South Africa, 2008: findings from death notification. [Internet]. Available: www.statssa.gov.za. (Cited 15 September 2011)

- Stead WW, Eichenholz A, Stauss HK.** 1955. Operative and pathologic findings in twenty four patients with syndrome of idiopathic pleurisy with effusion, presumably tuberculosis. *American Review of Respiratory Disease* 71:473-502.
- Stead WW, Senner JW, Reddick WT, Lofgren JP.** 1990. Racial differences in susceptibility to infection by *Mycobacterium tuberculosis*. *The New England Journal of Medicine* 322:422-427.
- Steer MS, Waxman I, Freedman S.** 1995. Chronic pancreatitis. *New England Journal of Medicine* 332:1482-1490.
- Stephens DS, Greenwood B, Brandtzaeg P.** 2007. Epidemic meningitis, meningococcaemia and *Neisseria meningitidis*. *Lancet* 369:2196-2210.
- Stewart BF, Siscovick D, Lind BK, Gardin JM, Gottdiener JS, Smith VE, Kitzman DW, Otto CM.** 1997. Clinical factors associated with calcific aortic valve disease. *Journal of the American College of Cardiology* 29:630-634.
- Stewart EA.** 2001. Uterine fibroids. *Lancet* 357:293-298.
- Stewart TD.** 1984. Pathologic changes in aging sacroiliac joints. A study of dissecting-room skeletons. *Clinical Orthopedics* 183:188-196.
- Steyn M, Scholtz Y, Botha D, Pretorius S.** 2013. The changing face of tuberculosis: Trends in tuberculosis-associated skeletal changes. *Tuberculosis* 93:467-474.
- Stollman NH, Raskin JB.** 1999. Diverticular disease of the colon. *Journal of Clinical Gastroenterology* 29:241-252.
- Streicher EM, Warren RM, Kewley C, Simpson J, Rastogi N, Sola C, Van der Spuy GD, Van Helden PD, Victor TC.** 2004. Genotypic and phenotypic characterization of drug resistant *Mycobacterium tuberculosis* isolates from rural districts of the Western Cape Province of South Africa. *Journal of Clinical Microbiology* 42:891-894.
- Stollman NH, Raskin JB.** 2004. Diverticular disease of the colon. *Lancet* 363:631-639.
- Strickland L, Letson GD, Muro-Cacho CA.** 2001. Gastrointestinal stromal tumors. *Cancer Control* 8:252-261.

- Stull MA, Clark LR, Reagan K, Green CE, Tracy CM, Goose PW, Suhocki PV, Twigg HL.** 1990. Bronchioloalveolar carcinoma of the lung. *American Journal of Roentgenology* 154:1318-1324.
- Saunders JB, Latt N.** 1993. Epidemiology of alcoholic liver disease. *Baillière's Clinical Gastroenterology* 7:555-579.
- Sugaya H, Moriishi J, Dohi M, Kon Y, Tsuchiya A.** 2003. Glenoid rim morphology in recurrent anterior glenohumeral instability. *The Journal of Bone & Joint Surgery* 85A:878-884.
- Sullivan RC, Francona NT, Kirshbaum JD.** 1940. Tuberculosis of the stomach. a clinical and pathologic study. *Annals of Surgery* 112:225-233.
- Sunderman FW, Boerner F.** 1949. Normal values in clinical medicine. WB Saunders, Philadelphia.
- Supply P, Mazars E, Lesjean S, Vincent V, Gicquel B, Locht C.** 2000. Variable human minisatellite-like regions in the *Mycobacterium tuberculosis* genome. *Molecular Microbiology* 36:762-771.
- Swensen SJ, Hartman TE, Williams DE.** 1994. Computed tomographic diagnosis of *Mycobacterium avium-intracellulare* complex in patients with bronchiectasis. *Chest* 105:49-52.
- Tang LM, Chen ST, Hsu WC, Lyu RK.** 1999. Acute bacterial meningitis in adults: a hospital-based epidemiological study. *QJM: An International Journal of Medicine* 92:719-725.
- Taylor GM, Goyal M, Legge AJ, Shaw RJ, Young D.** 1999. Genotypic analysis of *Mycobacterium tuberculosis* from medieval human remains. *Microbiology* 145:899-904.
- Terada N, Arai Y, Kinukawa N, Terai A.** 2008. The 10-year natural history of simple renal cysts. *Urology* 71:7-12.
- Thomas GAO, Rhodes J, Ingram JR.** 2005. Mechanisms of disease: nicotine – a review of its actions in the context of gastrointestinal disease. *Nature Clinical Practice, Gastroenterology & Hepatology* 2:536-544.
- Tomashefski JF, Davies P, Boggis C, Greene R, Zapol WM, Reid LM.** 1983. The pulmonary vascular lesions of the adult respiratory distress syndrome. *American Journal of Pathology* 112:112-126.

Thompson T, Evans W. 1930. Paradoxical embolism. *QJM: An International Journal of Medicine* 23:135-152.

Thorpe A, Neal D. 2003. Benign prostatic hyperplasia. *Lancet* 361:1359-1367.

Thwaites GE. 2009. Tuberculosis of the central nervous system in adults. In HS Schaaf & A Zumla (eds.), *Tuberculosis. A comprehensive clinical reference*, pp. 401-412, Saunders Elsevier, Philadelphia.

Thwaites GE, Bang ND, Dung NH, Quy HT, Oanh TT, Thoa NTC, Hien NQ, Thuc NT, Hai NN, Lan NTN, Lan NN, Duc NH, Tuan VN, Hiep CH, Chau TTH, Mai PP, Dung NT, Stepniewska K, White NJ, Hien TT, Farrar JJ. 2004. Dexamethasone for the treatment of tuberculous meningitis in adolescents and adults. *New England Journal of Medicine* 351:1741-1751.

Thwaites GF, Chau TTH, Mai NTH, Drobniewski F, McAdam K, Farrar J. 2000. Tuberculous meningitis. *Journal of Neurology, Neurosurgery & Psychiatry* 68:289-299.

Tile M. 1988. Pelvic ring fractures: should they be fixed? *Journal of Bone and Joint Surgery* 70B: 1-12.

Török ME, Yen NTB, Chau TTH, Mai NTH, Phu NH, Mai PP, Dung NT, Chau NVV, Bang ND, Tien NA, Minh NH, Hien NQ, Thai PVK, Dong DT, Anh DTT, Thoa NTC, Hai NN, Lan NN, Lan NTN, Quy HT, Dung NH, Hien TT, Chinh NT, Simmons CP, de Jong M, Turgut M. 2001. Multifocal extensive spinal tuberculosis (Pott's disease) involving cervical, thoracic and lumbar vertebrae. *British Journal of Neurosurgery* 15:142-146.

Trapnell JE, Duncan EHL. 1975. Patterns of incidence in acute pancreatitis. *British Medical Journal* 2:179-183.

Travis WD, Lubin J, Ries L, Devesa S. 1996. United States lung carcinoma incidence trends. Declining for most histologic types among males, increasing among females. *Cancer* 77:2464-2470.

Tsolaki AG, Gagneux S, Pym AS, Goquet de la Salmoniere YL, Kreiswirth BN, Van Soolingen D, Small PM. 2005. Deletions classify the Beijing/W strains as a distinct genetic lineage of *Mycobacterium tuberculosis*. *Journal of Clinical Microbiology* 43:3185-3191.

Turgut M. 2001. Multifocal extensive spinal tuberculosis (Pott's disease) involving cervical, thoracic and lumbar vertebrae. *British Journal of Neurosurgery* 15:142-146.

- Turken O, Kunter E, Sezer M, Solmazgul E, Cerrahoglu K, Bozkanat E, Ozturk A, Ilvan A.** 2002. Hemostatic changes in active pulmonary tuberculosis. *International Journal of Tuberculosis and Lung Disease* 6:927-932.
- Turner RT.** 2000. Skeletal response to alcohol. *Alcoholism: Clinical and Experimental Research* 24:1693-1701.
- Tuyns AJ, Pequignot G.** 1984. Greater risk of ascitic cirrhosis in females in relation to alcohol consumption. *International Journal of Epidemiology* 13:53-57.
- Underwood JCE.** 2004. General and Systemic Pathology. Osteoarticular and connective tissues: Osteomyelitis. Churchill Livingstone, Edinburgh, pp. 712-713.
- Utsinger PD.** 1985. Diffuse idiopathic skeletal hyperostosis. *Clinical Rheumatic Disease* 11:325-351.
- Van der Merwe AE, Steyn M, Maat GJR.** 2010. Adult scurvy in skeletal remains of late 19th century mineworkers in Kimberley, South Africa. *International Journal of Osteoarchaeology* 20:307-316.
- Van der Merwe AE, Weston DA, Oostraa RJ, Maat GJR.** 2013. A review of the embryological development and associated developmental abnormalities of the sternum in the light of a rare palaeopathological case of sternal clefting. *HOMO – Journal of Comparative Human Biology* 64:129-141.
- Van Embden JDA, Cave MD, Crawford JT, Dale JW, Eisenach KD, Gicquel B, Hermans P, Martin C, McAdam R, Shinnick TM, Small PM.** 1993. Strain identification of *Mycobacterium tuberculosis* by DNA fingerprinting: Recommendations for a standardized methodology. *Journal of Clinical Microbiology* 31:406-409.
- Van Embden JDA, Van Gorkom T, Kremer K, Jansen R, Van Der Zeijst BAM, Schouls LM.** 2000. Genetic variation and evolutionary origin of the direct repeat locus of *Mycobacterium tuberculosis* complex bacteria. *Journal of Bacteriology* 182:2393-2401.
- Vanhoenacker FM, De Backer AI, Op de Beeck B, Maes M, Van Altena R, Van Beckevoort D, Kersemans P, De Schepper AM.** 2004. Imaging of gastrointestinal and abdominal tuberculosis. *European Radiology Supplements* 14:E103-E115.

- Van Rie A, Beyers N, Gie RP, Kunneke M, Zietsman L, Donald PR.** 1999. Childhood tuberculosis in an urban population in South Africa: burden and risk factor. *Archives of Disease in Childhood* 80:433-437.
- Van Soolingen D, Qian L, de Haas PE, Douglas JT, Traore H, Portaels F, et al.** 1995. Predominance of a single genotype of Mycobacterium tuberculosis in countries of East Asia. *Journal of Clinical Microbiology* 33:3234-3238.
- Van't Hoog AH, Laserson KF, Githui WA, Meme HK, Agaya JA, Odeny LO, Muchiri BG, Marston BJ, DeCock KM, Borgdorff MW.** 2011. High prevalence of pulmonary tuberculosis and inadequate case finding in rural western Kenya. *American Journal of Respiration and Critical Care Medicine* 183:1245-1253.
- Venkataramana NK.** 2011. Hydrocephalus Indian scenario – a review. *Journal of Pediatric Neurosciences* 6:S11-S22.
- Verdy M, Guimond J, Fauteux, Aube M.** 1978. Prevalence of hyperostosis frontalis interna in relation to body weight. *The American Journal of Clinical Nutrition* 31:2002-2004.
- Vigorita VJ.** 1999. Orthopaedic pathology. Hypertrophic (Pulmonary) Osteoarthropathy. Lippincott Williams & Wilkins, Philadelphia, pp. 275-278.
- Virmani R, Avolio AP, Mergner WJ, Robinowitz M, Herderick EE, Cornhill JF, Guo SY, Liu T, Ou DY, O'Rourke M.** 1991. Effect of aging on aortic morphology in populations with high and low prevalence of hypertension and atherosclerosis. *American Journal of Pathology* 139:1119-1129.
- Vollenhoven B.** 1998. Introduction: the epidemiology of uterine leiomyomas. *Baillière's Clinical Obstetrics and Gynaecology* 12:169-176.
- Waldron T, Rogers J.** 1990. An epidemiologic study of sacroiliac fusion in some human skeletal remains. *American Journal of Physical Anthropology* 83:123-127.
- Walter T, Olivares M, Pizarro F, Muñoz C.** 1997. Iron, anemia and infection. *Nutrition Reviews* 55:111-124.
- Wang HS, Chen WS, Su WJ, Lin JK, Lin TC, Jiang JK.** 1998. The changing pattern of intestinal tuberculosis: 30 years' experience. *International Journal of Tuberculosis and Lung Disease* 2:569-574.

- Wapler U, Crubézy E, Schultz M.** 2004. Is cribra orbitalia synonymous with anemia? Analysis and interpretation of cranial pathology in Sudan. *American Journal of Physical Anthropology* 123:333-339.
- Warf BC.** 2005. Hydrocephalus in Uganda: the predominance of infectious origin and primary management with endoscopic third ventriculostomy. *Journal of Neurosurgery: Pediatrics* 102:1-15.
- Warren RM, Victor TC, Streicher EM, Richardson M, Beyers N, Gey van Pittius NC, Van Helden PD.** 2004. Patients with active tuberculosis often have different strains in the same sputum specimen. *American Journal of Respiratory and Critical Care Medicine* 169:640-614.
- Warren RM, Gey van Pittius NC, Barnard M, Hesselning A, Engelke E, De Kock M, Gutierrez MC, Chege GK, Victor TC, Hoal EG, Van Helden PD.** 2006. Differentiation of *Mycobacterium tuberculosis* complex by PCR amplification of genomic regions of difference. *International Journal of Tuberculosis and Lung Disease* 10:818-822.
- Watts HG, Lifeso RM.** 1996. Current concepts review. Tuberculosis of Bones and Joints. *Journal of Bone and Joint Surgery* 2:288-298.
- Weinfeld RM, Olson PN, Maki DD, Griffiths HJ.** 1997. The prevalence of diffuse idiopathic skeletal hyperostosis (DISH) in two large American Midwest metropolitan hospital populations. *Skeletal Radiology* 26:222-225.
- Wells CD, Cegielski JP, Nelson LJ, Laserson KF, Holtz TH, Finlay A, Castro KG, Weyer K.** 2007. HIV infection and multidrug-resistant tuberculosis – The perfect storm. *The Journal of Infectious Diseases* 196:S86-107.
- Wenger JD, Hightower MW, Facklam RR, Gaventa S, Broome CV, Bacterial Meningitis Study Group.** 1990. Bacterial meningitis in the United States, 1986: report of a multistate surveillance study. *The Journal of Infectious Diseases* 162:1316-1323.
- Western Cape Government Health.** 2013. Annual Report 2012/2013. [Internet]. Available: http://www.westerncape.gov.za/assets/departments/health/annual_report_2012-13_full-11h00.pdf. [2014, 4 July]
- Westerveld LA, Quarles van Ufford HME, Verlaan JJ, Oner FC.** 2008. The prevalence of diffuse idiopathic skeletal hyperostosis in an outpatient population in the Netherlands. *Journal of Rheumatology* 35:1635-1638.

- Weycker D, Edelsberg J, Oster G, Tino G.** 2005. Prevalence and economic burden of bronchiectasis. *Clinical Pulmonary Medicine* 12:205-209.
- Wicky S, Wintermark M, Schnyder P, Capasso P, Denys A.** 2000. Imaging of blunt chest trauma. *European Radiology* 10:1524-1538.
- Wiles NJ, Lingford-Hughes A, Daniel J, Hickman M, Farrell M, Macleod J, Haynes JC, Skapinakis P, Araya R, Lewis G.** 2007. Socio-economic status in childhood and later alcohol use: systemic review. *Addiction* 102:1546-1563.
- Williams JK, Adams MR, Klopfenstein HS.** 1990. Estrogen modulates responses of atherosclerotic coronary arteries. *Circulation* 81:1680-1687.
- Williamson DF, Forman MR, Binkin NJ, Gentry EM, Remington PL, Trowbridge FL.** 1987. Alcohol and body weight in United States adults. *Journal of Public Health* 77:1324-1330.
- Wilink TBM, Quick CRG, Day NE.** 1999. The association between cigarette smoking and abdominal aortic aneurysms. *Journal of Vascular Surgery* 30:1099-1105.
- Witt MA, Lipshultz LI.** 1993. Varicocele: a progressive or static lesion? *Urology* 42:541-543.
- Wolbers M, Farrar JJ.** 2011. Timing of initiation of antiretroviral therapy in human immunodeficiency virus (HIV)-associated tuberculous meningitis. *Clinical Infectious Diseases* 52:1374-1383.
- Wood R, Liang H, Wu H, Middelkoop K, Oni T, Rangaka MX, Wilkinson RJ, Bekker LG, Lawn SD.** 2010. Changing prevalence of tuberculosis infection with increasing age in high-burden townships in South Africa. *International Journal of Tuberculosis and Lung Disease* 14:406-412.
- Woodring JH, Vandiviere HM, Fried AM, Dillon ML, Williams TD, Melvin IG.** 1986. Update: the radiographic features of pulmonary tuberculosis. *American Journal of Roentgenology* 146:497-506.
- World Health Organization. Communicable Diseases: Tuberculosis.** 2011. [Internet] Available: http://www.searo.who.int/en/Section10/Section2097/Section2106_10678.htm.
- World Health Organization. Global Tuberculosis Control: Surveillance, Planning, Financing.** 2010. [Internet]. Available: http://www.who.int/tb/publications/global_report/en/index.html.

- Wynne-Davies R.** 1975. Congenital vertebral anomalies: aetiology and relationship to spina bifida cystica. *Journal of Medical Genetics* 12:280-288.
- Wynn Jones H, Beckles VLL, Akinola B, Stevenson AJ, Harrison WJ.** 2011. Chronic haematogenous osteomyelitis in children. *Journal of Bone and Joint Surgery* 93B:1005-1010.
- Xia F, Poon RTP, Wang SG, Bie P, Huang XQ, Dong JH.** 2003. Tuberculosis of pancreas and peripancreatic lymph nodes in immunocompetent patients: experience from China. *World Journal of Gastroenterology* 9:1361-1364.
- Xu X, Yu R, Qiu L, Shen J, Dong F, Chen Y.** 2011. Gallbladder tuberculosis: CT findings with histopathologic correlation. *Korean Journal of Radiology* 12:196-202.
- Yach D.** 1988. Tuberculosis in the Western Cape Health Region of South Africa. *Social Science & Medicine* 27:683-689.
- Yang Z, Kong Y, Wilson F, Foxman B, Fowler AH, Marrs CF, Cave MD, Bates JH.** 2004. Identification of risk factors for extrapulmonary tuberculosis. *Clinical Infectious Diseases* 38:199-205.
- Yao Q, Altman RD, Brahn E.** 2009. Periostitis and hypertrophic pulmonary osteoarthropathy: report of 2 cases and review of the literature. *Seminars in Arthritis and Rheumatism* 38:458-466.
- Yerokin AP.** 1979. Classification and frequency of varicocele in children. *Klinicheskaia Khirurgiia* 6:45.
- Yoon SS, Charny CK, Fong Y, Jarnagin WR, Schwartz LH, Blumgart LH, DeMatteo RP.** 2003. Diagnosis, management, and outcomes of 115 patients with hepatic hemangioma. *Journal of the American College of Surgeons* 197:392-402.
- Yoskovitch A, Kantor S.** 2001. Cervical osteophytes presenting as unilateral vocal fold paralysis and dysphagia. *The Journal of Laryngology & Otology* 115:422-424.
- Youmans GP.** 1979. Tuberculosis. Saunders, Philadelphia.
- Yu G, Hsieht C, Peng J.** 1988. Risk factors associated with the prevalence of pulmonary tuberculosis among sanitary workers in Shanghai. *Tubercle* 69:105-112.

- Zaman SN, Melia WM, Johnson RD, Portmann BC, Johnson PJ, Williams R.** 1985. Risk factors in development of hepatocellular carcinoma in cirrhosis: prospective study of 613 patients. *Lancet* i:1357-1360.
- Zerbi P, Schønau A, Bonetto S, Gori A, Costanzi G, Duca P, Vago L.** 2001. Amplified *in situ* hybridization with peptide nucleic acid probes for differentiation of *Mycobacterium tuberculosis* complex and nontuberculous *Mycobacterium* species on formalin-fixed, paraffin-embedded archival biopsy and autopsy samples. *American Journal of Clinical Pathology* 116:770-775.
- Zhan F, Wang CJ, Lin JZ, Zhong PJ, Qui WZ, Lin HH, Liu YH, Zhao ZJ.** 2010. Isolated splenic tuberculosis: a case report. *World Journal of Gastrointestinal Pathophysiology* 1:109-111.
- Zhang YQ, Shi J, Rajakumar G, Day AL, Simpkins JW.** 1998. Effects of sex and estradiol treatment on focal brain ischemia. *Brain Research* 784:321-324.
- Zhou XJ, Rakheja D, Yu X, Saxena R, Vaziri ND, Silva FG.** 2008. The aging kidney. *Kidney International* 74:710-720.
- Zink A, Haas CJ, Reischl U, Szeimies U, Nerlich AG.** 2001. Molecular analysis of skeletal tuberculosis in an ancient Egyptian population. *Journal of Medical Microbiology* 50:355-366.
- Zink AR, Sola C, Reischl U, Grabner W, Rastogi N, Wolf H, Nerlich AG.** 2003. Characterization of *Mycobacterium tuberculosis* complex DNAs from Egyptian mummies by spoligotyping. *Journal of Clinical Microbiology* 41:359-367.
- Zignol M, Hosseini MS, Wright A, Lambregts-van Weezenbeek C, Nunn P, Watt CJ, Williams BG, Dye C.** 2006. Global incidence of multidrug-resistant tuberculosis. *Journal of Infectious Diseases* 194:479-485.

Addenda

Addendum A:Standard formula for embalming at the Division Anatomy and Histology, SU.

The following formula has been in use at the Division of Anatomy and Histology for several years and is ideal for South African conditions.

<u>Reagent</u>	<u>Quantity</u>
Ethanol	15.0L
Thymol	40.0g
Poli-ethylene glycol 400	12.0L
Formalin	1.5L
Phenol	1.5L
Water	<u>15.0L</u>
	~ 45.0L

(Approximately 40.0 L of embalming fluid is needed to embalm one cadaver.)

Addendum B:Weights of the lungs and hearts of the cadaver cohort (n=127)

<i>Cadaver Ref. Nr</i>	<i>Right Lung (g)</i>	<i>Left Lung (g)</i>	<i>Heart (g)</i>	<i>Cadaver Ref. Nr</i>	<i>Right Lung (g)</i>	<i>Left Lung (g)</i>	<i>Heart (g)</i>
K01-10	1330.0	380.0	290.0	K15/11	520.0	430.0	150.0
K02-10	1080.0	1000.0	340.0	K18/11	470.0	390.0	230.0
K03-10	850.0	880.0	230.0	K31/11	710.0	500.0	140.0
K04-10	680.0	610.0	150.0	K38/11	900.0	570.0	220.0
K05-10	590.0	510.0	220.0	K40/11	300.0	340.0	200.0
K06-10	680.0	750.0	200.0	K41/11	440.0	50.0*	220.0
K10-10	1110.0	980.0	230.0	K42/11	1200.0	640.0	300.0
K12-10	1060.0	800.0	240.0	K43/11	640.0	520.0	170.0
K13-10	750.0	760.0	260.0	K44/11	890.0	730.0	280.0
K16-10	790.0	450.0	160.0	K46/11	710.0	1070.0	250.0
K18-10	700.0	550.0	160.0	K47/11	1060.0	810.0	390.0
K19-10	720.0	640.0	170.0	K52/11	1340.0	610.0	250.0
K30-10	680.0	530.0	240.0	K53/11	870.0	720.0	440.0
K36-10	710.0	590.0	180.0	K55/11	720.0	820.0	230.0
K38-10	590.0	460.0	240.0	K59/11	540.0	600.0	170.0
K40-10	1320.0	730.0	210.0	K62/11	700.0	520.0	190.0
K42-10	1110.0	900.0	270.0	K63/11	640.0	500.0	240.0
K45-10	910.0	960.0	220.0	K64/11	580.0	530.0	180.0
K47-10	630.0	510.0	210.0	K65/11	400.0	590.0	200.0
K80-09	460.0	500.0	190.0	K69/11	380.0	540.0	140.0
K81-09	760.0	780.0	270.0	K70/11	460.0	350.0	110.0
K82-09	590.0	610.0	250.0	K72/11	640.0	730.0	160.0
K83-09	690.0	600.0	240.0	K74/11	180.0	480.0	170.0
K87-09	400.0	460.0	180.0	K75/11	390.0	620.0	240.0
K89-09	1200.0	790.0	280.0	K76/11	600.0	560.0	150.0
K95-09	1060.0	280.0	570.0	K80/11	810.0	240.0	120.0
K96-09	730.0	850.0	220.0	K82/11	390.0	320.0	260.0
K99-09	490.0	240.0	170.0	K101/11	1410.0	950.0	220.0
K100-09	1130.0	690.0	300.0	K116/11	490.0	600.0	120.0
K101-09	700.0	300.0	220.0	K120/11	640.0	490.0	140.0
K102-09	530.0	390.0	150.0	K121/11	950.0	1020.0	220.0
K104-09	990.0	890.0	180.0	K124/11	600.0	650.0	160.0
K106-09	840.0	820.0	300.0	K125/11	580.0	600.0	220.0
K108-09	580.0	400.0	170.0	K126/11	910.0	890.0	200.0
K110-09	530.0	340.0	130.0	K129/11	420.0	360.0	160.0
K112-09	1080.0	1050.0	220.0	K130/11	300.0	270.0	150.0
K113-09	990.0	1120.0	240.0	K138/11	610.0	580.0	200.0
K115-09	590.0	550.0	240.0	K140/11	580.0	650.0	250.0
K118-09	540.0	870.0	310.0	K148/11	700.0	620.0	160.0
K119-09	720.0	600.0	170.0	K25-12	1220.0	940.0	210.0
K05/11	950.0	Pneumonectomy	170.0	K26-12	780.0	1160.0	220.0
K06/11	660.0	640.0	150.0	K27-12	1140.0	1350.0	250.0

<i>Cadaver Ref. Nr</i>	<i>Right Lung (g)</i>	<i>Left Lung (g)</i>	<i>Heart (g)</i>	<i>Cadaver Ref. Nr</i>	<i>Right Lung (g)</i>	<i>Left Lung (g)</i>	<i>Heart (g)</i>
K10/11	550.0	600.0	220.0	K28-12	580.0	440.0	200.0
K13/11	850.0	660.0	130.0	K31-12	530.0	470.0	210.0
K42-12	720.0	510.0	170.0	K76-12	840.0	860.0	320.0
K43-12	2020.0	1270.0	300.0	K77-12	860.0	700.0	150.0
K46-12	550.0	490.0	310.0	K78-12	690.0	550.0	270.0
K49-12	620.0	1260.0	300.0	K79-12	460.0	430.0	140.0
K50-12	920.0	490.0	220.0	K81-12	900.0	790.0	140.0
K43-12	2020.0	1270.0	300.0	K82-12	760.0	680.0	110.0
K46-12	550.0	490.0	310.0	K83-12	1160.0	980.0	340.0
K49-12	620.0	1260.0	300.0	K86-12	580.0	540.0	180.0
K50-12	920.0	490.0	220.0	K87-12	940.0	880.0	370.0
K51-12	680.0	1220.0	420.0	K93-12	680.0	540.0	390.0
K52-12	480.0	820.0	220.0	K94-12	910.0	470.0	300.0
K57-12	1090.0	890.0	230.0	K97-12	830.0	770.0	250.0
K58-12	1480.0	1270.0	400.0	K98-12	1070.0	880.0	420.0
K60-12	700.0	650.0	110.0	K99-12	1060.0	630.0	600.0
K61-12	780.0	880.0	250.0	K100-12	600.0	720.0	230.0
K62-12	920.0	860.0	280.0	K101-12	960.0	570.0	160.0
K64-12	1050.0	740.0	260.0	K104-12	440.0	360.0	270.
K66-12	930.0	1020.0	110.0	K106-12	1700.0	760.0	470.0
K69-12	1360.0	950.0	190.0	K107-12	970.0	680.0	150.0
K73-12	960.0	1130.0	190.0	K119-11	1550.0	1200.0	480.0
K74-12	680.0	760.0	140.0	K124-12	870.0	990.0	220.0
K75-12	780.0	890.0	290.0				

* Part of lung remained attached in the hemithorax

Addendum C:Cardiac valve measurements in the 2012 cadaver cohort (n=43)

<i>Cadaver Ref. Nr.</i>	<i>Sex</i>	<i>Aortic Valve (AV) mm</i>	<i>Pulmonary Valve (PV) mm</i>	<i>Mitral Valve (MV) mm</i>	<i>Tricuspid Valve (TV) mm</i>
K05/11	F	60	75	85	112
K06/11	M	58	71	84	118
K10/11	F	64	54	93	108
K13/11	F	60	70	75	113
K15/11	M	70	58	115	103
K18/11	F	76	60	83	120
K31/11	M	68	79	100	112
K38/11	M	80	81	105	110
K40/11	F	57	71	86	120
K41/11	F	59	70	69	88
K42/11	M	68	82	80	159
K43/11	F	50	55	80	96
K44/11	M	75	65	86	113
K46/11	M	70	65	130	99
K47/11	M	80	90	120	125
K52/11	M	74	77	84	126
K53/11	M	95	98	110	102
K55/11	M	65	66	85	108
K59/11	M	67	90	93	130
K62/11	M	84	76	68	118
K63/11	M	67	65	80	99
K64/11	F	68	65	90	110
K65/11	F	75	82	79	124
K69/11	F	60	56	72	125
K70/11	F	67	74	93	110
K72/11	M	58	80	95	111
K74/11	M	95	63	99	123
K75/11	M	68	83	97	118
K76/11	F	60	57	88	104
K80/11	M	74	78	90	115
K82/11	F	67	62	103	97
K101/11	M	65	88	80	118
K116/11	F	60	63	95	103
K120/11	F	55	70	77	100
K121/11	M	73	91	84	153
K124/11	F	60	67	78	102
K125/11	M	63	62	*	99
K126/11	M	74	71	100	126
K129/11	M	80	75	104	130
K130/11	F	75	60	103	80
K138/11	M	85	57	95	125
K140/11	F	77	74	90	149
K148/11	M	68	79	98	133

* Valve could not be accurately measured

Addendum D:Cardiac valve measurements in the 2013 cadaver cohort (n=44)

<i>Cadaver Ref. Nr.</i>	<i>Sex</i>	<i>Aortic Valve (AV) mm</i>	<i>Pulmonary Valve (PV) mm</i>	<i>Mitral Valve (MV) mm</i>	<i>Tricuspid Valve (TV) mm</i>
K25/12	M	70	73	81	123
K26/12	M	65	70	80	112
K27/12	M	72	80	104	*
K28/12	F	72	75	110	104
K31/12	M	65	70	86	131
K42/12	F	52	56	106	104
K43/12	M	86	93	113	148
K46/12	M	63	67	98	111
K49/12	M	72	77	92	107
K50/12	F	65	70	94	125
K51/12	M	62	83	*	115
K52/12	M	54	63	*	129
K57/12	M	82	67	86	114
K58/12	M	70	80	104	114
K60/12	F	56	59	93	93
K61/12	M	71	78	88	138
K62/12	F	65	62	96	98
K64/12	M	65	70	117	119
K66/12	F	66	67	88	104
K69/12	M	57	64	74	146
K73/12	M	68	75	85	121
K74/12	F	46	53	74	90
K75/12	M	67	80	81	138
K76/12	M	68	85	92	132
K77/12	F	55	78	81	109
K78/12	M	60	67	82	124
K79/12	F	62	70	96	92
K81/12	M	66	68	90	101
K82/12	M	75	78	89	130
K83/12	M	58	56	98	114
K86/12	F	51	65	82	106
K87/12	M	66	97	*	130
K93/12	M	77	72	74	111
K94/12	M	57	52	83	95
K97/12	M	68	80	83	116
K98/12	M	71	67	93	103
K99/12	M	67	103	83	143
K100/12	F	68	71	87	111
K101/12	M	65	59	79	113
K104/12	F	63	60	77	94
K106/12	M	71	90	106	152
K107/12	F	64	65	96	122
K119/11	M	74	93	105	142
K124/12	M	71	81	102	131

* Valve could not be accurately measured

Addendum E:Body weights and estimated body mass index (BMI) of the cadavers (n=127)

<i>Cadaver Ref. Nr.</i>	<i>Weight (kg)</i>	<i>Body Mass Index (BMI)</i>	<i>Cadaver Ref. Nr.</i>	<i>Weight (kg)</i>	<i>Body Mass Index (BMI)</i>	<i>Cadaver Ref. Nr.</i>	<i>Weight (kg)</i>	<i>Body Mass Index (BMI)</i>
K01-10	49.5	11.5	K31/11	*	---	K50-12	50.5	39.8
K02-10	52.4	13.7	K38/11	38.6	7.9	K51-12	42.6	9.1
K03-10	44.6	10.4	K40/11	31.9	29.1	K52-12	31.9	24.4
K04-10	34.0	12.7	K41/11	41.3	36.1	K57-12	64.6	19.4
K05-10	47.4	11.8	K42/11	52.5	15.2	K58-12	49.3	11.5
K06-10	39.7	13.5	K43/11	30.5	30.0	K60-12	46.5	35.1
K10-10	43.0	12.0	K44/11	63.4	10.0	K61-12	46.6	12.0
K12-10	49.2	14.0	K46/11	45.6	9.6	K62-12	59.9	24.8
K13-10	47.1	10.3	K47/11	51.3	23.6	K64-12	42.1	9.0
K16-10	36.1	24.9	K52/11	*	---	K66-12	28.0	13.7
K18-10	*	---	K53/11	*	---	K69-12	53.8	17.3
K19-10	41.6	35.1	K55/11	*	---	K73-12	34.4	7.2
K30-10	71.0	12.5	K59/11	39.9	9.2	K74-12	27.8	29.7
K36-10	40.7	9.3	K62/11	46.6	8.4	K75-12	48.9	11.5
K38-10	43.5	11.2	K63/11	45.9	10.8	K76-12	69.2	13.6
K40-10	42.7	9.8	K64/11	64.5	19.7	K77-12	42.3	31.9
K42-10	46.1	10.1	K65/11	*	---	K78-12	46.6	13.0
K45-10	62.4	17.7	K69/11	27.8	13.2	K79-12	53.2	42.3
K47-10	43.0	11.0	K70/11	46.7	32.8	K81-12	29.7	6.9
K80-09	*	---	K72/11	41.1	11.6	K82-12	54.2	12.5
K81-09	*	---	K74/11	*	---	K83-12	55.0	13.1
K82-09	*	---	K75/11	*	---	K86-12	43.6	40.0
K83-09	*	---	K76/11	*	---	K87-12	67.1	20.7
K87-09	*	---	K80/11	48.0	14.7	K93-12	60.8	14.4
K89-09	*	---	K82/11	40.0	34.3	K94-12	34.8	7.8
K95-09	*	---	K101/11	*	---	K97-12	46.8	10.5
K96-09	44.0	23.1	K116/11	*	---	K98-12	72.1	17.4
K99-09	33.2	12.0	K120/11	*	---	K99-12	47.8	11.6
K100-09	46.2	12.7	K121/11	*	---	K100-12	45.1	35.9
K101-09	34.4	9.1	K124/11	*	---	K101-12	30.0	6.8
K102-09	27.8	18.5	K125/11	40.9	8.7	K104-12	45.0	23.7
K104-09	36.8	28.7	K126/11	46.5	10.6	K106-12	70.5	13.2
K106-09	48.4	14.0	K129/11	52.8	19.5	K107-12	41.3	15.9
K108-09	36.5	26.5	K130/11	34.7	14.5	K119-11	*	---
K110-09	33.4	12.4	K138/11	50.3	24.8	K124-12	47.7	8.0
K112-09	33.0	6.2	K140/11	40.5	33.5			
K113-09	49.5	10.7	K148/11	27.4	6.8			
K115-09	37.5	8.8	K25-12	47.4	10.7			
K118-09	48.4	10.3	K26-12	46.4	9.5			
K119-09	50.3	37.0	K27-12	49.7	10.8			
K05/11	33.4	24.4	K28-12	32.7	25.5			
K06/11	39.1	9.0	K31-12	72.7	13.0			
K10/11	52.2	37.2	K42-12	52.8	34.5			
K13/11	25.0	19.0	K43-12	52.5	9.6			
K15/11	33.0	12.3	K46-12	44.2	11.6			
K18/11	50.9	21.5	K49-12	49.8	9.7			

* Weight is unavailable; --- BMI undetermined

Addendum F:Protocol for the standard Hematoxylin and Eosin technique for Paraffin Sections

The reagents used are Eosin Y (*acid red 87*) Cl 45380 as well as Mayer's hematoxylin.

Solution A:

Hematoxylin	1.0 g
Distilled water	1000.0 mL
Potassium or ammonium alum	50.0 g
Sodium iodate	0.2 g
Citric acid	1.0 g
Chloral hydrate SLR	50.0 g
Chloral hydrate AR	30.0 g

Method:

1. Immerse in Xylene for 2 minutes x 2
2. Immerse in absolute (100%) alcohol for 1 minute x 2
3. Immerse in 96% alcohol for 1 minute x 2
4. Immerse in 70% alcohol for 1 minute
5. Wash in tap water for 2 minutes
6. Stain in Haematoxylin for 4 minutes
7. Wash in running tap water for 3 minutes
8. Stain in Eosin for 2.30 seconds
9. Wash in running tap water for 2 minutes
10. Immerse in 70% alcohol for 0.20 seconds
11. Immerse in 96% alcohol for 0.15 seconds x 2
12. Immerse in absolute (100%) alcohol for 0.15 seconds x 2
13. Immerse in Xylene for 0.30 seconds
14. Immerse for a second time in Xylene for 1 minute
15. Mount the slides with DPX mounting medium and a cover slide

Results:

Nuclei	-	Blue/black	Cytoplasm	-	Shades of pink
Muscle	-	Pinkish-red	RBC	-	Orange
Fibrin	-	Deep pink			

Addendum G:Protocol for the Ziehl-Neelsen technique for acid-fast bacteria**Solution A:**

Basic fuchsin	0.5 g
Absolute alcohol	5.0 g
5% aqueous phenol	100 mL

Solution B:

Hydrochloric acid	10.0 g
70% alcohol	1000.0 mL

Solution C (stock solution):

Methylene blue	1.4 g
95% alcohol	100.0 mL

Solution D (working solution):

Methylene blue	10.0 mL
Tap water	90.0 mL

Method:

1. Deparaffinise the sections in xylene for 3 minutes and hydrate in different graded alcohols for 1 minute each. The alcohols used are: 70%, 96% and absolute alcohol
2. Rinse the sections in distilled water
3. Add carbol fuchsin to the sections and place the sections in an incubator for 1 hour. The temperature of the incubator needs to be maintained at between 56-60°C
4. Rinse in distilled water
5. Use 1% acid alcohol for differentiation
6. Wash and rinse in running tap water for 5 minutes
7. Add the methylene blue as counterstain for approximately 30 seconds
8. Rinse in running tap water
9. Dehydrate through graded alcohols (70%, 96% and absolute alcohol)
10. Clear the sections in xylene and mount in DPX medium

Results:

Mycobacteria	-	Red
Background	-	Blue

Addendum H:Protocol for the Perls' Prussian blue reaction for ferric iron**Ferrocyanide Solution:**

1% aqueous potassium ferrocyanide	20.0 mL
2% aqueous hydrochloric acid	20.0 mL

Method:

1. Deparaffinise sections
2. Depending on the amount of ferric iron present, treat the sections with acid ferrocyanide solution for 10 to 30 minutes
3. Wash with distilled water
4. Stain the nuclei with 0.5% aqueous neutral red or 0.1% nuclear fast red
5. Rinse briefly with distilled water
6. Dehydrate the sections
7. Clear in xylene and mount

Results:

Nuclei	-	Red
Ferric iron	-	Blue

Addendum I:Protocol for the Martius Scarlet Blue (MSB) technique for fibrin

The reagents used are Martius yellow (*acid yellow 24*) CI 10315, brilliant crystal scarlet (*acid red 44*) CI 16250 and soluble methyl blue (*acid blue*) CI 42780.

Solution A:

Martius yellow	0.5 g
Phosphotungstic acid	2.0 g
95% alcohol	100.0 mL

Solution B:

Brilliant crystal scarlet	1.0 g
Glacial acetic acid	2.0 mL
Distilled water	100.0 mL

Solution C:

Phosphotungstic acid	1.0 g
Distilled water	100.0 mL

Solution D:

Methyl blue	0.5 g
Glacial acetic acid	1.0 mL
Distilled water	100.0 mL

Solution E:

Glacial acetic acid	1.0 mL
Distilled water	100 mL

Method:

1. Deparaffinise sections
2. With the use of iodine and sodium thiosulfate procedure, remove any mercury present in the sections
3. Stain the nuclei by means of the celestine blue-hematoxylin treatment
4. Differentiate the sections in 1% acid alcohol
5. Wash in tap water
6. Rinse the sections in 95% alcohol
7. Stain for 2 minutes in the Martius yellow solution
8. Rinse well in distilled water
9. Stain for 10 minutes in the brilliant crystal scarlet
10. Rinse well in distilled water
11. Use the phosphotungstic solution to remove the reddish stained collagen
12. Rinse well in distilled water
13. Stain the collagen with the methyl blue solution
14. Rinse well in 1% acetic acid
15. Dehydrate the sections
16. Clear in xylene and mount

Results:

Nuclei	-	Blue
Erythrocytes	-	Yellow
Muscle	-	Red
Collagen	-	Blue
Fibrin fibrin)	-	Red (ranges from yellow to blue depending on the age of the

Addendum J:Protocol for the Periodic Acid-Schiff (PAS) technique**Solution A:**

Periodic Acid	1.0 g
Deionized or distilled water	100.0 mL

Method:

1. Deparaffinise sections
2. Oxidise the sections with periodic acid for 5 minutes
3. Rinse well in deionized water
4. Stain the sections with the Schiff reagent for 15 minutes
5. Rinse well in running tap water for 5 to 10 minutes
6. Use Mayer's hematoxylin to stain for nuclei
7. Dehydrate the sections
8. Clear in xylene and mount

Results:

Glycogen	-	Magenta
Glycoproteins	-	Magenta
Nuclei	-	Blue

Addendum K:Protocol for the Verhoeff's method for elastic fibers**Solution A:**

Hematoxylin	5.0 g
Absolute alcohol	100.0 mL

Solution B:

Ferric chloride	10.0 g
Distilled water	100.0 mL

Solution C (Lugol's iodine solution):

Iodine	1.0 g
Potassium iodide	2.0 g
Distilled water	100.0 mL

Solution D (working solution):

Solution A	20.0 mL
Solution B	8.0 mL
Solution C	8.0 mL

Method:

1. Deparaffinise the sections
2. Stain with Verhoeff's solution for 15 to 30 minutes
3. Wash in water
4. Use the 2% aqueous ferric chloride to differentiate the elastic fibers (appear black)
5. Wash in water
6. Wash in 95% alcohol to remove staining caused by the iodine
7. Use von Gieson as a counterstain (Eosin may also work)
8. Blot to remove the excess stain
9. Dehydrate the sections
10. Clear in xylene and mount

Results:

Elastic fibers and nuclei	-	Black
Collagen	-	Red
Other tissue	-	Yellow

Addenda L:

A summary of the distribution of systemic TB lesions in the cadaver cohort (n=127)

Cadaver Reference Number	Systemic Tuberculosis Lesion Distribution										
	Pulmonary	Lymph Nodes	Cardiovascular	Brain	Gastrointestinal	Hepatic	Pancreatic	Splenic	Renal	Genital	Skeletal
K01-10	+	-	-	Did not evaluate brains from the first cadaver cohort	-	-	-	-	-	-	-
K02-10	+	-	-		-	-	-	-	-	-	-
K03-10	+	-	-		-	-	-	-	-	-	-
K04-10	+	-	-		-	-	-	-	-	-	-
K05-10	-	-	-		-	-	-	-	-	-	-
K06-10	+	-	-		-	-	-	-	-	-	-
K10-10	+	-	-		-	-	-	-	-	-	-
K12-10	+	-	-		-	-	-	-	-	-	-
K13-10	+	-	-		-	-	-	-	-	-	-
K16-10	+	-	-		-	-	-	-	-	-	-
K18-10	+	-	-		-	-	-	-	-	-	-
K19-10	+	-	-		-	-	-	-	-	-	+
K30-10	+	-	-		-	-	-	-	-	-	-
K36-10	-	-	-		-	-	-	-	-	-	-
K38-10	+	-	-		-	-	-	-	-	-	-
K40-10	+	-	-		-	-	-	-	-	-	-
K42-10	+	-	-		-	-	-	-	-	-	-
K45-10	+	-	-		-	-	+	-	-	-	-
K47-10	-	-	-		-	-	-	-	-	-	-
K80-09	-	-	-		-	-	-	-	-	-	-
K81-09	+	-	-		-	-	-	-	-	-	-
K82-09	+	-	-		-	-	-	-	-	-	-
K83-09	+	-	-		-	-	-	-	-	-	-
K87-09	+	+	-		-	-	+	-	+	-	-
K89-09	+	-	-		-	-	-	-	-	-	-
K95-09	+	-	-		-	-	-	-	-	-	-
K96-09	+	-	-		-	-	-	-	-	-	-
K99-09	-	-	-		-	-	-	-	-	-	-
K100-09	+	-	-		-	-	-	-	-	-	-
K101-09	+	-	-		-	-	-	-	-	-	-
K102-09	+	-	-		-	-	-	-	-	+	-
K104-09	+	-	-		-	-	-	-	-	-	-
K106-09	+	-	-		-	-	-	-	-	-	-
K108-09	-	-	-		-	-	-	-	+	-	-
K110-09	+	-	-		-	-	-	-	-	-	-
K112-09	+	-	-		-	-	-	-	-	-	-
K113-09	+	-	-		-	-	-	-	-	-	-
K115-09	+	-	-		-	-	-	-	-	-	-
K118-09	-	-	-		-	-	-	-	-	-	-
K119-09	-	-	-		-	-	-	-	-	+	-

Cadaver Reference Number	Systemic Tuberculosis Lesion Distribution										
	Pulmonary	Lymph Nodes	Cardiovascular	Brain	Gastrointestinal	Hepatic	Pancreatic	Splenic	Renal	Genital	Skeletal
K05-11	+	-	-	-	-	-	-	-	-	-	-
K06-11	-	-	-	-	-	-	-	-	-	-	-
K10-11	-	-	-	-	-	-	-	-	-	-	-
K13-11	+	-	-	-	-	-	-	+	-	-	-
K15-11	+	-	-	-	-	-	-	-	-	-	-
K18-11	-	-	-	-	-	-	-	-	-	-	-
K31-11	+	-	-	-	-	-	-	-	-	-	-
K38-11	-	-	-	-	-	-	-	-	-	-	-
K40-11	-	-	-	-	-	-	-	-	-	-	-
K41-11	+	-	-	-	-	-	-	-	-	-	-
K42-11	-	-	-	-	-	-	-	-	-	-	-
K43-11	-	-	-	-	-	-	-	-	-	-	-
K44-11	-	-	-	-	-	-	-	-	-	-	-
K46-11	+	-	-	-	-	+	-	+	-	-	-
K47-11	+	-	-	-	-	-	-	-	-	-	-
K52-11	+	+	-	-	-	+	-	-	-	-	-
K53-11	+	-	-	-	-	-	-	-	-	-	-
K55-11	+	-	-	-	+	+	-	-	-	-	-
K59-11	+	-	-	-	-	-	-	-	-	-	-
K62-11	+	-	-	-	-	-	-	-	-	-	-
K63-11	-	-	-	-	-	-	-	-	-	-	-
K64-11	+	-	-	-	-	-	-	+	+	-	-
K65-11	+	+	-	-	-	+	-	-	+	-	-
K69-11	+	-	-	-	-	-	-	-	-	-	-
K70-11	+	-	-	-	-	-	-	-	-	-	-
K72-11	-	-	-	-	-	-	-	+	-	-	-
K74-11	-	-	-	-	-	-	-	-	-	-	-
K75-11	+	-	-	-	-	-	-	-	-	-	-
K76-11	-	-	-	-	-	-	-	-	-	-	-
K80-11	+	-	-	-	-	-	-	-	-	-	-
K82-11	+	-	-	-	-	-	-	-	-	-	-
K101-11	+	-	-	-	-	-	-	-	-	-	-
K116-11	+	-	-	-	-	-	-	+	-	-	-
K120-11	+	-	-	-	-	-	-	+	-	-	-
K121-11	+	+	-	-	-	+	-	+	+	-	-
K124-11	+	+	-	-	-	+	-	+	-	-	-
K125-11	+	-	-	-	-	-	-	-	-	-	-
K126-11	+	-	-	-	-	-	-	-	-	-	-
K129-11	+	-	-	-	-	-	-	-	-	-	-
K130-11	-	-	-	-	-	-	-	-	-	-	-
K138-11	+	-	-	-	-	+	-	-	-	-	-
K140-11	+	+	-	-	-	+	-	+	+	-	-
K148-11	+	-	-	-	-	-	-	-	-	-	-

Cadaver Reference Number	Systemic Tuberculosis Lesion Distribution										
	Pulmonary	Lymph Nodes	Cardiovascular	Brain	Gastrointestinal	Hepatic	Pancreatic	Splenic	Renal	Genital	Skeletal
K25-12	+	-	-	-	-	+	+	+	+	-	-
K26-12	+	-	-	-	-	+	+	+	+	-	-
K27-12	+	-	-	-	-	-	-	-	-	-	-
K28-12	+	-	-	-	-	-	-	-	-	-	-
K31-12	-	-	-	-	-	-	-	-	-	-	-
K42-12	+	-	-	-	-	+	-	+	-	-	-
K43-12	+	-	-	-	-	-	-	-	-	-	-
K46-12	+	-	-	-	-	-	-	-	-	-	-
K49-12	+	-	-	-	-	+	-	+	+	-	-
K50-12	+	-	-	-	-	-	-	-	-	-	-
K51-12	+	-	-	-	-	-	-	-	-	-	-
K52-12	+	-	-	-	-	-	-	-	-	-	-
K57-12	+	-	-	-	-	-	-	-	-	-	-
K58-12	-	-	-	-	-	-	-	-	-	-	-
K60-12	+	-	-	-	+	-	-	+	-	-	-
K61-12	+	+	-	-	-	-	-	-	-	-	-
K62-12	-	-	-	-	-	-	-	-	-	-	-
K64-12	+	-	-	-	-	-	-	-	-	-	-
K66-12	+	-	-	-	-	-	-	-	-	-	-
K69-12	+	-	-	-	-	-	-	-	-	-	-
K73-12	+	-	-	-	-	-	-	-	-	-	-
K74-12	+	-	-	-	-	-	-	+	+	-	-
K75-12	+	-	-	-	-	-	-	+	+	-	-
K76-12	+	-	-	-	-	-	-	-	-	-	-
K77-12	+	+	-	-	-	-	-	-	-	-	-
K78-12	+	-	-	-	-	-	-	-	-	-	-
K79-12	-	-	-	-	-	-	-	-	-	-	-
K81-12	+	-	-	-	-	-	-	-	-	-	-
K82-12	+	-	-	-	-	-	-	-	-	-	-
K83-12	-	-	-	-	-	-	-	-	-	-	-
K86-12	-	-	-	-	-	-	-	+	-	-	-
K87-12	+	-	-	-	-	-	-	-	-	-	-
K93-12	-	+	-	-	-	-	-	-	-	-	-
K94-12	-	-	-	-	-	-	-	-	-	-	-
K97-12	+	-	-	-	-	-	-	-	-	-	-
K98-12	+	-	-	-	-	-	-	-	-	-	-
K99-12	+	+	-	-	-	-	-	-	-	-	-
K100-12	+	+	-	-	-	-	-	-	-	-	-
K101-12	+	-	-	-	-	-	-	-	-	-	-
K104-12	-	-	-	-	-	-	-	+	-	-	-
K106-12	+	-	-	-	-	-	-	-	-	-	-
K107-12	+	-	-	-	-	-	-	-	-	-	-
K119-11	+	+	-	-	-	-	+	+	-	-	-
K124-12	+	-	-	-	-	-	-	-	-	-	-

“felix qui potuit rerum cognoscere causas”

Fortunate he, who was able to learn the causes of things